AD-760 265

THEORY AND CALCULATION OF FEED UNITS OF LIQUID-PROPELLANT ROCKET ENGINES

B. V. Ovsyannikov, et al

Foreign Technology Division
Wright-Patterson Air Force Base, Chio

28 February 1973

FTD-MT-24-1524-72

FOREIGN TECHNOLOGY DIVISION

THEORY AND CALCULATION OF FEED UNITS OF LIQUID-PROPELLANT ROCKET ENGINES

by

B. V. Ovsyannikov and
B. I. Borovskiy

Approved for public release;
distribution unlimited.

UNCLASSIFIED

Security Classification

DOCUMENT CONTROL DATA - R & D

(Security classification of title, body of abstract and indexing annotation must be entered when the overall report is classified)

1. ORIGINATING ACTIVITY (Corporate author) Foreign Technology Division Air Force Systems Command U. S. Air Force	2a. REPORT SECURITY CLASSIFICATION UNCLASSIFIED 2b. GROUP

3. REPORT TITLE

THEORY AND CALCULATION OF FEED UNITS OF LIQUID-PROPELLANT ROCKET ENGINES

4. DESCRIPTIVE NOTES (Type of report and inclusive dates)

Translation

5. AUTHOR(S) (First name, middle initial, last name)

B. V. Ovsyannikov, B. I. Borovskiy

6. REPORT DATE 1971	7a. TOTAL NO. OF PAGES<br~~170~~ 793	7b. NO. OF REFS 161
8a. CONTRACT OR GRANT NO. b. PROJECT NO. c. d. 771-04-01	9a. ORIGINATOR'S REPORT NUMBER(S) FTD-MT-24-1524-72 9b. OTHER REPORT NO(S) (Any other numbers that may be assigned this report)	

10. DISTRIBUTION STATEMENT

Approved for public release; distribution unlimited.

11. SUPPLEMENTARY NOTES	12. SPONSORING MILITARY ACTIVITY Foreign Technology Division Wright-Patterson AFB, Ohio

13. ABSTRACT

21 08
21 08.1

DD FORM 1 NOV 68 1473

UNCLASSIFIED

Security Classification

EDITED MACHINE TRANSLATION

FTD-MT-24-1524-72

THEORY AND CALCULATION OF FEED UNITS OF LIQUID-PROPELLANT ROCKET ENGINES

by: B. V. Ovsyannikov and B. I. Borovskiy

English pages: 770

Source: Teoriya i Raschet Agregatov Pitaniya Zhidkostnykh Raketnykh Dvigateley, Izd-vo Mashinostroyeniye, Moscow, 1971, pp. 1-540.

Requester: FTD/PDTA-5

This document is a SYSTRAN machine aided translation, post-edited for technical accuracy by: Robert D. Hill

TABLE OF CONTENTS

U. S. BOARD ON GEOGRAPHIC NAMES TRANSLITERATION SYSTEM

Block	Italic	Transliteration	Block	Italic	Transliteration
А а	*А а*	A, a	Р р	*Р р*	R, r
Б б	*Б б*	B, b	С с	*С с*	S, s
В в	*В в*	V, v	Т т	*Т т*	T, t
Г г	*Г г*	G, g	У у	*У у*	U, u
Д д	*Д д*	D, d	Ф ф	*Ф ф*	F, f
Е е	*Е е*	Ye, ye; E, e*	Х х	*Х х*	Kh, kh
Ж ж	*Ж ж*	Zh, zh	Ц ц	*Ц ц*	Ts, ts
З з	*З з*	Z, z	Ч ч	*Ч ч*	Ch, ch
И и	*И и*	I, i	Ш ш	*Ш ш*	Sh, sh
Й й	*Й й*	Y, y	Щ щ	*Щ щ*	Shch, shch
К к	*К к*	K, k	Ъ ъ	*Ъ ъ*	"
Л л	*Л л*	L, l	Ы ы	*Ы ы*	Y, y
М м	*М м*	M, m	Ь ь	*Ь ь*	'
Н н	*Н н*	N, n	Э э	*Э э*	E, e
О о	*О о*	O, o	Ю ю	*Ю ю*	Yu, yu
П п	*П п*	P, p	Я я	*Я я*	Ya, ya

* ye initially, after vowels, and after ъ, ь; e elsewhere. When written as ё in Russian, transliterate as yё or ё. The use of diacritical marks is preferred, but such marks may be omitted when expediency dictates.

FOLLOWING ARE THE CORRESPONDING RUSSIAN AND ENGLISH

DESIGNATIONS OF THE TRIGONOMETRIC FUNCTIONS

Russian	English
sin	sin
cos	cos
tg	tan
ctg	cot
sec	sec
cosec	csc
sh	sinh
ch	cosh
th	tanh
cth	coth
sch	sech
csch	csch
arc sin	$\sin^{-1}$
arc cos	$\cos^{-1}$
arc tg	$\tan^{-1}$
arc ctg	$\cot^{-1}$
arc sec	$\sec^{-1}$
arc cosec	$\csc^{-1}$
arc sh	$\sinh^{-1}$
arc ch	$\cosh^{-1}$
arc th	$\tanh^{-1}$
arc cth	$\coth^{-1}$
arc sch	sech^{-1}
arc csch	csch^{-1}
rot	curl
lg	log

All figures, graphs, tables, equations, etc. merged into this translation were extracted from the best quality copy available.

Theory and Calculation of Feed Units of Liquid-Propellant Rocket Engines. B. V. Ovsyannikov, and B. I. Borovskiy, Moscow, "Machine Building," 1971, 540 pages, plus 2 inserts.

In the book information on the theory and hydraulic design of pumps and turbines of turbopump units [TU] (THA) of liquid-propellant rocket engines [LPRE] (ЖРД) is given. Principles of the general theory of vane machines are given. The basic calculated relations for the design of the flow part of pumps and turbines are derived. The selection of the basic parameters of turbopump units is substantiated, and conditions of their operation are analyzed. Methods of the calculation of pumps and turbines of LPRE are briefly set forth. Examples of the calculation are given.

The book is written in accordance with the curriculum and is intended as a manual for students of aviation, machine-building and polytechnic colleges who are specializing in engines of flight vehicles.

The book can also be useful for engineers and technicians who are engaged in the calculation, design and operation of engine installations.

The book has nine tables, 350 figures and a bibliography of 161 names.

Reviewers are Doctor of Technical Sciences V. F. Chebyevskiy and the Department of Turbine Construction of KAI.

PREFACE

In the book problems of the theory and hydraulic design of pumps and turbines of turbopump units of liquid-propellant rocket engines are discussed. In connection with the fact that used in turbopump units of LPRE are the vane machines of different forms - axial-flow turbines and pumps, radial (centrifugal) pumps, radial (centripetal) turbines, hydroturbine, - in the book principles of the general theory of vane machines are given. This made it possible to avoid repetitions in the derviation of the fundamental relations and in the account of information of the profiling and calculation of the flow area of pumps and turbines.

Considerable attention is given in the book to the cavitation calculation of pumps, which provides the reliability of the engine installation, and also to the calculation of the energy characteristics of pumps and turbines.

Examined as a basic is the screw-centrifugal pump the most typical for the LPRE, and features of the calculation of pumps of the oxidizer and fuel are examined. Information on the selection and calculation of turbines of TU for engines of different designs is given in the book.

In the final section the selection of parameters of turbopump units is substantiated, and conditions of their operation are analyzed. An examination of these questions is conducted in

quite general and brief form, since a study on the specific designs of the feed and control of the engine is the object of a special course.

The terminology and designations are accepted taking into account the general approach to pumps and turbines as well as to vane machines; at the same time widely used are terms and designations recommended by the Committee of Technical Terminology of the Academy of Sciences of the USSR and most widespread in technical, academic and scientific literature.

Equations and numerical values are given in conformity with the International System of Units [SI] (CH). The actual data and numerical values are given on the basis of Soviet and foreign publications. Examples of the calculations have purely a systematic nature and do not refer to any specific engine.

In the account of the many problems the authors drew on the experience of industrial pump building and turbine construction. Furthermore, the material given in the textbook written by one of authors is partially used (B. V. Ovsyannikov, "Theory and Calculation of Pumps of Liquid-Propellant Rocket Engines" M., Oborongiz, 1960).

In view of the fact that in a number of colleges an abbreviated academic course is studied, part of the material which can be reduced in such cases is printed in brevier.

For the facilitation of the independent work of the students, besides the material of manual in the book a large quantity of graphic dependences is given, examples of calculations are given and a sufficiently detailed bibliography is given.

Chapters 1 and 2 in a larger part were written by B. V. Ovsyannikov, and the remaining chapters were written by the authors together; the total scientific editing of the book was done by B. V. Ovsyannikov.

The authors express their gratitude to these reviewers: Doctor of Technical Sciences V. F. Chebyevskiy, Candidates of Technical Sciences M. K. Maksutova, A. P. Tunakov and L. V. Goryunov for their valuable observations made during the review of the manuscript, and also to Doctors of Technical Sciences O. N. Yemin, K. V. Kholshchevnikov, V. A. Tselikov, Candidates of Technical Sciences N. S. Yershov and N. I. Kravchik for the useful advice expressed by them in the survey of individual sections of the manuscript.

The authors will be grateful to readers for critical observations both with respect to the essence of the discussed questions and with respect to the method of presentation. We ask that observations be sent to: Moscow, B-66, 1st Basmannyy Lane, 3, Publishing House "Machine-Building."

NOTATIONS

a - speed of sound; dimension of the minimum cross section of the cascade;

b - width of the meridian cross section of the vane machine (pump, turbine);

c - absolute velocity of the motion of liquid or gas;

C - cavitation power-speed coefficient;

D, d - diameter;

F, f - area;

G - mass flow rate of fluid or gas;

H - pressure, or increase in specific energy of fluid or gas;

h - height;

$\bar{H}$ - coefficient of pressure;

i - angle of attack; enthalpy;

k - coefficient which considers the effect of the finite number of blades;

L - specific work; decrease in energy of fluid or gas;

$\bar{L}$ - operating factor;

N - power;

n_s - power-speed coefficient (for a pump with bilateral inlet it is determined according to half the flow rate);

n_s^* - power-speed coefficient determined from the entire flow rate;

p - pressure;

Q - volumetric flow rate of fluid or gas;

q - flow-rate parameter;

R, r - radius;

R - gas constant;

T - temperature;

t - pitch;

u - circumferential velocity;

v - flow velocity; specific volume;

w - relative speed;

z - number of blades; number of stages of the turbine or pump;

ε - degree of admission (degree of intake);

η - efficiency;

ν - coefficient of kinematic viscosity of fluid;

ξ - coefficient of the local resistances;

ρ - mass density of fluid or gas;

σ - coefficient of total pressure;

ω - angular velocity; frequency of rotation;

ζ - loss factor.

SUBSCRIPTS

ад - adiabatic - refers to parameters of the ideal adiabatic process;

вн - internal;

вт - hub-refers to parameters of the cross section of blades in hub;

вх - inlet

вых - outlet;

г - hydraulic or geometric;

гидр - hydraulic (hydraulic resistance);

д - disk;

кав - cavitation;

кр - critical;

мех - mechanical;

н - pump;

п - peripheral;

пол - polytropic;

р - calculated; flow;

с - refers to parameters of nozzle cascade;

ср - average;

сра - separation;

т - theoretical; turbine;

тр - friction;

у - refers to parameters of packing (leakage);

ш - screw conveyer;

m - refers to meridian projections of speeds and cross sections;

r - refers to radial projections of speeds;

u - refers to circumferential projections of speeds and to parameters called parameters on the circumference of a turbine wheel;

z - refers to axial projections of speeds, moments with respect to the axis and so on;

∞ - refers to all parameters determined on the basis of the assumption that the number of the blades is infinitely large.

CHAPTER 1

APPLICATION OF PUMPS AND TURBINES IN LIQUID-PROPELLANT ROCKET ENGINES

1.1. BASIC PARAMETERS OF FEED SYSTEMS OF COMPONENTS IN LIQUID-PROPELLANT ROCKET ENGINES

The liquid-propellant rocket engine [LPRE] (ЖРД) is an engine designed for the creation of thrust with short-term action. Usually the operating time of the engine is measured in seconds or minutes. In the LPRE propellants consisting of the liquid components, liquid fuel and liquid oxidizer, are used. The mass fuel consumption consists of kilograms and thousands of kilograms per second. The magnitude of the mass fuel consumption is determined by the thrust and specific thrust of the engine:

$$G_{\Sigma} = R/R_{уд}, \tag{1.1}$$

where G_{Σ} is the mass fuel consumption, i.e., the total consumption of the components - oxidizer ($G_{ок}$) and fuel, ($G_{гор}$)

$$G_{\Sigma} = G_{ок} + G_{гор}; \tag{1.2}$$

R is thrust in Newtons (N);

$R_{уд}$ is specific thrust in N/(kg/s).

The specific thrust of the LPRE, depending on the selected components, varies usually within 2500-4000 N/(kg/s). Let us estimate approximately the fuel consumption in the LPRE. If we accept for the LPRE $R_{уд}$ = 3300 N/(kg/s), then for each 10 kN of thrust 3 kg/s of fuel consumption will be required.

The mass flow rate of each of the components can be determined by the total consumption G_{Σ} and the selected value of the correlation coefficient of the components

$$\varkappa = G_{ок}/G_{гор}. \tag{1.3}$$

By means of equations (1.2) and (1.3) we will obtain

$$G_{ок} = \frac{\varkappa}{1+\varkappa} G_{\Sigma}; \tag{1.4}$$

$$G_{гор} = \frac{G_{\Sigma}}{1+\varkappa}. \tag{1.5}$$

As a rule, κ is greater than unity (usually κ = 2-4), and therefore the flow rate mass of the oxidizer $G_{ок}$ is greater than the fuel consumption $G_{гор}$. The volume flow rate of the component is found in terms of the mass flow rate and density

$$Q_{ок} = G_{ок}/\rho_{ок}; \tag{1.6}$$

$$Q_{гор} = G_{гор}/\rho_{гор}, \tag{1.7}$$

where $Q_{ок}$ and $Q_{гор}$ are the volumetric flow rates of the oxidizer and fuel, respectively;

$\rho_{ок}$ and $\rho_{гор}$ are the densities of the oxidizer and fuel.

Usually the density of the oxidizer (derivatives of nitric acid, liquid oxygen, etc.) is more than the density of the fuel (kerosene, alcholos, etc.), and therefore the difference in the volumetric flow rates of the oxidizer and fuel is less than the difference in their mass flow rates.

The volumetric flow rates of components consist in units and dozens of liters per second for engines with moderate thrust (up to 300 kN) and hundred of liters per second for high-thrust engines.

The feed pressure of the working component $p_{вых}$ is determined by the combustion chamber pressure $p_к$, by the drop on injectors $\Delta p_ф$ and by the resistance of the hydraulic line from the outlet of the pump to injectors, which with passage of the component (as a rule, this is fuel) through the cooling jacket of the combustion chamber can be great (up to 40-60 bar):

$$p_{вых} = p_к + \Delta p_ф + \Delta p_{маг.вых}. \quad (1.8)$$

With a combustion chamber pressure of 100-150 bar, drops on the injectors of 5-20 bar, and a resistance of hydraulic line of 15-20 bar, the value of the required feed pressure can be 150-220 bar.

Depending on the layout of the feed system of the engine, the feed of components of fuel into the combustion chamber of the LPRE can be achieved by a displacement of components from the tank by high-pressure gas or with the aid of pumps. In accordance with this, the feed systems of fuel components of the LPRE are divided into two groups:

1) pressurized systems;

2) pumping systems.

In pressurized systems (Fig. 1.1) any pressure chamber is utilized for the fuel feed into the combustion chamber. Used as a pressure chamber is a gas pressure tank (air, nitrogen) or a unit which produces gas by means of the combustion of powder ([SFPA] (ПАД) - solid fuel pressure accumulator) or liquid components of any propellant ([LFPA] (ЖАД) - liquid fuel pressure accumulator).

A characteristic of the pressurization system consists in the fact that the tanks with the components are under high pressure, which exceeds the combustion chamber pressure. Therefore, it is necessary to make the tanks thick-walled. At high pressures in the combustion chamber and with considerable quantities of fuel being consumed during the operating time (which is characteristics of engines of high thrust or long useful life), the tanks in the pressurized feed systems will be extremely heavy, unacceptable for a rocket. Therefore, for the LPRE with high pressure in the combustion chamber, which operate for a relatively long time or which have high thrust, pumping feed systems are always used.

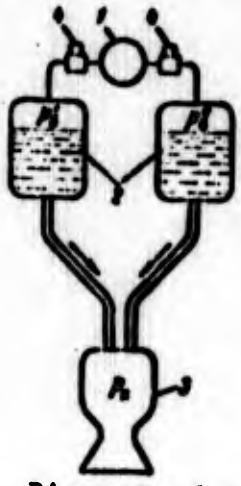

Fig. 1.1. Diagram of the pressurized feed system of fuel components of the LPRE; 1 - pressure chamber; 2 - tanks with components; 3 - combustion chamber; 4 - reduction valves.

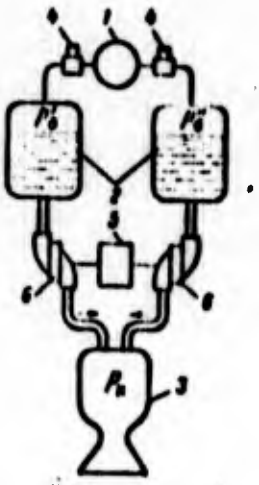

Fig. 1.2. Diagram of the pumping feed system of components of fuel of the LPRE: 1 - pressure chamber; 2 - tanks with components; 3 - combustion chamber; 4 - reduction valves; 5 - engine for drive of pumps; 6 - pumps.

In the pumping feed system within the fuel tanks, for example, with the aid of a gas pressure cylinder, the low pressure necessary to provide noncavitation operation of the pumps is maintained. The pressure necessary for fuel feed into the combustion chamber is created by the pumps (Fig. 1.2) being set into motion from the engine - usually from the turbine. Subsequently the unit which consists of the pumps and engine

will be called the pumping unit. If in the pumping unit a turbine is used as an engine, then we will call such unit a turbopump unit, or in abbreviated form, [TU] (THA). The working medium of the turbine is the gas obtained in the gas generator of the engine with the combustion of components of fuel of the engine or with the decomposition of any substance (for example, hydrogen peroxide).

The pump feed of fuel components in the LPRE was proposed by K. E. Tsiolkovsky as long ago as 1914. The pumping feed system is considerably more complex than the pressurized system, but at high quantities of expendable fuel and high feed pressures the pumping system is more preferable, since the weight of the entire power-supply system of the LPRE, including tanks of the components, will be less. Even at a combustion chamber pressure which exceeds 30-50 bars, it is inexpedient to use the pressurized feed system of components in the LPRE. (The exception is with micromotors - engines with low thrust and low duration of operation used for controlling satellites and spaceships in which a pressurized system is used).

The pumping feed system of components at the present time is the most widespread feed system of components in the LPRE. In the pumping feed system the pump should feed the necessary flow of the component, and in this case the pressure of the component should be raised from a low pump inlet pressure to a high pressure which exceeds the combustion chamber pressure [see equation (1.8)], i.e., the pump should provide an increase in the mechanical energy of the pumped fuel component.

An increase in the mechanical energy of 1 kg of the mass of liquid passed through the pump is called the pump head and is

designated H.[1] For a noncompressible fluid it is possible to write

$$H = \frac{p^*_{вых} - p^*_{вх}}{\rho} \frac{дж}{кг}, \qquad (1.9)$$

or

$$H = \left(\frac{p_{вых}}{\rho} + \frac{c^2_{вых}}{2}\right) - \left(\frac{p_{вх}}{\rho} + \frac{c^2_{вх}}{2}\right) = \frac{p_{вых} - p_{вх}}{\rho} + \frac{c^2_{вых} - c^2_{вх}}{2}, \qquad (1.10)$$

where p* and p are the full and static pressures of the component fuel, respectively; c - speed of the component; subscripts "вх" and "вых" refer to parameters of the component at the inlet into the pump and at the outlet from it.

Usually $c_{вх}$ = 5-10 m/s, and $c_{вых}$ = 10-20 m/s. At identical or close values of $c_{вх}$ and $c_{вых}$, it is possible to write

$$H = \frac{p_{вых} - p_{вх}}{\rho}. \qquad (1.11)$$

The value of the required outlet pressure $p_{вых}$ (feed pressure of the component) is estimated by equation (1.8). For determining the required pump heads H, let us discuss the estimate of the magnitude of the available inlet pressure of the pump $p_{вх}$.

Inlet pressure of the pump $p_{вх}$ (Fig. 1.3) is determined by the tank $p_б$, the level of the liquid column, the inertia head and the flow friction of the main line feeding the component to the pump, and the flow velocity at the inlet.

---

[1] In hydraulics the mechanical energy of 1 kg of liquid is called the liquid head. If we disregard the energy of the position, then the liquid head will be determined by equation $\frac{p^*}{\rho} = \frac{p}{\rho} + \frac{c^2}{2}$. The pump head is an increase in the liquid head passed through the pump.

Let us designate by the letter θ the angle between the direction of motion of the rocket (axis of the rocket) and the direction of the force of gravity (see Fig. 1.3). In the determination of the inlet pressure of the pump, it is necessary to consider the acceleration only tangential with respect to the flight trajectory. The acceleration, normal with respect to the trajectory, leads to a nonuniformity of pressure on the cross section of the pipeline, but will not have effect on the value of the mean pressure.

Fig. 1.3. Diagram of pump arrangement in a rocket.

For the liquid which flows along the tube, the inertial force in this cross section will be equal to

$$P_j = \gamma f l j,$$

where l is the level of the liquid column above the cross section of the inlet;

j is the tangential acceleration of the rocket;

f is the cross-sectional area of the tube.

The value of inertia pressure will be

$$p_j = \gamma l j.$$

Correspondingly, the gravitational pressure of the fluid column will be equal to $\rho g l \cos\theta$.

The sum of the gravitational and inertia pressures can be presented in the form

$$\rho g l \cos\theta + \rho j l = \rho l (g \cos\theta + j).$$

Taking all factors into account, the inlet pressure of the pump will be equal to

$$p_{вх} = p_б + \rho l (g \cos\theta + j) - \Delta p_{конв.вх} - \psi \frac{c_{вх}^2}{2}. \qquad (1.12)$$

During the rocket flight the inlet pressure of the pump does not remain constant but is changed with a change in the acceleration of the rocket and level of fluid in the tank.

Figure 1.4 shows the approximate dependence of the inlet pressure of the pump on the flight time of the rocket in the powered flight trajectory when the engine is operating. With the rocket launch $p_{вх}$ is usually 2-6 bar. During the motion of the rocket pressure $p_{вх}$, in being changed, can pass through the minimum, since the gravitational pressure falls in connection with a decrease in the level of the liquid column l, and inertial pressure rapidly increase in proportion to an increase in the acceleration of the rocket (tank pressure $p_б$ is virtually not changed).

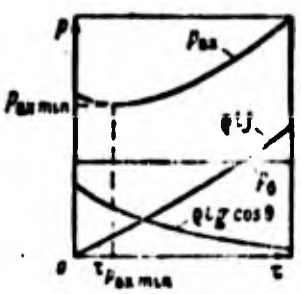

Fig. 1.4. Approximate dependence of inlet pressure of pump on the flight time of the rocket.

Let us note that the inlet pressure $p_{вх}$ is an important parameter of the pumping feed system of the LPRE. At low pressure $p_{вх}$ at the inlet of the pump cavitation can arise (see Section 3.3), which leads to a disruption of the pump - drop in pressure created by the pump and consumption. Therefore, it is important to design the pump so that it would possess the necessary anticavitation properties, i.e., would be able to operate without cavitation stalling at the assigned inlet pressure.

By knowing the required outlet pressure of the pump $p_{вых}$ and the available inlet pressure $p_{вх}$, it is possible to evaluate according to equation (1.11) the required pump head. Since the $p_{вх}$ is incomparably less than the pressure $p_{вых}$, the pump head H is virtually determined by the outlet pressure. Usually the required value of the pressure is 10,000-30,000 J/kg. Since the density of the fuel is less than the density of the oxidizer, the pump head of the fuel is greater than the pump head of the oxidizer. For pumps operating on liquid hydrogen (which has a very low density), the required head reaches a value of 250,000-400,000 J/kg. It hence follows that the pumps of the LPRE should be high-pressure pumps.

The power consumed by the pump can be calculated according to equation

$$N_{\text{н}} = \frac{GH}{\eta_{\text{н}}},$$

where G - the mass flow rate of the component through the pump;

$\eta_{\text{н}}$ - the efficiency of the pump. The more the efficiency of the pump, the less the required power. Usually $\eta_{\text{н}} = 0.5\text{-}0.8$.

At the assigned values of the required head and efficiency, the power consumed by pump is determined by the mass flow rate of the component (thrust of the engine). The power of pumps of the LPRE can reach 20,000-40,000 kW and more.

Let us formulate in more detail the basic requirements for pumps of the LPRE and engines being used for their drive.

1.2. REQUIREMENTS FOR PUMPING UNITS OF LIQUID-PROPELLANT ROCKET ENGINES

1.2.1. GENERAL REQUIREMENTS.

Let us formulate the basic, most general requirements for pumping units of the LPRE which consist of pumps and an engine for their drive:

1) the pumping unit should provide the continuous feed of the necessary quantity of components into the combustion chamber under an assigned pressure with as high an efficiency as possible;

2) the overall dimensions and mass of the pumping unit should be a minimum, and, consequently, the angular velocity of the unit should be as maximal as possible;

3) the cost of the manufacture of the pumping unit should be a minimum;

4) the pumping unit should provide normal operation of the engine in different conditions.

These general requirements for the pumping unit are defined concretely and supplemented depending on the purpose and schemes of the LPRE. Additional requirements are more precisely formulated in the examination of the specific feed system of the LPRE.

Having enumerated the general requirements for the pumping unit, let us formulate additional requirements for pumps of LPRE and engines used for their drive.

1.2.2. REQUIREMENTS FOR PUMPS

The requirements for pumps are almost wholly defined by such parameters of the engine plant as thrust, combustion chamber pressure, physicochemical properties of the components, tank pressure, and so on. These requirements are:

1) the pump should be adapted for operation with aggressive fluids, which are the high-boiling and low-boiling (cryogenic) oxidizers of propellants of the LPRE: nitric acid and its derivatives, hydrogen peroxide, liquid fluorine, liquid oxygen, and so on.

In operating with oxidizers the friction between the parts of the pump is inadmissible, which leads to the local heating of internal parts of the pump, inflammation and even explosion of the pump. In view of this the pumps in which there are friction pairs can prove to be unsuitable for the LPRE;

2) pumps of the LPRE should possess high anticavitation properties, i.e., they should be efficient at low pressures at the inlet. The less the permissible inlet pressure of the pump, the less the necessary tank pressure of the component, and this leads to a decrease in the mass of the tank and decrease in the mass of the entire engine plant;

3) the pump should have such a characteristic (dependence of the pressure created on the fluid flow rate) which would provide the stable operation of the feed system both on the basic and transient operating modes of the engine.

In the operation of the pump there should be eliminated the possibility of the stalling of the conditions or the onset of oscillations of parameters of the pump (pressure, flow rate) under the effect of low probable deviations in the resistance of the feed system.

These are the basic, general requirements for pump of the LPRE. In isolated special cases these requirements can be modified, and new specific requirements can appear.

1.2.3. REQUIREMENTS FOR ENGINES OF THE DRIVE OF PUMPING UNITS

Let us formulate additional requirements for engines of the pump drive of LPRE, taking into account that many requirements for the engine were included in the general requirements for the pumping unit:

1) the drive engine should have a high angular velocity and, as a rule, provide drive to the pumps without using special devices transmitting the torque (for example, a gear train);

2) in the engine such an energy source which does not require a considerable increase in the mass of the rocket should be utilized. In the case when the working medium used is ejected into the atmosphere, in passing the combustion chamber of the LPRE, the engine of the pump drive should have high power coefficients referred to the unit mass of the expendable working medium;

3) the engine should be easily transferred from one mode to another.

Taking into account the requirements formulated above, let us explain which types of pumps and engines will be best suitable for their use in liquid-propellant rocket engines.

1.3. COMPARISON OF PUMPS AND ENGINES OF DIFFERENT TYPES

1.3.1. PUMPS

There are many types of the pumps which operate according to different principles and constructively are different from each other.

Let us analyze briefly the operating principle and basic properties of pumps in connection with the requirements given to pumps of the feed system of LPRE. We will examine only mechanical pumps. For the pumping of the current-conduction fluids, in particular, metals, electrical and electromagnetic pumps of different types are used.

According to the operating principle, mechanical pumps can be divided into four basic groups: positive-displacement, frictions pumps, jet, and vane.

1.3.1.1. Positive-Displacement Pumps

Positive-displacement pumps operate according to the principle of displacement. Fluid in these pumps is forced into the delivery line by any moving control. The pressure being developed by the positive-displacement pump depends on the flow friction of force main after the pump and is virtually limited only by the clearance leakage and strength of parts of the pump.

Basically positive-displacement pumps of three types are used (see source [29]):

1. Piston (Fig. 1.5), in which the displacement of the fluid into the high-pressure area and also the suction of the fluid are produced by the piston being set into motion with the

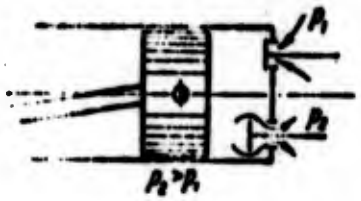

Fig. 1.5. Diagram of a piston pump.

aid of a crankgear from the shaft of any engine. The suction and displacement are achieved through the controllable or automatic valves.

2. Gear or helical (Fig. 1.6).

These pumps are arranged in such a way that the rotors, made in the form of serrated gears or screws, being rotated with a small clearance in the pump casing, cut off from the intake annulus the volume of fluid which fell into the cavity between the teeth and housing, and it is ejected into the cavity of increased pressure.

Fig. 1.6. Diagram of a gear pump.

3. Rotary (Fig. 1.7).

Rotary pumps are arranged in such a way that the vanes, which are moved in radial grooves of the eccentrically rotating rotor, cut off the fluid from the intake annulus and transfer it to the cavity of increased pressure.

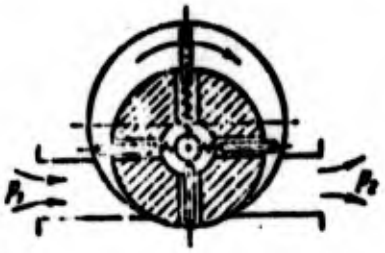

Fig. 1.7. Diagram of a rotary pump.

The major advantages of the positive-displacement pumps are:

1) the possibility of obtaining high pressures;

2) the independence of the rate of discharge of the feed pressure. The theoretical characteristic of these pumps (dependence of the pressure being developed by the pump on the flow which flows through the pump, not allowing for a change in the value of the clearance leakage) is a vertical line (Fig. 1.8);

3) high efficiency;

4) possibility of operation with a two-phase fluid.

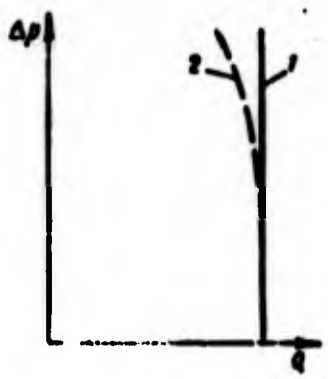

Fig. 1.8. Standard characteristics of positive-displacement pumps: 1 - theoretical; 2 - real characteristic.

Positive-displacement pumps with small clearances between the operating unit and housing are self-priming pumps, i.e., such pumps which can operate without priming, evacuating first the gases and vapors and then the fluid.

The deficiencies inherent to the positive-displacement pumps are:

1) large masses and overall dimensions, especially with high flow rates;

2) small angular velocity (due to the danger of great wear), especially in the case of the use in the crankgear transmission. As a consequence of this, for positive-displacement pumps limited productivitv with the assigned mass and dimensions is characteristic;

3) the presence of rubbing surfaces can lead to the localized heating, which is inadmissible with the pumping of oxidizers of fuels of LPRE.

The field of application of positive-displacement pumps as the basic (low flow rates and high pressures) coincides with the field of application of the displacement feed (low momenta), which has advantages with respect to the mass and structural simplicity. Sometimes the positive-displacement pumps can be used as bench pumps.

1.3.1.2. Friction Pumps

In friction pumps the mobile working element carries the fluid away because of the presence of forces of viscosity. Figure 1.9 gives a disk friction pump, which consists of feed 1, disk wheel 2 and spiral branch 3 (see sources [26] and [28]).

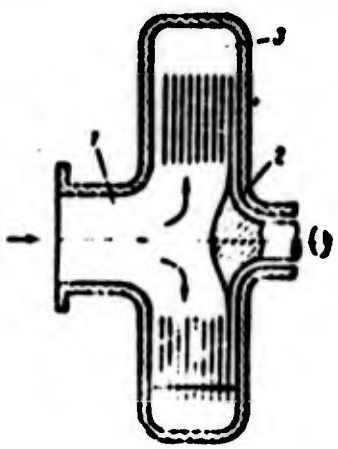

Fig. 1.9. Diagram of a friction pump: 1 - feed; 2 - disk wheel; 3 - branch.

The disk wheel consists of several thin disks fastened to each other by rivets on the periphery in such a way that between the disks there remains small clearances for the passage of the fluid. The operating principle of the disk pump consists in the following. During rotation of the wheel the fluid, which is located in the clearance between the disks, is twisted as a result of the friction against the disks, owing to which a pumping effect is created.

The advantages of the disk pumps consist in their high anticavitation qualities. Disk pumps can operate at lower inlet pressures than, for example, vane pumps. This is explained by the fact that with the flow of the entering edges of the disks there appears less evacuation than with the flow of the vanes.

Shortcomings of disk friction pumps are:

1) low efficiency (usually less than 0.4);

2) large overall dimensions with high flow rates and pressures;

3) great dependence of the pump performance of physical properties and temperature of the component of fuel being pumped.

These shortcomings restrict the use of disk pumps as the basic pumps of LPRE. They can be used as the auxiliary stages of pumps for the improvement of their anticavitation qualities. Pumps which are the combination of the friction pump and vane pump deserve attention.

1.3.1.3. Jet Pumps

The jet pump (ejector) (see further Fig. 3.103) includes nozzles 1, mixing chamber 2, diffuser 3 and converging nozzle

section 4. Fluid under high pressure (ejection fluid) is fed to the nozzle 1. Entering into the input part of the mixing chamber is the ejected fluid with low pressure and speed. In nozzle 1 the ejection fluid increases its kinetic energy because of a pressure drop and then enters into the mixing chamber. In the mixing chamber in the process of mixing, an energy transfer occurs from the ejection fluid to that being ejected.

As a result of this at the output of mixing the mechanical energy of one kilogram of the mass of the mixed fluid becomes more than the energy of the ejected fluid at the mixing chamber inlet. In the diffuser the pressure of the mixed fluid increases up to pressure p_3 larger than p_1. The advantage of jet pumps consists in their structural simplicity and reliability. Jet pumps can be used in LPRE as auxiliary (booster) pumps in front of the main pumps for an increase in anticavitation qualtities of the pumping feed system (see sources [34] and [36]).

Shortcomings in jet pumps:

1) low efficiency;

2) low pressures, which they can provide.

1.3.1.4. Vane Pumps.

A vane pump is a variety of a vane machine. In the vane pump the conversion of mechanical energy on the pump shaft into energy of the fluid is accomplished in the rotating channels formed by the blades. For vane pumps the streamline flow of the rotating blades by the flow of the fluid is characteristic. Vane pumps are divided into two basic types, centrifugal (see, further Fig. 3.20) and axial pumps (see further Fig. 3.69).

In the centrifugal pump the displacement of the particle of fluid in the rotor occurs with a considerable increase in its

distance from the axis of rotation. In the energy conversion in the centrifugal pump, a great role is played by the Coriolis force of inertia. In the axial pump the displacement of the particle of fluid occurs with an insignificant change in its distance from the axis. In the energy conversion in axial pumps the dominant role is played by the circulation flow of the baldes. Besides centrifugal and axial pumps, there are vane pumps of the intermediate type - mixed-flow pump.

Centrifugal pumps are usually used in required pressures exceeding 1000 J/kg.

The field of application of single-stage axial pumps as the basic, as a rule, refers to less pressures and especially high consumptions - exceeding 150-200 *l*/s. If we use multistage axial pumps, it is possible to obtain sufficiently high pressures. In the LPRE the axial pumps are used basically as first stages of the pumps; specifically, receiving wide application was the helical-type pump (worm conveyor) (see further Fig. 2.67). The rotor wheel of the worm conveyor has 2-3 long blades encompassing the hub at an angle exceeding 180°. The blade of the worm conveyor is profiled along the height according to a definite law. The worm conveyor creates low pressure but can provide high flow rates. A shortcoming in the helical-type pump is the low efficiency, which reaches 0.5. Worm conveyors possess good anticavitation properties. Therefore, helical-type pumps found use in the LPRE as the stages which improved the anticavitation properties of pumps of the LPRE (see sources [13] and [35]).

Vane pumps have the following positive properties:

1) the possibility of providing virtually any pressures and fluid flow rates;

2) the possibility of operating at high angular velocities;

3) the small mass of the pump;

4) the small overall dimensions of the pump;

5) the possibility of operating on aggressive fluids as a result of the absence of friction pairs;

6) the convenience of drive from electric motors and turbines;

7) the minimum number of moving parts.

The disadvantages of vane pumps are:

1) a comparatively small value of efficiency of the pump (usually not more than 0.8-0.85);

2) change in the pressure being developed by the pump with a change in the flow rate.

A variety of centrifugal vane pumps is the vortex pump (see Fig. 1.10 and source [25]). The wheel with small vanes milled out on the periphery is rotated in the housing so that between the housing and the wheel there is an annular channel of constant section. The inlets and outlets (see Fig. 1.10) are separated by a cross connection adjacent (with small clearance) to the wheel. Fluid is caught by the vanes, passes along the vane channel and is thrown out into the annular channel of the housing. Moving along the annular channel, before leaving the pump fluid repeatedly enters into the vane channels. To a certain extent, the vortex pump acts as a multistage centrifugal pump.

The advantage of the vortex pump consists in the fact that at this circular velocity of the wheel the pressure of the vortex pump is higher than that of the centrifugal pump (almost two

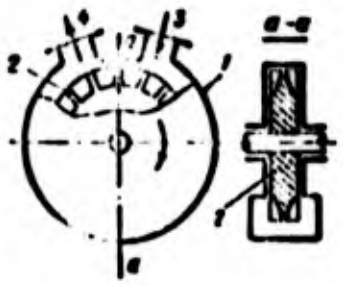

Fig. 1.10. Diagram of a vortex pump: 1 - housing; 2 - rotor wheel; 3 - inlets; 4 - outlet.

times). Vortex pumps possess good absorptivity. With low productivity (up to 10 *l*/s) the vortex pump can have a higher efficiency than the centrifugal pump, and when Q > 1(*l*/s the efficiency of the vortex pumps is less than that of the centrifugal vane pump.

From the brief examination of the different types of pumps it may be concluded that sometimes all the examined forms of the pumps can find use in the feed systems of the LPRE. But with comparatively high flow rates of the aggressive liquid, vane pumps most fully satisfy the requirement given to pumps of feed systems of the LPRE, and therefore vane pumps found extensive use in feed systems of the LPRE. With further presentation of the course, the theory and calculation of vane pumps will be examined in detail.

Let us note the feature of contemporary pumps of the LPRE. Characteristic at the present time is the use of combined vane pumps, which consist of a different type of vane stages. In the combined vane pumps the best properties of each of the types of vane pumps are used. The most widespread is the combination of the worm-conveyor stage with the centrifugal installed on one shaft (see source [35]). Such a pump is called a worm-centrifugal (see further Fig. 3.1). It possesses high anticavitation and delivery qualities.

In the feed system the LPRE, the combination of the worm-centrifugal pump with auxiliary (booster) jets or vane pumps also finds use (see Section 3.3.8).

1.3.2. ENGINES FOR PUMP DRIVE

It is possible to use two engine types as engines for the pump drive:

1) heat engines;

2) electric motors.

The use of electric motors for the pump drive of LPRE at the present time is made difficult due to the absence of light and powerful electric power sources aboard the rocket. It is doubtful that with the development of sources of electrical energy which directly use chemical, nuclear or solar energy, electric motors will be used for the pump dirve in LPRE.

Virtually at the present time for the pump drive, only heat engines are used. For heat engines installed on the rocket, aboard the flight vehicle there should be a reserve of fuel and oxidizer.

If we examine the two possible forms of heat engines - piston engine and turbine plant - in the relation of their conformity to requirements given to engines for the pump drive of the LPRE the turbine will have a clear advantage.

The turbine makes it possible to obtain high power with a small mass of construction; and the high angular velocity, absence of a crankgear, and consequently, unbalanced force of inertia, and the direct-flow course of the working medium cause the low mass of the turbine.

Another advantage of the turbine is the ease of its connection with the vane pumps. The turbine makes it possible to obtain the high energy per unit of the consumption of the working medium, and this is very important, as it will be shown below in the case the LPRE with the ejection of the working medium of the turbine passing by the combustion chamber. Problems of the control of the turbine are also solved comparatively easily.

Therefore, the turbine is the only type of engine being used for the pump drive of the LPRE. The contemporary turbopump unit (TU) consists of worm-centrifugal pumps for feeding components of the fuel and turbine. Figure 1.11 shows the TU of the liquid-propellant rocket engine RD-107 (see source [27]), and Fig. 1.12 shows the TU of the aircraft LPRE XRL-99, which feeds the components of the fuel - liquid oxygen and ammonia. The turbine operates on vapors of hydrogen peroxide. The frequency of rotation of the TU reaches at the present time 3000-4000 $1/s$ and above (see source [33]).

GRAPHIC NOT REPRODUCIBLE

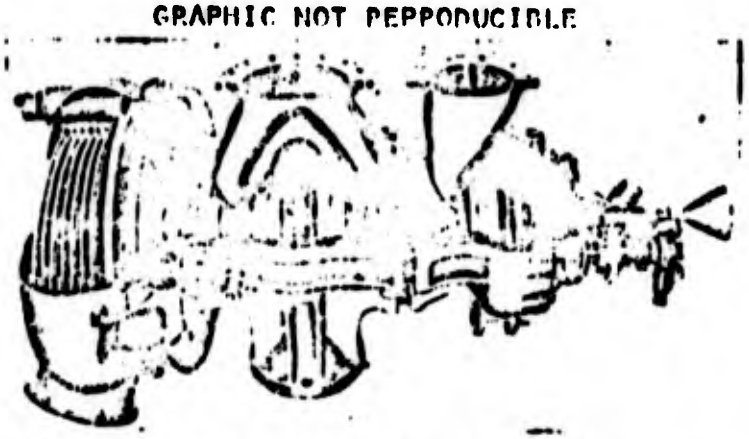

Fig. 1.11. Turbopump unit of the LPRE RD-107.

Given on Fig. 1.13 is a longitudinal cross section of a turbopump unit of the American engine J-2 for the feeding of liquid hydrogen. The hydrogen pump consists of a preliminary pump and seven-stage axial pump.

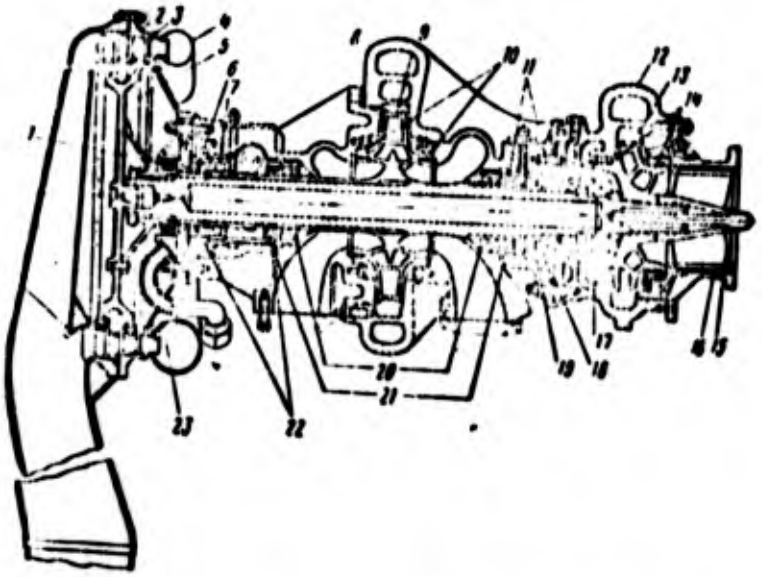

Fig. 1.12. Turbopump unit of the aircraft Liquid-propellant Rocket Engine XRL-99: 1 - Seal; 2 - Turbine casing; 3 - Nozzle unit; 4 - Inlet manifold of turbine; 5 - Turbine disk; 6 - Thrust ring of bearing; 7 - Bearing; 8 - Diffuser of fuel pump; 9 - Impeller of fuel pump; 10 - Seal of fuel pump; 11 - Seal; 12 - Diffuser of the oxidizer pump; 13 - Impeller of oxidizer pump; 14 - Seal of the oxidizer pump; 15 - Preliminary pump; 16 - Housing of preliminary pump; 17 - Seal; 18 - Thrust ring of bearing; 19 - Bearing; 20 - Seal of fuel pump; 21 - Fuel and oil drain; 22 - Seal; 23 - Drain of steam and gas.

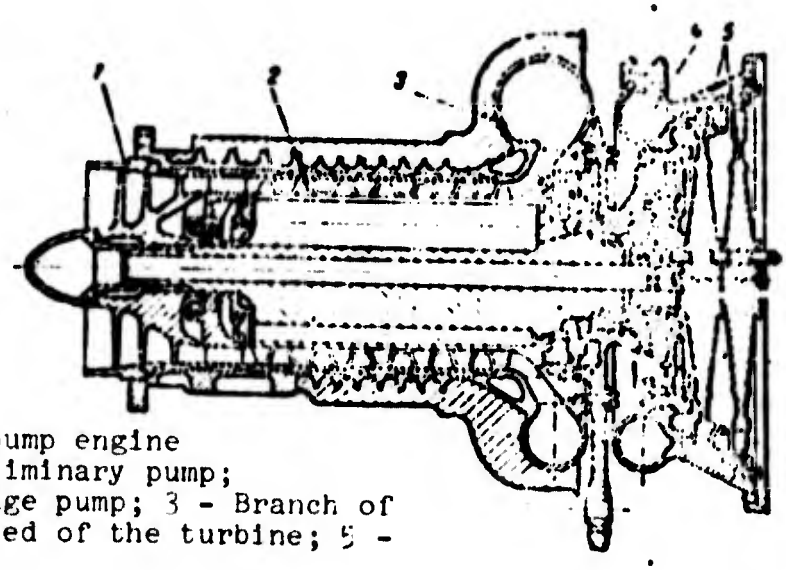

Fig. 1.13. Turbopump engine unit J-2: 1 - Preliminary pump; 2 - Axial multistage pump; 3 - Branch of axial pump; 4 - Feed of the turbine; 5 - Turbine wheel.

Figure 1.14 (see source [27]) shows the turbopump engine unit RZ-2 with reducing angular velocity (from the turbine to pumps) by pinion drive. The use of the pinion drive makes it possible to obtain the optimum angular velocities for pumps and the turbine, but it considerably complicates the construction and makes it heavier.

Depending on the scheme of the feed system of the LPRE the turbopump unit should satisfy these or different operating conditions. Features of the turbines and pumps of the LPRE can be explained only in the examination of standard patterns of the feed systems of the LPRE.

GRAPHIC NOT REPRODUCIBLE

Fig. 1.14. Turbopump unit with pinion drive from the turbine to pumps of the engine RZ-2: 1 - Worm conveyor of oxidizer pump; 2 - The centrifugal wheel of the oxidizer pump; 3 - Branch of oxidizer pump; 4 - Centrifugal wheel of fuel pump; 5 - Branch of fuel pump; 6 - Two-stage turbine; 7 - Pinion drive from turbine to pumps; 8 - Drive gears of the units.

1.4. SCHEMES OF FEED SYSTEMS OF LPRE WITH TURBOPUMP FEEDING OF THE FUEL

Let us analyze the basic standard patterns of the feed systems of LPRE with a turbopump unit. The scheme of the feed system causes specific requirements for pumps and turbines. Parameters of the pumps and turbines can greatly differ depending on the scheme of the feed system of the LPRE. The feed system affects the operating conditions and parameters of the turbine especially greatly.

The operating conditions of a turbine will substantially differ depending on whether or not after the turbine gas is fed to the combustion chamber. Let us accept this as the basic criterion for the classification of the feed systems of LPRE with a TU. According to this criterion, the feed systems can be divided into groups (Fig. 1.15). Figure 1.15 gives the short names of schemes of the feed system. These names are conditional and are introduced for convenience.

The scheme of the feed system with the gas feed after the turbine into the combustion chamber will be called the scheme with the *precombustion-chamber turbine*, and the scheme without the feed of the turbine gas into the combustion chamber will be called the scheme with the *autonomous (independent) turbine*.

In the diagram with the precombustion-chamber turbine the outlet pressure of the turbine (counterpressure) is great, and it is determined by the pressure of the combustion chamber of the LPRE.

In the scheme with the autonomous turbine the counterpressure is considerably less, since the gas after the turbine is ejected into the atmosphere, passing by the combustion chamber. The LPRE with an autonomous turbine is widely used in rocket technology.

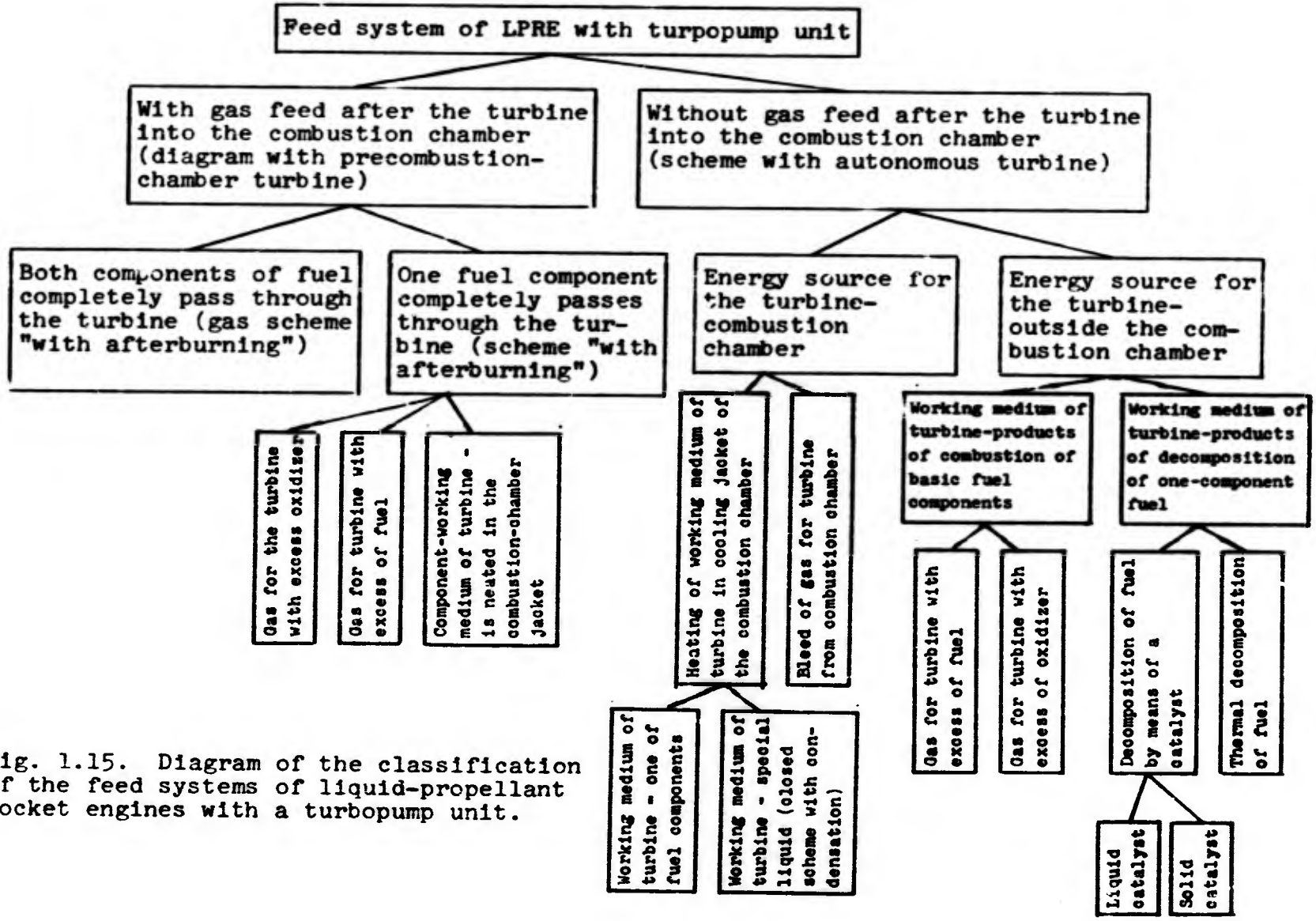

Fig. 1.15. Diagram of the classification of the feed systems of liquid-propellant rocket engines with a turbopump unit.

The development of the LPRE began from engines made according to scheme of this group, from which we will begin a more detailed examination of the feed systems.

1.4.1. FEED SYSTEMS WITH AUTONOMOUS TURBINE

After the autonomous turbine the gas enters into the special nozzles (sometimes these are the control nozzles of rocket control) and is ejected through them into the atmosphere, creating an additional thrust. If only one of the components of fuel is cryogenic, then in front of the entrance into the nozzles the gas is used for evaporation in the heat exchanger of a definite quantity of cryogenic component intended for the tank pressurization with this component (see source [30]). If one of the components of fuel is high-boiling (noncryogenic), then part of the gas after the turbine can be used for the tank pressurization with this component.

The energy source of the autonomous turbine can be connected with the combustion chamber of the engine and can be independent of it. In the first case the turbine operates on gas taken from the combustion chamber (see source [35]), with a subsequent temperature decrease up to that permissible for the turbine (for example, by means of injection of one of the fuel components), or on gas obtained by the gasification of a special liquid in the cooling jacket of the combustion chamber.

Both of these methods of the use of the combustion chamber as the energy source for the turbine did not find use in the LPRE. The first method is not used because the solution to the problem of the gas bleed is complex and decreases the strength and reliability of the combustion chamber and the second means - in view of its complexity and an increase in the mass of the engine.

In the scheme with the energy source of the turbine, independent of the combustion chamber, gas for the turbine is obtained in a special gas generator. Figure 1.16 gives a diagram of the feed system of the LPRE with an autonomous turbine, to which gas is fed from the gas generator, which operates on the basic components of fuel. Such a scheme is basic for the LPRE with an autonomous turbine. Part of the components after the pumps is directed to the gas generator. The gas after the turbine is used for the evaporation of part of the component going to the pressurization tank.

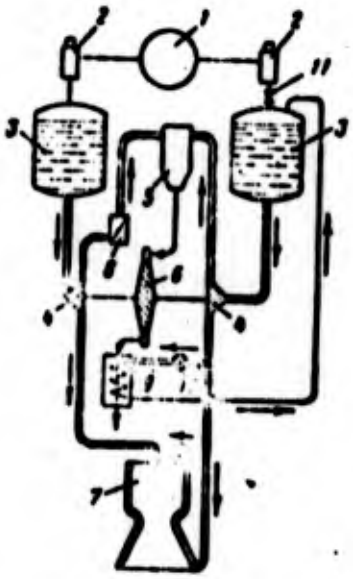

Fig. 1.16. Diagram of a liquid-propellant rocket engine with an autonomous turbine and heat exchanger in which is utilized the heat of exhaust gases of the turbine for the evaporation of the fuel component going to the pressurization tank: 1 - pressure accumulator; 2 - reduction valves; 3 - tanks; 4 - pumps; 5 - gas generator; 6 - turbine; 7 - combustion chamber; 8 - thrust regulator; 9 - heat exchanger; 10 - valve; 11 - return valve.

The gas generator operates with considerable excess of one of the components in order to obtain gas with the temperature permissible for the turbine from considerations of strength (usually 800-1200° K). Depending on whether the gas generator operates with the fuel excess or oxidizer excess, the gas approaching the turbine blades will be reducing or oxidizing. Used most frequently in the scheme with the autonomous turbine is the reducing gas, since the oxidizing gas at high temperatures possesses great oxidizing properties, which are dangerous for metallic parts.

By the gas bled after the turbine, the tank of that fuel component on the excess of which the gas generator operates is pressurized.

In the creation of gas generators which operate on the basic components of fuel considerable difficulties arose in due time. Therefore, LPRE with gas generators in which utilized were special liquids, chemically unstable substances were widespread: hydrogen peroxide, nitromethane, isopropylnitrate and others, which were gasified in the presence of a liquid or solid catalyst or by means of thermal decomposition. A solid catalyst is present in the gas generator, and a liquid catalyst is fed to the gas generator as a gasified substance by a pump or by displacement from the tank (Fig. 1.17).

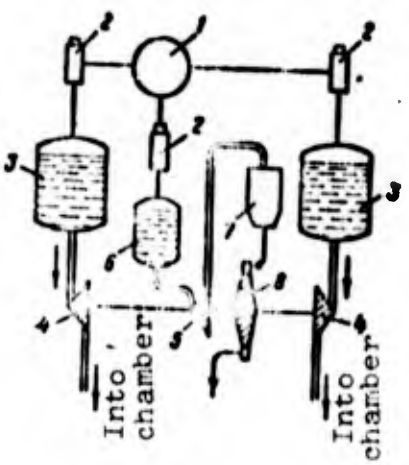

Fig. 1.17. Diagram of the feed system of liquid-propellant rocket engines with pump feed of the monopropellant into the gas generator of the autonomous turbine: 1 - accumulator; 2 - reduction valves; 3 - tanks with working components; 4 - pumps of working components; 5 - pump of monopropellant for the turbine; 6 - tank with fuel for turbine; 7 - gas generator; 8 - turbine.

In all schemes of the feed systems of the LPRE with an automonous turbine, the specific thrust of the engine is lowered as a result of the expenditure of fuel for the obtaining of gas being ejected after turbine into the atmosphere with a lower rate than the discharge velocity from the main nozzle. Besides that, the chemical energy of this gas is not used in the engine entirely, since in this gas the oxidizer or combustible are

present in the form of a vapor, and in the case of the reducing gas, which possesses larger value of RT, there are also products of the partial oxidation of the fuel.

For an increase in the cost-effectiveness of the LPRE with the autonomous turbine, the gas flow rate through the turbine should be as less as possible, i.e., the autonomous turbine is low-flow. With the assigned power of the turbine equal to the power being consumed by the pumps, the requirement for low consumption means that the turbine should create as great a specific work as possible - the power referred to the gas flow rate, i.e., from unity of the gas flow rate as great a work as possible should be taken.

It is possible to remove much work from a unit of gas flow rate if the gas has high energy. Since the gas temperature is limited by the strength of the turbine, it is possible to increase the energy of the gas by an increase in its pressure. The outlet pressure from the autonomous turbine is comparatively low (2-5 bar), and therefore at the high pressure of gas at the inlet the autonomous turbine has a high degree of a depressurization $\delta = p_0^*/p_2$ (where p_0^* and p_2 are the total pressure of gas at the inlet into the turbine and static pressure at the outlet respectively). Usually $\delta = 20\text{-}50$. Thus, the autonomous turbine is low-flow with a high degree of pressure drop δ.

Pumps in the feed system with the autonomous turbine should possess high efficiency since a decrease in the efficiency increases the required power for their drive and, correspondingly, the gas flow rate through the turbine. The relative gas consumption for the autonomous turbine (ratio of flow through the turbine to the total consumption of the components) depends on the thrust of the engine and combustion chamber pressure and is 2-6%. The specific thrust of the engine with the

autonomous turbine falls approximately so much as a result of the ejection of the turbine gas into the atmosphere.

The specific thrust of the engine $P_{уд.д}$ in the presence of the autonomous turbine for the pump drive is determined thus:

$$P_{уд.д} = \frac{G_к P_{уд.к} + G_т P_{уд.т}}{G_к + G_т},$$

where $P_{уд.к}$ is the specific thrust of the chamber;

$G_к$ is the gas flow rate through the chamber;

$G_т$ is the gas flow rate through the turbine;

$P_{уд.т}$ is the specific thrust of the exhaust nozzle of the turbine.

With the assigned initial pressure in front of the turbine and the assigned power, the specific thrust of the engine will depend on the outlet pressure from the turbine. With an increase in the outlet pressure, the required gas flow rate through the turbine will be increased, and the specific thrust of the exit nozzle of the turbine will be increased.

In practice the dependence of the specific thrust of the engine on the outlet pressure is slight, and the outlet pressure p_2, is selected in order to insure a supercritical pressure differential in the nozzle of the turbine, or assign it on the basis of the assigned thrust of nozzles of the turbine as control nozzles, or finally obtain value p_2, taking into account the requirements of the pressurized system.

1.4.2. FEED SYSTEMS WITH A PRECOMBUSTION-CHAMBER TURBINE

In the case of the use of a feed system with a precombustion-chamber turbine, a reduction in the specific thrust of the LPRE is completely eliminated due to the fuel consumption for the

feed of the turbine. Having especially great advantage is the scheme with the precombustion-chamber turbine at high pressures in the combustion chamber (above 100-120 bar).

Figure 1.18 shows a scheme of the feed system with a precombustion-chamber turbine with a gas generator which operates on the basic fuel components. One of the components is completely passed through the gas generator, and the other is added in the quantities necessary for obtaining the necessary temperature in front of the turbine. The gas generator can operate both with an excess of fuel (reducing gas generator) (see Fig. 1.18) and also with an excess of oxidizer (oxidizing gas generator) (Fig. 1.19). The bulk of the second component enters in a liquid state directly into the combustion chamber. In the chamber there occurs afterburning of the component, which completely occurred in gasified form through the turbine in conjunction with the component entering into the combustion chamber in the liquid phase.

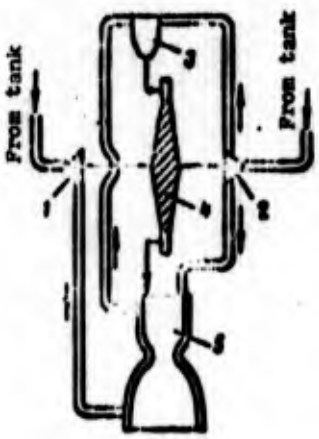

Fig. 1.18. Scheme of the feed system of the LPRE with the precombustion-chamber turbine operating on gas with an excess of fuel: 1 - fuel pump; 2 - the oxidizer pump; 3 - reducing gas generator; 4 - turbine; 5 - combustion chamber.

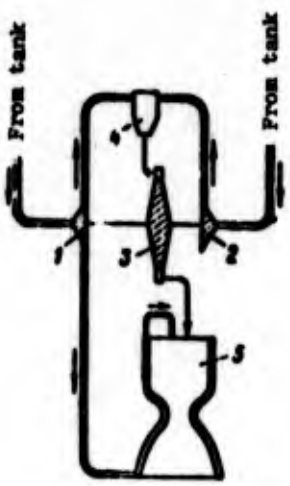

Fig. 1.19. Scheme of the feed system of the LPRE with the precombustion-chamber turbine operating on gas with an excess of oxidizer: 1 - fuel pump; 2 - oxidizer pump; 3 - turbine; 4 - oxidizing gas generator; 5 - the combustion chamber.

On the basis of these specific operating conditions of the combustion chamber, this scheme of the feed can be called still the scheme "with afterburning." For realization of the operation by this scheme the pressure in front of the turbine should be more than the combustion-chamber pressure. Therefore, pumps of the feed system with the precombustion-chamber turbine should provide higher pressures than in the system with an autonomous turbine. In a number of cases it is advantageous to have a separate pump feeding the gas generator with feed to it of part of the component after the main pump (Fig. 1.20).

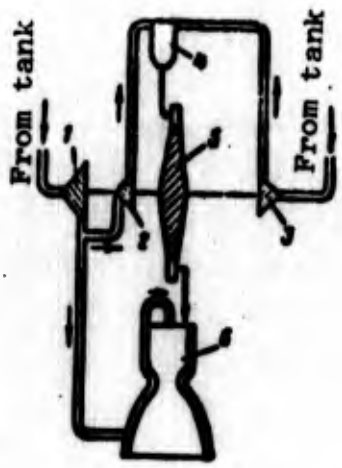

Fig. 1.20. Scheme of the feed system of the LPRE with the precombustion-chamber turbine operating on gas with an excess of oxidizer and having an additional (gas-producing) fuel pump: 1 - fuel pump; 2 - additional fuel pump; 3 - the oxidizer pump; 4 - gas generator; 5 - turbine; 6 - combustion chamber.

In system with the precombustion-chamber turbine at the assigned pressure in the combustion chamber the pressure in front of the turbine is determined from the condition of the balance (equality) of power being consumed by the pumps and the power of the turbine at the selected gas temperature in front of the turbine. Since through the precombustion-chamber turbine there passes a high gas flow rate, the precombustion-chamber turbine is high-flow. With a high gas flow rate, for the producing of the necessary power a small pressure differential on the turbine is sufficient. Therefore, the precombustion-chamber turbine is a turbine with a low degree of a pressure drop (δ = 1.3-1.8, i.e., the pressure in front of the

precombustion-chamber turbine exceeds only by 30-80% the pressure behind the turbine). Let us recall that in the case of the autonomous turbine the pressure in front of the turbine exceeds by 20-50 times the pressure behing the turbine. It is desirable to have less pressure and temperature before the precombustion-chamber turbine, since the presence of the gas generator and high-pressure pipelines at the high gas temperature lowers the reliability of the LPRE and increases its weight.

The efficiency of the pumps and turbine, without affecting the specific thrust of the LPRE from the precombustion-chamber turbine, affects the mass and reliability of the engine plant. The less the efficiency, the higher the pressure and gas temperature in front of the turbine (in the gas generator) should be in order to insure the balance of powers of the TU. Let us note that pressure behind the pump of the gas generator of the turbine (see Fig. 1.20) is the maximum pressure in the channel of the engine. Therefore, the requirement for high efficiencies of pumps and turbines is completely compulsory for the LPRE with afterburning.

The logical development of the circuit with afterburning is the scheme in which into the combustion chamber enter both components in a gasified form. This scheme can be called "gas"; it is shown on Fig. 1.21. The gas scheme of the LPRE makes it possible to realize the higher pressures in the combustion chamber. For the gasification of the components two gas generators are used, one of which operates with an excess of fuel, and the other operates with an excess of oxidizer. For the realization of gas scheme it is advantageous to have two precombustion-chamber turbines (in the case of spontaneous ignition components this requirement is compulsory). Each of the turbines can drive one pump, and then in the feed system there will be two TU (see source [32]), but it is possible to install turbines on one shaft with the pumps, and then

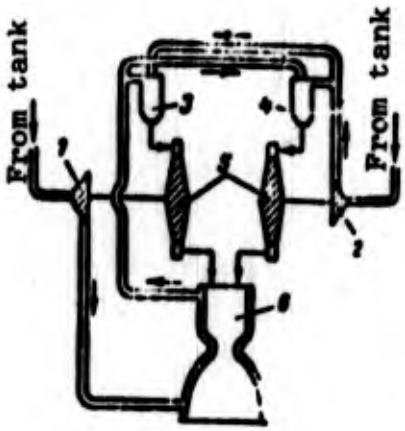

Fig. 1.21. Scheme of the feed system of a LPRE with two precombustion-chamber turbines (gas diagram "with afterburning."): 1 - fuel pump; 2 - oxidizer pump; 3 - reducing gas generator; 4 - oxidizing gas generator; 5 - turbine; 6 - combustion chamber.

constructively one TU will be obtained. At different pressures in the gas generators it can prove to be advisable to have separate pumps feeding the gas generators with a feed in them of part of the components after the basic pumps.

The operating conditions and requirements of the pumps and turbines of the scheme are the same as those in circuit with afterburning. In the gas scheme it is possible to lower substantially the pressure and temperature in front of the turbine as compared with the circuit with afterburning, since the gas flow passing through the turbines is great (is equal to the flow of the components). The scheme of the LPRE with the precombustion-chamber turbine can be fulfilled without gas generator (Fig. 1.22). In this case the gasification of one of the components occurs in the cooling jacket of the combustion chamber. The turbine which operates by this scheme can be called the precombustion-chamber regenerative turbine. This scheme is implemented in the American engine RL-10 (see source [31]), where used as the fuel is liquid hydrogen, which is gasified in the combustion-chamber jacket and enters into the turbine. At high combustion-chamber pressures the power selected from the chamber in the cooling system proves to be insufficient to provide the necessary power of the turbine. This circumstance restricts the use of this scheme.

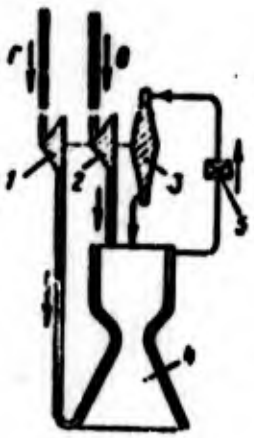

Fig. 1.22. Scheme of a LPRE with the heating of the working medium of the turbine in the cooling jacket of the combustion chamber: 1 - pump of the component which is the working medium of the turbine; 2 - pump of the second component; 3 - turbine; 4 - combustion chamber; 5 - valve device.

An examination of schemes of the feed of the LPRE with a turbopump unit shows that requirements for the pumps and turbines, the conditions of their operation and the parameters greatly differ depending on the selected scheme of the feed system of the LPRE. Subsequently, (see Section 5.1) features of the process and calculation of pumps and turbines operating in the LPRE of different schemes will be examined in more detail.

CHAPTER 2

PRINCIPLES OF THE GENERAL THEORY OF VANE MACHINES

2.1. DEFINITION OF A VANE MACHINE

The centrifugal pump, axial pump and axial-flow turbines are the preferred forms of machine units used in feed systems of liquid-propellant rocket engines [LPRE] (ЖРД). Moreover, in feed systems of LPRE radial inward-flow turbines are used (see source [63]). All these units are vane machines according to the operating principle. An examination of the general theory of vane machines makes it possible to determine the general regularities and properties necessary for understanding the processes occurring in vane machines of different types making up the turbopump units of the LPRE.

In technology the terms "vane machine," "blade machine" or "turbomachine" denote the machine in which there occurs the conversion of external mechanical energy (energy on the shaft) into energy of the flowing liquid (gas) or vice versa - the conversion of energy of a liquid (gas) into the external mechanical energy accomplished with streamline flow by the flow of liquid of a rotating vane cascade (vane ring). The rotating vane cascade is the operating unit of a machine, and whence there occurs the name vane or vane machine. The vanes are fastened on the wheel disk. The disk with the vanes will

be called the rotor. Finally, the definition of a vane machine can be formulated thus:

A vane machine is a machine in which there occurs a change in the flow of energy of the liquid or gas in the process of the streamline flow of vanes of a rotating rotor.

Given on Fig. 2.1 is a diagram of the rotor of a vane machine in general form. The rotor is fastened to the shaft. The wheel is rotated with an angular velocity ω, and, therefore, any point of the wheel moves with a circular velocity u:

$$u = \omega R, \tag{2.1}$$

where R is the radius of the selected point.

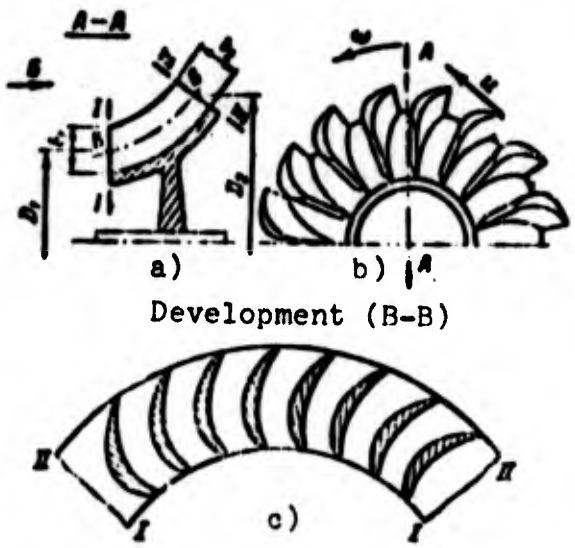

Fig. 2.1. Diagram of the wheel of a diagonal vane machine: a) meridian cross section; b) view along the arrow б; c) development of the cross section of blades of the surface rotation with the generatrix B-B.

The fluid flow[1] moves from cross section I-I (inlet) to cross section II-II (output from the wheel). Usually the rotor of the vane machine is depicted as a meridian cross section (see Fig. 2.1a), i.e., a cross section with the plane passing through the axis (on Fig. 2.1 the cross section along A-A) and by a projection on a plane which coincides with the plane of rotation (see Fig. 2.1b). But these projections frequently do not expose forms of the vanes, and therefore we use an additional cross section, namely, the cross section by the surface which is the surface of rotation the generatrix of which coincides with the center line of the meridian cross section (line B-B on Fig. 2.1a). When this surface is a plane, cylindrical or conical, its development is depicted on the plane of the drawing without distortion. Usually, in order to obtain the planar image of the cross section of the vanes, more complex surfaces passing through the axes of the channels are replaced by sections of conical or cylindrical surfaces.

Figure 2.1 shows the surface scanning of rotation with the generatrix B-B (see Fig. 2.1c) (for the image on the plane the surface of rotation with the curvilinear generatrix is replaced by a conical surface). In this case the cross sections of the vanes form the airfoil cascade.

The vane machines are widely used in technology and have a different purpose and design. In view of the diversity of the varieties of vane machines, let us make their classification according to a number of most important criteria.

---

[1]By liquid in this section we will understand as the moving medium. It can be true liquid or gas (vapor).

2.2. CLASSIFICATION OF VANE MACHINES

2.2.1. DIVISION OF VANE MACHINES INTO ENGINE MACHINES AND EXECUTOR MACHINES

The classification of vane machines can be conducted according to a whole series of criteria. One of the most important criteria is that the machine consumes or issues energy. In other words, is it an executor machine or engine machine? According to this criterion, the division of the vane machines is conducted in Table 2.1.

Table 2.1. Division of vane machines into engine machines and executor machines.

Vane engine machine (machine with the power consumption)	Vane executor machine (machine with power consumption)
Hydraulic turbines	Pumps
Steam turbines	Compressors
Gas turbines	Ventilators
Turboexpanders	Blowers
Wind motors	Propellers
Water-pressure wheels	Screw propellers
	Vane hydraulic brake

Let us say that at the present time created for hydraulic systems are reversible units which can operate under conditions of the pump and under conditions of the turbine, i.e., be utilized both as an executor machine and as an engine machine. The group of the combined machines can be referred to as hydraulic couplings or turbocouplings, which include the pump and turbine. Air and screw propellers refer to the vane engine machines, since they utilize the power fed to them for the rejection of masses of air or water and thereby create the thrust force.

Characteristic for the vane machine is the flow of moving liquid about the impeller vanes without a change in the volume of internal cavities of the machine. Hydraulic volumetric machines (see section 1.3.1.1), in which the liquid is forced out by vanes from a closed volume (i.e., different rotary pumps with vanes), it is not possible to consider as vane machines, although constructively they can have a rotor and vanes. Water-filled wheels of a different kind refer to a special group of hydraulic engines, which also we will not call vane machines. These wheels are driven only under the action of the gravity of water. Of the water wheels only pressure-filled wheels - the simplest water turbines - can be referred to as vane machines.

2.2.2. DIVISION OF VANE MACHINES ACCORDING TO THE SCHEME OF THE DEVICE

The vane machine, as a rule, consists of rotating rotors and fixed feed and discharge devices made in the form of nozzles, stators, jackets, collectors, and so on. The presence of the rotor is compulsory for any vane machine, and the feed and discharge devices can be absent; for example, there are no propeller and wind motor.

A characteristic criterion for division by the scheme of the device is the direction of the flow of the working medium relative to the axis of rotation. In accordance with this, vane machines are divided into:

a) radial (Fig. 2.2), in which the flow lines of liquid in the rotor form the flow surfaces close to the planes perpendicular to the axis of rotation, i.e., the generatrix of the stream surface on the major portion of its length is perpendicular to the axis (B-B on Fig. 2.2);

b) axial (Fig. 2.3), in which the flow lines of liquid form the flow surfaces close to the coaxial circular cylindrical surfaces, i.e., the generatrix of the flow surfaces is parallel to the axis (B-B on Fig. 2.3);

c) diagonal (see Fig. 2.1), in which the flow lines form the surfaces of revolution with the generatrix inclined toward the axis at an arbitrary angle.

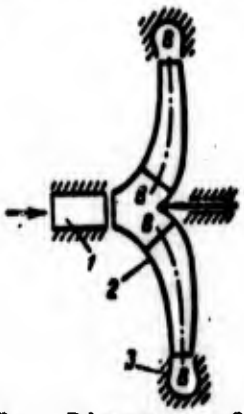

Fig. 2.2. Diagram of a radial vane machine: 1 - guide vane at the inlet into the rotor; 2 - rotor; 3 - guide vane at outlet from the rotor.

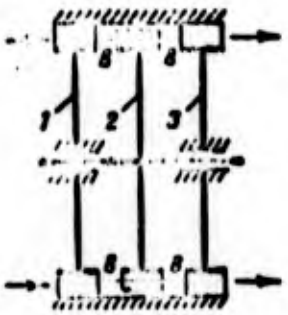

Fig. 2.3. Diagram of the axial vane machine: 1 - guide vane at the inlet into the rotor; 2 - rotor; 3 - guide vane at the outlet from the rotor.

On the diagrams given on Figs. 2.2 and 2.3, the numeral 1 designates the guide vane at the inlet to the rotor, and numeral 2 - the rotor and numeral 3 - the guide vane at the outlet from the rotor.

The radial and diagonal machines, in turn, are subdivided into centrifugal and centripetal (Figs. 2.4 and 2.5, respectively). In centrifugal machines displacement of the particle occurs with an increase in its distance from the axis of rotation. In centripetal vane machines the particle of liquid is moved from larger radii to smaller, i.e., with a decrease in the distance from the axis of rotation.

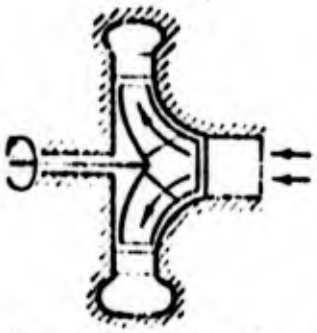

Fig. 2.4. Diagram of a centrifugal radial vane machine.

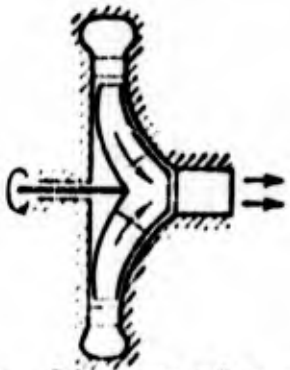

Fig. 2.5. Diagram of a centripetal radial vane machine.

Vane engine machines and vane executor machines can constructively be made as radial (diagonal) and axial. Vane machines in which the flow part can be formed from elements of the axial and radial machines are used.

As will be shown further (see sections 2.12.3 and 2.12.5), the selection of the specific scheme of the vane machine is determined by the relationship of the frequency of rotation of the rotor volume flow rate and specific work.

2.2.3. SEPARATION OF VANE MACHINES ACCORDING TO THE NUMBER OF STAGES

Let us accept the number of stages as the following criterion of classification.

We will call the stage of the vane machine the combination of the rotor with the feed and discharge devices. Consequently, shown on Figs. 2.2, 2.3 and 2.4 were single-stage vane machines. In technology multistage vane machines are frequently used. Multistage machines can include both axial and radial stages in different combinations. The number of stages of the vane machine is determined by the number of rotors. Thus, Fig. 2.6 shows a diagram of an axial two-stage vane machine. Figure 2.7 shows a diagram of a two-stage vane machine whose first stage is axial and the second - radial.

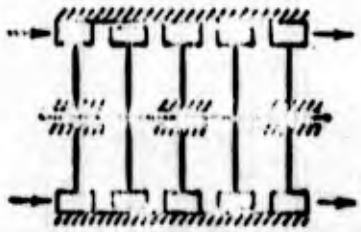

Fig. 2.6. Diagram of a two-stage axial vane machine.

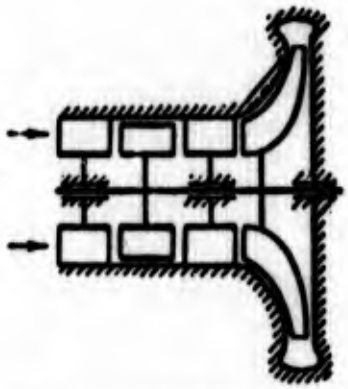

Fig. 2.7. Diagram of a two-stage combined vane machine.

A large number of stages (which can be measured in the dozens) have axial-flow compressors and steam turbines of fixed systems. In feed systems of the LPRE the number of stages of the vane machines usually does not exceed two. This, in turn, is connected with the high angular velocities of vane machines of the LPRE and with the requirement for the limitation of their mass.

For feed with high pressure of liquid hydrogen, which has a low density, high pressure is necessary. The number of stages of the pump in this case substantially increases and can reach 4-8 (see Fig. 1.13).

Let us examine briefly the basic stages of development of vane machines.

2.3. BASIC STAGES OF DEVELOPMENT OF VANE MACHINES

The water-filled wheel and the simplest wind wheel are the earliest engine devices operating according to the principle of vane machines (see source [43]).

The theoretical bases of the calculation of hydraulic vane machines were laid by Danil Bernoulli and Leonard Euler. A large role was played by D. Bernoulli's work which was published in 1733, "Hydraulics, or a Report About the Forces and Motion of Liquids."

In 1750 a Hungarian scholar, Segner, invented the reactive hydraulic turbine - the so-called "Segner wheel." L. Euler in 1754 published the work "A More Complete Theory of the Machines Driven by the Action of Water", where it gave the theory of Segner's wheel and developed the general positions of the theory of vane hydraulic engines. There Euler expressed the idea about the use of a turbine which consists of a guide vane and rotor.

The 19th century is characterized by the rapid development and extension of vane machines. Vane pumps, ventilators, hydraulic and steam turbines received especially widespread acceptance at the end of the 19th century in connection with the development of high-speed electric motors and electric generators.

The development of gas turbines was retarded by the absence of heat-resistant materials and highly effective compressors. A great contribution to the development of gas turbines was made by Russian scientists and engineers. In 1892 P. D. Kuz'minskiy developed project and constructed the first gas turbine of continuous action in the work. A great significance for the development of steam turbines was in the transactions of the Swedish engineer Gustav Laval and English engineer Charles Parsons.

The development of aviation caused the producing of propellers - vane machine-motors. N. Ye. Joukowski's service in the matter of the producing of vane machines and, specifically, propellers is great. The theory created by him during the

years of 1890-1900 of the airfoil lift became principle for calculating not only the wings of aircraft, but also vanes of turbines, propellers and pumps.

In the USSR the production of steam turbines, centrifugal pumps and hydroturbines was started as long ago as in 1921 according to the plan of GOELRO (State Commission for the Electrification of Russia). At the present time in all branches of Soviet technology vane machines are used.

Vane machines play an important role in aviation technology. The gas-turbine engine - the engine which has the turbine and compressor as the necessary component parts - is the basic type of the contemporary aircraft engines. The producing of liquid rocket engines required the use of centrifugal and axial pumps for the fuel feed and turbines for the pump drive.

The calculation and design of the contemporary vane machine require a great amount of knowledge. In a whole number of scientific and designer collectives the questions of the theory and practice of vane machines are successfully worked out.

2.4. BASIC PROPERTIES OF VANE MACHINES

Let us examine which features and advantages over other types of machines vane machines possess and which conditioned their extremely wide application.

Let us list the basic, most general properties of vane machines.

1. Continuity of action. Vane machines are machines of continuous but not cyclic action, and they pass per unit time a large quantity of working medium; therefore, they possess good specific indexes - specific mass, specific volume, and so on.

2. High speeds of the operating unit. The rotor wheels of the vane machines can have high circular velocity. The more the circular velocity will be, the more the work per unit of flow of the working medium will be, as follows from the Euler equation (see further Section 2.7.1). The strength of the material of the rotor places a limit to the increase in the circular velocity, since at high speeds immense inertia forces act on the rotor.

At the present time the maximum circular velocity of centrifugal compressors approach 500-600 m/s, and circular velocities of turbines operating in more difficult temperature conditions, 350-450 m/s. At such circular velocities the rotors of the small-size turbines and compressors have a rotation frequency of the order of 3000-10,000 *l*/s. The greatest rotation frequency (up to 10,000 *l*/s) are in turbines of refrigerators. Because of the high values of the rotation frequency, vane machines have, as a rule, small values of specific mass, i.e., the mass per unit of power.

3. The possibility of the achievement in one unit of practically umlimited powers and flows of the working medium. Thus, at the present time the turbine is an engine capable of developing the highest power during a prolonged time. The power of separate steam turbines and hydroturbines reaches 500-800 thousands of kW. At the same time, in instrument manufacture turbines whose power is measured in several watts are used.

Large industrial ventilators pump through thousands of cubic meters of air per second, and water pumps pump dozens of cubic meters of water per second; at the same time, there are vane pumps with a productivity of less than 0.1 *l*/s.

4. The possibility of the achievement of high efficiency. The efficiency, i.e., the ratio of the useful power to that available for contemporary vane machines can reach a value of 0.8-0.9. Vane machines of aviation gas-turbine engines - turbines and axial-flow compressors - have efficiency values sometimes exceeding 0.9.

5. Equilibrium. It is principally possible to provide the the operation of a vane machine without the action of the unbalanced force of inertia. The unbalanced forces of inertia in vane machines can appear only as a result of errors during the manufacture. In practice they are reduced to the permissible minimum by the dynamic rotor balancing of machines. In the [TU] (THA) of LPRE the rotor can be balanced to within 10^{-4} N·m. The equilibrium of the machine is a valuable performance feature. Loads on supports, frame and foundation are sharply dycreased, and the entire construction can be made lighter. Included in this is the considerable advantage of vane machines over reciprocating engines having a crankgear which is always unbalanced.

6. High reliability and easy servicing, which are valuable performance characteristics of vane machines.

7. The convenience of connection with electric motors, generators, etc. Vane machines as the machines of rotary motion are easily connected with electrical machines. Moreover, the drive of the vane machine requiring power (compressor, pump) from the vane machine-engine (turbine) is easily carried out by their direct uniting. Such units are widely common in technology. The present course is dedicated to the theory and calculation of a unit of such form, a turbopump unit of a liquid-propellant rocket engine. True, sometimes in the TU of an LPRE a gear train between the pumps and the turbine is used (see Fig. 1.14), but this scheme is not typical for contemporary LPRE.

This does not exhaust all the characteristic properties of vane machines. Above only most considerable and general features for all types of vane machines were shown. In each special case of the use of a vane machine there are its features and the advantages and shortcomings of it in comparison with other types of machines.

2.5. PARAMETERS OF VANE CASCADES

The vane cascades (vane rings) which form the stage of the vane machine are three-dimensional, but if the stage is cut by the coaxial surfaces of revolution, distant along the normal at an infinitesimal distance (for example, for the axial machine - cylindrical surfaces), then we will obtain the elementary stage of the vane machine consisting in the scan of two-dimensional plane vane airfoil cascades.

In the theory of vane machines, frequently instead of the examination of the available, in actuality, flow of three-dimensional unsteady fluid flow around the vanes one is limited to the examination of the two-dimensional steady flow of foil cascades on a number of cross sections, i.e., the idealized schemes of flow (with the cylindrical flow surfaces for axial machines and flat flow surfaces for purely radial machines) are examined.

The plane vane cascade consists of plane single vane profiles. Let us examine the basic parameters of the single plane vane profile and plane vane cascade.

Figure 2.8 shows a single vane profile. The locus of the centers of circles inscribed into the profile forms the camber line. In general any point of profile can be assinged by two coordinates - x and y. The x-axis is usually directed along the line connecting the outermost point of the camber line, called

the chord. The concave part of the profile is called the trough, and the convex part - the back. The coordinates of points which form the back have the subscript "c", and the coordinates of points forming the trough - the subscript "к".

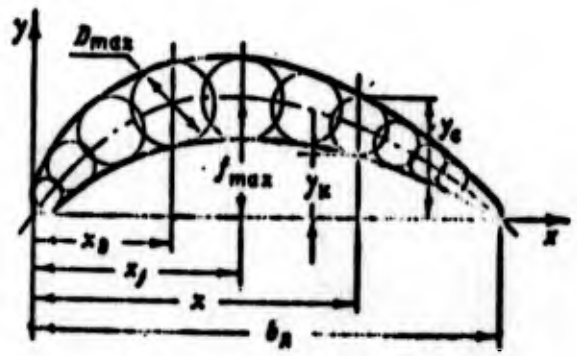

Fig. 2.8. Vane profile with the designation of the basic dimensions.

For the assignment of the profile these concepts are still utilized:

Quantity D_{max} is the maximum profile thickness or the maximum diameter of the circumference inscribed into the outline of the profile; f_{max} is the maximum deflection of the chamber line or the greatest distance of the chamber line from the chord.

Frequently all values which characterize the profile are assigned in relative coordinates, in fractions of chord $b_л$. For example, the relative maximum thickness $\bar{D}_{max} = D_{max}/b_л$ and so on. The leading and trailing edges of the profile can be made rounded off or sharp.

Figure 2.9 shows a plane straight airfoil cascade, and Fig. 2.10 shows a plane circular airfoil cascade. The plane straight airfoil cascade is obtained with the scanning of the

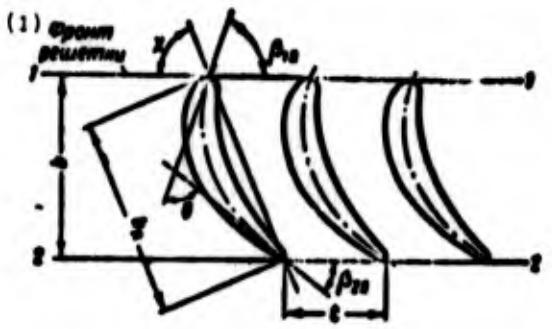

Fig. 2.9. Two-dimensional airfoil vane cascade.
KEY: (1) Front of cascade.

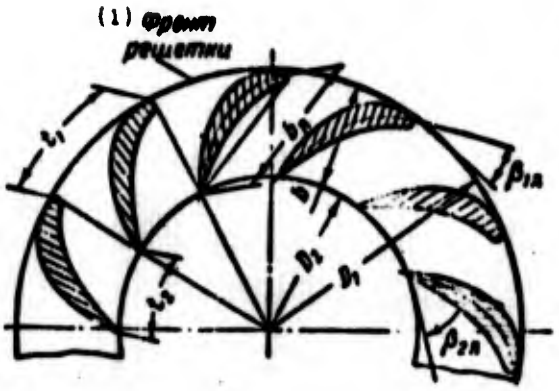

Fig. 2.10. Two-dimensional circular vane cascade.
KEY: (1) Front of cascade.

cross section of vanes of the axial machine by the cylindrical surface with the axis coinciding with the axis of rotation. The plane circular airfoil cascade is obtained with the cross section of the vanes of the radial machine by the plane perpendicular to the axis of rotation.

The line passing through the extreme points of the leading edges is called the input front of the airfoil cascade (line 1-1 on Fig. 2.9). The line passing through the extreme points of the trailing edges of the plane vane cascade forms the leading front of the cascade (line 2-2 on Fig. 2.9). In the plane cascade the front is a straight line, and in the plane circular cascade it is a circle.

Distance along the front between the appropriate points of the adjacent profiles is called the cascade spacing t. For a foil cascade the pitch at the inlet into the cascade is equal to the pitch at the output from it. For the circular cascade the values of pitches at the inlet into the cascade and at output from it differ between each other (see Fig. 2.10). The angle made up by the chord of the profile and front of the airfoil cascade is called the setting angle χ (see Fig. 2.9).

For the airfoil cascade let us introduce the concept of the width of the cascade b. The width of the cascade is the distance along the normal between fronts of the cascade. The plane airfoil vane cascade will be completely assigned by the profile, the angle of setting and the cascade spacing. For the assignment of the plane circular vane cascade, it is necessary to know still the diameter of the circle at the inlet into the cascade or at the outlet from it.

For investigating the flow through the plane vane cascade, the inlet and outlet angles of the cascade profile play an important role. Usually the inlet angle of the profile in the cascade $\beta_{1л}$ is defined as the angle composed by tangent to the camber line at its initial point and the inlet front of the cascade (see Fig. 2.9 and 2.10). The outlet angle of the cascade profile will be designated $\beta_{2л}$.

The angle θ (see Fig. 2.9) characterizes the angle of curvature of the profile:

$$\theta = 180° - (\beta_{1л} + \beta_{2л})°.$$

An important parameter of the airfoil cascade is its solidity or the ratio of chord to the pitch:

$$\bar{b}_л = \frac{b_л}{t}$$

or the inverse ratio, called the relative pitch:

$$\bar{t}_a = \frac{t}{b_a}.$$

Frequently the solidity and the relative pitch are determined from the value of the width of the cascade:

$$\bar{b} = \frac{b}{t} \quad \text{and} \quad \bar{t} = \frac{t}{b}.$$

Plane vane cascades can form channels of various shapes. The form of the vane channel of the cascade can be judged if between adjacent profiles we inscribe the circles so that they would touch both profiles (Fig. 2.11). The centers of these circles form the center line of the vane channel. If the center line of the channel is straightened, then the envelopes of the inscribed circles form a straight axial vane channel.

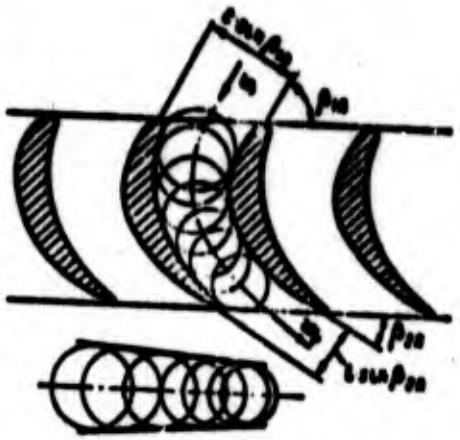

Fig. 2.11. Convergent vane cascade.

The cascades whose vane channels are narrowed (convergent cascades, see Fig. 2.11) provide the acceleration of the fluid flow. The cascades which provide the acceleration of flow but already in supersonic flow include such cascades the vane channels of which first become narrow and then expand (see further Fig. 4.17).

For subsonic speeds the vane cascades with divergent vane channels are diffuser cascades which provide the braking of the fluid flow (Fig. 2.12).

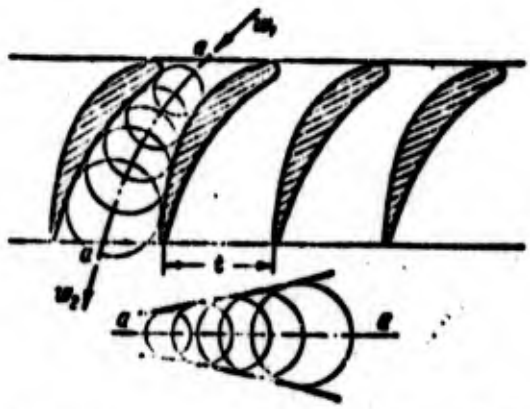

Fig. 2.12. Diffuser vane cascade.

The cascade can have identical flow areas at the inlet and outlet. Such cascades (Fig. 2.13) are used in impulse vane machines (see further section 2.9).

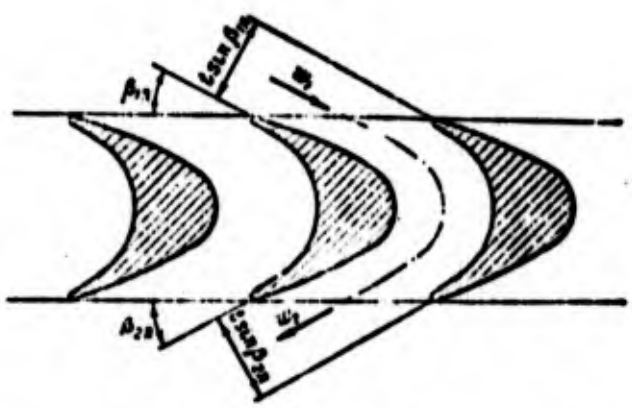

Fig. 2.13. Cascade for impulse vane machines.

Turbine cascades as a rule are convergent, and the cascades of compressors and pumps are diffuser. Impulse cascades are used in both machines.

2.6. KINEMATIC RELATIONSHIPS FOR VANE MACHINES

2.6.1. BASIC INFORMATION

With the hydrodynamic computation of cascades of vane machines problems of two forms, the so-called direct and inverse problems, are solved. The direct problem is the determination of the velocity field of fluid flow through the given cascade at the assigned boundary conditions. The inverse problem is the construction of cascades which satisfy the definite optimum law of the velocity distribution. In the solution of the direct and inverse problems, in general it is necessary to examine the three-dimensional flow and in connection with the airfoil cascades - the two-dimensional flow. For the solution of these problems it is necessary to make sufficiently laborious calculations. Elements of the two-dimensional theory of flow in airfoil cascades will be given below. In the present section we will examine the velocities averaged over the cross section, i.e., we will proceed from the one-dimensional theory of flow. In spite of obvious simplification of the pattern of flow, the one-dimensional theory makes it possible to examine many laws governing vane machines.

In general the vector of the absolute velocity $\vec{c}$ can be expanded into three components: circular - $\vec{c}_u$, radial - $\vec{c}_r$ and axial - $\vec{c}_z$ (Fig. 2.14).[1] The circular velocity component lies

[1]Subsequently, for the sake of simplicity in recording, we will write the sign of the vector above the symbol which designates the speed only when it is absolutely necessary.

in the plane of rotation and is directed along the line of the vector of the circular velocity. Radial and axial components c_r and c_z lie in the plane which is called the meridian plane. This plane passes through the axis of rotation of the vane machine. We will designate the projections of speeds on this plane by the subscript "m".

The meridian velocity component c_m is the sum of the radial and axial components (see Fig. 2.14):

$$\vec{c}_m = \vec{c}_r + \vec{c}_z.$$

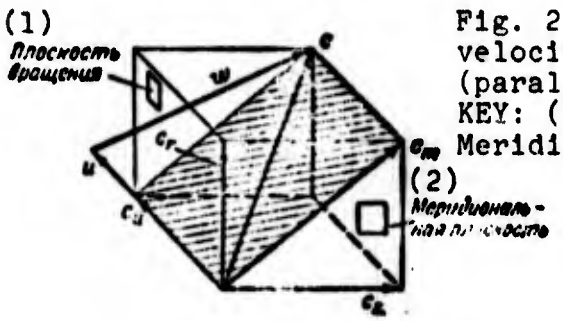

Fig. 2.14. Expansion of absolute velocity into its components (parallelpiped of absolute velocity). KEY: (1) Plane of rotation; (2) Meridian plane.

The absolute velocity c is completely determined by the meridian component c_m and circular velocity component c_u:

$$\vec{c} = \vec{c}_m + \vec{c}_u.$$

The circular component c_u characterizes the "twisting" of the flow and is connected directly with the value of specific work, as will be shown below. The meridian component c_m is determined by the volumetric fluid flow rate through the vane machine and by the cross section normal to the direction of component c_m, which we will designate F_m. In practice the flow cannot fill the whole cross section due to the presence of separation zones. In general

$$F_m = \alpha F_{mp},$$

where α is the coefficient of narrowing ($\alpha \leq 1$);
F_{mp} is the calculated flow area.

Usually we assume that $\alpha = 1$. The velocity c_m will be found from the equation of continuity:

$$G = \rho c_m F_m, \tag{2.2}$$

where G is the mass flow rate in kg/s;
ρ is density in kg/m^3.

For ρ = const

$$c_m = \frac{Q}{F_m}, \tag{2.3}$$

where Q is the volume flow rate in m^3/s.

By knowing the absolute velocity of fluid c and the circular velocity of the wheel (velocity of following) u, it is easy to find, by applying the general rule of the addition of velocities of complex motion, the speed of the fluid relative to the moving vane - the relative speed w:

$$\vec{w} = \vec{c} - \vec{u}. \tag{2.4}$$

These three vectors lie in one plane shaded on Fig. 2.14. Transferring this plane to the plane of the drawing, we can obtain for any vane machine the scheme of the speeds or the velocity triangle, i.e., the construction showing the vector coupling of absolute, relative and circular velocities. For a purely axial vane machine the meridian velocity component is equal to the axial, and for a purely radial machine it is equal to the radial component speed, i.e.,

for the axial machine $c_r = 0$ and $c_m = c_z$,

and for the radial machine $c_z = 0$ and $c_m = c_r$.

Consequently, for the axial vane machine, the parallelepiped obtained in the expansion of the vector of absolute velocity into components (see Fig. 2.14) will be replaced by the parallelogram located in the plane tangent to the coaxial cylindrical surface (Fig. 2.15). In this plane the construction of velocity schemes for the axial machine will be produced.

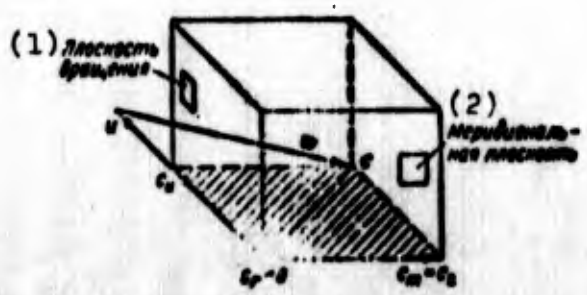

Fig. 2.15. Expansion of absolute velocity into its components for the axial vane machine.
KEY: (1) Plane of rotation; (2) Meridian plane.

For a purely radial vane machine the parallelepiped of the vector of absolute velocity (see Fig. 2.14) is replaced by the parallelogram in plane of which is the plane of rotation, and the construction of the velocity will be produced (Fig. 2.16).

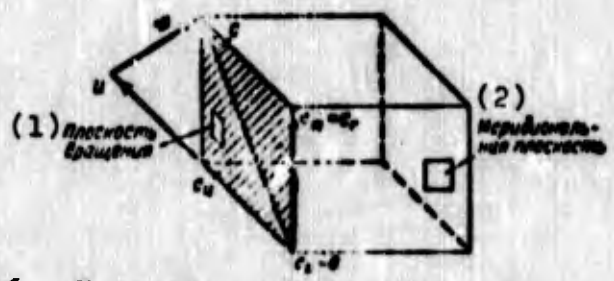

Fig. 2.16. Expansion of absolute velocity into its components for the radial vane machine.
KEY: (1) Plane of rotation; (2) Meridian plane.

2.6.2. INLET INTO THE WHEEL

We will assume that the vector of the absolute inlet velocity of the vane channels c_1 is known, or that it is possible to find it. In general it is determined by two components - meridian c_{1m} and circular c_{1u}. The meridian component is determined by the value of the volume flow rate Q and the flow area of the wheel normal to meridian velocity component directly in front of the vanes F_{1m} [see equation (2.3)].

The circular velocity component at the inlet c_{1u} is found from conditions of the flow of fluid in the feed device.

For the inlet into the wheel it is possible to record the relation:

$$\vec{w}_1 = \vec{c}_1 - \vec{u}_1,$$

where u_1 is the circular velocity on the mean diameter of the leading edges of the vanes.

Velocities c_1, w_1 and u_1 in the plane passing through vectors c_{1m} and u_1. In the construction of schemes this plane is combined with the plane of the drawing. Let us accept the direction of vertical line in the plane of the drawing as the meridian direction (direction of velocity c_{1m}), and then the circular velocity u_1 is depicted as a section of the horizontal line, and w_1 will be found as the difference in vectors c_1 and u_1 (Fig. 2.17).

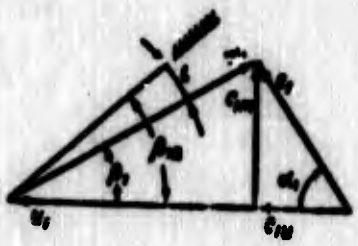

Fig. 2.17. Velocity triangle at the inlet into the wheel of the vane machine.

Angle α_1 is the angle between the direction of the flow in absolute motion and the direction of the circular velocity.

The angle β_1 is the angle between the direction of the flow in relative motion determined by vector w_1 and the direction of the circular velocity - for a turbine and the opposite direction - for a pump. In general the angle β_1 cannot coincide with the angle of inclination of the vane $\beta_{1л}$. The angle i - between the direction of flow in relative motion at the inlet into the vane and the direction of the leading edge of the vane - is called the angle of attack. Consequently, the angle of attack i is determined by the angle between the velocity vector w_1 and tangent to the camber line of vane at the inlet.

2.6.3. FLOW ALONG VANE CHANNELS OF THE WHEEL AND AT THE OUTLET FROM THE WHEEL

In order to find the absolute velocity of fluid at any point of the vane channel at a certain distance from the inlet to the vanes, it is necessary to produce a vectorial addition of the relative velocity of the fluid in channel w and the velocity of following u. The relative velocity w at any radius within the vane channel is found according to the direction which is determined in the first approximation according to the direction of the center line of the vane (angle $\beta_л$) and according to the value of the meridian velocity component $c_{m\,л}$ (Fig. 2.18). The assumption relative to the fact that the direction of the profile tangent to the center line is parallel to the relative speed, strictly speaking, correct only for the lattice which consists of an infinitely large number of infinitely thin profiles. If necessary the velocity vectors which correspond to this design scheme will be noted by the sign ∞ ($z = \infty$).

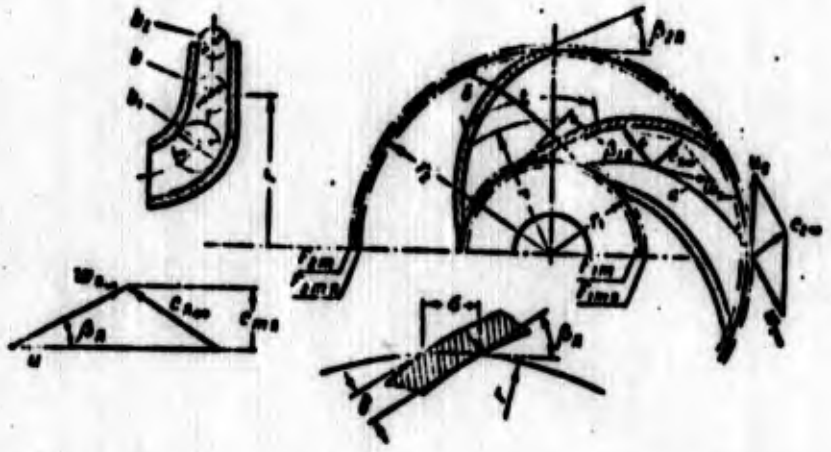

Fig. 2.18. Plotting of velocity triangles in vane channels and at the outlet from the wheel of a centrifugal pump.

For determining the value of the averaged velocity within the vane channel, it is necessary to consider the profile thickness together with the thickness of the boundary layer displacement. With detached flow one should consider the thickness of the separation zone.

In the first approximation, especially for machines in which the flow areas are commensurable with the cross section encumbered by the vanes, only the thickness of the vanes (for example, in pumps) is considered.

Let us conduct the determination of the meridian velocity, taking into account the thickness of the vanes in the cross section of the wheel located on an arbitrary radius in the example of a centrifugal wheel (see Fig. 2.18). Let us designate the flow area of the wheel (radius r) F_m, and the flow cross-sectional area at the same radius r, taking into account the thickness of the vanes, will be designated $F_{m\,л}$. Ratio $F_m/F_{m\,л}$ is the coefficient of contraction of the cross section; let us designate it k. Cross sections F_m and $F_{m\,л}$ can be calculated by the vane pitch t ($t = 2\pi r/z$, where z is the number of vanes); then

$$k=\frac{F_m}{F_{m\,л}}=\frac{s\delta b}{s(t-\sigma)b}=\frac{t}{t-\sigma}; \qquad (2.5)$$

$$F_{m\,л}=\frac{F_m}{k}=\frac{2\pi rb}{k}. \qquad (2.6)$$

Here σ is the thickness of the vanes determined on a circular arc (approximately chordwise). The connection between the normal thickness δ and thickness σ is easily established from an examination of Fig. 2.18:

$$\delta = \frac{\delta}{\sin \beta_л}. \qquad (2.7)$$

To find the meridian velocity, taking into account the thickness of the vanes in the cross section of the wheel located on an arbitrary radius, let us use the equation directly ensuing from equation (2.3):

$$c_{m\,л} = c_m k, \qquad (2.8)$$

where k, taking into account expressions (2.4) and (2.6), can be recorded in the form

$$k = \frac{1}{1 - \frac{\delta}{t \sin \beta_л}}. \qquad (2.9)$$

Here $c_{m\,л}$ is the meridian velocity taking into account the thickness of the vanes; and c_m is the meridian velocity not allowing for the thickness of the vanes.

The relative velocity in the arbitrary cross section of the wheel, taking into account the thickness of the vanes, is found by plotting the velocity triangle according to the known velocities $c_{m\,л}$ and u and according angle $\beta_л$ (see Fig. 2.18) or from the relation

$$w_л = \frac{c_{m\,л}}{\sin \beta_л}. \qquad (2.10)$$

The outlet velocity triangles from the wheel are constructed just as for the arbitrary cross section but not allowing for contraction of the cross section by the vanes.

Figure 2.18 shows the relative location of the velocity vectors of the relative, migratory and absolute motion in the example of the centrifugal vane machine (pump) for the arbitrary and outlet radii. Also shown there are flow lines of the fluid for the wheel of the centrifugal pump (when $z = \infty$) in the relative (a) and absolute (b) motion.

2.6.4. EXAMPLES OF THE PLOTTING OF VELOCITY SCHEMES

Figure 2.19 shows the basic sections of the stage of an axial vane machine (axial pump). Such cross sections are the meridian section (a) and the development of the cylindrical cross section of the vane cascades (b) (diameter of the cylinder is equal to the mean diameter of the stage, its generatrix is I-I). In general the stage of the axial pump has a guide device at the inlet and a stator at the outlet. The guide device provides the necessary torsion of the flow at the inlet into the wheel (c_{1u}). The stator is a diffuser device which converts kinetic energy into pressure energy.

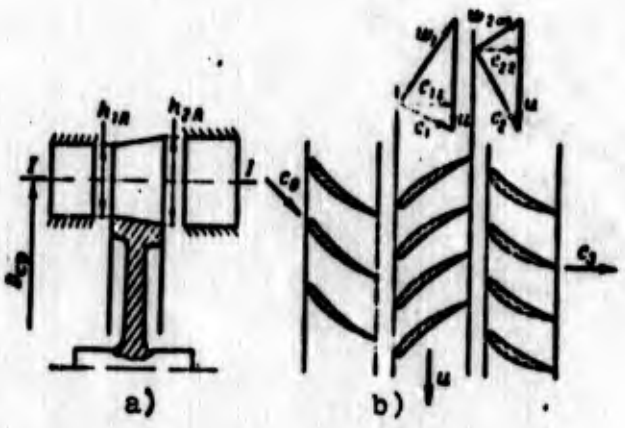

Fig. 2.19. Characteristic cross sections of the stage of the axial pump and velocity triangles: a) meridian cross section; b) development of the cylindrical cross section with the generatrix I-I.

The plotting of velocity schemes (triangles) (Fig. 2.20) will be carried out for the mean diameter D_{cp}. Let us assume that the fluid flow at the inlet into the wheel has a circular component c_{1u} (frequently it is equal to zero). The meridian component (in this case axial) is found from the relation

$$c_{1m} = \frac{Q_1}{F_{1m}}. \tag{2.11}$$

In this case F_{1m} is the ring cross section with a height of h_{1n} :

$$F_{1m} = \pi D_{c_1} h_{1n}. \tag{2.12}$$

By knowing the volumetric flow rate or having defined it as the quotient of the division of the mass flow rate for the density:

$$Q_1 = \frac{G_1}{\rho_1}, \tag{2.13}$$

let us find the velocity value $c_{1z} = c_{1m}$:

$$c_{1z} = c_{1m} = \frac{Q_1}{\pi D_1 b_1}. \tag{2.14}$$

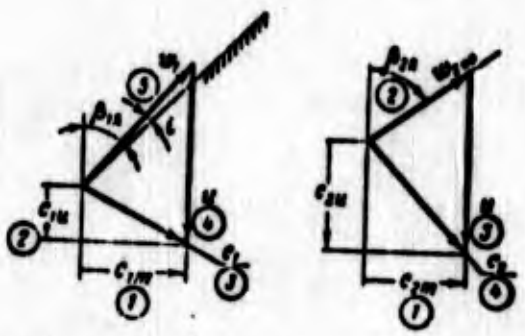

Fig. 2.20. Plotting velocity triangles for an axial pump.

Having two projections of absolute velocity c_{1u} and c_{1z} and knowing the value and direction of the circular velocity u, let us plot the velocity triangle at the inlet into the vane cascade. On Fig. 2.20 the order of the plotting is noted by numerals in circles. The direction w_1 is determined by the relationship of velocities c_1 and u and in general can comprise the angle of attack i tangent to the profile at the inlet of the vane.

For the plotting of the velocity triangle at the outlet from the axial vane cascade, let us find the value of the axial component of absolute velocity. It is determined by the volumetric fluid flow rate and the flow cross-sectional area at the outlet from the cascade:

$$c_{2z} = c_{2m} = \frac{Q_2}{F_{2m}}, \qquad (2.15)$$

where F_{2m} is the flow cross-sectional area at the outlet from the cascade:

$$F_{2m} = \pi D_{cp} b_2 \sin \beta_2. \qquad (2.16)$$

Besides the value of the axial velocity component, the flow direction at the outlet from the cascade is known in the first approximation. We will consider that the direction of the relative outlet velocity from the vane channel coincides with the outlet angle of the vanes (design scheme $z = \infty$). Then the velocity triangle is completely defined (see Fig. 2.20). The absolute velocity at the outlet from the wheel c_2 is found with respect to the value and direction.

Let us give the plotting of schemes of velocities for an axial-flow turbine. Figure 2.21 shows the necessary projections

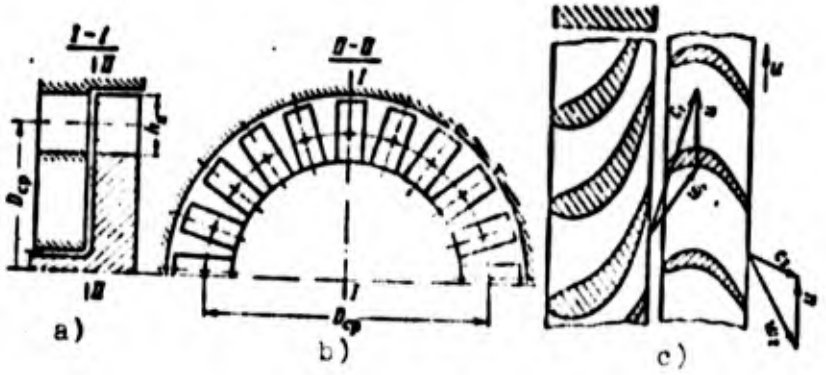

Fig. 2.21. Characteristic cross sections of an axial-flow turbine and velocity triangles: a) meridian cross section; b) cross section in a scheme; c) development of a cylindrical cross section (increased two times in comparison with a and b).

which expose the form and dimensions of the axial-flow turbine - the meridian cross section along I-I, the cross section in scheme II-II and the development of cylindrical cross section with a diameter equal to the mean diameter of the turbine.

The guide device at the inlet into the turbine, usually called the nozzle box, providing the expansion of gas and its acceleration, should insure such a direction of absolute inlet velocity to the turbine wheel (α_1) in order to obtain a large value of the circular component c_{1u}. Thus, the velocity $\vec{c}_1$ is assigned. In other respects the plotting does not require explanation. Figure 2.21 gives plans of the velocities directly near the profiles, and Fig. 2.22 gives combined schemes of the velocities for the inlet into the rotor and outlet from it.

Let us observe the plotting of the schemes of velocities for the radial inward-flow turbine, the wheel of which is a circular vane cascade. Installed in front of the rotor is a nozzle box, which provides the acceleration of flow to the velocity c_1.

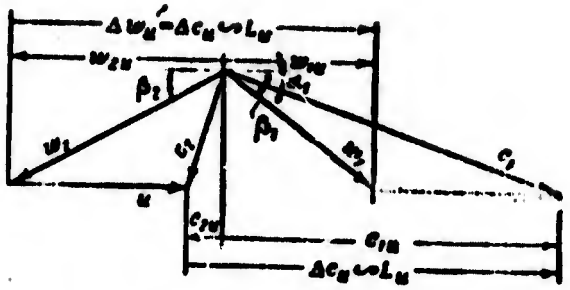

Fig. 2.22. Velocity triangles for an axial-flow turbine.

Figure 2.23 shows the basic sections which expose the form and relationship of dimensions of the nozzle box and radial wheel. Such cross sections are the meridian cross section (I-I) and cross section in the scheme (II-II).

For a radial vane machine the axial component of absolute velocity is equal to zero:

$$c_z = 0.$$

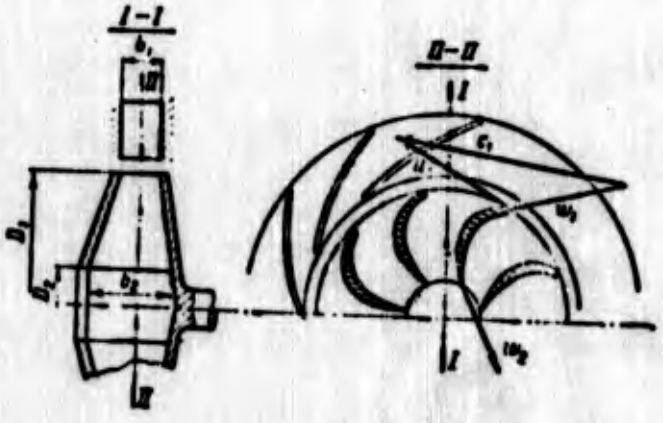

Fig. 2.23. Characteristic cross sections of a radial-flow turbine.

At the inlet into the turbine the flow should have a considerable circular component c_{1u} created by the guide (nozzle) apparatus installed in front of the wheel. The value c_{1u} should be assigned. The meridian component (in this case radial) is found from the relation general for all vanes (2.11).

For the radial machine F_{1m} is the cylindrical cross section with a width along the generatrix equal to the width of the circular vane cascade b_1 and is equal to:

$$F_{1m} = \pi D_1 b_1. \tag{2.17}$$

According to the known value of volumetric flow rate at the inlet into the wheel, let us find the velocity $c_{1r} = c_{1m}$:

$$c_{1r} = c_{1m} = \frac{Q_1}{\pi D_1 b_1}, \tag{2.18}$$

where $Q_1 = \frac{G_1}{\rho_1}$.

Having two projections of absolute velocity c_{1u} and c_{1r} and knowing the value and direction of the circular velocity, we plot the velocity triangle at the inlet into the circular cascade. As a result of the plotting we find the value and direction of the relative speed w_1 (Fig. 2.24).

Instead of c_{1u} and Q_1, the velocity at the outlet from the nozzle box c_1 and angle α_1, which determines the direction of velocity c_1, can be assigned. Then the plotting of the velocity

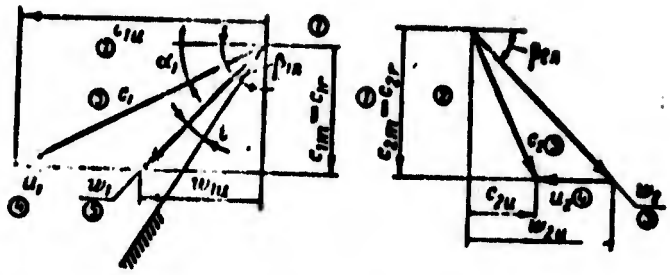

Fig. 2.24. Plotting of velocity triangles for a radial-flow turbine.

triangle is carried out in the following manner: we plot the velocity c_1 at angle α_1 (see Fig. 2.24), and we subtract vector $\vec{u}_1$ from the vector $\vec{c}_1$ and obtain the vector $\vec{w}_1$.

To find the absolute velocity at the outlet from the wheel, let us conduct the plotting of the velocity triangle.

The meridian (radial) component of absolute velocity at the outlet from the wheel is found from the known formula:

$$c_{2r} = c_{2m} = \frac{Q_2}{F_{2m}} = \frac{Q_2}{\pi D_2 b_2}, \qquad (2.19)$$

where $Q_2 = \frac{G_2}{\rho_2}$.

Besides the radial velocity component, u_2 and the direction of flow at the outlet from the wheel are known. The angle of inclination of the vector of relative speed is taken equal to the output angle of the vanes $\beta_{2л}$ ($z = \infty$). Then the value and direction of the absolute outlet velocity of the wheel will be determined by the plotting of the velocity triangle presented on Fig. 2.24.

Having selected the basic procedures of the plotting of the schemes of velocities for wheels of the vane machines, let us pass to the development of the fundamental principles ensuing from the law of the conservation of momentum for the wheel of the vane machine.

2.7. FUNDAMENTAL PRINCIPLES WHICH ENSUE FROM THE LAW ON MOMENTUM

2.7.1. EULER EQUATION FOR VANE MACHINES

Between the fluid flow and impeller blades a force interaction is achieved. This interaction indicates in the final result the fact that on vanes of the rotating wheel there acts a difference in forces of pressure on both sides of the vane; otherwise it is not possible to transmit energy from the wheel to the fluid and vice versa. For the pump (compressor) this pressure difference determines the moment of resistance on the shaft and for the turbine - the torsional moment.

For an example, Fig. 2.25 gives the pressure distribution along the cross section of the vane channel of the wheel of the centrifugal pump. As a result of the nonuniformity of the pressure distribution with the steady nature of the relative flow of fluid through the rotor, the absolute motion of the fluid through the rotor will have a nonstationary nature. In fact, each particle of the rotor periodically passes by the point connected with the housing. The instantaneous absolute velocity at this point will be cyclically changed in accordance with the pressure distribution (relative speed) in the vane channel. Consequently, in the absolute flow the feature of the steady motion, the constancy of the velocity at a particular point of space, will

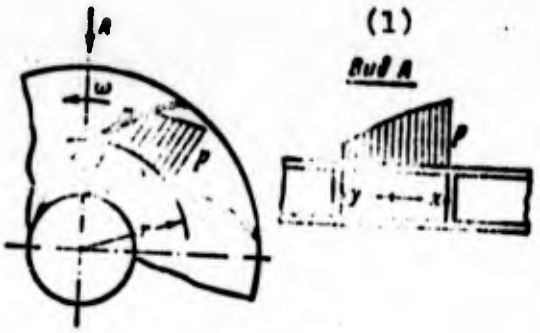

Fig. 2.25. Approximate pattern of the pressure distribution along the cross section of the vane channel of the centrifugal wheel. KEY: (1) form A.

not be held. But, by examining the averaged velocities, it is possible to use the fundamental laws of mechanics for the steady motion to the flow of fluid relative to the fixed coordinates called the absolute fluid flow.

For determining the total moment which acts on the rotor during the flow of fluid through it, let us use the theorem about the moment of momentum.

The moment of the resultant of external forces applied to the chosen contour of the fluid is equal to a change in the moment of momentum of the mass of fluid flowing per unit time through this contour.

Let us use the theorem about the moment of momentum for the radial vane machine, although it is correct for any machine.

Let us take the contour limited by surfaces F_1, F_2 and $F_к$, i.e., including all the channels with the exception of the vanes themselves (Fig. 2.26).

Taking into account the nonstationary nature of absolute motion in the rotor, let us find the average (in mass) value of the moment of the circular velocity component:

$$\overline{c_u r} = \frac{1}{Q}\int c_u r dQ. \qquad (2.20)$$

Let us record the equation of the theorem about the moment of momentum relative to the axis of rotation in the form

$$G(\bar{c}_{2u}r_2-\bar{c}_{1u}r_1)=M_z \ [\text{N}\cdot\text{m}]. \qquad (2.21)$$

where G is the mass fluid flow rate per second; M_z is the resultant moment of the external forces.

In general the resultant moment of external forces consists of the moment of surface forces - moment $M_л$ from the effect of the rotor (surface $F_к$ on Fig. 2.26) on the chosen volume of fluid - and moments M_{F_1} and M_{F_2} of surface forces acting over boundary surfaces F_1 and F_2. Of the volumetric forces only the forces of gravity (weight) will be external, but as a result of the axial symmetry they give relative to the axis a moment equal to zero. Of the surface forces which act on boundary surfaces, moments M_{F_1} and M_{F_2} relative to the axis of rotation can give only tangential stresses, i.e., the forces of friction caused by the turbulent exchange of momenta. The forces of pressure on the boundary surfaces as normal forces do not give the moment with respect to the axis:

$$M_z=M_л+M_{F_1}+M_{F_2}. \qquad (2.22)$$

The moment which acts on the chosen volume of the fluid on the side of the rotor in general is the moment of the surface forces, i.e., the forces of pressure and forces of friction. In more detail the nature of the acting forces is explained later in an examination of the relative flow thorugh the rotor of the vane machine.

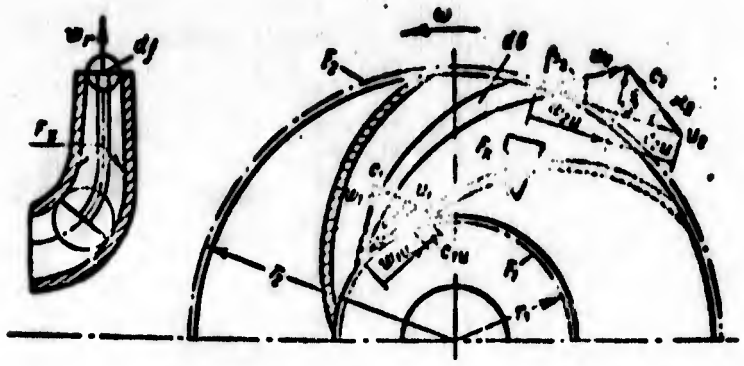

Fig. 2.26. Diagram of the flow of fluid through the wheel of a centrifugal vane machine.

Equation (2.21) shows that a change in the moment of momentum of the fluid in absolute motion through the wheel of the pump is equal to the resultant moment of forces acting on the chosen volume of the fluid. By disregarding the moments of the surface forces which act along surfaces F_1 and F_2, we restrict the rotor of the vane machine, and on the internal surfaces, which restrict vanes in width, we will obtain that the moment acting on the side of the vanes on the fluid will be equal to

$$M_л = G(\vec{c}_{2u}r_2 - \vec{c}_{1u}r_1) \text{ [N·m]}. \tag{2.23}$$

The moment from the effect of flow on the rotor will be opposite in sign:

$$M_u = -M_л. \tag{2.24}$$

According to the value of the moment M_u, it is possible to define the power of the rotor of the vane machine as the product of the moment and the frequency of rotation. Let us call it the circular power:

$$N_u = M_u\omega \left[\frac{\text{N·m}}{\text{s}} = \frac{\text{J}}{\text{s}} = \text{W}\right]. \tag{2.25}$$

In referring the power to the mass flow rate per second, we will obtain the expression for the specific work of the vane machine. The specific work is the energy transmitted to the turbine wheel by a urit of mass of fluid (1 kg) or transmitted by the wheel of a pump to a unit of mass of fluid (1 kg):

$$L_u = \frac{N_u}{G} \quad \left[\frac{W}{kg/s} = \frac{J \cdot s}{s \cdot kg} = \frac{J}{kg}\right]. \tag{2.26}$$

If we express L_u by the moment M_u, then we will obtain

$$L_u = \frac{M_u \omega}{G}. \tag{2.27}$$

In substituting the developed expression for M_u [formulas (2.23) and (2.24)], we will obtain

$$L_u = \bar{c}_{1u} u_1 - \bar{c}_{2u} u_2 \left[\frac{J}{kg} = \frac{m^2}{s^2}\right]. \tag{2.28}$$

The equation written in this form is called the Euler equation for vane machines. It is correct for all types of vane machines. For axial vane machines $u = u_1 = u_2$, and the Euler equation will be recorded in the simplest form:

$$L_u = u(\bar{c}_{1u} - \bar{c}_{2u}). \tag{2.29}$$

An analysis of the Euler equation shows the following.

1. The specific work of the vane machine, expressed in J/kg, does not depend on the kind of the working medium, since the physical parameters of the working medium do not enter into this

formula. This work depends only on the value of the circular components of absolute velocities and circular velocities of the rotation of the rotor.

2. The work is transmitted to the rotor from the fluid (i.e., the energy of the fluid is decreased) when $\bar{c}_{1u}u_1 > \bar{c}_{2u}u_2$, and vice versa, the rotor transmits the work, i.e., it increases the energy of the fluid when $\bar{c}_{2u}u_2 > \bar{c}_{1u}u_1$. The vane machines, which transmit energy from the fluid to the rotor operate under conditions of the engine-turbine. The vane machines which transmit external mechanical energy to the gas or fluid are actuating machines and operate under conditions of the compressor or pump.

Consequently, for the turbine the Euler equation will be recorded in this form:

$$L_u = \bar{c}_{1u}u_1 - \bar{c}_{2u}u_2 \left[\frac{\text{J}}{\text{kg}}\right]^1, \qquad (2.30)$$

where L_u is the specific circular work of the turbine[2], i.e., the energy transmitted to the rotor by one kilogram of fluid.

In the pump or compressor the energy is transmitted from the rotor to the fluid; correspondingly we will obtain

$$H_T = -L_u;$$
$$H_T = \bar{c}_{2u}u_2 - \bar{c}_{1u}u_1 \left[\frac{\text{J}}{\text{kg}}\right]. \qquad (2.31)$$

---

[1]The line (averaging sign) over c_{1u} and c_{2u} will subsequently be omitted.

[2]Term "circular" means "on the circumference of the rotor" on the vanes"; thereby it is emphasized that we are speaking about the specific work of the vane cascade and not the machine as a whole.

where $H_т$ is specific theoretical (circular) pressure or the energy transmitted by the rotor of 1 kg of mass of the fluid which passed through the pump or compressor (which will subsequently be called compressor vane machines). The notations L_u and $H_т$ are introduced for convenience and are conventional for the turbines and pumps.

3. The specific work of the vane machine will be more, the greater the circular velocity component c_u and circular velocity u entering into first terms of equations (2.30) and (2.31). In the case of the turbine this means the need for the provision by the nozzle box of such a direction of velocity c_1 in order that the circular component c_1 would have a large value. In the case of the compressor vane machine the necessary value c_{2u} is provided by a deviation in the flow in the rotor, i.e., by the angle of the impeller vanes at the outlet $\beta_{2л}$: the more $\beta_{2л}$, the more c_{2u} will be. The large value of the circular velocity u_1 for the turbine and u_2 for the pump can be obtained at the high frequency of rotation ω or at large diameters of the rotor D_1 for the turbine and D_2 for the pump.

4. The specific work of the vane machine on the circumference of the rotor will be more if the circular velocity component, which enters into the second term of (2.30) and (2.31), will have a different sign than the circular velocity component in the first term of these equations.

For the pump and compressor this means that with the twist of the flow at the inlet to the side opposite the rotation, the pressure of the machine will be increased, and with twist of the flow to the side of rotation it will be decreased.

For the turbine the torsion of the flow at the outlet from the rotor to the side of rotation decreases the work of

the turbine. The presence of the circular velocity component at turbine outlet, directed to the side opposite the rotation, increases the work of the turbine; however, it lowers its economy, as will be shown further.

2.7.2. FORCES WHICH ACT ON THE VANE PROFILE OF AN AXIAL CASCADE

The Euler equation does not reveal the nature of the forces acting on the rotor of the vane machine from the side of the fluid. For axial vane machines the nature of the forces which act on the side of the fluid on the impeller vanes is determined by the theorem of N. Ye. Joukowski about forces which act on a streamlined profile.

Let us examine, following N. Ye. Joukowski, the forces acting on the vane profile of an axial cascade of a unit length in relative steady motion. In the examination of the streamline flow of a single profile, the concept of averaged relative speed w_{cp} is introduced.

The relative averaged flow velocity w_{cp} is the average vector from values of relative velocity at infinity in front of the vane and behind it (Fig. 2.27):

$$w_{cp} = \sqrt{w_z^2 + \left(\frac{w_{1u} + w_{2u}}{2}\right)^2}; \qquad (2.32)$$

$$\operatorname{tg}\beta_{cp} = \frac{w_z}{w_{u\,cp}} = \frac{2w_z}{w_{1u} + w_{2u}}. \qquad (2.33)$$

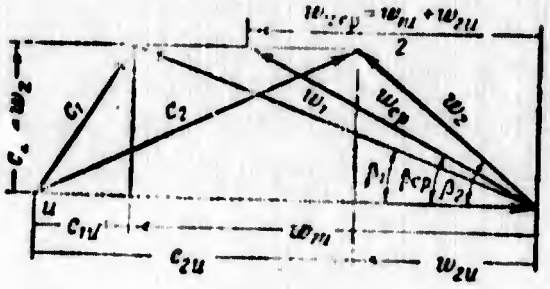

Fig. 2.27. Combined velocity triangles at the inlet into the axial cascade and at the outlet from it.

As N. Ye. Joukowski showed, the force F, which appears with the streamline flow of the vane profile, can be determined according to the value of circulation of the relative speed around the profile[1]:

$$F = \rho \Gamma_{л\,w} w_{cp} \qquad (2.34)$$

(The force intensity is determined for the profile of unit length, and therefore the dimensionality of the forces is N/m).

Here $\Gamma_{л\,w}$ - is circulation along the contour ABCD (Fig. 2.28):

$$\Gamma_{л w} = \int w\,ds = t(c_{1u} - c_{2u}). \qquad (2.35)$$

Equation (2.34) expresses N. Ye. Joukowski's theorem.

The force with which the flow of nonviscous fluid acts on the profile is equal to the product of the density ρ of the fluid, circulation $\Gamma_{л\,w}$ of the relative velocity on the contour ABCD encompassing the profile, and the average flow velocity at infinity.

---

[1]N. Ye. Joukowski's theorem about forces acting on a wing profile and cascade is derived in detail in courses in gas dynamics [37] and [38].

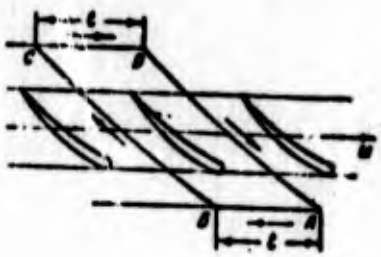

Fig. 2.28. The determination of circulation around the vane in an axial vane machine.

This force is called lift, and its direction is perpendicular to the direction of the velocity w_{cp} (Fig. 2.29). This means that the lift, i.e., the force of pressure of the fluid on the profile, directed perpendicular to the averaged flow velocity, appears as a result of the imposition of the circulation flow on the flow determined by the assigned flow rate.

In this case on the convex side of the profile the velocity increases, and the pressure drops, and on concave side the opposite is true. A pressure differential , which acts on the profile, creates lift. The lift can be expanded into a circular component F_u and axial component F_z.

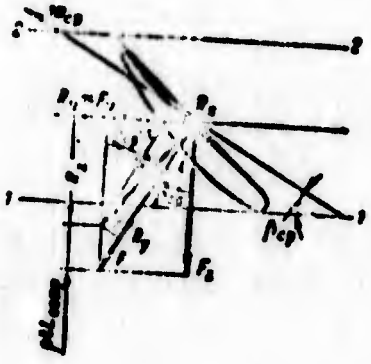

Fig. 2.29. Forces which act on the streamlined profile.

In vane machines the total circumferential force F_{uz}, which acts on the vanes, creates a torque on the shaft. Therefore, for vane machines very important is the conclusion following from N. Ye. Joukowski's theorem about the fact that the circumferential force which acts on the vanes is proportional to the circulation of the relative velocity along the contour, which encompasses the profile and passes through the axes of the vane channels and circular arcs at the inlet into the cascade and at the outlet from it. For the real fluid the force of action on the profile will be changed.

Figure 2.29 also depicts the scheme of forces which act on the profile of the axial cascade in a real viscous fluid at the same velocity w_{cp} (in general values of the averaged velocity and circulation will also be changed).

In courses in gas dynamics [37] and [38] it is shown that

$$R_a = F_a; \tag{2.36}$$

$$R_t = F_t - \varrho l L_{c.mp}, \tag{2.37}$$

where L_{comp} is the work of force R_x (drag) referred to the mass unit of fluid and improved on the path being passed by the profile relative to the fluid per unit time (w_{cp}):

$$L_{comp} = \frac{R_x w_{cp}}{\varrho l w_{t\,cp}} = \frac{R \sin \chi}{\varrho l \sin \beta_{cp}}. \tag{2.38}$$

where R is the resultant force of reaction of the flow; R_x is the force which acts in the direction of the velocity w_{cp} (drag).

Thus, the viscosity effect was revealed both directly - in the form of the appearance of an additional resisting force (drag), and in an implicit form - by means of the change in velocities and circulation.

The ratio of the drag to the lift is called the inverse quality of the profile and is equal to the tangent of the angle χ (χ - the angle formed by force R and normal to the direction w_{cp}):

$$\operatorname{tg}\chi = \frac{R_x}{R_y}, \tag{2.39}$$

where R_y is the force normal to the direction w_{cp} (lift).

Let us determine the moment of the rotor of the vane machine first, not allowing for the interaction of the profiles:

$$M_a = zR_a r_{cp} b_a =$$
$$= z\Gamma_a w r_{cp} (w_{cp} b_a \sin\beta_{cp}) = \frac{\eta}{2\pi} z\Gamma_a w. \tag{2.40}$$

With motion of the vane (rotation) the power referred to the profiles of the unit length will be equal to

$$N_a = zR_a u = zRu \sin(\beta_{cp} + \chi). \tag{2.41}$$

The work which occurs for 1 kg of mass of fluid (for a pump - theoretical pressure H_T), determined in the calculated cross-section (on radius r), for the section of the vane with a length dr will be equal to

$$H_T = \frac{N_R dr}{\rho dQ} = \frac{zRu \sin(\beta_{cp} + \chi)}{\rho dQ} dr,$$

where dQ is the volumetric fluid flow included between the two cylindrical surfaces with radii r and r + dr:

$$dQ = z b_1 c_m dr; \qquad (2.42)$$

taking this into account

$$H_T = \frac{Ru \sin(\beta_{cp} + \gamma)}{u c_m} = \frac{Ru \sin(\beta_{cp} + \chi)}{u w_{cp} \sin \beta_{cp}} \left[\frac{J}{kg}\right]. \qquad (2.43)$$

As is known from aerodynamics, the airfoil lift of a unit length is equal to

$$R_y = c_y b_1 R \frac{w_{cp}^2}{2}, \qquad (2.44)$$

and since

$$R = \frac{R_y}{\cos \chi},$$

then

$$R = \frac{c_y \rho b_1 w_{cp}^2}{2 \cos \chi}. \qquad (2.45)$$

By substituting expression (2.45) for R into equation (2.43), we obtain

$$H_T = c_y \frac{b_1}{t} \frac{u}{c_m} \frac{w_{cn}^2}{2} \frac{\sin(\beta_{cp} + \chi)}{\cos \chi} \left[\frac{J}{kg}\right]. \qquad (2.46)$$

From relation (2.46) it follows that the specific energy of the elementary axial stage of the vane machine is proportional to the coefficient of airfoil lift and to the cascade solidity. By knowing the airfoil lift coefficient and being assigned the cascade solidity, it is possible to calculate H_T.

To calculate the interaction of profiles, introduced is the coefficient which considers the distinction in the coefficient of the airfoil lift in the cascade $c_{y\ реш}$ from the lift coefficient of the unit profile:

$$\rho = \frac{c_{y\ реш}}{c_{y\ отд}}. \qquad (2.47)$$

In practice this method of the calculation of specific work of a vane machine is applicable for widely spaced cascades ($b_п/t < 1$): for dense cascades the interaction of the profiles will be greatly expressed, and the lift coefficients, obtained during testing of separate profiles, will not characterize the work of the profile in the cascade. Furthermore, it is necessary to keep in mind that the nature of the streamline flow of the profile in the machine even with widely spaced cascades differs from the nature of the streamline flow of the profile in the wind tunnel, i.e., from the conditions under which c_y is usually determined.

The method of calculation of the value of specific work of the vane machine, based on relations (2.43) and (2.46), is applied only in the calculation of axial pumps, hydroturbines and screws with low cascade solidity.

2.7.3. CONNECTION OF THE MOMENT OF THE WHEEL OF A RADIAL VANE MACHINE WITH THE MOMENT OF THE CORIOLIS FORCES OF INERTIA

Let us examine the nature of the forces acting on the side of the fluid on the vane of a radial (diagonal) machine in the relative steady motion. In the radial vane machines together with the aerodynamic forces, determined by Joukowski's theorem, of great significance (and, frequently, the basic) are the inertial forces of the fluid.

In examining the relative motion of the fluid in the rotating wheel, in essence, we examine the flow of fluid relative to the evenly rotating coordinates fastened to the wheel, i.e., the flow in the noninertial coordinate system. In this case added to the volumetric forces which act on the fluid, which is located in the wheel, besides the forces of gravity (weight), are the forces of inertia from the movable and Coriolis accelerations, i.e., the centrifugal and Coriolis forces of inertia.

Centrifugal forces pass through the axis and therefore do not give the moment with respect to the axis of rotation. The Coriolis forces of inertia in radial vane machines give the moment with respect to the axis.

As is known, with the motion of the fluid along the channel of the rotating wheel the Coriolis (rotary) acceleration, which acts on the fluid, is connected with the change in the direction of relative velocity w and a change in the velocity u. The Coriolis acceleration is imparted to the fluid by the vanes (walls of the channel) through elastic forces (forces of pressure). The Coriolis force of inertia is equal to the force which acts on the fluid on the side of the vanes and directed in an opposite

direction. Acting on the vanes is not the Coriolis force themselves, but the forces of pressure counterbalancing it. In the case of the pump the moment from the Coriolis forces in the form of the moment of forces of pressure is counterbalanced by the external moment applied to the rotor.

We record the moment of the Coriolis force of inertia, which acts from the fluid on the wheel, in the integral form

$$M_{u\,s} = \int_V r F_{u\,s} \rho dV, \qquad (2.48)$$

where F_{ku} is the circular component of vector of the Coriolis force of inertia referred to the unit mass; V is the volume of the chosen fluid element; F_{ku} is equal to the circular component of the vector of Coriolis acceleration taken with the opposite sign:

$$\vec{F}_{u\,s} = -\vec{j}_{u\,s}.$$

From the examination of Fig. 2.30, where the vectors of velocity and acceleration for the motion of the stream along the diagonal rotor are shown (see also Fig. 2.32), it follows that

$$j_{u\,s} = 2(\vec{\omega} \times \vec{w}_r) = 2\omega w_r \sin(\hat{\omega w_r}); \qquad (2.49)$$

since the angle between ω and w_r is equal to 90°, then according to the value

$$F_{u\,s} = -2\omega w_r. \qquad (2.50)$$

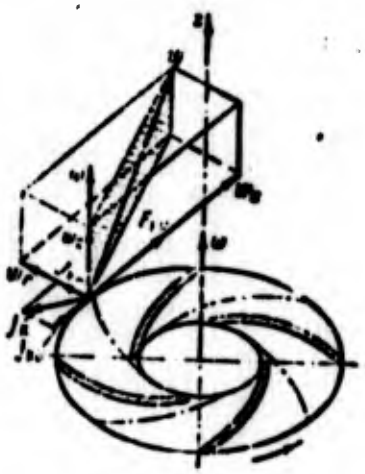

Fig. 2.30. Determination of the Coriolis force of inertia in a centrifugal vane machine.

The elementary volume dV can be presented in this form:

$$dV = dr\, b\, r\, d\varphi. \tag{2.51}$$

By substituting expressions (2.50) and (2.51) for F_{ku} and dV into equation (2.48) and passing over to the definite integrals, we obtain

$$M_{u.s} = -\int_{r_1}^{r_2}\int_{0}^{b}\int_{0}^{2\pi} r^2 2\omega w_{rl}\, dr\, b\, d\varphi. \tag{2.52}$$

According to the equation of continuity the mass flow rate for all radii is a constant value:

$$C = \int_{0}^{b}\int_{0}^{2\pi} r w_{rl}\, b\, d\varphi;$$

then

$$M_{u.s} = -G 2\omega \int_{r_1}^{r_2} r\, dr = -G\omega(r_2^2 - r_1^2) = \\ = -G(u_2 r_2 - u_1 r_1). \tag{2.53}$$

Let us transform formula (2.23), utilizing the relations ensuing from the triangles of averaged velocities (see Fig. 2.24):

$$\vec{c}_{1u}=\vec{w}_{1u}+\vec{u}_1 \text{ and } \vec{c}_{2u}=\vec{w}_{2u}+\vec{u}_2.$$

We will obtain the following equation for the moment acting on the side of the vanes on the fluid:

$$M_{\text{л}}=G(w_{2u}r_2-w_{1u}r_1)+G(u_2r_2-u_1r_1); \tag{2.54}$$

taking into account expression (2.53), we obtain

$$M_{\text{л}}=G(w_{2u}r_2-w_{1u}r_1)+M'_{\text{к}\,z}, \tag{2.55}$$

where $M'_{\text{к}\ z}$ is the moment which acts on the fluid on the side of the rotor equal in magnitude but opposite in sign to the moment $M_{\text{к}\ z}$ [see expression (2.53)].

The first term in equation (2.55) can be represented in terms of circulation of the flow $\Gamma_{\text{л}\ w}$ in the relative motion around the contour ABCD, which includes the profile of the vane (Fig. 2.31)[1]

$$M_{\text{л}}=-G\frac{z}{2\pi}\Gamma_{\text{л}\,w}+M'_{\text{к}\,z}. \tag{2.56}$$

---

[1]Subsequently (in Section 2.10.1) it will be shown that the relative flow in the rotor of the radial vane machine is vortex (nonpotential). Hence, the contour of the calculation $\Gamma_{\text{л}\ w}$ cannot be taken arbitrarily as any contour encompassing the profile of the vane. We will understand by the circulation of the relative velocity $\Gamma_{\text{л}\ w}$ as the circulation along the contour ABCD, i.e., on the contour passing through axes of the vane channels and circular arcs at the inlet into the circular cascade and at the outlet from it.

Fig. 2.31. Determination of circulation around the vane in a centrifugal vane machine.

The moment applied to the rotating rotor in value is equal to the moment which acts on the flow from the rotor but opposite to it in sign:

$$M_в = \frac{a}{2\pi} z\Gamma_{отн} + M_{вн} \qquad (2.57)$$

or in the expanded form:

$$M_в = G(w_{1u}r_1 - w_{2u}r_2) + G(u_1r_1 - u_2r_2). \qquad (2.58)$$

The first term of (2.58) is the moment which appears as a result of the streamline flow of fluid flow about the vanes and proportional to the circulation, calculated according to the relative speed, the number of vanes and the mass fluid flow rate. The pressure distribution over the vane profile, which corresponds to the circulation of relative velocity, can be obtained by means of the scavenging of fixed vane velocities by the flow with velocities and angles of incidences corresponding to the relative velocity.

The second term of equation (2.58) expresses the moment appearing on the wheel of the vane machine from the effect of the Coriolis forces of inertia. Under the effect of the circular

component of the Coriolis force of inertia, the fluid attempts to move in a circular direction. The vanes prevent the movement of the fluid under the action of the force of inertia and on the vanes there will appear a pressure difference which equalizes the force of inertia and creates an additional torsional moment for the turbine and moment of resistance for the pump.

Consequently, in the radial vane machine the total pressure differential on the vanes appears as a result of the effect of two factors: the streamline flow of flow about the vanes in relative motion and the effect of the Coriolis forces of inertia. A pressure difference on the vanes leads to the emergence of the moment on the rotor relative to the axis of rotation.

For the axial vane machine, assuming that the inlet and outlet of the fluid occurs on one radius, we have

$$u_2 = u_1.$$

The second term of (2.58) in this case will be equal to zero. This means that the moment on the impeller vanes of the axial vane machine is determined only by the streamline flow of the fluid flow about the vanes in relative motion. The value of this moment depends on the value of circulation of the fluid around the contour passing over the center lines of the vane channels and segments of the circular arcs at inlet and outlet equal to the pitch [compare formulas (2.57) and (2.58)]:

$$M_z = \frac{\rho}{2\pi} z\Gamma_{1,2}; \quad M_z = Gr(w_{1u} - w_{2u}).$$

The value of the circulation is determined by expression (2.35) in accordance with Fig. 2.28. In the axial vane machine the Coriolis forces of inertia will not give the moment applied to the rotor with respect to the axis of rotation, since they are radial forces passing through the axis (Fig. 2.32).

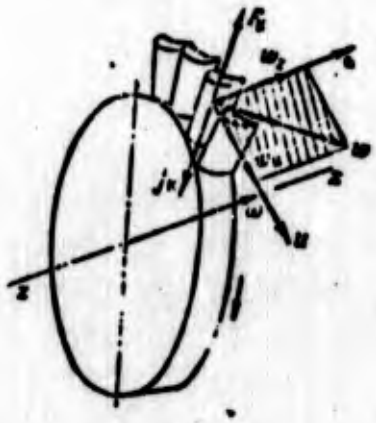

Fig. 2.32. Determination of the Coriolis force of inertia in an axial vane machine.

For the pump or compressor, in accordance with expressions (2.27) and (2.58), the equation for theoretical pressure will be recorded thus:

$$H_t = (w_{2u}u_2 - w_{1u}u_1) + (u_2^2 - u_1^2)\left[\frac{J}{kg}\right]. \qquad (2.59)$$

Correspondingly, for the turbine we will obtain

$$l_t = (w_{1u}u_1 - w_{2u}u_2) + (u_1^2 - u_2^2). \qquad (2.60)$$

The first terms in equations (2.59) and (2.60) express the specific work of the rotor connected with the moment from the circulation of relative velocity on the contour ABCD

(see Fig. 2.31). We will conditionally call these terms the specific work connected with the circulation forces. The second terms express the specific work of the rotor determined by the moment connected with the Coriolis forces of inertia. Let us conditionally call these terms in equations (2.59) and (2.60) the specific work of the Coriolis forces. The equations take the general form for all the vane machines.

For the axial machine the second terms of equations (2.59) and (2.60) will be equal to zero.

When $u_2 = u_1 = u$

$$H_t = u(w_{1u} - w_{2u})$$
and $$L_u = u(w_{1u} - w_{2u}).$$

In the axial vane machine the rotor will accomplish work only in such a case when as a result of the streamline flow of the impeller vanes the direction of the relative velocity, i.e., the circulation of the relative speed will be different from zero [see equation (2.40)].

Vane cascades of the axial machines should be profited quite thoroughly. For them great significance is in the selection of the perfected shape and camber, the optimum value of the angle of incidence and other parameters connected with the provision of the assigned circulation (work).

In radial vane machines the dominant role in the producing of the moment on the rotor is played by the Coriolis force of inertia, the work of which does not depend on the shape of the vanes but depends on their radial extent. The greater the difference in the circular velocity, the more the value of the Coriolis forces, and the less the role the flow in the relative motion plays.

With the unsuccessful profile of the vane and with nonoptimal angles of incidences the losses in any vane machine will increase, but in an axial machine simultaneously with this the circulation (work) decreases; for a radial machine this does not have considerable importance. Furthermore, in a radial machine losses in the rotor comprise a small fraction of all the losses. Hence, in radial machines approximation methods of the construction of the vanes, which are based mainly on design and technological considerations are used extensively.

Let us note that because of the energy transfer by the inertial forces in channels of the centrifugal compressor machine (pump), it is possible to obtain a pressure increase in the rotor wheel with convergent flow of the flow along the vane channel (in the absence of diffuser flow). For convergent flows less values of hydraulic losses and less stringent requirements for the shape of the profiles which form the vane channels are characteristic.

Effects of the Coriolis forces of inertia and the streamline flow of vanes in relative motion can be added, i.e., increase the total pressure difference on the vane, and can be subtracted from each other by decreasing the pressure difference on the vanes (see source [49]). This depends on the direction of flow of the vanes, the direction of rotation and the direction of flow with respect to the axis, i.e., on what kind of radial machine is examined, i.e., centripetal or centrifugal.

Figures 2.33 and 2.34 depict diagrams of flow, respectively, for the centrifugal and centripetal vane machines which operate under conditions of the pump (compressor) and turbine.

The pressure in the vane channel caused by the Coriolis force of inertia is marked $p_к$. The direction of the increase in

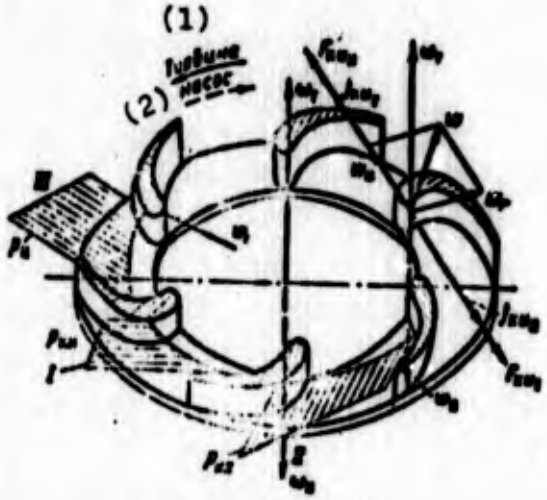

Fig. 2.33. Explanation of the operating principle of a centrifugal vane machine.
KEY: (1) Turbine; (2) Pump.

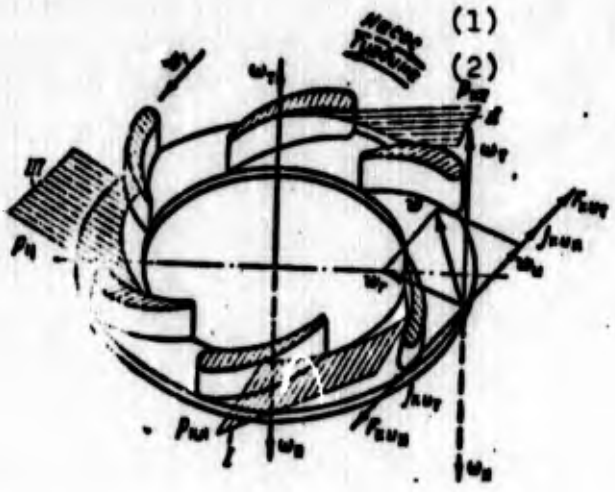

Fig. 2.34. Explanation of the operating principle of the centripetal vane machine.
KEY: (1) Pump; (2) Turbine.

pressure $p_к$ coincides with the direction of the circular component of the Coriolis force of inertia.

The pressure distribution, caused by the flow of the fixed vane profile, quantitatively determined by the circulation of relative velocity on the contour ABCD (see Fig. 2.31), is marked $p_ц$ (see Figs. 2.33 and 2.34).

With the streamline flow of the common vane profile (for example, that depicted on Figs. 2.33 and 2.34) with a small angle of incidence on the blade face an increased pressure is formed, and on the back a reduced pressure is formed. In accordance with this Figs. 2.33 and 2.34 show the pressure distribution on the vane channel $p_ц$, caused by the streamline flow of the vane profile. For an example, the greatly bent profile is taken. (In the case of the pump the profile is bent according to rotation).

The directions of rotation of the rotor in the work of the assigned profile in turbine conditions ($c_{1u} > c_{2u}$) and in pumping conditions ($c_{2u} > c_{1u}$) will be the opposite (on Figs. 2.33 and 2.34 the angular velocities for these cases are designated $\omega_т$ and $\omega_н$, respectively). Hence, the directions of the circular components of Coriolis force of inertia for the turbine and pump will also be the opposite. Figures 2.33 and 2.34 show the pressure distribution on the vane channel, which appears from the Coriolis forces of inertia, by these diagrams: for the turbine - $p_{к.т}$ and for the pump - $p_{к.н}$.

In the case of inward-flow turbine (see Fig. 2.34) the total pressure difference acting on the vane profile will be more than in the case of centripetal pump, since in the turbine the directions of the increase in pressures from the

Coriolis forces of inertia and from the streamline flow of the vane coincide (see Fig. 2.34). In the centripetal pump the pressure difference on the vanes will be less other conditions being equal, since an increase in pressure from the Coriolis force of inertia and from the steramline flow of the vanes occurs in different directions. As a result of this the specific work for the inward-flow turbine will be more than that for the centripetal pump at the same values of the relative velocity of the inlet into the cascade, the angle incidence of angular velocity , and so on.

For the centrifugal vane machine the picture will be different (see Fig. 2.33). In view of the fact that the directions of the Coriolis forces of inertia for the pump and turbine will be opposite, diagrams $p_{к.н}$ and $p_{к.т}$ will differ. For the pump a pressure increase from the Coriolis forces of inertia is directed from the convex to the concave side of the vane, i.e., just as this occurs in the case of the pressure distribution appearing with the streamline flow of the vanes (having the profile and conditions of flow depicted in Fig. 2.33) by the flow in relative motion. Consequently, for the centrifugal pump (see Fig. 2.33) these effects will be added and for the turbine, subtracted.

The specific work of the centrifugal vane machine, other conditions being equal, will be more for the pump but less for the turbine. This follows from equations (2.59) and (2.60): in centrifugal machines $u_2 > u_1$, and the second term in the equation for the pump is positive; for centripetal machines $u_1 > u_2$, and in this case the second term of the equation for calculation of the specific work of the turbine is also positive.

Hence it is possible to make a practical conclusion that, as a rule, it is not advantageous to use centrifugal turbines and centripetal pumps. However, with the small radial extent of the vanes (small difference between u_1 and u_2) the effect of the Coriolis force of inertia is small, and in this case the use of centrifugal turbines and centripetal pumps can prove to be advisable

With the considerable difference in dimensions of the inlet and outlet of the redial vane machine the effect of the term $(u_2^2-u_1^2)$ in equations (2.59) and (2.60) can be determining.

For the radial rotor with straight vanes (Fig. 2.35) when $w_1 = w_2$, the theoretical pump pressure is completely determined by the work of the rotor connected with the moment from Coriolis forces of inertia.

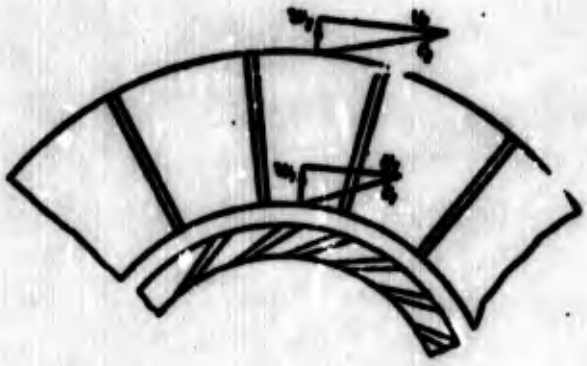

Fig. 2.35. Diagram of flow in a centrifugal pump with a guide device at the inlet.

From equation (2.59) it follows that in this case

$$H_t = u_2^2 - u_1^2. \qquad (2.61)$$

Let us discuss in more detail the relationship between the works from the circulation forces caused by the circulation of the relative speed and from the Coriolis forces of inertia in centrifugal pumps (see source [50]) and the inward-flow turbines, which are the preferred types of radial machines in the LPRE.

Let us examine first the centrifugal pump. Let us designate the specific work transferred with the aid of circulation forces $H_{ц}$, and the specific work transferred by means of Coriolis forces of inertia, - $H_{кор}$. Then equation (2.59) takes this form:

$$H_т = H_ц + H_{кор}; \quad H_ц = w_{2u}u_2 - w_{1u}u_1;$$
$$H_{кор} = u_2^2 - u_1^2.$$

The ratios $H_{ц}$ to $H_т$ and $H_{кор}$ to $H_т$ characterize the portions of energy transferred to the fluid, respectively, by means of circulation and Coriolis forces:

$$h_ц = \frac{w_{2u}u_2 - w_{1u}u_1}{w_{2u}u_2 - w_{1u}u_1 + u_2^2 - u_1^2}; \tag{2.62}$$

$$h_{кор} = \frac{u_2^2 - u_1^2}{w_{2u}u_2 - w_{1u}u_1 + u_2^2 - u_1^2}. \tag{2.63}$$

From velocity triangles at the inlet into the rotor and at the outlet from it (see Fig. 2.26), it follows that

$$w_{1u} = -(u_1 - c_{1u}); \quad w_{2u} = -(u_2 - c_{2u});$$
$$c_{2u} = u_2 - c_{2m}\operatorname{ctg}\beta_{2л}. \tag{2.64}$$

where $\beta_{2л}$ is the angle of the vanes at the outlet from the rotor.

Having transformed expressions (2.62) and (2.63) by means of relations (2.64), it is possible to obtain

$$h_{ц} = 1 - \frac{1 - \left(\frac{D_1}{D_2}\right)^2}{1 - q - \frac{c_{1u}}{u_1}\left(\frac{D_1}{D_2}\right)^2}; \qquad (2.65)$$

$$h_{кор} = \frac{1 - (D_1/D_2)^2}{1 - q - \frac{c_{1u}}{u_1}\left(\frac{D_1}{D_2}\right)^2}. \qquad (2.66)$$

In equations (2.65) and (2.66) the letter q denotes the complex $(c_{2m}/u_2)\text{ctg}\,\beta_{2л}$, called the flow parameter. The values $h_{ц}$ and $h_{кор}$ are determined by the ratio of diameters of the inlet into the rotor and outlet from it (D_1/D_2), by the flow parameter q and by the relative twist of flow at the inlet c_{1u}/u_1.

The dependence of $h_{ц}$ and $h_{кор}$ on these parameters is shown by Fig. 2.36. The ratio $D_1/D_2 = 1$ corresponds to the axial pump the specific work of which $H_т$ is created only by the circulation forces: $h_{ц} = 1$; $h_{кор} = 0$. With a decrease in D_1/D_2 and increase in q and c_{1u}/u_1, the portion of energy transferred with the aid of the circulation forces $h_{ц}$ is decreased, and the portion of energy transferred with the aid of the Coriolis forces $h_{кор}$ is increased.

For pumps with the ratio $D_1/D_2 < 0.5$-0.6 and $q > 0$ (the latter corresponds to rotors with the angle $\beta_{2л} < 90°$) $h_{ц}$ becomes

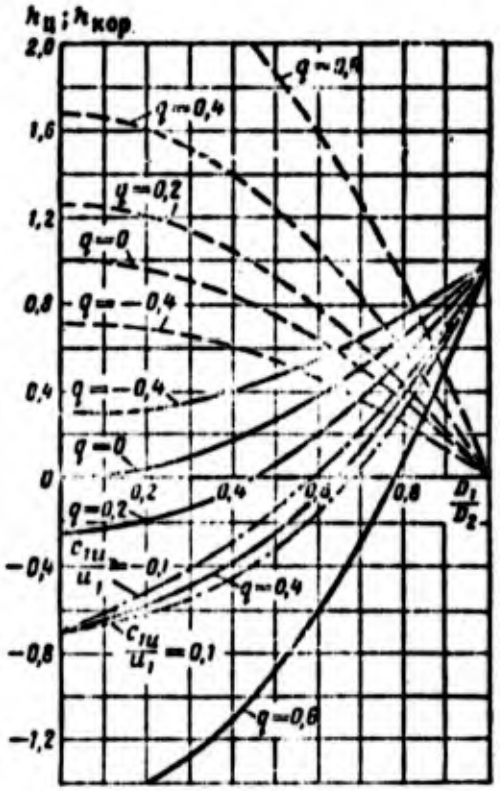

Fig. 2.36. Dependence of the relative work of Coriolis forces of inertia $h_{кор}$ and relative work of circulation forces h_u on the ratio of diameters D_1/D_2, q and c_{1u}/u_1 for the centrifugal pump: ——— h_u } when $c_{1u}/u_1 = 0$; -.-.-.- $h_{кор}$ }

-.-.-. h_u when $c_{1u}/u_1 \neq 0$.

negative, and $h_{кор}$ is more than unity, i.e., in the process of the flow of fluid about the vanes the energy is not transferred, but, on the contrary, is subtracted from it (the energy is transferred from the fluid to the rotor). The rotor transfers the energy of the fluid only by means of the balancing of Coriolis forces, compensating the energy taken from the fluid by means of circulation forces. For these pumps the geometric parameters of the profile of the vane and conditions of flow (angles of incidences do not have a noticeable effect on the external criteria.

In the case of pumps when $D_1/D_2 > 0.5$ the energy transfer of the fluid when $h_u > 0$ and $h_{кор} > 0$, i.e., specific work is created by both Coriolis and circulation forces. For such

pumps the profiling of the impeller vanes and the provision of favorable angles of incidences are already of vital importance.

Let us examine the inward-flow turbine. Having designated the specific work transferred by the circulation forces by $L_ц$, and the specific work transferred by Coriolis forces by $L_{кор}$, let us present equation (2.60) in the form

$$L_т = L_{кор} + L_ц; \quad L_ц = w_{1u}u_1 - w_{2u}u_2;$$
$$L_{кор} = u_1^2 - u_2^2.$$

Then

$$l_т = \frac{L_ц}{L_т} = \frac{w_{1u}u_1 - w_{2u}u_2}{w_{1u}u_1 - w_{2u}u_2 + u_1^2 - u_2^2}; \qquad (2.67)$$

$$l_{т.р} = \frac{L_{т.р}}{L_т} = \frac{u_1^2 - u_2^2}{w_{1u}u_1 - w_{2u}u_2 + u_1^2 - u_2^2}. \qquad (2.68)$$

From the velocity triangles (see Fig. 2.24) it follows that

$$w_{1u} = c_{1u} - u_1; \quad w_{2u} = c_{2u} - u_2; \quad c_{1u} = c_1 \cos\alpha_1. \qquad (2.69)$$

Solving equations (2.67) and (2.68) in conjunction with (2.69), we obtain

$$l_т = 1 - \frac{1 - (D_2/D_1)^2}{\frac{\cos\alpha_1}{u_1/c_1} - \frac{c_{2u}}{u_2}\left(\frac{D_2}{D_1}\right)^2}; \qquad (2.70)$$

$$l_{кор} = \frac{1-(D_2/D_1)^2}{\frac{\cos\alpha_1}{u_1 c_1} - \frac{c_{2u}}{u_2}\left(\frac{D_2}{D_1}\right)^2}. \qquad (2.71)$$

The values of l_u and $l_{кор}$ depend on the angle of the departure of flow from the nozzle box α_1 and on the ratio of diameters D_2/D_1, the ratio of velocities u/c_1 and relative twist of the flow at the outlet of the rotor c_{2u}/u_2 (Fig. 2.37). With an increase in the ratio u_1/c_1 the portion of work of the Coriolis forces is increased, and the portion of work of the circulation forces is decreased. At high values of u_1/c_1 the value of l_u becomes negative, and $l_{кор}$ becomes more than unity. However, under conditions which usually correspond to inward-flow turbines ($u_1/c_1 < 1$) the energy is transferred to the rotor both by the work of the circulation and the Coriolis forces ($l_u > 0$, $l_{кор} > 0$). Therefore, for the inward-flow turbines usually important are a profile of vane and the provision for favorable angles of incidences.

2.7.4. AXIAL AND RADIAL FORCES ACTING ON THE ROTOR OF THE VANE MACHINE

Besides the torsional moment (moment of resistance), on the side of the fluid axial and radial forces can act on the rotor.

For determining the axial thrust, let us use the theorem about the momentum: the resultant of the external forces applied to any contour of fluid is equal to the change in the momentum of the mass of fluid passing per unit time through this contour.

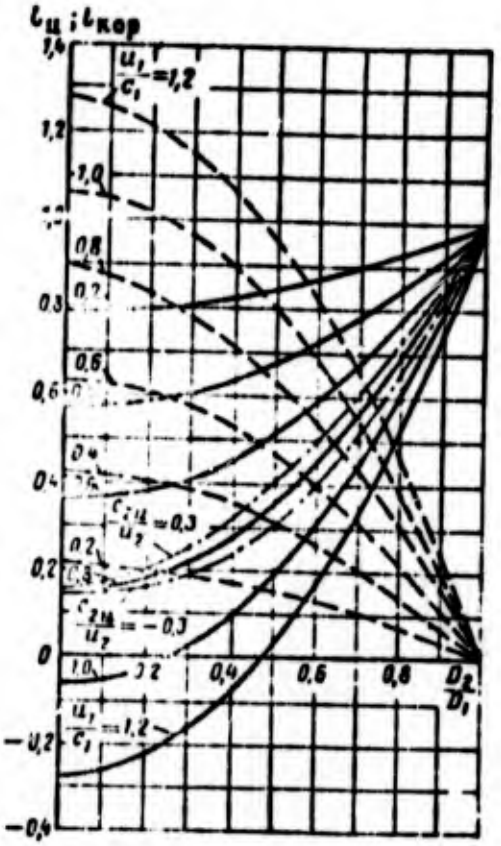

Fig. 2.37. Dependence of the relative work of Coriolis forces of inertia $l_{кор}$ and relative work of circulation forces l_u on the ratio of diameters D_2/D_1, u_1/c_1 and c_{2u}/u_2 for the inward-flow turbine ($\alpha_1 = 20°$):

——— l_u } when $c_{2u}/u_2 = 0$;

-.-.-.-. $l_{кор}$ }

-.-.-.-. l_u when $c_{2u}/u_2 \neq 0$.

Let us take the contours distinguished on Fig. 2.38 by the dashed line. The contour abcde (see Fig. 2.38I) encompasses the rotor of the pump; contour aabb (see Fig. 2.38CII) encompasses the turbine rotor. In the projection on the z axis we will obtain

$$R_z = \int_{F_z} p\,dF_z + G(c_{1z} - c_{2z}), \qquad (2.72)$$

where R_z is the force which acts on the rotor in an axial direction (positive direction R_z coincides with direction c_{1z}); F_z is the projection of the contour on the plane perpendicular to the z axis; c_{2z} is the axial component of the velocity from the rotor of the outlet; c_{1z} is the axial component of the velocity of the inlet into the rotor.

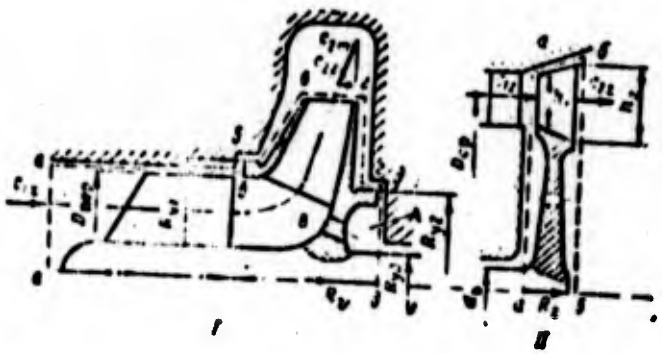

Fig. 2.38. Determination of the axial forces which act on rotors of vane machines: I - screw-centrifugal pump; II - axial-flow turbine.

Let us determine the pressure p subsequently.

During off-design conditions or partial admission (removal), as a result of the unsymmetric pressure distribution and velocities over the circumference of the rotor, i.e., due to the disturbance of the axial symmetry of the flow, an additional radial hydrodynamic force acting on the wheel appears. This radial stress is quite complex to define, since the pressure distribution and velocities in off-design conditions with the unsymmetric pattern of flow through the rotor is usually impossible to calculate. For the specific forms of vane machines there are empirical formula . The determination of axial and radial stresses will be examined in more detail in Section 5.3.

2.8. FUNDAMENTAL RELATIONS WHICH ENSUE FROM THE LAW OF THE CONSERVATION OF ENERGY

Equations (2.59) and (2.60), based on the law about the moment of momentum, do not reveal the relation between parameters of the fluid with its flow along channels of the flow area of the vane machine. Such a relation can be established from the law of the conservation of energy.

If we disregard the change in energy of the position for flow in vane machines (in view of the small absolute dimensions of elements of the machine), then the equation of the conservation of energy without the feed of external mechanical energy and external heat will be recorded in the form

$$i + \frac{c^2}{2} = \text{const}. \qquad (2.73)$$

For the compressible fluid (gas), which is subordinated to the equation of state in the form (ideal gas) $p/\rho = RT$; $t = c_p T$, the equation of the conservation of energy will be recorded thus:

$$c_p T + \frac{c^2}{2} = \text{const.} \qquad (2.74)$$

For the incompressible fluid during its flow without friction, the internal energy remains constant during the mutual transition of energy from one form to another ($T = \text{const}$), and the energy equation (Bernoulli equation) will be recorded in the form

$$\frac{p}{\rho} + \frac{c^2}{2} = \text{const.} \qquad (2.75)$$

Equation (2.73) is correct for the flow with friction (hydraulic losses), since the work of friction passes over to heat and increases the enthalpy of the fluid. The nature of losses in individual kinds of vane machines will be examined further (see Section 2.13). In the case of the use of equation (2.73) for processes of flow with friction, it is necessary to determine the enthalpy according to the real state of the fluid.

For incompressible fluids in the examination of processes of the flow with friction, one usually operates purely with mechanical and not thermal values. Even during flow with friction a change in temperature of the fluids is small. For an examination of flow with friction we use the energy equation recorded in the form

$$\frac{p_1}{\rho} + \frac{c_1^2}{2} = \frac{p_2}{\rho} + \frac{c_2^2}{2} + L_{\text{comp}}. \qquad (2.76)$$

For irrotational flow, equations (2.75) and (2.76) are valid for the entire flow.

With the removal of mechanical energy the equation of the conservation of energy will be recorded in the form

$$i_1 + \frac{c_1^2}{2} = i_2 + \frac{c_2^2}{2} + L, \qquad (2.77)$$

where L is the removed specific energy (specific work). With the feed of energy instead of L we will have H_T with the opposite sign.

For the incompressible fluid equation (2.77) can be recorded thus:

$$\frac{p_1}{\rho} + \frac{c_1^2}{2} = \frac{p_2}{\rho} + \frac{c_2^2}{2} + L + L_{comp}. \qquad (2.78)$$

Equations (2.77) and (2.78) are valid for the fixed coordinate system, i.e., for the absolute flow (flow in fixed elements of vane machines).

Let us examine how equations (2.77) and (2.78) are transformed for flow in the rotor, i.e., for the flow relative to the evenly rotating coordinates.

For the steady relative motion of fluid, the equation of motion in the Euler form in projections toward the direction of movement of the particle will be recorded thus:

$$F_s - \frac{1}{\rho}\frac{dp}{ds} = \frac{d}{ds}\left(\frac{w^2}{2}\right), \qquad (2.79)$$

where ds is the element of the line flow (Fig. 2.39); F_s - the component of the mass forces in the direction of motion of the particle referred to a unit of mass.

During relative motion the centrifugal forces of inertia refer to the mass forces - from the rotation of the coordinates

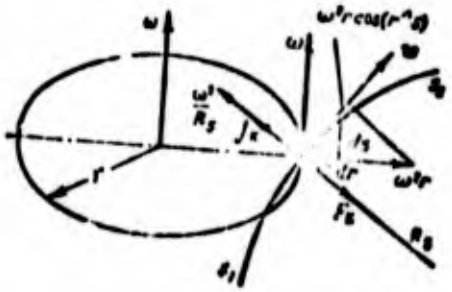

Fig. 2.39. Derivation of the energy equation.

and due to the curvature of the flow line - and the Coriolis force of inertia [the effect of gravity (weight) and acceleration of the rocket to flow in the rotor are disregarded].

The component of the centrifugal force from rotation of the coordinates (see Fig. 2.39) will be equal to

$$\omega^2 r \cos(\hat{rds}) = \omega^2 r \frac{dr}{ds}.$$

The projections of centrifugal force w^2/R_s, which appears as a result of the curvature of the flow line, and the Coriolis force $F_к$ in the direction of the movement will be equal to zero, since these forces are perpendicular to the direction of the relative velocity, i.e., the direction of the movement. Then

$$F_s = \omega^2 r \frac{dr}{ds}.$$

Substituting the value F_s into equation (2.79), we obtain

$$\omega^2 r \frac{dr}{ds} - \frac{1}{\rho}\frac{dp}{ds} - \frac{d}{ds}\left(\frac{w^2}{2}\right) = 0; \qquad (2.80)$$

having multiplied equation (2.80) by ds and changing signs, we obtain

$$-\omega^2 d\left(\frac{r^2}{2}\right) + \frac{1}{\rho} dp + d\left(\frac{w^2}{2}\right) = 0. \qquad (2.81)$$

Integrating equation (2.81) for the calculated cross sections 1-1 and 2-2, we obtain for the compressible fluid

$$\frac{w_1^2 - u_1^2}{2} - \frac{w_2^2 - u_2^2}{2} = \int_1^2 \frac{dp}{\rho}; \qquad (2.82)$$

for the incompressible fluid

$$\frac{w_1^2 - u_1^2}{2} - \frac{w_2^2 - u_2^2}{2} = \frac{p_2 - p_1}{\rho}, \qquad (2.83)$$

or

$$\frac{w_2^2 - u_2^2}{2} + \frac{p_2}{\rho} = \frac{w_1^2 - u_1^2}{2} + \frac{p_1}{\rho}. \qquad (2.84)$$

In such a form the energy equation (not allowing for losses) can be applied for the stream of the fluid flowing in the rotating rotor, i.e., for the stream of fluid in the field of inertial forces of the rotary motion.

Taking into account the hydraulic losses, equation (2.82) will be recorded thus:

$$\int_1^2 \frac{dp}{\rho} = \frac{w_1^2 - u_1^2}{2} - \frac{w_2^2 - u_2^2}{2} - L_{comp}; \qquad (2.85)$$

for the incompressible fluid

$$\frac{p_2 - p_1}{\rho} = \frac{w_1^2 - u_1^2}{2} - \frac{w_2^2 - u_2^2}{2} - L_{comp}.$$

For the axial vane machines ($u_1 = u_2$) equation (2.85) will be recorded in the form

$$\int_1^2 \frac{dp}{\rho} = \frac{w_1^2 - w_2^2}{2} - L_{\text{гидр}}. \qquad (2.86)$$

Forms of the Specific Energy Transferred by the Rotor of Fluid

From the velocity triangles, for example, for a centrifugal pump (see Fig. 2.26), we obtain

$$w_1^2 = u_1^2 + c_1^2 - 2c_1 u_1 \cos\alpha_1; \qquad (2.87)$$

$$w_2^2 = u_2^2 + c_2^2 - 2c_2 u_2 \cos\alpha_2. \qquad (2.88)$$

Subtracting equation (2.87) from (2.88) and having multiplied all terms by 1/2, we obtain

$$\frac{w_2^2 - w_1^2}{2} = \frac{u_2^2 - u_1^2}{2} + \frac{c_2^2 - c_1^2}{2} - (c_{2u}u_2 - c_{1u}u_1).$$

The theoretical pressure according to the Euler equation (2.31) is equal to

$$H_T = c_{2u}u_2 - c_{1u}u_1.$$

By comparing this expression with the preceding equation, we will obtain the expression for H_T in the converted form:

$$H_T = \frac{w_1^2 - w_2^2}{2} + \frac{u_2^2 - u_1^2}{2} + \frac{c_2^2 - c_1^2}{2} \left[\frac{J}{kg}\right]. \qquad (2.89)$$

Equation (2.89) is recorded for the compressor vane machine. For the inward-flow turbine it will be recorded in the form

$$L_{\text{т}} = \frac{w_2^2 - w_1^2}{2} + \frac{u_1^2 - u_2^2}{2} + \frac{c_1^2 - c_2^2}{2} \left[\frac{\text{J}}{\text{kg}}\right]. \qquad (2.90)$$

Let us show the physical meaning of each term in equations (2.89) and (2.90), and let us introduce some new concepts in the example of the equation written for the radial compressor machine.

An increase in the kinetic energy of the fluid in absolute motion will comprise the dynamic head of the rotor

$$H_{\text{дин}} = \frac{c_2^2 - c_1^2}{2} \left[\frac{\text{J}}{\text{kg}}\right]. \qquad (2.91)$$

Let us use the energy equation of relative motion (2.85) to the flow of the compressible fluid through the rotor:

$$\int_1^2 \frac{dp}{\rho} = \frac{w_1^2 - w_2^2}{2} + \frac{u_2^2 - u_1^2}{2} - L_{\text{comp}},$$

where $\int_1^2 \frac{dp}{\rho}$ is an increase in the potential energy.

We will call this value the static head of the rotor

$$H_{\text{ст}} = \int_1^2 \frac{dp}{\rho} = \frac{w_1^2 - w_2^2}{2} + \frac{u_2^2 - u_1^2}{2} - L_{\text{comp}} \left[\frac{\text{J}}{\text{kg}}\right]; \qquad (2.92)$$

for the incompressible fluid

$$H_{\text{ст}} = \frac{p_2 - p_1}{\rho} = \frac{w_1^2 - w_2^2}{2} + \frac{u_2^2 - u_1^2}{2} - L_{\text{comp}}. \qquad (2.93)$$

Let us note that the losses decrease only the static head without changing the dynamic head.

In comparing expressions (2.89), (2.91) and (2.92), we conclude that

$$H_т = H_{ст} + H_{ст} + L_{сопр}. \qquad (2.94)$$

Let us analyze expression (2.92) for the static head in more detail. Term $(w_1^2-w_2^2)/2$ is the change in kinetic energy of the fluid in relative motion and shows that a pressure increase can be achieved by the stagnation of flow in relative motion.

The term $(u_2^2-u_1^2)/2$ is the portion of work of the rotor spent for the displacement of the mass of fluid from smaller radii to larger in the field of inertial forces of rotary motion. This work is quantitatively half of the work produced by the Coriolis force of inertia [see formulas (2.59) and (2.60)], and it is connected with an increase in the potential energy in the moving fluid from the region of low pressure at smaller radii into the high-pressure region at larger radii.

For a radial wheel with straight vanes (see Fig. 2.35), when $w_1 = w_2$, equation (2.89) will be recorded in the form

$$H_т = \frac{c_2^2-c_1^2}{2} + \frac{u_2^2-u_1^2}{2}. \qquad (2.95)$$

In this case $c_{2m} = c_{1m}$ and

$$\frac{c_2^2-c_1^2}{2} = \frac{c_{2u}^2-c_{1u}^2}{2} = \frac{u_2^2-u_1^2}{2}.$$

In this case, as was shown earlier [see formula (2.61)], the theoretical pressure

$$H_t = u_2^2 - u_1^2.$$

Half of the theoretical pressure consists of an increase in the kinetic energy and half - a theoretical increase in the potential energy.

On the basis of the above, the work of the rotor connected with the Coriolis forces of inertia can be understood as the work spent for the displacement of the particles of fluid to larger radii, for a larger energy level (potential energy) - the second term of the right side of equation (2.95), and to an increase in the kinetic energy as a result of the increase in the velocity of following - the first term of the right side of the equation (2.95).

For the axial pump expressions (2.89) and (2.93) are simplified:

$$H_t = \frac{w_1^2 - w_2^2}{2} + \frac{c_2^2 - c_1^2}{2}; \qquad (2.96)$$

$$H_{cr} = \frac{w_1^2 - w_2^2}{2} - L_{comp}. \qquad (2.97)$$

For the turbine (centripetal) the change in the potential energy L_{CT} with passage of the rotor will be equal to the change in kinetic energy in relative motion, to the work returned to the rotor in the moving of the fluid from larger radii (greater pressures) to smaller radii (less pressures), and to the work spent for the overcoming of the resisting forces:

$$L_{c_1} = \frac{w_2^2 - w_1^2}{2} + L_{comp} + \frac{u_1^2 - u_2^2}{2}. \qquad (2.98)$$

For the axial-flow turbine

$$L_{c_1} = \frac{w_2^2 - w_1^2}{2} + L_{comp} \qquad (2.99)$$

Let us designate the third term of the right side of equation (2.90)

$$\frac{c_1^2 - c_2^2}{2} = L_{тех};$$

then

$$L_0 = L_{cr} + L_{тех} - L_{comp}. \qquad (2.100)$$

Equations (2.94) and (2.100) visually show which form of energy of the fluid is changed in work of the rotor of the vane machine.

2.9. FUNDAMENTAL RELATIONS OBTAINED FROM THE ONE-DIMENSIONAL (STREAM) THEORY OF CHANNEL FLOW OF THE ROTOR OF VANE MACHINES

Let us introduce the concept about the kinematic degree of reaction of the rotor of the vane machine. The kinematic degree of reaction of the rotor determines the type of vane machine and makes it possible to evaluate its basic properties without carrying out a detailed calculation.

Let us define the kinematic degree of the reaction of the rotor as the ratio of a theoretically possible change in the potential energy $\left(\int_1^2 \frac{dp}{\rho}\right)_т$ when $L_{comp} = 0$ to the total variation in energy of 1 kg of mass of fluid passing through the rotor.

For the rotor of the pump which operates on incompressible fluid, the expression for the degree of reaction will be recorded thus:

$$\rho_к = \frac{(H_{ст})_т}{H_т} = \frac{\left(\frac{p_2 - p_1}{\rho}\right)_т}{\left(\frac{p_2 - p_1}{\rho}\right)_т + \frac{c_2^2 - c_1^2}{2}} = \frac{\frac{w_1^2 - w_2^2}{2} + \frac{u_2^2 - u_1^2}{2}}{H_т}. \qquad (2.101)$$

For the turbine rotor the expression for the degree of reaction will be recorded thus:

$$\rho_к = \frac{(L_{ст})_т}{L_т} = \frac{\left(\int_1^2 \frac{dp}{\rho}\right)_т}{\left(\int_1^2 \frac{dp}{\rho}\right)_т + \frac{c_1^2 - c_2^2}{2}} = \frac{\frac{w_2^2 - w_1^2}{2} + \frac{u_1^2 - u_2^2}{2}}{L_т}. \qquad (2.102)$$

The kinematic degree of reaction is the very characteristic parameter of the vane machine. Let us analyze the connection of the operation of the rotor of the vane machine and degree of reaction in more deteil.

We will assume that for the pump and compressor the value of the twist at the inlet $c_{1u} = 0$, i.e., that they have a radial inlet, and for turbine, on the contrary, let us assume the value

of the twist at the outlet $c_{2u} = 0$, i.e., we will consider that it has a radial outlet (minimum losses with the outlet velocity). In this case the pressure or specific work on the circumference of the rotor will be expressed by one term in the appropriate Euler equations (2.31) and (2.30): $H_T = c_{2u}u_2$ (pump and compressor) or $L_u = c_{1u}u_1$ (turbine).

In presenting the material in this section, we will examine the ideal vane machine without losses, i.e., we will assume that

$$H_T = H_{ст} - H_{сг} \quad (L_{сопр} = 0). \tag{2.103}$$

The angle of incidence everywhere in this section will be taken as equal to zero. Furthermore, we will assume that there is an equality of the meridian velocities at the inlet and outlet: $c_{1m} = c_{2m} = c_m$ (which is frequently held in practice).

The expression for the kinematic degree of reaction of the rotor with the adopted assumptions can be presented (for the pump and compressor) in the form of

$$\rho_к = \frac{H_{к.т}}{H_T} = \frac{H_T - H_{ст}}{H_T}, \text{ and } H_{ст} = \frac{c_2^2 - c_1^2}{2}.$$

Let us write c_2^2 as the sum:

$$c_2^2 = c_{2u}^2 + c_{2m}^2;$$

$c_1^2 = c_{2m}^2$, since it is accepted that $c_{1u} = 0$.

Taking into account these relations we obtain

$$H_{дин} = \frac{c_{2u}^2}{2}. \qquad (2.104)$$

The expression for the static head takes this form:

$$H_{ст} = H_т - H_{дин} = c_{2u}u_2 - \frac{c_{2u}^2}{2} = \frac{c_{2u}(2u_2 - c_{2u})}{2}, \qquad (2.105)$$

and the expression for the degree of reaction

$$\rho_к = 1 - \frac{c_{2u}}{2u_2}. \qquad (2.106)$$

Similar expressions can be obtained for the structural behavior and degree of reaction of the turbine rotor:

$$L_{ст} = \frac{c_{1u}(2u_1 - c_{1u})}{2}; \quad \rho_к = 1 - \frac{c_{1u}}{2u_1}. \qquad (2.107)$$

The twist of the flow, which determines the value of the transmitted or obtained specific work, will be designated c_u, understanding by this for the turbine $c_{1u} = c_u$, and for the pump $c_2 = c_u$.

In accordance with this let us write:

$$H_т = c_u u \qquad (2.108)$$

and

$$L_т = c_u u. \qquad (2.109)$$

where u is the circular velocity at the outlet from the rotor - for the pump, or the circular velocity at the inlet into the rotor - for the turbine; for generality we will write u without the corresponding subscripts.

As before, by value H_T we will understand as the energy transmitted by the rotor to the mass of fluid per 1 kg, and by L_u - the work returned to the rotor with a mass of the fluid equal to 1 kg.

Subsequently, for the pump and turbine we will write

$$\eta_r = 1 - \frac{c_u}{2u} = 1 - \frac{\bar{c}_u}{2}. \qquad (2.110)$$

Let us call ratio $c_u/u = \bar{c}_u$ the relative twist. Let us introduce the concept about the coefficient of theoretical pressure (for the pump) or the coefficient of circular work (for the turbine).

For the pump the coefficient of theoretical pressure is the ratio of theoretical pressure to the square of the circular velocity:

$$\bar{H}_T = \frac{H_T}{u^2}. \qquad (2.111)$$

For the turbine, correspondingly, the coefficient of the circular work is the ratio of the circular work to the square of the circular velocity:

$$\bar{L}_u = \frac{L_u}{u^2}. \qquad (2.112)$$

For the pump without twist at the inlet the coefficient of theoretical pressure is equal to the relative twist [see equation (2.31)]:

$$\bar{H}_t = \frac{c_u}{u} = \bar{c}_u. \qquad (2.113)$$

For the turbine without twist at the outlet the coefficient of circular work [see equation (2.30)] is also equal to the relative twist:

$$\bar{L}_u = \frac{c_u}{u} = \bar{c}_u. \qquad (2.114)$$

Let us examine equation (2.110) in general form for any vane machine.

1) $c_u = 0$: $\bar{c}_u = \frac{c_u}{u} = 2$; $\bar{H}_t = \bar{L}_u = 2$:

in this case $c_u = 2u$;

$$H_{ст} = L_{ст} = \frac{c_u(2u - c_u)}{2} = 0; \quad H_t = L_u = 2u^2;$$
$$H_{дин} = L_{дин} = H_t = L_u = 2u^2.$$

Consequently, for the purely active vane machine the energy conversion occurs only by means of a change in the kinetic energy of the working medium.

The velocity triangles for this case in the example of axial machines are shown, respectively, for the pump and turbine on Figs. 2.40a and 2.41a. The relative velocities at the outlet from the rotor and at the inlet into the rotor are equal to each other. For the pump the angle of the inlet into the rotor is equal to arctg c_m/u and the angle of the outlet from the rotor is equal to 180° - arctg c_m/u (for the turbine - vice versa).

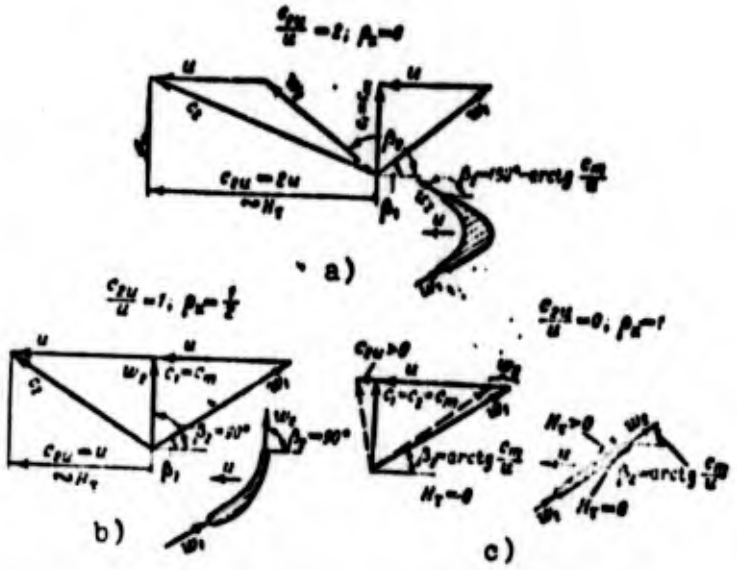

Fig. 2.40. Velocity triangles and profiles of vanes of an axial pump.

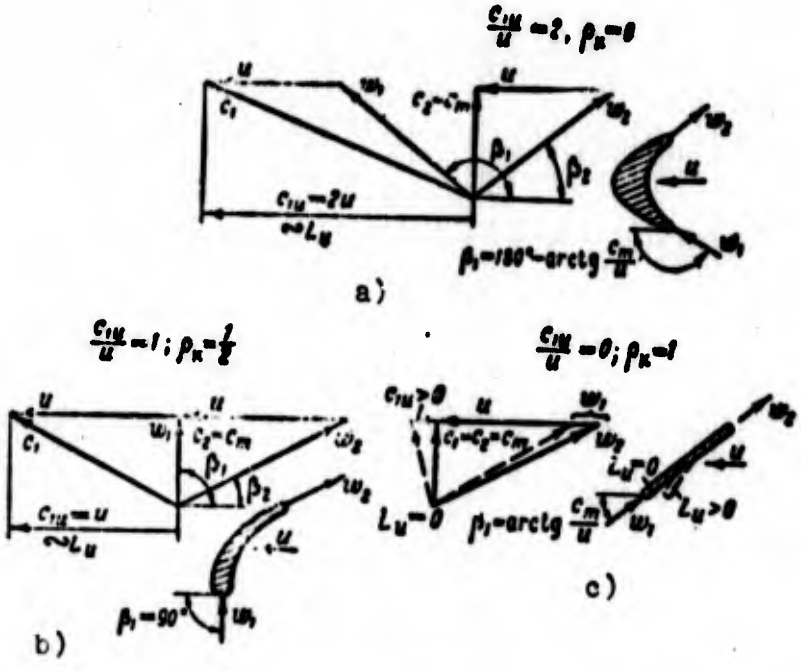

Fig. 2.41. Velocity triangles and profiles of vanes of an axial-flow turbine.

The profile of the vane is symmetrical.

2) $\varphi_u = \frac{1}{2}$; $\bar{c}_u = \frac{c_u}{u} = 1$; $\bar{H}_T = \bar{L}_u = 1$;

in this case $c_u = u$;

$$H_{cT} = L_{cT} = \frac{c_u^2}{2} = \frac{u^2}{2}; \quad H_{вых} = L_{вых} = \frac{c_u^2}{2} = \frac{u^2}{2};$$
$$H_T = L_u = u^2.$$

The velocity triangles for the pump and turbines which correspond to this case are plotted on Fig. 2.40b and 2.41b. Relative velocities of the outlet from the wheel of the pump and at the inlet into the turbine wheel have an angle of inclination equal to the angle of inclination of the vanes, $\beta = 90°$. The angle at the inlet into the pump and at the turbine outlet is equal to arctg c_m/u. The shape of the vane is unsymmetric.

3) $\varphi_u = 1$ when $\bar{c}_u = \frac{c_u}{u} = 0$, since $c_u = 0$ and $u \neq \infty$;

in this case

$$H_{cT} = L_{cT} = 0; \quad H_{вых} = L_{вых} = 0;$$
$$H_T = L_u = 0.$$

The velocity triangles for the pump and turbines which correspond to this case are plotted on Fig. 2.40c and 2.41c by solid lines.

With passage through the rotor the flow does not change its direction and velocity. The flow angle β = arctg c_m/u. The profile of the vane takes the form of a plate.

Profiles in the form of a plate are applied in pumps and turbines, but at the positive angle of incidence for the pump (the angle of the vane is more than the flow angle) and negative for the turbine (the angle of the vanes is less than the flow angle). In this case $\rho_к$ will be less than unity. The profiles which correspond to the degrees of reaction close to unity are widely applied (on Fig. 2.40c and 2.41c they are shown by a dashed line); there by a dashed line the velocity triangles, inlet for the pump and inlet for the turbine, which correspond to conditions $1 > \rho_к > 1/2$, are plotted.

The profiles of vanes for the pump and for the turbine are similar to each other but are oriented differently. The same profile in principle can operate under conditions of the compressor (pump) and under conditions of the turbine, but in this case different guide devices are necessary, and the direction of rotation relative to the camber will be the reverse (compare Figs. 2.40 and 2.41). Generally speaking, the shape of the leading edges should also be different, but there are specially designed hydraulic machines which can operate both in turbine and pump conditions (the so-called reversible units).

If along the axis of the abscissa we plot the value of the relative twist $\bar{c}_u$, along the axis of the ordinates we plot conditionally upward the relative pressures $\bar{H}$, i.e., the pressures referred to u^2 (all values referred to u^2 are noted from above by a line), including the coefficient of theoretical pressure of the compressor vane machine $\bar{H}_т$, and along the axis of ordinates downward we plot the relative work $\bar{L}$ transmitted to the turbine rotor (including the coefficient of circular work $\bar{L}_u$), then we will obtain the graphs given on Fig. 2.42.

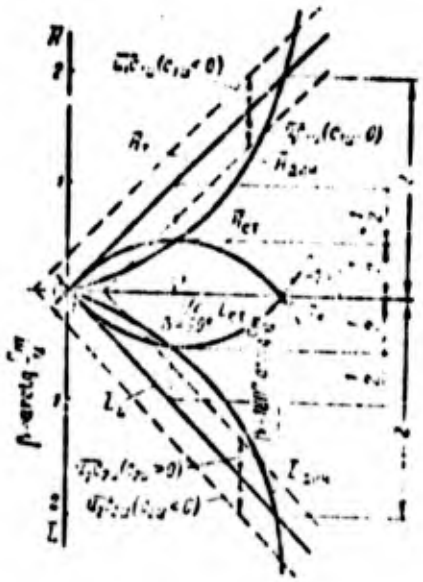

Fig. 2.42. Dependence of the coefficients of pressure and work on the relative twist of the flow, the degree of reaction and the angle of the vanes.

Let us note again that $\bar{H}_T$ (for $c_{1u} = 0$) and $\bar{L}_u$ (for $c_{2u} = 0$) are nothing else than the relative twist $\bar{c}_u$. We plot along the axis of the abscissa also the degree of reaction, and in accordance with the velocity triangles given on Figs. 2.40 and 2.41 we plot the angles of the vanes - for the pump the outlet and for the turbine - the inlet.

From an examination of the graphs given on Fig. 2.42 (c_{1u} for the pump and c_{2u} for the turbine are equal to zero), it is possible to make the following conclusions:

1) the more the relative twist is in absolute value, the less the degree of reaction;

2) the smaller degrees of reaction and larger relative twists correspond to the larger values and larger coefficients of theoretical pressure and circular work;

3) the maximum value of the static head or change in the potential energy takes place when $\rho_H = 0.5$ and at the slope

angle of the vanes of 90° (for the compressor machine - at the outlet and for the turbine - at the inlet);

4) the camber of the vanes increases with a decrease in the degree of reaction (see Figs. 2.40 and 2.41);

5) with the negative degrees in reaction ($\rho_н < 0$) with an increase in the angle up to values greater than ($180° - \text{arctg } c_m/u$), the coefficient of theoretical pressure (work) of the vane machine will increase, but in this case in the impeller channels of the compressor (pump) the pressure will drop and in channels of the turbine - increase, which is undesirable;

6) with the degrees of reaction more than unity ($\rho_н > 1$) the vane machines (when $c_{1u} = 0$ for the pump and $c_{2u} = 0$ for the turbine) those functions for which they were intended cannot be fulfilled, i.e., the compressor will operate only under the conditions of the turbine, i.e., accomplish work because of the energy of the fluid, and the turbine will operate under conditions of the compressor, i.e., increase the energy of the fluid because of external mechanical energy.

Figures 2.43 and 2.44 give velocity triangles for rotors of radial vane machines - respectively, for the centrifugal pump and the inward-flow turbine - for different degrees of reaction ($\rho_н = 0$; 1/2 and 1). Plotted in these figures are the diagrammatic representations of profiles of vanes of radial vane machines. From these representations it is possible to judge the profile of the vane for any value of the degree of reaction.

In Figs. 2.43c and 2.44c plotted by a dashed line are diagrammatic representations of profiles and velocity triangles

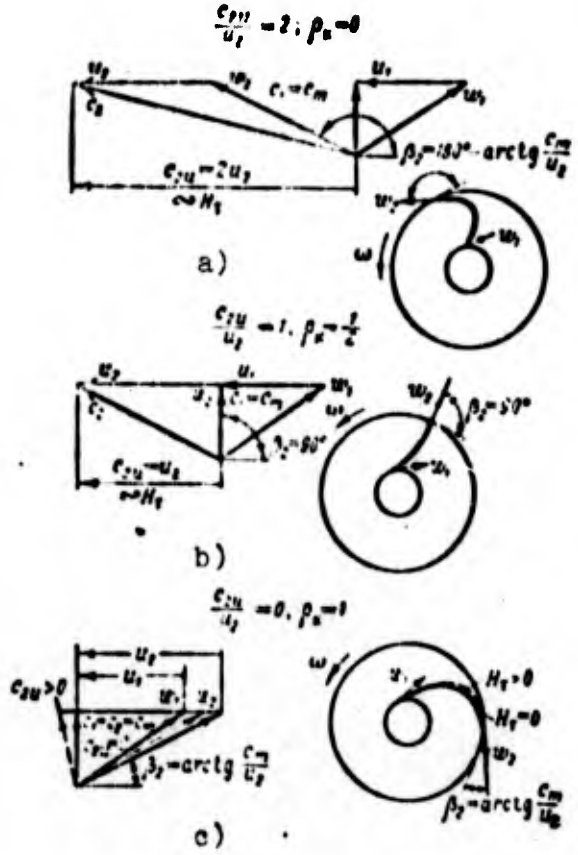

Fig. 2.43. Velocity triangles and diagrammatic representations of profiles of vanes of a centrifugal pump ($c_{1u} = 0$).

for $1 > \rho_н > 1/2$. It is evident that for the pump when $\rho_н < 0.5$ the vane is bent back in the direction of the rotation, and when $\rho_н > 0.5$ - opposite the direction of rotation (for the turbine - vice versa).

Everything said above is correct when $c_{1u} = 0$ (for the pump) and $c_{2u} = 0$ (for the turbine). If for the pump $c_{1u} \neq 0$ (respectively, for the turbine $c_{2u} \neq 0$), then the relationships of pressures and degrees of reaction will be different.

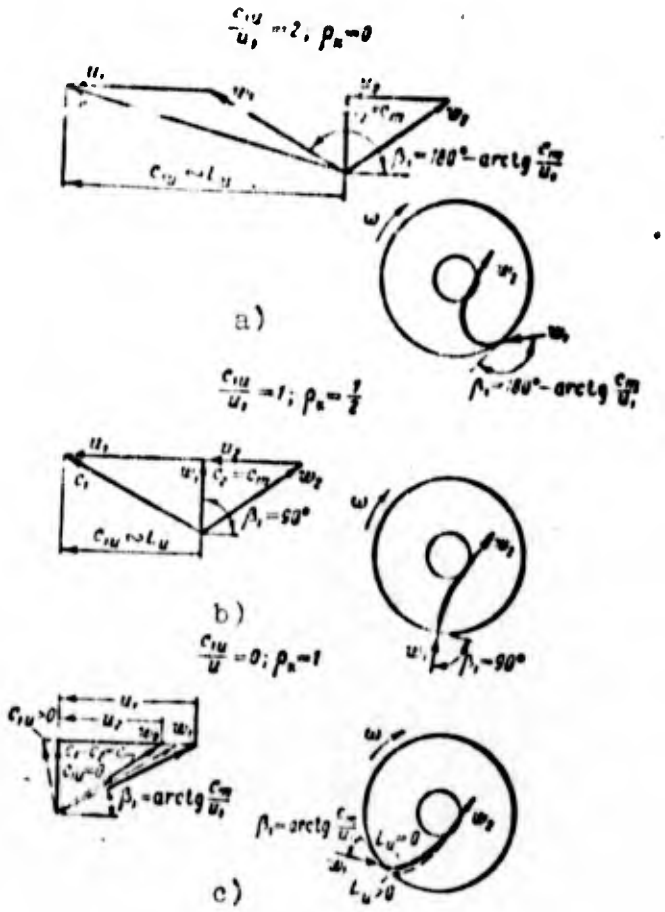

Fig. 2.44. Velocity triangles and diagrammatic representation of profiles of vanes of an inward-flow turbine ($c_{2u} = 0$).

Plotted on Fig. 2.42 by a dashed line are lines $\bar{H}_T$ and $\bar{L}_u$ for the cases of twist opposite to the direction of the rotation and of twist in the direction of the rotation (at the inlet - for the pump and at the outlet - for the turbine).

The twist opposite to the direction of rotation ($c_{1u} < 0$ - for the pump and $c_{2u} < 0$ - for the turbine) increases the energy

transmitted to the fluid or tapped near it. The twist in the direction of rotation decreases the work of the vane machine (see Fig. 2.42). The lines which correspond to the coefficients of theoretical pressure (work) are displaced by the value $\bar{u}_1 c_{1u}$ or, correspondingly, the value $\bar{u}_2 \bar{c}_{2u}$. Here $\bar{u}_1 = u_1/u_2$ and $\bar{u}_2 = u_2/u_1$. By means of "twisting" to the side opposite to the direction of rotation, it is possible to obtain pressure from the pump with the degree of reaction $\rho_н = 1$ (in this case $c_{2u} = c_{1u}$) and even when $\rho_н > 1$.

According to the value of relative twist $\bar{c}_u$ or the degree of reaction connected with it, taking into account the nature of the curves given on Fig. 2.42, it is possible to select the type of vane machine depending on its purpose and evaluate its properties in the most general form.

So, if a vane machine with a high value of the operating factor is necessary, with a high specific power (the power per unit of consumption of the working medium) with the limited value u_2, then one should use the vane machine with a high relative twist $\bar{c}_u$, i.e., an active vane machine. The high efficiency of such a machine is difficult to obtain, since values of velocities of the flowing of the working medium in it (at an assigned circular velocity) will be high. On the other hand, a high value of efficiency should be expected from a machine with low relative twist, but the work of the stage in this case will be small, and therefore such machines are most frequently made multistage.

From an examination of the passage of the curves given on Fig. 2.42, it is possible to make other conclusions. If, for example, at the compressor outlet only kinetic energy

of the flow (for example, of a blower) is necessary, then it is advantageous to use vane machines of low reaction. If at the outlet basically potential energy (high pressures and low speeds) is necessary, then one should prefer the reactive vane machines (pumps for fluid).

When selecting the type of vane machine, one proceeds from a large number of design, economic and operating requirements. Only examples of the general approach to the selection of the type of the vane machine on the basis of its properties expressed in general form were mentioned here. Considerations of strength frequently play decisive role. For radial machines on the basis of conditions of strength, it frequently proves to be advisable to use the rotor with radial vanes (pumps for the pumping of liquid hydrogen, the superchargers, inward-flow turbines) - $\beta_{1л}$ for the turbine and $\beta_{2л}$ for the pump = 90°.

Subsequently, when we analyze the requirements for pumps and turbines of the LPRE, we will discuss in more detail the selection of their parameters connected with the coefficient of theoretical pressure (work) or the degree of reaction.

2.10. ELEMENTS OF THE TWO-DIMENSIONAL THEORY OF FLOW IN AIRFOIL CASCADES

2.10.1. METHODS OF SOLVING PROBLEMS OF THE TWO-DIMENSIONAL THEORY OF FLOW IN AIRFOIL CASCADES

The direct problem of the two-dimensional theory consists in determining the velocity field of the fluid $v_x = v_x(x, y)$; $v_y = v_y(x, y)$ for the assigned airfoil cascade. The case of the potential, i.e., irrotational flow is of special interest. Irrotational flow is the flow the particles of which do not rotate about its axis. The importance of the case of irrotational flow is determined by the fact that with the flowing around by flow of airfoil and fixed circular cascades, the rotation of the particles is practically absent almost in the entire flow, with the exception of regions of a small extent, where a sharp change in the velocity value occurs and where, consequently, the angular velocity of rotation of the liquid particles Ω is significant.

In the flow around the blades such regions are the boundary layer on the body, the wake behind edges of the blades, and the shock wave. In the boundary layer the velocity is changed from zero on the surface of the body to considerable velocity on the boundary layer. Particles rotating in the boundary layer enter into the wake behind the body. Found in the wake are vortices which are formed as a result of the separation and contraction of the boundary layer.

With nondetached flow of the body, thicknesses of the boundary layer and wake appear small as compared to dimensions of the body. In the first approximation they can be excluded from the examination, and the examination of the streamline flow of the body by a real fluid can be replaced by an examination of the irrotational flow by an ideal (nonviscous) fluid. The regularities obtainable here are close to the real ones.

In the case of a rotating circular cascade, the problem is complicated by the fact that the flow in relative motion is vortical and rotational; in absolute motion the flow is considered to be irrotational. All the transformations are conducted according to the ratio to absolute motion, and the effect of the pump rotation is considered as the introduction of the flow of constant vorticity ($-\omega$).

As is known from hydrodynamics, the condition of the potentiality of the flow is written in the form

$$\Omega = \frac{1}{2}\left(\frac{\partial v_y}{\partial x} - \frac{\partial v_x}{\partial y}\right) = 0,$$

or

$$\frac{\partial v_x}{\partial y} = \frac{\partial v_y}{\partial x}. \qquad (2.115)$$

It is known that if condition (2.115) is satisfied, then there is such a function $\varphi = \varphi(x, y)$ by which it is possible to express v_x and v_y in the following form:

$$v_x = \frac{\partial \varphi}{\partial x}; \quad v_y = \frac{\partial \varphi}{\partial y}.$$

The function φ is called the velocity potential. The introduction of the velocity potential φ facilitates the problem of the definition of v_x and v_y with irrotational flow, since instead of two unknowns (v_x and v_y) it is possible to operate with one unknown function φ.

The equation of continuity for two-dimensional flow is written in the form

$$\frac{\partial(\rho v_x)}{\partial x} + \frac{\partial(\rho v_y)}{\partial y} = 0.$$

If the medium is incompressible or if the compressibility of the medium can be disregarded ($M \leq 0.3$-0.4), then equation of continuity will be written in the form

$$\frac{\partial v_x}{\partial x} + \frac{\partial v_y}{\partial y} = 0,$$

or

$$\frac{\partial v_x}{\partial x} = -\frac{\partial v_y}{\partial y}.$$

Then instead of variables v_x and v_y it is possible to use the function $\psi = \psi(x, y)$, called the stream function, with which v_x and v_y are connected in the following manner:

$$v_x = \frac{\partial \psi}{\partial y}; \quad v_y = \frac{\partial \psi}{\partial x}.$$

If the flow is the potential and incompressible, then for determining v_x and v_y it is possible to use the function φ and function ψ.

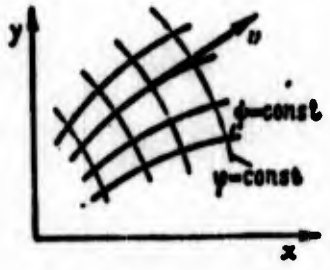

Fig. 2.45. Flow lines (ψ = const) and lines of equal potential (φ = const).

Figure 2.45 depicts lines φ = const and ψ = const. The property of these lines consists in the fact that the flow velocity $\vec{v}$ is normal to line φ = const and is tangent to the line ψ = const. Line φ = const is called the line of equal potential, and line ψ = const - the flow line. The change in the function φ along the normal to the line of equal potential determines the velocity:

$$\frac{\partial \varphi}{\partial n} = v.$$

It is possible to show that the velocity potential φ and the stream function ψ are harmonic functions. This makes it possible to present them in the form of the sum of harmonic functions:

$$\varphi = \varphi_1 + \varphi_2 + \varphi_3 + \ldots;$$
$$\psi = \psi_1 + \psi_2 + \psi_3 + \ldots.$$

In other words, the solution of the complex flow can be presented as the sum of solutions of simple flows on which the complex flow is decomposed. Such simple flows, called "characteristics" are three flows: parallel flow, flow from the point source (or to the point flow) and the flow around the vortex (Fig. 2.46).

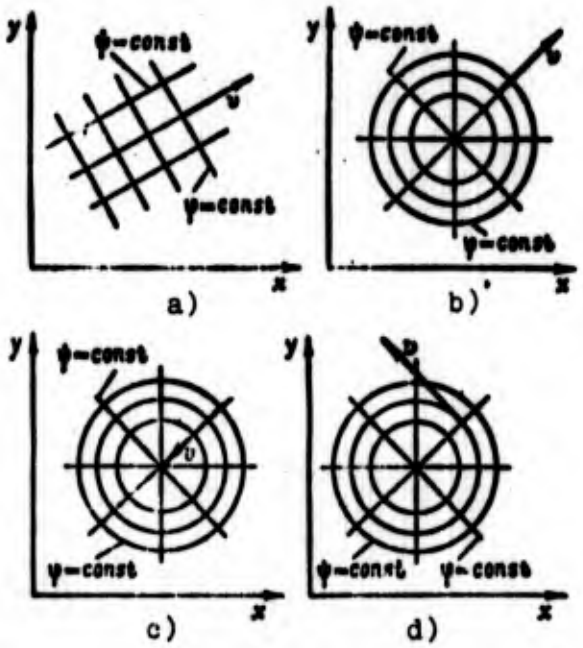

Fig. 2.46. System of characteristics: a) plane-parallel flow; b) flow from a point source; c) flow toward a point flow; d) flow around the vortex.

For each of these simple flows the expressions of the velocity potential φ and the stream function ψ are known. In the solution to the problem of the flow of the vanes, the vane is replaced by such a system of features which satisfies the boundary conditions: the flow lines adjacent to the surface of the vane coincide with the contour of the vane, and the point of descent of fluid from the vane coincides with the trailing edge of the vane (condition of nonseparated flow).

Then the solution to the problem will be found by means of the summation of the flow encountering the vanes and the flow created by the system of features replacing the vane. This method is called the method of characteristics. The method of characteristics makes it possible to solve the problem for the flow of a vane of any form. The difficulty consists in the determination of the intensity of the system of characteristics, in which the boundary conditions are satisfied. The conducting of a number of

the successive approximations, which increase the volume of the calculations is necessary. At the present time this difficulty is overcome by the use of a computer.

Subsequently, we will use source [60], in which on the basis of the method of characteristics the problem of the angles of lag of the flow from the direction of the vanes for a circular cascade, taking into account the variable height of the channel is solved.

Another method of calculation of the streamline flow is the method of conformal transformations, in which the detailed theory of the complex variable functions is used. The problem of the flow of the simple figure - circumference, is solved. The solution by the method of conformal transformations is transferred to the streamline flow of the vane of assigned form. The complexity of the method consists in the selection of the complex function which would reflect the contour of the vane into the circumference.

At the present time this problem is solved for some special cases. For example, mapping functions for the airfoil cascade composed of linear segments and for the circular cascade with vanes which are cross sections of the logarithmic spiral are found. In the presence of a mapping function the solution of the problem is facilitated by use of a computer.

The method of characteristics and the method of the conformal transformations can be used and for cascades of variable width, and the compressibility of the medium can also be taken into account.

There are the approximate, so-called "channel" methods of calculation (see source [61]) of the streamline flow of the vanes. In the vane channel of the airfoil and fixed circular cascade approximate lines of equal potential are constructed; in the rotating circular cascade approximately constructed are lines normal to the flow lines in relative motion and are assigned by the velocity distribution law along these lines.

The channel method makes it possible to consider the compressibility effect of the medium at high subsonic speeds of flow. Having determined the velocity field $v = v(x, y)$ from the solution of the problem of the streamline flow of the cascade vanes, it is possible to find the pressure field $p = p(x, y)$. In this case the energy equation for an ideal fluid is used.

2.10.2. VELOCITY FIELDS AND PRESSURE FIELDS WITH THE STREAMLINE FLOW OF VANE CASCADES

A detailed study on methods of the solution of problems of two-dimensional flow in cascades goes beyond the limits of the present course. This question is analyzed in detail in a number of the books (see, for example, sources [20] and [61]). In the present section let us examine the patterns of flow in vane cascades obtained as a result of a solution by means of the two-dimensional theory of problems of the determination of the velocity field with the streamline flow of specific cascades. Let us simultaneously describe a number of experimental results on the measurement of velocity and pressure fields in vane cascades.

2.10.2.1. Flow in an Airfoil Vane Cascade

Source [2] gives results of the calculation by the method of conformal mappings of potential streamline flow of the compressor cascade the profile of the vane which is given on Fig. 2.47a. The cascade had a relative pitch of $t/b = 1$ and an angle of incidence of the profiles of $\chi = 45°$. The graph of the velocity distribution over the development of the contour of the profile for the different angles of incidence is given on Fig. 2.47b. The streamlime flow with positive angles of incidence (which correspond to inleakage to the concave side of the profile) was examined. In the streamline flow with the zero angle of incidence, the velocity quite sharply increases from a zero value at the tip of the branching off (critical point) up to a maximum value on the back of the profile and somewhat smaller value on the concave side. Then the

velocity is smoothly decreased toward the trailing edge in view of the diffusivity of the cascade. With an increase in the angle of incidence the flow pattern is changed. The critical tip is somewhat displaced to the side of the trough. Near it along the back a sharp peak of velocity is formed. The flow is accelerated with the streamline flow of the leading edge of a profile. Then the velocity is sharply decreased. This rapid decrease in the velocity corresponds to the positive pressure gradient, and the boundary-layer separation (for such cascades when $i \geq 8\text{-}10°$) can be observed. Prior to the appearance of separation the velocity distribution, obtained theoretically, agrees well with the experimental data, with the exception of the trailing edge, where a wake is formed.

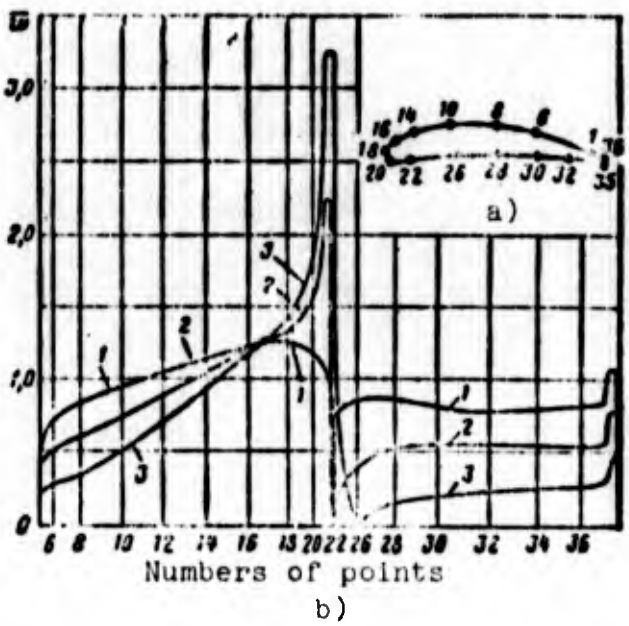

Fig. 2.47. Distribution of dimensionless velocity $\bar{w}$ along the profile of the compressor (pumping) axial cascade at different angles of incidences: 1 - $i = 0°$; 2 - $i = 10°$; 3 - $i = 20°$.

Figure 2.48 gives the profile of the active turbine operating cascade TR-1A and the velocity distribution along the development of the contour of the profile (see source [61]), obtained by the calculated method (channel method of Samoylovich-Sherstyuk) - lines and experimentally - points. The angle of the inlet of flow

$\beta_1 = 21°$, and the relative cascade spacing $\bar{t} = 0.585$; $\lambda_{w_2} = 0.76$. The velocity near the vane back considerably exceeds the velocity of the face. On the vane back near the trailing edge, the calculation indicates the existence of a small diffuser section (according to results of experiments such a section is absent).

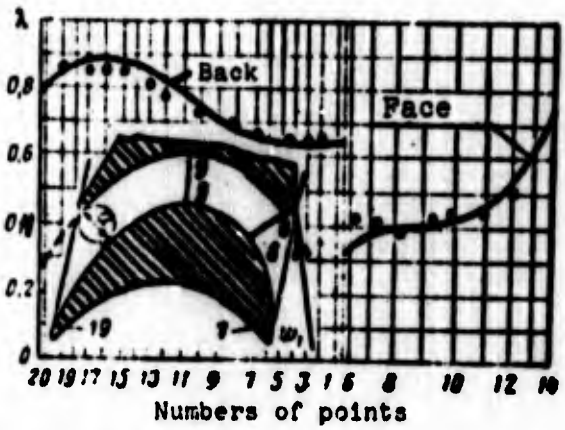

Fig. 2.48. Distribution of the reduced velocity λ along the profile TR-1A of the turbine active axial cascade.

On Fig. 2.49 for the same profile experimental diagrams of the distribution of pressure on the contour of the profile at different inlet angles of the flow and at different M_{w_2} numbers are given (see source [2]). At the small angle of the inlet ($\beta_1 = 18°$) in the inlet section of the back there appears a diffuser flow, and at large angles of the inlet near the whole back a convergent flow appears. The region of minimum pressure is located near the trailing edge. The pressure of the face considerably exceeds the pressure of the back. The velocity everywhere remains subsonic and barely affects the nature of the pressure distribution. It is noticeable only that the region of minimum pressure with a velocity increase is moved toward the trailing edge.

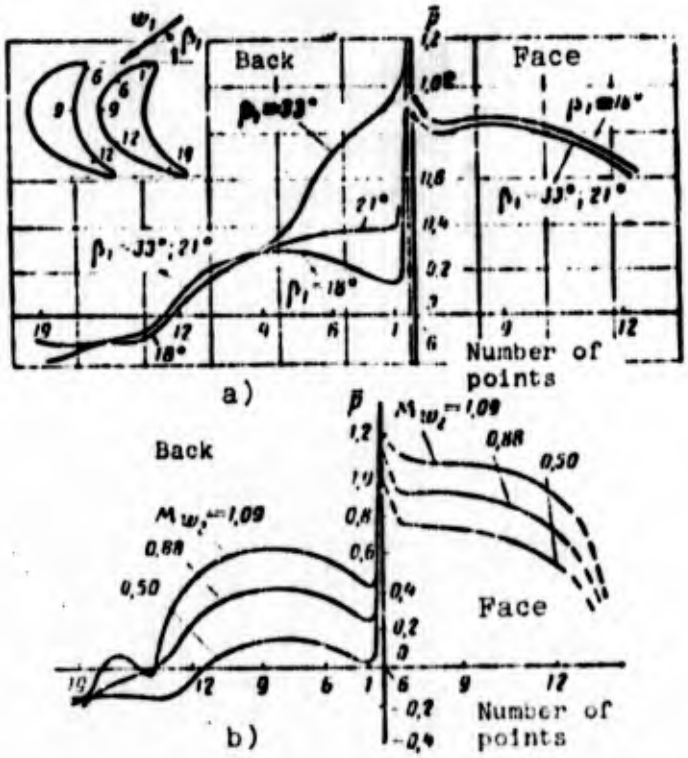

Fig. 2.49. Distribution of the dimensionless pressure $\bar{p}$ on the profile TR-1A of the turbine axial cascade: a) at different flow angles β_1; b) at different numbers M_{w_2} ($\beta_1 = 18°$).

Figure 2.50a (see source [24]) gives diagrams of the pressure distributions on the profile of the reactive cascade. A change in the pressure bears a smoother nature than that of the active cascade. The circular projections of forces of pressure on the profile determine the value of the circumferential force. A pressure differential on both turbine profiles is created basically due to the presence of rarefaction on the back.

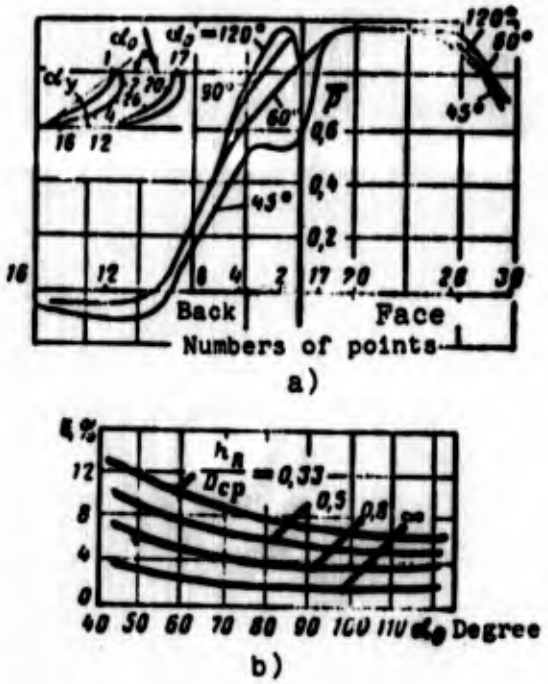

Fig. 2.50. Distribution of dimensionless pressure $\bar{p}$ on the profile of a turbine reactive axial cascade (a) at different flow angles α_0, and the dependence of the loss factor in the reactive cascade (b) on the flow angle α_0 (b/t = 1.35; M = 0.5).

2.10.2.2. Flow in a Circular Revolving Cascade

The flow in rotating circular cascades has a more complex nature, since the flow along vane channel occurs in the field of inertial forces. Let us find the velocity distribution law in the cross section of the vane channel for the rotating circular cascade ($c_z = w_z = 0$). Let us isolate in the vane channel the elementary fluid volume with the mass dm = ρbdnds, where b is the width of the channel in a direction perpendicular to the plane of the drawing (Fig. 2.51).

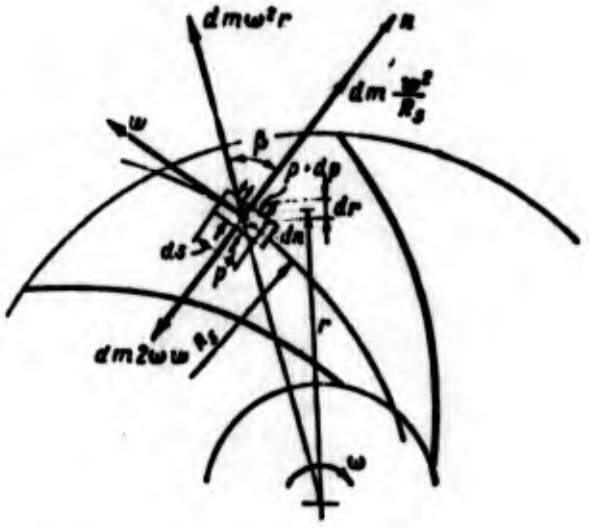

Fig. 2.51. Determination of the change in velocity over the width of the vane channel of the wheel of the radial vane machine.

Let us examine the equilibrium of the elementary fluid volume in the direction of the normal to the flow line in relative motion (see source [54]). Acting on the chosen element are the following forces, which have components in the direction of the normal:

the surface forces (pressure) the total component of which is equal to

$$P_n = (p + dp)bds - pbds = dpbds;$$

the component of the centrifugal force of inertia which appears in view of the presence of the centripetal acceleration due to the rotation of the wheel

$$dm\omega^2 r \cos \beta;$$

the centrifugal force of inertia which appears in view of the presence of centripetal acceleration due to the curvature of the flow line

$$dm \frac{w^2}{R_s};$$

the Coriolis force of inertia

$$dm2w\omega.$$

The sum of all these forces is equal to zero:

$$-dpbds + dm\omega^2 r \cos\beta + dm\frac{w^2}{R_s} - dm2w\omega = 0. \qquad (2.116)$$

Having divided and multiplied the first term of the left side of the equation by ρdn, having reduced all terms by dm = ρdsdnb, and having replaced cos β = dr/dn, we obtain

$$-\frac{dp}{\rho dn} + \frac{\omega^2 r dr}{dn} + \frac{w^2}{R_s} - 2\omega w = 0. \qquad (2.117)$$

Assuming the energy of the streams on the pitch to be constant, which is correct for the absolute potential, although nonstationary, motion (see source [38]), from equation (2.81) we obtain the following relation:

$$w\frac{dw}{dn} = -\frac{dp}{\rho dn} + \frac{\omega^2 r dr}{dn}. \qquad (2.118)$$

In accordance with expression (2.117) this relation is transformed thus:

$$\frac{dw}{dn} = 2\omega - \frac{w}{R_s}. \qquad (2.119)$$

Let us conduct the integration of equation (2.119), having considered that the radii of curvature of all the streams are equal to radius of the vane ($R_s = R_л$):

$$\int_{w_{cp}}^{w} \frac{dw}{2\omega R_л - w} = \int_0^n \frac{dn}{R_л}. \qquad (2.120)$$

We assume that on the center line of the channel (n = 0) $w = w_{cp}$. Integrating equation (2.120), we obtain

$$\frac{2\omega R_л - w}{2\omega R_л - w_{cp}} = e^{-\frac{n}{R_л}}.$$

With the expansion of $e^{-n/R_л}$ in series

$$e^{-\frac{n}{R_л}} = 1 - \frac{n}{R_л} + \frac{n^2}{2R_л^2} - \ldots,$$

if we are limited to two first terms (since $n/R_л << 1$), then after conversions we obtain

$$w = w_{ср}\left(1 - \frac{n}{R_л}\right) + 2\omega n. \qquad (2.121)$$

From equation (2.121) it follows that a change in the velocity across the channel is subordinate to the linear law. The high velocity appears near the rear (nonoperative) side of the vane, and the lower velocity - near the leading (operative) side. Using equations (2.81) and (2.121), it is possible to find the theoretical pressure distribution in the vane channel.

Let us show on an example of radial vane that the difference in the velocities, expressed by the second term of the right side of equation (2.121), determines the transfer by the wheel of the moment equal to moment from Coriolis forces.

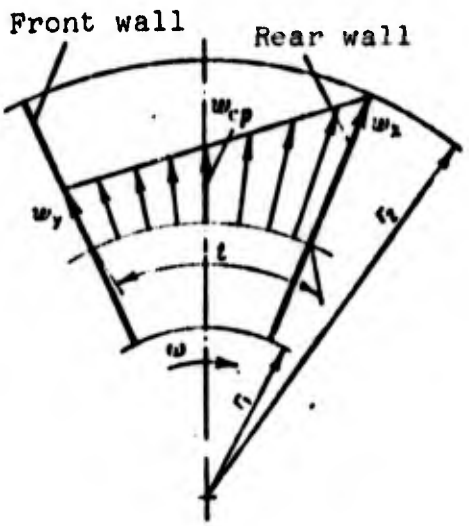

Fig. 2.52. Theoretical velocity distribution over the width of the vane channel of the wheel of the radial vane machine.

Figure 2.52 shows diagrams of the relative velocity which correspond to the circular cascade with radial vanes. The velocity in the nonoperative side is called w_x and in the operative side, w_y.

From formula (2.121) it follows that

$$w_x = w_{cp} + 2\omega\frac{t}{2} = w_{cp} + \omega t; \tag{2.122}$$

$$w_y = w_{cp} - 2\omega\frac{t}{2} = w_{cp} - \omega t. \tag{2.123}$$

On radius r a pressure differential on the vane will be found from equation (2.81):

$$\frac{p_x - p_y}{\rho} = \frac{\Delta p}{\rho} = \frac{w_y^2 - w_x^2}{2},$$

or taking into account expressions (2.122) and (2.123),

$$\Delta p = \rho 2\omega t w_{cp}. \tag{2.124}$$

The moment from the pressure differential is found from the relation

$$M = -\int_{r_1}^{r_2} r\Delta p b z_n dr. \tag{2.125}$$

By substituting expression (2.124) into (2.125), we obtain

$$M = -\int_{r_1}^{r_2} 2\omega\rho t w_{cp} b z_n r dr. \tag{2.126}$$

By replacing in equation (2.126) $\rho t w_{cp} b z_n$ in terms of the mass flow rate G, we obtain

$$M = -2G\omega\int_{r_1}^{r_2} r dr. \tag{2.127}$$

Integrating (2.127), we obtain expression (2.53), i.e., the moment M is the moment of the Coriolis forces transferred from the wheel of the fluid. The specific energy transmitted by the wheel, in accordance with this moment, will be determined by the previously derived formula (2.61).

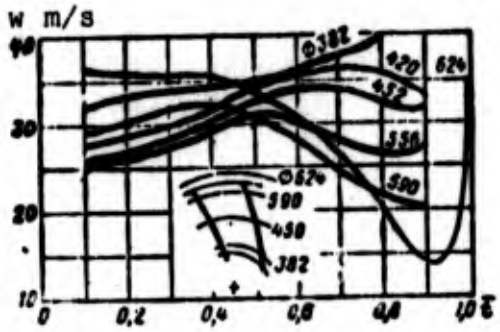

Fig. 2.53. Real velocity distribution over the vane channel of the wheel of radial vane machine.

Figure 2.53 (see source [52]) shows the velocity distribution in the wheel of the centrifugal compressor at different radii. The velocity distribution, which corresponds to the calculated scheme of flow, takes place at the input radii and in the middle of the channel; on the output radii the real pattern of flow greatly differs from that calculated.

Approximately the same velocity distribution was observed in the wheel of the pump (see source [52]). Deviation from the design scheme of the flow is connected with the lag of flow from the direction of the vanes as a result of the inertia of the fluid and the presence of forces of viscosity (separation zones and secondary flows).

2.10.3. DEFLECTING PROPERTIES OF VANE CASCADES

At the outlet from the cascade the fluid flow can have a direction different from the direction of the tangent to the camber line of the profile due to two basic reasons.

The first reason is the development of inertia of the fluid, and the second is connected with the effect of the boundary-layer thickness, the presence of separation zones etc., i.e., with the

effect of viscous forces in the streamline flow of the cascade. The action of the inertial and viscous forces is developed together, but it is systematically more convenient to examine their effect on the cascade flow separately. A deviation in the flow from the direction of the cascade as a result of the inertia of the flow would be developed in the flow of an ideal fluid.

2.10.3.1. The Effect of the Inertia of Fluid on the Deflecting Properties of Cascades

Any cascade comprised of profiles with angles $\beta_{2л} \neq \beta_{1л}$ (and with inleakage with the angle of attack not equal to zero, and when $\beta_{2л} = \beta_{1л}$), changes the direction of the flow. In this case the flow, as a result of its inertia, attempts to keep the initial direction, as a result of which the flow passing through the cascade is turned at a smaller angle than the angle of curvature of the profile.

In a straight cascade (axial machine) for the observer, who moves together with the fluid flow, a deflection in the flow would be explained by the fact that the centrifugal forces of inertia, which appear as a result of the curvature of the profile, near the outlet from the cascade deflect the flow in the direction from the center of the curvature. At the outlet from the cascade the pressure on both sides of the profile is equalized and the surplus pressure from the concave side near the end of the profile no longer counterbalances the centrifugal force of inertia. A deflection in the flow from the assigned geometric direction of flow at the outlet from the cascade will take place for any cascade - fixed and rotating, straight and circular. The more the cascade density, the less the direction of flow will be distinguished from the direction given by the cascade. The more widely spaced the cascade (the less its solidity), the greater the effect this phenomenon will have.

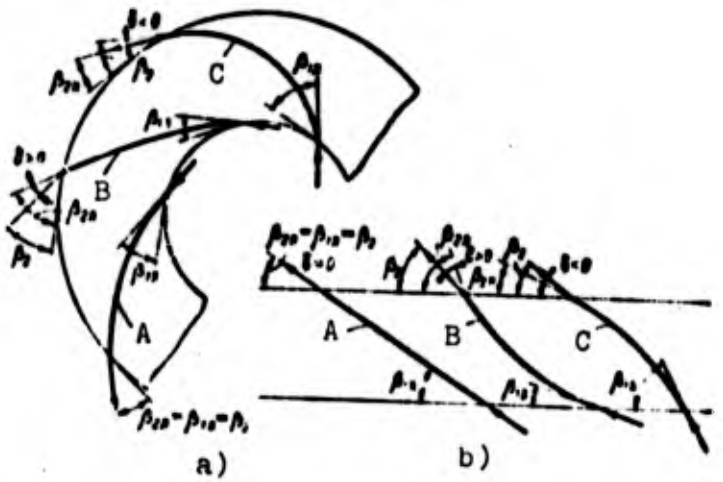

Fig. 2.54. Diagram of the deflection of flow by a fixed circular cascade (a) and an airfoil (straight) cascade (b).

Figure 2.54 shows a diagram of the change in angles at the inlet into straight and circular cascades of constant width and at the outlet from them [circular cascade (see Fig. 2.54a) can be conformally mapped (with the retention of the angles) into an airfoil cascade (see Fig. 2.54b)]. If the outlet angles of the camber line of the profile are greater than the inlet angles (see Fig. 2.54b, profile B), then the flow will emerge at a smaller angle than the angle $\beta_{2л}$ ($\delta = \beta_{2л} - \beta_2 > 0$). If the outlet angles are less than the inlet (see Fig. 2.54b, profile C), then the flow will emerge with a larger angle than angle $\beta_{2л}$ ($\delta < 0$). At an invariable angle of the profile the flow is not deflected ($\delta = 0$) (see Fig. 2.54b, profile A).

In the rotating circular cascades, the deviation in the flow is also affected by the Coriolis forces of inertia. Therefore, the effect of the final number of vanes quite greatly affects the work of the radial compressor machines.

Let us examine briefly the physical phenomena explaining the additional deviation in the flow from the direction of the vanes in centrifugal pumps and compressors.

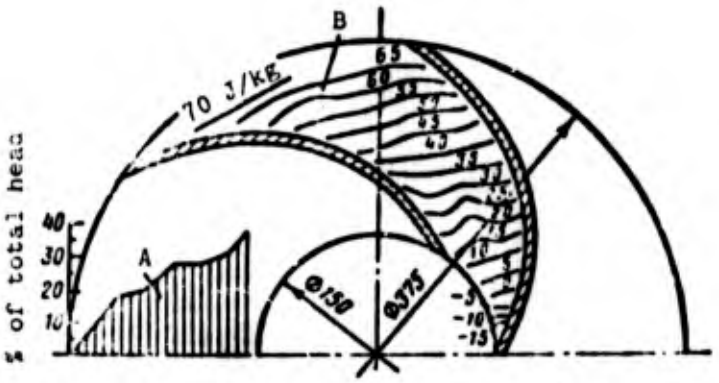

Fig. 2.55. Energy difference of the pressure on both sides of the impeller vane (A) and energy difference of the pressure in wheel and at the inlet into the wheel of the pump (B): $\omega = 70$ 1/s.

The pressure differential on the impeller vane of the centrifugal pump is connected with the streamline flow of the vane in relative motion and with the presence of Coriolis forces of inertia. In the outlet section of the wheel from both sides of the outlet edges of the vane the pressure is equalized. An experiment confirms this (see Fig. 2.55, where data on the energy difference of pressure on the front and rear walls of impeller vanes of the centrifugal pump were given).

Such a pressure distribution along the vane means that in the outlet part of the vane channel the Coriolis force of inertia $F_{и}\, u_2$ is not counterbalanced by the forces of pressure and moves the fluid in a circular direction to the side opposite to the direction of rotation, changing the direction of the flow (see Figs. 2.56 and 2.57, where represented schematically are the forces acting on the particle of fluid and the basic kinematic relationships for the wheel with bent-back blades). Due to the pressure balance near the ends of the blades the fluid is "undertwisted." In practice this denotes that the flow "slips," i.e., it seemingly obtains a circular component in a direction opposite to the direction of rotation and emerges at an angle different from the angle of the blades (see Fig. 2.57).

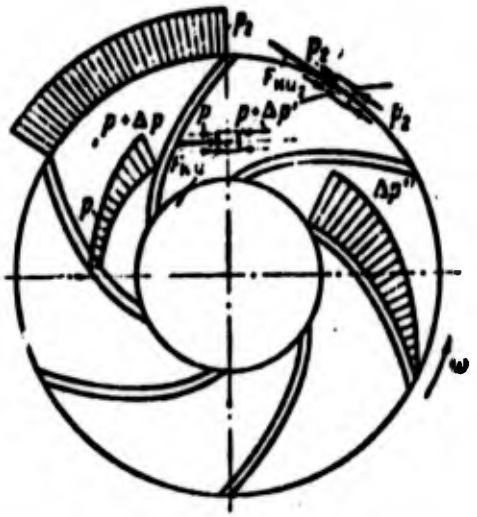

Fig. 2.56. Forces which act on a particle of fluid in the vane channel and at the outlet from the centrifugal pump.

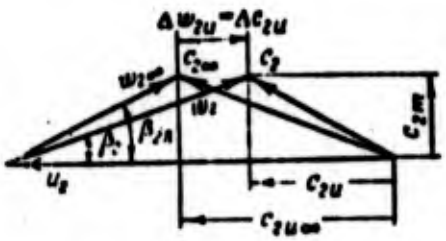

Fig. 2.57. Velocity triangles at the outlet from the wheel taking into account and not taking into account the effect of the finite number of blades.

An increase in the energy of the fluid as a result of the effect on the flow of the wheel of the vane machine, which corresponds to the mechanical energy actually taken from the wheel, is found from the Euler equation, into which there should be substituted the real value c_{2u}:

$$H_T = c_{2u}u_2 - c_{1u}u_1. \qquad (2.128)$$

Let us designate the theoretical pressure which corresponds to the circular velocity component calculated from the scheme $z = \infty$, $H_{T\infty}$:

$$H_{T\infty} = c_{2u\infty}u_2 - c_{1u}u_1. \qquad (2.129)$$

The value $H_{T\infty}$ is the pressure which theoretically could be transmitted to the fluid if the scheme of flow $z = \infty$ would be realized. For centrifugal pumps the distinction of H_T from $H_{T\infty}$ is great (sometimes it is 30-40%).

Let us introduce the concept about the coefficient considering the distinction in values of H_T and $H_{T\infty}$:

$$k_z = H_T/H_{T\infty}. \qquad (2.130)$$

The relationships of H_T and $H_{T\infty}$ is most greatly affected by the number of the blades. Therefore, this coefficient is called the coefficient considering the finite number of blades.

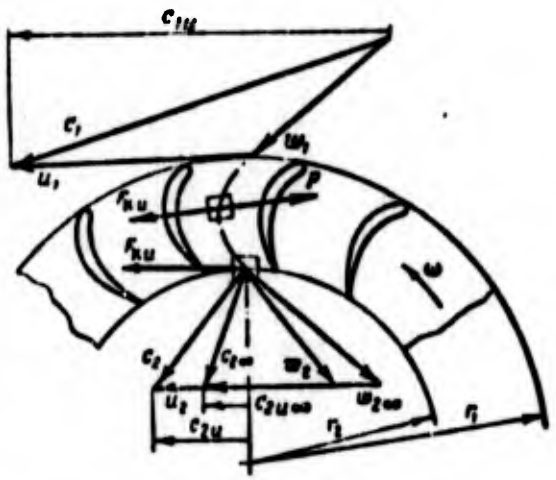

Fig. 2.58. Forces acting on a particle of fluid in the vane channel and at the outlet from the wheel of the inward-flow turbine.

In the radial inward-flow turbines, which have outlet from the wheel in the form of a cylindrical surface of radius r_2 (Fig. 2.58), the flow by virtue of its inertia also differs from the direction of the blades. Because of the pressure balance at the ends of the blades, the Coriolis force of inertia is not counterbalanced by the forces of pressure and deflects flow, whereupon this deflection will occur in the direction of rotation. The flow in the wheel of an inward-flow turbine is "undertwisted." Just as it usually is in the case of a centrifugal compressor machine, this circumstance will decrease the work which is evident from the velocity triangles (see Fig. 2.58, on which for clarity the magnitude of deflection is excessive):

$$L_u = c_{1u}u_1 - c_{2u}u_2 < L_{u\infty} = c_{1u}u_1 - c_{2u\infty}u_2.$$

In turbines the number of blades is usually greater than that in compressors and pumps, and therefore in turbines a deviation in the flow from the direction of the blades is insignificant. In inward-flow turbines with an axial outlet the effect of the inertia of fluid does not directly affect the deviation in the flow at the outlet, but can influence the redistribution of velocities on the radius. The latter fact is confirmed by experiments (see source [46]).

In the rotating circular cascades the angle of deflection of the flow, connected with the tendency to maintain the direction, and the angle of deflection of flow caused by rotation (effect of Coriolis forces), can be added and subtracted from each other. Thus, for instance, for the centrifugal machine at angles of inleakage less than the outlet angles of the blades (diffuser cascade), the angles of deflection of the flow are totaled ($\delta = \beta_{2л} - \beta_{1л} > 0$, see Fig. 2.54a, profile B). At angles of inleakage greater than the outlet angles of the blades (convergent cascade), the deviation in the flow connected with the tendency to maintain the direction can exceed the deviation caused by the rotation, and $\delta < 0$ can take place (see Fig. 2.54a, profile C). In this case the real value c_{2u} will be more than $c_{2u\infty}$, and H_T can be more than $H_{T\infty}$ (see source [59]; see also Section 3.1.1.3).

2.10.3.2. Viscosity Effect on Deflecting Properties of Cascades

The direction of the rate of flow of the boundary layer of a profile coincides with the direction of the tangent to the profile. But the dissymmetry of the boundary-layer development in the vane channel leads to a deflection in the flow. The direction of the flow velocity will be deflected to the side of surface with a smaller value of the boundary-layer thickness. For example, the flow at the outlet from the diffuser cascade deviates to the side of the concave surface of the blade as a result of an increase in the boundary-layer thickness, its swelling and separation on the

blade back. In dense cascades this phenomenon can have a greater effect than the undertwist of the flow as a result of the limited denseness. The separation zones lead to an increase in the relative velocity and, in turn, to a deviation in c_{2u} from the calculated value.

The deviation of the actual direction of the outlet velocity from the cascade from the calculated direction can also be connected with a number of other factors, for example, as will be subsequently shown, with the deviation of the flow in an oblique section of the turbine cascades at supercritical differentials. A distinction in theoretical pressure or theoretical specific work of the vane machine from the calculated theoretical pressure (work) can take place also as a result of the fact that in the design scheme (specifically, when $z = \infty$) flows with a uniform velocity distribution are examined, whereas in actuality the flows of the vane channels have an uneven distribution of velocities (see Fig. 2.53).

Subsequently, in presenting the material in concrete forms of vane machines formulas for calculating the finite number of blades will be given.

2.11. CALCULATION OF THE THREE-DIMENSIONAL NATURE OF FLOW IN THE CALCULATION OF VANE MACHINES

For the calculation of machines with the blades of large extent along the normal to the stream surface, it is necessary to know the change in parameters of the fluid in the clearances in front of the blades and behind the blades. In the twisted flows which flow in the space limited by the surfaces of rotation (walls of the housing, fairings, jacket, etc.), the inertial forces which appear with bending by the flow of the contours of the housing are counterbalanced by forces of pressure, and, therefore, the pressure and other parameters of gas along the normal to the flow will be nonuniform.

Calculation of the three-dimensional spatial flow of fluid presents great difficulties. Therefore, it is necessary to resort to simplifying representations. Thus, for instance, it is considered advisable thus to design the stage of a vane machine in order that the flow lines of fluid will form stream surfaces close to the surfaces of rotation; in this case it is possible to expect a decrease in the losses and, moreover, the calculation of the machine is simplified, since it is possible to use results of wind-tunnel tests of airfoil cascades more reliably.

An experiment shows that velocities along the normal do not exceed 5-6% of the meridian velocity. Consequently, in calculating the parameters in the boundary cross sections of the vane ring (at the inlet and outlet), one considers a change in the parameters characteristic for the state of equilibrium of the fluid in the direction of the normal to the stream surface, i.e., one imposes the requirement of the absences of deflection of the stream surfaces from the surfaces of rotation:

$$c_n = 0 \ (c_r = 0).$$

The work of the wheel of the vane machine is determined by the schemes of velocities at the inlet and outlet. The velocity triangles for the vane machine will be completely assigned for all cross sections along the normal (for the axial machine - on the radius), if the law of the change along the normal of the circular components $c_{1u}(n)$ and $c_{2u}(n)$, meridian components $c_{1m}(n)$ and $c_{2m}(n)$ and circular velocity $u(n)$, i.e., a total of five variables are assigned. Consequently, kinematics of the flow at the inlet into the stage and at the outlet from it for each cross section along the normal will be described by five equations.

The equilibrium conditions, recorded for cross sections of the flow at the inlet into the rotor and at the outlet from it, are two equations of five necessary for the full assignment of the flow

at the inlet into the machine and at the outlet from it. The third equation will be the law of the change in circular velocity along the radius:

$$u = \omega r.$$

It is advantageous to assign by the fourth equation the energy distribution along the normal to the stream surface (according to height or width of the blade). Frequently the obtaining of constant work (pressure) according to the blade height is attained. In this case in all cross sections of the blade along the normal identical energy will be fed or removed, which will eliminate the interaction of the streams on each other, which can lead to added losses. The fifth equation, generally speaking, can be arbitrary; it will determine finally the form of the stage of the vane machine. In practice a change in parameters of the fluid along the normal are considered with sufficiently high blades: $D_{cp}/h_n < 5\text{-}8$.

Let us discuss the derivation of the balance equation. Let us examine the equilibrium of the elementary volume of fluid in the noninertial coordinate system, i.e., in the coordinate system connected with this volume.

Acting on the fluid volume in the clearance of the vane machine (Fig. 2.59), which possesses a circular velocity component c_u and a meridian velocity c_m, are the centrifugal forces of inertia and a pressure difference. The angular velocity of the rotation of the coordinate system is equal to c_u/r.

The expression for the centrifugal force of inertia, which acts on the volume element in the rotating coordinate system will be recorded thus:

$$N = \frac{\rho c_u^2 df dn}{r},$$

where df is the area of element in the plane tangent to the flow line.

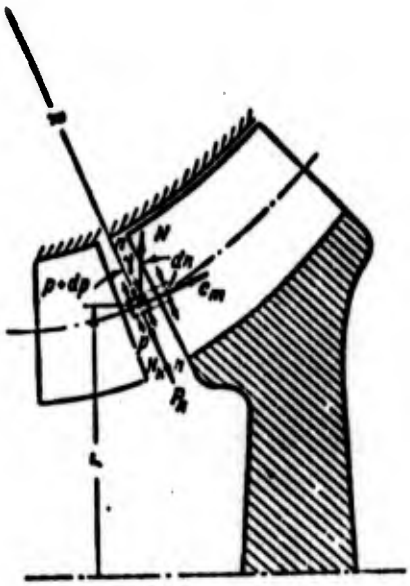

Fig. 2.59. Derivation of the balance equation.

Due to the presence of the curvature of the flow lines, acting on the particle of fluid in the clearance in the coordinate system, which moves together with the particle, will also be the centrifugal force N_R:

$$N_R = \frac{\rho c_m^2 df dn}{R}.$$

The total force component of pressure along the normal will be equal to

$$P_n = (p + dp)df - pdf = dpdf.$$

Since we examined the volume element which does not move relative to the coordinate system, the Coriolis force of inertia is equal to zero.

In the mobile coordinate system the particle is in equilibrium, and the sum of the projections of forces on the direction of the normal n-n is equal to zero:

$$N \cos \gamma - N_R - P_n = 0,$$

or in the expanded form

$$\frac{\rho c_u^2 df dn \cos\gamma}{r} = dpdf + \frac{\rho c_m^2 df dn}{R};$$

finally we obtain

$$\frac{dp}{dn} = \rho \frac{c_u^2}{r} \cos\gamma - \rho \frac{c_m^2}{R}. \qquad (2.131)$$

Equation (2.131) is called the balance equation along the normal.

For an axial machine, assuming $\gamma = 0$ and $R = \infty$, i.e., disregarding the streamline curvature in the meridian plane, we obtain

$$\frac{dp}{dr} = \rho \frac{c_u^2}{r}. \qquad (2.132)$$

From the equation of the conservation of energy for an incompressible fluid (2.78) (if we disregard the heat supply and the change in energy of the position and consider the losses in all the streams to be identical) it follows that

$$\frac{dp}{dn} = -\rho \frac{dL_i}{dn} - \rho \frac{d}{dn}\left(\frac{c^2}{2}\right), \qquad (2.133)$$

where i is the subscript which designates the cross section of the blade.

By comparing expressions (2.131) and (2.133), we obtain

$$\frac{d(c^2)}{dn} + 2\frac{c_u^2}{r}\cos\gamma - 2\frac{c_m^2}{R} = -2\frac{dL_i}{dn}. \qquad (2.134)$$

When $L_i(n) = \text{const}$ or $L_i = 0$

$$\frac{d(c^2)}{dn} + 2\frac{c_u^2}{r}\cos\gamma - 2\frac{c_m^2}{R} = 0. \qquad (2.135)$$

For the axial machines

$$\frac{d(c^2)}{dr} + 2\frac{c_u^2}{r} = 0. \qquad (2.136)$$

Replacing c^2 in expression (2.135) by $(c_u^2 + c_m^2)$, we obtain

$$\frac{d(c_m^2)}{dn} + \frac{d(c_u^2)}{dn} + 2\frac{c_u^2}{r}\cos\gamma - 2\frac{c_m^2}{R} = 0, \qquad (2.137)$$

or for the axial machine, where $c_m = c_z$, since $dn = dr$,

$$\frac{d(c_z^2)}{dr} + \frac{1}{r^2}\left[r^2\frac{d(c_u^2)}{dr} + 2c_u^2 r\right] = 0;$$

we finally obtain

$$\frac{d(c_z^2)}{dr} + \frac{1}{r^2}\frac{d[(c_u r)^2]}{dr} = 0. \qquad (2.138)$$

This equation establishes the dependence of the circular and axial velocity comporents on the radius in clearances of the axial vane machine.

When $dL_i \neq 0$ equation (2.134) correspondingly will be recorded in the form

$$\frac{d\left(c_z^2\right)}{dr} + \frac{1}{r^2}\frac{d\left[\left(c_u r\right)^2\right]}{dr} = -2\frac{dL_i}{dr}. \qquad (2.139)$$

The calculation of the change in parameters along the normal to the stream surface is produced mainly in axial machines, since in axial machines (specifically, in precombustion-chamber turbines of liquid-propellant rocket engines) the blades are relatively long: $D_{cp}/h_л = 5\text{-}8$. Moreover, in diagonal machines the pressure increase caused by presence of c_u is partially counterbalanced by the pressure increase due to the curvature of the flow lines in the meridian cross section (see Fig. 2.59).

For a purely radial machine $R = \infty$, $\gamma = 90°$ (direction of the normal is parallel to the leading edge of the rotor), and therefore equations (2.134) and (2.133) take the following form:

$$\frac{d(c^2)}{dn} = -2\frac{dL_i}{dn}; \qquad (2.140)$$

$$\frac{dp}{dn} = 0. \qquad (2.141)$$

Consequently, pressures at the inlet into the radial wheel and at the outlet from it with the accepted assumptions will be constant along the width of the blade.

Let us examine the basic procedures of the radial profiling of axial machines.

2.11.1. THE PROFILING OF THE BLADES OF AXIAL PUMPS ALONG THE RADIUS

The stage of the axial pump is a combination of the elementary stages located on different radii. Operating conditions of these elementary stages are considerably different.

Conditions of radial equilibrium, which are advantageously maintained at the inlet into the operating cascade and at the outlet from it in order to avoid losses connected with the radial leakage, will give two equations for determining the kinematics of flow in the stage. In accordance with formulas (2.138) and (2.139), these equations for the axial pump will be recorded thus:

$$\frac{d(c_{1r}^2)}{dr} + \frac{1}{r^3}\frac{d[(c_{1u}r)^2]}{dr} = 0; \qquad (2.142)$$

$$\frac{d(c_{2r}^2)}{dr} + \frac{1}{r^3}\frac{d[(c_{2u}r)^2]}{dr} = 2\frac{dH_{rl}}{dr}. \qquad (2.143)$$

The law of the change in circular velocity in radius $u = \omega r$ is the third equation. The fourth and fifth conditions additionally being formulated determine finally the form of the stage. In the absence of a guide device at the inlet into the axial rotor ($c_{1u} = 0$), which is typical for axial pumps of liquid-propellant rocket engines, four equations are completely sufficient in order to determine the form of the stage. Let us examine the specific laws of profiling of cascades of the stage of axial pumps.

2.11.1.1. Stage with Constant Circulation

Assuming that at the inlet into the rotor and at the outlet from it the potential (irrotational) flow takes place, we obtain the fifth condition:

$$\Gamma = c_u r = \text{const}, \tag{2.144}$$

consequently, $c_{1u}r = \text{const}$ and $c_{2u}r = \text{const}$.

The presence of irrotational flow at the inlet into the rotor and at the outlet from it means that the energy feed on the radius is constant [i.e., $H_{T\ i}(r) = \text{const}$]:

$$H_{T\ i}(r) = \omega(c_{2u}r - c_{1u}r) = \text{const}. \tag{2.145}$$

Sometimes such stages are called stages with a free vortex, since the irrotational flow around the vortex is described by equation (2.145), which expresses the constancy of circulation around the vortex.

From equations of radial equilibrium (2.142) and (2.143), it follows that when $c_{1u}r = \text{const}$ we have $c_{1z}(r) = \text{const}$, and when $c_{2u}r = \text{const}$ we have $c_{2z}(r) = \text{const}$, since $H_{T\ i}(r) = \text{const}$.

Thus, in the ideal case the stage of the axial pump with the constancy of circulation is characterized by the uniformity of the axial velocities. In the absence of twist at the inlet ($c_{1u} = 0$) [see equation (2.132)] the inlet pressure along the radius will also be uniform.

Figure 2.60 shows a change in the pressure and circular velocity components of the fluid along the radius for the stage with constant circulation and axial inlet. At the outlet from blades of the rotor wheel the pressure along the radius, in accordance with equation (2.131), is increased. Integration of equation (2.131) gives

$$\frac{p_2(r) - p_{2\,cp}}{\rho} = \frac{c_{2u\,cp}^2}{2}\left(1 - \frac{r_{cp}^2}{r^2}\right). \tag{2.146}$$

If the stator, which stands behind the rotor, completely deflects the flow in an axial direction, then the pressure behind it will be uniform (see p_3 on Fig. 2.60).

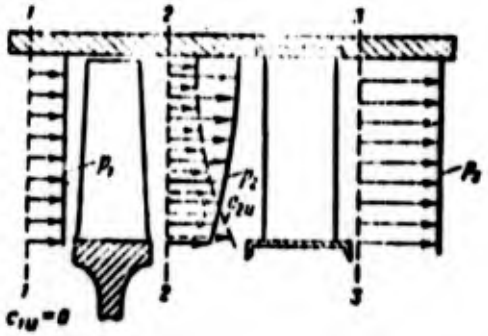

Fig. 2.60. The change in the pressure and circular velocity components of flow along the radius in the stage of the axial pump with constant circulation ($c_u r$ = const).

The degree of the reaction of the stage with constant circulation will be variable along the radius. In general when $c_{1u} \neq 0$ the expression for the degree of reaction will be recorded in the form [it can be derived similar to formula (2.106)]

$$\Omega_r = 1 - \frac{c_{1u} + c_{2u}}{2w}. \qquad (2.147)$$

By multiplying the numerator and denominator of the second term of the right side of formula (2.147) by r, we obtain

$$\Omega_r = 1 - \frac{rc_{1u} + rc_{2u}}{2wr}.$$

Consequently, for this stage (rc_{1u} and rc_{2u} according to the condition are constant) we obtain

$$\Omega_r = 1 - \frac{\text{const}}{r^2}, \qquad (2.148)$$

i.e., the larger the radius, the more the degree of reaction.

The coefficient of theoretical pressure (theoretical pressure referred to the square of the current circular velocity) is also changed along the radius. For this stage $H_{T\,1}(r)$ = const, and therefore,

$$\eta_{T1} = \frac{\text{const}}{r^2}, \qquad (2.149)$$

i.e., the coefficient of theoretical pressure is changed inversely proportional to the square of the radius.

The velocity triangles for different cross sections are different (Fig. 2.61). Parameters in the mean section are indicated by the subscript "ср," in the peripheral cross section - "п," and in the hub - "вт."

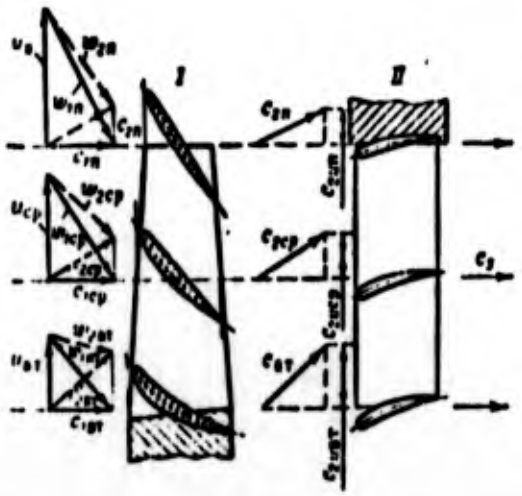

Fig. 2.61. Velocity triangles and cross sections of blades at different radii of the stage of the axial pump ($c_u r$ = const).

A change in the angle β_1 can be established from the velocity triangles:

$$\operatorname{tg}\beta_1 = \frac{c_{1z}}{u} = \frac{c_{1z}}{\omega r}.$$

When $c_{1z}(r)$ = const (c_{1u} = 0)

$$\operatorname{tg}\beta_1 = \frac{\text{const}}{r}, \text{ or } r\operatorname{tg}\beta_1 = \text{const}. \qquad (2.150)$$

At the zero angle of incidence r tg $\beta_{1п}$ = const. This relation means that the leading edge of the blades of the stage should be twisted along the spiral surface (as is known, the equation of the spiral surface r tg $\beta_п$ = const). But the entire surface of the blade of the stage, made according to the law $c_u r$ = const, does not coincide with the spiral surface. Let us find the dependence of the outlet angle of the blade from the radius (disregarding the deflection of flow from the direction of the blade):

$$\operatorname{tg}\beta_{2\pi} = \frac{c_{2a}}{u - c_{2u}} = \frac{c_{2a}}{u - \frac{c_{2u} \cdot r_1}{r}}.$$

After the elementary conversions, assuming $c_{2z} = c_{2z\ cp} = \text{const}$, we obtain

$$\operatorname{tg}\beta_{2\pi} = \frac{\text{const} \cdot r}{\text{const}' \cdot r^2 - \text{const}''}.$$

The smaller the radius, the larger $\beta_{2\pi}$, i.e., the more the profile will bend (see Fig. 2.61), and the larger the setting angle.

The major advantage of the stage with constant circulation is in the low hydraulic losses, i.e., in the high efficiency and the constancy of pressure on the radius. The high efficiency and constancy of pressure on the radius make it possible to utilize such stages as the pressure stages of multistage axial pumps. Such pumps, according to conditions of strength, should be made with short blades.

In this case $\bar{d}_{вт} = d_{вт}/D_{cp}$ will be 0.5-0.7.

A shortcoming of stages with constant circulation is the fact that at the assigned circular velocity the pressure quality of the stage is low, since the coefficients of theoretical pressure of the peripheral cross sections are low.

In the case of long blades the abrupt change in setting angles and the degree of reaction on the radius is also a shortcoming in these stages. In the root cross sections the degree of reaction can take negative values, which leads to reduction in the efficiency.

2.11.1.2. Stage with the Constant Coefficient of Theoretical Pressure on the Radius

For the constancy of the coefficient of theoretical pressure when $c_{1u} = 0$, the twist at the outlet should be proportional to the radius (fourth necessary equation):

$$\bar{H}_{T\,1} = \frac{c_{2u}}{u} = \text{const},$$

or

$$\frac{c_{2u}}{r} = \text{const}. \qquad (2.151)$$

In this case the entire mass of the fluid at the outlet from the rotor is rotated around the axis of the rotor with the law of the distribution of circular velocity components as near the rotating solid. The stage with the constant coefficient of theoretical pressure is called also the stage with a change in the twist on the radius "according to the law of the solid," or "according to the law of the forced vortex." In this case the pressure of the elementary stage will be increased in proportion to the square of the radius:

$$H_{T\,1} = \text{const} \cdot r^2, \qquad (2.152)$$

or

$$H_{T\,1} = \text{const} \cdot u^2.$$

The pressure is rapidly increased towards the periphery. The integration of equation (2.132) gives the dependence

$$\frac{p_1(r) - p_{1cp}}{\rho} = \frac{c_{2u\,cp}^2}{2}\left(\frac{r^2}{r_{cp}^2} - 1\right). \qquad (2.153)$$

The comparison of formulas (2.146) and (2.153) makes it possible to draw the conclusion about the different nature of the change in pressure for two laws of radial profiling - $c_u r = \text{const}$ and $c_u/r = \text{const}$.

Having assumed that $r \to \infty$, we will obtain that the pressure with the law $c_u r = \text{const}$ approaches a finite value (see Fig. 2.60) and with law $c_u/r = \text{const}$ - to a infinite value.

When $c_{1u} = 0$ and $c_{1z}(r) = \text{const}$ the profiling of the leading edge of the rotor blade of the axial pump does not depend on the form of the stage and should be made according to a spiral surface $r \operatorname{tg} \beta_{1л} = \text{const}$, since the input velocity triangles (see Fig. 2.61) in this case are identical for all forms of the stages.

A change in the setting angle of the profile on the radius with profiling according to the law $c_u/r = \text{const}$ is less than that with profiling according to the law $c_u r = \text{const}$.

With the profiling of the blades according to the law $\bar{H}_{т\,i} = \text{const}$ the kinematic degree of reaction will be constant on the radius:

$$\rho_к = 1 - \frac{c_{2u}}{2u} = 1 - \frac{\text{const}' \cdot r}{2\omega r} = \text{const}. \qquad (2.154)$$

2.11.1.3. Other Forms of Stages of Axial Pumps

It is possible to use other forms of axial wheels with the law of profiling different from $c_u r = \text{const}$ or $c_u/r = \text{const}$.

In general the law of profiling can be recorded in the form

$$c_u r^m = \text{const}, \qquad (2.155)$$

where m is changed from +1 to -1.

It is obvious that $m = 1$ corresponds to law $c_u r = \text{const}$, and $m = -1$ corresponds to the law $c_u/r = \text{const}$.

The rotors profiled according to the law c_u = const (m = 0) are called semivortical. It is obvious that the theoretical pressure in this case is changed in proportion to the radius:

$$H_{T\,1} = c_{2u}u = \text{const} \cdot r. \tag{2.156}$$

The coefficient of theoretical pressure $\bar{H}_T$ for such a wheel will be decreased with an increase in the radius:

$$\bar{H}_{T\,1} = \frac{\text{const}}{r}. \tag{2.157}$$

In pumps of liquid-propellant rocket engines the axial vane wheel made on a spiral surface is widespread; such a wheel is called a spiral-screw wheel.

2.11.1.4. Spiral-Screw Axial Stage

Figure 2.62 gives the main notations for the cascade of the spiral-screw wheel of constant pitch. The pitch, i.e., the axial displacement of helical line on the length of the full circumference is designated by the letter s. The angle of the blade and the pitch are connected by the relation $\text{tg}\,\beta_л = s/\pi D$. The length of the plate which forms the blade is designated by the symbol $b_л$, and the distance between the corresponding points on the circumference - the cascade pitch - is denoted by the letter t:

$$t = \frac{\pi D}{z}. \tag{2.158}$$

where z is the number of the blades.

Two- or three-entry screw conveyors (two or three blades) are commonly used. Figure 2.62 shows the cascade of a two-entry screw conveyor, i.e., spiral-screw wheel with two blades. The width of the vane channel is designated by the letter a:

$$a = (t - \sigma) \sin \beta_л. \tag{2.159}$$

where $$\sigma = \frac{\delta}{\sin \beta_л};$$

σ - the thickness of the blade in the plane of rotation;

δ - the normal thickness of the blade.

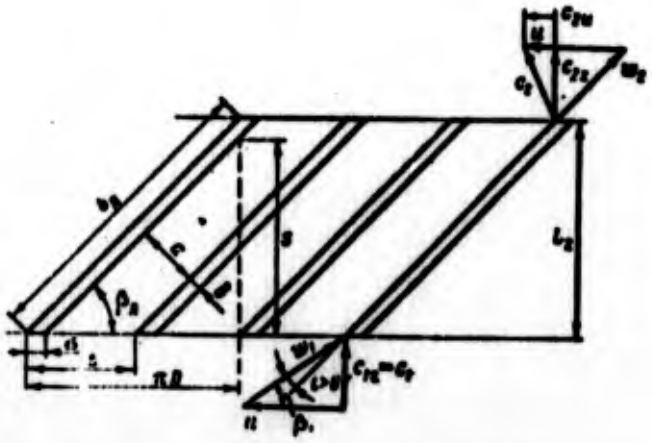

Fig. 2.62. The cascade and velocity triangles of a spiral-screw wheel of constant pitch.

The development of the cylindrical cross section of the screw conveyor of constant pitch is the cascade of direct plates. Therefore, the deflection in the flow by such a cascade (see Section 2.9) will be observed only at positive angles of incidences ($\beta_л > \beta_1$). The greater the angle of incidence, the greater the pressure of the screw conveyor (Fig. 2.63).

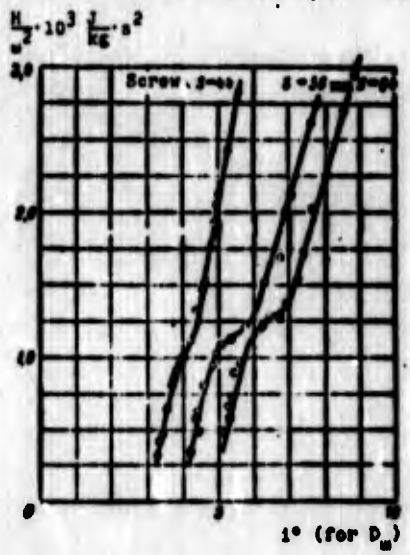

Fig. 2.63. Experimental dependence of pressure of a screw conveyor on the incidence.

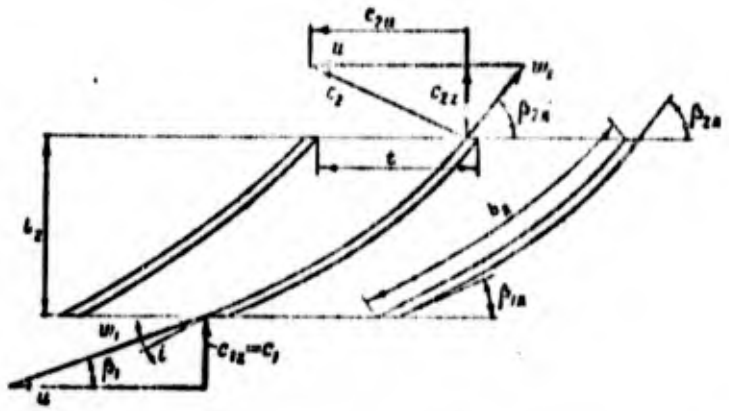

Fig. 2.64. Development of a cylindrical cross section and velocity triangles of a screw conveyor of variable pitch.

If the angle of the blades is increased from the inlet to the outlet (in this cylindrical cross section), then such a wheel will be called a screw conveyor of variable pitch. The blade of such a screw conveyor will be the spiral surface of variable pitch. The development of the cylindrical cross section of the screw conveyor of variable pitch is represented on Fig. 2.64.

Even in the absence of twist at the inlet into a screw conveyor (the most typical case when using a screw conveyor as a preliminary pump of the liquid-propellant rocket engine) the angle of attack is changed on the radius. Let us show this:

$$\operatorname{tg} i = \operatorname{tg}(\beta_л - \beta_1) = \frac{\operatorname{tg}\beta_л - \operatorname{tg}\beta_1}{1 + \operatorname{tg}\beta_л \operatorname{tg}\beta_1}; \quad \operatorname{tg} i = \frac{\frac{s}{2\pi r} - \frac{c_{1z}}{\omega r}}{1 + \frac{s c_{1z}}{2\pi\omega r^2}}, \tag{2.160}$$

since

$$\operatorname{tg}\beta_л = \frac{s}{2\pi r}; \quad \operatorname{tg}\beta_1 = \frac{c_{1z}}{u} = \frac{c_{1z}}{\omega r}.$$

The smaller the r, the larger the angle of attack. When $c_{1z}(r) = \text{const}$, constant on the radius is the relation

$$\frac{\operatorname{tg}\beta_1}{\operatorname{tg}\beta_л} = \frac{2\pi c_{1z}}{\omega s}. \tag{2.161}$$

The velocity c_{2z} is variable on the radius (Fig. 2.65), but the mean-flow velocity at the inlet and outlet are identical: $c_{1z} = c_{2z} = c_z$ (when $d_{вт}$ = const along the length).

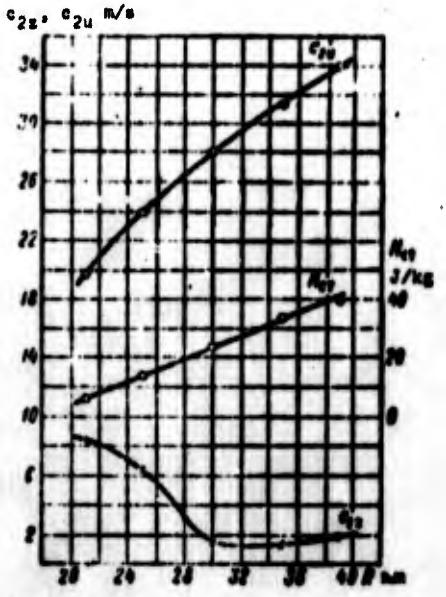

Fig. 2.65. Experimental dependences c_{2u}, c_{2z} and $H_{ст}$ on the radius R for the screw conveyor.

From the velocity triangle (Fig. 2.66) it follows that

$$c_{z0} = u \operatorname{tg} \beta_л = \frac{\omega r s}{2\pi r} = \frac{\omega s}{2\pi}, \qquad (2.162)$$

where c_{z0} is the axial velocity at the zero angle of incidence, i.e., with zero theoretical pressure (the effect of the thickness of the blade in the outlets of the given section will be disregarded).

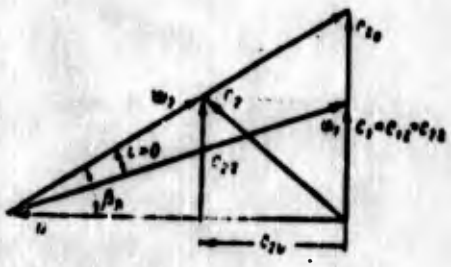

Fig. 2.66. Velocity triangles for the screw conveyor.

When i = 0 the theoretical pressure $H_T = 0$, since $c_{2u} = 0$; c_{z0} obviously corresponds to the maximum flow rate Q_0 for this screw conveyor; Q_0 is the flow rate at which the flow enters into the blade with a zero angle of attack ($H_T = 0$).

Taking into account equation (2.162), the relation (2.161) is recorded thus:

$$\frac{\operatorname{tg}\beta_1}{\operatorname{tg}\beta_n} = \frac{c_z}{c_{z0}}.$$

Let us designate this ratio by the letter q, and we will call it the flow parameter:

$$q = \frac{c_z}{c_{z0}} = \frac{\operatorname{tg}\beta_1}{\operatorname{tg}\beta_{2a}} = \frac{c_z}{u\operatorname{tg}\beta_{2a}} = \frac{c_z}{u}\operatorname{ctg}\beta_{2a} = \frac{Q}{Q_0} = \frac{2\pi c_z}{\omega s}. \qquad (2.163)$$

When s = const, q(r) = const.

For the screw conveyor of variable pitch, q will be recorded in the form

$$q = \frac{c_z}{c_{z0}} = \frac{\operatorname{tg}\beta_1}{\operatorname{tg}\beta_{2a}} = \frac{c_z}{u}\operatorname{ctg}\beta_{2a} = \frac{Q}{Q_0} = \frac{2\pi c_z}{\omega s_2}, \qquad (2.164)$$

where c_{z0} and Q_0 correspond to the zero pressure of the screw conveyor of variable pitch ($H_T = 0$).

The theoretical pressure in this cross section of the screw conveyor is found from the Euler equation (when $c_{1u} = 0$):

$$H_{T\,1} = c_{2u1}u_1. \qquad (2.165)$$

Figure 2.65 shows the experimental dependences c_{2u}, c_{2z} and H_{cT} on the radius.

Since in all the cross sections an increase in energy is different, the theoretical pressure of the stage will be defined as the average pressure integral according to the flow:

$$H_T = \frac{2\pi \int_{r_{BT}}^{R_n} r c_{2zi} H_{Ti} dr}{Q}, \qquad (2.166)$$

where i is the sign of any intermediate cross section between d_{BT} and D_n (Fig. 2.67).

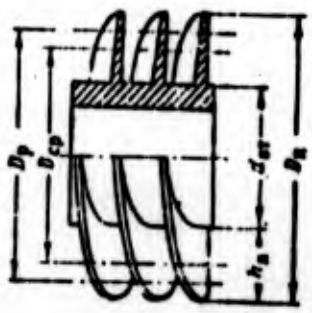

Fig. 2.67. Spiral-screw wheel (screw conveyor).

In an experimental study [47] $H_{T\,i}$ and H_T for an individual screw-type pump were determined from equations (2.165) and (2.166) on the basis of the velocity fields c_{2zi} and c_{2ui} measured experimentally. The diameter at which $H_{T\,i}$ was equal to H_T was taken as the calculated. The calculated diameter was larger than the mean quadratic and arithmetic mean:

$$D_p = \frac{\sqrt{3D_n^2 + d_{BT}^2}}{2} \qquad (2.167)$$

(see Fig. 2.67). This is explained by the nature of dependence $H_{T\,i}$ on r and by the fact that at the outlet near the hub the zone of countercurrents was observed. For the screw conveyor, being used as a stage of the screw-centrifugal pump, in view of the effect of the centrifugal wheel on the zone of return currents, the value of the calculated diameter is less than that for the screw-type pump, and it can be taken as the arithmetic mean:

$$D_p = D_{cp} = \frac{D_n + d_{BT}}{2}. \qquad (2.168)$$

For this diameter we will construct velocity triangles, examining the joint operation of the screw conveyor and centrifugal wheel. The theoretical pressure of the screw conveyor H_T will be expressed by the flow parameter q and the circular velocity on the calculated diameter by u_p (assuming $c_{1z\,p} = c_{2z\,p}$):

$$H_T = u_p^2(1 - q). \qquad (2.169)$$

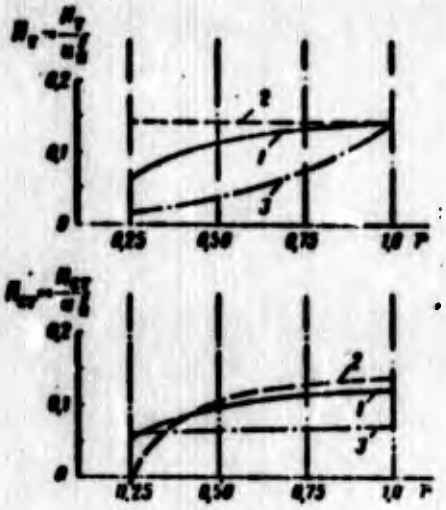

Fig. 2.67a. Calculated dependences of the coefficient of pressure on the radius for three axial wheels when $\bar{d}_{вт} = 0.25$ and $\operatorname{tg} \beta_{2л} = 0.3$: 1 - spiral-screw wheel; 2 - wheel with $c_u r = \text{const}$; 3 - wheel with $c_u/r = \text{const}$.

Figure 2.67a gives graphs of the change in the coefficient of pressure depending on a radius for three axial wheels: spiral-screw wheel, the wheel designed according to the law $c_u r = \text{const}$, and the wheel designed according to the law $c_u/r = \text{const}$. A comparison is conducted with the same coefficient of pressure on the periphery.

In relation to the provision for noncavitation work of the centrifugal wheel, the wheel designed according to the law $c_u/r = \text{const}$ and the spiral-screw wheel used as preliminary pumps have a favorable passage of the dependence $\bar{H}_{ст} = f(r)$, since the dimensionless static head is changed little on the cross section. For the wheel with $c_u r = \text{const}$ the static head in the hub sharply falls, owing to which a cavitation zone at the outlet from the wheel can appear. The spiral-screw wheel has a technological advantage over other wheels in view of the simplicity of geometric form of the blades (spiral surface). Therefore, as a preliminary pump of pumps of the liquid-propellant rocket engines usually used is a spiral-screw wheel as that which provides the favorable distribution of parameters on the cross section and which is simple to manufacture, although hydraulic losses in these wheels are considerable.

2.11.2. THE PROFILING OF THE BLADES OF AXIAL-FLOW TURBINES ON THE RADIUS

2.11.2.1. Stage with Constant Circulation

The profiles of turbine blades when $D_{cp}/h_л \leq 7\text{-}8$ are flowed around under substantially different conditions. Such blades (let us call them conditionally "long") can be found in turbines of liquid-propellant rocket engines with the gas feed into the combustion chamber (in precombustion-chamber turbines). The flow at the outlet from the nozzle box has a large circular velocity component - twist.

With a constant pressure along the radius at the inlet into the nozzle cascade the pressure at the outlet will increase toward the periphery. This will mean that the degree of pressure drop in the nozzle box will be changed along the radius (Fig. 2.68). With long blades, moreover, the circular velocity is noticeably changed. With the profiling of the blades at different radii all this should be taken into consideration (see source [57]).

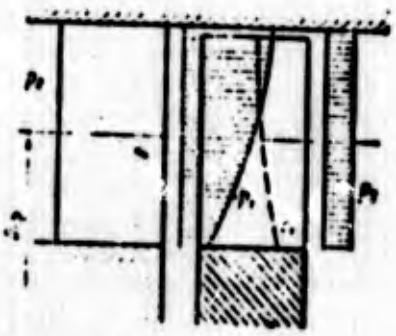

Fig. 2.68. Change in the pressure and velocity along the radius in the axial clearance of the stage of an axial-flow turbine.

Let us examine the work of the stage in which there should be fulfilled the condition of constancy of the circulation of velocity over height at the inlet into the rotor blades and at the outlet from them:

$$c_{1u}r = \text{const}; \tag{2.170}$$

$$c_{2u}r = \text{const}. \tag{2.171}$$

These conditions are the fourth and fifth equations determining the kinematics of flow in the stage. From conditions (2.170) and (2.171) there ensues the condition of the constancy of work on the radius (L_u = const):

$$L_u = \omega(c_{1u}r - c_{2u}r).$$

From equation (2.138) it follows that with $c_{1u}r$ = const

$$c_{1z}(r) = \text{const}.$$

Thus, in the stage of the axial-flow turbine with constant circulation, just as in the stage of the axial pump, the flow has a constant axial velocity c_{1z} along the radius.

From equation (2.139) it follows that with $c_{2u}r$ = const and L_u = const the axial component of the velocity at the outlet from the blades will be constant:

$$c_{2z}(r) = \text{const}.$$

Let us recall that all the relations of this section were obtained for an incompressible fluid. Let us say that a density change along the radius leads to the appearance of a radial component and a certain disturbance of the uniformity of flow.

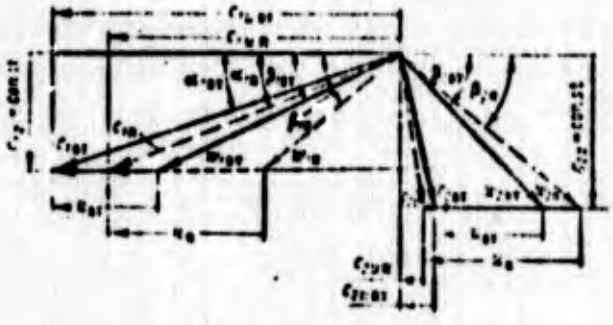

Fig. 2.69. Velocity triangles of the stage of the turbine profiled according to the law $c_{1u}r$ = const for two cross sections - peripheral (dashed line) and hub (solid line).

Figure 2.69 gives the velocity triangles for the peripheral and hub sections. From them it is possible to judge a change in the angles of the blades with a change in the radius, assuming in the first approximation that the flow angles coincide with the angles of the blades.

Figure 2.70 shows the change in the degree of reaction of the stage with $c_{1u}r$ = const, L_u = const over the height of the blade, and profiles of the blades of peripheral and hub cross sections are given.

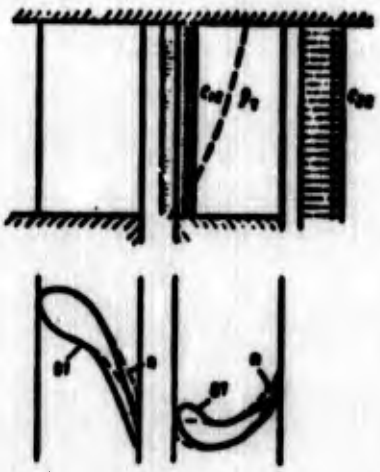

Fig. 2.70. Shapes of blades and a change in parameters along the radius for the stage of the turbine profiled according to the law $c_{1u}r$ = const.

The advantage of the method of the design of the stage according to the law $c_u r$ = const consists in the fact that in this case low hydraulic losses are provided (this is explained by the uniformity of the axial velocities). The great change in angles of the blades and the possibility of the appearance of negative reaction in the root are shortcomings of this method of the design of the stage.

2.11.2.2. Stage with Constant Angle α_1

For precombustion-chamber turbines of liquid-propellant rocket engines, it is advantageous to use stages whose angle α_1 is constant along the radius, i.e., the nozzle blades are not

twisted, and, consequently, they are simpler to produce. Thus, the law α_1 = const is the fourth equation determining the velocity triangles of the stage. Parameters at the outlet are assigned by the fifth equation.

Equation (2.136) is converted into the following form:

$$\frac{dc_1^2}{dr} + 2\frac{c_1^2}{r}\cos^2\alpha_1 = 0,$$

since $c_u = c_1 \cos \alpha_1$.

After the integration of this equation we obtain

$$c_{1u} r^{\cos^2 \alpha_1} = \text{const}.$$

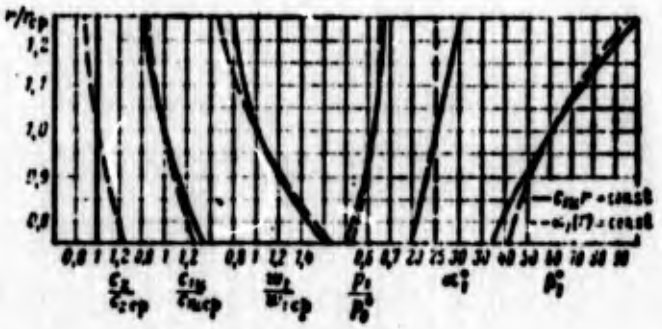

Fig. 2.71. Comparison of the change in parameters of stages of the turbine profiled according to laws $c_{1u}r$ = const and $\alpha_1(r)$ = const (dashed line) (see source [21]).

On Fig. 2.71 the comparative graphic representations, which show a change in parameters along the height of the blade for stages profiled according to laws $c_{1u}r$ = const and $c_{1u}r^{\cos^2 \alpha_1}$ = const $\alpha_1(r)$ = const].

With the method of profiling $\alpha_1(r)$ = const (see Fig. 2.71) considerable nonuniformity of the axial velocities occurs.

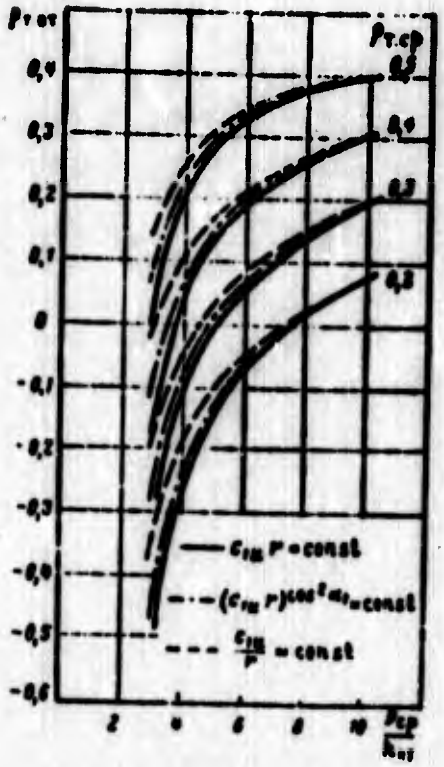

Fig. 2.72. Dependence of the degree of reaction in the hub of the turbine on the relative height of the blades with a different degree of reaction on the mean diameter and different laws of profiling.

Upon consideration of the losses, the angle of nozzle blades should be increased toward the periphery (see source [6]).

Figure 2.72 shows the dependence of the degree of reaction in the hub on the relative height of the blades with a different degree of reaction on the mean diameter and different laws of profiling.

According to data of experimental studies (for example, [41] and [56]) the use of blades profiled over height when $D_{cp}/h_л \leq 5\text{-}6$ leads to a noticeable gain in efficiency (up to 5-6%). When $D_{cp}/h_л > 8\text{-}10$ an increase in the efficiency will be insignificant.

Stages designed according to different laws of profiling different from laws $c_{1u}r = \text{const}$ and $\alpha_1(r) = \text{const}$ can be used. In general turbine blades, just as the blades of pumps, are designed on the basis of relation (2.155).

2.12. SIMILARITY OF BLADE MACHINES

2.12.1. GENERAL INFORMATION

In connection with the fact that some processes in vane machines do not yield to theoretical calculation, the experimental study of vane machines acquires special importance. During tests it is necessary to process experimental data in such a way that results of the study of the specific machine could be used with the calculation and design of other machines. Moreover, it is necessary to deal with tests of vane machines on model working media, in model conditions or with model tests of the vane machine of other dimensions. Primarily, this is caused for the following reasons: the impossibility of the use of a natural working medium as a result of its agressiveness and toxicity and the undesirability of the use of complex and expensive equipment in the testing of natural models of high power in natural conditions. The processing of experimental material, the selection of the model working medium, model conditions and dimensions of the model are carried out in accordance with laws of the theory of similar phenomena (see source [53]).

The similar phenomena are phenomena of an identical physical nature for which relations of similar parameters characterizing these phenomena are identical at similar points and at similar moments of time (the latter condition refers to the unsteady processes).

Phenomena of an identical physical nature are understood as such phenomena which are described by the same system of equations and which can be characterized by the same physical parameters. Phenomena of a different physical nature can be mathematically described by systems of equations of an identical structure. In this case the similar phenomena or mathematical analogy are indicated. The method of analogy is also applied in the study of

processes in vane machines (see source [48]). For example, the method of electrical analogy is used for the investigating of the flow of blade profiles.

The theory of similitude establishes that for similar phenomena the dimensionless complexes, called the similarity criteria, composed of parameters characterizing this phenomenon (characteristic parameters), are identical. In order that the phenomena are similar, a necessary and sufficient condition is the provision of equality of the so-called determining similarity criteria. In other words, with the equality of the characteristic criteria the phenomena will be similar, and the similar indeterminate criteria (operating factors, efficiency and so on) will be identical. Each indeterminate criterion can be expressed in the form of a function of the characteristic criteria.

The characteristic criteria include such criteria which include parameters entering into conditions of uniqueness, i.e., into conditions reducing the phenomenon to this specific case. Conditions of the uniqueness in a strict mathematical form can be obtained from the solution of the problem of existence and from the uniqueness of the solution of the system of equations describing this phenomenon. However it is not always possible to obtain this solution. Moreover, the very system of equations which describes the phenomenon is frequently unknown, and in the compilation of the criteria it is necessary to operate not with the system of equations but with the parameters characterizing this phenomenon. Usually the conditions of uniqueness include boundary and initial conditions, geometric characteristics of the system, and numerical values of physical constants, i.e., those parameters whose values can be selected during the experiments.

On the basis of the theory of similitude, let us find the similarity criteria for vane machines. The working medium of the pump is the fluid the compressibility of which can be disregarded. The working medium of the turbine is compressed gas. Therefore,

the parameters which characterize processes in the pump and turbine will be different. In connection with this, let us examine the similarity criterion separately for the machine operating on incompressible fluid (for example, for a pump) and for the machine operating on a compressible fluid (for example, for the turbine).

2.12.2. SIMILARITY OF PUMPS

Let us examine the case when cavitation is absent or does not affect the pressure and power of the pump. Then the process in the pump and its effectiveness will be characterized by the following parameters:

a) Geometric Parameters of the Pump

These parameters include all parameters determining the dimensions and design of the inlet, the wheel and the discharge device, including the surface roughness and structural clearances. These parameters are divided into dimensional: $D_{вх}$ (diameter of the inlet), D_2, Δ, b, etc. - with the dimensionality in meters, and dimensionless: θ (structural angles of elements), z (number of impeller vanes, number of diffuser vanes, etc.).

b) Hydrodynamic Parameters of the Pump

H - pump head in J/kg (or in m^2/s^2);
N - pump power[1] in W (or in $m^2 \cdot kg/s^3$);
G - mass of the working medium passing through the pump per unit time, in kg/s;
ω - frequency of rotation of the pump in s^{-1};
τ - characteristic time interval in s.

[1]In Section 2.12 the power and efficiency are understood as the internal power and internal efficiency (see Section 2.15).

c) Parameters of the Working Medium

ρ - density in kg/m^3;
μ - dynamic viscosity in $N \cdot s/m^2$ [or in $kg/(m \cdot s)$].

Thus, all the characteristic parameters can be expressed by dimensional units: m, s, and kg. Let us take the three parameters according to the number of the basic dimensionality. These parameters should have an independent dimensionality, i.e., such that the dimensionality of each parameter could not be expressed in terms of the dimensionality of the other two. As such parameters let us select parameters D_2 (or any other dimensional geometric parameter), ω and ρ.

The characteristic parameters as follows from the theory of similitude can be reduced to the dimensionless complexes whose quantity will be less than the quantity of the parameters themselves by the number of parameters with an independent dimensionality. In this case the n characteristic parameters give n - 3 dimensionless complexes. The dimensionless complexes are obtained as a result of the division of the characteristic parameters by the product $D_2^{\alpha}\omega^{\beta}\rho^{\gamma}$. Values of exponents α, β and γ are determined from the condition of the dimensionality of the complex.

From the geometric parameters we will obtain the following dimensionless complexes: $D_{вх}/D_2$, Δ/D_2, b/D_2, θ, z and so on. These complexes in their totality comprise the condition of the full geometric similarity of the pumps. The pumps which have identical values of the indicated complexes will be geometrically similar.

The hydrodynamic parameters, including parameters of the working medium, form the dimensionless complexes, which for geometrically similar pumps are the similarity criteria:

1) Euler's criterion $Eu = \bar{H} = \frac{H}{u_2^2}$;

2) power criterion $\bar{N} = \frac{N}{\rho\omega^3 D_2^5}$ or the efficiency of the pump η;

3) flow criterion $\bar{Q} = \frac{Q}{\omega D_2^3}$;

4) Reynold's criterion $Re = \frac{\omega D_2^2}{\nu}$;

5) criterion of homochronism $Ho = \tau\omega$.

For an example, let us give the derivation of Euler's criterion (dimensionless complex of pressure):

$$\frac{H}{D_2^{\alpha}\,\rho^{\beta}\gamma}\left[\frac{m^2/s^2}{m^{\alpha}\,\frac{1}{s^{\beta}}\,\frac{kg^{\gamma}}{m^{3\gamma}}}\right];$$

in order that the dimensionless expression would be obtained, the following equations should be valid:

$$2 - \alpha + 3\gamma = 0;\ -2 + \beta = 0;\ -\gamma = 0.$$

Solving these equations, we obtain $\alpha = 2$; $\beta = 2$; consequently, the dimensionless complex

$$\frac{H}{D_2^2\omega^2} = \text{const}\ \frac{H}{u_2^2} = \bar{H}.$$

For geometrically similar pumps the determinate criteria (see Section 2.12.1) are $\bar{Q}$, Re and Ho, and the indeterminate criteria are $\bar{H}$ and $\bar{N}$ (or η). The relation between the indeterminate and determinate criteria is recorded in the form

$$\bar{H},\ \bar{N}\ (\text{or } \eta) = f(\bar{Q},\ Re,\ Ho). \qquad (2.172)$$

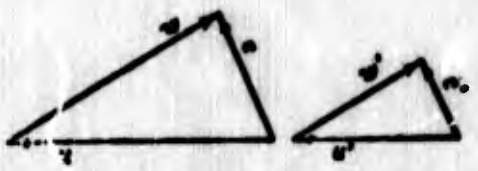

Fig. 2.73. Similar velocity triangles.

The determinate criterion $\bar{Q}$ for geometrically similar pumps is the criterion of kinematic similarity. The kinematics similarity of flows will take place when at similar points of the flows the velocities will be proportional, and their vectors will have identical directions. For flows in the rotating channels this means the similarity of the velocity triangles (Fig. 2.73). For such flows the condition of kinematic similarity will be recorded in the form

$$\frac{c}{c_M} = \frac{w}{w_M} = \frac{u}{u_M},$$

where the subscript "м" means "model."

Let us show that the flow criterion $\bar{Q}$ is actually the criterion of the kinematic similarity of geometrically similar pumps. Let us examine the cross section in front of the inlet into the centrifugal pump in which the twist of the flow is absent, i.e., $c_1 = c_{1m}$ (right triangle of velocities). Understood by velocity c_1 the average speed in the cross section.

Let us express the flow Q in terms of the velocity $c_1 = c_{1m}$ [see equation (2.3)]:

$$Q = \pi D_1 b_1 c_1.$$

Then it is possible to record that

$$\bar{Q} = \frac{\pi}{2} \frac{D_1}{D_2} \frac{b_1}{D_2} \frac{c_1}{u_1}.$$

With the equality of criteria $\bar{Q}$ of geometrically similar pumps ($\bar{Q} = \bar{Q}_M$), we obtain

$$\frac{c_1}{u_1} = \frac{c_{1M}}{u_{1M}}, \text{ or } \frac{c_1}{c_{1M}} = \frac{u_1}{u_{1M}}.$$

This indicates the fulfillment of the conditions of kinematic similarity with the equality of the flow criteria $\bar{Q}$.

The criterion of homochronism Ho characterizes the similarity of the passage of processes in time. For steady processes the need for the criterion Ho disappears. Then equation (2.172) will be recorded in the form

$$\bar{H},\ \bar{N}\ (\text{or } \eta) = f(\bar{Q},\ Re), \tag{2.173}$$

The Reynold's criterion Re, as is shown in hydrodynamics, characterizes the ratio of forces of inertia in fluid to the forces of viscosity. The equality of the Reynold's criterion Re of geometrically similar pumps determines their similarity in the relationship between the forces of inertia and forces of viscosity.

At large values of the Re criterion the effect of the forces of viscosity on the flow weakens (in comparison with the inertial forces). Usually at $Re > 10^6$ the Re criterion virtually does not affect the dimensionless complex of pressure (see source [55]), and at $Re > 10^7$ - the power criterion $\bar{N}$ and efficiency η, i.e., the region of self-similarity on Re approaches. For the region of self-similarity on the Re criterion expression (2.173) takes the form

$$\bar{H},\ \bar{N}\ (\text{or } \eta) = f(\bar{Q}). \tag{2.174}$$

With the geometric similarity of model and natural pumps and with equal or self-similar values of the Reynold's criterion, parameters of the natural pump can be found from test data of the model pump, reduced to the criterial form of (2.173) or (2.174).

For similar conditions $\bar{Q} = \bar{Q}_M$ the flow through the natural pump will be expressed by the flow of the model pump in the following manner:

$$Q = Q_M \frac{n}{n_M}\left(\frac{D_2}{D_{2M}}\right)^3 = Q_M \frac{n}{n_M}\chi^3, \tag{2.175}$$

where χ is the coefficient of the ratio of linear dimensions of the nature and the model - the scale of modeling.

In the similar conditions $\bar{Q} = \bar{Q}_M$ Euler's criterion $Eu(\bar{H})$, the power criterion $\bar{N}$ and the efficiency η will be equal for the model and nature. Then in similar conditions the pressure, the power and the efficiency of the natural pump will be determined according to the formulas:

$$H = H_M\left(\frac{\omega}{\omega_M}\right)^2\chi^2; \tag{2.176}$$

$$N = N_M\frac{\rho}{\rho_M}\left(\frac{\omega}{\omega_M}\right)^3\chi^5; \tag{2.177}$$

$$\eta = \eta_M. \tag{2.178}$$

If it is necessary to design a pump with a flow Q and pressure H, geometrically similar to the model pump with parameters Q_M, H_M and ω_M, then by means of equations (2.175)-(2.178) it is possible to find the necessary coefficient χ and the necessary frequency of the rotation ω and determine the power and efficiency of the designed pump.

In the study of pumps of the liquid-propellant rocket engines tests of models of natural pumps usually are not carried out. This is explained by the comparatively small dimensions of pumps of liquid-propellant rocket engines. However, tests on model fluids, most frequently in water are used extensively. In this case the conversion of parameters from the model fluid to the natural is also produced according to equations (2.175)-(2.178), in which it is assumed that $\chi = 1$.

In testings of the pump on the same working medium in different conditions, the similarity of the conditions is maintained, as follows from the equation (2.175) when $Q/\omega = \text{const}$. Maintained in similar conditions will be the ratios

$$\frac{H}{\omega^2} = \text{const}; \quad \frac{N}{\omega^3} = \text{const} \text{ and } \eta = \text{const}.$$

Frequently in the producing of the reduced model of the natural pump, it is not possible to insure the geometric similarity over the surface roughness and structural clearances, for example, in the packings of the wheel. In this case the incomplete geometric similarity of the model and natures or the approximate modeling are indicated.

As was already mentioned, the complexes $\bar{H}$, $\bar{N}$, $\bar{Q}$, Re and Ho retain the properties of similarity criteria only for pumps geometrically similar. For pumps of complexes not geometrically similar $\bar{H}$, $\bar{N}$, $\bar{Q}$, Re are used as dimensionless complexes and have the following names: $\bar{H}$ is the dimensionless pressure (or the coefficient of pressure), $\bar{N}$ is the dimensionless power (or normalized power), $\bar{Q}$ is the coefficient of flow and Re is Reynolds number. The dimensionless complexes $\bar{H}$, $\bar{N}$, $\bar{Q}$, and Re are widely used in the generalization of these objects not similar geometrically. Their convenience consists in the fact that with the transition to these complexes the number of variables with which it is necessary to operate during the study is decreased.

2.12.3. POWER-SPEED COEFFICIENT OF THE PUMP

Having divided $\bar{Q}^{1/2}$ by $\bar{H}^{3/4}$, having multiplied the obtained result by $2^{3/2} \cdot 193.3$[1]), we will obtain the dimensionless complex, which establishes the relationship of the three basic parameters characterizing the work of the pump:

$$n_s = 2^{3/2} \cdot 193{,}3 \frac{n\sqrt{Q}}{H^{3/4}} = 193{,}3 \frac{n\sqrt{Q}}{H^{3/4}}. \qquad (2.179)$$

The complex n_s is called the power-speed coefficient of the pump. For geometrically similar pumps the complex n_s is the dimensionless number. Having expressed the criterion $\bar{H}$ by the criterion $\bar{Q}$ and Re [see equation 2.173], it is possible to transform the expression (2.179) to the following form:

$$n_s = \text{const} \frac{\sqrt{\bar{Q}}}{f'(\bar{Q}, \text{Re})}.$$

The latter equation shows that in the case of the geometrically similar pumps having equal values or values self-similar on $\bar{H}$ of the criterion Re, the complex n_s is connected only with the flow criterion $\bar{Q}$. And since the flow criterion $\bar{Q}$ determines the kinematic similarity, then for such pumps the power-speed coefficient will be the criterion of kinematic similarity, and it can be used instead of the criterion $\bar{Q}$. For geometrically dissimilar pumps the complex $\bar{Q}$ loses the sense of the dimensionless number, and, consequently, the complex n_s loses properties of the dimensionless number.

The power-speed coefficinet n_s found wide application in the theory of pumps as a complex which connects the basic parameters

---

[1]The dimensionless coefficient 193.3 is introduced in order that the numerical value n_s, calculated according to equation (2.179), would coincide with value n_s calculated in the system of units kgf, m, s, r/min according to equation $n_s = 3.65n\frac{\sqrt{Q}}{H^{3/4}}$.

of the pump - H, Q and ω. It is used in the generalization of experimental data of geometrically dissimilar pumps - for the systematization of the standard calculated coefficients and geometric relationships of pumps. In particular, with the aid of the power-speed coefficient it is possible to characterize approximately the geometric form of the meridian section of the wheel of the pump (Fig. 2.74). According to data given in Fig. 2.74, it is possible to judge how the form of wheel is changed with an increase in n_s. With small n_s we have pumps of low power-speed factor - the meridian section of the channel of the wheel is narrow and long. With an increase in n_s the channel widens itself, the ratio b_2/D_2 increases, the diameters of the outlet and inlet are connected, ratio D_0/D_2 increases, and the wheel is gradually converted from a radial into a diagonal and then into an axial type of wheel.

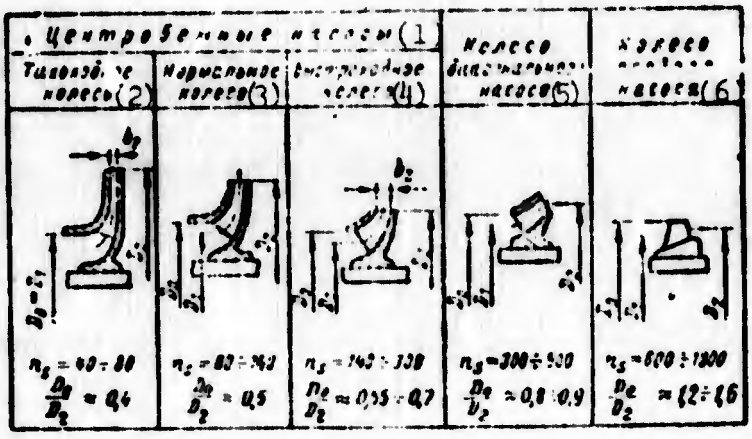

Fig. 2.74. Approximate form of the meridian section of wheels of centrifugal pumps with the different values of the power-speed coefficient (see source [9]).
KEY: (1) Centrifugal pumps; (2) Low-speed wheel; (3) Normal wheel; (4) High-speed wheel; (5) Wheel of mixed-flow pump; (6) Wheel of axial pump.

However, there is no unique relationship between the geometric relationships of the wheel (D_0/D_2, b_2/D_2 etc.) and the power-speed coefficient of the pump n_s. The geometric relationships are affected by other parameters of the pump, which are selected when designing independently of value n_s (see source [39]). Thus, for instance, to provide for high anticavitation properties of the pump, it is necessary to increase the diameter of the inlet into the wheel D_0 and width of the wheel b_1. And this at the same value n_s leads to an increase in the ratio D_0/D_2 and b_2/D_2.

In pumps of liquid-propellant rocket engines the selection of parameters which affect the geometric relationships of the wheel and the calculated coefficients is produced in a wider range than in pumps of general mechanical engineering. Thus, the angle of the outlet from the wheel of the pump of liquid-propellant rocket engines is changed from 25° to 90°, and in wheels of pumps of the general mechanical engineering - from 20° to 30°. As a result of this in pumps of liquid-propellant rocket engines the power-speed coefficient n_s only very approximately characterizes the geometric relationships of the wheel and determines the calculated coefficients. In pumps of general mechanical engineering and the dependence between the geometric relationships and the calculated coefficients can be stricter.

Let us note that for the multistage pumps the power-speed coefficient n_s is calculated not for the entire pump but for the stage of the pump. If the stage of the pump has a bilateral inlet, the value n_s is determined from the flow arriving at one inlet. The power-speed coefficient can be calculated also according to the entire flow through such a wheel (see source [40]); then it will be designated n_s^*. For stages of the bilateral inlet the relation between n_s^* and n_s is expressed thus: $n_s^* = \sqrt{2}n_s$, and for the stages of the one-way inlet $n_s^* = n_s$.

2.12.4. SIMILARITY OF TURBINES

Let us find the dimensionless number for a turbine. The work and effectiveness of the process in the stage of a turbine is characterized by the following parameters:

a) Geometric Parameters of a Turbine

Just as for the pump, the geometric parameters of a turbine include all parameters determining the dimensions and design of all elements of the turbine, including the foughness and structural clearances. These are the linear dimensions of the turbine ($D_{ср}$, $h_л$, Δ, etc.), angular dimensions ($\alpha_{1л}$, $\beta_{2л}$, etc.), and the number of blades of the wheel and nozzle box ($z_к$, $z_с$).

b) Gas-Dynamic Parameters of the Turbine

G - mass of gas passing through the turbine per unit time in kg/s; N - energy of the turbine in W (or in $m^2 \cdot kg/s^3$); $L^*_{ад}$ - adiabatic work of the turbine in J/kg (or in m^2/s^2); $L_{1ад}$ - adiabatic work of expansion in the nozzle box in J/kg (or in m^2/s^2); p^*_0 - total pressure at the inlet into the turbine in N/m^2 [or in $kg/(m \cdot s^2)$]; T^*_0 - total temperature at the inlet into the turbine in °K; ω - frequency of rotation of the turbine in s^{-1}; τ - characteristic time interval in s.

c) Characteristics of the Working Medium at the Inlet into the Turbine

ρ^*_0 - the density of the gas determined from the stagnation parameters in kg/m^3; R - gas constant in $J/(kg \cdot °K)$ [or in $m^2/(s^2 \cdot °K)$]; c_p - specific heat of the gas at constant pressure in $J/(kg \cdot °K)$ [or in $m^2/s^2 \cdot °K$)]; λ_0 - coefficient of the thermal conductivity of gas in $W/(m \cdot °K)$ [or in $kg \cdot m/(s^3 \cdot °K)$]; μ_0 - the dynamic viscosity of the gas in $N \cdot s/m^2$ [or in $kg/(m \cdot s)$].

Let us select $D_{ср}$, T_0^*, ω, and ρ_0^* as the parameters with independent dimensionality. Then from the geometric parameters we will obtain the dimensionless complexes $h_л/D_{ср}$, $\Delta/D_{ср}$, etc., $\alpha_{1л}$, $\beta_{2л}$ etc, and $z_н$, and $z_с$. These complexes in their totality comprise the condition of the total geometric similarity of turbines.

The gas-dynamic parameters and characteristics of the working medium give after the definite conversions the dimensionless complexes, which for geometrically similar turbines are the dimensionless number:

1. Flow criterion $\bar{G} = \frac{G}{\rho_0^* D_{ср}^3}$.

2. Power criterion $\bar{N} = \frac{N}{\rho_0^* \omega^3 D_{ср}^5}$ or the efficiency of the turbine η.

3. The criterion of reaction of the stage $\frac{L_{ол}}{L_{ад}^*} = (1 - \rho_т)$, where $\rho_т$ is the thermal degree of reaction of the stage (see Section 4.2.1.2).

4. $k = \frac{p_0^*}{\rho_0^* R T_0^*}$ -- coefficient which considers the distinction in the imperfect gas from the thermodynamically ideal gas, for which $\xi = 1$.

Subsequently, we will accept that the working medium of the turbine can be considered a thermodynamically ideal gas.

5. The criterion of kinematic similarity $u/c_{ад}$, where $u = \frac{\omega D_{ср}}{2}$, $c_{ад} = \sqrt{2L_{ад}^*}$.

6. The Reynold's number $Re = \frac{\rho_0^* c_{ад} b}{\mu_0}$, which determines the similarity in the relationships between the forces of inertia and forces of viscosity in the fluid which flows in elements of the turbine.

7. The criterion $k = c_p/c_v$, which determines the similarity of the relationships between the specific heats of the gas.

8. The normalized velocity

$$\lambda_{c_{1a}} = \frac{c_{1a}}{a_{kp}}, \text{ or } \lambda_{c_{1a1}} = \frac{c_{1a1}}{a_{kp}}, \text{ or } \lambda_u = \frac{u}{a_{kp}},$$

where $a_{kp} = \sqrt{2\frac{k}{k+1}RT_0^*}$; $c_{1a1} = \sqrt{2L_{1a}}$ — the adiabatic exhaust gas velocity from the nozzle box.

The normalized velocity λ is uniquely connected with the Mach number M through k. Therefore, instead of the normalized velocity it is possible to use the Mach number, for example, $M_{c_{1ад}} = c_{1ад}/a_1$, where a_1 is the speed of sound determined from the parameters at the outlet from the nozzle box at the discharge velocity $c_{1ад}$.

The criterion $\lambda_{c_{1ад}}$ (or $M_{c_{1ад}}$) characterizes the compressibility of the working medium. In conjunction with the criterion k, it determines the density ratio of the gas at similar points of geometrically similar turbines. The value $\lambda_{c_{1ад}}$ (or $M_{c_{1ад}}$) governs losses of special form, namely, the wave losses connected with shock waves.

9. The Prandtl number $Pr = \frac{\mu c_p}{\lambda_g}$, which determines the similarity of the transfer of heat in the gas. In turbines with the uncooled elements of flow area, the effect of this criterion can be disregarded.

10. The criterion of homochronism $Ho = \tau\omega$. The criterion Ho for steady states drops out of the examination.

One should note the generality of the recording of expressions for the flow $\bar{G}(\bar{Q})$, power ($\bar{N}$) criteria and Re number for vane machines (turbines and pumps).

For turbines the determinate criteria are $u/c_{ад}$, Re, k, $\lambda_{c_{lад}}$ (or $M_{c_{lад}}$) and Ho, and the indeterminate - $\bar{G}$, $\bar{N}$ (or η) and $\rho_т$. For the steady-state process of geometrically similar turbines the relationship between the indeterminate and determinate criteria is recorded in the form

$$\bar{G},\ \bar{N}\ (\text{or } \eta),\ \varepsilon_т = f(u/c_{ад},\ \mathrm{Re},\ \lambda_{c_{ад}},\ k), \tag{2.180}$$

or

$$\bar{G},\ \bar{N}\ (\text{or } \eta),\ \varepsilon_т = f(u/c_{ад},\ \mathrm{Re},\ \lambda_{c_{lад}},\ k). \tag{2.180'}$$

At large Reynolds numbers ($Re = 10^5$-10^6) the effect of the Re number on the indeterminate criteria can be disregarded, since virtually when $Re > 10^5$-10^6 the region of self-similarity on the Reynolds' number approaches. In this case equation (2.180) takes the following form:

$$\bar{G},\ \bar{N}\ (\text{or } \eta),\ \varepsilon_т = f(u/c_{ад},\ \lambda_{c_{ад}},\ k). \tag{2.181}$$

It would be possible to give similar considerations for the compressor.

If geometrically similar turbines are tested on the same gas (k = idem), then equation (2.181) will be recorded in the form

$$\bar{G},\ \bar{N}\ (\text{or } \eta),\ \varepsilon_т = f(u/c_{ад},\ \lambda_{c_{ад}}). \tag{2.182}$$

For determining the parameters of turbines, testing of turbines on model gases (air, freon) is carried out (see source [58]). In this case the geometric similarity is undoubtedly observed but values k for the natural and model gases cannot be maintained equal. This leads to the incomplete (approximate) similarity. The effect of the deviation from condition k = idem, as can be disregarded with the conversion of parameters of the

turbine $\bar{G}$, $\bar{N}$ (or η) from the model to the natural gas if the difference in values of k does not exceed 10-15%.

For geometrically dissimilar turbines the complexes $\bar{G}$, $\bar{N}$, $\rho_т$, $u/c_{ад}$, Re, k, $\lambda_{c_{ад}}$ (or $M_{c_{ад}}$) lose the sense of the dimensionless number. They are used as dimensionless complexes and have unlike the criteria, the following names: the normalized flow and power ($\bar{G}$ and $\bar{N}$), the degree of reaction $\rho_т$, the ratio of velocities $u/c_{ад}$, Reynolds number Re, the normalized velocity $\lambda_{c_{ад}}$ (or number $M_{c_{ад}}$), the adiabatic index k.

With the disturbance of the geometric similarity in the relation of roughnesses and clearances, the incomplete geometric similarity, the effect of which is considered with the conversion of data of the test of the model in nature, is discussed.

2.12.5. POWER-SPEED COEFFICIENT OF THE TURBINE

With the aid of the criteria $\bar{G}$ and $u/c_{ад}$, it is possible to make up the complex which will also be the dimensionless number of geometrically similar turbines:

$$\Pi = 2^{3/4}\bar{G}^{1,2}\left(\frac{u}{c_{ад}}\right)^{3,2} = \frac{u\sqrt{G\bar{R}_0^*}}{L_{ад}^{*3,4}},$$

or, bearing in mind the dependence (2.180') for $\bar{G}$:

$$\Pi = \frac{u\sqrt{G\bar{R}_0^*}}{L_{ад}^{*3,4}} = f\left(\frac{u}{c_{ад}}, \mathrm{Re}, \lambda_{c_{1ад}}, k\right). \qquad (2.183)$$

Equation (2.183) shows that at equal or self-similar values of Re, $\lambda_{c_{1ад}}$ and equal k, the criterion Π can be considered as the criterion of the kinematic similarity of geometrically similar turbines instead of the criterion $u/c_{ад}$.

Having multiplied and divided the criterion П by the density of gas at the outlet from the nozzle box $\rho_{1ад}$, which corresponds to the discharge velocity $c_{1ад}$, we will obtain

$$\Pi = \frac{\omega\sqrt{Q_{1ад}}}{L_{ад}^{*3/4}}\sqrt{\frac{Q_{1ад}}{g_0}} = \frac{\omega\sqrt{Q_{1ад}}}{L_{ад}^{*3/4}} = \varphi(\lambda_{c_{1ад}}, k), \qquad (2.184)$$

where $Q_{1ад}$ is the volumetric gas flow rate at the inlet into the turbine wheel calculated from parameters of the adiabatic process.

The dimensionless complex $\frac{\omega\sqrt{Q_{1ад}}}{L_{ад}^{*3/4}}$, multiplied, by analogy with expression (2.179), by 193.3, is called the power-speed coefficient of the stage of the turbine and is designated $n_{s\,т}$. On the basis of equation (2.184) it is possible to record:

$$n_{s\,т} = 193{,}3\frac{\omega\sqrt{Q_{1ад}}}{L_{ад}^{*3/4}} = \frac{\Pi \cdot 193{,}3}{\varphi(\lambda_{c_{1ад}}, k)}. \qquad (2.185)$$

Thus, the expression of the power-speed coefficient for the turbine is recorded similar to the expression of the power-speed coefficient for the pump.

The last expression makes it possible to conclude that for geometrically similar turbines the power-speed coefficient $n_{s\,т}$ under specific conditions (at equal or self-similar values of Re and $\lambda_{c_{1ад}}$ and equal k), just as criterion n_s, is the criterion of kinematic similarity.

The criterion Но and the power-speed coefficient $n_{s\,т}$ are not used for geometrically similar turbines. It finds use in the study of geometrically dissimilar turbines. Thus, the power-speed coefficient of the turbine $n_{s\,т}$, just as the power-speed coefficient of the pump n_s, is used for the characteristic of the shape of the meridian section of the turbine wheel (Fig. 2.75). With an increase in $n_{s\,т}$ the span of the blade of the wheel increases, and

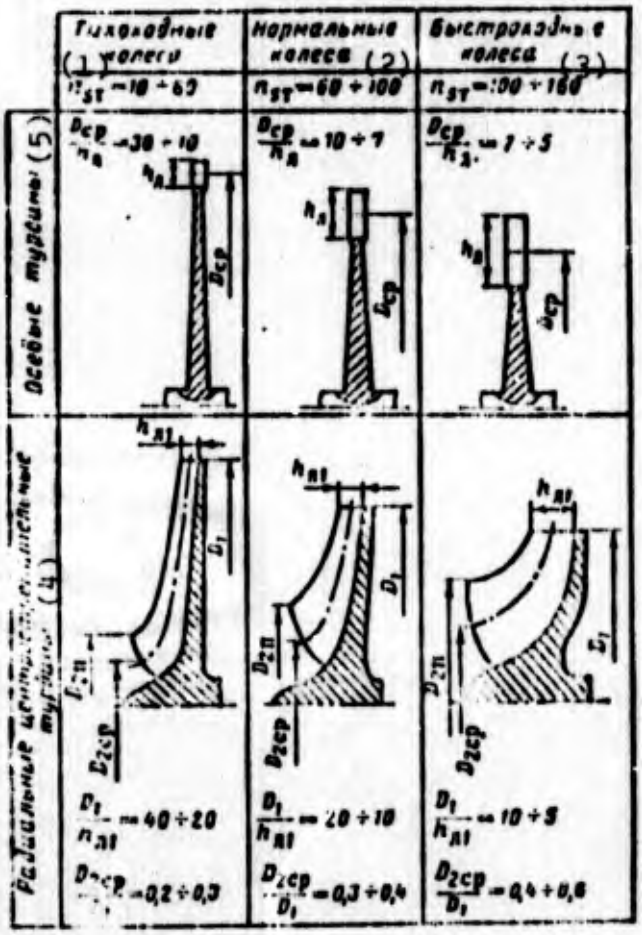

Fig. 2.75. Approximate form of the meridian section of wheels of the axial and inward-flow turbine with the different values of the power-speed coefficient.
KEY: (1) Slow-speed wheels; (2) Normal wheels; (3) High-speed wheels; (4) Radial inward-flow turbines; (5) Axial-flow turbines.

the ratio of diameters of the radial turbine D_{2cp}/D_1 increases. Turbines with $n_{s\,т} < 60$ are made, as a rule, with an incomplete gas feed along the circumference of the wheel (partial admission) for an increase in span of the blade.

However, there is no strict unique relation between the geometric relationships of the turbine wheel and value $n_{s\,т}$. The geometric relationships of the wheel are affected by other parameters which are selected in the calculation independently of $n_{s\,т}$. In order to show this, let us express the volume flow rate $Q_{лад}$ in the following manner:

$$Q_{1a1} = \pi D_{cp} h_{\pi 1} \varepsilon c_{1a1} \sin \alpha_1, \qquad (2.186)$$

where D_{cp} and $h_{\pi 1}$ are for the axial-flow turbine the mean diameter of the wheel and span of the rotor blade at the inlet, and for the radial inward-flow turbine - the outside diameter of the wheel and width of the blade on the outside diameter: ε is the degree of admission of the turbine (see Section 4.3.3.1).

Having substituted expression (2.185) into equation (2.186), we obtain after transformations

$$\frac{h_{\pi 1}}{D_{cp}} = \frac{n_{s\tau}^2}{(193{,}3)^2 \cdot 8 \cdot 2\pi \cdot \varepsilon \sqrt{1 - c_\tau \left(\frac{u_{cp}}{c_{a\tau}}\right)^2} \sin \alpha_1}.$$

The last expression shows that with an increase in the power-speed coefficient, other conditions being equal, a broadening of the channel of the wheel in the meridian section occurs. But the value of the ratio $h_{\pi 1}/D_{cp}$ is affected by the selection of the ratio of velocities $u/c_{ад}$, the degree of reaction $\rho_т$, the angle of the nozzle box α_1 and the degree of the admission ε.

Subsequently, in the study of course we will encounter coefficients $n_{s\,т}$ and n_s complexes whose use facilitates the solution of some problems of the theory.

Figures 2.74 and 2.75 show the wheels of vane machines which have different values n_s and $n_{s\,т}$. Pumps of the liquid-propellant rocket engines usually have n_s = 30-100. Moreover, corresponding to the fuel pumps are smaller values of $n_{s\,т}$ and to the oxidizer pumps, i.e., large, since the volume flow rate Q of the oxidizer pump is more and the pressure H is less than the corresponding values for the fuel pump (see Section 1.1). Therefore, fuel pumps have wheels with a narrower and longer meridian section. Autonomous turbines of liquid-propellant rocket engines, made

axial, have $n_{s\,T} < 60\text{-}80$, and the precombustion-chamber turbines - $n_{s\,T} > 80$, and therefore wheels of the precombustion-chamber axial-flow turbines have longer blades than those of the autonomous turbines.

2.13. LOSSES IN VANE MACHINES

2.13.1. CLASSIFICATION OF BASIC FORMS OF LOSSES

In an ideal vane machine without an external heat exchange and friction, the operating conditions are an ideal adiabatic process, i.e., the isentropic process which subsequently we will conditionally call the adiabatic process.

With the realization of the operating conditions in a real vane machine, irreversible losses of mechanical energy take place. Losses of mechanical energy can be divided into four groups: a) internal losses, b) high-speed outlet losses, c) losses connected with leakages of the working medium, d) mechanical (external) losses.

a) Internal Losses

By internal losses we will understand as all losses within the vane machine leading to a change in the state of the working medium. This group of losses includes the losses connected with friction and separation (in turbines and compressors upon the reaching of transonic speeds - also wave losses). The internal losses connected with the flow in vane cascades, feeds and removals will be called hydraulic. Let us call the added losses connected with work of the wheel of the vane machine disk losses. The internal losses should also include the power losses, which lead to a change in the state of the working medium in connection with its leakage, for example, the preheating of the working medium with its throttling in the clearances and with subsequent mixing with the main flow.

If the fluid overflowing through the clearances (leakage) is not mixed with the main flow, and, consequently, does not change the state of the working medium, then the losses appearing in this case will not be referred to internal losses. As an example of such losses can be the leakages of fluid through the drainage into the atmosphere.

The real processes of flow in the vane machine are processes with the heat feed, i.e., polytropic processes.

b) High-Speed Outlet Losses

The kinetic energy of the fluid, calculated from the outlet velocity in individual forms of vane machines (specifically, in turbines of liquid-propellant rocket engines), is conditionally taken as the lost energy. This energy can be considered as lost in the sense that it cannot be converted into the useful work of this vane machine. These losses, which are called high-speed outlet losses, are calculated according to the escape velocities of the gas from the vane machine:

$$L_c = \frac{c_2^2}{2}. \qquad (2.187)$$

c) Losses Connected with Leakages of the Working Medium

The power being projected or consumed by the machine also affects the loss (leakage) of the working medium. The quantity of working medium, according to which the available or useful power of the vane machine is calculated, can differ from the quantity of the working medium passing through the wheel of the vane machine, due to the presence of its clearance leakages, which separate the wheel from the housing.

In pumps and compressors part of the fluid escaping from the wheel passes along clearances and can again enter into the inlet into the wheel. The energy obtained by this part of the fluid in the wheel is dissipated and in the form of thermal energy can again be fed to the main flow of the fluid. In the turbine not all the fed quantity of gas proceeds to the wheel - part of it can escape through the axial and radial clearances between the wheel and housing. In connection with this, the effective power will be less than the energy calculated according to the fed quantity of gas.

The quantity of leaking fluid with the known designs and parameters of the machine can be designed. The value of the fluid leakage in general is calculated from the following formulas:

<u>for the incompressible fluid</u>

$$G_y = \mu f_y \sqrt{2g\Delta p_y}. \qquad (2.188)$$

where μ is the coefficient of flow of the packing slot; f_y is the cross-sectional area of the slot; Δp_y is the pressure differential for the packing;

<u>for the compressible fluid</u>

$$G_y = \mu f_y a_{kp} \rho_{kp} q(\lambda_y). \qquad (2.189)$$

where the critical parameters are calculated according to parameters of gas in front of the packing, and the given flow is taken as a function of the degree of pressure drop in the packing:

$$q(\lambda_y) = f(\pi_y).$$

Let us specify that the losses enumerated characterize the work of the separate vane machine - the pump, turbine or turbopump unit. In the examination of the engine installation as a whole, some losses of the individual vane machine cannot be losses for the installation. Thus, for instance, the high-speed energy of

the gas at the turbine exhaust can be used for producing an augmented thrust. The mechanical energy of the fluid which passed into thermal energy is a loss for the pumps but is not a loss for the engine installation as a whole, since it increases the enthalpy of the fuel in the chamber. For schemes with the precombustion-chamber turbine this consideration will be correct for the turbine.

The individual forms of the losses can be calculated, but the theory, as a rule, gives only the structure of the equation, and the calculated coefficients are basically determined by means of experimental study.

d) Mechanical (External) Losses

Mechanical (external) losses include losses in bearings, in the contact end packings of the shaft, sealing rings, the expenditure of energy to the drive of impellers, and so on.

Mechanical losses are not connected with the operating process and do not affect directly the state of the working medium of the machine, although the heat of mechanical losses by means of the heat feed can be transferred to the working medium.

The power expended on mechanical losses is called with the power of mechanical losses.

2.13.2. INTERNAL LOSSES IN VANE MACHINES

Let us examine the hydraulic losses, i.e., losses in vane cascades and in the channels of feeds and removals.

2.13.2.1. Hydraulic Losses

A. LOSSES IN VANE CASCADES

Energy losses during cascade flow can be divided into three groups, which we conditionally call: profile (primary) losses, end (secondary) losses and additional losses.

Profile losses are energy losses which appear with the flow around of plane vane cascade. Profile losses consist of:

1) boundary-layer friction;

2) losses to the formation of vortex zones with the flow around of the profile and outlet edges (separation losses);

3) wave losses connected with the passage of the flow through shock waves.

These losses in the case of axial machines and fixed elements of radial machines can be determined most accurately by a wind-tunnel test of the vane cascade.

Tip losses are losses caused by the limitation of the circular vane cascade over the span (width). These losses are revealed by a comparison of results of the wind-tunnel test of the fixed circular vane cascade and airfoil cascade with length preventing the effect of the limiting surfaces. These losses include the following:

1) friction losses in end surfaces which restrict the cascade along the span (width) and losses to the formation of pair vortices;

2) losses connected with the disturbance of the main flow with the gas leakage through the radial clearance from one side of the blade to the other in the case of blades without a shroud (Fig. 2.76);

3) fan losses, i.e., losses connected with the nonoptimal cascade density in off-design cross sections;

Fig. 2.76. Leakage of fluid (gas) in blades without a shroud.

4) losses connected with the diffusivity of the meridional cross.

For the additional losses let us refer to the losses connected with the joint operation of guide and losses connected with the rotation of the operating cascade, namely:

1) losses caused by the transiency and nonuniformity of flow (loss for the alignment of the velocity field) after the cascade;

2) losses connected with the flow which appears in the boundary layer due to the rotation of the cascade.

a) Boundary Layer and Profile Losses in Vane Cascades

Profile losses are determined by the boundary-layer flow. The flow pattern and boundary-layer losses depends both on the shape of the blade and the velocity.

In this section we will discuss the clarification of the structure of the boundary layer and examine the nature of profile losses at subsonic speeds in order to reveal the general laws governing the flow around of blades of low-pressure turbines and pumps. Features of the flow and losses at supersonic speed, characteristic for high-differential turbines, will be examined further in Chapter 4.

Figure 2.77 shows schematically the pressure distribution obtained by calculation (see source [62]) and boundary layer for the turbine and pump cascades comprised of infinitely thin profiles with an identical relative pitch and setting angle.

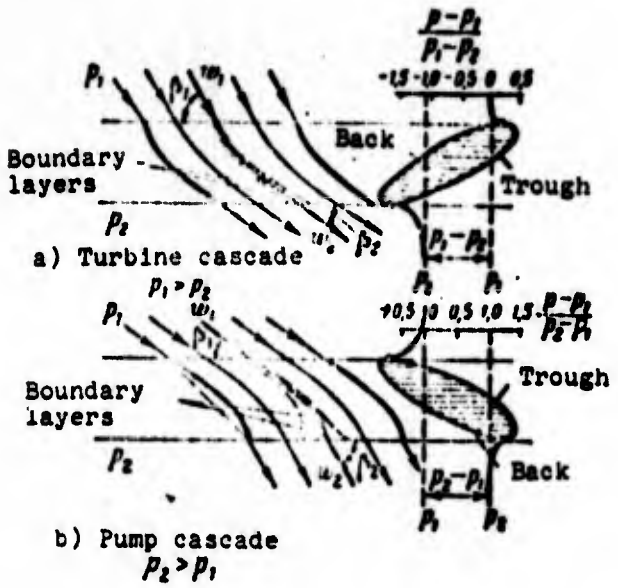

Fig. 2.77. Pressure distribution and boundary layer on blades of the turbine and pump axial cascades.

In the turbine cascade on both sides of the blade almost on the entire contour pressure decrease occurs. In the pumping cascade almost on the entire blade a pressure increase is observed. In the turbine cascade with a pressure decrease the boundary layer thickness remains small along the entire width of the blade, and separation does not appear. In a pump cascade the boundary layer thickness, due to a pressure increase along the flow, rapidly increases, and on both sides of the blade boundary-layer separation occurs. This leads to the narrowing of the cross section of the vane channel. Losses of the diffuser cascade noticeably exceed losses of the convergent cascade.

Figure 2.78 gives results of the calculation of the coefficient of losses (see source [62])

$$\zeta = \frac{p^*_{1w} - p^*_{2w}}{\rho \frac{w_{1z}^2}{2}}, \qquad (2.190)$$

where w_{1z} is the axial velocity; p^*_{1w} and p^*_{2w} are the total pressures in the relative motion.

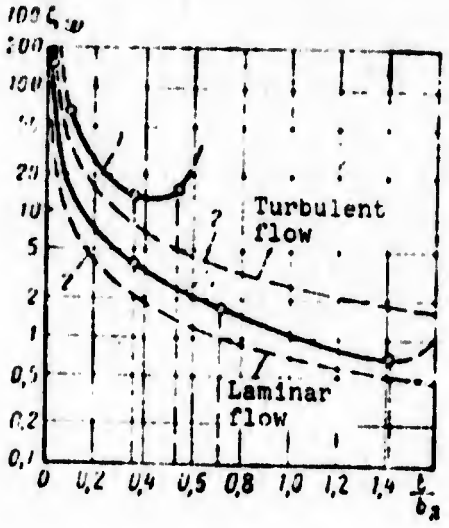

Fig. 2.78. Dependence of the loss factor on the relative pitch for pump and turbine casades and for the cascade of plates at the zero angle of incidence: 1 - pump cascade; 2 - cascade of plates; 3 - turbine cascade.

The angle of deflection (angular difference of the flow at the inlet into the cascade and at the outlet from it) in all the cascades is equal to 25°. Therefore, the pressure differential on the blade at low values of the relative pitch is low, and at $t/b_л$ the blades are less bent than at large values of $t/b_л$. At small values of $t/b_л$ the loss factor is great for all cascades, since these are the dense cascades in which the friction losses are great. At large values of $t/b_л$ an increase in the losses is connected with large bending of the blades and boundary-layer separation. The optimum relative pitch, which corresponds to the minimum losses, is less for the pump cascade (see Fig. 2.78). On Fig. 2.78 the loss factors for the turbulent and laminar conditions of the flow around the cascades of plates with the same relative pitch and with a zero angle of attack are also plotted.

Convergent cascades have loss factors greater than those with the laminar flow of the plates but less than those under turbulent conditions. Diffuser cascades have the greatest loss factors.

The frictional resistance is less with laminar flow. With the separation of the flow the losses increase, and therefore it is desirable to design blades and select operational conditions so that the laminar boundary layer would have a large extent and in order that the separation zones would be absent.

The cascades of centrifugal pumps, as a rule, are diffuser, and therefore the growth of the boundary layer and its separation are observed in these cascades more frequently. At the positive incidences common for centrifugal pumps, as shown in Fig. 2.79, the separation of flow occurs toward the end of the blade from its back side. At this place the kinetic energy of liquid particles of the boundary layer will be insufficient for the overcoming of a pressure differential.

Let us examine in more detail the pattern of boundary-layer flow in the example of certain turbine profiles.

Figure 2.80 gives a schematic representation of a boundary layer on the profile of a reactive convergent cascade at subsonic speeds. The reactive convergent cascades are used in turbines, in particular, in nozzle boxes, and in the rotor of the precombustion-chamber turbine of liquid-propellant rocket engines. The leaking-in flow is divided by the profile into two parts. Point a is called the branch point or stagnation point. In it the velocity is equal to zero, and the pressure reaches a maximum value.

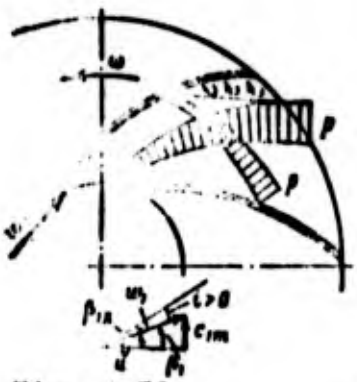

Fig. 2.79.

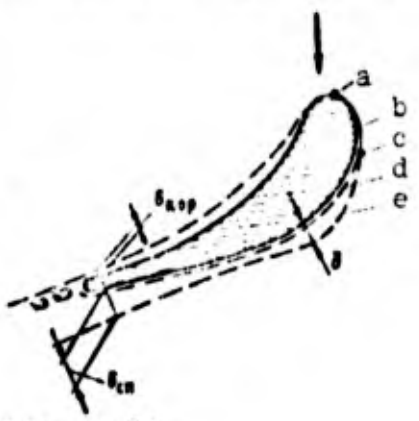

Fig. 2.80.

Fig. 2.79. Possible vortex zones with the flow around of the impeller vanes of a centrifugal pump with positive incidences.

Fig. 2.80. Schematic representation of a boundary layer on the profile of a reactive cascade: a) branch point; b) laminar boundary layer; c) transition point; d) laminar sublayer; e) turbulent layer.

On the trough, beginning from point a, the boundary layer thickness gradually increases. It is nearer to the outlet in the convergent section, where the flow is accelerated, and the boundary layer becomes thin. On the back of profile the thickness of the layer usually slowly builds up, noticeably increasing in the section of the oblique section. In this section the separation of flow from the profile is possible. Depending on the flow conditions and the profile, the boundary layer can be laminar, turbulent or mixed.

Figure 2.80 depicts the pattern of the boundary-layer flow when the boundary layer on the trough and on the back near the branch point is laminar, and then on the back it passes over to turbulent with a thin laminar sublayer. With considerable convergence of the vane channel, the transition point of the laminar boundary layer into the turbulent layer can be located in the oblique section.

In individual cascades with a low degree of reaction and at the positive angles of incidence in the outlet part of the back diffuser flow, the swelling of the boundary layer and its separation (Fig. 2.81) can take place. Separation gives rise to the formation of vortices with the return current near the surface. The vortex cores pass over into the main flow and attenuate in it. Energy is spent on the reconstruction of the vortices, and profile losses with the flow around the blades increase. At negative angles of incidence separation zones can appear also near the surface of the trough.

In turbines of liquid-propellant rocket engines active cascades (see Fig. 2.13). With the subsonic flow around the profile of the active cascade in the boundary layer usually it is also possible to distinguish three sections (Fig. 2.82): laminar (b), turbulent (c) with laminar sublayer (d), and the separation region (f). Their extent greatly depends on the angle incidence. At positive angles of incidence the transition point (c) and separation zone (f) approach the inlet.

Fig. 2.81.

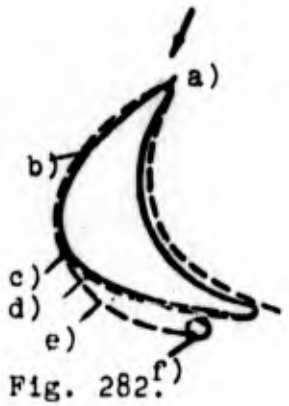

Fig. 282.

Fig. 2.81. Schematic representation of the flow with separation in the blade back.

Fig. 2.82. Schematic representation of the boundary layer on the profile of the active cascade (see designations in Fig. 2.80): f) separation zone.

A comparison of the pressure distribution along the profile of the blades of the active and reactive cascades (see Figs. 2.49 and 2.50) shows that with the flow around impulse blade a deeper lowering of pressure on the blade back and a great peak of pressure on the side of the trough at the inlet into the blade are observed. With such a pressure distribution in the trailing edge of the impulse blade there takes place the diffuser flow, which is accompanied by the detached flow. At a small angle of the inlet the diffuser region appears at the outlet part of the back.

The Reynolds number affects the losses with the flow around the blade profiles ($Re = \frac{wb_n}{\nu}$). The less Re (when $Re \leq 10^5$), the more the losses. As a rule, at numbers $Re > 10^5$ the roughness more noticeably affects the magnitude of losses than do the flow conditions determined by the Re number. In vane machines of liquid-propellant rocket engines, usually $Re > 10^5$.

With large roughnesses the losses in the cascade noticeably increase. At the mean-square height of the roughnesses to 5 um the quality of the finish has little effect on losses in the

cascade, since the roughnesses of the surface are covered by a laminar sublayer (see source [45]). Usually the flow area of the pump, the internal surfaces of the housing and disks of the wheel are made with a finish of V6 (average height of the roughness is 10 μm) and above. After casting such a finish is reached by special treatment. An increase in the purity leads to an increase in the efficiency of the pump. Thus, a decrease in the roughness from 135 down to 20 μm can lead to an increase in efficiency of 6-10% (see source [51]). The flow area of the turbine, as a rule, is made with a purity of V7 (average height of the roughness is 6.3 μm) and above, and surfaces of the disk and housing are made with a purity of V6. The less the absolute dimensions of the vane machine, the greater the surface roughness is necessary.

Considerable losses appear in the flow around the outlet edges. The edge losses, commensurable with friction, refer also to profile losses. Emerging from the cascade, the flow undergoes sudden expansion and behind the edge vortex separation zones appear (see Fig. 2.80). The thicker the trailing edge and the denser the cascade, the greater the edge losses. The flow escaping from the cascade is considerably nonuniform (Fig. 2.83).

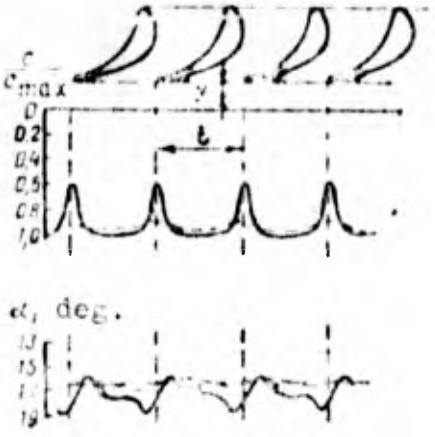

Fig. 2.83. Flow parameters at the outlet from the cascade: —— y/t = 0.1; ---- y/t = 1.8.

b) End (Secondary) Losses

Let us examine in succession all the losses which refer to end losses.

1) Losses of friction on cylindrical surfaces which limit the vane channel in height. Pair vortex.

The friction on the external and internal limiting surfaces leads to the stagnation of the velocity in these walls, the presence of the velocity gradient and the developed boundary layer; in general the frictional effect on the external and internal surfaces is different, but the basic regularities should be similar. These friction losses are determined by the flow conditions and the surface condition and can be estimated according to common equations taking into account the Reynolds number. In the total balance of losses their portion is considerable only in the small height of the blade. The presence of friction on the limiting surfaces with flow along the vane channels, which are always curvilinear, causes parasitic vortex flows called pair vortices.

The pressure distribution along the vane channel of the cascade (for an example, the turbine cascade is taken) will be different on the average by the height of the cross section (I-I in Fig. 2.84) and for the restricting surfaces (cross sections II-II and III-III in Fig. 2.84). For greater definition an examination is conducted for the cascade which has a ring which encompasses the blades and rotates together with them (the so-called shroud).

Near the surfaces which limit the blade in height, the rate of flow will be less and a pressure increase on the blade face of these surfaces will also be less than in the middle of the channel. Consequently, acting on the particles of gas which are located at

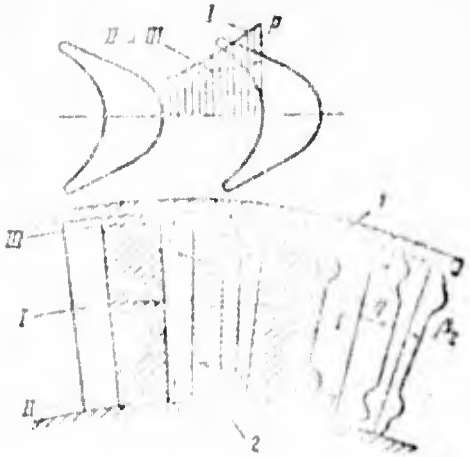

Fig. 2.84. Diagram of secondary flow in the vane channel: 1 - boundary layer; 2 - diagram of relative velocity (conditionally turned into the plane of the drawing).

the blade face near the limiting face surfaces (cross sections II-II and III-III) in a radial direction will be the pressure differential moving them towards the limiting surfaces. By virtue of the continuity of flow along the limiting surfaces, motion of the boundary layer of gas from the blade face to the back will begin. This moving boundary layer is braked by the main flow and will swell near the blade back (see Fig. 2.84), where conditionally shown to the right is the boundary-layer thickness). In turn, this boundary layer moving along the limiting wall pushes aside the boundary layer on the blade back toward the middle of the channel. As a result the thickened boundary layer is separated from the surface of the back in the form of two cores.

[illegible] nature of the motion of the boundary layers leads to the appearance in the blade channel of two differently directed vortex flows, called pair vortices. The pair vortex is a parasite vortex flow. Let us give [illegible] representation about the [illegible] on the main flow is a simplified [illegible] three-dimensional flow in the vane channels [illegible].

[illegible] of weight in the reconstruction of these [illegible] reasonable value. On Fig. 2.84 is [illegible] picture of the change in

efficiency of the streams η and outlet angles of the flow β_2. The greatest losses are observed at places of the boundary layer thickening on the blade back. At these places the outlet flow angle increases, which is explained by the boundary-layer separation. The less the span of the blade, and the more its width, the greater the part of the main flow is occupied by a pair vortex and the greater the relative percentage of power losses.

Losses to the pair vortex sharply increase when pair vortices are linked with each other. In this case the magnitude of the losses begins to depend on the relative span of the blade. This begins with relation $h_л/b_л \leq 1\text{-}1.5$. Because of this the short turbine blades of the TU of the liquid-propellant rocket engine must be made quite narrow.

Losses to the pair vortex are connected with the presence of the pressure gradient across the vane channel. Therefore, all factors which facilitate an increase in the pressure differential on the blades simultaneously increase the losses to secondary flows. Such factors are, for example, the curvature of the profile, being characterized by angle $[180° - (\beta_{1л} + \beta_{2л})°]$, and the positive angles of incidence.

The effect of the span of the blade on the level of the losses can be observed in Fig. 2.50b, where the loss factor for different relative spans are plotted. A reduction in the span of the cascade sharply increases the losses.

In vane channels of pumps there also appears the pair vortex - the parasitic vortex motion caused by the effect of the walls restricting the channel over the height or width.

Figure 2.85 shows the pair vortex in the cross section of the vane channel of the centrifugal pump. The pair vortex is removed by the main flow.

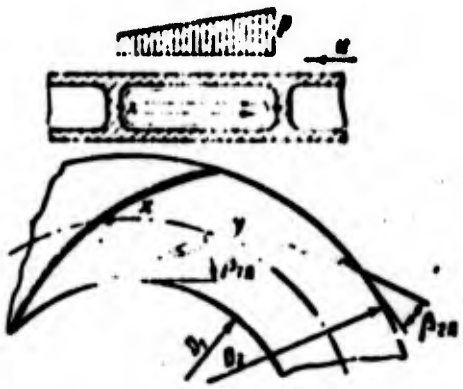

Fig. 2.85. [illegible] channels of [illegible] wheel.

2) Losses connected with leakage through the radial clearance.

The nature of secondary flows in the presence of a radial clearance becomes complicated. Gas leaks through the radial clearance from the face, i.e., from the cavity of high pressure, to the blade back (see Fig. 2.76). Here the flow of the leakage gas under the action of the pair vortex and the main flow is convoluted, forming an unpaired vortex. It is advantageous to have a closed radial clearance, i.e., to use shrouds for the blades of the vane channel on the periphery (see Fig. 2.84) and closed wheels of centrigual pumps (see further Fig. 3.8a).

3) The fan losses which appear in the long vane rings in connection with the fact that the optimum blade pitch (see 'd') is selected only for any one calculated cross section.

Fan losses can be lowered, using blades with a variable chord, for example, for axial machines - with a chord increasing on the radius.

4) Losses connected with the diffusivity of the meridional section of the blades.

For the smooth outline of the flow area of the blade machines, it is frequently necessary to introduce the diffusivity of the meridian section of the rotor blades (Fig. 2.86). The introduction of diffusivity leads to added losses. The scavenging of stationary blades showed that the secondary losses depend on the expansion angle of the meridian section λ.

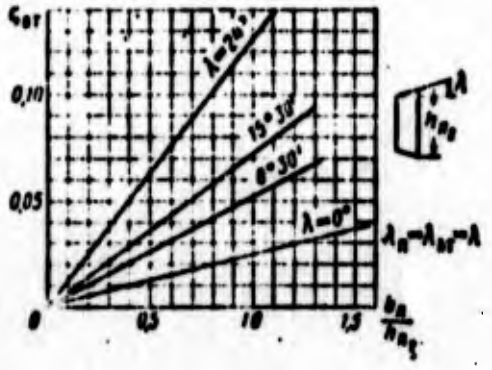

Fig. 2.86. Dependence of secondary losses on $b_л/h_{л_2}$ at different angles of diffusivity of the meridian section (see source [10]).

Figure 2.86 gives test data of blades with a shroud when $\lambda_л = \lambda_{вт} = \lambda$. Plotted along the axis of the ordinates is the coefficient of secondary losses; $b_л$ is the width of the blade; $t_л/b_л = 0.65$ - the relative pitch of the cascade; $\beta_{1л} = 35°$ - inlet angle; $\rho_т = 0$-15% - reaction of the cascade. The boundary layer in the limiting surfaces in the direction of the gas flow, as a result of diffusivity, is thickened, and detached flow is possible.

The effect of the height of the cascade on losses can be judged from Fig. 2.50b, where experimental data on the loss factor at a different value of the relative height ($h_{л_2}/D_{ср}$) are given.

c) Additional Losses

1) Losses connected with the transiency of the flow.

Losses to the transiency of flow are connected with the balancing of the field of velocities and pressures in the flow of

gas which escapes from the cascade. The distrubance of the axial symmetry of the cascade flow, which can take place in off-design conditions or technological errors during the manufacture of cascades or feeding and discharge channels, also leads to a noticeable increase in the losses.

The transiency of the flow is explained, furthermore by the periodic change in the arrangement of operating cascade relative to the guide (see source [44]). Flowing about operating cascade in this case is the nonuniform flow due to the presence of edge traces with a periodicity depending on the number of the guide vanes and frequency of rotation of the rotor (see Fig. 2.83).

2) Losses connected with radial leakage due to the rotation of the cascade.

With rotation there can arise losses from the leakage in the operating cascade, which appears under the action of inertial forces. Acting on the fluid which flows on the cascade in relative motion are the centrifugal and Coriolis forces of inertia.

In axial machines the Coriolis force of inertia acts in a radial direction, coinciding with the centrifugal force of inertia (see Fig. 2.32). The rotation of rotor blades can change the magnitude of the profile and secondary losses in view of the effect of the centrifugal and Coriolis forces of inertia on the boundary layer.

d) Coefficients Which Evaluate Losses in Vane Cascades

Usually losses in the vane cascades are estimated by a lowering of the total pressure (stagnation pressure), although other coefficients are used [see, for example, formula (2.190)].

The ratio of the total pressure at the outlet from the cascade to the total pressure at the inlet into it is called the coefficient of the total pressure

$$\sigma = \frac{p_2^*}{p_1^*}. \qquad (2.191)$$

In turbines it is accepted to define losses in cascades by velocity factors. In nozzle cascades the velocity factor for the stream is the ratio of the real discharge velocity to the adiabatic velocity:

$$\varphi = \frac{c_1}{c_{1ад}}.$$

In the operating cascades the velocity factor for the stream is the ratio of the real outlet velocity to the adiabatic:

$$\psi = \frac{w_2}{w_{2ад}}.$$

With nonuniform flow the velocity factor is ratio of the averaged real velocity to the velocity in the absence of losses. Averaging for the determination of the flow rate, momentum and kinetic energy should be produced differently, since the flow rate is proportional to the first stage, the momentum proportional to the second, and the energy proportional to the third stage of the velocity.

In experiments, depending on the procedure taken for the tests each of these three velocity factors can be determined. Their magnitude, generally speaking, will be different, but usually this distinction is small.

Between coefficients σ and ϕ or ψ in gas dynamics the following relation is established:

$$\sigma_1 = \left[\frac{1 - \frac{k-1}{k+1}\left(\frac{\lambda_{c_1}}{\varphi}\right)^2}{1 - \frac{k-1}{k+1}\lambda_{c_1}^2}\right]^{\frac{k}{k-1}} \frac{\pi(\lambda_{c_{1ad}})}{\pi(\lambda_{c_1})}, \qquad (2.192)$$

where

$$\pi(\lambda_{w_{2a}}) = \frac{p_1}{p_0^*} \quad \text{and} \quad \pi(\lambda_{w_1}) = \frac{p_1}{p_1^*};$$

$$\varphi = \left[\frac{1 - \frac{k-1}{k+1}\left(\frac{\lambda_{w_2}}{\lambda_{w_{2a}}}\right)^2}{1 - \frac{k-1}{k+1}\lambda_{w_2}^2}\right]^{\frac{k}{k-1}} = \frac{\pi(\lambda_{w_{2a}})}{\pi(\lambda_{w_2})}. \qquad (2.193)$$

The loss factor in the cascade can be also determined according to the following equation:

$$\zeta_1 = 1 - \frac{c_1^2}{c_{1a}^2} = 1 - \varphi^2 \qquad (2.194)$$

or

$$\zeta_2 = 1 - \varphi^2. \qquad (2.195)$$

The efficiency of the cascade is determined by the ratio of the squares of velocities:

$$\eta_1 = 1 - \zeta_1 = \varphi^2. \qquad (2.196)$$

Profile losses can be determined by the scavenging or spill of airfoil cascades. The sum of the profile and secondary losses for axial machines is determined by the scavenging or spill of circular cascades. All losses in the cascades can be determined only by way of the measurement of the fields of total pressures in the operating machine, which is always associated with considerable difficulties. In the calculation of vane machines the additional coefficients, considering the end (secondary) losses in the cascades are frequently introduced. The determination of these coefficients and their numerical value will be given in further sections.

B. LOSSES IN FEEDS AND REMOVALS

Losses in the feed and removal channels can bead to two forms of losses: losses of friction and losses from the local resistances.

The losses of friction in complex channels of feeds and removals can be defined as losses in pipelines of arbitrary form by means of the determination of losses in the equivalent pipeline of round cross section with the same hydraulic radius.

The diameter of such a tube will be found from the known equation

$$D_r = \frac{4F}{\Pi}, \tag{2.197}$$

where F is the cross-sectional area of the channel; Π - wettable perimeter of the channel.

Then the losses of friction in the channel (when ρ = const or M < 0.3-0.4) will be equal to

$$\frac{\Delta p^*}{\rho} = \frac{p_1^* - p_2^*}{\rho} = \lambda \frac{l}{D_{r.cp}} \frac{c_{cp}^2}{2} \left[\frac{J}{kg}\right], \tag{2.198}$$

where c_{cp} is the average rate of the flow; l - length of the channel; ρ - the average density; $D_{r.cp}$ the average hydraulic diameter.

For channels λ is found depending on the Reynolds number and relative roughness of walls of the channel.

When $Re > 5 \cdot 10^3 \left(Re = \frac{c_{cp} D_r}{\nu}\right)$

$$\lambda = 0{,}316 \frac{1}{Re^{0.25}} - \text{for the smooth walls}$$

and $\lambda = \frac{1}{\left(1.74 + 2\lg\frac{D_r}{2k}\right)^2}$ for the rough walls,

where k is the absolute roughness.

Losses connected with the local resistance include losses to the local change in the cross sections, losses to the mixing of the streams, losses to the rotation of the flow, and losses connected with the diffusivity of the channel. For example, in centrifugal pumps attributed to the local losses can be losses to the rotation in the case of - elbow-shaped or semispiral feed (see further Fig. 3.2) and losses to the mixing at the outlet of the flow from the wheel into the spiral removal.

Losses to local resistances are estimated according to the general equation

$$\frac{p_1^* - p_2^*}{\rho} = \zeta \frac{c^2}{2} \left[\frac{J}{kg}\right], \qquad (2.199)$$

where ζ is the coefficient of local resistance; c is the characteristic rate of flow in the channel (usually in front of the local resistance).

Specific values of coefficients of local resistances are found experimentally. The experimental data are classified in handbooks. For vane machines of liquid-propellant rocket engines little experimental data on coefficients of local losses is published. Some data will be given subsequently - with the presentation of specific material on pumps and turbines of liquid-propellant rocket engines.

An estimate of channel losses can be produced also by means of coefficients of total pressure [see formula (2.191)].

2.13.2.2. Disk Losses

A. LOSSES OF DISK FRICTION

In the rotation of a wheel disk of a vane machine additional energy is expended; let us call it the power of disk losses.

With the rotation of the disk, the fluid (gas) in the clearance also begins to be rotated as a result of the action of forces of friction. The diagram of the circular velocity components of flow in the clearance between the wheel disk and the housing is given in Fig. 2.87. The presence of a circular velocity component in the fluid in the clearance leads to the appearance of radial flow of the fluid in the clearance. The approximate form of the flow line in the meridian plane of the radial wheel is shown in Fig. 2.88.

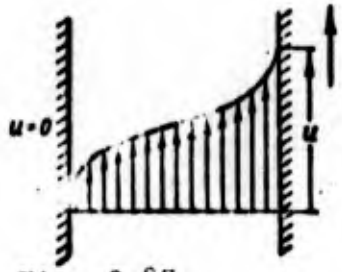

Fig. 2.87.

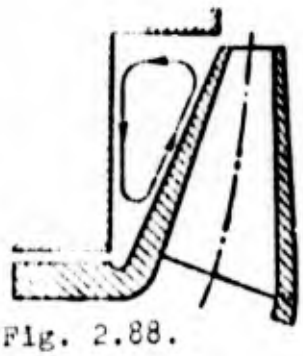
Fig. 2.88.

Fig. 2.87. Diagram of the circular velocity components of flow in an axial clearance between the wheel disk and housing.

Fig. 2.88. Flow line of fluid in the axial clearance between the wheel disk and housing.

The antitorque moment of the wheel of the vane machine appears as a result of friction. Imparted to the fluid is the moment and, since the twisted fluid moves toward the periphery and new portions of the fluid will continuously approach the rotary disks, the expenditure of energy to friction in view of the pumping action of the disks constitutes a noticeable value.

Let us derive the dependence of the power of friction of the disk on parameters of the wheel for an incompressible fluid.

Conditions of friction of the disk can be considered turbulent, and then the tangential stress τ will be proportional to the product of the density of the fluid and the kinetic energy calculated according to the relative velocity of the surface and fluid. In this case the relative velocity of the fixed fluid and wheel is the circular velocity, and τ will be equal to

$$\tau = C'_{тр.д} \rho \frac{u^2}{2} \left[\frac{N}{м^2}\right],$$

where $C'_{тр.д}$ is the coefficient of friction; ρ is the density of the fluid in the clearance.

The moment of friction can be found by means of the integration:

$$M_{тр.д} = \int_0^{r_2} \tau r 2\pi r dr,$$

where r_2 is the external radius of the disk, or

$$M_{тр.д} = \pi C'_{тр.д} \rho \omega^2 \int_0^{r_2} r^4 dr.$$

After integration we obtain

$$M_{тр.д} = C_{тр.д} \rho r_2^5 \omega^2 \ [N \cdot м], \qquad (2.200)$$

where $C_{тр.д}$ is the coefficient of friction of the disk, which includes all the constants.

The power of the disk friction is determined from the equation

$$N_{тр.д} = 2 M_{тр.д} \omega \ [W] \qquad (2.201)$$

(coefficient 2 considers the friction along both sides of the disk), or

$$N_{тр.д} = 2C_{тр.д}\rho r_2^5\omega^3 \text{ [W]}. \quad (2.202)$$

As follows from equation (2.202), the power of friction of the lateral surfaces of the wheel is proportional to the fifth power of the radius and to the cube of the angular velocity.

The coefficient of friction $C_{тр.д}$ is determined depending on the Reynolds number. For smooth disks, assuming that the angular velocity of the rotation of the fluid in the clearance is equal to half of the angular velocity of the wheel, taking the experimental data into account, we will obtain for $Re > 10^5$ (see source [42])

$$C_{тр.д} = \frac{0{,}039}{\sqrt[5]{Re}}. \quad (2.202a)$$

The Re number is calculated according to the equation

$$Re = \frac{r_2^2\omega}{\nu}. \quad (2.202b)$$

B. OTHER LOSSES REFERRED TO THE DISK

Let us refer to the group of losses conditionally called the disk, apart from the losses of disk friction, also losses connected with the feed of the working medium to the wheel not along the entire circumference but only on part of it (losses to admission, see Section 4.5.2.2). Let us also refer some power losses connected with the work of the wheel in off-design conditions to disk losses, for example, in pumps of the loss of "hydraulic stagnation" with low flow rates (see Section 3.1.2.2).

The presence of disk losses in pumps increases the required driving power. The presence of disk losses in turbines decreases the effective power of the turbine. Disk losses turn into heat and, if we disregard the external heat exchange, then this heat

will be entirely fed to the working fluid. The name "disk losses" means that these losses refer to the rotor (to the stage) as a whole. The expenditure of work to disk losses will be determined by the equation

$$l_{\text{д}} = \frac{N_{\text{д}}}{G} \left[\frac{\text{J}}{\text{kg}}\right]. \qquad (2.203)$$

2.14. BASIC THERMODYNAMIC RELATIONSHIPS AND THERMAL DIAGRAMS USED IN THE EXAMINATION OF PROCESSES IN VANE MACHINES

Let us examine the basic thermodynamic relationships for processes in vane machines occurring with friction and, as a result of this, with the heat feed to the fluid. In this case, for the sake of simplicity in the calculations, we will assume that the inlet velocity of the vane machine is equal to the outlet velocity of vane machine ($c_1 = c_2$).

By the work of resistance L_{comp} [see equation (2.78)] we will understand as all the internal losses.

For flow without external heat exchange

$$dl_{\text{comp}} = dQ.$$

Having used the equation of the first law of thermodynamics and examining the vane machine as a whole, we will obtain

$$i_2 - i_1 = \int_1^2 v\,dp + l_{\text{comp}}. \qquad (2.204)$$

By comparing equation (2.204) with (2.77) when $c_1 = c_2$, and designating the energy transmitted to the fluid or selected from the fluid (taking into account the work of friction), as the internal work of the vane machine, respectively, for the pump (compressor) we will obtain

$$H_{\text{н}} = i_2 - i_1 = \int_1^2 v\,dp \quad L_{\text{...}}; \tag{2.205}$$

for the turbine

$$L_{\text{т}} = i_1 - i = \int_2^1 v\,dp \quad L_{\text{...}}. \tag{2.206}$$

For the gases which satisfy the equation of state pv = RT, for the adiabatic process (pv^k = const) we will obtain

$$H_{ад} = i_{2д} - i_1 = c_p(T_{2д} - T_1) = \int_1^{2д} v\,dp =$$

$$= \frac{k}{k-1}(p_2 v_{2д} - p_1 v_1) = \frac{k}{k-1} RT_1 \left[\left(\frac{p_2}{p_1}\right)^{\frac{k-1}{k}} - 1\right]; \tag{2.207}$$

$$L_{ад} = i_1 - i_{2д} = c_p(T_1 - T_{2д}) = \int_{2д}^1 v\,dp =$$

$$= \frac{k}{k-1}(p_1 v_1 - p_2 v_{2д}) = \frac{k}{k-1} RT_1 \left[1 - \left(\frac{p_2}{p_1}\right)^{\frac{k-1}{k}}\right]. \tag{2.208}$$

For the pump (compressor) the adiabatic pressure is the minimum pressure which must be transmitted to the fluid for a pressure increase up to the assigned magnitude. For the turbine the adiabatic work is a theoretical available work. In turbines as theoretical available work accepted more frequently is the work of the adiabatic expansion from the input stagnation parameters to the output static parameters:

$$L_{0,1} = i_1^* - i_{2д}. \tag{2.209}$$

This work is the maximum theoretical work with the full use of the outlet velocity.

The real processes are polytropic processes with the heat feed as a result of the work of friction. With the heat feed the volume of compressible liquid (gas) increases. In this case

the work of the expansion and work of compression also increase. This is visually evident with the representation of the process in the vane machine in the pv-diagram.

In order to explain the features of the occurrence of processes in turbines operating on gases and vapors and in pumps for the compressible and incompressible fluids, let us examine in p-v coordinates the phase state for the component in the most general case (Fig. 2.89). The line A-кр-B is a boundary curve. The curve A-кр determines the specific volume of the saturated fluid, and curve кр-B - the specific volume of the saturated vapors (point "кр" is the critical point). The remaining lines are isotherms. At high temperatures the overheated steam medium is close to the state of an ideal gas. The isotherm in this case is depicted in coordinates p-v as a hyperbola: its equation is pv = RT.

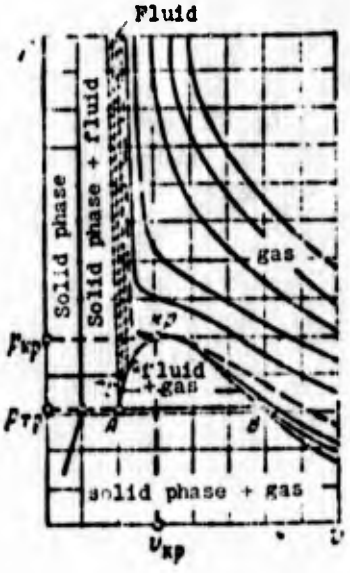

Fig. 2.89. Representation of isotherms in coordinates p-v for different phases of the substance.

At less temperatures the vapors do not behave as ideal gases. For the equation of the isotherm of vapors (imperfect gas) many equations are proposed. Typical for this region is the equation of van der Waals:

$$\left(p+\frac{a}{v^2}\right)(v-b)=RT, \qquad (2.210)$$

where a and b can be considered as constants only in the small temperature range.

In general

$$a = f(p, T) \text{ and } b = f(p, T).$$

The region shaded in Fig. 2.89 is the region of the fluid medium where a change in the pressure barely leads to a change in the specific volume, although a certain decrease in the volume almost always takes place. For individual fluids, for example, for hydrogen, the compressibility, i.e., a change in the specific volume, is considerable. In turbines of liquid-propellant rocket engines usually used as the working medium are combustion gases and overheated vapors at such parameters when their state is close to the state of an ideal gas. Sometimes (for example, when vapors of liquid metal are utilized) it is necessary to design the turbine for the operating with moist vapor.

Let us examine the representation in the pv-diagram of the process in a turbine operating on gas or steam (Fig. 2.90).

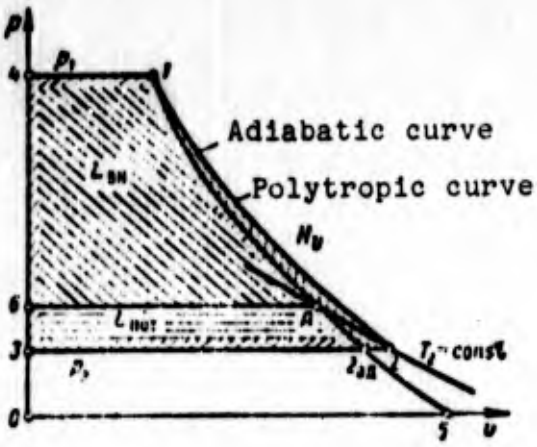

Fig. 2.90. Representation of the process in the turbine in coordinates p-v.

The adiabatic work of the turbine in coordinates p-v as a difference in enthalpy $i_1 - i_{2_{ад}}$ will be depicted as the area $1\text{-}2_{ад}\text{-}3\text{-}4$, where line $1\text{-}2_{ад}$ corresponds to the adiabatic curve.

The real process of the expansion occurs with the heat feed: the line depicting this process will be the polytropic curve pv^n with the index $n < k$. The line of polytropic curve 1-2 with the heat feed passes more slopingly than does the adiabatic curve. The specific volumes additionally increase as a result of the heat feed. Consequently, the work of expansion of the gas (let us call it conditionally polytropic)

$$l_{пол} = \int_1^2 v\,dp \tag{2.211}$$

will be depicted in coordinates p-v with an area 1-2-3-4. It is the actual available work. This work is greater than work of the adiabatic expansion:

$$l_{пол} > l_{ад}.$$

The difference in the polytropic and adiabatic works is the additional work of the volumetric expansion, obtained as a result of the heat feed from the work of friction H_v:

$$l_{пол} = l_{ад} + H_v, \tag{2.212}$$

where H_v is the part of the work of friction being returned, which is realized in the form of an additional work of expansion, and therefore the designation corresponds to an increase in energy (letter H). Usually H_v is 15-20% of the entire work of friction.

The difference L_{conp} and H_v is the irreversible lost part of the entire work of friction:

$$l_{пот} = L_{conp} - H_v. \tag{2.213}$$

The difference in entire available work of expansion $L_{пол}$ and the entire work of friction L_{conp} will determine the internal work of the turbine [see equation (2.206)]:

$$l_{ад} - L_{conp} = l_1 - l_2 = L_i. \tag{2.214}$$

From equations (2.212), (2.213) and (2.214) it follows that

$$l_{вн} = l_{ад} - l_{пот}. \qquad (2.215)$$

The internal work of the turbine can also be shown in coordinates p-v. The enthalpy i in coordinates p-v (see Fig. 2.90) will be graphically depicted as the area 0-4-1-5; the enthalpy i_2 - the area 0-6-A-5, where point A is found by the intersection of the isotherm T_2 with the adiabatic curve passing through point 1. The area 1-A-6-4 is proportional to the difference of the enthalpies $i_1-i_2 = L_{вн}$. The area 3-6-A-$2_{ад}$ corresponds to the real expenditure of mechanical energy to friction $L_{пот}$. The total negative work is equal to the sum of areas 3-6-A-$2_{ад}$ and 1-2-$2_{ад}$.

In practice for calculations of vane machines more frequently is-diagrams are used, although in them all components of the balance of works are not shown, in particular, the additional work of the volumetric expansion is not shown.

In many cases the use of is-diagrams makes it possible to show most simply and visually the process in the blade machines. For such working media, as steam, imperfect gases and liquid, the use of an is-diagram considerably simplifies the calculations, since the relationship of the parameters for these substances is frequently difficult to represent in an analytical form. The is-diagrams are used especially extensively for calculations of a turbine.

Figure 2.91 shows the representation of the process in the turbine in i-s coordinates. Point 1 corresponds to the static parameters of the inlet, and point 1* - to the stagnation parameters of the inlet. Point $2_{ад}$ characterizes the state of the gas with its adiabatic expansion up to pressure p_2, point $2^*_{ад}$ - the state of the gas at the turbine exhaust with the adiabatic process according to the stagnation parameters. Point 2 corresponds to the actual process of the gas expansion (taking into account all the internal losses).

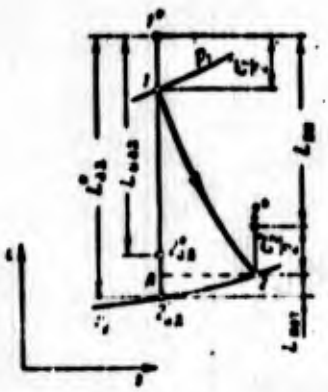

Fig. 2.91. Representation of the process in the turbine in i-s coordinates.

The difference in enthalpies $i_1^* - i_{2_{ад}}$ characterizes the available adiabatic work $L_{ад}^*$ (point A in Fig. 2.90 corresponds to point A in Fig. 2.91). The difference in enthalpies $i_1^* - i_{2_{ад}}^*$ corresponds to the energy $L_{u\ ад}$ which would be selected for the gas and transferred to the wheel during an ideal adiabatic process.

The segment $i_{2_{ад}}^* - i_{2_{ад}}$ characterizes the energy loss with an outlet velocity in an ideal turbine. The difference in the enthalpies $i_1^* - i_2^*$ characterizes the internal work of the turbine $L_{вн}$. Work $L_{вн}$ corresponds to the total variation in the gas energy. (When $c_1 = c_2$, as was accepted in the examination of process in the pv-diagram, $L_{вн} = i_1 - i_2$).

Segment $2\text{-}2_{ад}$ corresponds to the mechanical energy $L_{пот}$ lost in connection with the presence of the work of friction. Work L_u, transmitted by the gas to the wheel, which is determined by the Euler equation (2.30), is more than work $L_{вн}$ by the magnitude of the work of disk losses (including losses with leakages):

$$L_u = L_{вн} + L_д. \qquad (2.216)$$

Let us examine the basic thermodynamic relationships for pumps (compressors). The most general case is the work of the pump on a compressible fluid, but the majority of the pumps operates on virtually an incompressible fluid.

The pump of liquid-propellant rocket engines, as a rule, pumps through an incompressible liquid. The representation of its process in coordinates p-v is presented in Fig. 2.92. Line 1-2 is simultaneously an isotherm, adiabatic curve and isochor. The area 1-2-3-4 is proportional to the pump pressure:

$$H = \frac{p_2 - p_1}{\rho} \left[\frac{J}{kg}\right].$$

The work of friction is not connected with an increase in the volume and can conditionally be shown as the area 1-1'-4'-4. Then in the pv-diagram the area 1'-2-3-4' will correspond to the theoretical pressure equal to the adiabatic pressure.

For the pump which pumps over the compressible fluid, for example, liquid hydrogen (and for the compressor), the process in the pv-diagram will be depicted in the manner which it is shown in Fig. 2.93.

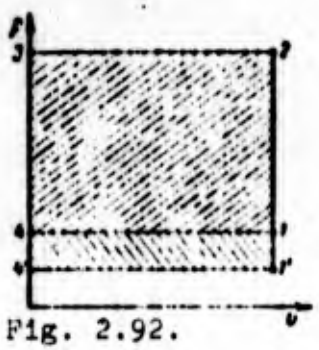

Fig. 2.92.

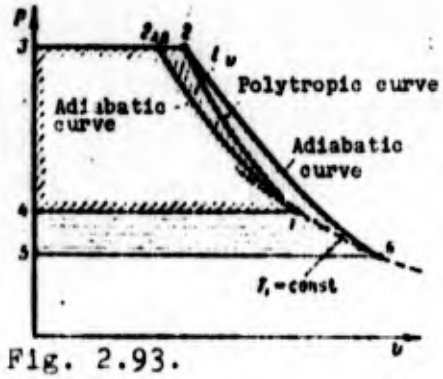

Fig. 2.93.

Fig. 2.92. Representation in coordinates p-v of process in the pump (for an incompressible fluid).

Fig. 2.93. Representation in coordinates p-v of the process in the pump (compressor) for a compressible fluid.

The area 1-$2_{ад}$-3-4 corresponds to the minimum work of compression (adiabatic). The heat feed as a result of losses of friction (including disk losses and heating as a result of the return of

leakages) increases the volume of the fluid being pumped through and additionally increases the work of the pump (compressor) up to value L_v.

The actual process of the pressure increase will be depicted as line 1-2, which corresponds to the polytropic curve, i.e., to the process with the heat feed (n > k). The value of the additional increase in work L_v will be depicted in the pv-diagram as area $1\text{-}2_{ад}\text{-}2$. The value L_v is not the only expenditure of work as a result of losses. The full expenditure of the work as a result of friction is the sum of the work strictly of friction and the additional work which arose in connection with an increase in the volume with the heat feed of friction:

$$L_{зат} = L_{тр} + L_v \tag{2.217}$$

The area 1-2-3-4 is proportional to the polytropic work $\int_1^2 v\,dp$, i.e., the work spent for an increase in the energy of the fluid with a pressure increase from p_1 to p_2:

$$H_{нас} = \int_1^2 v\,dp = \int_1^{p_2} v\,dp + L_v = H_{ад} + L_v \tag{2.218}$$

This value should be called the pressure of the pump (compressor), since it corresponds to a real increase in the specific energy of the fluid. The total internal work spent for the pressure increase of 1 kg of mass will be depicted as the area 5-6-2-3 in accordance with equation (2.205) as a difference in the enthalpies

$$H_{нас} = i_2 - i_1.$$

Point 6 will be found by the intersection of the isotherm T_1 = const carried out through point 1 with the adiabatic curve passing through point 2. The horizontally shaded area 1-2-6-5-4

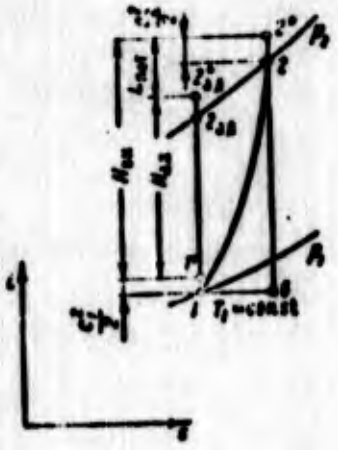

Fig. 2.94. Representation of the process in a pump (compressor) in coordinates i-s.

characterizes the frictional work L_{comp}. The full expenditure of energy in connection with the losses of friction and the feed (as a result of this) of heat to the fluid corresponds to the area 4-1-$2_{ад}$-2-6-5.

The process in the pump (compressor) in coordinates i-s depicted in Fig. 2.94. The adiabatic process is depicted as the line parallel to the axis of ordinates. The total increase in the energy of the fluid during the adiabatic process corresponds to a difference in enthalpies of $i^*_{2_{ад}} - i^*_1$. The minimally necessary increase in energy up to assigned outlet pressure (not allowing for high-speed output energy) is characterized by the segment $H_{ад} = i_{2_{ад}} - i^*_1$.

The real process with the preheating of the fluid as a result of all losses is depicted as line 1-2. The difference in enthalpies of i^*_2-i^*_1 corresponds to an increase in the total energy of the fluid $H_{вн}$ (when $c_2 = c_1$, $H_{вн} = i_2$-i_1, as was accepted in the plotting of the pv-diagram, see Fig. 2.93).

The difference in the total variation of energy of the fluid and change in the energy during the adiabatic process (i^*_2-$i^*_{2_{ад}}$) characterizes the irreversible expenditure of energy directly to the work of friction L_{comp} and, connected with this, to the additional work of compression in connection with an increase in the volume of fluid L_v [see equation (2.217)]. (Point 6, see Fig. 2.93, is transferred for clarity also in Fig. 2.94).

In connection with the losses and an increase in the volume of fluid, it is necessary to expend higher energy in order to obtain the assigned parameters p_2 and c_2 at the outlet. With the realization of the real process in the pump (compressor), besides

the mechanical energy, the internal energy of the working medium, is unavoidably increased and the entropy is increased, which is undesirable since this leads to an increase in the required external energy transferred by the wheel of fluid.

Directly in the flow area of the wheel (compressor) of fluid there is transferred the energy $H_т$, which calculated according to the Euler equation (2.31), is less than $H_{вн}$. Part of the energy from the drive engine is transferred to the fluid in the form of heat from losses of friction of the disk, heat from the return of leakages, i.e., from the fluid which already obtained earlier the energy in wheel and having higher energy:

$$H_т = H_{вн} - H_д, \tag{2.219}$$

where $H_д$ is the energy (thermal) fed to the fluid because of disk losses (including the heat feed as a result of the return of the leakages).

The real increase in the specific mechanical energy corresponds to the polytropic work of compression:

$$H_{ад}(H) = H_{вн} + L_v = \int_1^2 v dp + \frac{c_2^2 - c_1^2}{2}. \tag{2.220}$$

Theoretical pressure $H_т$ exceeds the real pressure by the value of the hydraulic losses in the flow area of the pump.

For the incompressible fluid the value $L_v = 0$ and real increase in the specific mechanical energy of the fluid (real pressure) is equal to the adiabatic pressure $H = H_{ад}$.

2.15. EFFICIENCIES OF VANE MACHINES

The power N_u expressed by equation (2.25) is not the power on the shaft. For the pump and compressor the power on the shaft (power input) will be more by the value of power connected with the expenditure, disk and mechanical losses.

For the turbine the power on the shaft (developed power), as a result of the same resistances, will be less. In order to find the available power of the vane machine, it is necessary to measure the torsional moment on the shaft and the frequency of rotation:

$$N = M_{\text{вращ}}\omega \text{ [W]}. \tag{2.221}$$

This means is used for determining the power during the testing of vane machines.

In the case of the design of a vane machine, it is necessary to calculate its power. To solve this problem by means of the calculated determination of the torsional moment or the total moment of resistance is sufficiently complicated. In the practice of the design of vane machines, the power is determined by means of the calculation of the available or required power and the evaluation of losses by the introduction of a number of efficiencies.

For the pump and compressor the minimum required power is defined as adiabatic useful power, i.e., the power which would be consumed by the pump (compressor) for an increase in pressure and velocity up to the assigned magnitudes in the absence of any losses:

$$N_{ад} = H_{ад}G, \tag{2.222}$$

where G is the fluid flow which enters into the system.

For the pump and compressor, which operate on compressible fluid, the real pressure is the polytropic pressure $H_{пол}$ [see equation (2.220)]. In connection with this, for compressor machines operating on gas and compressible fluids, it is possible to introduce the concept about the polytropic net power (ocasionally it is also referred to as hydraulic):

$$N_{\text{под}} = HG. \qquad (2.223)$$

In the work on an incompressible fluid the concepts $N_{\text{ад}}$ and $N_{\text{пол}}$ coincide, since the heat feed of the losses does not change the volume of fluid in the process of delivery. In compressors it is more frequently accepted to define the net power as the adiabatic, since its value is determined from the input parameters and outlet pressure without a detailed calculation of the compressor.

For the turbine the available power, as the maximum value of energy which can be selected from the fluid per unit time, is determined by the product of the adiabatic work of the expansion of 1 kg of gas calculated from the stagnation parameters at the inlet and the static parameters at the outlet (see Fig. 2.91), by mass gas flow rate, applied to the turbine:

$$N^{\circ}_{\text{ад}} = L^{\circ}_{\text{ад}} G. \qquad (2.224)$$

The available power of the turbine - is the maximally possible power which the turbine would develop in the absence of any losses. The real available power of the turbine is the power calculated from the polytropic work:

$$N^{\circ}_{\text{пол}} = L^{\circ}_{\text{пол}} G. \qquad (2.225)$$

As a rule, the calculation of efficiency is conducted according to the adiabatic available power, which is considerably more convenient, since its value is easily determined from the input parameters and inlet pressure without a detailed calculation of the turbine.

Let us introduce the concept about the efficiencies evaluating the different losses with the realization of the process in the vane machine. In this section let us conduct the classification of efficiencies and give their definition. The dependence of the

efficiencies on the design parameters and parameters of the conditions will be examined in an account of the material relating to pumps and turbines of liquid-propellant rocket engines.

2.15.1. HYDRAULIC EFFICIENCY OF VANE MACHINES. CIRCULAR EFFICIENCY OF THE TURBINE

Let us call the hydraulic (adiabatic) efficiency for pumps (compressors) the ratio of the adiabatic pressure to the theoretical pressure:

$$\eta_h = \frac{H_{ad}}{H_т}. \tag{2.226}$$

Since

$$H_т = H_{ad} + L_g + L_{comp.unpot.vacuum} \tag{2.227}$$

then

$$\eta_h = 1 - \frac{L_g + L_{comp.unpot.vacuum}}{H_т} = 1 - \frac{L_{u\ t.unpot.vacuum}}{H_т}.$$

The hydraulic (adiabatic) efficiency estimates the losses connected with the heat feed from all losses and purely hydraulic losses in the flow area of the pump.

When operating on an incompressible fluid the hydraulic efficiency estimates only the hydraulic losses in the flow area of the pump, which are determined by the hydraulic resistances:

$$\eta_г = \frac{H}{H_т} = 1 - \frac{L_{comp.unpot.vacuum}}{H_т}. \tag{2.228}$$

When operating on a compressible liquid a similar efficiency will be the polytropic efficiency:

$$\eta_{г(пол)} = \frac{H}{H_т}. \tag{2.229}$$

For the turbine the hydraulic (adiabatic) efficiency is determined as the ratio of circular work L_u^* determined from the

stagnation parameters, i.e., the sum of work L_u, the ideal gas with passage over the flow area of the turbine, and kinetic energy at the outlet, to the available adiabatic work:

$$L_u^* = L_u + \frac{c_2^2}{2}. \tag{2.230}$$

Thus L_u^* is the work which the gas would complete during the full use of the high-speed energy with the deduction of hydraulic losses:

$$\eta_r = \frac{L_u^*}{L_{ad}^*} = 1 - \frac{L_{comp.пр.т.part} - H_g}{L_{ad}^*} = 1 - \frac{l_{пр.т.пот.part}}{L_{ad}^*}. \tag{2.231}$$

The hydraulic efficiency of the turbine estimates the irreversible expenditure of energy to hydraulic losses in the flow area of the turbine. Sometimes it is called the efficiency according to stagnation parameters. The hydraulic polytropic efficiency of the turbine will be determined by the ratio

$$\eta_{r(пол)} = \frac{L_u}{L_{пол}^*} = 1 - \frac{L_{comp.пр.т.part}}{L_{пол}^*}.$$

For the turbines used as drive engines, there is great significance in the circular efficiency, which is the ratio of the circular work to the adiabatic available work:

$$\eta_u = \frac{L_u}{L_{ad}^*} = 1 - \frac{L_{пот.пр.т.part} + \frac{c_2^2}{2}}{L_{ad}^*}. \tag{2.232}$$

The circular efficiency of the turbine estimates the irreversible expenditure of energy for hydraulic losses in the flow area of the pump and for high-speed losses (energy losses with the outlet velocity).

Let us refine the concept about the circular power (power on the circumference of the wheel), [see formula (2.25)].

For the pump

$$N_e = H_t G'. \tag{2.233}$$

The circular power of the pump is value of the mechanical energy transmitted by the wheel per unit time (1 s) to the mass of fluid G' kg passing through the wheel of the pump.

For the turbine

$$N_e = L_e G'. \tag{2.234}$$

The circular power of the turbine is value of mechanical energy transmitted to the wheel per unit time (1 s) by a mass of fluid of G' kg passing through the turbine wheel.

2.15.2. INTERNAL AND DISK EFFICIENCY OF VANE MACHINES

The ratio of the adiabatic presure to the internal pressure will consist of the internal efficiency of the pump (compressor):

$$\eta_{oi} = \frac{H_{ad}}{H_{oi}} = 1 - \frac{L_{w.s}}{H_{oi}}. \tag{2.235}$$

In accordance with the is-diagram given in Fig. 2.94:

$$\eta_{oi} = \frac{i_1^0 - i_{2_{ad}}^0}{i_1^0 - i_{2_{oi}}^0}. \tag{2.236}$$

The internal efficiency of the pump estimates all the energy losses with the exception of mechanical losses.

The ratio of the internal work of the turbine to the adiabatic will be the internal efficiency of the turbine.

$$\eta_{oi} = \frac{L_{oi}}{L_{oi}^0} = 1 - \frac{L_{w.s} + \frac{c_2^2}{2}}{L_{oi}^0}. \tag{2.237}$$

In accordance with the is-diagram given in Fig. 2.91:

$$\eta_{oi} = \frac{i_1^* - i_2^*}{i_1^* - i_{2ad}}. \qquad (2.238)$$

The internal efficiency of the turbine estimates all the energy losses except the mechanical (including the energy losses with the outlet velocity).

Let us call the ratio of theoretical pressure of the wheel to the internal pressure the disk efficiency of the pump:

$$\eta_д = \frac{H_t}{H_{to}} = 1 - \frac{L_д}{H_{to}}, \qquad (2.239)$$

where $L_д = N_д/G'$ - disk losses.

Let us call the ratio of the internal work of the turbine to the circular work the disk efficiency of the turbine:

$$\eta_д = \frac{L_{to}}{L_u} = 1 - \frac{L_д}{L_u}. \qquad (2.240)$$

For the pump the internal efficiency can be represented as the product of the hydraulic and disk efficiency:

$$\eta_{oi} = \eta_г \eta_д. \qquad (2.241)$$

For the turbine the internal efficiency can be represented as the product of the circular and disk efficiency:

$$\eta_{oi} = \eta_u \eta_д. \qquad (2.242)$$

2.15.3. MECHANICAL EFFICIENCY

Let us introduce the concept about the internal power of the vane machine. The internal power of the pump will be called the power consumed by the pump in the absence of mechanical losses:

$$N_{вн}=H_{вн}G', \tag{2.243}$$

where G' is the mass flow rate through the wheels of the pump, which exceeds by the value of the leakages the flow being fed into the system:

$$G'=G+G_y.$$

The internal power of the pump can be represented as the sum of the circular power and power of the disk losses:

$$N_{вн}=N_к+N_д. \tag{2.244}$$

The total power being consumed by the pump will be more than $N_{вн}$ by the value of the power of mechanical losses:

$$N_в=N_{вн}+N_{мех}. \tag{2.245}$$

The total power of the pump can be represented also as the sum of the circular power, the power of the disk losses and the power of the mechanical losses:

$$N_в=N_к+N_д+N_{мех}. \tag{2.246}$$

The ratio of the internal power to the total power consists of the mechanical efficiency of the pump $\eta_{мех}$:

$$\eta_{мех}=\frac{N_{вн}}{N_в}. \tag{2.247}$$

Let us call the internal power of the turbine the product of internal work on the real mass flow rate through the turbine wheel:

$$N_{т.вн}=L_{вн}G'. \tag{2.248}$$

The flow rate G' differs from the flow rate, suitable for the turbine by the value of leakages. Usually

$$G' = G - G_y \qquad (2.249)$$

(sometimes the gas flow rate through the turbine wheel can increase in connection with the inleakage).

The internal power of the turbine can be represented as the difference in the circular power and power of the disk losses:

$$N_{in} = N_u - N_d. \qquad (2.250)$$

The effective power of the turbine N_T is less than the internal by the value of the mechanical losses:

$$N_T = N_{in} - N_{mech}. \qquad (2.251)$$

The effective power of the turbine can be represented also as a difference in the circular power and the power of disk and mechanical losses:

$$N_T = N_u - N_d - N_{mech}. \qquad (2.252)$$

The ratio of the effective power to the internal power will be the mechanical efficiency of the turbine:

$$\eta_{mech} = \frac{N_T}{N_{in}}. \qquad (2.253)$$

The portion of strictly mechanical losses is usually very low, but in taking into account the power for driving the impellers for the pump it can consist of a noticeable value. The value of the mechanical efficiency of the turbine of liquid-propellant rocket engines is taken equal to unit, referring all the mechanical losses in the turbopump unit to the pumps.

2.15.4. POWER AND FLOW EFFICIENCY OF VANE MACHINES

The ratio of the useful adiabatic power to the total power will be the power efficiency of the pump, or simply the efficiency of the pump:

$$\eta_n = \frac{N_{ад}}{N_в}. \tag{2.254}$$

Having substituted into this formula the expression for the adiabatic energy (2.222), having replaced the total power by the internal power and the mechanical efficiency, and having expressed the internal power according to equation (2.243), we will obtain

$$\eta_n = \eta_{гн}\eta_{мех}\frac{G}{G'}. \tag{2.255}$$

Let us call the ratio of the mass flow rate which enters into the system to the flow rate through the wheels of the pump, G/G', the flow efficiency of the pump (compressor) and designate it η_p:

$$\eta_p' = G/G'. \tag{2.255}'$$

Then the efficiency of the pump can be represented in the form of the product:

$$\eta_н = \eta_{гн}\eta_p\eta_{мех}.$$

The product

$$\eta_{гн}\eta_p = \frac{H_{ад}G}{H_{тн}G'} = \frac{N_{ад}}{N_{тн}} = \eta_{тн}N \tag{2.256}$$

can be called the internal power efficiency.

If we develop the expression for $\eta_{ВН}$, we will obtain that the efficiency of the pump is the product of the particular efficiencies - hydraulic, disk, mechanical and flow:

$$\eta_н = \eta_г\eta_д\eta_p\eta_{мех}. \tag{2.257}$$

In the calculations of the pumps (compressors), it is convenient, by utilizing the statistical data, to be assigned the efficiencies of the pump or particular efficiencies and calculate the power input on the basis of the assigned magnitudes of required head and flow rate.

From equations (2.222) and (2.254) it follows that

$$N_{\text{н}} = \frac{H_{\text{т}} G}{\eta_{\text{н}}} = \frac{H_{\text{т}} G}{\eta_{\text{г}} \eta_{\text{г}} \eta_{\text{г}} \eta_{\text{мех}}}. \qquad (2.258)$$

The ratio of the effective power of the turbine to the available adiabatic power will comprise the power efficiency of the turbine, or simply the efficiency of the turbine:

$$\eta_{\text{т}} = \frac{N_{\text{т}}}{N_{\text{ад}}^{\text{т}}}. \qquad (2.259)$$

Having substituted into equation (2.259) the expression for adiabatic power (2.224), having replaced the total power by the internal power and the mechanical efficiency, and having expressed the internal energy according to equation (2.248), we obtain

$$\eta_{\text{т}} = \eta_{\text{ви}} \eta_{\text{мех}} \frac{G'}{G}. \qquad (2.260)$$

Let us call the ratio of the mass flow rate through the turbine wheel to the flow rate, which enters into the system, G'/G, the flow efficiency of the turbine and designate it $\eta_{\text{р}}$. Then the efficiency of the turbine can be represented in the form of the product:

$$\eta_{\text{т}} = \eta_{\text{ви}} \eta_{\text{р}} \eta_{\text{мех}}, \qquad (2.261)$$

or, having developed the expression for $\eta_{\text{ви}}$ [see formula (2.241)], we will obtain that the efficiency of the turbine is the product of the particular efficiences, circular, disk, flow and mechancial:

$$\eta_{\text{т}} = \eta_{\text{к}} \eta_{\text{д}} \eta_{\text{р}} \eta_{\text{мех}}. \qquad (2.262)$$

The flow efficiency of the turbines is always greater than the efficiency of the pumps, since in the pump through the seals there flows the fluid of the same density, and in turbines there always flows the gas which was already expanded in the flow area. Furthermore, with the identical absolute magnitude of the clearances their relative effect in the pump can be more than that in the turbine, in view of the less absolute dimensions of the pump.

In the calculations of the turbine it is convenient, by utilizing statistical data, to be assigned the efficiency of the turbine or particular efficiency and calculate the effective power on the basis of the assigned adiabatic work and available gas flow rate through the turbines. From equations (2.224) and (2.259) it follows that

$$N_{\text{т}} = L_{ад}^{*} G_{\text{т}} \eta_{\text{т}}. \tag{2.263}$$

In the calculation of turbines the concept about the internal power efficiency is sometimes introduced:

$$\eta_{\text{т.i}} = \eta_{\text{г}} \eta_{\text{р}} \eta_{\text{л}} = \frac{N_{\text{вн}}}{N_{\text{ад}}^{*}}. \tag{2.264}$$

Table 2.2 gives the accepted designations of pressures (works), powers and efficiencies.

Table 2.2. Designations of pressures (works), powers and efficiencies of vane machines of liquid-propellant rocket engines.

No.	Pump			
	Name	Designation	Formula	Dimensionality
	1. Pressures			
1	Real	H	$(p_2^{*} - p_1^{*})/\varrho$	J/kg
2	Theoretical (circular)	$H_{\text{т}}$ ($H_{\text{ш}}$)	$c_{2u}u_2 - c_{1u}u_1$	J/kg
3	Theoretical (circular) with an infinitely large number of blades	$H_{\text{т}\infty}$	$c_{2u\infty}u_2 - c_{1u}u_1$	J/kg

Table 2.2. (continued).

4	Internal	H_{ra}	$i_2^* - i_1^* = \frac{N_{in}}{Gi'}$	J/kg
	II. Powers			
1	Useful	N_{uo3}	HG	W
2	Circular	N_3	$H_1 Gi'$	W
3	Internal	N_{in}	$H_{in} Gi'$	W
4	Disk losses	$N_д$	$H_д Gi'$	W
5	Mechanical losses	$N_{мех}$	—	W
6	Total	$N_в$	$\frac{HG}{\eta_в}$	W
	III. Efficiencies			
1	Hydraulic	$\eta_г$	$\frac{H}{H_1}$	—
2	Disk	$\eta_д$	$H_1' H_{in}$	—
3	Internal	η_{in}	$\frac{H}{H_{in}} = \frac{HG'}{N_{in}} = \eta_г \eta_д$	—
4	Mechanical	$\eta_{мех}$	$N_{in}/N_в$	—
5	Flow	$\eta_р$	G/G'	—
6	Internal power	$\eta_{in} N'$	$\frac{HGi}{N_{in}} = \eta_г \eta_д \eta_р$	—
7	Total power	$\eta_в$	$\frac{N_{uo3}}{N_в} = \frac{HG}{N_в} = \eta_{in} \eta_р \eta_{мех} = \eta_г \eta_д \eta_р \eta_{мех}$	—

No.	Name	Designation	Formula	Dimensionality
	Pump for compressible fluid			
	1. Work			
1	Adiabatic	$H_{ад}$	$i_{2ад}^* - i_1^* = \int_1^{2_{ад}} v dp + \frac{c_2^2 - c_1^2}{2}$	J/kg

Table 2.2. (continued).

2	Polytropic (real)	H	$\int_1^2 vdp + \frac{c_2^2 - c_1^2}{2}$	J/kg
3	Theoretical (circular)	$H_т$ (H_∞)	$c_{2u}u_2 - c_{1u}u_1$	J/kg
4	Theoretical (circular with an infinitely large number of blades	$H_{т\infty}$	$c_{2u\infty}u_2 - c_{1u}u_1$	J/kg
5	Internal	$H_{ин}$	$i_2^* - i_1^*$	J/kg
6	Additional work as a result of volumetric expansion	L_p	$\int_1^2 vdp - \int_{2t}^2 vdp$	J/kg
	II. Powers			
1	Useful adiabatic	$N_{ад}$	$H_{ад}Q$	W
2	Useful polytropic	$N_{пол}$	HQ	W
3	Circular	N_∞	$H_тQ'$	W
4	Internal	$N_{ин}$	$H_{ин}\rho i'$	W
5	Disk losses	$N_д$	$H_д\rho i'$	W
6	Mechanical losses	$N_{мех}$	—	W
7	Total	$N_в$	$\frac{H_{ад}\rho Q}{\eta_{ин}}$	W
	III. Efficiencies			
1	Hydraulic (adiabatic)	$\eta_г$	$H_{ад}/H_т$	—
1a	Hydraulic (polytropic)	$\eta_{г.пол}$	$H/H_т$	—
2	Disk	$\eta_д$	$H_т/H_{т\infty}$	—
3	Internal	$\eta_{ин}$	$H_{ад}H_{ин} = \eta_г\eta_д$	—
4	Mechanical	$\eta_{мех}$	$N_{ин}/N_в$	—
5	Flow	$\eta_р$	Q/Q'	—
6	Internal power	$\eta_{ин}N$	$\frac{N_{ад}}{N_{ин}} = \eta_{ин}\eta_р = \eta_г\eta_д\eta_р$	—
7	Total power	$\eta_в$	$\frac{N_{ад}}{N_в} \quad \frac{H_{ад}Q}{N_в} \quad \eta_г\eta_д\eta_р\eta_{мех}$	—

Table 2.2. (continued).

No.	Turbine			
	Name	Designation	Formula	Dimensionality
	I. Pressures			
1	Adiabatic	L^*_{ad}	$i^*_1 - i_{2ad} = \int_{p_{ad}}^{1} v dp + \frac{c_1^2}{2}$	J/kg
2	Polytropic	L^*_{pol}	$\int_{p}^{1} v dp + \frac{c_1^2}{2}$	J/kg
3	Circular	L_u	$c_{1u}u_1 - c_{2u}u_2$	J/kg
4	Total circular	L^*_u	$L_u + (c_2^2/2)$	J/kg
5	Internal	L_{in}	$i^*_1 - i^*_2$	J/kg
6	Additional work of volumetric expansion	H_p	$\int_{p}^{1} v dp - \int_{p_{ad}}^{1} v dp$	J/kg
	II. Powers			
1	Available adiabatic	N^*_{ad}	$L^*_{ad}G$	W
2	Available polytropic	N^*_{pol}	$L^*_{pol}G$	W
3	Circular	N_u	L_uG'	W
4	Internal	N_{in}	$L_{in}G'$	W
5	Disk losses	N_d	L_dG'	W
6	Mechanical losses	N_{mech}	—	W
7	Effective	N_e	$L^*_{ad}G\eta_e$	W
	III. Efficiencies			
1	Hydraulic (adiabatic)	η_h	L_u/L^*_{ad}	—
1a	Hydraulic (polytropic)	$\eta_{h.pol}$	L_u/L^*_{pol}	—
2	Circular (blade)	η_u	L_u/L^*_{ad}	—
3	Disk	η_d	L_{in}/L_u	—
4	Internal	η_{in}	L_{in}/L^*_{ad}	—
5	Mechanical	η_{mech}	N_i/N_{in}	—
6	Flow	η_p	G'/G	—
7	Internal power	$\eta_{in}N$	$\frac{N_{in}}{N^*_{ad}} = \eta_{in}\eta_p = \eta_u\eta_d\eta_p$	—
8	Effective power	η_e	$\frac{N_e}{N^*_{ad}} = \eta_u\eta_d\eta_p\eta_{mech}$	—

Figures 2.95 and 2.96 for clarity depict the approximate balances of powers, respectively, for the pump and turbine. The relationships of the width of the separate regions correspond to the relationships of the powers. By taking the ratios of the corresponding values of the width of these regions, it is possible to judge the individual forms of efficiency.

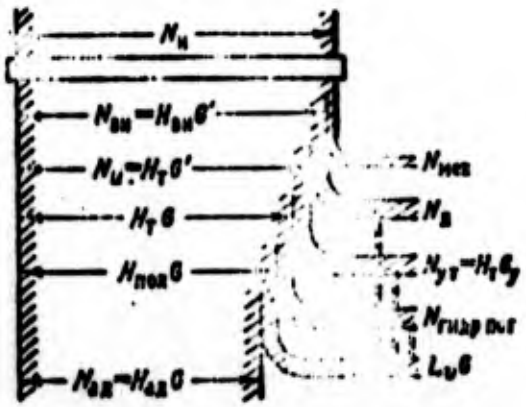

Fig. 2.95. Balance of powers for a pump (when operating on a compressible fluid).

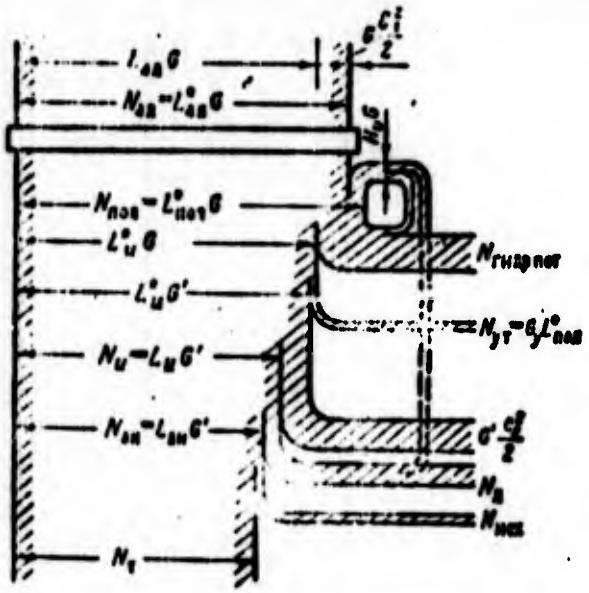

Fig. 2.96. Balance of powers for a turbine.

As follows from Table 2.2 and Figs. 2.95 and 2.96, there is a complete analogy between the efficiency of the pump and the efficiency of the turbine.

CHAPTER 3

PUMPS OF LIQUID-PROPELLANT ROCKET ENGINES

3.1. CENTRIFUGAL PUMPS

3.1.1. LAYOUT OF THE DEVICE. OPERATING UNITS OF THE PUMP, HYDRAULIC LOSSES IN THE PUMP

As a pump of a liquid-propellant rocket engine [LPRE] (ЖРД) the pump having two rotors - axial (screw conveyor) and centrifugal, is usually used. Subsequently, we will call such a pump screw-centrifugal pump. The purpose of screw conveyor is to improve the anticavitation and energy qualities of the pump. Figure 3.1 depicts the structural scheme of a screw-centrifugal pump.

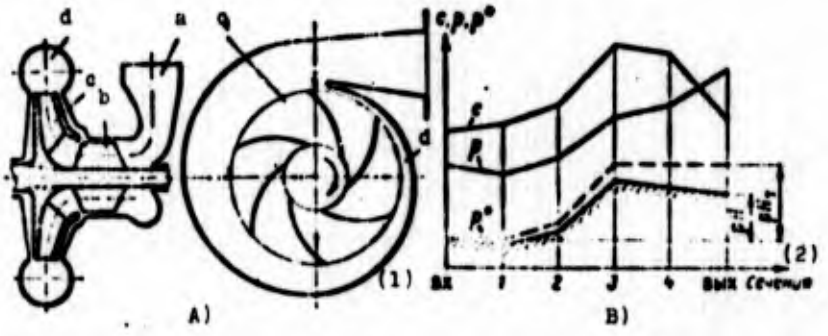

Fig. 3.1. Diagram of a screw-centrifugal pump (A) and graphs of the change in parameters of the fluid along the length of the flow area (B).
KEY: (1) Inlet; (2) Outlet of cross section.

The flow area of the screw-centrifugal pump consists of the following elements (see Fig. 3.1A): feed a; screw conveyor b; centrifugal wheel c, occasionally referred to as an impeller, and removal d.

Figure 3.1B shows the change in the flow parameters of the fluid - velocity c, pressure p and total pressure p* along the length of the flow area of the pump. Section вх-1 characterizes the change of the parameters in the feed. Because of the introduction of convergence in inlet the pressure of the fluid somewhat drops, and the velocity increases. The total mechanical energy of the fluid - total pressure p* - will be lowered due to the presence of hydraulic losses. With the flow of the fluid without losses, the total pressure in the inlet part will remain constant (dashed line on Fig. 3.1B).

In the screw conveyor (section 1-2) the total pressure is increased as a result of the feed of external energy; usually in this case the static pressure and kinetic energy increase.

The basic increase in the total pressure as a result of the transfer of the fluid of external energy is accomplished in the centrifugal wheel (section 2-3) and the pressure and velocity in this case increase. In the removal, which consists of a spiral collector (section 3-4) and conical diffuser (section 4-вых), the conversion of kinetic energy into pressure occurs. As a result of hydraulic losses, the total pressure will be reduced.

The total pressure will be increased only in the axial and centrifugal pumps, and in the remaining elements the total pressure is decreased due to the presence of losses. The difference in the total pressures at the inlet and outlet for the incompressible fluid characterizes the real pressure of the pump H.

The real pressure is determined in experiments by means of the measurement of pressures and velocities before the inlet into the pump and at outlet from it in accordance with equation (1.10). The velocity is not usually measured directly but is calculated from the measured value of the volume flow and known area of the pipelines in the inlet and outlet sections of the pump.

For this pump, in terms of the known dimensions and values of velocities at the outlet from the centrifugal wheel, the theoretical pressure $H_т$ is easily calculated [see equation (2.31)].

The real pressure of the pump can be found by calculation means successively subtracting from $H_т$ the values of hydraulic losses over the entire flow channel of the pump: $H = H_т - L_{гидр.пот}$. But this means is laborious and does not give very reliable results, since values of the calculated loss factor can be estimated only approximately (see source [13]). The tentative value of the real pump pressure is determined more simply by using the concept of the hydraulic efficiency of the pump (see section 2.15.1):

$$H = H_т \eta_г. \qquad (3.1)$$

3.1.1.1. Feed of the Pump

The feed serves to provide for feed to the wheel of the pump with the assigned velocity and definite direction. It should satisfy the following requirements:

1) provide the axisymmetric flow of the fluid at the inlet into the screw conveyor with as uniform distribution of velocities and pressures as possible;

2) provide the velocity recommended for the inlet into the screw conveyor, usually equal to 5-10 m/s;

3) provide the necessary direction of the velocity - most frequently, axial;

4) have a minimum of hydraulic losses.

On the basis of these requirements the feed is usually fulfilled with the convergent (narrowing) section, where there occurs an increase in the velocity to 15-30% (in the accelerated flow a more uniform velocity field and less possibility for the flow separation are obtained).

Four forms of feeds are distinguished[1] (Fig. 3.2): conical straight connecting piece a - axial feed; elbow-shaped intake pipe b; circular intake pipe c and semispiral intake pipe d.

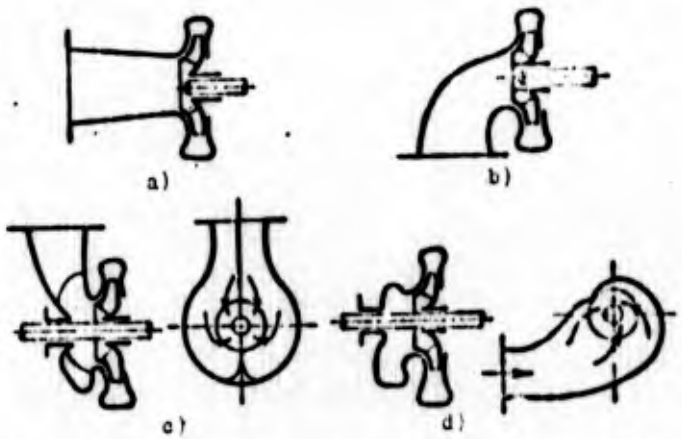

Fig. 3.2. Inlet devices of pumps: a) axial feed; b) elbow-shaped feed; c) circular feed; d) semispiral feed.

To provide for the axisymmetric flow and uniform velocity distribution, it is most advantageous to have a straight conical connecting piece, axial feed, but it requires a cantilever arrangement of the pump, and therefore in the turbopump unit [TU] (THA) of the LPRE it is rarely used. The use of such a connecting

[1]Feeds of the centrifugal and screw-centrifugal pumps virtually do not differ from each other.

piece is advantageous when it is structurally possible to carry out a transition of the pipeline directly into the connecting piece of the pump without rotation.

The elbow-shaped connector, although it does not provide a uniform velocity distribution, is structurally simple and is frequently used in turbopump units for the cantilever arranged pumps. The most widespread are circular and semispiral feeds.

As the experiments showed (see sources [87, 102]), at the inlet velocities $c_{вх}$ = 5-8 m/s a change in the feed virtually does not affect the energy performance of the pump. At large inlet velocities the effect of the feed on the performance can be affected noticeably. The feed in pumps of the LPRE affects basically the cavitation parameters of the pump. With an increase in losses in the feed the pressure at the inlet into the screw conveyor is decreased, which makes the anticavitation qualities of the pump worse.

An increase in the nonuniformity of the flow at the outlet from the feed also has a negative effect on the cavitation parameters of the pump (see source [106]). For the velocity distribution in the feed at low flow rates and at the overexpanded inlets nominal flow rates are affected by the twisted return currents coming out of the screw conveyor. In the presence of circular and semispiral feeds, return currents are quenched in the removal, and the twist is not transferred to the inlet pipeline, but in the case of the use of axial and elbow-shaped feeds the twist is transferred to the inlet pipeline.

During the calculations it is possible to accept values of the coefficients of local resistance for the axial feed ξ = 0.2-0.3; for the elbow-shaped - ξ = 0.8-1.0; for the circular and semispiral - ξ = 1.3-1.4 (see source [85]). These values correspond to convergence 20-30%.

As a rule, the form of the inlet is determined by the total structural layout of the turbopump unit.

One of the possible variants of circular feed is shown on Fig. 3.3. The diameter of the feed D is determined by the outside diameter of the screw conveyor $D_ш$, and the diameter d - by the diameter of the liner of the screw conveyor $d_{вт}$: $D = (1.02\text{-}1.05)D_ш$; $d = (1.05\text{-}1.1)d_{вт}$. The diameter of the inlet into the feed $D_{вх}$ is selected on the basis of the condition of the provision for an increase in the velocity from the inlet into the feed to the outlet from the connecting piece by 15-20%: $D_{вх} = (1.07\text{-}1.1)\sqrt{D^2 - d^2}$.

The basic dimensions of the connecting piece are assigned in fractions of a diameter $D_{вх}$. On the section from the inlet into the connecting piece up to cross section I-I, the velocity increases by 2-4% by means of a decrease in the area of this cross section. The areas of other cross sections of the feed vary in proportion to the angle ϕ:

$$F_\varphi = \frac{F_{I-I}}{2}\left(1 - \frac{\varphi}{\pi}\right).$$

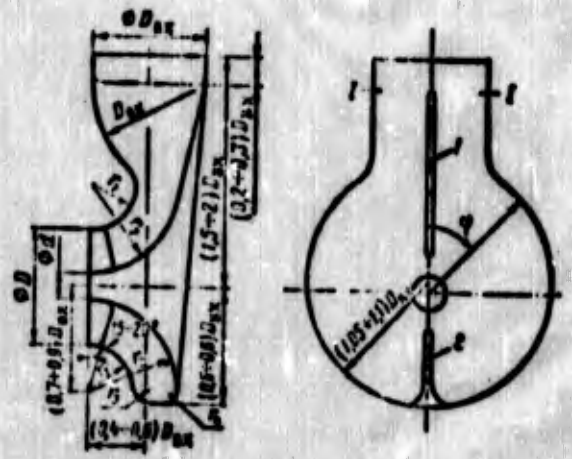

Fig. 3.3. A possible variant of the circular feed: 1 - separating fin; 2 - guide fin.

The form of the cross sections is selected from the condition of the provision for a smoothness of the internal surfaces of the feed. For the uniform feed of the fluid to the screw conveyor in the feed, separating fin 1 and guide fin 2 are fulfilled.

3.1.1.2. Rotors

Figure 3.4 gives the scheme of rotors of a screw-centrifugal pump, and the characteristic cross sections are shown: 1-1 - inlet into the screw conveyor; 2ш-2ш - outlet from the screw conveyor; 1ц-1ц - inlet into the centrifugal wheel; 2-2 - outlet from the centrifugal wheel. Subsequently, the designations of the cross sections will be used as subscripts for the parameters. The subscript "ш" in a number of cases is omitted if the parameters at the outlet from the screw conveyor are examined on the periphery (п), at the calculated diameter (р) and near the liner of the screw conveyor (вт). The subscript "ц" is omitted in those sections where only the centrifugal wheel is examined.

A. SCREW-CONVEYOR WHEEL

At the assigned operating mode of the pump, i.e., at the known flow Q and angular velocity ω, it is possible to construct a velocity triangle at the inlet into screw conveyor for any radius (see Fig. 2.62 and Fig. 2.64). The angle between the direction of the relative velocity and the reverse direction of the circular β_1 (see Fig. 2.62 and Fig. 2.64), i.e., the flow angle at the inlet into the screw conveyor is determined by the operating mode, i.e., by the angular velocity and the fluid flow rate. Usually this angle in screw conveyors of LPRE does not exceed 6-8°.

The screw conveyor should raise the pressure in front of the centrifugal wheel in order to insure its noncavitation operation, and therefore the screw conveyor is a reactive axial wheel. The screw conveyors obtained especially widespread use in pumps of LPRE.

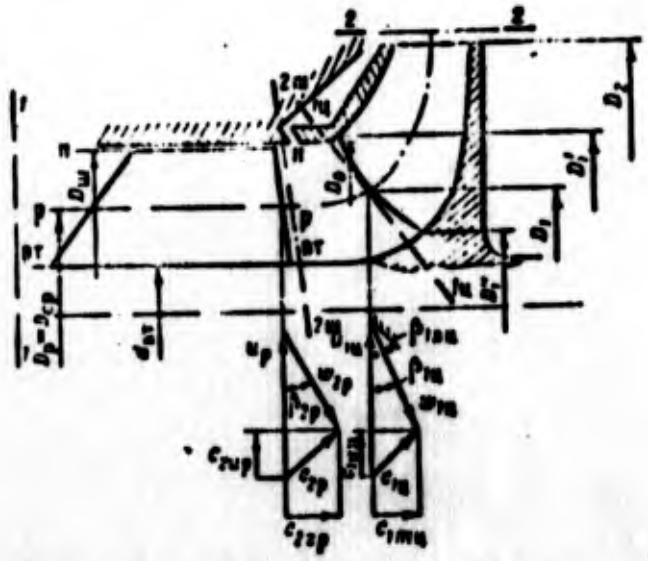

Fig. 3.4. Designations of basic dimensions of the screw-centrifugal pump and velocity triangles at the outlet from the screw conveyor and at the inlet into the centrifugal wheel.

Screw-conveyor wheels are simple to produce and possess as a preliminary pump of the centrifugal wheel a favorable nature of the change in the parameters along the radius (see Section 2.11.1.4).

In screw conveyors of LPRE dense cascades are used ($b_л/t > 1.5$). For such cascades we will consider that the flow at the outlet from the preliminary pump takes the direction of the blades; thus, on Fig. 2.62 $\beta_2 = \beta_л$, and on Fig. 2.64 $\beta_2 = \beta_{2л}$.

B. CENTRIFUGAL WHEEL

a) Angles of the Impeller Vanes

The flow, having left the wheel of the screw conveyor, enters into the centrifugal wheel. Disregarding the losses, it is assumed that the flow in space between the screw conveyor and the blades of the centrifugal wheel is achieved according to the law $c_u r = \text{const}$. Under this assumption and the assumption about the

fact that the streams flow, not mixing, along the known circular component of absolute velocity at the outlet from the preliminary pump, it is possible to find the circular velocity component at the inlet into the centrifugal wheel:

$$c_{1u} = \frac{c_{2u} r_2}{r_a}.$$

The meridian component of absolute velocity remains constant or is decreased. Plotted on Fig. 3.4 are the velocity triangles - at the outlet from the screw conveyor (for the arithmetic mean diameter) and at the inlet into the centrifugal wheel (for the mean diameter of the leading edge). For the screw conveyor, which operates with the centrifugal wheel, the arithmetic mean diameter can be taken as the calculated (see Section 2.11.1.4).

According to the plotted velocity triangle, the angle of entry of the flow into the centrifugal wheel $\beta_{1ц}$ is determined. The magnitude of this angle determines the value of the inlet angle of the blades: $\beta_{1л.ц} = \beta_{1ц} + i_ц$. Usually it is taken at $i_ц = 0\text{-}15°$. In this range of the change in $i_ц$ the energy and cavitation properties of the centrifugal wheels weakly depend on the angle of incidence. This is evident from Fig. 3.5, where given are the experimental data on the effect of the angle of incidence on the head, efficiency and inlet pressure $p_{срв}$, upon which there begins cavitation separation. It is advantageous to have the angle $\beta_{1л.ц}$ sufficiently large, since in this case the degree of the diffusivity of the vane channel will be decreased.

Blades at the outlet can have different angles $\beta_{2л}$ in the plane of rotation. The wheels, generally speaking, can have blades of three basic types:

a) $\beta_{2л} < 90°$; b) $\beta_{2л} = 90°$; c) $\beta_{2л} > 90°$ (see Fig. 2.43).

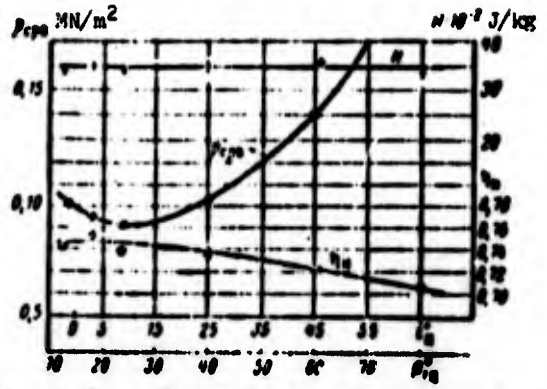

Fig. 3.5. Experimental dependence of separation pressure, head and efficiency of the centrifugal pump on the angle of incidence at the inlet into the wheel.

Let us examine which wheels having different outlet angles satisfy more the requirements given to pumps of LPRE.

1. On the basis of the requirement for obtaining the minimum hydraulic losses of the pump:

a) it is advantageous to have a large portion of static head, since losses in the process of the transformation of large values of kinetic energy into pressure energy in the discharge devices are great; consequently, it is more preferable to have $\beta_{2л} \leq 90°$ and $\rho_{н} \geq 0.5$ (see Fig. 2.42).

b) it is necessary to select the optimum shape of the vane channel in the plane of rotation. Figure 3.6 shows shapes of a channel in the plane of rotation with the straightening of the axis (equivalent diffuser). With comparatively small $\beta_{2л}$ the angle of taper of channel is less, and consequently, the possibility for the separation of flow is less, and the possibility for the appearance of return currents, especially at large ratios D_1/D_2 is less. When $\beta_{2л} < \beta_{1л}$ the cascade will become convergent. At the too narrow angles of $\beta_{2л}$, the channel can be (especially with low ratios D_1/D_2) very narrow and long, which, in turn, leads to an increase in the hydraulic losses. On the basis of the most

favorable hydraulic shape of the channel in the plane of rotation it is advantageous to select angles $\beta_{2л}$ within the limits of 20-40°.

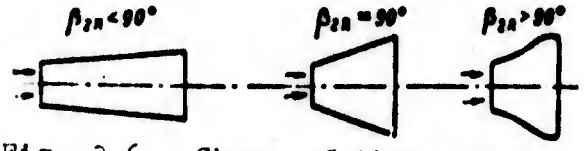

Fig. 3.6. Shape of the expanded vane channel of the wheel at different angles $\beta_{2л}$.

2. It is necessary to bear in mind that with a decrease in $\beta_{2л}$ and an increase in the static head (see Fig. 2.42) the losses connected with leakage of the fluid from the outlet cavity (great outlet pressures from the wheel) increase.

3. One should remember that the absolute value of $H_{т\infty}$ at this circular velocity is small at narrow angles $\beta_{2л}$. Figure 3.7 gives the dependences $\bar{H}_{т\infty}$ and $\bar{H}$ - the coefficients of theoretical pressure when $z = \infty$ and the pressure of the centrifugal pump - from the angle $\beta_{2л}$.

In order to obtain high pressure from the wheel with a small angle $\beta_{2л}$, it is necessary to increase the circular velocity, and this leads to great friction losses of the disk. The coefficient of theoretical pressure when $z = \infty$ is determined from the equation $\bar{H}_{т\infty} = H_{т\infty}/u_2^2$, or when $c_{1u} = 0$, using expression $H_{т\infty} = c_{2u\infty}u_2$ and the relations resulting from the velocity triangle at the outlet from the centrifugal wheel, we will obtain

$$\bar{H}_{т\infty} = 1 - q, \qquad (3.2)$$

where $q = (c_{2m}/u_2)\operatorname{ctg}\beta_{2л}$ is the flow parameter.

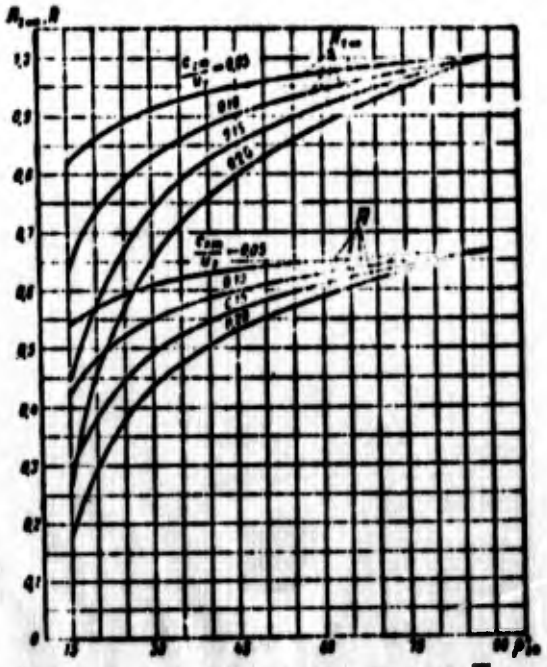

Fig. 3.7. Dependences of $\bar{H}_{T\infty}$ and $\bar{H}$ on $\beta_{2л}$.

The coefficient of pressure in the design conditions is determined from the equation

$$\bar{H} = k_z \eta_г (1 - \varphi), \tag{3.3}$$

where k_z is the coefficient which considers the effect of the number of blades (see Section 2.10.3).

Usually for pumps when $D_1/D_2 \leq 0.55$

$$k_z \eta_г = 0{,}6 \div 0{,}68, \tag{3.4}$$

and for pumps when $D_1/D_2 > 0.55$

$$k_z \eta_г = (1{,}35 \div 1{,}5)\left(1 - \frac{D_1}{D_2}\right). \tag{3.5}$$

Figure 3.7 shows that at low values c_{2m}/u_2 the increase in $\beta_{2л}$ up to values which exceed 40-50° is inexpedient, since the pump pressure in this case is changed little. For large values

c_{2m}/u_2 one should select the larger angles $\beta_{2л}$ up to 90°. But at the same time, let us specify that for wheels with a large ratio D_1/D_2 exceeding 0.6 small angles $\beta_{2л}$ = 15-20° are sometimes used for an increase in the cascade density of the wheel.

4. On the basis of the requirements for obtaining the continuously falling pressure pump characteristic [dependence H = f(Q)], which provide static stability of the pump system, as will be shown subsequently, it is more preferable to have angles $\beta_{2л} \leq 30\text{-}40°$.

5. For the transfer of the maximum energy to a unit of mass of fluid it is more preferable to have large angles $\beta_{2л}$ ($\beta_{2л} > 90°$), which provides greater pressure at the same circular velocity. But in the relation to the strength the blades radial at the outlet ($\beta_{2л} = 90°$) possess considerable advantage, since they do not undergo great bending moments from the action of centrifugal forces.

The circular velocity in pumps of LPRE do not usually exceed 200-250 m/s, and, as a rule, these pumps were underloaded in a strength relation, and therefore on the basis of conditions of strength the use of angles $\beta_{2л} < 90°$ is completely possible.

Taking into account the requirements formulated above for the magnitude of the angle $\beta_{2л}$, it is possible to consider that the optimum magnitude of the angle $\beta_{2л}$ for pumps lies within limits of 20-60°. Usually for pumps of LPRE the value $\beta_{2л}$ =30-50°, and the value $\varphi_н$ is close to 0.75-0.65.

For pumps which pump hydrogen which possesses low density, high pressures (large coefficients of pressure) are necessary. Therefore, for a reduction in the overall dimensions of hydrogen pumps the value $\beta_{2л}$ in these pumps is selected equal to 90°, i.e., blades with a radial outlet part, which also satisfy the

conditions of strength at increased circular velocities are used. For hydrogen pumps the circular velocity can reach values of 350-450 m/s (see source [107]).

b) The Types of Wheels

In pumps of LPRE most frequently encountered are double shrouded rotors having driven and driving disks (front and rear cover walls) (Fig. 3.8a); but single shrouded (see Fig. 3.8b) and unshrouded (see Fig. 3.8c) wheels can be encountered.

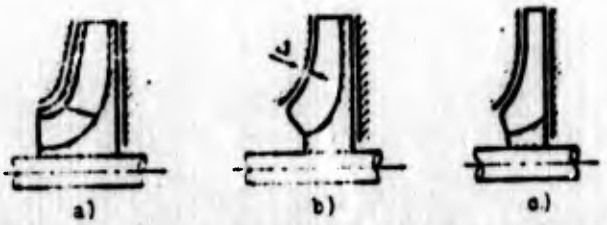

Fig. 3.8. Types of centrifugal wheels: a) double shrouded; b) single shrouded; c) unshrouded.

Usually the efficiency of a pump with double shrouded wheels is more than the efficiency of a pump with the single shrouded or unshrouded wheel. In unshrouded wheels there appear losses connected with the leakage of the fluid through the axial clearance Δ from one side of the blades to the other. Single shrouded and unshrouded wheels must be made with a small axial clearance, since with an increase in the clearance the efficiency of the pump which has such wheels is decreased (see source [68]). Pumps with double shrouded wheels are little sensitive to axial clearance. This makes it possible to maintain the clearance with less accuracy which gives structural advantages to such pumps. Unshrouded wheels are simpler in a technological respect.

c) Profiling of the Impeller Vanes

Widespread use has been obtained by the construction of the center line of the impeller vane by the circular arc (cylindrical

blades). For wheels with a ratio $D_1/D_2 \leq 0.5\text{-}0.55$, for which the dominant role in the energy transfer is played by the Coriolis and not the circulation forces (see Section 2.7.3), the selection of the simple shape of the blade is completely substantiated. Experience shows that wheels with cylindrical blades, as a rule, are equivalent in cost effectiveness to wheels of blades of a more complex shape. In a technological respect cylindrical blades are the most simple.

For centrifugal wheels with large ratios of diameters ($D_1/D_2 > 0.6$) the role of the circulation forces in the energy transfer increases. This requires the use of aerodynamically more perfected shapes of blades. Such wheels can be made with three-dimensional blades, i.e., with blades of twofold curvature. The method of the construction of such blades is presented in work [13].

Let us discuss the construction of the center line of the cylindrical blade (see source [15]). Circles with diameters D_1 and D_2 are drawn (Fig. 3.9). On the circle of diameter D_2 the arbitrary point G is selected, and it is connected with the center of the circle O. From radius OG the angle equal to the sum of the angles $\beta_{1л} + \beta_{2л}$ is plotted. At this angle the radius OK of the circle of diameter D_1 is drawn. Point G is connected with point K and line GK is continued up to the intersection with the circle of diameter D_1 at point B. Drawn from point G is the ray at angle $\beta_{2л}$, which is plotted to the left of line OG. From the middle of line GB a perpendicular is erected up to its intersection at point M with the ray drawn from point G. Point M will be the center from which one should draw the arc forming the center line of the blade - arc BG.

It is easy to show that the arc BG is inclined toward the circle of diameter D_1 at an angle $\beta_{1л}$ and toward the circle of diameter D_2 at angle $\beta_{2л}$. Having designated the angle OGB by symbol ψ, we obtain

$$\angle OKB = \vartheta_{1л} + \vartheta_{2л} + \psi;$$
$$\angle OBK = \angle OKB = \vartheta_{1л} + \vartheta_{2л} + \psi;$$
$$\angle MBG = \angle MGB = \vartheta_{2л} + \psi;$$
$$\angle OBM = \angle OBK - \angle MBG = \vartheta_{1л} + \vartheta_{2л} + \psi - \vartheta_{2л} - \psi = \beta_{1л}.$$

Correspondingly,

$$\angle LBP = \angle OBM = \beta_{1л} \text{ and } \angle NGQ = \angle MGO = \beta_{2л}.$$

It is also possible to constuct the center line of the blades by two circles, a parabola, etc., but for this angles at the inlet and outlet - $\beta_{1л}$ and $\beta_{2л}$ - and the angle of inclusion of blade θ.

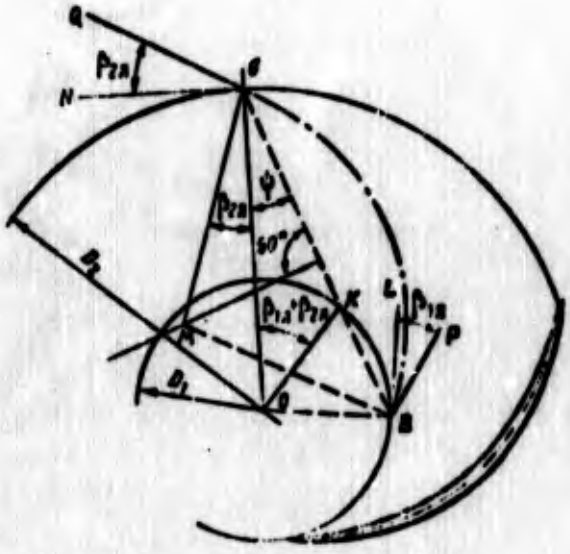

Fig. 3.9. Profiling of the blades of a centrifugal wheel.

From the center line of the profile it is necessary to plot the profile thickness δ. The law of the change in the profile thickness is assigned. The maximum profile thickness is located approximately on the middle of the center line. Usually $\delta_{max}/b_л$ = 0.05-0.08; for an improvement in the anticavitation qualities of the wheel leading edge is sharpened on a length equal to 0.2-0.3 from the length of the blade. For the purpose of

decreasing the blocking of the cross section the leading edge is also made sharpened; the sharpening occupies approximately the same length as that at inlet. At a distance of the pitch $t = \pi D_2/z$ the following blade is similarly constructed. The obtained vane channels must be checked. The law of the change in the flow area should be smooth and approach the samples recommended in practice.

The flow area of the vane channel, which is perpendicular to lines of current in relative motion, is approximately determined by the area of the trapesoid, the center line of which is equal to the diameter of the circumference inscribed into the vane channel (see Fig. 2.12), and the height is equal to the width of the wheel in the meridian section b on the radius corresponding to the selected point on the center line of the vane channel. The diameter of the circumference inscribed into vane channel conditionally replaces the distance along the normal between the two adjacent profiles.

Having a high hydraulic efficiency are rotor wheels whose change in the flow area of the vane channel depending on the radius passes through the maximum at approximately one-third of the length of the channel; value Δ should be 10-20% of $F_{s=0}$ (Fig. 3.10). With a similar change in the flow area of the vane channel the area of diffuser flow is decreased.

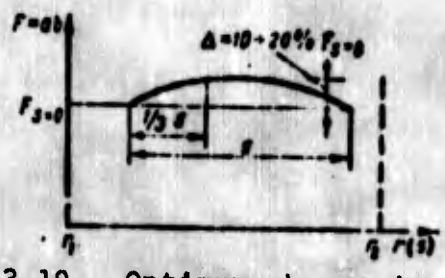

Fig. 3.10. Optimum change in the flow passage cross-sectional area of the vane channel of the centrifugal wheel along the radius.

3.1.1.3. Theoretical Pressure of a Screw-Centrifugal Pump Taking into Account the Finite Number of the Blades

For determining the theoretical pump pressure, or, in other words, the specific energy transmitted to the fluid, we take the boundary cross sections at the inlet into the screw conveyor and at outlet from the centrifugal wheel. Then the theoretical pressure of the screw-centrifugal pump (if we accept the scheme of the wheels with an infinitely large number of blades) is calculated in accordance with equations (2.31) and (2.59).

In the presence of a screw conveyor the specific energy transferred to the fluid by the centrifugal wheel will be less by the value of the specific energy transferred to the fluid screw conveyor. The theoretical pressure of the centrifugal wheel should be calculated taking into account the circular component at the inlet into the wheel:

$$H_{T\infty} = H_{T\infty 2} + H_{T\infty 1},$$

or $$H_{T\infty} = (c_{2u}u - c_{1u}u)_\infty + (c_{2u\infty}u_2 - c_{1u}u_1)_\infty.$$

Under the assumption that the flow between the screw conveyor and the centrifugal wheel obeys the law $c_u r$ = const, we obtain

$$(c_{2u}u)_\infty = (c_{1u}u_1)_\infty$$

and then

$$H_{T\infty} = (c_{2u\infty}u_2)_\infty - (c_{1u}u)_\infty.$$

When $c_{1u\ \infty} = 0$ the equation is simplified:

$$H_{T\infty} = c_{2u\infty}u_2. \qquad (3.6)$$

Consequently, the theoretical pressure of the screw-centrifugal pump is determined by the outlet parameters of the centrifugal wheel, i.e., just as if there is one centrifugal wheel, under the condition that $c_{1u\ ц} = 0$.

In view of the inertness of the fluid, it is not possible to transmit from the wheel with the finite number of blades the energy corresponding to $H_{T\infty}$. The energy distinct from $H_{T\infty}$ and equal to H_T (see Section 2.10.3) is transferred to the fluid:

$$H_T = k_z H_{T\infty}.$$

For the case where $c_{1u\ ш} = 0$, we will have

$$r_{2ш} = k_z r_{2u\infty}, \qquad (3.7)$$

and the coefficient of pressure $\bar{H} = k_z \eta_г \bar{H}_{T\infty}$ [see equation (3.3)]. The relation between H_T and $H_{T\infty}$ was established by a whole number of researchers on the basis of calculated or experimental dependences (see for example, source [15]).

The most theoretically substantiated data on coefficient k_z and theoretical pressure H_T can be obtained in the solution to the problem of the flow of the circular cascade of the centrifugal wheel. In source [60] this problem for the potential incompressible flow is solved by the method of singularities. The spaciousness of the cascade (variable width of the blade) was considered by the introduction of the system of flows whose intensity was changed depending on the width of the blade.

For training purposes the determination of coefficient k_z of the screw centrifugal pumps can be conducted according to data given in works [60] and [100] (Figs. 3.11-3.13), even if the geometric parameters of the wheels differ somewhat from those for which the data in these works are obtained.

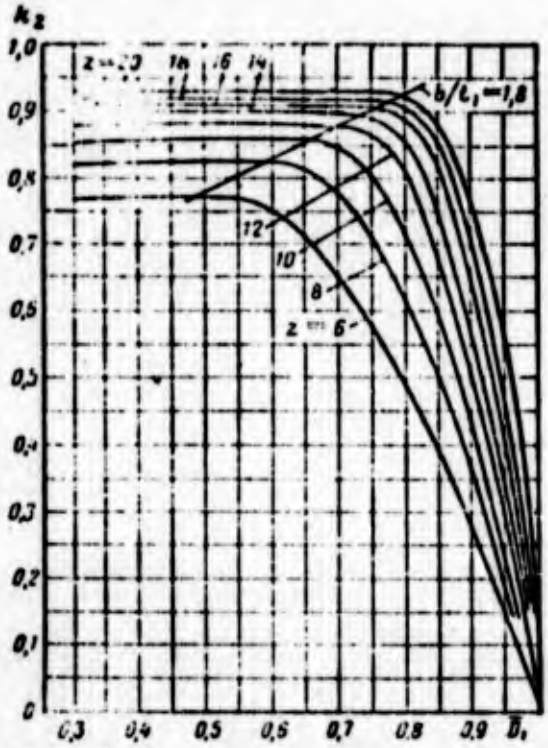

Fig. 3.11.

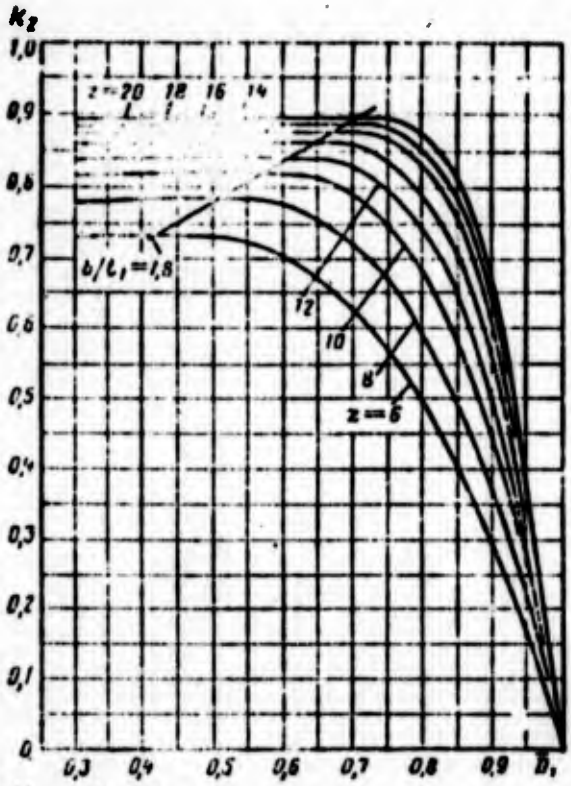

Fig. 3.12.

Fig. 3.11. Dependence of coefficient k_z on the relative diameter $\bar{D}_1 = D_1/D_2$ and the number of blades z (when $\beta_{2л} = 30°$, $c_{2m}/u_2 \leq$ ≤ 0.2 and $\beta_{1л} = 28°$).

Fig. 3.12. Dependence of coefficient k_z on the relative diameter $\bar{D}_1 = D_1/D_2$ and the number of blades z (when $\beta_{2л} = 60°$, $c_{2m}/u_2 \leq$ ≤ 0.2 and $\beta_{1л} = 28°$).

Let us examine in more detail the effect of parameters of the pump on k_z. The effect of the operating mode of the pump on coefficient k_z is important in the range $c_{2m}/u_2 < 0.15$-0.2 (see Fig. 3.14, borrowed from source [60]), which is of practical interest. The number of blades considerably affects the coefficient k_z. With an increase in the number of blades z the coefficient k_z increases (Fig. 3.15).

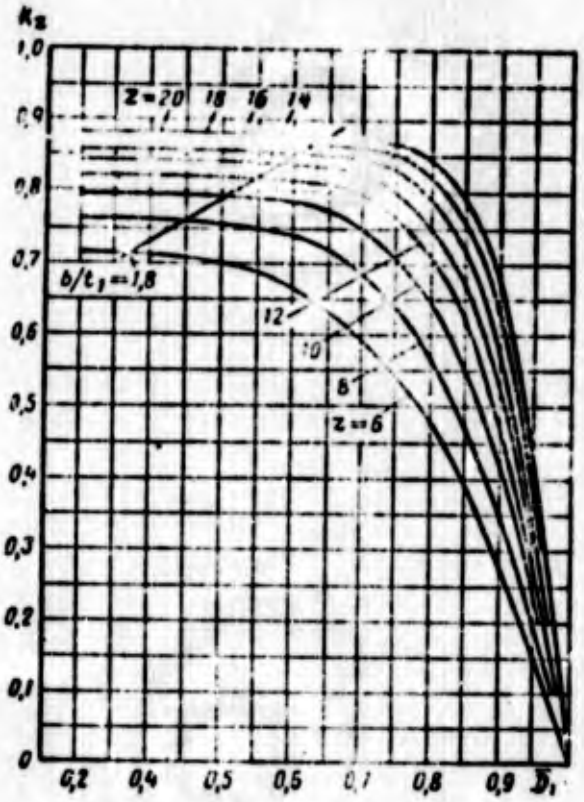

Fig. 3.13. Dependence of coefficient k_z on the relative diameter $\bar{D}_1 = D_1/D_2$ and the number of blades z (when $\beta_{2л} = 90°$, $c_{2m}/u_2 \leq$ ≤ 0.2 and $\beta_{1л} = 28°$).

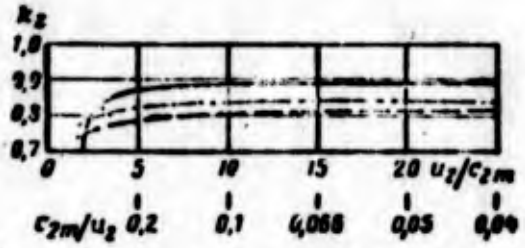

Fig. 3.14. Effect on coefficient k_z of the ratio of the velocities u_2/c_{2m} ($\bar{D}_1 = 0.8$; $\beta_{1л} = 28°$; z = 16): —— $\beta_{2л} = 30°$; -·- $\beta_{2л} = 60°$; --- $\beta_{2л} = 90°$

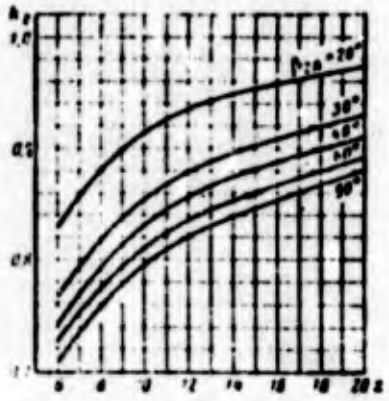

Fig. 3.15. Effect on coefficient k_z of the number of blades z and angle $\beta_{2л}$ ($\beta_{1л}$ = 20-28°; b/t_1 = 1.8-1.9).

As regards the relative diameter $\bar{D}_1 = D_1/D_2$, its effect is felt only with the low cascade density of the wheel, beginning from denseness $b_л/t_1 < 1.8$-1.9 (t_1 - the cascade pitch at the inlet) (see Figs. 3.11-3.13). With the usually accepted number of blades z = 6-12 the effect of $\bar{D}_1$ is developed in the region $\bar{D}_1 > 0.5$-0.6. With an increase of the number of blades the value $\bar{D}_1$, beginning from which k_z falls, is increased. Therefore, at large values of $\bar{D}_1$, for an increase in k_z it is necessary to increase the number of the blades. In the limit when the relative diameter of the circular cascade of the wheel $\bar{D}_1 \to 0$, the cascade density becomes so low that it does not exert a deflecting effect on the flow, and $k_z \to 0$.

With an increase in the angle of blades at the outlet $\beta_{2л}$ coefficient k_z is monotonically decreased (Fig. 3.16). This is explained by an increase, with an increase in $\beta_{2л}$, of a pressure differential on the blade (increase in the load) similar to an increase in the load with a decrease in the number of blades. The greatest effect $\beta_{2л}$ is developed in the region of the low values of the angle ($\beta_{2л} < 40$-$50°$) and in the region of large angles ($\beta_{2л} > 110$-$120°$).

If in the case of diffuser wheels [$F_1/F_2 \leq 1$ ($\beta_{2л} > \beta_{1л}$)] there will always be $\bar{H}_т < \bar{H}_{т\infty}$, $0 \leq k_z < 1$ and angle $\delta = \beta_{2л} - \beta_2$ is positive, then in the case of convergent wheels [$F_1/F_2 > 1$ ($\beta_{2л} < \beta_{1л}$)] the theoretical pressure $\bar{H}_т$ can exceed the theoretical

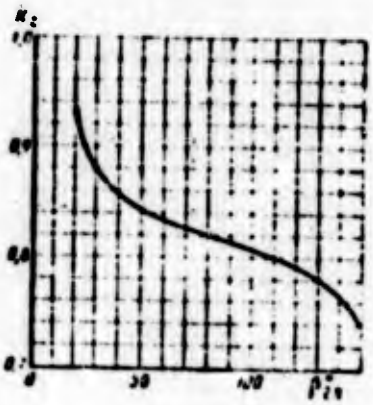

Fig. 3.16. Dependence of coefficient k_z on the angle $\beta_{2л}$ ($\bar{D}_1 = 0.5$; $\beta_{1л} = 28°$; $z = 12$)

pressure with an infinite number of blades $\bar{H}_{T\infty}$ or be equal to it ($\bar{H}_T \geq \bar{H}_{T\infty}$) (see Section 2.10.3 and Fig. 2.54). In this case the angle of lag δ will be negative or equal to zero ($\delta \leq 0$), and k_z can take values equal to unity or larger than unity (Fig. 3.17) and also negative: $k_z \geq 1$; $k_z < 0$. The possibility of obtaining the indicated values δ, $\bar{H}_T$ and k_z, which ensue from the theory, is confirmed experimentally (see source [59]).

Figure 3.17 depicts the experimental values of δ, $\bar{H}_T$ and k_z for the convergent cascade of the centrifugal wheel ($F_1/F_2 = 2.2$). They are calculated according to the measured angle of flow at the outlet; the wheel worked in free space without a spiral branch pipe (see source [82]). The nature of the change $\bar{H}_T$ and k_z according to $\bar{c}_{2m} = c_{2m}/u_2$ corresponds to the nature of their change predicted by the theory (see source [60]).

At large values of c_{2m} the theoretical pressure $\bar{H}_T$ becomes more than $\bar{H}_{T\infty}$, and, consequently, k_z becomes more than unity, and δ is negative. When $\bar{c}_{2m} = \operatorname{tg} \beta_{2л}$, when $\bar{H}_{T\infty} = 0$, value k_z, in accordance with equation (2.130), is equal to infinity.

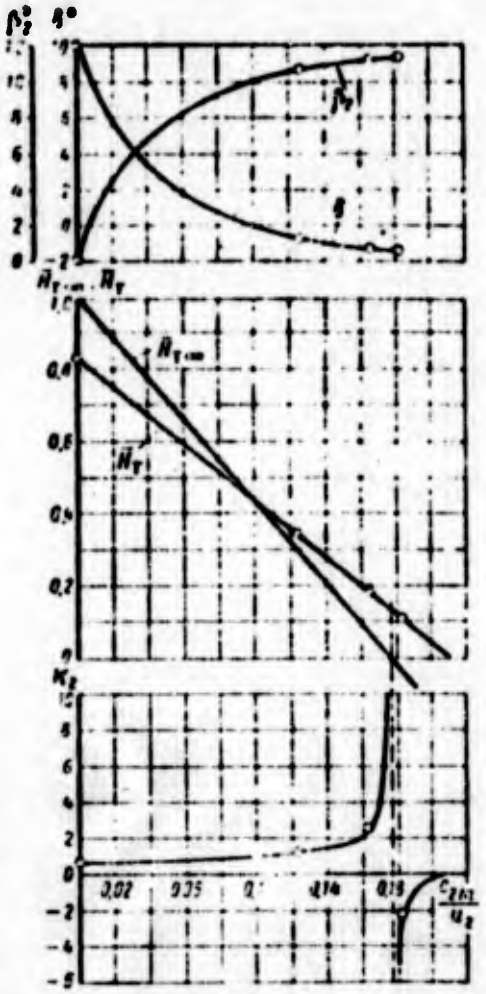

Fig. 3.17. Dependence of the angle of lag of flow δ at the outlet from the centrifugal wheel and coefficients k_z, $\bar{H}_{T\infty}$, and $\bar{H}_T$ on ratio c_{2m}/u_2 for the convergent cascade of the centrifugal wheel ($F_1/F_2 = 2.2$).

When $\bar{c}_{2m} > \operatorname{tg} \beta_{2л}$ the value $\bar{H}_{T\infty}$ takes the negative values, $\bar{H}_T$ remains positive, and then k_z becomes negative. At the point $\bar{H}_T = 0$ the value k_z takes a zero value.

3.1.1.4. Branch Pipe of the Pump

A. GENERAL INFORMATION

The branch pipe serves for the collection of the fluid coming out of the wheel, its direction into the system, and the conversion

in this case of the kinetic energy of flow into the pressure energy. This is necessary because the flow at the outlet from the wheel has a velocity of 150-200 m/s and sometimes it is more, i.e., it possesses high kinetic energy, while for the feed system of the LPRE high pressures (15-30 MN/m^2) and the low speed of the fluid at the outlet from the pump ($c_{вых}$ = 6-15 m/s) are necessary. The high speeds of motion of the fluid in the system lead to high hydraulic losses. Furthermore, the hydraulic impact with the action of the automation elements of the LPRE (velocity is quenched down to zero) will be more at a higher initial velocity.

The available kinetic energy for conversion into pressure energy in the discharge device is equal to

$$\frac{c_2^2}{2} - \frac{c_{вых}^2}{2}.$$

At values $\beta_{2л}$ common for pumps, equal to 30-50°, it consists in the design conditions of 25-35% of the entire theoretical pressure of the pump.

The branch pipes have the following requirements:

1) converting the kinetic energy of the fluid flow into static head with minimum losses;

2) insuring the uniform field of velocities and pressures, creating conditions for the steady relative motion of the fluid through the wheel and for the reduction in the radial stresses;

3) having the smallest possible dimensions.

The branch pipe of a single-stage pump (Fig. 3.18) usually consists of a circular vaneless diffuser (section 2-2'), a spiral collector (section 2'-3) and a conical diffuser (3-4)

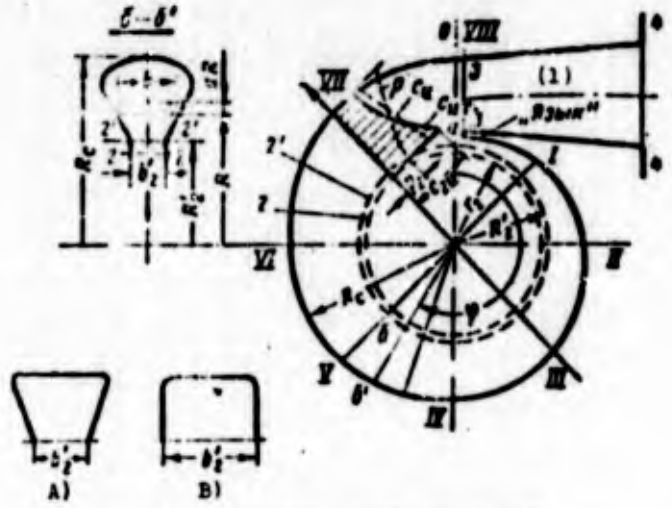

Fig. 3.18. Spiral branch pipe.
KEY: (1) "Tongue."

Besides the vaneless diffuser, the branch pipe can include even a vane diffuser (Fig. 3.19). Technologically the vane diffuser is complex, but during its use increase strength and rigidity of the housing, and the efficiency at the precalculated point can also be increased.

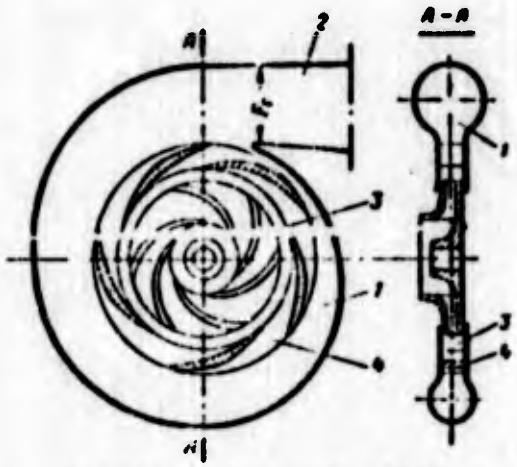

Fig. 3.19. Diagram of a pump with a circular vane diffuser: 1 - spiral collector; 2 - conical diffuser; 3 - circular vaneless diffuser; 4 - circular vane diffuser.

The vaneless diffuser plays an auxiliary role in pumps of LPRE. It separates the wheel of the pump from vanes of the vane diffuser or from the "tongue" of the spiral part of the branch pipe. Converted in it into potential energy is the insignificant portion of the kinetic energy of the flow.

In compressors and blowers the vaneless diffuser has an independent importance. In the vane and conical diffusers there occurs the conversion into pressure of virtually the entire available kinetic energy of the flow. The spiral collector is intended for the collection of the fluid coming out of the wheel and its direction through the conical diffuser into the main delivery line. In conical diffuser basically the conversion of kinetic energy into potential energy occurs.

The branch pipes of multistage pumps, besides the indicated elements, include reverse guiding vanes II (Fig. 3.20), which are intended for the removal of fluid from one stage of the pump to the other.

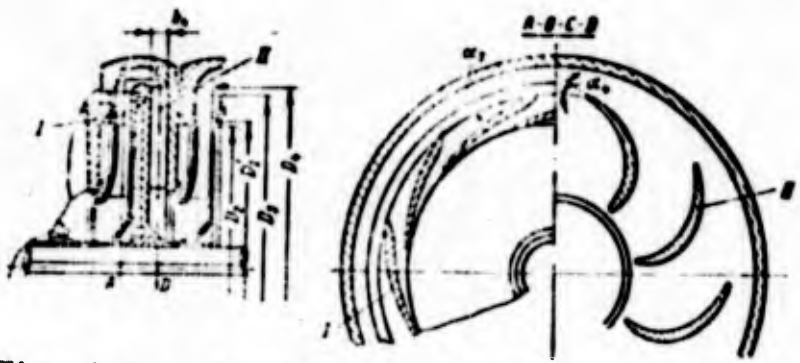

Fig. 3.20. Multistage centrifugal pump: I - circular vane first-stage diffuser; II - guiding vane between the first and second stages.

Let us examine in more detail the flow in the elements of discharge devices.

B. VANELESS ANNULAR DIFFUSER

At the inlet into the plane vaneless diffuser, which is annular space at the outlet from the wheel (Fig. 3.21), the flow has the rate $c_2 = \sqrt{c_{2u}^2 + c_{2m}^2}$ equal to the escape velocity of the fluid from the wheel. The rates c_{2m} and c_{2u} (velocity components c_2) are determined respectively from equations (2.3) and (3.7). As a rule, c_{2u} is considerably more than c_{2m}, and therefore in diffuser elements of the branch a pressure increase occurs basically because of a decrease in circular velocity component c_{2u}.

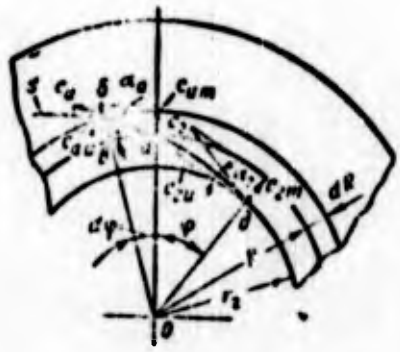

Fig. 3.21. Determination of the flow line of fluid in a circular vaneless diffuser.

Let us examine how velocities c_{2m} and c_{2u} in the plane vaneless diffuser are decreased. A decrease in the velocity c_{2m} is reached by an increase in the flow area with an increase in the radius:

$$\frac{c_m}{c_{2m}} = \frac{F_{2m}}{F_m} = \frac{2\pi r_2 b_2}{2\pi R b}. \qquad (3.8)$$

Hence when $b = b_2$ we obtain

$$\frac{c_m}{c_{2m}} = \frac{r_2}{R}, \qquad (3.9)$$

i.e., the meridian velocity component c_m is decreased inversely proportional to the radius of the vaneless diffuser.

Let us establish the dependence of the circular component c_{2u} on the radius R from the moment-of-momentum equation (2.21), assuming that the wall friction of the diffuser is absent:

$$G(c_{2u}r_2 - c_u R) = 0.$$

Hence we will obtain

$$\frac{c_u}{c_{2u}} = \frac{r_2}{R}. \qquad (3.10)$$

Consequently, the circular velocity component c_u will be decreased with an increase in the radius (Fig. 3.22).

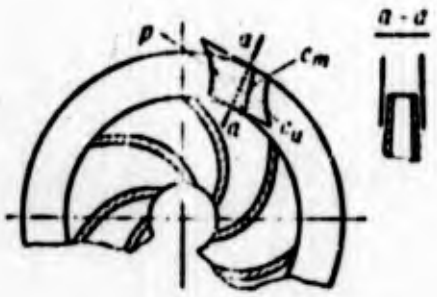

Fig. 3.22. Distribution of pressure and velocities in a circular vaneless diffuser.

The ratio $c_m/c_u = \operatorname{tg}\alpha$ determines the inclination of the flow line. With the aid of expressions (3.9) and (3.10), we obtain

$$\operatorname{tg}\alpha = \frac{c_m}{c_u} = \frac{c_{2m}}{c_{2u}} = \operatorname{tg}\alpha_2. \qquad (3.11)$$

i.e., the flow line in the vaneless diffuser retains the initial angle α_2.

Let us find the expression for the flow line. The flow passing from radius R (see Fig. 3.21) to radius R + dR follows along line s, which is the flow line with the angle equal to α_2. From the elementary triangle aбв we obtain

$$\frac{dR}{Rd\varphi}=\operatorname{tg}\alpha_2.$$

Hence let us record the differential equation of the flow line in polar coordinates:

$$\frac{dR}{R}=\operatorname{tg}\alpha_2 d\varphi.$$

Integrating this equation within limits from r_2 (correspondingly, $\phi = 0$) to the current values R and ϕ, we obtain

$$\int_{r_2}^{R}\frac{dR}{R}=\operatorname{tg}\alpha_2\int_0^{\varphi}d\varphi;\quad \ln\frac{R}{r_2}=\varphi\operatorname{tg}\alpha_2;$$

$$R=r_2e^{\varphi\operatorname{tg}\alpha_2}. \qquad (3.12)$$

Equation (3.12) is the equation of the logarithmic spiral, passing through the point $\phi = 0$ and $R = r_2$. Thus, the flow line in the vaneless diffuser of constant width is the logarithmic spiral. The less the angle α_2 (the more c_{2u} in comparison with c_{2m}), the more the length of the flow line s (see Fig. 3.21) and the larger the path the particle of fluid passing from radius r_2 to radius R of the vaneless diffuser passes. Friction increases the angle of inclination of the spiral α.

Let us define how the pressure increases in the vaneless diffuser (not allowing for friction). From the Bernoulli equation (2.75) we obtain

$$p-p_2=\rho\left(\frac{c_2^2}{2}-\frac{c^2}{2}\right).$$

After the substitution into this equation of expressions (3.9) and (3.10), we find:

$$p-p_2=\rho\frac{c_2^2}{2}\left[1-\left(\frac{r_2}{R}\right)^2\right]. \qquad (3.13)$$

With an increase in the radius the pressure in the vaneless diffuser is increased (see Fig. 3.22). For the conversion in the vaneless diffuser of a considerable part of the kinetic energy of flow into potential energy, it is necessary to increase the external radius of the diffuser, considerably increasing its radial extent. Therefore, as a basic diffuser device the vaneless diffuser in pumps of the liquid-propellant rocket engine is not used. Moreover, pumps of liquid-propellant rocket engines have a small ratio c_{2m}/c_{2u} (small value α_2 = 5-10°), and this, as was already mentioned, leads to the great length of the flow line, and, therefore, to great friction losses of the fluid against the walls of the diffuser.

Losses in vaneless diffusers of pumps of liquid-propellant rocket engines are usually not calculated separately. These refer to losses in the spiral part of the branch or to losses in the vane diffuser. In pumps of liquid-propellant rocket engines the external radius of the vaneless diffuser R_2' is usually equal to $(1.05\text{-}1.15)r_2$.

C. VANE ANNULAR DIFFUSER

The vane annular diffuser is made in the form of a circular cascade installed between walls (see Fig. 3.19). The liquid jet is deflected by the blades from the trajectory of free motion along the logarithmic spiral. The trajectory in the particles of fluid is obtained more steeply. With the same radial displacement the circular velocity component in the vane diffuser is decreased more greatly than it is in the vaneless. A decrease in c is basically provided by a decrease in c_{2u}, since value c_m is generally comparatively small.

The shape of the blade (Fig. 3.23) is selected so that the angle $\alpha_{3л}$ would be more than the angle $\alpha_{2л}'$, determined by the inclination of absolute velocity to the circular direction with a

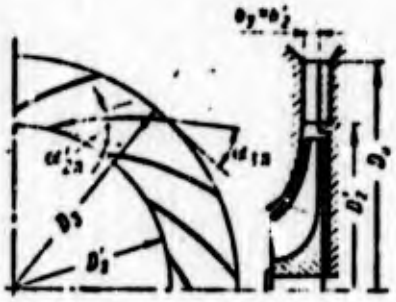

Fig. 3.23. Diagram of a circular vane diffuser.

free flow of fluid. The vane channel in this case is expanded, and the angle of expansion should not exceed 8-10°.

The expansion ratio of the vane diffuser is equal to (see Fig. 3.23):

$$\frac{F_3}{F_2'} = \frac{\pi D_3 k_3' b_3 \sin \alpha_{3a}}{\pi D_2' k_2' b_2' \sin \alpha_{2a}}, \qquad (3.14)$$

where k_3 is the coefficient of narrowing of the section by the blades at the outlet; k_2' is the coefficient of narrowing of the section by blades at the inlet.

It is recommended to select the width of the vane diffuser b_2' somewhat larger than the width of the flow area of the wheel:

$$b_2' = (1{,}1 \div 1{,}2) b_3.$$

This makes it possible to compensate for the inaccuracy in the relative location of the wheel and diffuser.

In channels of the vane diffuser the stagnation of flow is achieved on a shorter path of the particle of fluid than in the vaneless annular diffuser, and therefore at the narrow angles of the outlet of the jet from the wheel hydraulic losses in the vane diffuser are less than those in a vaneless annular diffuser. The number of blades is usually 5-12.

The installation of the vane diffuser complicates the design of the pump, but sometimes its use is desirable from a structural point of view, since the vane diffuser can insure great rigidity and strength of the pump casing with thin walls.

The outlet velocity from the vane diffuser is found from the known angle of inclination of the center line of the blades to the circular direction and according to the known meridian velocity component:

$$c_{3m} = \frac{Q}{\pi D_3 b_3}; \tag{3.15}$$

$$c_{3u} = \frac{c_{3m}}{\sin \alpha_{3л}} \text{ and } c_{3u} = \frac{c_{3m}}{\operatorname{tg} \alpha_{3л}}. \tag{3.16}$$

The velocity behind the blades will be less, since the meridian component is lowered due to an increase in the cross-sectional area:

$$c_{3m} = \frac{Q}{\pi D_3 b_3}.$$

The circular component will not be changed:

$$c_{3u} = c_{2u};$$
$$c_3 = \sqrt{c_{3u}^2 + c_{3m}^2}. \tag{3.17}$$

The pressure increase in the vane diffuser is determined from the energy equation

$$p_3 - p_2 = \rho\left(\frac{c_2'^2}{2} - \frac{c_3^2}{2}\right) - L_{гидр}.$$

Assuming that $k = 1$ and $c_2' = c_{2m}'/\sin \alpha_{2л}'$ - (angle of attack is equal to zero), we obtain that

$$p_3 - p_2 = \rho \frac{c_3'^2}{2}\left[1 - \left(\frac{D_2' \sin \alpha_{2л}'}{D_3 \sin \alpha_{3л}}\right)^2\right] - L_{\text{с.в}}$$

Since $\alpha_{3л} > \alpha_{2л}'$, then with identical dimensions in the vane diffuser a larger pressure increase than in the vaneless diffuser is achieved [see equation (3.13)]. The flow in the vane diffuser and losses in it are calculated as in the vane circular cascade if ratio $b_л/t_{ср} < 1$ (here $b_л$ is the length of the blade; $t_{ср}$ is the pitch at the mean diameter of the vane diffuser). When $b_л/t_{ср} > 1$ the vane diffuser is considered as a system of the channels. The losses in it are determined from equations of hydraulics (see Section 2.13.2.1).

Usually vane diffusers have $D_3/D_2' = 1.35\text{-}1.45$; $b_3/b_2' = 1$ (see source [ ]). The angle of the blades at outlet from the diffuser $\alpha_{3л}$ is taken to be 12-15° larger than angle $\alpha_{2л}'$. The center line of the diffuser vanes is outlined by a circular arc. The method of construction of the center line is similar to the method of construction of the center line of blades of the centrifugal wheel (see Section 3.1.1.2). The maximum thickness of the blade is located approximately on its middle. The leading edge of the blade is rounded off by a larger radius than is the trailing edge.

After the construction of the blades, it is necessary to be convinced of the fact that the angle of the equivalent conical diffuser, which has a length equal to the length of the vane diffuser and flow areas equal with it, does not exceed 10-12°. If the angle proves to be more, then for a decrease in its losses it must be decreased down to permissible values by means of a decrease in the angle $\alpha_{3л}$ or increase in the ratio of diameters D_3/D_2' and number of blades z.

D. SPIRAL COLLECTOR

The spiral collector is widely used in centrifugal pumps. The circular and meridian velocities of flow in it will be decreased with an increase in the radius (see Fig. 3.18). As a result of this a certain increase in the pressure along the radius occurs. An additional increase in the cross section for the conversion of kinetic energy $c_{2u}^2/2$ into pressure energy (geometric diffuser effect), as a rule, is not provided, since that increases the losses in the collector.

If in the outlet section of the collector the average velocity is equal to c_3, then the pressure increase in it is determined from the energy equation:

$$p_3 - p_2' = \rho\left(\frac{c_2'^2}{2} - \frac{c_3^2}{2}\right) - L_{\text{loss}},$$

where c_2' is velocity at the inlet into the collector (outlet from the vaneless diffuser).

Let us derive the fundamental relations for calculating the spiral collectors. Let us assume that the fluid flow through the element of the arc of the outlet circumference of the wheel is proportional to the angle of the coverage of this arc. Let us designate Q_ϕ as the flow through the arc аб (see Fig. 3.18) of the circle described by radius R_2':

$$Q_\varphi = \frac{\varphi}{2\pi} Q, \qquad (3.18)$$

where ϕ is the angle of coverage of arc аб, and Q is the fluid flow which enters from the wheel into the spiral.

The flow through the elementary cross section $df = bdR$ (see sketch on the upper left on Fig. 3.18) is designated

$$dQ_\varphi = c_u\, df = c_u b\, dR.$$

The flow through the whole cross section 6-6′ is also equal to Q_ϕ:

$$Q_\phi = \int_{R_2}^{R_c} dQ_\phi = \int_{R_2}^{R_c} c_u b dR. \qquad (3.19)$$

Having substituted here the expression for Q_ϕ from equation (3.18), we obtain

$$\frac{\varphi}{2\pi} Q = \int_{R_2}^{R_c} c_u b dR.$$

Hence there results the basic equation for calculating spiral collectors, which establishes the relationship of the current angle ϕ and geometric parameters b and R_c:

$$\varphi = \frac{2\pi}{Q} \int_{R_2}^{R_c} c_u b dR. \qquad (3.20)$$

The last equation is the basic equation for the design of the collector. If we assign the law of the change in c_u and width b along radius R, then from equation (3.20) the dependence of the radius of spiral R_c on the angle ϕ is determined. The cross section of the spiral can be circular (see Fig. 3.18), pear-shaped (see Fig. 3.18), trapesoidal (see Fig. 3.18A), rectangular (see Fig. 3.18B) and so on. The simplest is the rectangular cross section ($b = b_2' = \text{const}$).

Collectors with a rectangular cross section are frequently used in screw-centrifugal pumps. The width of the collector b_2' is selected on the basis of the width of the wheel. It can be more or less than the width of the wheel $b_д$, taking into account the thickness of disks of the wheel, but not less than the width

of the flow area of the wheel b_2 (Fig. 3.24). When $b_2' = b_2$ there is eliminated the appearance of vortex zones in the region shaded by faces of the disks. But with the width of the spiral b_2' exceeding the width of the wheel b_2, the energy of the jets flowing from disks of the wheel is used. Collectors with a width of b_2' larger than b_2 are usually used:

$$b_2' = b_2 + (0{,}04 \div 0{,}06) D_2.$$

An experiment shows (see source [91]) that an increase in the width of the collector, which will be accompanied, other conditions being equal, by a decrease in the height of cross sections of the collector, does not have a substantial effect on parameters of the pump.

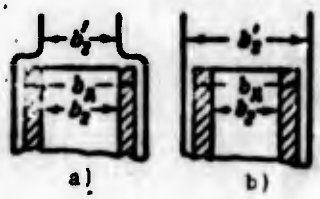

Fig. 3.24. Narrow (a) and wide (b) inlets into the spiral collector.

Let us examine the scheme of the calculation in which we proceed from the fact that the external wall of the collector should not have a disturbing effect on the flow. In this case the contour of the external wall of the spiral should coincide with the direction of flow lines of the fluid which moves from the wheel in free space. As is known, the free flow at the outlet from the wheel, not allowing for friction, obeys the law $c_u R = \text{const}$.

Assuming that $c_u R = c_{2u} r_2$, from equation (3.20) we obtain

$$\varphi = \frac{2\pi c_{2u} r_2}{Q} \int_{R_2'}^{R_c} b \frac{dR}{R}.$$

When $b = b_2' = \text{const}$

$$\varphi = \frac{2\pi c_{2m} r_2 b}{Q} (\ln R_c - \ln R_2'); \quad \ln \frac{R_c}{R_2'} = \varphi \frac{Q}{2\pi c_{2m} r_2 b}.$$

Taking into account that

$$\frac{Q}{2\pi r_2 b} = c_{2m} \frac{b_2}{b},$$

we obtain

$$\ln \frac{R_c}{R_2'} = \varphi \frac{b_2}{b} \operatorname{tg} \alpha_2;$$

$$R_c = R_2' e^{\varphi \frac{b_2}{b} \operatorname{tg} \alpha_2}; \qquad (3.21)$$

$$R_{c\max} = R_2' e^{2\pi \frac{b_2}{b} \operatorname{tg} \alpha_2}, \qquad (3.22)$$

Equation (3.21) for the external radius of the spiral of the rectangular cross section of constant width is the equation of the logarithmic spiral. The external wall of the spiral coincides with the flow line of fluid in the case of the absence of losses [see equation (3.12)].

The presence of losses in the spiral collector, caused by the wall friction and the nonuniformity of flow at the outlet from the wheel (inlet into the collector) and in the collector (losses to eddy viscosity in the flow) leads to a distinction in distribution of velocities and pressures in the collector from their distribution in the case of the absence of losses ($c_u R = \text{const}$).

Figure 3.25 gives the experimentally obtained velocity field in cross sections of the collector. It is evident, in particular, that the velocity c_u is decreased more slowly than according to the law $c_u R = \text{const}$, - in general according to the law $c_u R^{\alpha} = \text{const}$

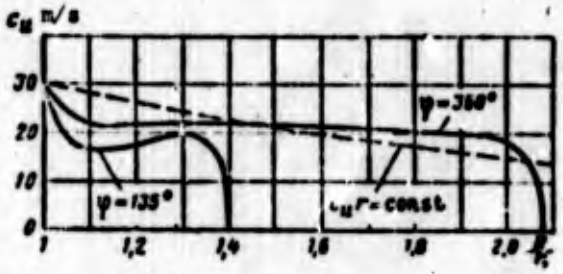

Fig. 3.25. Theoretical (dashed line) and experimental curves of the change in the circular velocity component of the flow c_u along the radius of the spiral collector.

($\alpha < 1$) (see source [75]). The mixing of the jets in the collector leads to the equalizing of the circular velocity on cross sections of the collector. This makes it possible to carry out calculation of the collector from the assumption of constant velocity c_c = const in all its cross sections.

Let us accept for the velocity c_c that velocity which would take place in the absence of losses ($c_u R$ = const) in the middle of the outlet section of the collector, i.e., on the radius

$$R_{cp} = \frac{R_{c\,max} + R_2'}{2}.$$

For the collector with a rectangular cross section b = const, by utilizing expression (3.22), it is possible to record:

$$R_{cp} = \frac{R_2'}{2}\left(1 + e^{2\pi \frac{b_2}{t}\operatorname{ctg}\alpha_2}\right).$$

Then

$$r_c = \frac{c_{u2}r_2}{R_{cp}} = r_{2a}\frac{2r_2}{R_2'}\left(1 + e^{2\pi \frac{b_2}{t}\operatorname{ctg}\alpha_2}\right)^{-1}.$$

The cross-sectional area of the outlet from the collector [inlet into the conical diffuser (see Fig. 3.18)] will be determined according to the equation

$$f_1=\frac{Q}{c_c}=\frac{QR_3'}{2\varepsilon_{2u}r_2}\left(1+e^{2\pi\frac{b_2}{b}\operatorname{ctg}\varepsilon_{2u}}\right). \qquad (3.23)$$

The areas of the intermediate cross sections are determined according to the area of the inlet into the conical diffuser f_3:

$$f_\varphi=(\varphi/2\pi)f_3, \qquad (3.24)$$

Since when b = const

$$f_\varphi=b(R_c-R_3'), \qquad (3.25)$$

Then, by substituting expression (3.25) into (3.24), we will obtain the following relation of the radius of collector R_c with the angle φ:

$$R_c=R_3'+(\varphi/2\pi)\frac{f_3}{b}. \qquad (3.26)$$

It should be noted that the operation of the pump with a small deviation in the actual contour of the external wall of the collector from that calculated is not greatly affected. However, deviation from the calculated area of the cross section of the inlet into the conical diffuser can affect the parameters of the pump (see source [91]).

E. CONICAL DIFFUSER

In the absence of a vane diffuser the basic stagnation of the flow is achieved in the conical diffuser. Its portion consists of 80-85% of the dynamic head converted into the static head in the discharge devices. The conical diffuser is made in the form of a widening connecting piece of variable cross section Fig. 3.26a). Its inlet section corresponds to the form of the cross section of the spiral collector, and the outlet section is usually made circular, since the conical diffuser will be joined directly with the pressurizing pipeline.

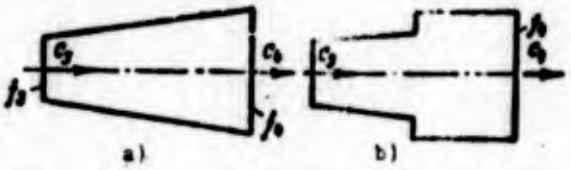

Fig. 3.26. Diagrams of conical diffusers: a) conical diffuser; b) stepped conical diffuser.

As studies showed (see source [91]), on the initial section of the diffuser it is advantageous not to increase the cross-sectional area. This leads to the equalizing of the velocity field and a decrease in the diffuser losses. It is possible to take the length of the section with a constant cross-sectional area on which the shape of the cross section of the inlet into the diffuser passes over to a circle equal to 0.2-0.35 of the length of the diffuser. The expansion ratio of the conical diffuser is characterized by the angle of opening γ°. The circular sections can have an opening angle 10-20°. The larger angles of opening lead to great losses connected with the boundary-layer separation.

In pumps of liquid-propellant rocket engines the large expansion ratios are used, since values of the escape velocities from the spiral $c_c = c_3$ are great and can reach 100-150 m/s. The average velocity in the outlet section of the spiral (at the inlet section of the conical diffuser) is found from the rate of discharge and the known value of the cross section.

The velocity $c_{вых}(c_4)$ in the outlet section of the conical diffuser determines the degree of its expansion:

$$\bar{f}_1 = \frac{f_3}{f_{вых}} = \frac{c_{вых}}{c_3}.$$

Then the pressure increase in the conical diffuser will be equal to

$$p_4 - p_1 = \varrho \frac{c_1^2}{2}\left(1 - \overline{f_3^2}\right) - L_{1\text{-}4}.$$

The length of the conical diffuser is usually limited to the value equal to $(2.5\text{-}6.5)d_3$, where d_3 is the equivalent diameter of the initial cross section of the diffuser $\left(d_3 = \sqrt{\frac{4}{\pi} f_3}\right)$.

If after the conical diffuser the velocity proves to be inadmissibly large (higher than 10-20 m/s), then a stepped conical diffuser is used (see Fig. 3.26b) or vane diffuser is placed at the outlet from the wheel. The use of a diffuser with a constant pressure gradient (diffuser with an increasing angle of expansion) deserves attention.

F. LOSSES IN THE COLLECTOR AND CONICAL DIFFUSER

During the calculations the losses in the spiral collector and in the conical diffuser are estimated totally with the use of statistical data. The calculation of losses in elements of the collector and conical diffuser by methods of hydraulics (see Section 2.13.2.1) is uncertain, since it does not consider, for example, the great nonuniformity of the field of velocities taking place in the collector and conical diffuser. Losses with the mixing of the jets which escape from the wheel with the flow which moves along the spiral collector should especially be noticeable. Because of the turbulence the velocities in the spiral along the cross section are equalized (law $c_u R^{\alpha} = \text{const}$, $\alpha < 1$), and the velocity c_2 escaping from the wheel has a higher value than the flow velocity which approached this cross section.

The sum of the losses in the collector and conical diffuser is expressed as the kinetic energy of the flow at the inlet into the collector. If the branch consists of a vaneless diffuser, collector and conical diffuser, then losses in such a branch are expressed as the kinetic energy of flow at the outlet from the wheel:

$$L_{отв} = \zeta_{отв} \frac{c_2^2}{2}. \qquad (3.27)$$

where $\zeta_{отв}$ = 0.18-0.22 (see source [95]) - the loss factor in branch. When $c_{1u\ ш} = 0$, disregarding the velocity c_{2m} (insignificant in comparison with c_{2u}), with the aid of expression (2.128) it is possible to record:

$$L_{отв} = \zeta_{отв} \bar{H}_т^2 \frac{u_2^2}{2}. \qquad (3.28)$$

3.1.1.5. Hydraulic Efficiency of the Pump

The hydraulic efficiency of the screw-centrifugal pump is the efficiency which evaluates the hydraulic losses in the flow area (see Section 2.15.1). The hydraulic efficiency of the screw-centrifugal pump can differ from the efficiency of the centrifugal pump not having a screw conveyor.

At small ratios D_1/D_2 ($D_1/D_2 \leq 0.5$-0.55), which is characteristic for small values of n_s ($n_s < 60$-80), the arrangement of screw conveyor has little effect on the hydraulic efficiency of the pump. With large ratios D_1/D_2 ($D_1/D_2 > 0.55$) the installation of the screw conveyor, as a rule, increases the hydraulic efficiency of the pump by 10-15% (see source [50]), and sometimes an increase in the efficiency reaches 20-30%.

At values of $D_1/D_2 > 0.55$ the efficiency of the centrifugal wheel decreases, and the installation of the screw preliminary pump makes it possible to hold it at a level of 0.82-0.85. This circumstance is very important for pumps of liquid-propellant rocket engines, since the centrifugal wheels of the pumps of liquid-propellant rocket engines of high thrusts have large ratios D_1/D_2. Therefore, the screw preliminary pump is frequently used not only for an increase in the anticavitation qualities of the pump, but also for an increase in efficiency.

The maximum values of hydraulic efficiency (Fig. 3.27), as experimental studies show, lie at values of relative "twist" at the inlet into the centrifugal wheel $c_{1u\,ц}/u_{1ц} = 0.3\text{-}0.4$. With an increase in $c_{1u\,ц}$ (which corresponds to the large pitch of the screw preliminary pump) increases the portion of energy transferred by means of the Coriolis force of inertia (see Fig. 2.36), and the portion of energy transferred by the wheel as a result of the circulation flow is decreased.

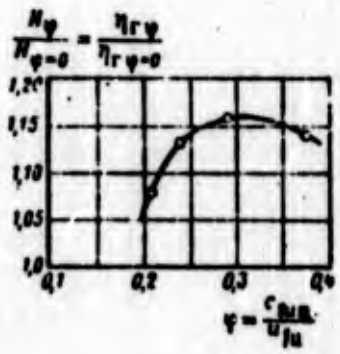

Fig. 3.27. Effect of twist at the inlet into the centrifugal wheel on the hydraulic efficiency and pressure of the screw-centrifugal pump.

Hydraulic losses with the transmission of energy by means of Coriolis forces are connected only with the rate of the flow, i.e., with the relative velocity, and it is decreased with an increase in $c_{1u\,ц}$ (see Fig. 3.4). As a result of this, the energy losses in the centrifugal pump are lowered. With a further increase in $c_{1u\,ц}$ (screw pitch) the portion of losses of the screw preliminary pump in the total energy balance increases, and the efficiency of the screw conveyor is somewhat less than the efficiency of the centrifugal wheel. Furthermore, at high values of $c_{1u\,ц}$ the losses on the section between the screw conveyor and the centrifugal wheel increase.

The effect of the shape of profiles of the blades of an axial preliminary pump and centrifugal wheel on the magnitude of the hydraulic efficiency of the screw-centrifugal pump is small:

The ratio

$$\frac{H_т - h_{гидр.вх.ш} - h_{гидр.отв}}{H_т} = \frac{H_{нас}}{H_т}\eta = \eta_{гв} \qquad (3.29)$$

is the efficiency of the screw-centrifugal wheel, where $H_{нас}$ is pressure of the screw-centrifugal wheel. Disregarding losses in the feed, it is possible to record:

$$\eta_г = \eta_{г.в}\eta_{отв}. \qquad (3.30)$$

It is difficult to calculate directly $\eta_{г.к}$; it can be determined with the aid of equations (3.28) and (3.30), finding the preliminarily hydraulic efficiency of the entire pump ($\eta_г$) and the efficiency of the branch:

$$\eta_{отв} = \frac{H_{отв} - h_{отв}}{H_{отв}} = \frac{H}{H_{отв}}.$$

For calculating the hydraulic efficiency of the pump, results of the generalization of statistical data are used. For pumps with the ratio of the diameters $D_1/D_2 \leq 0.55$ the hydraulic efficiency $\eta_г = 0.82$-0.85. When $0.55 < D_1/D_2 \leq 0.8$

$$\eta_г = (1,1 \div 1,15)\left(1,3 - \frac{D_1}{D_2}\right). \qquad (3.31)$$

3.1.2. LEAKAGE LOSSES IN A PUMP. DISK AND MECHANICAL LOSSES

3.1.2.1. Leakage Losses in Pumps

A. GENERAL INFORMATION

In the most general case leakages of fluid in the centrifugal pump can occur along three channels (Fig. 3.28):

1) through the front seal, which separates the cavity of high pressure from the cavity of low pressure (Q_{y1});
2) through the discharging openings (Q_{y2});
3) through the seal along the shaft (Q_{y3}).

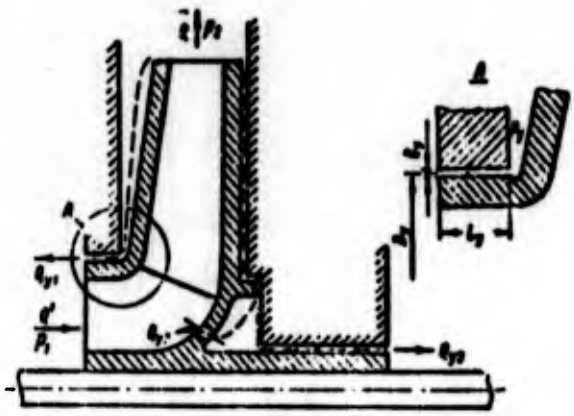

Fig. 3.28. Diagram of leakages of fluid from the pressure cavity of the centrifugal pump.

There can be no discharging openings, and therefore leakage Q_{y2} is not necessary for all pumps.

It is attempted to make the seal on the shaft, which separates the flow area of the pump from the drainage cavities, as a rule, with full sealing, using contact seals, and impellers; in this case the leakage virtually occurs through the drain holes into the inlet into the pump, the tank or the atmosphere.

In unshrouded wheels the fluid leakage from the pressure cavity into the intake cavity can occur through clearance between the blades, and the housing. The presence of a cover disk, or shroud, eliminates the overflowing through the blades from the forcing side to the nonoperative side, but does not remove the total leakage from the pressure cavity into the intake cavity.

In the designing of a turbopump unit of a liquid-propellant rocket engine [LPRE] (ЖРД), it is important to know quantity of fluid running off from the cavity of high pressure:

$$Q_y = Q_{y1} + Q_{y2} + Q_y.$$

The method of calculation of the amount of fluid which escapes through the seal is given in the example of a slot ring seal, which separates the cavity of high pressure from the cavity of low pressure on the driven disk of the centrifugal wheel (see Fig. 3.28A).

The leakage Q_{y1} depends on the flow passage cross-sectional area of the slot in the seal, the design of the seal (sharpness of edges, etc.) and the pressure differential.

The flow through the slot with an assigned pressure differential is found according to the known equation:

$$Q_{y1} = \mu f_y \sqrt{2\frac{p_y - p_1}{\rho}},$$

or

$$Q_{y1} = \mu \pi D_y \delta_y \sqrt{2L_y}. \qquad (3.32)$$

where μ is the coefficient of flow; f_y - the flow area of the seal; D_y - the diameter on which the seal is located; δ_y - value of the radial clearance; p_y - pressure in front of the seal; p_1 - pressure at the inlet into the wheel; L_y - energy lost by the fluid with overflowing through the seal.

Let us express L_y in terms of the static head of the wheel:

$$L_y = \frac{p_y - p_1}{\rho} = \frac{p_2 - p_1}{\rho} - \frac{p_2 - p_y}{\rho} = H_{st} - \frac{p_2 - p_y}{\rho}, \qquad (3.33)$$

where p_2 is pressure at the outlet from wheel.

The term $(p_2 - p_y)/\rho$ in equation (3.33) characterizes the pressure difference at the outlet from the wheel and in front of the seal.

In order to calculate the leakage through the seal, one should first find the pressure in front of the seal p_y, which is determined by the law of motion of the fluid in the clearance between the rotating wheel and pump casing.

B. DETERMINATION OF PRESSURE IN THE CLEARANCE BETWEEN THE ROTATING WHEEL AND PUMP CASING

The pressure distribution in the clearance between the wheel and the pump casing depends on the nature of the motion of the fluid in the clearance. Directly at the wall of the wheel the fluid is rotated together with the wheel. Near the wall of the housing the fluid is immobile. It is obvious that the interlayers of the fluid in the clearance are driven by forces of viscosity, but they have a circular velocity less than the circular velocity of the wheel on this radius. An approximate diagram of circular velocities (in the cross section of the clearance by the cylinder of an arbitrary radius) is shown on Fig. 2.87.

With the rotation of the fluid in the clearance, its motion in a radial plane appears. Under the action of centrifugal forces the layers of fluid adjacent to the wheel will be moved to a larger radius. Under the effect of increased pressure at the outlet from the wheel, along the wall of the housing motion from the periphery to the axis will begin. An approximate diagram of the meridian

velocity of the motion of fluid in the axial clearance is represented on Fig. 3.29, and the flow line for the centrifugal pump is given on Fig. 2.88. The velocity distribution in the clearance is affected by the "twist" of the main flow at the outlet from the wheel c_{2u}. With the flow of the fluid through the seal, the diagram of the meridian velocity in the axial clearance will be unsymmetric (see Fig. 3.29).

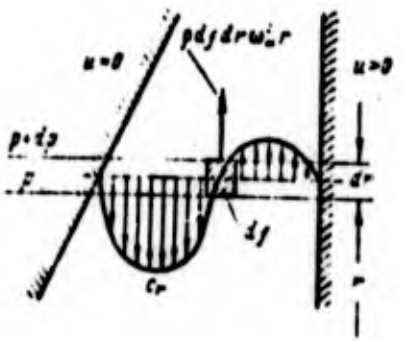

Fig. 3.29. Diagram of meridian velocity in the axial clearance between the disk and the pump casing.

As a first approximation let us find the pressure in front of the seal for the case where the fluid leakage through the seal, in view of the smallness of the flow of effluent fluid, will not noticeably affect the distribution of velocities and pressures in the clearance. In this case the average angular velocity of the rotation of fluid will be equal to half of the angular velocity of rotation of the wheel (see source [9]):

$$\omega_{cp.ж} = \frac{\omega}{2}.$$

Let us find the law of the change in pressure along the radius in the clearance for particles of fluid which is in radial equilibrium. Acting on the fluid element, which is in radial equilibrium, in the coordinate system connected with this element, is the centrifugal inertial force $\rho\omega^2_{cp.ж}\, r df dr$ and the pressure difference dp (see Fig. 3.29).

From the equation of radial equilibrium [see equation (2.131)] it follows that

$$\frac{dp}{dr} = \rho \omega^2_{ср.ж} r. \qquad (3.34)$$

Integrating this equation from r (moving radius) to r_2 and replacing $\omega^2_{ср.ж} = \omega^2/4$, we obtain

$$p_2 - p = \rho \frac{\omega^2}{4} \frac{r_2^2 - r^2}{2},$$

whence the pressure in the clearance in radial equilibrium will be equal to

$$p = p_2 - \rho \frac{\omega^2 r_2^2 - \omega^2 r^2}{8},$$

or

$$p = p_2 - \rho \frac{\omega^2 r_2^2}{8}\left[1 - \left(\frac{r}{r_2}\right)^2\right]. \qquad (3.35)$$

By knowing the radius R_y on which seal is located, let us find the pressure in front of the seal p_y (see Fig. 3.28):

$$p_y = p_2 - \rho \frac{\omega^2 r_2^2}{8}\left[1 - \left(\frac{R_y}{r_2}\right)^2\right]; \qquad (3.36)$$

hence we will obtain the pressure difference:

$$p_2 - p_y = \rho \frac{\omega^2 r_2^2}{8}\left[1 - \left(\frac{R_y}{r_2}\right)^2\right] \qquad (3.37)$$

and the corresponding pressure lost in the seal:

$$L_y = H_{ст} - \frac{\omega^2 r_2^2}{8}\left[1 - \left(\frac{R_y}{r_2}\right)^2\right], \qquad (3.38)$$

where $H_{ст} = H_{кол} - H_{дин}$; taking equations (2.104) and (3.29) into account, we obtain

$$H_{ст} = H_1 \eta_{г.к} - (r_{2ж}^2/2) \quad (\text{when } r_{1ж} = r_{2ж}). \qquad (3.39)$$

Figure 3.30 depicts the pressure distribution in the clearance and wheel.

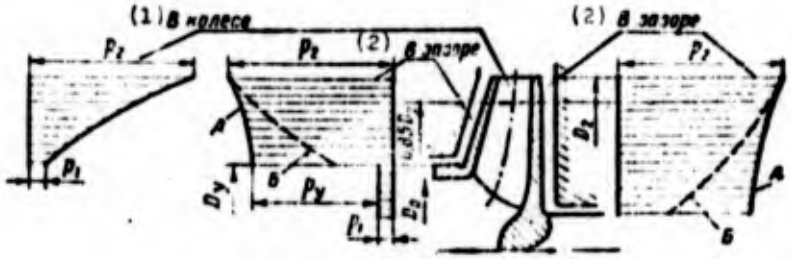

Fig. 3.30. Diagrams of pressures in the axial clearance between the disk and pump casing and in the flow area of the wheel: А - not allowing for leakages; Б - taking leakages into account.
KEY: (1) In the wheel; (2) In the clearance.

The value of pressure L_y lost in seal can be made more accurate by means of an account of the effect of leakages through the axial clearance and the effect of the circular flow velocity at outlet from the wheel c_{2u}. In work [67], taking this effect into account, the dependence for the pressure difference on radius r_2 and moving radius r of axial clearance is obtained. By assuming that at the inlet into the axial clearance the circular velocity of the fluid is equal to the circular flow velocity at the outlet from the wheel, it is possible to present the indicated dependence in the form

$$p_2 - p \quad (k_y e^{2,3[\alpha(r_{2u}/u_2) + \beta(r/r_2)]}, \qquad (3.40)$$

where p is the pressure on the moving radius r; k_y, α and β are the coefficients which depend on the flow through the seal Q_{y1} (Fig. 3.31).

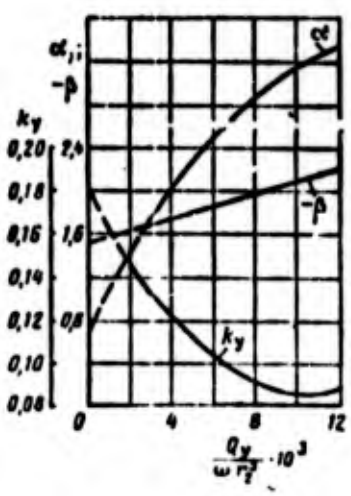

Fig. 3.31. Dependence of coefficients k_y, α and β on the value of leakages through the axial clearance.

In the region where $r \geq 0.85r_2$, it is possible to accept the linear dependence of the difference $p_2 - p$ on radius r:

$$p_2 - p = 0.17(p_2 - p_{r=0.85r_2})\left(1 - \frac{r}{r_2}\right). \quad (3.41)$$

Assuming that $r = R_y \leq 0.85r_2$, let us find the pressure difference at the outlet from the wheel and in front of the seal:

$$p_2 - p_y = \psi k_y \rho^{2,3}[\omega_{2u}^2 + \beta(R_y, r_2)] \quad (3.42)$$

and the pressure corresponding to this difference

$$L_y = H_{cr} = k_y \rho^{2,3}[\omega_{2u}^2 + \beta(R_y, r_2)]. \quad (3.43)$$

Since the pressure L_y depends on leakages Q_{y1} (in terms of coefficients k_y, α and β), and the value of leakages Q_{y1}, in turn, depends on L_y [see equation (3.32)], then value Q_{y1} will be determined as a result of several approximations.

The calculation according to equation (3.40) shows that the presence of leakages through the axial clearance lowers the pressure in the clearance and in front of the seal (see Fig. 3.30).

C. DETERMINATION OF THE COEFFICIENT OF FLOW μ

The coefficient of flow μ in equation (3.32) is the ratio of the flow through this seal Q to the theoretical flow rate Q_T through the opening with the same cross-sectional flow area:

$$\mu = \frac{Q}{Q_T}.$$

The introduction of the coefficient of flow μ makes it possible to reduce the complex nature of the outflow through the clearance of the seal to the case of the outflow through the opening.

If value Q_{y1} is determined experimentally, then, by knowing the pressure in front of the seal p_y and pressure at the inlet into the wheel p_1, the coefficient μ can be defined by equation (3.32) as an experimental value.

The coefficient of the flow μ is determined by the magnitude of the hydraulic resistances of the seal. The greater these resistances, the less the flow through the seal at the assigned pressure differential. Hence for a decrease in the flow through the seals, an attempt is made to increase the hydraulic losses along the channel, increasing the resistances artificially by the introduction of sharp edges, sudden expansions, sharp turns and so on.

Figure 3.32 gives approximate data on the magnitude of the coefficient of the flow μ for three forms of slit seals when l_y/δ_y = 100-200.

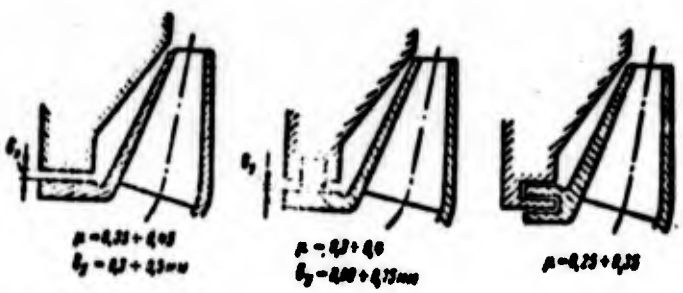

Fig. 3.32. Diagrams of the seals of the centrifugal wheel and values of the coefficient of flow μ for these seals.

In the determination of leakages through the discharging openings (Q_{y2}), we assume μ = 0.8. Studies (see, for example, source [90]) show that the magnitude of the leakages is affected also by the angular velocity of the shaft. Futhermore, with large pressure differentials on the seal high rates of flow appear in it, which lead to cavitation. With cavitation in the seal the value of the leakages is decreased (see source [65]).

D. CALCULATION OF THE IMPELLER SEAL OF THE SHAFT

In the turbopump unit [TU] (THA) of the LPRE the hydrodynamic seals of the shaft - impeller seals, are widely used (Fig. 3.33). The impeller seal serves for the prevention of the entering of fluid from the cavity of high pressure ($p_{2имп}$) into the gas cavity of low pressure ($p_{1имп}$).

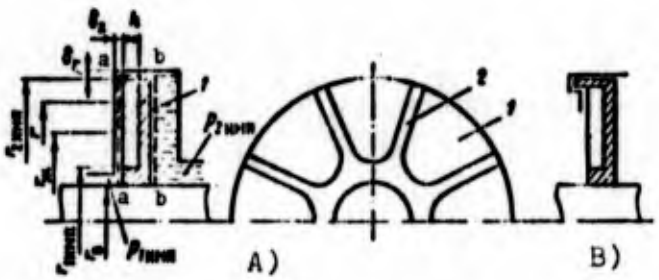

Fig. 3.33. Diagram of impeller seals of a shaft with unshrouded A) and shrouded B) impellers: 1 - disk of the impeller; 2 - blade of the impeller.

In the TU the impeller seals separate the cavities of the pumps and cavity of the turbine and also cavities of the pumps and cavities which are connected with the atmosphere - drainage cavities.

The impeller seal is a wheel (impeller) which is installed in the housing with small axial (δ_z) and radial (δ_r) clearances. The shape of the impeller vanes (radial, bent back or forward) does not affect the effectiveness of the seal, since through the impeller there is no flow of fluid. From technological considerations the blades of the impeller are made radial. The number of blades is selected at 6-8.

The impellers can be unshrouded (see Fig. 3.33A) and shrouded according to the outside diameter (see Fig. 3.33B) (see source [69]). The use of shrouded impellers decreases the incidence of

the gas into the cavity filled with fluid. The blades of the impeller draw in the fluid in rotation with the angular velocity $\omega_{ж}$. The pressure distribution in the axial clearance filled with fluid is determined by this angular velocity. Integrating the expression (3.34), we obtain

$$p_{2имп} - p_{имп} = \rho\alpha\omega^2 \frac{r^2_{2имп} - r^2}{2}, \qquad (3.44)$$

where $\alpha = (\omega_{ж}/\omega)^2$. Assuming $r = r_{ж}$, let us find the expression for the pressure differential on the seal:

$$p_{2имп} - p_{1имп} = \rho\alpha\omega^2 \frac{r^2_{2имп} - r^2_{ж}}{2}. \qquad (3.45)$$

It is obvious that the maximum pressure differential held by the seal will take place in the case of the full filling of channels of the impeller ($r_{ж} = r_{1имп}$):

$$(p_{2имп} - p_{1имп})_{max} = \rho\alpha\omega^2 \frac{r^2_{2имп} - r^2_{1имп}}{2}. \qquad (3.46)$$

With a differential which exceeds the maximum, the impeller seal becomes nonhermetic: fluid from cavity $p_{2имп}$ will penetrate into the cavity $p_{1имп}$. With the aid of relation (3.46) the required radial dimensions of the impeller at the assigned pressures $p_{2имп}$ and $p_{1имп}$ in the cavities being sealed are found.

Coefficient α in expressions (3.44), (3.45) and (3.46) depends on the width of the blade of the impeller h and axial clearance δ_z. The more the width of the blade and the less the axial clearance, the less the angular velocity of the fluid $\omega_{ж}$ will be distinguished from the angular velocity of the impeller ω (Fig. 3.34) (see source [69]). Usually $\alpha = 0.78$-0.82.

The power consumed by the impeller with a completely filled seal (maximum pressure differential) depends on the viscosity of the fluid, dimensions of the impeller and angular velocity ω. This power can be expressed by the power of the friction of a smooth disk $N_{тр.д}$ [see equation (2.202)]:

$$N_{имп} = K_{имп} N_{ср.т};$$
$$N_{имп} = K_{имп} C_{имп} \rho \omega^3 r_{2имп}^5; \qquad (3.47)$$

where

$$C_{имп} = 0{,}03 / \sqrt[4]{Re_{имп}}$$

when $Re_{имп} = \omega r_{2имп}^2 / \nu > 10^5$;

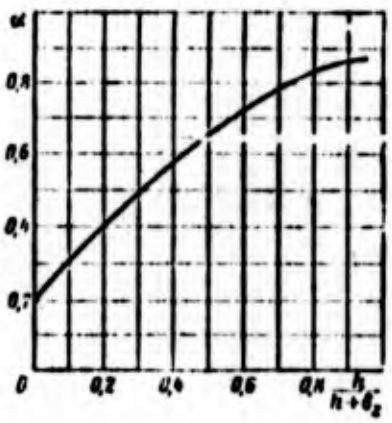

Fig. 3.34. Determination of the coefficient α of the impeller seal.

$K_{имп}$ is the coefficient which considers the friction of blades of the impeller and the external cylindrical surface against the fluid.

The processing of experimental data carried out by the authors (see source [69] gives the following dependence of the coefficient $K_{имп}$ on ratio $h/(h + \delta_z)$ in the range $h/(h + \delta_z) = 0.15$-0.80:

$$K_{имп} = 3 - 2\frac{h}{h + \delta_z}. \qquad (3.48)$$

A decrease in the pressure differential on the seal down to $0.5\,(p_{2имп} - p_{1имп})_{max}$ (incomplete filling of the impeller) leads to an insignificant decrease in the consumed power - by a total of 15-20%.

The power consumed by the impeller at the assigned pressure differential $(p_{2имп} - p_{1имп})_{max}$ is determined with the aid of expressions (3.46) and (3.47):

$$N_{нас} = 0{,}078 K_{нас} n^{1.5} \left\{ \frac{2(p_{нас} - p_{вх})_{max}}{\varepsilon \left[1 - \left(\frac{d}{D_1}\right)^2_{нас}\right]} \right\}^{2.5} \frac{1}{\varphi^{0.5}} \cdot \qquad (3.49)$$

From equation (3.49) it follows that at the assigned pressure differential an increase in the angular velocity of impeller decreases the consumed power, since the diameter of the impeller is decreased. An increase in the density of the fluid also leads to a decrease in the power. Therefore, in pumps of LPRE which have high angular velocities, the impeller seals had an extensive application.

The power expended for the drive of the impeller goes for the preheating of the fluid which fills the impeller. In connection with the small exchange of fluid in the impeller with fluid in the housing, the preheating of the fluid proves to be considerable. In the case of the use of cryogenic components of fuels of LPRE, this can lead to the boiling up of the component and the loss of airtightness. Thus, as a rule, impeller seals are used for the high-boiling liquids.

3.1.2.2. Disk Losses in Pumps

In the operation of the pump the expenditure of the power connected with disk losses is unavoidable. In pumps of LPRE besides the power losses connected with the friction of external surfaces of the wheel against the fluid (which bears the general nature for all vane machines, see Section 2.13.2.2), the expenditure of the energy for hydraulic stagnation ($N_{г.т}$) refers to the disk losses:

$$N_д = N_{тр.д} + N_{г.т}.$$

With the flows less than the calculated ($Q_p = Q_{\eta_{н\ max}}$) at the inlet into the wheel and at outlet from it intense return currents are observed (see source [101]). The return currents of fluid increase the friction surface. The jets which obtained twist in

the wheel penetrate the flow without twist or with less twist. Due to the presence of eddy viscosity, the twist of the effluent jets is decreased. The total reduction of the moment of momentum of the fluid will correspond to the moment of resistance of wall friction of the housing. Consequently, reverse flows increase the moment of resistance. The basic effect on losses of hydraulic stagnation is rendered by return output currents from the wheel, since the "tongue" of the spiral exerts considerable resistance to the return currents. The quantitative evaluation of these losses is extremely difficult and are detected only experimentally when $Q < (0.7\text{-}0.8)Q_p$.

The expenditure of power for the friction of disk is determined by equation (2.202). If value $C_{тр.д}$ is substituted into equation (2.202), then we will finally obtain

$$N_{тр.д} = \text{const} \cdot \omega^{2.8} r_2^{4.6}. \tag{3.50}$$

3.1.2.3. Mechanical Losses in Pumps

Mechanical losses in a pump (loss in bearings, contact seals and impeller seals) depend on the specific design of the pump. It is possible to consider approximately

$$N_{подш} + N_{уп} = (0{,}005 \div 0{,}01) N_н. \tag{3.51}$$

In general the dependence of the power expended for friction in contact seals and bearings can be represented in the form

$$N_{подш} + N_{уп} = \text{const}_1 \cdot \omega + \text{const} \cdot \omega^2. \tag{3.52}$$

Losses in bearings are proportional to the square of the angular velocity. Losses in the contact seals (in sealing rings, packing glands) are usually proportional to the angular velocity in the first power. The final nature of the dependence is determined by the specific design of the pump.

The basic portion of the power of mechanical losses of a pump consists of the power expended for the drive of the impellers (see Section 3.1.2.1), which, as a rule, are used in contemporary TU.

3.1.3. EFFICIENCY OF A PUMP

3.1.3.1. Flow Efficiency of a Pump

We convert the equation for the flow of a pump (see the equation given in Table 2.2), recorded in the form

$$\eta_p = \frac{1}{1 + (Q_y/Q)}. \tag{3.53}$$

Let us assume that leakages in the pump occur through two identical seals of the wheel; then it is possible to record [see equations (3.32), (3.38), (3.39)]:

$$Q_y = 2\mu_y \pi D_y b_y \sqrt{\eta_{г.ц} H_T - \frac{c_{2u}^2}{2} - \left|1 - \left(\frac{D_y}{D_2}\right)^2\right| \frac{u_2^2}{8}}. \tag{3.54}$$

Expressing H_T by the flow parameter of the pump q_p, which corresponds to the design conditions [see equation (3.3)], and transforming with the aid of equation (2.179) expression (3.54), we obtain

$$\frac{Q_y}{Q} = 1{,}33 \cdot 10^{6} \mu_y \frac{b_y}{D_y} \left(\frac{D_y}{D_1}\right)^2 \left(\frac{D_1}{D_2}\right)^3 \frac{A}{[k_z \eta_г (1 - \varphi_p)]^{1/3} n_s^{*2}}, \tag{3.55}$$

where

$$A = \left\{\eta_{г.ц} k_z (1 - \varphi_p) - \frac{1}{2}[k_z (1 - \varphi_p)]^2 - \frac{1}{8}\left[1 - \left(\frac{D_1}{D_2}\right)^2 \left(\frac{D_1}{D_2}\right)^2\right]\right\}^{1/2};$$

n_s^* - the power-speed coefficient of the pump calculated over the entire flow through the pump Q.

Having substituted expression (3.55) into equation (3.53), we will obtain

$$\eta_p = \frac{1}{1 + 1{,}33 \cdot 10^{6} \frac{k_1}{D_2} \left(\frac{D_2}{D_1}\right)^4 \left(\frac{D_1}{D_2}\right)^2 \frac{\lambda}{[k_2 \eta_r (1 - \varphi_p)]^{5/3} n_s^{*2}}}. \qquad (3.56)$$

The design equation (3.56) for the flow efficiency includes the ratio of diameters of the centrifugal wheel D_1/D_2. It is possible to record that

$$\frac{D_1}{D_2} = \left(\frac{D_1}{D_0}\right)\left(\frac{D_0}{D_2}\right) = 0{,}47 \frac{D_1}{D_0} K_{D_0} \sqrt[3]{\frac{Q}{i n}}, \qquad (3.57)$$

where D_0 is the diameter of the inlet into the wheel;

$$K_{D_0} = 2{,}13/k_1 \sqrt[3]{Q/n}, \qquad (3.58)$$

- the coefficient of the diameter of the inlet[1] (as will be shown further, this coefficient is determined in the calculation of the pump for cavitation); i is the number of inlets into the wheel.

After the transformation of equation (3.57) with the use of equations (2.179) and (3.3), we will finally obtain

$$\frac{D_1}{D_2} = 0{,}007 \frac{\varphi K_{D_0}}{\sqrt[3]{i}} \sqrt{k_2 \eta_r (1 - \varphi_p)}\, n_s^{*4/3}, \qquad (3.59)$$

where

$$\varphi = D_1/D_0.$$

Figure 3.35 depicts the dependence of the flow efficiency of the pump η_p on the power-speed coefficient n_s^* and flow parameter q_p.

---

[1]The dimensionless coefficient 2.13 in equation (3.58) is introduced in order that the numerical value K_{D_0}, calculated according to this equation, would coincide with value K_{D_0}, calculated according to formula $K_{D_0} = D_0/\sqrt[3]{Q/n}$, where n is in r/min.

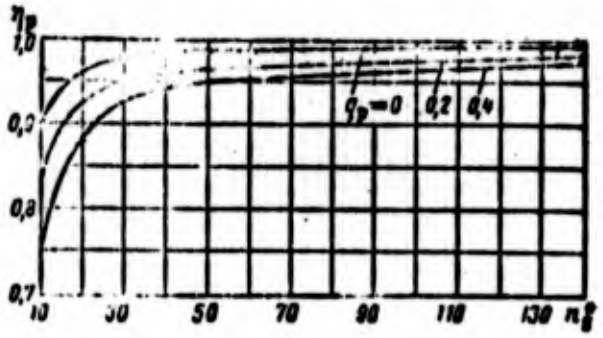

Fig. 3.35. Dependence of flow efficiency for pumps with one-way and two-way inlets on the power-speed coefficient n_s^* and flow parameter q_p (K_{D_0} = 5.2-8.0).

During the calculations values of the product $k_z\eta_r$ and values $\eta_{r.н}$ were determined from equations given in Section 3.1.1. Values of the remaining parameters which enter into the equations (3.57) and (3.59) were accepted as the following: $\mu = 0.4$; $\delta_y/D_y = 0.85 \times 10^{-3}$; $D_y/D_1 = 1.4$; $\Phi = 0.9$.

The dependence given on Fig. 3.35 can be used for the preliminary evaluation of the flow efficiency of the pump. With an increase in n_s^* the value η_p increases, which can be explained by the growth in Q with an increase in n_s^* with an approximately invariable value Q_y. An increase in the flow parameter q_p leads to a decrease in η_p, since there occurs an increase in the static head of the wheel and pressure in front of the seal. With an increase in K_{D_0} the diameter of the seal is increased and the leakages increase, and therefore η_p decreases. However, when K_{D_0} = 5:8 the effect of K_{D_0} is small, and with precomputations it can be disregarded.

3.1.3.2. Disk Efficiency of the Pump

In design conditions ($Q_p = Q_{\eta_{н\ max}}$) disk losses of the pump consist only of losses of disk friction. Then the equation for

disk efficiency will be recorded thus:

$$\eta_д = \frac{H_т}{H_{вн}} = 1 - \frac{L_{тр.т}}{H_{вн}} = 1 - \frac{N_{тр.т}}{\rho g H_{вн}} = 1 - \frac{N_{тр.т}}{(\rho i + \rho i_т) H_т + N_{тр.т}}.$$

Let us substitute into this equation the expression for the power of disk friction (2.202). After the transformations similar to the transformations carried out in Section 3.1.3.1, we will obtain the design equation for the disk efficiency:

$$\eta_д = 1 - \frac{C_{тр.т}}{C_{тр.т} + 1{,}3 \cdot 10^{-5} n_г^{3/2} [k_z (1 - q_р)]^{5/2} n_s^{*2} + 17{,}2 \mu \frac{\delta_т}{D_т} \left(\frac{D_т}{D_1}\right)^2 \left(\frac{D_1}{D_2}\right)^2 k_z (1 - q_р) A}. \quad (3.60)$$

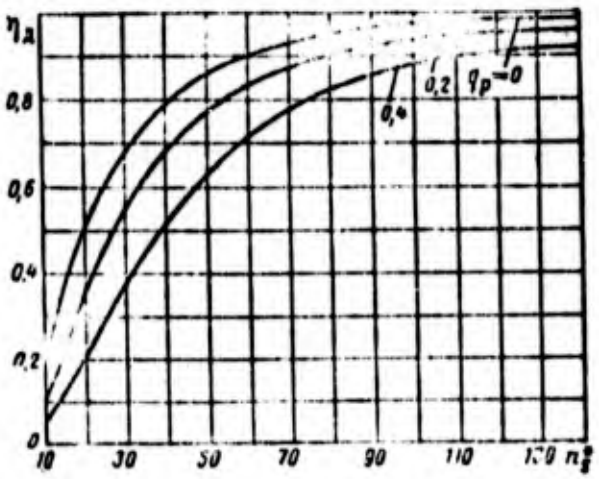

Fig. 3.36. Dependence of disk efficiency for pumps with one-way and two-way inlets on the power-speed coefficient n_s^* and flow parameter $q_р$ of K_{D_0} = 5.2-6.0.

Figures 3.36 and 3.37 depict the dependences of the disk efficiency $\eta_д$ on n_s^* and $q_р$ at different values of K_{D_0}, obtained with the aid of equation (3.60). In the calculations values $k_z \eta_г$, $\eta_{г.к}$, μ, $\delta_т/D_т$, and $D_т/D_1$ were defined in the same way as in Section

3.1.3.1. The hydraulic efficiency of the pump $\eta_г$ was determined from the equations given in Section 3.1.1.5. The coefficient of friction of the disk $C_{тр.д}$ is accepted equal to 0.002, which corresponds to Re = $3 \cdot 10^6$.

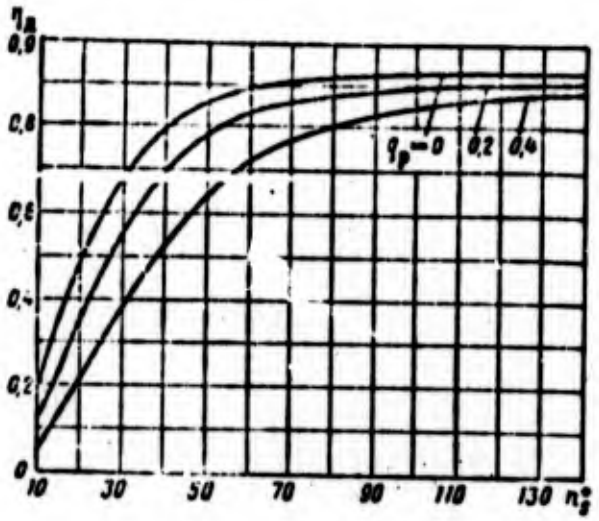

Fig. 3.37. Dependence of disk efficiency for pumps with one-way and two-way inlets on the power-speed coefficient n_s^* and flow parameter $q_р$ when K_{D_0} = 8.

3.1.3.3. Internal Power Efficiency of the Pump

The internal power efficiency of the pump $\eta_{вн\ N}$ is defined as the product

$$\eta_{вн.N} = \eta_г \eta_д \eta_р.$$

Having substituted expressions (3.56) and (3.60) into this equation, we obtain

$$\eta_{вн.N} = \frac{\eta_г}{1+1{,}33 \cdot 10^{6}\mu\left(\frac{D_3}{D_1}\right)^2\left(\frac{D_1}{D_2}\right)^3 \frac{(\ldots D_3).4}{[k_2\eta_г(1-q_р)]^{\ldots 2}n_s^{*\ldots}} + \frac{7{,}7\cdot 10^{\ldots}\ldots C_{тр.д}}{[\eta_г k_2(1-q_р)]^{5{,}3}n_s^{*\ldots}}}. \qquad (3.61)$$

The dependences of $\eta_{вн\ N}$ on n_s^* and q_p at different K_{D_0} are represented on Figs. 3.38-3.40. With an increase in n_s^* the quantity $\eta_{вн\ N}$ increases, but at a definite value of n_s^* the quantity $\eta_{вн\ N}$ begins to be decreased, since ratio D_1/D_2 reaches high values at which $\eta_г$ greatly decreases [see equation (3.31)].

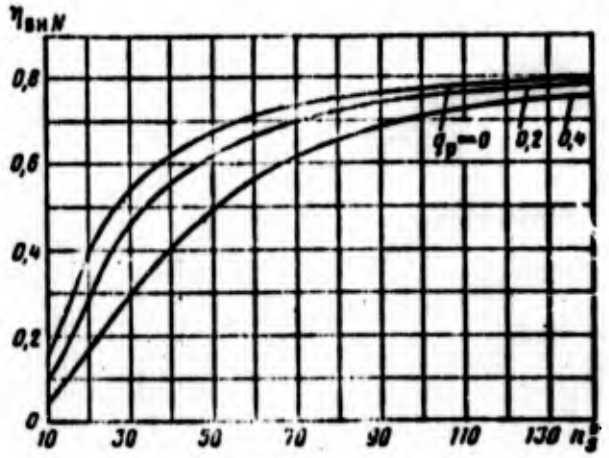

Fig. 3.38. Dependence of internal power efficiency for pumps with one-way and two-way inlets on the power-speed coefficient n_s^* and flow parameter q_p when $K_{D_0} = 5.2$.

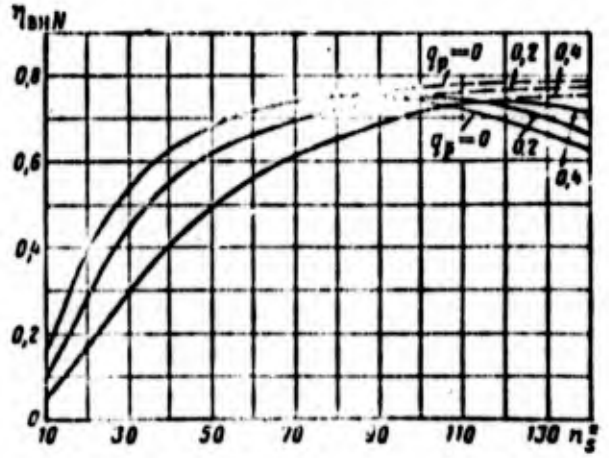

Fig. 3.39. Dependence of internal power efficiency for a pump on the power-speed coefficient n_s^* and flow parameter q_p when $K_{D_0} = 6.5$: —— - one-way inlet; – – – - two-way inlet.

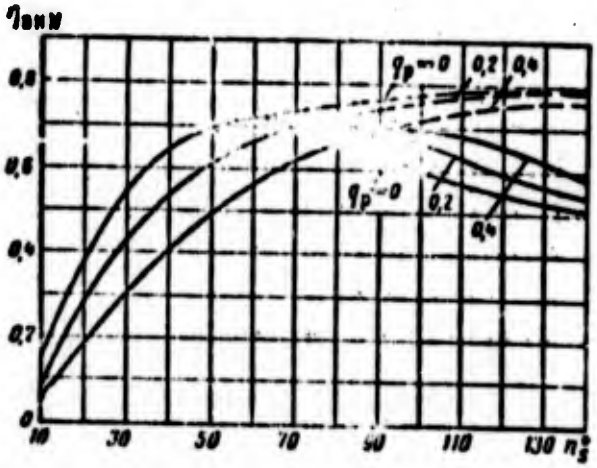

Fig. 3.40. Dependence of internal power efficiency for the pump on the power-speed coefficient n_s^* and flow parameter q_p when $K_{D_0} = 8$: —— - one-way inlet; - - - - two-way inlet.

3.1.3.4. Mechanical Efficiency of the Pump

The mechanical efficiency of the pump is determined by the expression

$$\eta_{мех} = 1 - \frac{N_{пот}}{N_в}.$$

In the absence in the pump of impeller seals, the mechanical efficiency of the pump, in accordance with equation (3.51), reaches the value $\eta_{мех} = 0.99\text{-}0.995$. The use of impeller seals leads to a reduction in the mechanical efficiency down to 0.95-0.97. These values can be used in the precomputations of full efficiency. It is more accurate to evaluate the mechanical efficiency of the pump with impeller seals possibly by means of the use of equation (3.47) for the energy consumed by the impeller.

3.1.3.5. Total Efficiency of the Pump

The total efficiency of the pump $\eta_н$ is defined as the product of the internal power of the efficiency $\eta_{вн}$ N and the mechanical efficiency $\eta_{мех}$:

$$\eta_н = \eta_{вн} \eta_{мех}. \tag{3.62}$$

3.1.4. ENERGY CHARACTERISTICS OF THE PUMP

3.1.4.1. Theoretical Characteristics of the Centrifugal and Screw-Centrifugal Pumps when z = ∞

The operation of the pump in the feed system of the LPRE is characterized by the frequency of rotation, the fluid flow rate, pressure and efficiency of the pump.

The efficiency of the pump and power are uniquely connected with the assigned Q and H:

$$N_н = \frac{\rho g H Q}{\eta_н} [W]. \tag{3.63}$$

In the LPRE the pump operates on different flow rates, since usually these engines are regulated according to thrust by a change in the flow rate. With a change in the thrust of the LPRE the flow rate through the pump can be changed from 10% to 120% of the computed value (see source [110]).

The parameters of the system and pump - flow rate, pressure, frequency of rotation and efficiency - are interconnected: a change in one of them produces a change in the other. The greatest interest is the dependences of pressure, efficiency and the power of the pump on the flow rate at a constant frequency of rotation and in the absence of the effect of cavitation on pressure and efficiency. We will call these dependences the energy characteristics of the pump.

A. DEPENDENCE OF THEORETICAL PRESSURE ON FLOW RATE

Let us examine the dependence of theoretical pressure on the flow rate, which can be called the theoretical pressure characteristic of the pump. The theoretical energy characteristics (for scheme $z = \infty$) are the same as those for the screw-centrifugal and centrifugal pumps with identical outlet geometric parameters ($\beta_{2л}$, b_2 and D_2).

The theoretical pressure with an infinitely large number of blades is determined from the Euler equation (on the assumption that $c_{1u} = 0$):

$$H_{T\infty} = u_2 c_{2u\infty}. \tag{3.64}$$

From the velocity triangle oab (Fig. 3.41) it follows that

$$c_{2u\infty} = u_2 - \frac{c_{2m}}{\operatorname{tg}\beta_{2л}}. \tag{3.65}$$

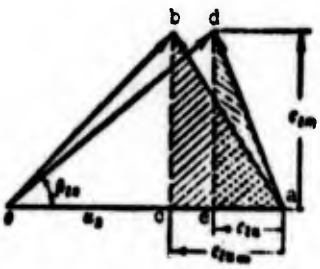

Fig. 3.41. Velocity triangles at the outlet from the wheel.

Having substituted expression (3.65) for $H_{T\infty}$ into the equation, we obtain

$$H_{T\infty} = u_2^2 - \frac{u_2 c_{2m}}{\operatorname{tg}\beta_{2л}}. \tag{3.66}$$

Using the relation

$$c_{2m} = \frac{Q}{\pi D_2 b_2},$$

we obtain

$$H_{T\infty} = u_2^2 - \frac{u_2 Q'}{\pi D_2 b_2 \operatorname{tg} \beta_{2л}}. \qquad (3.67)$$

Let us investigate equation (3.67). For this pump at the constant frequency of rotation (u_2 = const), equation (3.67) is the equation of a straight line in coordinates $H_{T\infty} = f(Q')$. Assuming that $Q' = 0$, we find the theoretical pressure with an infinitely large number of blades for the zero flow rate:

$$H_{T\infty} = u_2^2.$$

When $\operatorname{tg} \beta_{2л} > 0$, which corresponds to $\beta_{2л} < 90°$, $H_{T\infty}$ can be equal to zero. Assuming in formula (3.67) that $H_{T\infty} = 0$, we find the appropriate flow rate:

$$u_2^2 - \frac{u_2}{\pi D_2 b_2 \operatorname{tg} \beta_{2л}} Q' = 0;$$

$$Q'_{H_{T\infty}=0} = \pi D_2 b_2 u_2 \operatorname{tg} \beta_{2л}. \qquad (3.68)$$

The velocity triangle for this case is shown on Fig. 3.42:

$$c'_{2\infty} = c'_{2r} = u_2 \operatorname{tg} \beta_{2л};$$

in this case $c''_{2u\infty} = 0$, and the pressure is equal to zero.

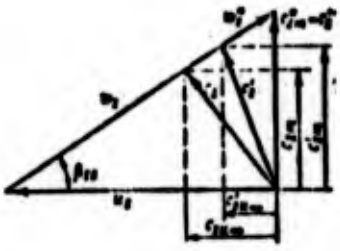

Fig. 3.42. Velocity triangles at the outlet from the wheel at different flow rates ($\beta_{2л} < 90°$).

Consequently, for blades of the centrifugal wheel, bent opposite to the rotation ($\beta_{2л} < 90°$), the dependence of theoretical pressure on the flow rate with an infinitely large number of blades $z = \infty$ is represented in coordinates $H_{T\infty} = f(Q')$ by a straight line,

which intercepts on the axis of the ordinates the segment equal to u_2^2 and on the axis of the abscissas, the segment equal to $\pi D_2 b_2 u_2 \operatorname{tg} \beta_{2л}$ (Fig. 3.43).

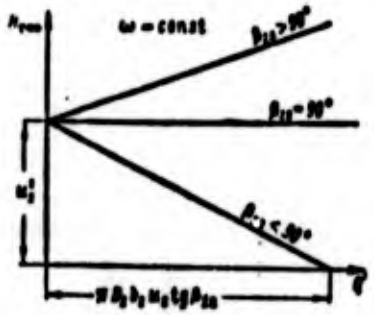

Fig. 3.43. Theoretical pressure characteristics of the pump at different angles of the blades.

With the radial blades at the outlet from the wheel $\beta_{2л} = 90°$ ($\operatorname{tg} \beta_{2л} = \infty$), from equation (3.57) it follows that

$$H_{T\infty} = u_2^2 = \text{const}.$$

In this case the pressure $H_{T\infty}$ does not depend on the flow rate and is depicted as a straight line parallel to the axis of the abscissas (see Fig. 3.43).

The velocity triangles at the outlet from the wheel when $\beta_{2л} = 90°$ for different flow rates are given on Fig. 3.44.

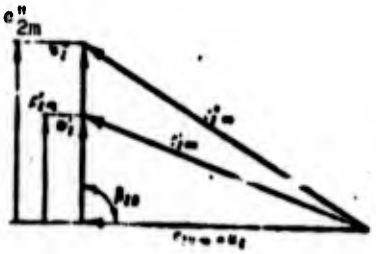

Fig. 3.44. Velocity triangles at the outlet from the wheel at different flow rates ($\beta_{2л} = 90°$).

When $\beta_{2л} > 90°$ the pressure $H_{T\infty} = f(Q')$ is also depicted as a straight line: $H_{T\infty}$ increases with an increase in the flow rate (see Figs. 3.43 and 3.45, on which depicted are velocity triangles for $\beta_{2л} > 90°$ at different flow rates).

Subsequently we will examine mainly characteristics of the pump having angles of blades at the outlet from the wheel $\beta_{2л} < 90°$ as the most typical for systems of the LPRE. The characteristic $H_{T\infty} = f(Q')$ can also be considered as the characteristic of a series of pumps, i.e., as values of $H_{T\infty}$ for pumps with different calculated flow rates.

a) Effect of Geometric Dimensions of the Wheel on the Theoretical Characteristic of the Pump

Let us examine the dependence of the course of the theoretical characteristic of the pump on the geometric dimensions of the wheel. In accordance with the theoretical characteristic, the real characteristic of the pump will be changed. A change in the outside diameter of the wheel D_2 leads to a parallel displacement of the line $H_{T\infty} = f(Q')$, since the segments being intercepted by it on the axis of the ordinates and the axis of the abscissas are proportional to D_2^2 (see Figs. 3.43 and 3.46).

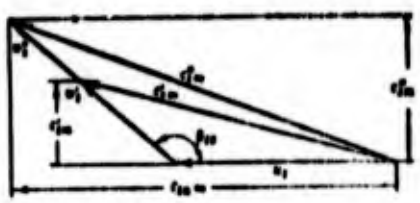

Fig. 3.45. Velocity triangles at the outlet from the wheel at different flow rates ($\beta_{2л} > 90°$).

An increase in the width of the wheel b_2 at outlet leads to a more slanting course of the characteristic (Fig. 3.47). The ordinate at $Q' = 0$ does not depend on b_2, and the segment intercepted by the line $H_{T\infty} = f(Q')$ on the axis of the abscissas increases in proportion to b_2.

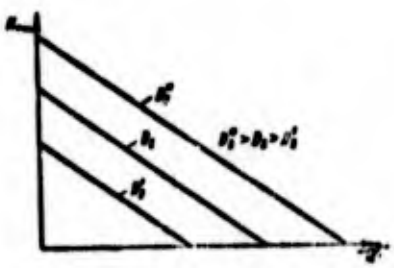

Fig. 3.46. Effect of the diameter of the wheel on the theoretical pressure characteristic of the pump.

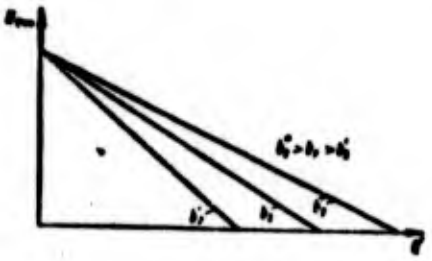

Fig. 3.47. Effect of the width of the wheel at outlet on the theoretical pressure characteristic of the pump.

b) Effect of Angular Velocity on the Theoretical Characteristic of the Pump

With a change in the angular velocity ω at the assigned geometric parameters, the inclination of the straight line $H_{T\infty} = f(Q')$ is changed (Fig. 3.48). With an increase in ω the line $H_{T\infty} = f(Q')$ will pass more steeply, since the segment being intercepted by the straight line on the axis of the ordinates is proportional to ω^2, and the segment on the axis of the abscissa is proportional to the value ω in the first degree (see Fig. 3.43). The equation of the theoretical characteristic for this pump can be recorded in the form [see equation (3.67)]

$$H_{T\infty} = A\omega^2 - BQ',$$

where A and B are constants of the pump.

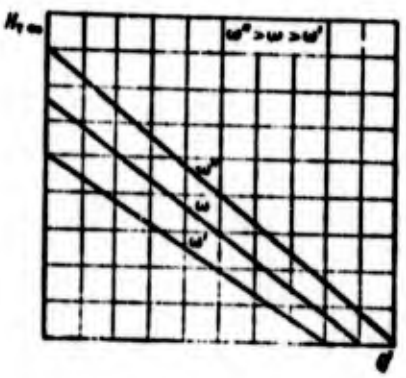

Fig. 3.48. Effect of angular velocity of the wheel on the theoretical pressure characteristic of the pump.

B. DEPENDENCE OF THE CIRCULAR POWER OF THE PUMP ON THE FLOW RATE

The theoretical circular power of the pump $N_{u\infty}$ is determined by theoretical pressure $H_{T\infty}$ and flow rate Q' through the wheel:

$$N_{u\infty} = \rho g H_{T\infty} Q'. \tag{3.69}$$

The dependence of the circular pump power on the flow rate for different values of $\beta_{2л}$ when ω = const is shown on Fig. 3.49.

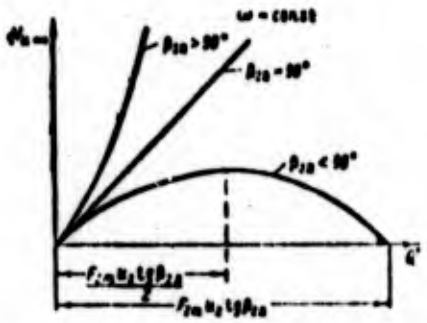

Fig. 3.49. Dependence of the circular pump power on the flow rate at different angles of the blades.

When Q' = 0, $N_{u\infty}$ = 0; if $\beta_{2л} < 90°$, then curve $N_{u\infty}$ passes through zero where $H_{T\infty}$ = 0, i.e., when

$$Q' = \pi D_2 b_2 u_2 \operatorname{tg}\beta_{2л} = F_{2m} u_2 \operatorname{tg}\beta_{2л}. \tag{3.70}$$

If $\beta_{2л}$ = 90°, then $N_{u\infty}$ increases in proportion to Q', since $H_{T\infty}$ = const.

If $\beta_{2л} > 90°$, then $N_{u\infty}$ increases faster with an increase in Q', since with an increase in Q', $H_{T\infty}$ increases.

For multimode engines in the selection of the turbine, for the pump it is more favorable to have a small change in the power according to the flow rate, since the turbine is selected according to the power corresponding to the maximum flow rate. According to conditions less in flow rate the turbine will be loaded little, and its efficiency can be lowered substantially. Consequently, pumps with blades bent back ($\beta_{2л} < 90°$) have in this respect an advantage over pumps with radial blades or blades bent forward.

3.1.4.2. Theoretical Pump Characteristics Taking into Account the Effect of the Finite Number of Blades

The dependence $H_T = f(Q')$ differs from the dependence $H_{T\infty} = f(Q')$ in view of the effect of the finite number of blades, which is considered as the coefficient $k_z = H_T/H_{T\infty}$ (see Section 3.1.1.3).

The coefficient k_z depends on the flow rate. For diffuser centrifugal wheel ($F_1/F_2 \leq 1$) the coefficient k_z is decreased with an increase in the flow rate in the region $c_{2m}/u_2 > 0.15$-0.2 (see Fig. 3.14). Such a nature of the dependence of k_z on c_{2m}/u_2 leads to the fact that the dependence of theoretical pressure H_T on c_{2m}/u_2 (or on Q') is close to a straight line, which is intersected with the straight line representing the dependence $H_{T\infty} = f(c_{2m}/u_2)$, in the region of negative pressures (point A on Fig. 3.50).

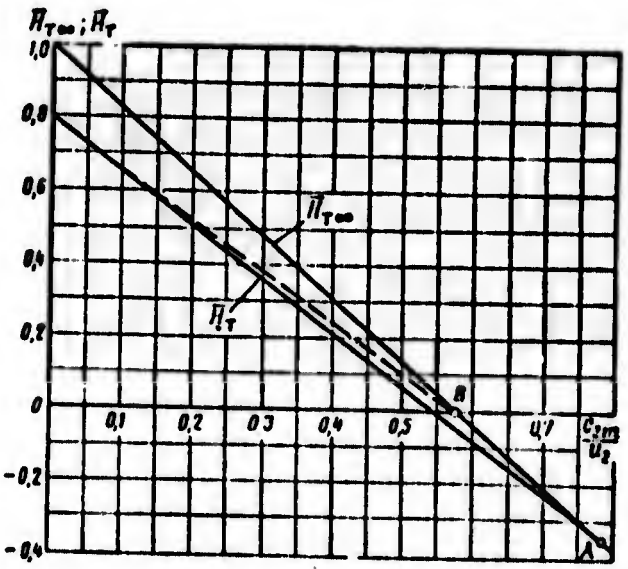

Fig. 3.50. Dependence of the theoretical pump pressure on the flow rate, taking into account the finite number of the blades.

The pressure H_T reaches a zero value with less flow rate than does pressure $H_{T\infty}$. In the range of the change in $c_{2m}/u_2 < 0.15$-0.2

the coefficient k_z is virtually constant and does not depend on the flow rate (see Fig. 3.14). Therefore, in the indicated range c_{2m}/u_2 the dependence $H_T = f(c_{2m}/u_2)$ will be close to a straight line (dashed line on Fig. 3.50), which is intersected with the straight line representing the dependence $H_{T\infty} = f(c_{2m}/u_2)$, at point $H_{T\infty} = 0$ (point B on Fig. 3.50).

Since usually in design conditions $(c_{2m}/u_2)_p = 0.05\text{-}0.1$, then coefficient k_z can be taken as constant in the range of the change in the flow rate from zero to a value which exceeds the calculated flow rate, at least, one and a half times. In this range there is found the region of the change in the flow rate, which is of practical interest (see source [110]).

Let us recall that the value k_z was determined (see Section 3.1.1.3) under the condition of circular symmetry of the flow and nonseparated streamline flow of the blades of the centrifugal wheel. This condition is realized with the calculated flow rate through the pump. At flow rates distinct from those calculated, the circular symmetry is disturbed and in the wheel separation zones can arise. Therefore, in off-design flow rates the value of the pump pressure H_T can differ somewhat from the value calculated with the aid of coefficient k_z.

The value H_T determines the expenditure of pump power for an increase in the energy of the fluid, i.e., it determines the circular operation of the pump:

$$N_u = \rho Q' H_T; \tag{3.71}$$

since $Q' = F_{2m}c_{2m}$, where $F_{2m} = \pi D_2 b_2$ is the flow passage cross-sectional area at the outlet from the wheel, and $H_T = c_{2u}u_2$,

$$N_u = \rho F_{2m} c_{2m} c_{2u} u_2 \text{ [W]}.$$

It is interesting to note that with the assigned value u_2 the circular pump power N_u is proportional to area ade of the velocity

triangles at the outlet from the wheel (see Fig. 3.41); this area is determined by the product $c_{2m}c_{2u}$. The theoretical circular power with an infinite number of blades $N_{u\infty}$ is correspondingly determined by the area of the triangle abc.

3.1.4.3. Real Characteristics of the Screw-Centrifugal Pump

A. GENERAL INFORMATION

In view of unavoidable losses, the real pump characteristics differ from the theoretical. Let us examine the real pressure pump characteristic - the dependence of pressure H on the flow rate Q through the pump at a constant frequency of rotation. The real pressure H differs from the theoretical by the magnitude of hydraulic losses: $H = H_T - L_{гидр.пот}$. The nature of the change in hydraulic losses and H_T with a change in the flow rate Q determines the shape of the characteristic $H = f(Q)$. Hydraulic losses depend on the magnitude and direction of the velocities with a change in the flow rate Q.

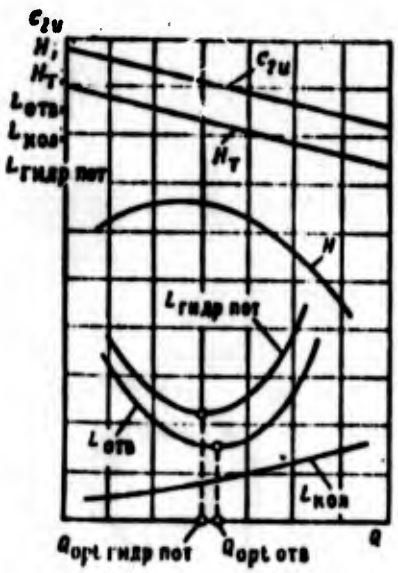

Fig. 3.51. Dependence of the change in hydraulic losses in the pump on the flow rate.

Figure 3.51 shows the nature of the change in hydraulic losses in the pump with their division into losses in the wheel $L_{кол}$ and losses in the branch $L_{отв}$. The design conditions of the pump Q_p is located near the minimum of hydraulic losses in the pump and in the branch.

Losses in the wheel increase with an increase in the flow rate, which is explained by an increase in the relative velocities in vane channels of the wheel. Losses in the branch have a clearly expressed minimum according to flow rate. In the case of the branch with a vane diffuser, this is connected with a change in the angle of incidence (by its deviation from the calculated value). When $Q < Q_p$ the angle of attack has large positive values and when $Q > Q_p$ large negative values: losses in the branch will be more than those in the design conditions (at the calculated angle of incidence).

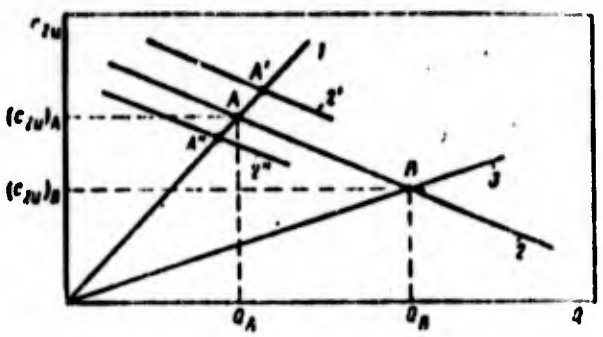

Fig. 3.52. Determination of the optimum twist of flow for the branch.

Let us examine the spiral branch. Losses in the branch would be located at a minimum level if the velocity c_2 at the outlet from the wheel (velocity c_2 can be replaced by its component c_{2u}, since $c_{2m} << c_{2u}$) was changed [see equation (3.23)] in proportion to the flow rate Q, i.e., if with an increase in Q the rate c_{2u} is increased (straight line 1 on Fig. 3.52). However, the wheel does not provide

such a law of the change in c_{2u} depending on Q: in actuality with an increase in the flow rate, the twist c_{2u} is decreased ($\beta_{2л} \leq 90°$) - line 2 on Fig. 3.52. Point A of the intersection of straight lines 1 and 2 corresponds to the flow rate $Q_{опт\ отв}$ close to the calculated flow rate Q_p.

Twist at the outlet from the wheel c_{2u} corresponds to the optimum for the branch. At less flow rates ($Q < Q_p$) see Fig. 3.51) the twist c_{2u} proves to be more than that necessary for the branch: cross sections of the branch are overexpanded. In conditions $Q > Q_p$ twist c_{2u} becomes less optimum for the branch: cross sections of the branch for these conditions are constricted.

The nonconformity of the velocity created by the wheel and the rate optimum for the branch leads to added losses, in particular, losses for the mixing of the fluid jet proceeding from the wheel at the velocity of c_2 with fluid jets in the branch having a velocity determined by cross sections of the branch.

Furthermore, losses take place during the streamline flow of the "tongue" of the spiral branch as a single blade. When $Q < Q_p$ the streamline flow occurs with an angle of attack larger and when $Q > Q_p$ smaller than that calculated. Large negative angles of incidence when $Q > Q_p$ lead to the separation of flow from the tongue. The region of separation is located in the diffuser of the branch; in this region cavitation phenomena can appear (see sources [64] and [91]), leading to a decrease in pressure and efficiency of the pump at high flow rates ($Q > Q_p$). Since the operating mode of the wheel with cavitation in the branch is not disturbed, then in this case there occurs no changes in the power being consumed by the pump, in comparison with the power in the absence of cavitation in the branch.

The nonconformity of the twist of the wheel c_{u2} to the twist optimum for the branch leads to the disturbance of the circular

symmetry of the pressures and velocities along the circumference of the wheel under conditions distinct from those calculated. Under conditions $Q < Q_p$, as studies show, the wheel of the pump begins to operate partially. The fluid proceeds from the wheel into the branch only by parts of the circumference of the wheel adjacent to the "tongue." On the remaining circular arc the flow rate is directed from the branch into the wheel. The energy obtained by the fluid in the wheel is expended for vortex formations in the branch and in the flow from the branch into the wheel. This leads to the appearance of added losses in the pump, called brake (see Section 3.1.2.2).

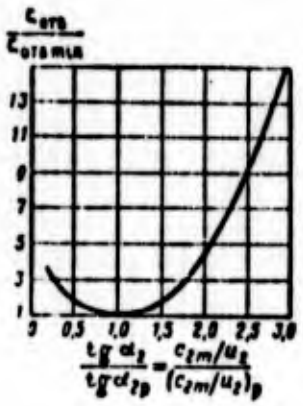

Fig. 3.53. Dependence of the loss factor in the spiral branch on the ratio $tg\ \alpha_2/tg\ \alpha_{2p}$.

Studies (see source [95]) show that there is the similarity in a change in losses in the branch under conditions different from those calculated. Conditions of the inlet into the spiral branch are characterized by the direction of the vector of absolute velocity determined by the tangent of the angle: $tg\ \alpha_2 = c_{2m}/c_{2u}$. The deviation of the operating mode of the branch from that calculated will be characterized by the distinction of $tg\ \alpha_2$ from the computed value $tg\ \alpha_{2p} = (c_{2m}/c_{2u})_p$. Figure 3.53 shows that with identical deviation of conditions from the calculated (equal ratios $tg\ \alpha_2/tg\ \alpha_{2p}$) for the branches identical ratios of the coefficient of losses to its value corresponding to the design conditions are observed:

$$\zeta_{отв}/\zeta_{отв\ min} = idem.$$

Subsequently we use this property of the spiral branches.

Let us subtract (with different Q) hydraulic losses in the wheel and branch from the value H_T:

$$H_T - L_{кол} - L_{отв} = H_T - L_{гидр.пот} = H. \qquad (3.72)$$

Then we will obtain the pressure characteristic of the pump $H = f(Q)$. The nature of change in H_T and $L_{гидр.пот}$, depending on the magnitude of flow, determines the shape of the curve $H = f(Q)$.

B. CALCULATED DETERMINATION OF PRESSURE CHARACTERISTICS OF THE PUMP

To plot the pressure characteristic, it is necessary to determine the theoretical pump pressure H_T and hydraulic losses under conditions different from those calculated. Since the losses in these conditions at the present time cannot be reliably determined by the calculation, then for calculating the pressure characteristics of the designed pumps it is possible to use the generalized characteristics of the pumps made. The generalization should be carried out with the aid of parameters which have the main effect on the pressure characteristic. Let us call such parameters the determining parameters.

Let us discuss in more detail the selection of the determining parameters. Let us divide the terms of the equation (3.72) by u_2^2. We will obtain

$$\bar{H} = \bar{H}_T - \bar{L}_{отв} - \bar{L}_{кол}. \qquad (3.73)$$

Let us determine from equation (3.28) losses in the branch:

$$L_{отв} = \frac{\zeta_{отв}}{2}\left(\frac{c_2}{u_2}\right)^2. \qquad (3.74)$$

The loss factor $\zeta_{отв}$, keeping in mind the dependence given on Fig. 3.53, can be expressed in the following form:

$$\frac{\zeta_{отв}}{\zeta_{отв\ min}} = f\left[\frac{c_{2m}/u_2}{(c_{2m}/u_2)_p}\right]. \qquad (3.75)$$

where $\zeta_{отв\ min}$ on the average is equal to 0.2 (see Section 3.1.1.4).

Having substituted equation (3.75) into expression (3.74), we obtain

$$\zeta_{отв} = 0{,}1 f\left[\frac{c_{2m}/u_2}{(c_{2m}/u_2)_p}\right]\left(\frac{c_2}{u_2}\right)^2. \qquad (3.76)$$

Let us express the losses in the wheel in fractions of the kinetic energy of the fluid in relative motion at the outlet from the wheel:

$$L_{кол} = \zeta_{кол}\left(\frac{w_2}{u_2}\right)^2 = \zeta_{кол}\left(1 + \frac{c_2^2}{u_2^2} - 2\frac{c_{2u}}{u_2}\right). \qquad (3.77)$$

Let us find the loss factor in the wheel $\zeta_{кол}$ from the expression for hydraulic efficiency in design conditions:

$$\eta_{г.р} = 1 - \frac{L_{отв.р} + L_{кол.р}}{H_{т.р}}. \qquad (3.78)$$

Solving equations (3.76), (3.77) and (3.78) together, we will obtain the expression for $\zeta_{кол}$. After the substitution of this expression into equation (3.77), we write:

$$L_{кол} = \frac{H_{т.р}(1-\eta_{г.р}) - 0{,}1\,(c_2/u_2)_p^2}{\left[1 + \left(\frac{c_2}{u_2}\right)_p^2 - 2\left(\frac{c_{2u}}{u_2}\right)_p\right]^2}\left[1 + \left(\frac{c_2}{u_2}\right)^2 - 2\frac{c_{2u}}{u_2}\right]^2. \qquad (3.79)$$

Let us transform expression (3.73) with the aid of relations (3.76) and (3.79). In this case, in view of the smallness c_{2m}, we will consider that $c_2 = c_{2u}$, and let us assume that $c_{1u} = 0$. Then the pump pressure referred to calculated is expressed in the following manner:

$$\frac{\bar{H}}{\bar{H}_p}=\frac{H}{H_p}=\frac{k_z\left(1-q_p\frac{Q}{Q_p}\right)}{k_z\eta_{r.p}(1-q_p)}-\frac{0{,}1\,k_z^2\left(1-q_p\frac{Q}{Q_p}\right)^2}{k_z\eta_{r.p}(1-q_p)}\,f\left[\frac{(1-q_p)\frac{Q}{Q_p}}{\left(1-q_p\frac{Q}{Q_p}\right)}\right]\cdot$$

$$\frac{\left[(k_z-k_z\eta_{r.p})(1-q_p)-0{,}1\,k_z^2(1-q_p)^2\right]\left[1-k_z(1-q_p)\frac{Q}{Q_p}\right]^2}{k_z\eta_{r.p}(1-q_p)[1-k_z(1-q_p)]^2}. \qquad (3.80)$$

Expression (3.80) shows that the pressure characteristic in relative coordinates $H/H_p = f(Q/Q_p)$ is determined by parameters $k_z\eta_{r.p}$, k_z and $q_p = \left(\frac{c_{2m}}{u_2}\right)_p \operatorname{ctg}\beta_{2л}$. Parameter $k_z\eta_{r.p}$ depends on the relative diameter of the centrifugal wheel of the pump $\bar{D}_1 = D_1/D_2$ (see Section 3.1.1.2). With a sufficient degree of accuracy for the examined question, it is possible to consider (with the given q_p), that k_z is also basically determined by the relative diameter $\bar{D}_1$ (see Section 3.1.1.3).

Thus, the determining parameters for the pressure characteristics in coordinates $H/H_p - Q/Q_p$ are the relative diameter $\bar{D}_1$ and flow parameter of the pump q_p. For pumps with a relative diameter of $\bar{D}_1 \leq 0.55$, parameters $k_z\eta_{r.p}$ and k_z are changed within sufficiently narrow limits ($\beta_{2л} \leq 90°$) (see Sections 3.1.1.3 and 3.1.1.2). Therefore, for the pressure characteristics of pumps with $\bar{D}_1 \leq 0.55$ the determining parameters will be only the flow parameter q_p.

The generalization of pump characteristics with $\bar{D}_1 \leq 0.55$ (Re > $> 10^5$) gives the following equation for calculating the head characteristic:

$$H/H_p = 1{,}06 + 0{,}8q_p\left(1-\frac{Q}{Q_p}\right) - 0{,}296\left(0{,}55-\frac{Q}{Q_p}\right)^2. \qquad (3.81)$$

The dependence of H/H_p on Q/Q_p at different q_p is given on Fig. 3.54. For a specific pump the coefficient of pressure $\bar{H}$ is proportional to ratio H/ω^2, and $\frac{Q}{Q_p} = \frac{Q_m}{(Q_m)_p}$. Then from equation (3.81) we will obtain the equation of the universal pressure pump

characteristic, i.e., the dependence of H/ω^2 on Q/ω:

$$\frac{H}{\omega^2} = A + B\frac{Q}{\omega} - C\left(\frac{Q}{\omega}\right)^2, \tag{3.82}$$

where

$$A = (0{,}97 + 0{,}8q_p)\left(\frac{H}{\omega^2}\right)_p;$$
$$B = (0{,}325 - 0{,}8q_p)(H/\omega^2)_p/(Q/\omega)_p;$$
$$C = 0{,}296\frac{(H/\omega^2)_p}{(Q/\omega)_p^2}.$$

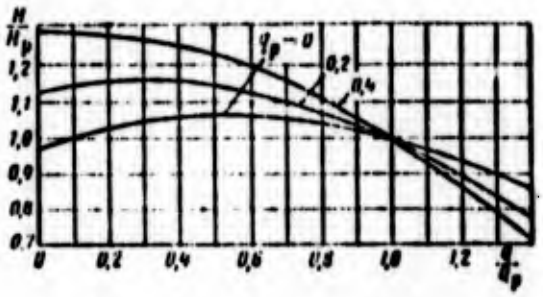

Fig. 3.54. The generalized pressure characteristics of pumps.

From expression (3.82) we will obtain the dependence of the pump head H on the flow rate Q and angular velocity ω, and the equation of the pressure pump characteristic when ω = const is

$$H = A\omega^2 + BQ\omega - CQ^2; \tag{3.83}$$
$$H = a + bQ - cQ^2,$$

where

$$a = A\omega^2; \quad b = B\omega; \quad c = C. \tag{3.84}$$

Figure 3.54 shows that with an increase in the flow parameter q_p the angle of inclination of the head characteristic at the calculated position is increased. With an increase in q_p the ratio H/H_p increases in the region $Q/Q_p < 1$ and is decreased in the region $Q/Q_p > 1$. The dependence (3.81) makes it possible to analyze the effect of geometric parameters of the pump on the form of its

head characteristic. The static stability of the pump feed system of the LPRE is connected with the form of the characteristic $H = f(Q)$, in particular, with its inclination, which characterizes the intensity of the change in the pump head with a change in the flow rate.

As it was said above, the form of characteristic is determined by the flow parameter q_p (see Fig. 3.54). Having expressed values $c_{2m\,p}$ and u_2 in terms of parameters of the pump, taking into account expression (3.3), we obtain the dependence

$$q_p = \frac{1}{1 + \frac{2\pi H_p' \operatorname{tg}\beta_{2л}}{Q_p \omega k_z \eta_{г.р}}}. \qquad (3.85)$$

Having established the effect on q_p of parameters which enter into equation (3.85), it is possible to observe their effect on the form of the head characteristic, being guided by the graph given on Fig. 3.54. In the calculation of the pump values Q_p and H_p are assigned. Then parameter q_p will increase with an increase in ω and $\eta_{г.р}$ and with a decrease in the width of the centrifugal wheel b_2 and angle $\beta_{2л}$. The quantity of the blades indirectly, by k_z, affects q_p. With an increase in the number of blades value k_z increases, and q_p also increases. In accordance with the effect of q_p on the form of the characteristic, it is possible to make the following conclusion: a decrease in b_2 and $\beta_{2л}$ and an increase in ω, $\eta_{г.р}$ and the numbers of blades z increase the angle of inclination of the head characteristic $H = f(Q)$ at the calculated position. In this case the pump head in the region $Q < Q_p$ is increased and is decreased in the region $Q > Q_p$. Let us note that the qualitative pattern of the effect of the geometric parameters of the pump on the form of the real head characteristic coincides with the pattern of the effect of these parameters on the form of the theoretical head characteristic (see Section 3.1.4.1).

Changing in the process of the calculation parameters b_2, $\beta_{2л}$, z and ω, it is possible to obtain the necessary form of the pressure pump characteristic. Let us analyze this question in more detail. For the calculated point of characteristic $H = f(Q)$, it is possible to record:

$$\left(\frac{dH}{dQ}\right)_p = \left[\frac{d\left(\frac{H}{H_p}\right)}{d\left(\frac{Q}{Q_p}\right)}\right]_p \cdot \frac{H_p}{Q_p}. \qquad (3.86)$$

Differentiating expression (3.81) with respect to Q/Q_p and assuming then that $Q/Q_p = 1$, we obtain

$$\left[\frac{d(H/H_p)}{d(Q/Q_p)}\right]_p = -0{,}8(0{,}33 + q_p). \qquad (3.87)$$

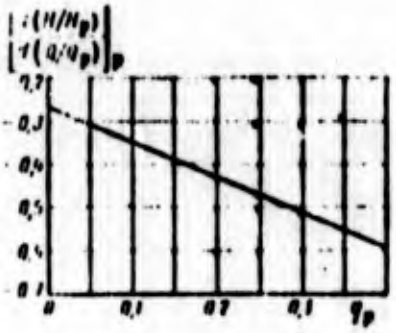

Fig. 3.55. Effect of the flow parameter on the angle of inclination of the head characteristic at the calculated position.

In graphic form the dependence (3.87) is given on Fig. 3.55. If it is necessary to design a pump with the assigned angle of inclination of the head characteristic at the calculated point $(dH/dQ)_p$, then it is necessary by equation (3.86) to determine the necessary value $\left[\frac{d(H/H_p)}{d(Q/Q_p)}\right]_p$, and then with the use of dependence (3.87) or the graph given on Fig. 3.55 one should determine the necessary value of the flow parameter q_p.

Parameters of the pump which provide the necessary value q_p will be determined from relation (3.85). Virtually it is possible

to vary values b_2 and $\beta_{2л}$. A change in the number of blades affects q_p insignificantly, and the angular velocity is usually determined from the calculation of the pump for cavitation, and it is attempted to obtain the hydraulic efficiency at a maximum under these conditions.

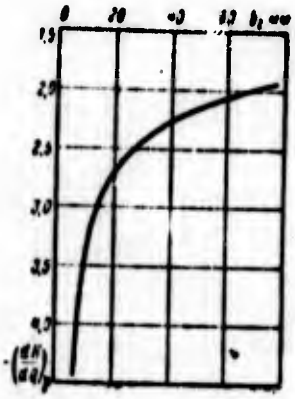

Fig. 3.56

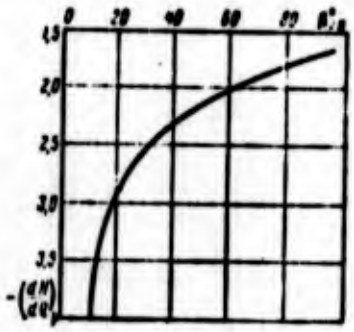

Fig. 3.57

Fig. 3.56. Example of the effect of the width of the blade at the outlet from the wheel on the angle of inclination of head characteristic at the calculated point (H_p = 5610 J/kg; Q = 80 l/s; ω = 1000 1/s; $\beta_{2л}$ = 22°).

Fig. 3.57. Example of the effect of $\beta_{2л}$ on the angle of inclination of the head characteristic at the calculated point (H_p = 5610 J/kg; Q = 80 l/s; ω = 1000 1/s; b_2 = 14 mm).

Figures 3.56 and 3.57, for an example, show within which limits it is possible to affect the angle of inclination of the head characteristic by a change in b_2 and $\beta_{2л}$.

C. DEPENDENCE OF THE EFFICIENCY OF PUMP ON THE FLOW RATE

The dependence of full efficiency of the pump $\eta_н$ on the flow rate Q at a constant angular velocity ω is called the efficiency-characteristic of the pump. In order to investigate the dependence of the full efficiency on the flow rate, let us present it in the

form of the product of the particular efficiencies:

$$\eta_н = \eta_г \eta_д \eta_р \eta_{мех}. \qquad (3.88)$$

With zero flow rate (Fig. 3.58) $\eta_г$ has a value different from zero, since the real pressure in this case is more than zero (see Fig. 3.54). Conditions of the maximum of hydraulic efficiency, due to a decrease in $H_т$, does not completely coincide with conditions (according to the flow rate) of the minimum hydraulic losses for pumps with $\beta_{2л} \leq 90°$ (see Fig. 3.51).

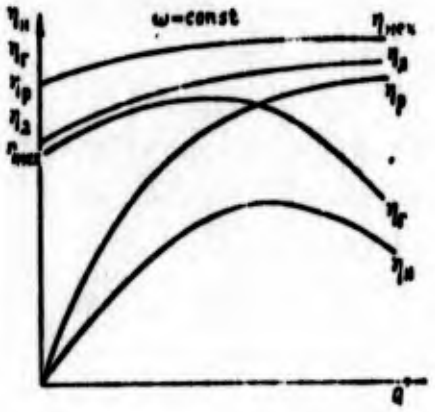

Fig. 3.58. Dependence of efficiencies of the pump on flow rate.

The disk efficiency [see equation (2.239)] with zero flow rate is low (see Fig. 3.58), since the internal energy $N_{вн}$ is determined by the value of the leakages, and the expenditure of energy to disk losses, including the energy of hydraulic stagnat[illegible] s great. With an increase in flow rate Q the internal energy [illegible]ases, and the losses of hydraulic stagnation are decreased, therefore disk efficiency will increase.

The flow efficiency $\eta_р$ with the approach of the flow through the pump for the zero value vanishes [see equation (3.53)], since leakages Q_y are not equal to zero. The value of the leakages at $Q = 0$ consists of the entire flow through the wheel. With an increase in the flow rate the quantity $\eta_р$ increases (see Fig. 3.58),

since the absolute value of the leakages remains approximately constant or is even decreased as a result of a decrease in the twist c_{2u} with an increase in $Q(\beta_{2л} < 90°)$. Mechanical losses do not depend on the flow rate, and the pump power increases with an increase in the flow rate, and therefore the mechanical efficiency $\eta_{мех}$ increases with an increase in Q (see Fig. 3.58).

The full efficiency which evaluates all the losses passes through the origin of the coordinates $\eta_н - Q$ and will have the maximum more to the right of the maximum of the hydraulic efficiency.

Since the hydraulic losses under conditions different from the calculated at the present time do not yield to the calculation, just as the losses to hydraulic stagnation, appearing under conditions of $Q < Q_p$, then for calculating the efficiency characteristic one should use, just as in the case of the head characteristics, results of the generalization of characteristics of the pumps made.

In the relative coordinates $\eta_н/\eta_{н.р} - Q/Q_p$ the efficiency characteristic of pumps with $\bar{D}_1 \leq 0.55$ and $\beta_{2л} \leq 90°(Re > 10^5)$ are generalized by the polynomial:

$$\frac{\eta_н}{\eta_{н.р}} = 2{,}69\frac{Q}{Q_p} - 2{,}65\left(\frac{Q}{Q_p}\right)^2 + 1{,}22\left(\frac{Q}{Q_p}\right)^3 - 0{,}26\left(\frac{Q}{Q_p}\right)^4. \qquad (3.89)$$

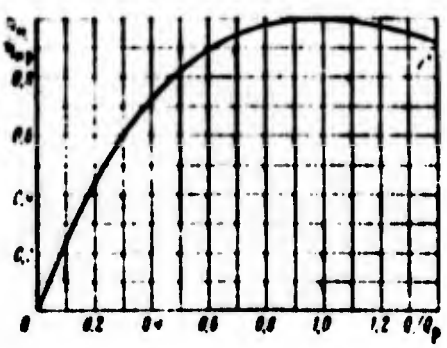

Fig. 3.59. Generalized dependence of the full efficiency of the pump on flow rate.

In graphic form this dependence is represented on Fig. 3.59. From equation (3.89) it is easy to find the equation of a universal efficiency characteristic of the pump $\eta_н = f(Q/\omega)$ and the characteristic $\eta_н = f(Q)$ at $\omega = const$:

$$\eta_н = A\frac{Q}{\omega} - B\left(\frac{Q}{\omega}\right)^2 + C\left(\frac{Q}{\omega}\right)^3 - D\left(\frac{Q}{\omega}\right)^4, \tag{3.90}$$

where

$$A = 2{,}69\frac{\eta_{н.р}}{(Q\omega)_р};\quad B = 2{,}63\frac{\eta_{н.р}}{(Q\omega)^2_р};$$

$$C = 1{,}22\frac{\eta_{н.р}}{(Q\omega)^3_р};\quad D = 0{,}26\frac{\eta_{н.р}}{(Q\omega)^4_р};$$

$$\eta_н = aQ - bQ^2 + cQ^3 - dQ^4, \tag{3.91}$$

where $a = A/\omega$; $b = B/\omega^2$; $c = C/\omega^3$; $d = D/\omega^4$.

D. THE REAL POWER PUMP PERFORMANCE

The power pump characteristic is called the dependence of power input $N_н$ on the flow rate Q. The power characteristic can be determined according to the head characteristic and efficiency characteristic. Keeping in mind equation (3.63) for the pump power, it is possible to record:

$$\frac{N_н}{N_{н.р}} = \frac{(Q/Q_р)(H/H_р)}{(\eta_н/\eta_{н.р})}.$$

Using this relation and relations (3.85) and (3.89), after the transformations we will obtain

$$\frac{N_н}{N_{н.р}} = \frac{1{,}06 + 0{,}8q_р\left(1 - \frac{Q}{Q_р}\right) - 0{,}26\left[0{,}55 - (Q/Q_р)\right]^3}{2{,}69 - 2{,}63(Q/Q_р) + 1{,}22(Q/Q_р)^2 - 0{,}26(Q/Q_р)^3}. \tag{3.92}$$

In graphic form the dependence (3.92) at different values of $q_р$ is represented on Fig. 3.60. It is evident that with an increase in $q_р$ the angle of inclination of the characteristic in relative coordinates is decreased.

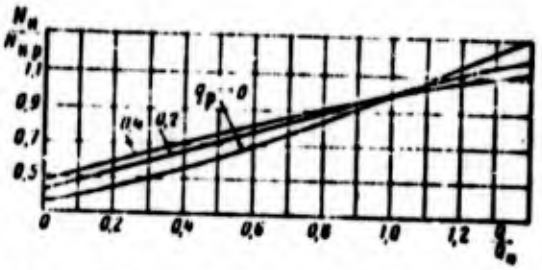

Fig. 3.60. Generalized power characteristics of pumps.

It was previously noted that a decrease in values b_2 and $\beta_{2л}$ and an increase in ω, $\eta_{г.р}$ and z lead to an increase in q_p. Consequently, such a change in the indicated parameters leads to a decrease in the slope angle of the power characteristic in relative coordinates. The slope of the power characteristic $N_н = f(Q)$ at the calculated point can be characterized in the following way:

$$\left(\frac{dN_н}{dQ}\right)_p = \frac{N_{н.р}}{Q_p}\left[\frac{d(N_н/N_{н.р})}{d(Q/Q_p)}\right]_p.$$

With an increase in q_p $\left[\frac{d(N_н/N_{н.р})}{d(Q/Q_p)}\right]_p$ is decreased, and the pump power $N_н$ is increased, since the full efficiency of the pump (Q_p, H_p and ω are assigned). However, for pumps with $n_s^* \geq 40$ an increase in q_p is accompanied by a decrease in the slope angle of power characteristic $N_н = f(Q)$.

E. FIELD OF ENERGY PUMP CHARACTERISTICS

In the practice of the use of screw-centrifugal pumps in feed systems of the LPRE, it is necessary to know the dependence of the pressure and full efficiency of the pump on the flow rate in the sufficiently wide frequency range of the rotation of the pump ω. Therefore, the pump should be characterized by the family of curves $H = f(Q)$ and $\eta = \varphi(Q)$, i.e., by the field of energy characteristics (Fig. 3.61).

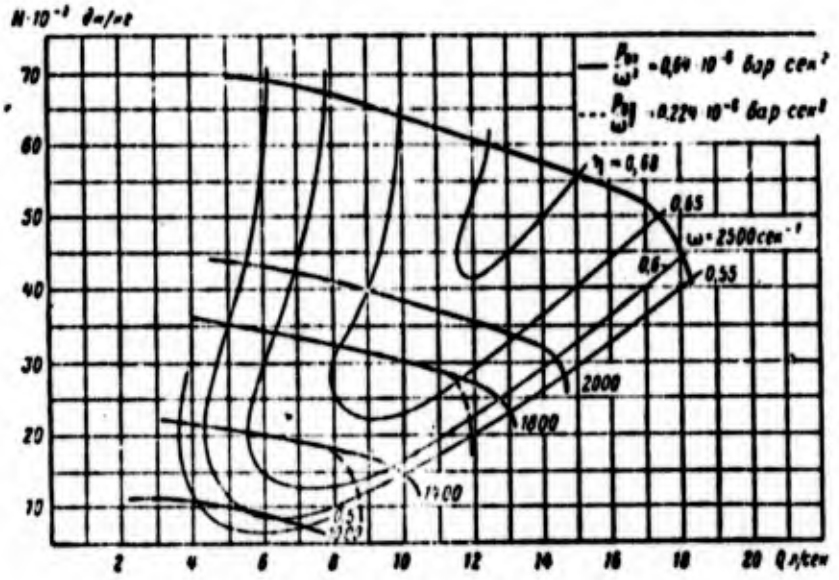

Fig. 3.61. Field of energy pump characteristics. Designations: дж/кг = J/kg; бар·сек^2 = bar·s^2; л/сек = l/s.

During a change in the frequency of rotation of the pump ω the value of criterion $Re = \omega D_2^2/\nu$ will be changed. In the region $Re > 10^5$ (see Section 2.12.2) Re does not affect the Euler's criterion $\bar{H} = H/u_2^2$ (self-similar region with respect to $\bar{H}$), and when $Re > 10^6$ the Re number does not virtually affect the internal power efficiency $\eta_{вн\ N}$ and the power criterion $\bar{N}_{вн} = N_{вн}/\rho\omega^3 D_2^5$ (self-similarity with respect to $\eta_{вн\ N}$ and $\bar{N}_{вн}$). The field of characteristics can encompass the range of the change in ω a; which Re is located in the self-similar region. Then (see Section 2.12.2) in similar conditions of the pump $Q/\omega = const$ the following relation will be maintained constant:

$$H/\omega^2 = const; \tag{3.93}$$

$$N_{вн}/\omega^3 = const; \tag{3.94}$$

$$\eta_{вн\ N} = const.$$

For similar conditions $Q/\omega = const$ with the aid of expression (3.93), we will obtain $H/Q^2 = const$, i.e., the lines of similar

conditions in coordinates H-Q will be determined by parabolas. Parabolas of similar conditions are lines of constant ratios $N_{вн}/\omega^3$ and $\eta_{вн\ N}$ (Fig. 3.62). On parabola the pump head H varies in proportion to ω^2, and the internal energy $N_{вн}$ in proportion to ω^3 [see relations (3.93) and (3.94)]. If values H and $N_{вн}$ at any value of ω are known, then with the aid of relations (3.93) and (3.94) it is possible to obtain values of the pressure and internal energy which correspond to another value of the frequency of rotation.

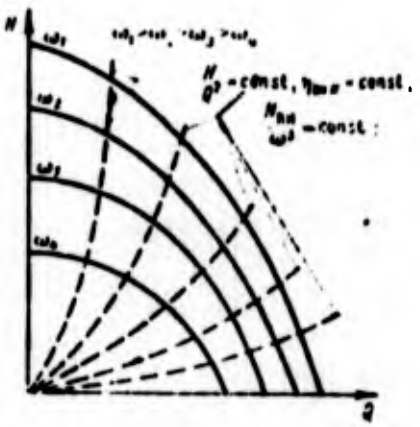

Fig. 3.62. Parabolas of similar conditions of the pump.

At low frequencies of rotation the criterion Re becomes less self-similar in value with respect to $N_{вн}(\eta_{вн\ N})$, i.e., $Re < 10^6$. In this case it is already impossible to disregard the effect of Re on $N_{вн}$ and $\eta_{вн\ N}$, and it is not possible to consider that in similar conditions Q/ω = const the value $N_{вн}$ is proportional to ω^3. Due to the effect of the power of disk friction (the effect of Re on the coefficient of the friction of the disk $C_{тр.д}$) [see equations (2.202) and (3.50)] the internal power will be decreased with a decrease in ω more slowly than with respect to the cube of the frequency of rotation. Therefore, the efficiency $\eta_{вн\ N}$ will not remain constant with a change in ω in similar conditions but will decrease with a decrease in ω. In connection with this in the region of small ω curves of constants $\eta_{вн\ N}$ will not coincide with parabolas of similar conditions H/Q^2 = const.

The noncoincidence of curves of constant full efficiencies η_H = const with parabolas of similar conditions will still be larger, since the dependence of mechanical losses in the pump on ω is also different from the cubic: with a decrease in ω the mechanical losses are decreased more gradually than with respect to the cube ω [see expressions (3.49) and (3.52)]. Therefore, with a decrease in ω in similar conditions the overall efficiency η_H, just as the internal power efficiency $\eta_{\text{EH N}}$, will be decreased. This will lead to the fact that in the region of small ω curves of constant full efficiencies will intersect the parabolas of similar conditions (see Fig. 3.61).

Let us note that in the region of very small ω, when the Re criterion becomes nonself-similar with respect to $\bar{H}(\text{Re} < 10^5)$, under conditions of Q/ω = const will condition H/ω^2 = const not be maintained, and curves H/Q^2 = const will not be curves of similar conditions.

Experience shows that for the pumps of LPRE, which, as a rule, correspond to high Re numbers and a low portion of mechanical losses in the power input, it is possible to consider that the curves η_H = const (N/ω^3 = const) coincide with parabolas of similar conditions H/Q^2 = const in the region of the change in the frequency of rotation $\omega > (0.5\text{-}0.6)\omega_p$. In this case it is possible to calculate the field of the energy pump characteristics of LPRE $H = f(Q)$ and $\eta_H = \varphi(Q)$ with the aid of relations (3.84) and (3.91).

Frequently the pump performance of LPRE is represented in the form of $H/\omega^2 = f(Q/\omega)$ and $\eta_H = \varphi(Q/\omega)$ (Fig. 3.63). Such characteristics are called universal characteristics; they do not depend on the frequency of rotation. Universal characteristics are calculated from equations (3.82) and (3.90).

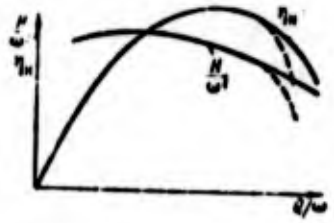

Fig. 3.63. Universal pump characteristics.

Sometimes the lines of constant efficiency η_H = const in the field of characteristics are closed in the region of large ω and high flow rates Q. A reduction in the full efficiency in these conditions (which graphically means the closing of lines of constant efficiency) should be explained by the emergence in these conditions of cavitation phenomena in the pump. In coordinates $H/\omega^2 - Q/\omega$ the cavitation is developed by an abrupt change in the nature of the course of the head characteristic and efficiency characteristic (dashed lines on Fig. 3.63; see also Fig. 3.61).

Energy characteristics can be obtained most reliably experimentally. Usually for the obtaining of the characteristics, tests of the pump in water are carried out. For pumps of LPRE which consume high power, the use of air (and other gases) as a model working medium deserves attention (see sources [78, 80, 84]). In this case in connection with the low air density a reduction of 80-100 times of the energy required for the pump drive is reached [see equation (3.63)].

F. FULL PUMP CHARACTERISTIC

For an examination of the individual problems of the joint operation of two pumps or the operation of the pump in the feed system of LPRE during transient conditions, it is necessary to know the full pump characteristic, i.e., the characteristic in all four quadrants of H-Q coordinates.

For an example Fig. 3.64 depicts the total characteristic of a centrifugal pump. The letters A, B and C designate the basic conditions. In each quadrant the direction of flow through the pump is shown.

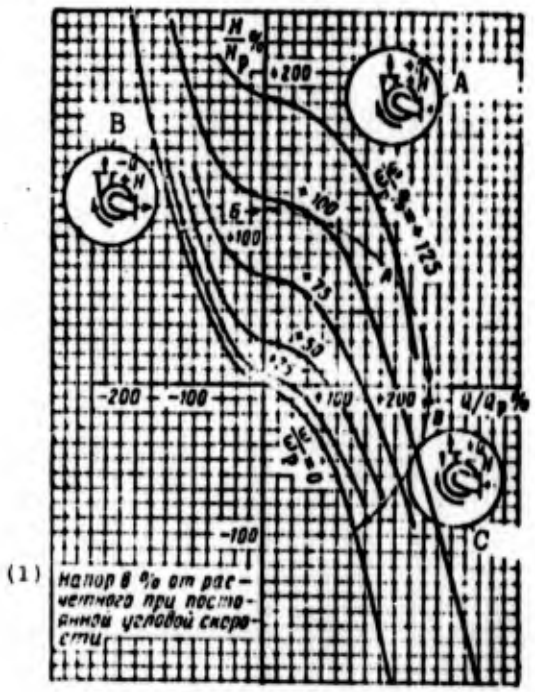

Fig. 3.64. Full characteristic of the centrifugal pump.
KEY: (1) Pressure in % of calculated pressure at constant angular velocity.

G. EFFECT OF THE SPIRAL BRANCH AND CENTRIFUGAL WHEEL ON OPTIMUM PARAMETERS OF THE PUMP

With definite flow the full efficiency of the pump η_H reaches a maximum (see Fig. 3.58). This flow is called the optimum pump flow, the operating mode in this flow - the optimum mode, and the corresponding parameters - the optimum parameters of the pump. The calculation of the pump is performed in the optimum mode, and therefore this mode in the calculation of the pump is called design mode.

With the final adjustment of the specific pump it can prove to be necessary to change the optimum parameters of the pump (Q_{opt} and H_{opt}). For example, it can prove necessary to increase the

pressure (when ω = const) or change the magnitude of the optimum flow rate. A change in the magnitude of the optimum flow rate will be required when the flow on which the pump will have to operate proves to be displaced relative to the optimum (for example, to the side of higher flow rates), which leads to an understating of the efficiency of the pump (see Fig. 3.58). An experiment shows (see sources [91], (105]) that in order to raise the pressure and change the optimum mode, there is no need to design the pump anew. It is sufficient to change somewhat the design of the pump during the period of final adjustment. Depending on which parameters of the pump should be changed, it is sufficient to change the centrifugal wheel with an invariable branch (D_2 = const) or change the branch with the same wheel. In order to determine correctly what precisely it is necessary to change, it is necessary to know how the wheel and branch affect the optimum parameters of the pump.

The optimum mode (see subsection A in the present section) is determined by the point of intersection of the relation

$$Q = k' c_{2u}, \tag{3.95}$$

which corresponds to the spiral branch, and the relation for the wheel

$$c_{2u}' = f(Q) \tag{3.96}$$

(see lines 1 and 2 on Fig. 3.52).

In expanded form we will obtain expression (3.96) from relation (3.23):

$$Q = 2f_1 \frac{r_2}{b_2} (1 + e^{2\pi (b_2 + \delta) \operatorname{tg} \beta_{2\text{л}}}) c_{2u} = k' c_{2u}. \tag{3.97}$$

where k' is the constant value for this branch.

Relation (3.97) can be named the characteristic of the throughput capacity of the branch.

Relation (3.96) takes the following form [see equations (3.7) and (3.65)]:

$$c_{2u} = k_z\left(u_2 - \frac{ctg\,\beta_{2л}}{\pi D_2 b_2}Q\right). \tag{3.98}$$

With a change in b_2, $\beta_{2л}$ and k_z(D_2 = const) the twist c_{2u} [determined by equation (3.98)] created by the wheel will be changed. Therefore, line 2 on Fig. 3.52, which corresponds to the wheel, will be shifted relative to the origin of coordinates (with an increase in b_2, $\beta_{2л}$ and k_z - from the origin of the coordinates, see lines 2' and 2"). With an invariable branch the optimum points will be found on the line corresponding to this branch. Then it is possible to record:

$$Q_{опт} = k'(c_{2u})_{опт}. \tag{3.99}$$

Let us express $(c_{2u})_{опт}$ in terms of the optimum pressure, keeping in mind that $H = c_{2u}u_2\eta_г$:

$$(c_{2u})_{опт} = \frac{H_{опт}}{u_2\eta_{г\,опт}}. \tag{3.100}$$

By substituting relation (3.100) into (3.99), we obtain

$$\frac{Q_{опт}}{\omega} = \frac{2k'}{D_2\eta_{г\,опт}}\frac{H_{опт}}{\omega^2} = k\frac{H_{опт}}{\omega^2}. \tag{3.101}$$

If changes in parameters of the wheel will have little effect on the value $\eta_{г\ опт}$, then k (when D_2 = const) will be a constant value for this branch, i.e., k = const (for this branch). Then [see equation (3.101)] changes in the wheel with an invariable branch lead to a displacement of the optimum mode in coordinates H/ω^2 - Q/ω along the line passing through the origin of the coordinates. An experiment confirms this conclusion (see source [91]).

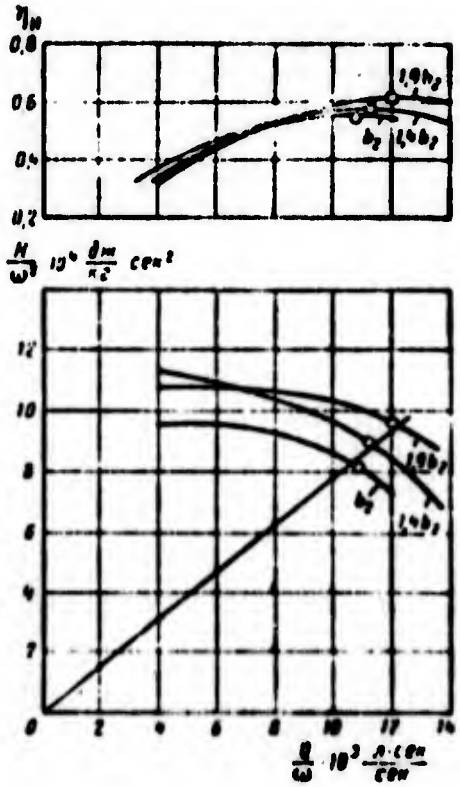

Fig. 365. Energy characteristics of pumps which differ from each other by the width of the centrifugal wheel at the outlet.

Figure 3.65 depicts the energy characteristics of versions of the pump which differ from each other only by the centrifugal wheel. Wheels have different values b_2. From the figure one can see that the optimum points on head characteristics are virtually located on one line. A change also in other geometric parameters of the centrifugal wheel ($\beta_{2л}$, $\beta_{1л}$, z and so on) and the screw conveyor leads to those results.

Experimental data (see Fig. 3.65) show that even a considerable change in parameters of the wheel has little effect on the value of the optimum flow, having basically an effect on the pressure. Therefore, it is possible to increase the pump head by a change in parameters of the wheel with an invariable branch. As a rule, b_2 and $\beta_{2л}$ are changed.

Drawing a line through the origin of the coordinates H-Q and the optimum point of the pump with the old wheel, according to the required pump head with the new wheel, let us find its optimum point. The values $\beta_{2л}$ and b_2 at which provided is the necessary pressure are determined according to the magnitude of the pressure. For the optimum points with the aid of (3.98) let us rewrite expression (3.100) in the form

$$H_{опт} = u_2^2 k_1 \eta_{г.опт} \left(1 - \frac{Q_{опт} c\lg \beta_{2л}}{u_2 D_2 b_2 \pi}\right). \qquad (3.102)$$

Substituting expression (3.101) into equation (3.102), we obtain the relation of the required head with values b_2 and $\beta_{2л}$:

$$H_{опт} = \frac{u_2^2 k_1 \eta_{г.опт}}{1 + \frac{k k_1 \eta_{г.опт} c\lg \beta_{2л}}{2\pi b_2}}. \qquad (3.103)$$

Let us now leave wheel constant, and we will change the branch (D_2 = const). With an increase in the intake area into the conical diffuser of the branch f_3, coefficient k' in expression (3.97) will increase and the characteristic of the throughput capacity of the branch will approach the axis Q (see line 3 on Fig. 3.52). In this case the optimum flow will increase ($Q_B > Q_A$), and value c_{2u} and, therefore, the pressure will be decreased. With a change in the branch the optimum points will be located on the line corresponding to this wheel (see Fig. 3.52).

In H-Q coordinates the optimum points are also located along the straight line [see equation (3.102)]. This conclusion is confirmed by the experimental data presented on Fig. 3.66, where shown are characteristics of variants of the pump differing from each other by the intake area into the conical diffuser f_3. Figure 3.66 shows that by a change in the branch (f_3) it is possible to achieve a considerable change in the optimum flow rate.

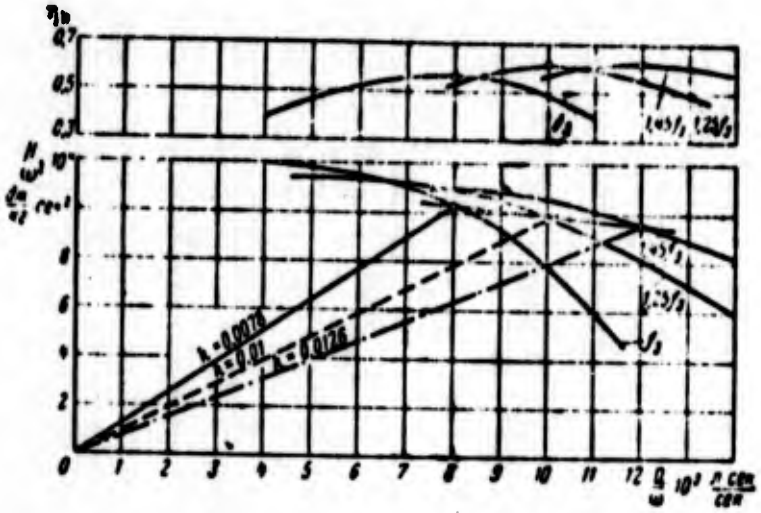

Fig. 3.66. Energy characteristics of pumps which differ from each other by the area of the outlet from the spiral collector.

A new optimum point is found on the line [see equation (3.102)] corresponding to the wheel and the required value Q_{opt}. In this case let us determine $k_z\eta_{r\ opt}$ according to equation (3.102) and the optimum parameters of the pump with the initial branch. The required flow rate Q_{opt} will determine the hermetic parameters of the branch.

Solving together expressions (3.101) and (3.102), we obtain

$$Q_{opt} = \frac{k_1 \frac{g}{\omega} H_{opt} k_z \eta_{r\ opt}}{1 + \frac{k k_z \eta_{r\ opt} \operatorname{ctg} \beta_{2p}}{2\pi b_2}}. \qquad (3.104)$$

According to value k [see equations (3.97) and (3.101)] let us find the necessary geometric parameters (f_3 and α_{2p}).

With a change in the wheel or branch the new value of the optimum efficiency can be evaluated with the aid of expressions (3.61) and (3.62), using the experimental value $k_z\eta_{r\ opt}$ found from parameters of the optimum mode of the initial variant of the pump. The energy characteristics are calculated with the use of relations (3.82) and (3.90).

We examined the question about how it is possible to increase the pressure by a change of only the wheel with the final adjustment of the pump. In practice it can be required to decrease the pump head (when ω = const). This can be achieved by decreasing b_2 or $\beta_{2л}$ when D_2 = const [see equation (3.103)]. But it is still possible to decrease the pressure more simply by the trimming of wheel, i.e., by a decrease in its diameter D_2. With the trimming of the wheel the space between the wheel and the branch increases, and, consequently, the nature of the flow entering into the branch is changed. The throughput capacity of the branch in this case is changed [coefficient k in equation (3.101) is changed]. Therefore, with the trimming of the wheel it is not possible to determine the pressure according to equation (3.103).

Experimental data show that with the reducing of the diameter of the wheel to ~8-10%, the optimum efficiency virtually remains constant, and the optimum pressure is decreased in proportion to the square of the diameter:

$$H'_{opt} = H_{opt}\left(\frac{D'_2}{D_2}\right)^2. \tag{3.105}$$

In this case the optimum flow rate will vary in proportion to the diameter in the first degree:

$$Q'_{opt} = Q\frac{D'_2}{D_2}, \tag{3.106}$$

where the prime denotes the parameters which correspond to the reduced diameter D'_2. Such a change in the flow rate can be explained in the following manner. The optimum pressure can be recorded in the form (3.102). Then

$$\frac{H_{opt}}{D_2^2} = k\eta_{г\,opt}\frac{\omega^2}{4}\left(1-\frac{2Q_{opt}}{\pi D_2 b_2 \omega D_2}\operatorname{ctg}\beta_{2л}\right); \tag{3.107}$$

$$\frac{H'_{opt}}{D'^2_2} = k'\eta'_{г\,opt}\frac{\omega^2}{4}\left(1-\frac{2Q'_{opt}}{\pi D'_2 b_2 \omega D'_2}\operatorname{ctg}\beta'_{2л}\right). \tag{3.108}$$

Since the left members of equations (3.107) and (3.108) are equal [see expression (3.105)], then their right sides are equal. Bearing in mind that the efficiency is not changed (trimming of the wheel does not exceed 8-10%), it can be concluded that $k_z\eta_{r\ opt} = k'_z\eta'_{r\ opt}$.

Therefore,

$$\frac{Q'_{опт}}{\pi D'_2 b'_2 \eta_{г} D_2} \operatorname{ctg}\beta'_{2л} = \frac{Q_{опт}}{\pi D_2 b_2 \eta_{г} D_2} \operatorname{ctg}\beta_{2л}. \qquad (3.109)$$

Since the meridian section of the centrifugal wheel becomes narrow toward the outlet, then with the reducing of D_2, b_2 will increase. Therefore, it is possible to consider that the area of the outlet from the wheel with its trimming will remain constant, i.e., $\pi D'_2 b_2 = \pi D_2 b_2$. With the small trimming of the wheel the outlet angle ($\beta'_{2л} \approx \beta_{2л}$) is little affected. Then from equation (3.109) we will obtain the expression (3.106). With the aid of expression (3.105), according to the necessary value H'_{opt} it is possible to determine the required diameter D'_2. Dependences (3.105) and (3.106) are valid not only for the optimum but also for other conditions. Consequently, with their aid it is possible to find the pressure pump characteristic $H = f(Q)$ and at a smaller diameter D'_2 the efficiency, as has already been said, can be accepted as being constant if the trimming of the wheel does not exceed 8-10%.

H. THE SELECTION OF THE CALCULATED FLOW RATE OF THE SCREW-CENTRIFUGAL PUMP WITH SMALL n_s^*

As a rule, in the calculation of a pump it is attempted to combine the assigned conditions of its operation $Q_{задан}$ with its optimum mode: $Q_{задан} = Q_p$. However, an experiment shows (see source [91]) that in certain cases (small n_s) for the obtaining of the maximally possible efficiency of the pump, it is advantageous to design a pump for a flow rate more than the assigned: $Q_p > Q_{задан}$.

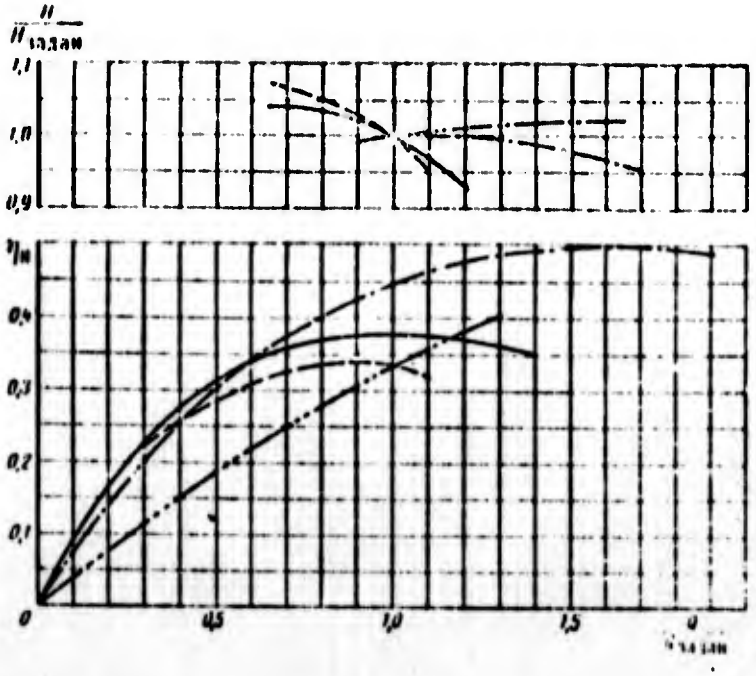

Fig. 3.67. Pump characteristics with $n_{s\ задан}^{*} = 30$ at different calculated flow rates:

——— $-Q_p/Q_{задан}=1$; – – – $Q_p/Q_{задан}=0,8$; – · – $Q_p/Q_{задан}=1,6$; ····· $Q_p/Q_{задан}=2,3$.

Figure 3.67 shows that with a definite displacement of the calculated flow rate from the assigned to the side of high flow rates, in this case when $Q_p = 1.6Q_{задан}$ (dot-and-dash line), in the assigned conditions a larger efficiency is reached than with the equality of the calculated and assigned flow rates. This gain in efficiency is explained by the fact that in the assigned conditions the hydraulic efficiency of the pump, calculated at higher than the assigned flow rate, will be more than at the calculated point, since the maximum value of the hydraulic efficiency corresponds to the flow rate less than the calculated (see Fig. 3.58).

With greater hydraulic efficiency the less diameter of the wheel D_2 is necessary for providing the assigned pressure $H_{задан}$

under the conditions of $Q_{задан}$. And this, in turn, leads to an increase in the full efficiency of the pump as a result of a decrease in the friction losses of the wheel against the fluid [see equation (2.202)]. It is natural that this increase in the efficiency will be more for pumps with small $n^*_{s\ задан}$ and large values of the flow parameter $q_{задан}$, in which friction losses of the wheel are great (see Fig. 3.36).

For determining the optimum value of the displacement of design conditions from the assigned to the side of higher flow rates, it is possible to proceed in the following manner. It is necessary to assign several values of the ratio of flow rates $Q_{задан}/Q_p$, for each of which according to equation (3.81) it is possible to determine ratio $H_{задан}/H_p$. This ratio makes it possible to determine the value of the power-speed coefficient of the pump in design conditions according to the value corresponding to the assigned:

$$n^*_{s\ p} = n^*_{s\ задан} \frac{\sqrt{Q_p / Q_{задан}}}{(H_p / H_{задан})^{3/4}}. \qquad (3.110)$$

According to value $n^*_{s\ p}$, the selected value $q_{задан} = q_p$ and value K_{D_0} known from the calculation of the pump for cavitation, let us determine with the aid of equation (3.62) and relations given on Figs. 3.38-3.40 the value of efficiency in the design conditions $\eta_{н.р}$. We use the value $\eta_{н.р}$ for determining the efficiency in the assigned conditions $\eta_{н.задан}$. For this let us use equation (3.89). The ratio $\eta_{н.задан}/\eta_{н.задан}$ ($\eta_{н.задан}$ - efficiency when $Q_p = Q_{задан}$) will characterize the gain in efficiency with displacement of the optimum characteristic. The ratio $Q_p/Q_{задан}$ at which $\eta_{н.задан}/\eta_{н.задан}$ reaches a maximum and is optimum. The calculations for $K_{D_0} = 5.2$-6.5 thus carried out (Fig. 3.68) show that it is virtually advantageous to design a pump for the flow rate higher than that assigned, beginning with the power-speed coefficient $n^*_{s\ задан} = 40$-60 and less. Such values of the power-speed coefficient correspond to pumps of the LPRE.

Specifically, the additional pumps which feed components into the gas generator of the engines with a precombustion-chamber turbine have values of $n^*_{s\ задан} = 10\text{-}20$.

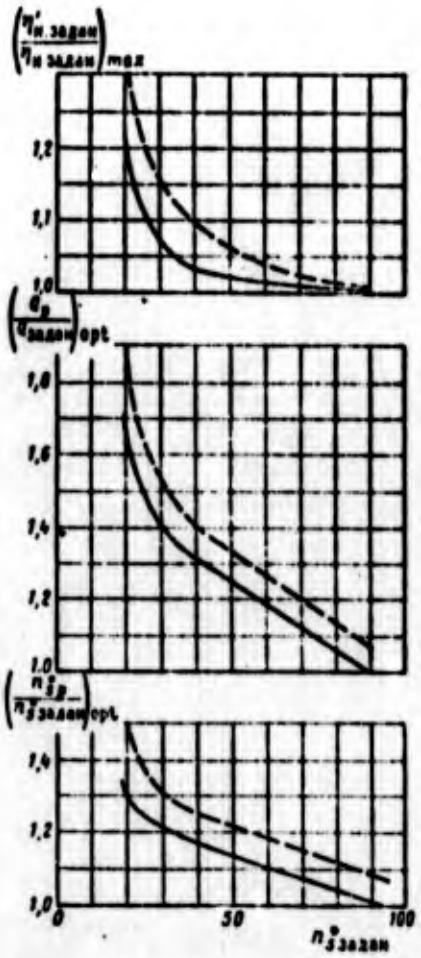

Fig. 3.68. Determination of the calculated flow rate, power-speed coefficient and maximum efficiency in the assigned conditions: —— - $q_p = 0$; - - - - $q_p = 0.2$.

The calculation of the pump for the flow rate higher than that assigned makes it possible, furthermore, to increase the width of the wheel b_2 at a low assigned flow rate, which decreases the hydraulic losses, since the possibility for the joining of boundary

layers in cover disks is eliminated. The large width facilitates the manufacture of the wheel.

3.2. AXIAL PUMPS

3.2.1. DESIGN OF AXIAL PUMPS

Axial pumps, as a rule, possess low pressure in one stage but are capable of pumping over great flows. In Section 3.1 the use of axial wheels as preliminary pumps was examined. Sometimes the axial pump can be used as an independent booster pump, which is installed directly in tank or near the tank (see Section 3.3.8). It has independent drive and is called a booster pump.

When using hydrogen as a fuel it is necessary to pump large volumetric flows even with comparatively low mass flow rates. For this purpose multistage axial pumps can be used. For example, in the engine J-2 (see Fig. 1.13) used for the pumping of liquid hydrogen is a seven-stage axial pump, which creates a pressure of $85 \cdot 10^5$ N/m^2 when Q = 500 l/s and ω = 2800 1/s (see source [30]).

Let us analyze the basic positions which refer to the axial pump in the example of the stage made in the form of an individual unit. A diagram of such a pump is given on Fig. 3.69.

In general the inlet of the pump consists of a feed and guide device. The feed is the intake pipe, which is constructively made similar to feeds of the centrifugal pump (see Fig. 3.2); on Fig. 3.69 the feed is not shown. The guide device a on Fig. 3.69 is the blade cascade, which provided the assigned direction of the inlet velocity into rotor wheel b. The guide device at the inlet can be absent. In the feed systems of LPRE the installation of a guide device at the inlet into pump, as a rule, is undesirable, since the deviation in the flow is connected with an increase in velocity and a decrease in the static pressure; futhermore, the

static pressure decreases as a result of losses in the flow of guide blades. The possibility for the emergence of cavitation phenomena at inlet into the pump in this case increases.

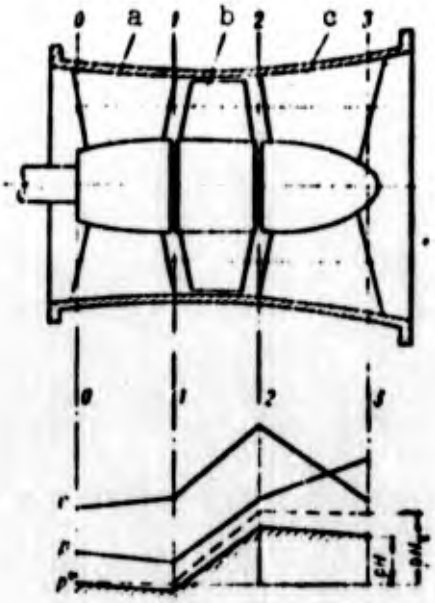

Fig. 3.69. Diagram of the axial pump and a change in the flow parameters along the length of the flow area.

The axial pump for an increase in the anticavitation qualities can also have a stage with high anticavitation qualities, in particular, the screw conveyor (see sources [113, 30] and Fig. 1.13). In this case the screw wheel will be the wheel of the first stage of the axial pump.

In the case of a multistage axial pump the role of the guide device at the inlet into the rotor wheel is served by the outlet stator of the preceding stage. Therefore, the diagram given on Fig. 3.69 can also be examined as the diagram of the intermediate stage of the multistage axial pump.

In general in the guide device there occurs the acceleration of the flow and a change in its direction. The total form of the change in the flow parameters along the length of the guide device - pressure p, velocity c, total pressure of the fluid p^* - is shown on Fig. 3.69. The total pressure of the fluid will decrease due to the presence of losses.

The rotor wheel b is the blade row fastened to the rotating shaft. In the rotor wheel to fluid will be fed energy - the value of total pressure p^* increases; as a rule, the velocity and pressure p also increase (see Fig. 3.69). Placed at the outlet from the rotor wheel is a blade cascade c in which the high-speed energy is partially converted into pressure. A deceleration in the outlet guide device is reached by means of a decrease in the circular and sometimes axial components of velocity. The blade cascade of the outlet guide device is frequently called a stator. In a multistage pump the stator of the previous stage plays a part in the guide device of the subsequent stage. Thus, along the length of the diffuser cascade the velocity will decrease, and the pressure will increase. The energy of the fluid (total pressure) will decrease due to the presence of hydraulic losses. Such a cascade plays a part in the diffuser device.

The axial pump cannot have a special branch. After rectification of the flow in the blade diffuser cascade, the flow from the pump casing can pass over directly into the pipeline or the following stage.

Sometimes, if the flow has a high speed (great twist), which is difficult to convert into pressure energy in the axial blade cascade with low losses, outlet devices in the form of a spiral collector and conical diffuser, as with a screw-centrifugal pump, can be used.

3.2.2. THEORETICAL PRESSURE AND DETERMINATION OF PARAMETERS OF THE ELEMENTARY AXIAL STAGE

In the present section we will examine the axial cascades of a single length. Such cascades form elementary axial stage, i.e., the stage, in which it is possible to disregard a change in parameters of the fluid over the height. Figure 3.70 shows the parameters, and velocity triangles of the elementary axial stage of the pump are depicted.

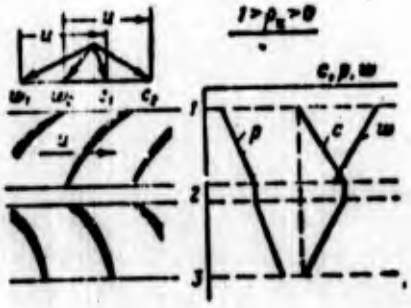

Fig. 3.70. Change in the flow parameters and velocity triangles for the elementary axial stage of the pump.

The theoretical pressure [see equations (2.31) and (2.59)] of such an axial stage is calculated according to equation

$$H_т = u(c_{2u} - c_{1u}) = u(w_{2u} - w_{1u}). \tag{3.111}$$

In hydrogen pumps from the stage it is necessary to obtain the maximum pressure and advantageously to increase maximally the circular velocity of the blades, for which the blades are arranged on large radii, i.e., is used a high hub-tip ratio. The span of the blade, as a rule, is small, and it sometimes reaches 8-10 mm.

For an increase in the pressure quality, it is advantageous to select the maximum angles of rotation of the flow and great denseness ($b_л/t_л > 1$). For the selection of parameters of the axial cascades of the pumps as a first approximation it is possible to draw on the experience of compressor manufacturing.

The generalization of experimental data on results of the blows of the compressor cascades made it possible to obtain the relation between the permissible value of the angle of rotation of the flow in the cascade $\Delta\beta = \beta_2 - \beta_1$, the cascade density $b_л/t_л$ and the outlet angle β_2 at the angle of incidence of $i = \pm 5°$ (Fig. 3.71).

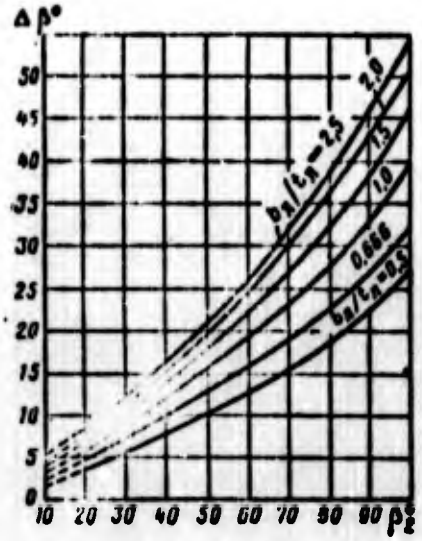

Fig. 3.71. Dependence of the permissible angle of rotation of the flow in the cascade on the flow angle at the outlet and the relative cascade pitch.

The limitation of the angle of rotation of the flow in the compressor cascade is connected with the advent of the boundary-layer separation from the surface of the blades. An increase in the cascade density leads to a decrease in the pressure difference on the concave and convex sides of the blade and makes it possible to increase the permissible degree of diffusivity and angle of rotation of the flow. Friction losses will be increased respectively.

Calculation of the finite number of blades can be produced by means of calculation of the lag angle δ (see Fig. 2.54). The value of the lag angle δ in the compressor cascades (diffuser) is usually equal to 3-5° and is calculated from empirical equations. For example, work [54] gives the following equation for the lag angle:

$$\delta^\circ = \frac{0{,}23\,(2\bar{b}_l)^2 - 0{,}002\,\beta_{2л}^\circ + 0{,}18}{\frac{1}{\theta}\sqrt{b_л/t_л} - 0{,}002},$$

where $\bar{B}_f$ is distance along the chord from the leading edge to the point which corresponds to the maximum bending deflection of the center line referred to the chord length; θ - angle of curvature of the profile: $\theta = [180° - (\beta_{1л} + \beta_{2л})°]$; $b_л$ - chord length; $t_л$ - cascade pitch.

For widely spaced cascades ($b_л/t_л < 1$) the calculation of H_T is frequently carried out on the basis of the airfoil lift, i.e., on the basis of N. Ye. Joukowski's theorem (see Section 2.7.2).

3.2.3. ENERGY CHARACTERISTICS OF AXIAL PUMPS

3.2.3.1. General Positions

Figure 3.54 depicts a change in the pump characteristic with different flow parameters q_p for the design mode. Lines for $q_p > 0.4$ will occur more steeply, which is characteristic for diagonal and axial pumps. For these pumps a sharp increase in the pressure is characteristic with a decrease in the flow rate in comparison with that calculated, and a sharp drop in pressure is characteristic with an increase in flow rate.

Figure 3.72 gives characteristics of the axial pump in the dimensionless parameters. The inflection of the pressure on the left side of the characteristic is characteristic for axial pumps and compressors and is explained by emergence in these conditions of vortex zones.

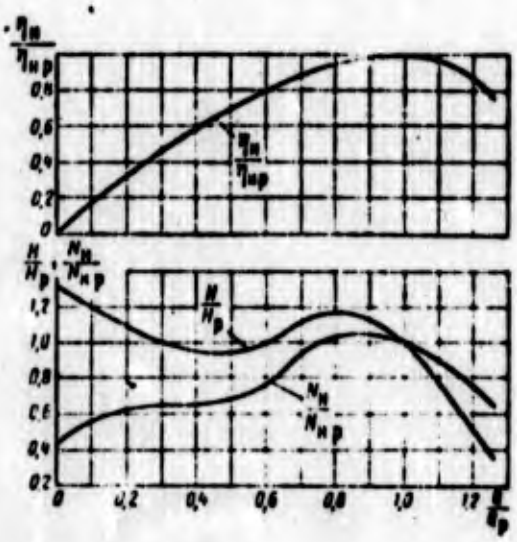

Fig. 3.72. Energy characteristics of an axial pump in relative coordinates.

The power of axial pumps sharply increases with a decrease in the flow rate. This is connected with the appearance of separation of vortex zones and the expenditure of power to "hydraulic stagnation" (see Section 3.1.2.2).

Let us examine in more detail the pressure characteristic of the screw axial pump. By knowing this characteristic, it is possible to evaluate the parameters of helical-type pump in the case of its use as an independent booster pump.

In the joint operation of the screw conveyor with the centrifugal wheel (screw-centrifugal pump) the centrifugal wheel affects the operation of the axial stage standing in front of it (see Section 2.11.1.4), and therefore characteristics of the isolated helical-type pump will differ from the characteristics of the screw conveyor in its joint operation with the centrifugal wheel. This distinction is explained basically by the fact that values of the calculated diameter for the separately standing screw conveyor and for the screw conveyor standing in front of the centrifugal wheel were different [see formulas (2.167) and (2.168)]. Helical-type pumps used in LPRE have a high cascade density. Therefore, the effect of the finite number of blades can be disregarded, i.e., it is possible to accept that

$$H_т = H_{т\infty}.$$

3.2.3.2. Theoretical Characteristic of the Helical-type Pump of Constant Pitch.

The theoretical pressure of the screw conveyor of constant pitch [see equation (2.169)] is written in the form

$$H_т = u_p^2\left(1 - \frac{c_{2u}}{u_p}\operatorname{ctg}\beta_{л.р}\right). \qquad (3.112)$$

Let us express H_T by the flow rate Q and geometric parameters of the screw conveyor.

It is easy to determine value c_{2z} from the following relations:

$$c_{2z} = \frac{Q}{F_{2z}};$$

$$F_{2z} = \frac{\pi D_m^2}{4} - \frac{\pi d_{sr}^2}{4} - \frac{D_m^2 - d_{sr}^2}{2} z \frac{\delta_p}{\sin \beta_{\lambda.p}}. \qquad (3.113)$$

where δ_p is the thickness of the blade at the calculated diameter (see Fig. 2.62).

By transforming this expression, we obtain

$$F_{2z} = h_\lambda \left(\pi D_{cp} - z \frac{\delta_p}{\sin \beta_{\lambda.p}} \right). \qquad (3.114)$$

Taking into account that

$$\operatorname{tg} \beta_{\lambda.p} = \frac{s}{\pi D_p},$$

let us express finally H_T [see equation (3.112)] in terms of the geometric parameters of the screw conveyor:

$$H_T = u_p^2 - \frac{u_2 Q \pi D_p}{s h_\lambda \left(\pi D_{cp} - \frac{z \delta_p}{\sin \beta_{\lambda.p}} \right)}. \qquad (3.115)$$

Let us investigate this expression: when Q = 0

$$H_{T\,Q=0} = u_p^2;$$

when $H_T = 0$

$$Q_{H_T=0} = \frac{sh_л\left(\pi D_{ср} - s\frac{b_р}{\sin\beta_{л.р}}\right)\omega}{2\pi}. \qquad (3.116)$$

From these relations it follows that the theoretical characteristic of the screw axial pump in corrdinates H_T - Q is the straight line intercepting along the axis of the ordinates the segment proportional to u_p^2 and along the axis of the abscissa – the segment proportional to expression (3.116) (Fig. 3.73).

The greater the helix angle $\beta_{л\ р}$, the more sloping the characteristic is. With an increase in the frequency of rotation, the value of theoretical pressure $H_{T\ Q=0}$ will increase more rapidly than $Q_{H_T=0}$, and the theoretical characteristic passes more steeply.

With a decrease in the flow rate the angle of attack increases, with an increase in the flow rate the angle of attack is decreased, and at the zero angle of incidence the theoretical pressure H_T is equal to zero ($Q = Q_{H_T=0}$). This characteristic can be also considered as the dependence $H_T = f(Q_p)$ for a series of screw conveyors with different calculated flow rates.

3.2.3.3. Actual Characteristics of a Helical-Type Pump

An analysis of experimental head characteristics of helical-type pumps showed that the majority of them takes the form of a straight line (see source [47]). Consequently, for the plotting of a characteristic it suffices to know two calculated points. The first calculated point is selected with zero flow rate. We will assume that $H_0 = kH_{T\ Q=0}$, where $k = \eta_г k_z$ is the experimental coefficient (k = 0.45-0.58).

The second point of the characteristic is determined for conditions $H_T = 0$, i.e., for conditions of the zero angle of

incidence. The expenditure of energy for the flow of fluid through the wheel will be determined by the expenditure of energy for the fluid friction against the walls of the wheel (flow of plates with zero angle of attack).

The power loss to friction [see equations (2.198)] is found from the expression

$$L_{\text{гидр.пот}} = \lambda \frac{b_{л.ср}}{D_г} \frac{c_{ср}^2}{2} \rho, \qquad (3.117)$$

where $b_{л\ ср}$ – the length of the blade on the mean diameter;

$D_г$ – the hydraulic diameter:

$$D_г = \frac{4 h_л a_{ср}}{2(h_л + a_{ср})}; \qquad (3.118)$$

here $a_{ср} = \frac{\pi D_{ср} - z(h_{ср} \sin \beta_{л.ср})}{z} \sin \beta_{л.ср}$ – the width of channel on the mean diameter;

$h_л$ – span of the blade.

The relative speed in the vane channel of the wheel under conditions of $Q_{H_т}=0$ retains the constant value:

$$w = \frac{Q_{H_т=0}}{h_л a_{ср} z}.$$

The drag coefficient λ is accepted within limits of 0.04-0.05 (see source [47]). Having plotted value $L_{\text{гидр.пот}}$, from the horizontal axis downward let us find the second point of the characteristic (see Fig. 3.73). Having connected both points, we will obtain the calculated real characteristic of the screw wheel.

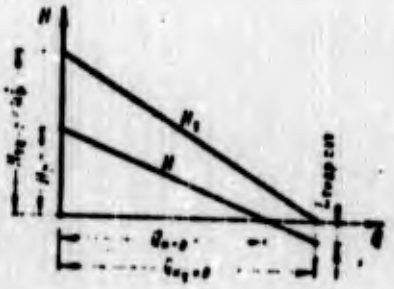

Fig. 3.73. Plotting of the head characteristic of a helical-type pump of constant pitch.

The real experimental characteristic of screw axial wheels is close to a straight line (Fig. 3.74). Sometimes the characteristic of a pump with a screw wheel has a sharp band characteristic for axial pumps with $q \approx 0.5$ (see Fig. 3.74), which is connected with the appearance at the outlet from the screw conveyor of return currents in the hub.

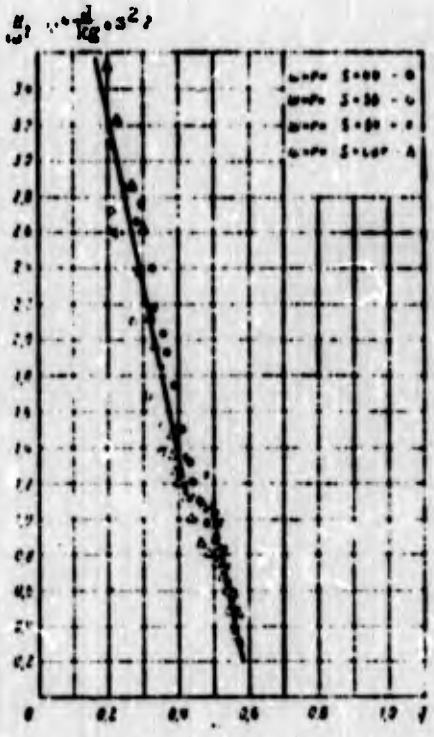

Fig. 3.74. Experimental dependence of pressure of the screw conveyor on the flow parameter for the helical-type pump of constant pitch.

Figure 3.75 shows the dependence of the efficiency of the screw conveyor on the flow rate (see source [47]) obtained during

the testing of an individual screw conveyor with a spiral branch i.e., taking into account losses in the branch.

With the aid of the relations obtained above, it is possible to determine approximately the head characteristic of the screw conveyor of variable pitch. For this it is sufficient to assume that

$$\lambda_{3.p} = \lambda_{2a.p}; \quad \lambda_{3.cp} = \lambda_{2a.cp} \text{ and } s = s_3.$$

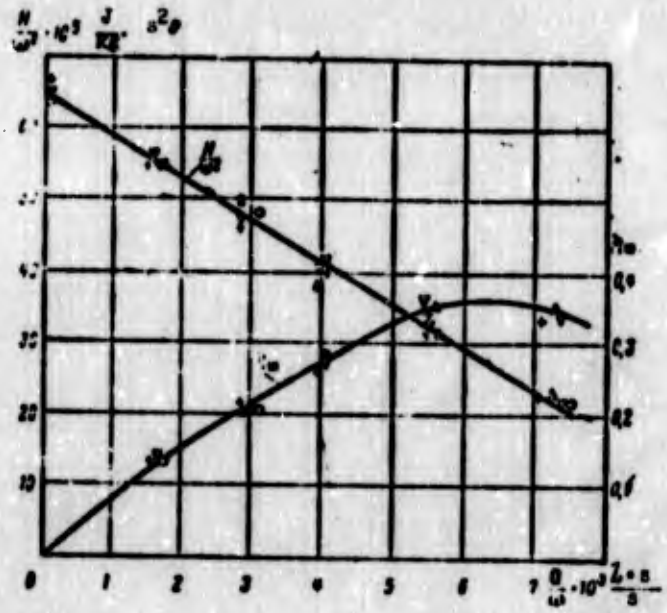

Fig. 3.75. Real energy characteristics of a helical-type pump.

3.3. CAVIATATION IN PUMPS OF LIQUID PROPELLANT ROCKET ENGINES

3.3.1. BASIC CONCEPTS

Cavitation is process of the disturbance of the continuity of fluid flow in the zone of reduced pressure, which consists in the formation of cavities filled with vapor and separated from the liquid by the gas. In the region of reduced pressures there appear tensile stresses, which lead to the rupture of the liquid.

Cavities, the cavitation caverns which are filled with vapors of fluid and separated from the fluid by the gas dissolved in it are formed.

The emergence and development of cavitation in the fluid is connected with the presence of the so-called "nuclei of cavitation." The physically pure and homogeneous fluid, free from the "nuclei of cavitation," absorbs the considerable tensile stresses. In commercial fluids there are always "nuclei of cavitation," and under the effect of tensile stresses cavitation phenomena appear. The "nuclei of cavitation" are those weak points in which the strength of the fluid is disturbed, and where cavitation phenomena appear.

According to most probable hypothesis (see source [88]), the nuclei of cavitation are the undissolved gas inclusions, including in pores and cracks of microparticles suspended in the fluid.

The development of cavitation in fluids is also affected by the quantity of dissolved and free gases which are being liberated in regions of reduced pressure and decrease the volumetric strength of the fluid (gas cavitation). In the presence of a two-phase medium the magnitude of the velocity of sound greatly decreases and the crises taking place during cavitation flows (flow restriction) can be the crises of sonic flows. Furthermore, the degree of development of cavitation can be affected by the thermodynamic properties of fluids (see further Section 3.3.4).

In entering into the region of higher pressures, the caverns "collapse," since the gases are partially dissolved and the vapor is condensed. The collapse of the caverns causes a local hydraulic impact, which, according to some theories, is cumulative, and which can lead to the failure (cavitation erosion) of the material of walls of the channels.

The emergence of cavitation leads to two basic negative consequences for hydraulic machines:

1) the collapse of the operating mode of the machine, i.e., a sharp reduction in the basic outlet parameters – H, Q and η_H (Fig. 3.76);

2) the errosive failure of the rotor wheel of the machine – usually in a continuous operation in cavitation conditions.

In pumps the cavitation appears with the pressure in front of the inlet into pump, which substantially exceeds the pressure of vaporization at this temperature of the fluid. This means that the region of minimum pressure is located within the flow area of the pump. A pressure drop within pump (in comparison with the inlet pressure) is connected first of all with the streamline flow of the inlet edges of the blades. In the streamline flow of the blades, just as with the flow of any profile, the region of reduced pressure is formed. At positive angles of incidences, which are common for pumps, the region of the reduced pressure appears from the nonoperative side of the inlet part of the blades (Figs. 3.77 and 3.78).

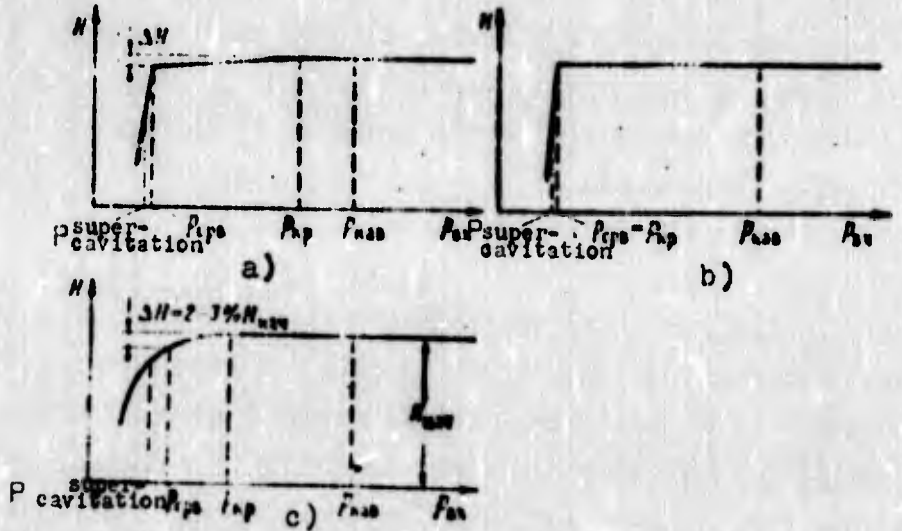

Fig. 3.76. Separation cavitation characteristics typical for: a) screw-centrifugal pumps; b) centrifugal pumps; c) axial pumps.

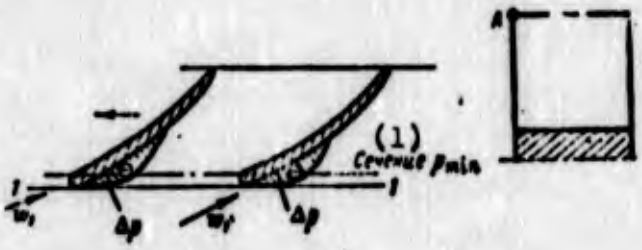

Fig. 3.77. Region of minimum pressures in the axial wheel.
KEY: (1) Cross section.

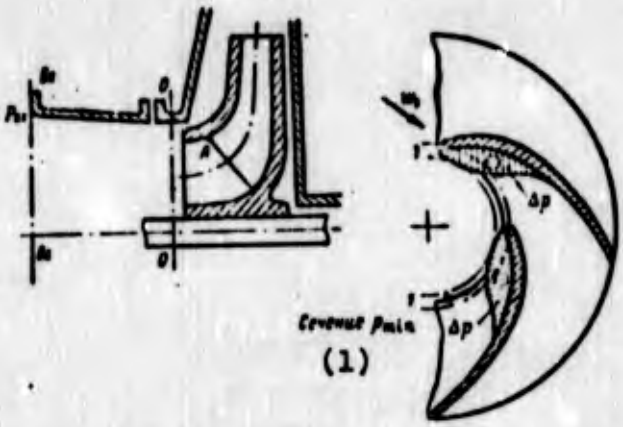

Fig. 3.78. Region of minimum pressures in a centrifugal wheel.
KEY: (1) Cross section.

Figure 3.79 gives curves of the pressure distribution along the back of the winged profile under different pressures in front of the profile p_1 (see source [88]). The curve $\frac{p_1 - p_n}{q\frac{w_1^2}{2}} = \infty$ corresponds to high pressures p_1 at inlet at which the cavitation is absent. With a decrease in pressure p_1 the absolute value of the minimum pressure on the back is decreased. At the defined value of p_1 the minimum pressure reaches the vapor pressure p_n, and cavitation appears. Since the pressure cannot fall below p_n, with a further decrease in p_1 an ever larger part of the back is occupied by the region with the pressure of the vapor pressure. This leads to reconstruction of the diagram of pressure on the back (see Fig. 3.79). The relative rarefaction on the back $\frac{p - p_1}{q\frac{w_1^2}{2}}$ is decreased, which leads to a decrease in lift of the profile.

Figure 3.80 depicts a change in the coefficients of lift c_y and drag c_x of the profile of the blade of the pump axial cascade

(b/t = 1.25) with a decrease in pressure p_1 obtained experimentally (see source [97]).

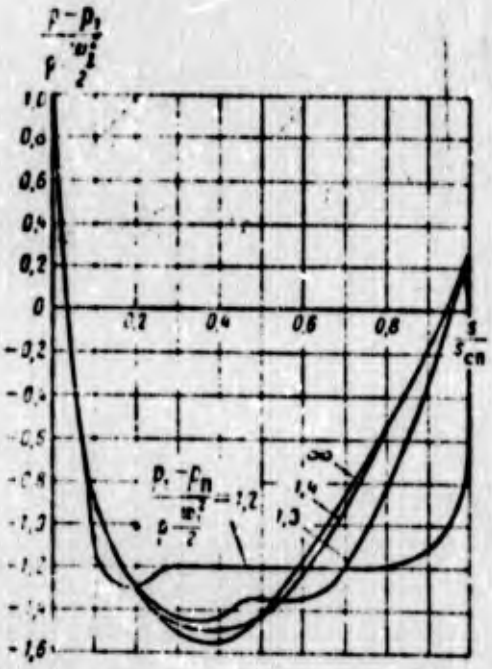

Fig. 3.79. Pressure distribution on the back of the winged profile at different pressures in front of the profile.

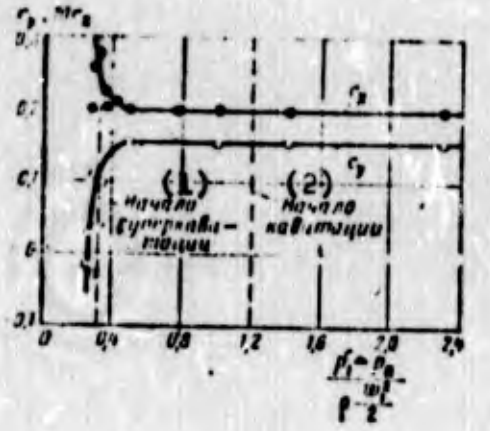

Fig. 3.80. Change in the coefficient of lift and airfoil drag of the blade of a pump axial cascade with a decrease in the inlet pressure.
KEY: (1) Beginning of supercavitation; (2) Beginning of cavitation.

Figure 3.80 shows the pressure of the beginning of cavitation. With the further development of cavitation (decrease in p_1), the replotting of the diagram of pressure on the back does not at first virtually affect the lift and drag, but at the defined value of p_1 the change in the diagram becomes considerable, and there occurs a sharp decrease in the lift down to zero and negative values, and an increase in the drag.

The cascade for which the lift decreases at less pressure possesses the best anticavitation properties. The more the rarefaction on the blade back, then at greater pressure in flow there will begin a lift decrease. Therefore, one should avoid the high angles of incidence, great load on the blade (great difference in blade pressures), and small cascade density, i.e., everything which can lead to greater rarefaction on the blade. The higher the speed of the flow flowing around the blade, the more the rarefaction will be on the blade (see Fig. 3.79). Hence, the point of the leading edges of the blade most distant from the axis of rotation can be the center of conception of cavitation (point A on Figs. 3.77 and 3.78).

Let us note that in the centrifugal wheel on the nonoperative side of the blade an additional pressure drop appears as a result of the effect of the Coriolis forces of inertia. Let us also note that in the centrifugal wheel the beginning cavitation in the region of the inlet into the blades will be rapidly developed, as a result of the fact that the motion on the inertia toward the periphery of the fluid is more dense that the vapor-gas caverns, and rarefaction increases.

The cavitation phenomena can appear also in elements of the feed-LPRE system, for example, in the units of automation, feeds etc. The appearance of cavitation zones is connected with the local decrease in pressure, which takes place at low pressures in the system or in transient conditions (for example, during starting).

Sometimes in centrifugal pumps cavitation can appear at the input part of the conical diffuser (at the "tongue"). Specifically, this is observed with high flow rate and at the large angles of blades. Cavitation in the branch is developed in the decrease in pressure of the pump with high flow rate (see Fig. 3.63) (pump power remains constant) (see sources [64, 91]).

3.3.2. Fundamental Principles Which Characterize Cavitation Conditions of the Pump

Let us record the fundamental principles characterizing cavitation conditions of the pump. These relations bear the total nature both for the axial or centrifugal and also for the screw-centrifugal pumps, i.e., for the inlets into the centrifugal and axial wheels.

Let us use the energy equation in relative motion for two cross sections: one cross section 1-1 (see Figs. 3.77 and 3.78) - directly in front of the inlet into the wheel, and the other - in the region of minimum pressure. The region of minimum pressure is located sufficiently close to the leading edge of the blades, and therefore for the centrifugal wheel it is possible to disregard a change in the circular velocity upon transition from the cross section in front of the inlet into the blades to the cross section where the pressure is equal to p_{min}. For axial pump the cross sections in question lie on one radius (see Fig. 3.77). The minimum pressure corresponds to the maximum rate of flow:

$$p_{min} + \varrho \frac{w_{max}^2}{2} = p_1 + \varrho \frac{w_1^2}{2}. \qquad (3.119)$$

Let us rewrite equation (3.119) in the form

$$\frac{p_1 - p_{min}}{\varrho} = \frac{w_{max}^2}{2} - \frac{w_1^2}{2}. \qquad (3.120)$$

Let us remove on the right side value $w_1^2/2$ from the brackets:

$$\frac{p_1 - p_{min}}{\varrho} = \frac{w_1^2}{2}\left[\left(\frac{w_{max}}{w_1}\right)^2 - 1\right]. \qquad (3.121)$$

Let us call the expression in the brackets the coefficient of the profile of rarefaction:

$$\lambda_{1\kappa a в} = \left[\left(\frac{w_{1\kappa a в}}{w_1}\right)^2 - 1\right] = \frac{p_1 - p_{\kappa a в}}{\rho\frac{w_1^2}{2}}. \qquad (3.122)$$

Then equation (3.122) will be rewritten in the form

$$p_1 - p_{\kappa a в} = \lambda_{1\kappa a в}\rho\frac{w_1^2}{2}. \qquad (3.123)$$

This value can be called the dynamic pressure drop during the flow of the blades.

During the cavitation mode the pressure in the fluid is reduced down to the pressure of p'_{min} which characterizes the cavitation onset; its value is connected with the pressure $p_п$ of the fluid vapors at this temperature. We will consider that the cavitation mode is characterized approximately by the equality $p'_{min} = p_п$.

Then

$$\lambda_{1\kappa a в} = \frac{p_{1\kappa a в} - p_п}{\rho\left(w_1^2/2\right)}. \qquad (3.124)$$

where $p_{1\kappa a в}$ is pressure in cross section 1-1, at which p_{min} reaches the pressure $p_{min} = p_п$.

Let us call value $\lambda_{1\kappa a в}$ the coefficient of cavitation (in hydraulics this coefficient is called the number of cavitation). This coefficient in essence is one of the forms of Euler's criterion, i.e., it is a constant value for geometrically similar pumps in similar conditions.

The condition of noncavitation operation for pumps results from expression (3.124) and will be recorded in the form

$$p_1 > p_{кав} = \lambda_{кав} \rho \frac{w_1^2}{2} + p_п. \qquad (3.125)$$

In practice during the testing of the pumps there can be determined not the pressure in front of the blades p_1 but the pressure at the inlet into the pump $p_{вх}$ (see Fig. 3.1, where conventional designations of the cross sections are given). In this case the condition of noncavitation operation of the pump is recorded in the form

$$p_{вх} > p_{кав} = \Delta p_{кав} + p_п = \lambda_{кав} \rho \frac{w_1^2}{2} + p_п, \qquad (3.126)$$

where $p_{кав}$ is the pressure at the inlet into the pump, at which the cavitation begins; $\Delta p_{кав} = p_{кав} - p_п$ - the cavitation pressure drop in conditions of the beginning of cavitation;

$$\lambda_{кав} = \frac{p_{кав} - p_п}{\rho \frac{w_1^2}{2}} = \frac{\Delta p_{кав}}{\rho \frac{w_1^2}{2}}. \qquad (3.127)$$

Here $\lambda_{кав}$ is the experimental coefficient which considers not only the rarefaction during the flow of the blades but also the nature of the flow of fluid from the inlet into the pump to the blades.

The emergence of cavitation is connected not only with the profile rarefaction on the blades, but also with an additional pressure drop of the fluid $\Delta p_{доп}$ from the place of the measurement of pressure $p_{вх}$ (in front of the feed) to the blades in view of a possible drop in the static pressure on this section as a result of losses, the convergence of the flow, and also in view of the nonuniform field of absolute velocities with the approach to the blade. An additional pressure drop (as compared with the mean

pressure at the inlet) will take place in the stream possessing the maximum speed;

$$\Delta p_{кав} = (m-1)\varrho\frac{c_{вх}^2}{2} - \zeta\varrho\frac{c_{вх}^2}{2} + \left[\left(\frac{F_{вх}}{F_1}\right)^2 - 1\right]\varrho\frac{c_{вх}^2}{2}; \qquad (3.128)$$

here m is the nonuniformity factor of the absolute velocity at the inlet: $m = c_{вх\ max}/c_{вх}$;

ζ – the coefficient of the pressure drop caused by hydraulic losses with the flow of fluid from inlet to the region of the minimum pressure;

$F_{вх}$ – the region at the inlet into the feed;

F_1 – the region in front of blades.

The relation $\Delta p_{кав}$ and $\lambda_{кав}$ with $\lambda_{разр}$ and $\Delta p_{доп}$ is established by the relation

$$\Delta p_{кав} = \lambda_{кав}\varrho\frac{w_1^2}{2} = \lambda_{разр}\varrho\frac{w_1^2}{2} + \Delta p_{доп}. \qquad (3.129)$$

The evaluation of cavitation qualities of wheels should be carried out from value $\lambda_{разр}$, and the corresponding evaluation of the entire pump – according to the value $\lambda_{кав}$.

Usually at the pressure of $p_{кав}$ the emergence of cavitation in pumps (initial stage of cavitation) still does not lead to a change in the outlet parameters of the pump H, Q and $\eta_н$ (see Fig. 3.76) - the concealed/latent cavitation. But in this case sometimes oscillatory phenomena can be observed (see source [153]). The stalling mode of the pump begins with more developed cavitation.

For pumps of LPRE it is important to avoid the cavitation stalling. In view of the comparatively short-term operation of these pumps is allowed their operation (without the fear of cavitation erosion) under conditions of the already beginning cavitation but without a substantial change in the parameters. Usually for the failure of the operating units of pumps during cavitation conditions considerable time is necessary.

On the basis of the aforesaid during the calculation and operation of pumps of LPRE it is important to know the minimum pressure at the inlet into the pump at which nonstalling operation of the pump is still provided.

By analogy with expression (3.126) we can record:

$$p_{cpo} = \lambda_{cpo} \varrho \frac{w_1^2}{2} + p_{n.} \qquad (3.130)$$

or

$$p_{cpo} = \Delta p_{cpo} + p_{n.}$$

where

$$\Delta p_{cpo} = \lambda_{cpo} \varrho \frac{w_1^2}{2} \qquad (3.131)$$

(Δp_{cpo} – pressure drop in cavitation separation conditions, which we will conditionally call cavitation pressure drop).

At the small pressure at the inlet into the pump p_{cpo} at the inlet into the wheel there will take place the pressure

$$p_{1cpo} = p_{cpo} - \Delta p_{sos.}$$

or, by analogy with expression (3.131),

$$p_{1cps} = \Delta p_{1cps} + p_s.$$

where

$$\Delta p_{1cps} = \lambda_{1cps} \rho \frac{w_1^2}{2}. \qquad (3.132)$$

The cavitation qualities of the wheel are determined by the coefficient λ_{1cps}, and the cavitation qualities of the pump – by the coefficient λ_{cps}.

Operating conditions of the pump without stalling will be recorded thus:

$$p_{s1} > p_{cps}.$$

The value p_{cps} is determined experimentally. According to this value the coefficient of cavitation in the separation conditions is found:

$$\lambda_{cps} = \frac{p_{cps} - p_s}{\rho \frac{w_1^2}{2}} = \frac{\Delta p_{cps}}{\rho \frac{w_1^2}{2}} = \frac{\Delta h_{cps}}{\frac{w_1^2}{2}}, \qquad (3.133)$$

where $\Delta h_{cps} = \frac{\Delta p_{cps}}{\rho}$.

To determine p_{cps} of this pump, the separation cavitation characteristic is taken.

The separation cavitation characteristic is called the dependence of the pump head on inlet pressure at a constant flow and constant frequency of rotation. Such characteristics are taken on special laboratory bench tests.

Figure 3.76 depicts the separation cavitation characteristics typical for the centrifugal (b), axial (c) and screw-centrifugal (a) pumps of LPRE. At the inlet pressure, designated on Fig. 3.76 by $p_{кр}$, the pump head begins to be reduced. A reduction in the pressure is connected with the already begun cavitation phenomena within the flow area of the pump (simultaneously with pressure the efficiency is lowered). We will call such conditions critical:

$$\lambda_p = \frac{p_{вх} - p_н}{\rho \frac{w_1^2}{2}} = \frac{\Delta p_{кр}}{\rho \frac{w_1^2}{2}}, \qquad (3.134)$$

where $\Delta p_{кр}$ is the pressure drop in the cavitation critical mode, subsequently called the cavitation pressure drop in the critical mode,

$$p_{вх} = \lambda_p \rho \frac{w_1^2}{2} + p_н. \qquad (3.135)$$

With the inlet pressure equal to $p_{срв}$, the pressure sharply drops (see Fig. 3.76). Also sharply decreasing are values of the efficiency and flow rate, which are not possible to maintain constant. This mode will be the separation mode [see equation (3.130)].

Thus, on the characteristic it is usually possible to distinguish two modes: the mode of the beginning of the change in outlet parameters of the pump (or critical mode) and the stalling mode (or separation mode). The concept of the two conditions for the separation cavitation characteristic was introduced by Professor S. S. Rudnev. The mode which corresponds to $p_{кр}$ is called by him the first critical mode, and the mode which corresponds to $p_{срв}$ - the second critical mode. The critical mode sometimes coincides with the separation mode (see Fig. 3.76b).

The stalling of the mode of the pump is connected with the developing cavitation zone, which is propogated along the length and width of the vane channel, which also leads to a sharp reduction in the pressure and flow rate through the pump.

It is desirable that the change in the pressure between the critical and separation modes (see Fig. 3.76a) would be minimum, since the region on the inlet pressure between $p_{кр}$ and $p_{срв}$ is the operating region.

Sometimes the modes of the stalling of the pump on characteristic $H = f(p_{вх})$ is not clearly developed (see Fig. 3.76c), but the value of the pressure (flow rate and efficiency) is sufficiently smoothly decreased with a decrease in the pressure. Such a course of the separation cavitation characteristic is observed sometimes in the testing of screw axial pumps, and in the case of centrifugal and screw-centrifugal pumps - when $D_1/D_2 > 0.5$. With such ratios D_1/D_2 the inlet conditions can affect the outlet parameters. In this case conditionally accepted as the stall pressure is such a pressure which corresponds to the drop in pressure by the established percent, depending on the requirements given to the engine plant; usually $\Delta H = 2\text{-}3\% H_{нач}$ for the basic pump and reaches 10% for the booster pump (see source [72]).

For axial and screw-centrifugal pumps it is possible to distinguish still the conditions at a pressure somewhat less than the separation ($p_{суперкав}$). During bench tests many pumps can operate sufficiently stable with sharply decreasing values of pressure and flow rate with an inlet pressure somewhat less than the separation, i.e., on the separation (left) branch of characteristic (see Figs. 3.76 and 3.80). This mode is called supercavitation. It is characterized by the fact that the cavitation cavern, having a length exceeding the length of the blade, is separated from the blades. The theoretical scheme of this mode is the separation cavitation streamline flow of the blades (supercavitation flow) (see source [93]).

Subsequently, we will distinguish four modes of the pump by the inlet pressure:

1) modes $p_{кав}$ of the beginning of cavitation (it corresponds to $\Delta p_{кав}$) – latent cavitation;

2) modes $p_{кр}$, during which noticeable is the sharp bending of the line $H = f(p_{вх})$ called the critical mode ($\Delta p_{кр}$);

3) conditions $p_{срв}$, during which the stalling of the modes is observed, separation modes ($\Delta p_{срв}$);

4) supercavitation modes $p_{суперкав}$ ($\Delta p_{суперкав}$).

Figure 3.81 gives the separation cavitation characteristics obtained during the testing of a screw-centrifugal pump on water. The upper two curves characterize the pump head, and the two lower curves – the pressure of the screw conveyor (determined by the measurement of the pressure on the housing between the worm conveyor and the centrifugal wheel). An experiment was carried out on deaerated water (black circles on Fig. 3.81) and on water with 2% air content (light circles).

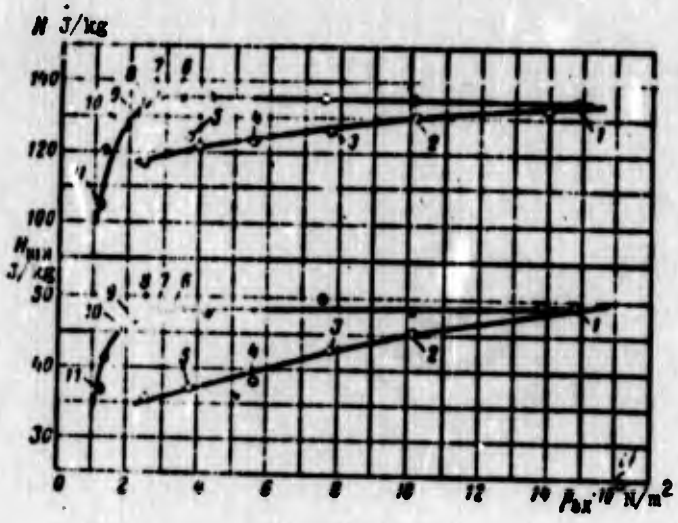

Fig. 3.81. Separation cavitation characteristics of the screw-centrifugal pump (upper curves) and screw conveyor (lower curves): ○ – deaerated water; ● – water with 2% air content.

Figure 3.82 gives photographs of cavitation zones in the screw wheel obtained during the experiment (the screw conveyor had a transparent housing). The numbers of points on the curves given on Fig. 3.81 correspond to the numbers of photographs. As is evident, cavitation zones appear near the hub of the wheel in the presence of air in water at higher pressures than in the operation of the pump on deaerated water. On deaerated water the cavitation cavern is produced on the periphery of the wheel, on the nonoperative side of the blade, and up to the stalling has clearly expressed boundaries. In the presence of air in the water, cavitation zones are located on the entire volume of the fluid.

To evaluate the anticavitation qualities of pumps of LPRE, greatest value has the value $\lambda_{cpв}$. For centrifugal pumps of LPRE the value $\lambda_{cpв}$ is 0.1-0.3, while for the screw centrifugal pumps - 0.02-0.05. In connection with this the cavitation stalling of the screw-centrifugal pump begins at considerably less inlet pressure than does the stalling of centrifugal pump (Fig. 3.83). This determined the wide application in the LPRE of screw-centrifugal pumps.

3.3.3. OPERATING CONDITIONS OF A PUMP WITHOUT CAVITATION STALLING

The problem of the provision of the operation of pumps without cavitation stalling has a decisive importance for LPRE, since the cavitation qualities of the pump determine the mass of the entire engine plant. The cavitation stalling of pumps at low pressures at the inlet ($p_{вх} < p_{cpв}$) leads to the cessation of the engine operation. A pressure increase at the inlet is connected with an increase in the mass, since the inlet pressure is provided by pressure in the tank of the flight vehicle.

The operating condition of the pump without cavitation stalling can be recorded in the form

[GRAPHIC NOT REPRODUCIBLE.]

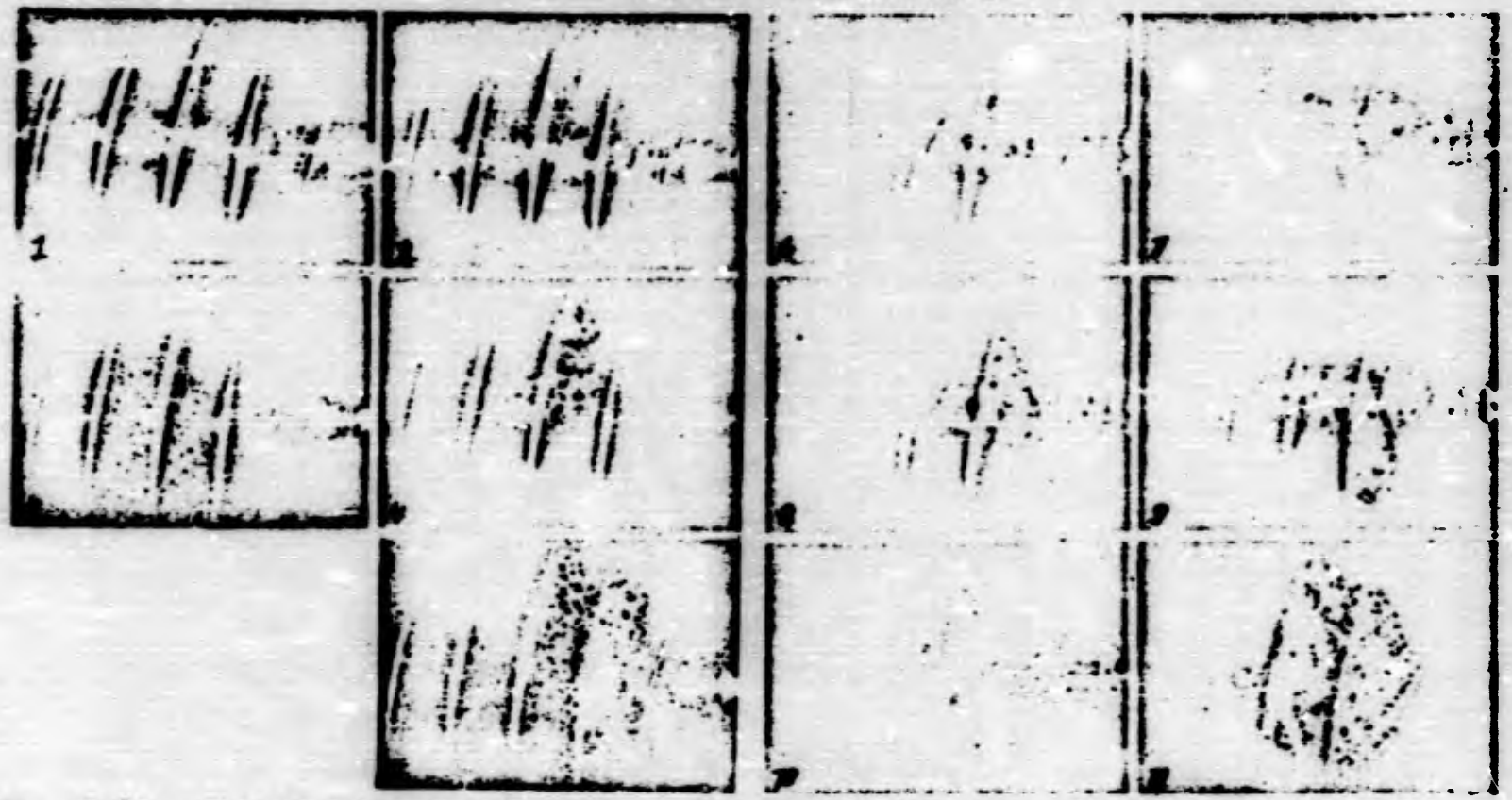

Fig. 3.82. Photographs of cavitation zones in the flow area of the screw conveyor (numbers of photographs correspond to numbers of points on Fig. 3.81). The motion of the flow is from left to right; the direction of the rotation is clockwise, if we look along the flow direction.

$$p_{вх} \geqslant p_{кр.п}. \qquad (3.136)$$

or

$$p_{вх} - p_п \geqslant \Delta p_{г.п} = \lambda_{гр.п} \varrho \frac{c_1^2}{2}. \qquad (3.137)$$

For the pumping system of LPRE the pressure $p_{вх}$ is determined by the tank pressure, the inertia and gravity heads and the value of the flow friction of the inlet main line (see Section 1.1):

$$p_{вх} = p_б + \varrho l g \left(\cos\theta - \frac{j}{g}\right) - \Delta p_{г.маг.вх} - \varrho \frac{c_{вх}^2}{2}. \qquad (3.138)$$

Fig. 3.83. Separation cavitation characteristics of the centrifugal pump ($H_ц$) and the same pump with a screw conveyor (screw-centrifugal pump, $H_{ш.ц}$).

Taking expression (3.138) into account, condition (3.137) of the operation without cavitation stalling can be thus recorded:

$$p_б + \varrho l g \cos\theta + j) - \Delta p_{г.маг.вх} - \varrho \frac{c_{вх}^2}{2} - p_п \geqslant \Delta p_{г.п} = \lambda_{гр.п} \varrho \frac{c_1^2}{2}. \qquad (3.139)$$

The left side of expression (3.139) is the available, or provided by the system, excess in inlet pressure of the pump above the vapor pressure, and the right side is the excess in pressure necessary for operation of the pump without stalling.

If generally it is not possible to allow the operation of the pump with beginning cavitation (for example, in the presence of the danger of cavitation erosion in the case of the continuous operation of the turbopump unit), then expression (3.126) will be rewritten in the form

$$p_{вх} - p_н > \Delta p_{кав} = \lambda_{кав} \rho \frac{w_1^2}{2}. \qquad (3.140)$$

Let us emphasize that for the pump, conditions of the beginning of cavitation $p_{кав}$ by the characteristic $H = f(p_{вх})$ in practice cannot be revealed.

If we transfer the term $\rho c_{вх}^2/2$ to the right side of expression (3.139), then expression (3.139) will be rewritten in the form

$$p_н + \rho(g \cos\theta \pm j) - \Delta p_{гидр.вх} - p_н > \Delta p_{нас}^* = p_{нас}^* - p_н. \qquad (3.141)$$

Then the left side of this expression will be the available excess in total pressure at the inlet into the pump above the vapor pressure, and the right side is the necessary excess in total pressure.

When designing an engine plant it is assumed always that the available excess in pressure is greater than that necessary by the value of the cavitation reserve $\Delta p_{зап}$:

$$p_{вх}^* - p_н - \Delta p_{зап} = \Delta p_{нас}^*. \qquad (3.142)$$

By introduction of the reserve of pressure $\Delta p_{зап}$, the imperfection of the methods for determining the necessary excess in pressure and the distinction in the cavitation properties of different copies of the same pump are considered. Usually $\Delta p_{зап}/\rho = \Delta h_{зап} = 10\text{-}30$ J/kg.

Expression (3.142) makes it possible to determine the value of the permissible cavitation of the pressure drop Δp^*_{cps} at the assigned tank pressure. From formulas (3.141) and (3.142) it follows that

$$p_б = \Delta p^*_{cps} + p_н + \Delta p_{маг} + \Delta p_{маг.ст} - \rho l (g \cos\theta + j). \qquad (3.143)$$

This expression makes it possible to determine the necessary tank pressure for the pump with the known value of the cavitation pressure drop Δp^*_{cps}. The tank pressure $p_б$ basically determines the wall thickness of the tank and, consequently, the mass of the tanks. The mass of the tanks comprises a considerable portion of the mass of the engine plant, and therefore the more the tank pressure will be the larger the dry mass the flight vehicle will have. Furthermore, it is necessary to strive for a decrease in pressure $p_б$ and for a reduction in the mass of the pressurized system of the tank. Let us examine in more detail the effect of the individual terms of expression (3.143) on the magnitude of the necessary tank pressure.

3.3.4. EFFECT OF PARAMETERS OF THE PUMP SYSTEM AND THE PUMPED FUEL COMPONENT ON THE MAGNITUDE OF TANK PRESSURE

The presence of gravitational and inertia backwaters makes it possible to use less tank pressure. For this it is advantageous to place the tanks of the components in front of the pump and, as far as possible, nearer to the nose of the rocket (see Fig. 1.3). To determine the necessary value of the tank pressure [see equation (3.143)] it is necessary for that point in time of operation of the flight vehicle when the term $\rho l(g \cos \theta + j)$ has a minimum value.

3.3.4.1. Effect of the Hydraulic System

For a decrease in the tank pressure, the flow friction of the section from tank to the inlet into the pump ($\Delta p_{\text{conp вх}}$) should be minimum, and this means that it is desirable to have a short pipeline, and one should avoid turns, an abrupt change in the cross sections and a high rate of flow of the fluid.

Furthermore, a decrease in the velocity at the assigned total pressure leads directly to an increase in the available excess in pressure at the inlet into the pump above the vapor pressure. However, with a decrease in the flow velocity, the dimensions and mass of the pipelines increase. Usually the velocity at the inlet into pump does not exceed 5-10 m/s.

3.3.4.2. Effect of the Anticavitation Qualities of the Pump.

The tank pressure necessary for nonseparation operation of the pump basically depends on the cavitation perfection of the pump, which determines the value $\Delta p^{*}_{\text{cpв}}$. The less $\Delta p^{*}_{\text{cpв}}$, the less $p_б$ will be. Therefore, when developing the turbopump unit of the LPRE it is especially important to obtain the small values of $\Delta p^{*}_{\text{cpв}}$ (see further section 3.3.7).

3.3.4.3. Effect of Physical Properties of the Fuel Component Being Pumped.

The necessary tank pressure largely depends on the physical properties of the fluid being pumped. The more the pressure of vaporization at the operating temperature of the fluid, the higher the tank pressure is necessary or the greater the cavitation perfection of the pump (low values $\Delta p^{*}_{\text{cpв}}$) is necessary, if the tank pressure is assigned.

Since the pressure of vaporization greatly depends on the temperature of the fluid, the calculation should be carried out

for the greatest temperature. Usually for noncryogenic fuels the maximum temperature is equal to 303-323°K (30-50°C).

The initial temperature in the tank for cryogenic components (oxygen, hydrogen, etc.) is the boiling temperature at atmospheric pressure, since the servicing of the rocket by these components is produced from capacities having drainage into the atmosphere. In flowing along the pipeline leading to the inlet into the pump, the fluid is warmed thoroughly. Consequently, the pressure of the vapor pressure usually exceeds the atmospheric pressure. The precise calculation of the temperature of the cryogenic component is sufficiently complex. In the first approximation, the pressure of the vapor pressure can be taken according to the temperature which exceeds the boiling point of the component at atmospheric pressure by 5-10°K.

It should be remembered that the necessary tank pressure depends on the density of the fluid ρ. Actually, expression (3.143) can be written thus:

$$p_6 = \rho\lambda_{1c}\frac{w_1^2}{2} + \rho\frac{c_{вх}^2}{2} + \rho L_{comp.\,at} + \rho\Delta h_{вс} - \rho j(x\cos\theta + l) + p_н. \tag{3.144}$$

Other conditions being equal, a change in the density ρ leads to a change in p_6. As a rule, the increase in ρ is accompanied by an increase in the value of the necessary tank pressure p_6. A significant role can be played by the thermodynamic properties of the fluid – such as the heat of vaporization, heat capacity and others. Let us examine this question in more detail.

For vaporization a certain heat reserve is necessary: intense vaporization without the external heat feed can occur only with overheated fluid. Virtually this means that the vaporization with cavitation appears with a pressure drop in the fluid up to a value somewhat less than the pressure of vaporization at this temperature.

Let us examine first the effect of the thermodynamic properties of the fluid on cavitation, not allowing for the gases which can be dissolved in the fluid. A pressure drop lower than the pressure which corresponds to the temperature of vaporization leads to a different degree of superheat – depending on the temperature and physical properties of the fluid.

Consequently, the inlet pressure at which there occurs cavitation stalling depends not only on the pressure of vaporization at this temperature and the additional pressure drop in the pump but also on the thermodynamic properties of the fluid, the value of its relative superheating, the heat of vaporization, surface tension, heat capacity, and thermal conductivity.

The approximate comparative evaluation of the cavitation properties of fluids can be produced on the basis of the following considerations (see source [18]). The available heat q for cavitation evaporation is determined by the amount of fluid from which it can be extracted (i.e., by parameters $V_ж$ and $\rho_ж$), by the heat capacity of the fluid $c_ж$ and the temperature of its superheating ΔT:

$$q = V_ж \rho_ж c_ж \Delta T. \qquad (3.145)$$

This heat is expended for the formation of any quantity of vapor determined by parameters $V_п$ and $\rho_п$:

$$q = V_п \rho_п r. \qquad (3.146)$$

where r is the heat of vaporization.

By equating expressions (3.145) and (3.146), we obtain

$$V_ж \rho_ж c_ж \Delta T = V_п \rho_п r. \qquad (3.147)$$

The cavitation intensity can be characterized by the volumetric ratio of the vapor formed to the volume of fluid. Let us designate

$$B = V_п / V_ж \qquad (3.148)$$

and let us call B the parameter of the cavitation intensity.

From equation (3.147) it follows that

$$B = \frac{V_п}{V_ж} = \frac{\rho_ж c_ж \Delta T}{\rho_п r}, \qquad (3.149)$$

where ΔT can be connected with the value of the pressure drop Δp.

A pressure drop lower than the pressure of the vapor pressure $p_п$ leads to the superheating of the fluid necessary for the development of the cavitation:

$$\Delta T = \frac{dT}{dp_п} \Delta p.$$

Consequently,

$$B = \frac{\rho_ж^2}{\rho_п} \frac{c_ж}{r} \frac{\Delta p' \rho_ж}{(d p_п / dT)}. \qquad (3.150)$$

Equation (3.150) shows that with the same drop in pressure energy $\Delta p/\rho_ж$ the parameter of cavitation intensity B increases with an increase in the ratio of the square of the density of the fluid to the vapor density and the ratio of the heat capacity of the fluid to the heat of vaporization and with a decrease in $dp_п/dT$.

Dependence $p_п = f(t)$ for a number of components is given on Fig. 3.84 . The more sloping the characteristic of the pressure

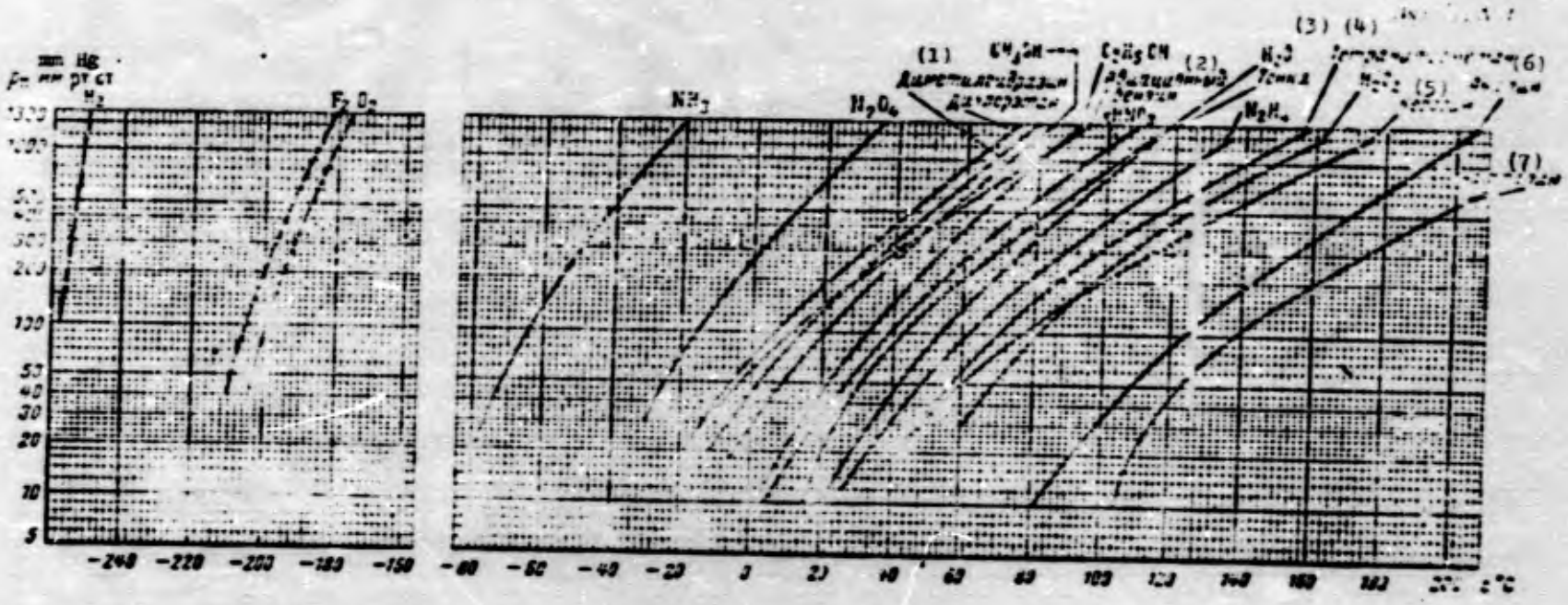

Fig. 3.84. Dependence of vapor pressure on temperature for different fluids.
KEY: (1) Dimethylhydrazine dichloroethane; (2) Aviation gasoline; (3) Tonka; (4) Tetranitromethane; (5) Kerosene; (6) Aniline; (7) Napthalene.

of vaporization on temperature occurs, the more the superheating of the fluid ΔT, i.e., the more the vapor is liberated. Since $dp_п/dT$ increases with an increase in the temperature (see Fig. 3.84), then hot liquids are relatively less inclined to cavitation. In operating on hot fluids the pump will have less cavitation pressure drop. However, the inlet pressure necessary for operation without cavitation stalling, in the case of the feed of hot fluids, will always be higher as a result of the pressure increase of vaporization with increased temperature.

For pumps of LPRE the effect of physical properties of fluids on their cavitation properties is important in connection with the fact that data of cavitation tests, obtained in operation of the pump on cold water, must be recalculated on natural fluids.

A comparison of the tendency of two fluids toward cavitation or the tendency toward the cavitation of just one fluid at different temperatures is possible by a comparison of parameters B with the same drop in the pressure energy $\Delta p/\rho_н$:

$$\frac{B_1}{B_2} = \frac{\left(\frac{v_н^2}{v_н}\frac{c_н}{r}\right)_1 \left(\frac{dp_н}{dT}\right)_1}{\left(\frac{v_н^2}{v_н}\frac{c_н}{r}\right)_2 \left(\frac{dp_н}{dT}\right)_1},$$

where the subscripts "1" and "2" refer either to different fluids or to just one fluid at different temperatures.

Table 3.1 gives a comparison of parameters B for some fluids with the parameter B for water.

The high-boiling fluids (nitric acid, kerosene), for which low values of $dp_п/dT$ are characteristic (see Fig. 3.84), correspond

Table 3.1

Parameters \ Name of Liquid	Water	Nitric Acid	Kero-sene	Liquid Nitrogen	Liquid Oxygen	Liquid Hydrogen
T°K	293	303	303	77	90	20
B/B Water	1	$0.12 \cdot 10^{-1}$	1.6	$0.36 \cdot 10^{-3}$	$0.25 \cdot 10^{-4}$	$0.55 \cdot 10^{-7}$

to values of parameter B, which are comparatively close to value B for water, i.e., the distinction in the thermodynamic properties of high-boiling fluids and water is unimportant for the process of cavitation.

Cavitation in the operation of pump on water and on high-boiling liquids will be developed almost equally, and values of $\Delta p^*_{cpB}/\rho$ in these cases will be close to each other.

Cryogenic fluids (nitrogen, oxygen, hydrogen) have large values of dp_n/dT (see Fig. 3.84) and, therefore, considerably smaller values of B than for water.

In the operation on cryogenic fluids the pump will have the best cavitation properties (smaller values of $\Delta p^*_{cpB}/\rho$) than in its operation on water. This theoretical conclusion is confirmed experimentally (Fig. 3.85) (see source [72]).

For determining the cavitation properties of a pump designed for operation on a high-boiling fluid, it suffices to conduct its tests on cold water, since the value of $\Delta p^*_{cpB}/\rho$ for the working high-boiling fluid can be accepted equal to the test value of the pump on water.

In the case of cryogenic pumps the results of their tests on water should be recalculated for the working cryogenic fluid (see source [72]):

$$\frac{\Delta p^{*}_{\text{сеп}}}{v} = \left(\frac{\Delta p^{*}_{\text{сеп}}}{\rho}\right)_{\text{вод}} - \left(\frac{\Delta p_{\text{ср}}}{\rho}\right)',$$

where $(\Delta p_{\text{ср в}}/\rho)'$ is the thermodynamic correction which considers a distinction in the thermodynamic properties of the working fluid and water.

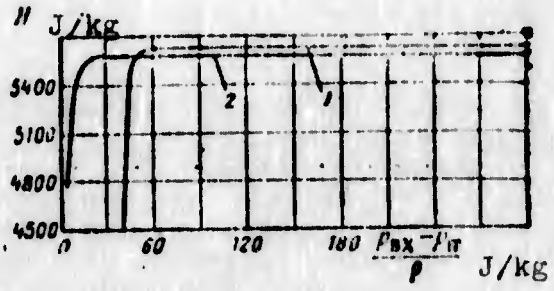

Fig. 3.85. Separation cavitation characteristics of a pump in its operation on water and liquid oxygen: 1 – water; 2 – liquid oxygen.

To obtain reliable cavitation characteristics of cryogenic pumps, it is necessary to carry out tests on working cryogenic fluids.

Effect of Dissolved and Undissolved Gases in the Fluid

The development of cavitation and cavitation parameters of the pump is affected by the content in the fluid of gases, undissolved and dissolved, which are liberated in the region of reduced pressure. Figure 3.81 depicts the separation cavitation characteristics of a pump in the presence of air in the water and without it.

When in the fluid free gas is present, the working medium of the pump becomes two-phase. As is known (see sources [71, 94]), the speed of sound in a two-phase medium becomes less than not only the speed of sound in a pure fluid but also the speed of sound in the gas contained in the two-phase medium.

Figure 3.86 (see source [94]) depicts the experimental dependence of the speed of sound in water-air and vapor-water media on the content of free air (vapor) in the mixture. It is evident that the speed of sound in certain cases can be 30-60 m/s. Such a speed of sound proves to be commensurable with the rates of flow in the pump. Therefore, in the pump, which operates on two-phase fluids it is possible to expect the crisis sonic phenomena (flow restriction, shock waves), which make its operation worse and lead to an increase in the separation pressure (an increase in $\Delta p^{*}_{\text{срв}}$).

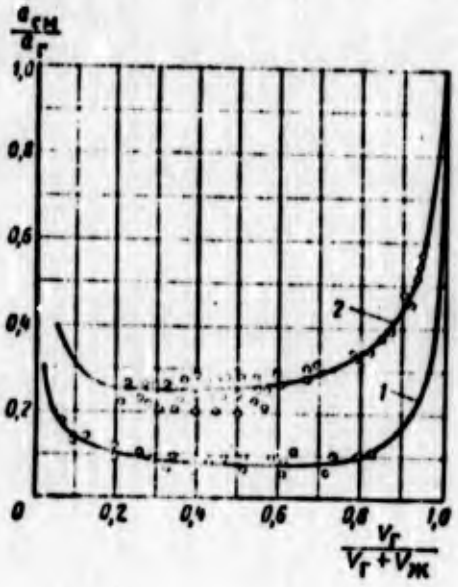

Fig. 3.86. Dependence of the speed of sound in water-air (1) and vapor water (2) mixtures on the content of air (vapor) in the mixture. [Pressure of water-air mixture is 1-2 bar; pressure of vapor-water mixture is 10 bar; subscripts "см" refer to the mixture; "ж" – to the fluid; "г" – to the gas (air or vapor); the speed of sound a in the vapor is equal to 606 m/s and in the air – 320 m/s.

3.3.5. PARAMETERS WHICH DETERMINE ANTICAVITATION PROPERTIES OF THE SCREW

3.3.5.1. Cavitation Coefficient $\lambda_{1\text{срв}}$

Into a correctly designed screw centrifugal pump (see further Section 3.3.7) its anticavitation properties are determined by a screw wheel. The cavitation coefficient of the screw conveyor $\lambda_{1\text{срв}}$[1]) depends on the rarefaction on blades of a screw conveyor,

[1]Parameters with subscript "1" correspond to the inlet into the screw conveyor and without a subscript – to the inlet into the screw centrifugal pump.

which depends, in turn, on the shape of profile, angle of the blades $\beta_л$, angle of incidence t, and the cascade density $b_л/t$. These parameters are changed along the radius of the screw conveyor (spatial lattice), which affects the value of $\lambda_{1cpв}$. For screw conveyors of constant pitch (s = const) with the cascade density on outside diameter $b_л/t > 1$ we obtain the equation (see source [74])

$$\lambda_{1cpв} = \frac{\pi}{1 - \bar{d}_{вт}^2} \sin(\beta_{л.п} - i_п) \sin i_п, \qquad (3.151)$$

where $\beta_{л.п}$ and $i_п$ are the angle of the blades and angle of attack, respectively, on the external (peripheral) diameter of the screw conveyor;

$$\bar{d}_{вт} = d_{вт}/D_п.$$

For similar screw conveyors ($\bar{d}_{вт}$ = idem; $\beta_л$ = idem) in kinematically similar conditions (i = idem), value $\lambda_{1cpв}$ = idem, i.e., it is the similarity criterion.

The denominator of the right side of equation (3.151) considers the spaciousness of the cascade of the screw conveyor. Equation (3.151) is valid for the screw-centrifugal pumps which operate on such components of fuels where the quantity of dissolved and free gases does not exceed 1-1.5% and which have the thermodynamic properties the effect of which on cavitation is close to the effect on cavitation of thermodynamic properties of water (see Section 3.3.4).

Expression (3.151) can also be used for the screw conveyor of variable pitch with the camber of profile on the mean diameter $\theta_{ср} = (\beta_{2л} - \beta_{1л})_{ср}$ up 4-6°. With the selected $i_{п.р}$ for the design

conditions ($i_{п.р}$ one should not select less than 2°-3°) equation (3.151) can be presented in the following form, using the relations resulting from the velocity triangle at the inlet into the screw conveyor when $c_{1u\,w} = 0$ (see Fig. 2.62 and 2.64):

$$\lambda_{1cpв} = \frac{\pi \sin i_{п.р}}{1 - d_{вт}^2} \frac{c_{1z}}{u_п} \Big/ \sqrt{1 + \left(\frac{c_{1z}}{u_п}\right)^2}, \qquad (3.152)$$

where c_{1z} is the mean velocity of the inlet into the screw conveyor; $u_п$ is circular velocity on the outside diameter of the screw conveyor.

With a decrease in ratio $c_{1z}/u_п$ the cavitation coefficient $\lambda_{1cpв}$ is decreased. However, experimental data show that below values of $c_{1z}/u_п = 0.06$-0.08 the coefficient $\lambda_{1cpв}$ can be considered constant (Fig. 3.87).

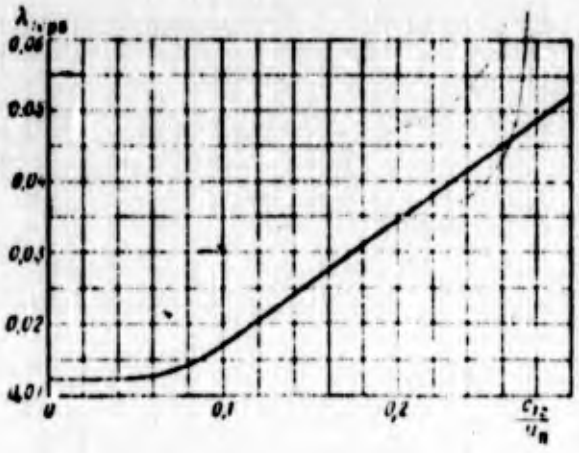

Fig. 3.87. Dependence of the cavitation coefficient in separation conditions of the screw-centrifugal pump on the ratio of the speeds $c_{1z}/u_п$ ($i_п \leq 4°$).

3.3.5.2. Cavitation Pressure Drop $\Delta p_{1cpв}$

Let us substitute for $\Delta p_{1cpв}$ expression (3.152) into equation (3.132); after the transformations it is possible to record:

$$\Delta p_{1cpв} = \varrho \frac{u_n^2}{2} \frac{\pi \sin i_{л.р}}{1 - \delta_{вт}^2} \frac{c_{1z}}{u_n} \sqrt{1 + \left(\frac{c_{1z}}{u_n}\right)^2}; \qquad (3.153)$$

$$\frac{\Delta p_{1cpв}}{\varrho u_n^2} = \frac{\pi \sin i_{л.р}}{2(1 - \delta_{вт}^2)} \frac{c_{1z}}{u_n} \sqrt{1 + \left(\frac{c_{1z}}{u_n}\right)^2}. \qquad (3.154)$$

Expression (3.154) shows that pumps with geometrically similar screw conveyors in kinematically similar conditions ($d_{вт}$ = idem; $i_{л.р}$ = idem; c_{1z}/u_n = idem) have identical ratios $\Delta p_{1cpв}/\rho u_n^2$.

3.3.5.3. Cavitation Drop in the Total Pressure $\Delta p^*_{cpв}$

The anticavitation perfection of a pump is characterized by the magnitude of the cavitation drop in the total pressure $\Delta p^*_{cpв}$. The less $\Delta p^*_{cpв}$, the less the tank pressure $p_б$ must be for non-separation operation of the pump [see equation (3.143)].

Let us record

$$\Delta p^*_{c1в} = p^*_{c1в} - p_в = p_{1cpв} + m\varrho \frac{c_{1z}^2}{2} + \Delta p^*_{нв.в} - p_в =$$

$$= \Delta p_{1cpв} + m\varrho \frac{c_{1z}^2}{2} + \Delta p^*_{нв.в}, \qquad (3.155)$$

where m is the variation factor of absolute velocity of the inlet into the screw conveyor; $\Delta p^*_{подв}$ - losses in the feed of the pump.

Let us substitute equation (2.199) into expression (3.155) for losses in feed; we obtain

$$\Delta p^*_{c1в} = \Delta p_{1cpв} + (m + k_{подв})\varrho \frac{c_{1z}^2}{2}. \qquad (3.156)$$

Having divided equation (3.156) by ρu_n^2, we obtain

$$\frac{\Delta p^{*}_{cpв}}{\rho u_{п}^{2}} = \frac{\Delta p_{1cpв}}{\rho u_{п}^{2}} + \frac{1}{2}(m + i_{вх.в})\left(\frac{c_{1z}}{u_{п}}\right)^{2}. \qquad (3.157)$$

For pumps with geometrically similar feeds and screw conveyors (similarity of pumps with respect to the inlet), as is evident from expressions (3.154) and (3.157), in kinematically similar conditions there is the equality of ratios $\Delta p^{*}_{cpв}/\rho u_{п}^{2}$.

Equation (3.157) shows that for an improvement in the anti-cavitation qualities of the pump, it follows to decrease the non-uniformity of the field of velocities at the inlet into the screw conveyor and attain the least losses in the branch.

3.3.5.4. Cavitation Power-Speed Coefficient

Expression (3.132) for $\Delta p_{1cpв}$ is converted to the form

$$\frac{\Delta p_{1cpв}}{\rho} = \lambda_{h.в} \frac{u_{п}^{2}}{2}\left[1 + \left(\frac{c_{1z}}{u_{п}}\right)^{2}\right]. \qquad (3.158)$$

Let us express the velocities $u_{п}$ and c_{1z} by the basic parameters of the pump – the volume flow rate and frequency of rotation

$$u_{п} = \frac{\pi D_{в}}{2} = \frac{\pi}{2} D_{э}\sqrt{1 + \bar{d}_{вт}^{2}}; \qquad (3.159)$$

$$c_{1z} = \frac{4Q}{\pi D_{э}^{2}}, \qquad (3.160)$$

where $D_{э}$ is the equivalent diameter of the inlet into the screw conveyor:

$$D_{э} = \sqrt{D_{к}^{2} - d_{вт}^{2}}; \quad \bar{d}_{вт} = \frac{d_{вт}}{D_{э}}.$$

Let us multiply and divide the right side of equation (3.158) by the ratio of velocities $(c_{1z}/u_n)^{2/3}$ and use expressions (3.159) and (3.160). Then we will obtain

$$\frac{\Delta p_{1\,cp\,0}}{\rho} = \omega^{4/3} Q^{2/3} \frac{\lambda_{1cp\,0}\left[1+\left(\frac{c_{1z}}{u_n}\right)^2\right](1+\bar{d}_{st}^2)^{2/3}}{2\pi^{2/3}\left(\frac{c_{1z}}{u_n}\right)^{2/3}}. \qquad (3.161)$$

or, having grouped the terms, we will have

$$\frac{\omega^{4/3} Q^{2/3}}{\frac{\Delta p_{1\,cp\,0}}{\rho}} = \frac{2\pi^{2/3}\left(\frac{c_{1z}}{u_n}\right)^{2/3}}{\lambda_{1cp\,0}\left[1+\left(\frac{c_{1z}}{u_n}\right)^2\right](1+\bar{d}_{st}^2)^{2/3}}. \qquad (3.162)$$

The right side of equition (3.162) for screw-centrifugal pumps geometrically similar with respect to the inlet in kinematically similar conditions is constant; then the complex of parameters on the left side of this equation will be the similarity criterion, with the aid of which the anticavitation qualities of pumps are estimated. Let us designate it C':

$$C' = \frac{\omega^{4/3} Q^{2/3}}{(\Delta p_{1\,cp\,0}/\rho)}.$$

In the form proposed by S. S. Rudnev, the criterion of anticavitation qualities of the pump is written, for example, for separation conditions thus:

$$C_{1\,sp} = 298 \frac{n\sqrt{Q}}{\left(\frac{\Delta p_{1\,cp\,0}}{\rho}\right)^{3/4}}. \qquad (3.163)$$

In connection with the analogy in the recording of equations for this criterion and for the power-speed coefficient n_s [see equation

(2.179)], criterion $C_{cpв}$ is called the cavitation power-speed coefficient.

In the technical system of units numerically equal for $C_{cpв}$ the quantity will be thus recorded:

$$C_{cpв} = 5{,}62\frac{n\sqrt{Q}}{\left(\frac{\Delta p^{*}_{cpв}}{\gamma}\right)^{3/4}},$$

where n is expressed in r/min; Q – in m^3/s; $\Delta p^{*}_{cpв}$ – in kgf/m^2; γ – in kg/m^3.

The cavitation power-speed coefficient can be determined for any conditions of cavitation. The advantage of using the cavitation power-speed coefficient $C_{cpв}$ [see equation (3.163)] consists in the fact that it connects the basic parameters of the pump Q and ω with the cavitation drop in the total pressure $\Delta p^{*}_{cpв} = \Delta p_{cpв} + \rho c^{2}_{вх}/2$. The less the cavitation pressure drop and inlet velocity, i.e., the better the anticavitation qualities of the pump, the larger the value of the cavitation power-speed coefficient. Let us focus attention to the fact that if $\Delta p_{cpв} = 0 (\lambda_{cpв} = 0$, which corresponds to the best cavitation qualities), then the value of the cavitation coefficient will not be equal to infinity and will be determined by the velocity of the fluid at the inlet.

3.3.6. CAVITATION DISCHARGE CHARACTERISTICS OF A SCREW-CENTRIFUGAL PUMP

The cavitation discharge characteristics of a pump in relative parameters are dependences of the cavitation drop in total or static pressure in separation conditions of the pump, referred to the square of the frequency of rotation, on the operating mode of the pump characterized by the ratio Q/ω.

Figure 3.88 gives the cavitation characteristic of the pump discharge. The convenience of using the cavitation characteristic consists in the fact that it does not depend on the frequency of rotation, the flow through the pump, density and temperature of the fluid.

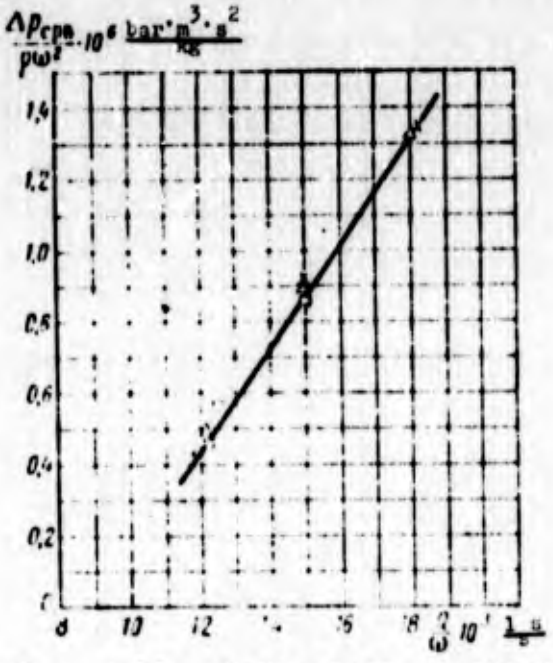

Fig. 3.88. Cavitation discharge characteristic of the pump.

With the aid of the cavitation discharge characteristic it is possible to determine the separation inlet pressure of the

pump for the conditions of its operation interesting to us. Let us assume, for example, that the discharge Q_1 of the fluid with density ρ_1, the frequency of the rotation ω_1 and the pressure of the vapor pressure $p_{п1}$ which corresponds to temperature T_1 are assigned. Let us determine the ratio Q_1/ω_1 and according to the characteristic determine the value $(\Delta p_{срв}/\rho\omega^2)_1$ corresponding to this ratio Q_1/ω_1. Hence we obtain the stall pressure

$$p_{вх\,кр} = \left(\frac{\Delta p_{срв}}{\rho\omega^2}\right)_1 \rho_1 \omega_1^2 + p_{п1}.$$

The possibility of plotting a cavitation characteristic in such coordinates ensues from the fact that $\Delta p_{срв}/\rho\omega^2$ is a constant value for similar conditions (Q/ω = idem).

If we use expressions (3.154), (3.157), (3.159), (3.160) and the relation

$$c_{вх} = \frac{Q}{F_{вх}}, \tag{3.164}$$

then, by substituting them into equation (3.131), we obtain

$$\frac{\Delta p_{срв}}{\rho\omega^2} = A_1\left(\frac{Q}{\omega}\right)^2 + A_2\frac{Q}{\omega}\sqrt{1 + A_3\left(\frac{Q}{\omega}\right)^2}, \tag{3.165}$$

where A_1, A_2, A_3 are constant values for this pump.

Equation (3.165) is the equation of the cavitation discharge pump characteristic.[1] In the region of low discharge (small ratio Q/ω) the cavitation characteristic can change its nature

---

[1] In connection with the small values A_1 and A_3, the cavitation discharge characteristic in the region of calculated values Q/ω is close to the linear (see Fig. 3.88).

determined by equation (3.165), which is the consequence of the change of the cavitation coefficient $\lambda_{1cpв}$ depending on $c_{1z}/u_п$ (see Fig. 3.87) connected with the presence of the reverse input currents with low discharge.

It is convenient to use the cavitation discharge characteristic for determining the stall pressure in the operation of the pump on different fluids (different densities ρ). As a rule, cavitation discharge characteristics are obtained by means of the removal of the stall characteristics of the pump (see Fig. 3.76) on water.

If the pump operates on fluids with gasses dissolved in them or free gases, then, besides the curve with zero content of the gas, on a graph curves with a different gas content will be plotted. The cavitation discharge pump characteristics with a different content in the fluid are determined from the stall characteristics obtained on water with a different content of gas dissolved in it or free gas (frequently - air).

3.3.7. SELECTION OF DESIGN PARAMETERS OF THE SCREW-CENTRIFUGAL PUMP WHICH PROVIDE ITS HIGH ANTICAVITATION QUALITIES

The high anticavitation perfection of the pump can be attained by means of the correct selection of design parameters of the screw conveyor.

3.3.7.1. Outside Diameter of the Screw Conveyor and Diameter of the Hub

A change in the outside diameter of the screw conveyor $D_ш$ other conditions being equal, leads to a change in the speeds c_{1z} and $u_п$, on the value of which $\lambda_{1cpв}$ (see Fig. 3.87) and $\Delta p^*_{cpв}$ [see equation (3.156)] depend. The complex dependence

of λ_{1cps} and Δp^*_{cps} on c_{1z} and u_n leads to the fact that with the defined (optimum) diameter D_w the best anticavitation qualities of the pump are attained.

By converting expression (3.163), we obtain

$$C_{cps} = 298 \left(\frac{\Delta p^*_{cps}}{\rho \omega^{4/3} Q^{2/3}} \right)^{-3/4}.$$

The maximum C_{cps} is reached with a minimum of the complex $\Delta p^*_{cps}/\rho\omega^{4/3}Q^{2/3}$. After the transformation of this complex by means of expressions (3.153) and (3.156), it is possible to be convinced of the fact that it is connected with two design factors: the coefficient of the equivalent diameter of the screw conveyor

$$K_{D_3} = 2{,}13 \frac{D_3}{\sqrt[3]{Q/\omega}}$$

and the coefficient of the diameter of the hub

$$K_{d_{sr}} = 2{,}13 \frac{d_{sr}}{\sqrt[3]{Q/\omega}}.$$

These coefficients determine the coefficient of the diameter of the screw conveyor

$$K_{D_w} = \sqrt{K^2_{D_3} + K^2_{d_{sr}}},$$

with the aid of which at known values of Q and ω it is possible to determine the diameter of the screw conveyor:

$$D_w = 0{,}47 K_{D_w} \sqrt[3]{Q/\omega}.$$

Coefficients $K_{D_э}$ and $K_{d_{вт}}$ are determined by the ratio of the velocities:

$$\frac{c_{1z}}{u_1} = \frac{24.3}{K'_{D_э}\sqrt{1+\left(\frac{K_{d_{вт}}}{K_{D_э}}\right)^2}}. \qquad (3.166)$$

The dependences of $C_{срв}$ on $K_{D_э}$ and $K_{d_{вт}}$ calculated with the aid of ratios (3.153), (3.156), and (3.163) are given on Fig. 3.89 for the screw-centrifugal pumps with different types of feeds. With an increase in $K_{D_э}$ (increase in $D_ш$) up to a certain limit the coefficient $C_{срв}$ increases.

The dependence of the optimum values $(K_{D_э})_{opt}$ and maximum value of the cavitation of the power-speed coefficient $(C_{срв})_{max}$ on $K_{d_{вт}}$ is given on Fig. 3.90. Optimum values of $K_{D_э}$ = 7-7.5, and $(C_{срв})_{max}$ reaches values of 4000-4500 at low values of $K_{d_{вт}}$. It is evident that an increase in losses in the feed (for example, the transition from an axial to a circular feed) decreases the value of $C_{срв}$ by 8-15%. With the aid of the graphs given on Fig. 3.90 it is possible to select the diameter of the screw conveyor $D_ш$ and evaluate the value $(C_{срв})_{max}$, since with the calculation the value $K_{d_{вт}}$ is easily determined: the diameter of the hub $d_{вт}$ is found from the precomputation of the pump spindle for strength (the transferred torsional moment), and Q and ω with the calculation are known.

For an increase in the anticavitation qualities of the pump (see Fig. 3.90) the diameter of the hub should be selected at a minimum, providing only the necessary strength of the shaft or structural feasibility. With the high requirements for anti-cavitation qualities of the pump one should select the diameter of the screw conveyor close to the optimum. If in this case

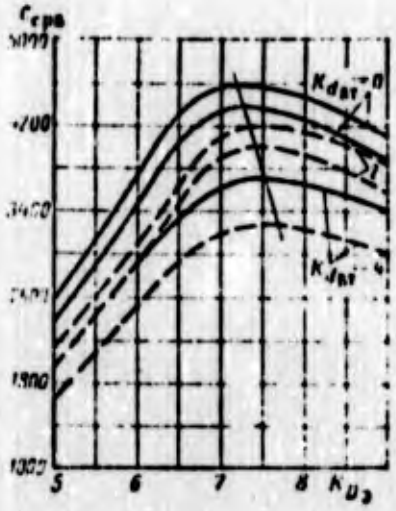

Fig. 3.89. Dependence of the cavitation power-speed coefficient C_{cps} of the screw-centrifugal pump on coefficients of the screw conveyor $K_{D_в}$ and $K_{d_{вт}}$ ($i_п \leq 4°$):
_____ - axial feed;
- - - - - - circular and semi-spherical feed.

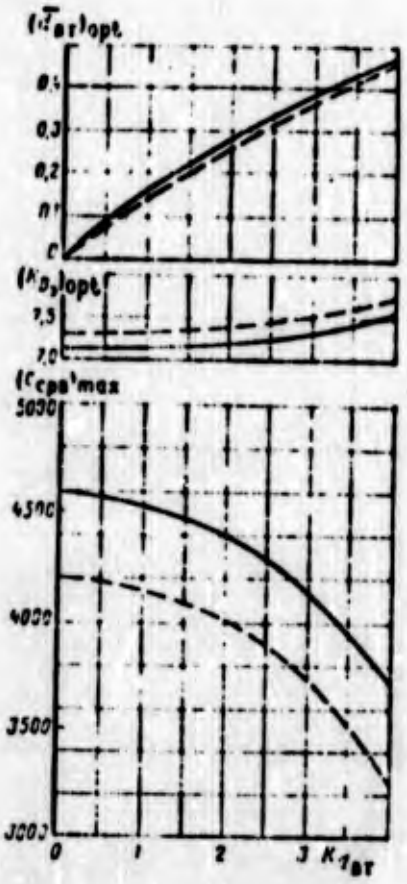

Fig. 3.90. Dependence of the maximum value of the cavitation power-speed coefficient of the screw-centrifugal pump and optimum values of coefficients of the screw conveyor $K_{D_в}$ and $\bar{d}_{вт}$ on $K_{d_{вт}}$ ($i_п \leq 4°$):
_____ - axial supply;
- - - - - circular and semi-spherical feeds.

there are obtained large values of $K_{D_ш}$, which lead to a considerable decrease in the efficiency of the pump (see Figs. 3.38-3.40), then one should pass from the design of the pump with identical diameters of the screw conveyor and inlet into the wheel ($D_ш = D_0$) (see Fig. 3.1) to the design with the diameter

of the screw conveyor greater than the diameter of the inlet into the wheel ($D_{sh} > D_0$) (Fig. 3.91). This will allow at high anticavitation qualities of the pump the obtaining of high efficiency.

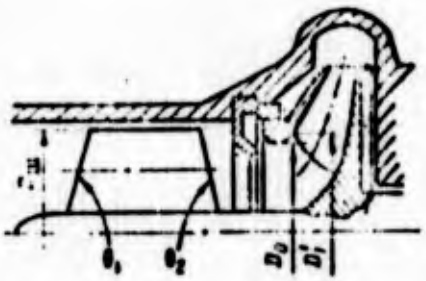

Fig. 3.91. Screw-centrifugal pump with exposed screw conveyor.

For an increase in the pressure quality of the screw conveyor it is sometimes necessary to increase the diameter of the hub at the outlet (increase in D_p); then it is advantageous to use a conical hub in the screw conveyor (see Fig. 1.12).

3.3.7.2. Determination of Pitch of the Screw Conveyor. Joint Operation of the Screw Conveyor and Centrifugal Wheel of the Pump

Studies (see sources [13, 75]) show that the anticavitation qualities of a screw-centrifugal pump will be determined by the screw conveyor if in the mode of cavitation stalling of the screw conveyor the pressure created by it is sufficient for nonstalling operation of the centrifugal wheel. In other words, the screw-centrifugal pump must be designed so that cavitation stalling of the screw conveyor would occur somewhat earlier than the stalling of the centrifugal wheel or simultaneously with it.

The condition of the simultaneous stalling is written as the equality of the total pressure at the outlet from the screw conveyor in stall conditions to the full stall pressure

of the centrifugal wheel for the most dangerous cross sections in the cavitation respect of the screw conveyor and wheel. Such cross sections for the screw conveyor and wheel are cross sections with the greatest speed of inleakage of flow, i.e., the outside diameter of the screw conveyor and peripheral diameter of the leading edges of the impeller vanes.

Let us assume that the stream leaving the screw conveyor at diameter $D_ш$ enters into the wheel at diameter D_1' (see Fig. 3.91). Then the condition of the simultaneity of stalling will be obtained from the equality of total energies of the mass unit of fluid (we disregard the losses) at the outlet from the screw conveyor and at the inlet into the wheel:

$$p_{п1} + \Delta p^{*}_{кр.ш} + \rho g H_{ш.п} = p_{п1ц} + \Delta p^{*}_{кр.ц}, \qquad (3.167)$$

where $H_{ш.п}$ is the pressure of the peripheral cascade of the screw conveyor; $p_{п1}$ and $p_{п1ц}$ - vapor pressures of fluid, respectively, at the inlet into the screw conveyor and at the inlet into the centrifugal wheel.

In general the pressures $P_{п1}$ and $p_{п1ц}$ are not equal, since the inlet temperature of the centrifugal wheel is higher than at the inlet into the screw conveyor - due to the preheating of the fluid by leakages which approach the inlet into the wheel and preheating as a result of losses in the screw conveyor.

In the operation of the pump in design conditions the difference in pressures of the vapor pressure can be disregarded. In this case equation (3.167) will be thus recorded:

$$\Delta p^{*}_{кр.ш} + \rho g H_{ш.п} = \Delta p^{*}_{кр.ц}. \qquad (3.168)$$

Let us divide equation (3.168) by $\rho u_п^2$:

$$\frac{\Delta p^{*}_{1\text{срв}}}{\rho u^{2}_{н}} + \frac{H_{ш.н}}{u^{2}_{н}} = \frac{\Delta p^{*}_{\text{срв.ц}}}{\rho u^{2}_{н}}, \tag{3.169}$$

where

$$\Delta p^{*}_{\text{срв.ц}} = \lambda_{\text{срв.ц}} \rho \frac{w^{2}_{1ц}}{2} + \rho \frac{c^{2}_{1ц}}{2};$$

$w_{1ц}$ and $c_{1ц}$ - the velocities at the peripheral diameter D'_1 of the leading edges of the centrifugal wheel; $\lambda_{\text{срв.ц}}$ - the cavitation coefficient of the centrifugal wheel in stall conditions.

Equation (3.169) is the equation of the joint operation of the screw conveyor and centrifugal wheel. Let us transform equation (3.169). From the velocity triangle at the inlet into the centrifugal wheel it is possible to record:

$$w^{2}_{1ц} = (u_{1ц} - c_{1uц})^{2} + c^{2}_{1mц}; \tag{3.170}$$

where

$$c^{2}_{1ц} = c^{2}_{1mц} + c^{2}_{1uц},$$

$$u_{1ц} = u_{н}(D'_1/D_{ш}).$$

Under the assumption that losses in the space between the screw conveyor and the wheel are absent, the flow will obey the law $c_u r$ = const; then

$$c_{1uц} = c_{2uп}\left(\frac{D_{ш}}{D_1}\right), \tag{3.171}$$

where $c_{2u\,п}$ is the twist of flow at the outlet from the screw conveyor - on the periphery.

Assuming that the axial velocity at the outlet from the screw conveyor c_{2z} ($c_{2z} = c_{1z}$) and meridian velocity at the

inlet into the centrifugal wheel $c_{1m\,ц}$ are invariable along the radius, we obtain

$$c_{1m\,ц} = \chi c_{1m}, \tag{3.172}$$

where

$$\chi = \frac{D_0^2}{4D_1 b_1}.$$

The cavitation coefficient of the centrifugal wheel can be recorded in the form (see source [13])

$$\lambda_{1\text{з.к}} = 0{,}053 + \left(1 - 0{,}38\frac{1}{\chi}\right)\frac{c_{1m}}{u_{1ц}} + \left(\frac{\delta}{\delta_0} - 0{,}615\right)\left(0{,}07 + 0{,}42\frac{c_{1m}}{u_{1ц}}\right), \tag{3.173}$$

where δ is the thickness of the leading edge of the blade of the centrifugal wheel; δ_0 - the thickness of the blade at a distance of 25 mm from the leading edge.

Equation (3.173) is obtained for the case of the absence of twist at the inlet into the centrifugal wheel, but the experimental data make it possible to conclude that it can also be used in the presence of twist.

The pressure of the screw conveyor $H_{ш.п}$ can be expressed in the following way:

$$H_{ш.п} = \eta_{г.ш.п}\frac{c_{2ш\,п}}{u_п}u_п^2, \tag{3.174}$$

where $\eta_{г.ш.п}$ - the hydraulic efficiency of the peripheral cascade of the screw conveyor.

Having substituted expressions (3.170), (3.171) and (3.172) into equation (3.169), we obtain

$$\frac{\Delta p^*_{1\,cpв\,п}}{\rho u_п^2} + v_{г.ш.п}\frac{c_{2u\,п}}{u_п} = \frac{1}{2}\lambda_{cpв.п}\left[\left(\frac{D_1}{D_ш} - \frac{c_{2u\,п}}{u_п}\frac{D_ш}{D_1}\right)^2 + \frac{\chi^2 c_{1z}^2}{u_п^2}\right] + \frac{1}{2}\left[\frac{\chi^2 c_{1z}^2}{u_п^2} + \left(\frac{D_ш}{D_1}\right)^2 \frac{c_{2u\,п}^2}{u_п^2}\right], \qquad (3.175)$$

where $\lambda_{cpв.ц}$ after the substitution of expressions (3.171) and (3.172) in (3.173), can be represented by the following equation:

$$\lambda_{cpв.ц} = 0{,}053 + \left(1 - 0{,}38\frac{1}{\chi}\right)\frac{D_ш}{D_1}\sqrt{\frac{\chi^2 c_{1z}^2}{u_п^2} + \left(\frac{D_ш}{D_1}\right)^2 \frac{c_{2u\,п}^2}{u_п^2}} + \left(\frac{\delta}{\delta_0} - 0{,}615\right)\left[0{,}07 + 0{,}42\frac{D_ш}{D_1}\sqrt{\frac{\chi^2 c_{1z}^2}{u_п^2} + \left(\frac{D_ш}{D_1}\right)^2 \frac{c_{2u\,п}^2}{u_п^2}}\right].$$

In equation (3.175) the value $\Delta p^*_{1cpв}/\rho u_п^2$, as a rule, is known from the cavitation calculation of the screw-centrifugal pump. From equation (3.175) it is possible to find that twist $c_{2u\,п}$ on the peripheral diameter of the screw conveyor at which the simultaneity of the cavitation stalling of the centrifugal wheel and screw conveyor is provided. This twist $c_{2u\,п}$ determines the required head of the screw conveyor.

Since twist $c_{2u\,п}$ enters also into the left and right sides of equation (3.175), it is solved by graphic means. First we determine for the number of values $c_{2u\,п}/u_п$ the sum $\frac{\Delta p^*_{1cpв\,п}}{\rho u_п^2} + \frac{H_{ш.п}}{H_п}$ - the left side of equation (3.175), and then we find the value $\Delta p^*_{cpв.ц}/\rho u_п^2$ - the right side of equation (3.175). The point of intersection of the corresponding dependences (Fig. 3.92) gives the value $c_{2u\,п}/u_п$, which satisfies equation (3.175). During calculations it is possible to consider that

$\eta_{г.ш.п}$ is equal to the efficiency of the screw conveyor $\eta_{г.ш} = 0.4\text{-}0.5$ (see sources [47, 74]).

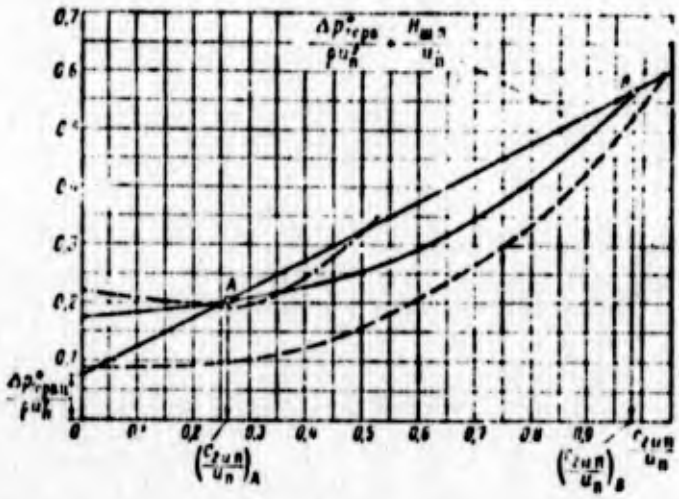

Fig. 3.92. Determination of the necessary twist of flow by the screw conveyor:

$\Delta p^{*}_{гра.ш}/\rho u_п^2$ — при $\chi=1$; $D_в/D_ш=1$; — при $\chi=0{,}5$; $D_в/D_ш=1$; — при $\chi=1$, $D_в/D_ш=0{,}78$.

Designation: при = when.

Figure 3.92 shows that equation (3.175) can satisfy two values of $c_{2u\ п}/u_п$ - larger and smaller (see points B and A on Fig. 3.92). The smaller value of $c_{2u\ п}/u_п$ is of interest to us, since to it corresponds less pressure of the screw conveyor.

According to the relative twist it is possible to determine the angle of the blade of screw conveyor on the periphery:

$$\operatorname{tg}\beta_{л.ш} = \frac{c_{1u}}{u_ш - c_{2u\ ш}} = \frac{c_{1u}\, u_ш}{1 - \frac{c_{2u\ ш}}{u_ш}}. \qquad (3.176)$$

The pitch of the screw conveyor at the outlet is determined according tc the equation

$$s_2 = \pi D_ш \operatorname{tg} \beta_{2л.л}. \qquad (3.177)$$

or, taking into account expression (3.176),

$$s_2 = \pi D_ш \frac{c_{1u}' u_ш}{1 - \frac{c_{2м.л}}{u_ш}}. \qquad (3.178)$$

The required head of the screw conveyor and magnitude of the pitch s_2 are affected by the ratio of areas of the outlet from the screw conveyor and inlet into the impeller vanes (coefficient χ) and the ratio of diameters of the screw conveyor and inlet into the blades of the centrifugal wheel $D_1'/D_ш$ [see equation (3.175)]. The decrease in χ (increase in the area of the inlet into the impeller vanes) decreases the value $\Delta p^*_{\text{срв.ц}}/\rho u_п^2$ - as a result of a decrease in $\lambda_{\text{срв.ц}}$ [see equation (3.173)], and, therefore, decreases the required head of the screw conveyor, angle $\beta_{2л.л}$ and pitch s_2.

In the case of the screw conveyor of constant pitch $s_1 = s_2 = s$; in this case the angle of attack decreases, which will favorably affect the anticavitation qualities of the screw conveyor and the entire screw-centrifugal pump. Thus, when designing a centrifugal wheel it is necessary to attempt to insure its high anticavitation qualities. Usually we assume that $\chi = 0.65$-0.8.

From expression (3.175) it is difficult to explain the effect of ratio $D_1'/D_ш$ on the necessary pressure of the screw conveyor. However, calculations show that within the usually encountered limits of values $D_1'/D_ш = 0.75$-1.1 the effect of the ratio $D_1/D_ш$ on the necessary pressure of the screw conveyor is small.

Figure 3.92 shows that the screw conveyor for the joint operation with the wheel should be designed with small values

of ratio $c_{2u\,п}/u_п$ not exceeding 0.2-0.3. In this case the coefficient of theoretical pressure of the screw conveyor $\bar{H}_{т.ш} = H_{т.ш}/u^2_{ср}$ reaches values of 0.5-0.7, and the degree of reaction at the mean diameter is 0.65-0.75. Consequently, it is necessary that the screw conveyor basically increase the static pressure at the inlet into the centrifugal wheel.

For the screw conveyor of constant pitch s = const, the pitch at the inlet s_1 should be equal to the pitch at the outlet s_2 calculated according to equation (3.178). The angle of the blades at the inlet will be equal to the angle of the blades at the outlet: $\beta_{1л.п} = \beta_{2л.п}$. Then the angle of attack on the outside diameter at the inlet will be found as the angular difference:

$$i_п = \beta_{1л.п} - \beta_{1п}, \qquad (3.179)$$

where $\beta_{1п}$ - the flow angle at the inlet on the periphery of the screw conveyor:

$$\beta_{1п} = \operatorname{arctg}(c_{1z}/u_п),$$

and the ratio $c_{1z}/u_п$ is determined with the anticavitation calculation of the screw conveyor (see further Section 3.4).

The angle of attack $i_п$ should not exceed 3°-5°. Its high value leads to a considerable deterioration in the anticavitation qualities of the screw-centrifugal pump [see equation (3.151)]. If the angle of attack $i_п$, calculated according to equation (3.179) when $\beta_{1л.п} = \beta_{2л.п}$, proves to be less than 3°-5°, then it is possible to discuss the screw conveyor of constant pitch: $s = s_1 = s_2$. Then the angle of the blade $\beta_{1л.п}$ and pitch of the screw conveyor s_1 will be found from expressions:

$$\beta_{1л.п} = \operatorname{arctg}\left(\frac{c_{1z}}{u_п}\right) + i_п; \qquad (3.180)$$

$$s_1 = \pi D_{ш1} \operatorname{tg} \beta_{1л}. \qquad (3.181)$$

If $i_п$ will be more than 3°-5°, then one should take the angle of attack as being equal to 2°-3° and use the screw conveyor of variable pitch with $s_1 < s_2$ calculated according to equation (3.178).

Let us recall that pressure of the screw conveyor of constant pitch is created because of the presence of the angle of incidence: the flow in the cascade of the screw conveyor is turned by an angle equal to the angle of attack. At zero angle of incidence the screw conveyor of constant pitch will not create pressure. In the screw conveyor of variable pitch the pressure is created both because of the presence of the angle of incidence and also due to the camber of the profile. In principle, at zero angle of incidence the screw conveyor of variable pitch will create pressure.

Technologically the screw conveyor of variable pitch is considerably more complex than the screw conveyor of constant pitch.

For an increase in the efficiency of the pump the use of the screw conveyor of variable pitch for producing the defined twist, at the inlet into the centrifugal wheel (see Section 3.1.1.5) (especially in the case of centrifugal wheels with $D_1/D_2 > 0.5$). This twist, as a rule, will correspond to higher pressure necessary for obtaining high anticavitation qualities of the pump. Therefore, the anticavitation qualities of the pump with such a screw conveyor can be somewhat worse.

3.3.7.3. Cascade Density of Screw Conveyor, Number of Blades, Length of the Blade and Other Design Parameters of the Screw Conveyor

Cavitation in the screw conveyor begins in the region of inlet. With the motion of the fluid along the vane channel the pressure increases, and vapor caverns disappear (vapor is condensed). For the disappearance of the cavern in the high-pressure region definite time is necessary. Therefore, a sufficient length of the vane channel of the screw conveyor is necessary in order that the cavern would disappear before leaving the screw conveyor and would not be extended to the outlet from it. The extension of the cavitation zone to the region of the outlet leads to a sharp drop in pressure of the screw conveyor and in connection with the insufficient inlet pressure of the centrifugal wheel - to the cavitation stalling of the centrifugal wheel and entire pump. The fact that with an increase in the cavitation zone in the wheel the pressure of the screw conveyor falls is shown by experimental data.

Figure 3.93 shows that with an increase in the cavitation zone (with a decrease in inlet pressure of the screw conveyor) pressure of the peripheral cascade of the screw conveyor is decreased, and, therefore, the pressure of the entire screw conveyor is decreased. The basic increase in the pressure in this case falls in the outlet part of the screw conveyor. Therefore, for the elevation in pressure of the screw conveyor to the value which corresponds to the absence of cavitation in the screw conveyor (high inlet pressure), it is necessary to increase the length of the screw conveyor and the length of the vane channel.

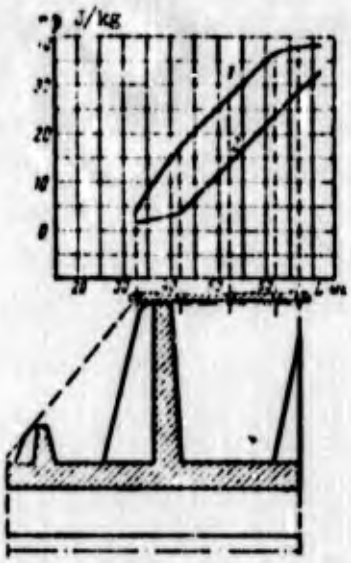

Fig. 3.93. Change in pressure energy along the length of the screw conveyor at different inlet pressures:
1 - $p_{вх} = 0.4$ MN/m^2;
2 - $p_{вх} = 0.072$ MN/m^2.

The cascade density of the screw conveyor, which is defined as the ratio of the length of the vane channel (length of the blade) of the screw conveyor to the pitch of the cascade of the mean diameter:

$$\tau_{cp} = \frac{b_{л.cp}}{t_{cp}}, \qquad (3.182)$$

is taken equal to 2-2.5. The cascade density of the screw conveyor, the number of the blades, and the length of the blade are connected with each other. Since

$$t_{cp} = \frac{\pi D_{cp}}{z_ш},$$

then, by taking expression (3.182) into account

$$\tau_{cp} = \frac{b_{л.cp} z_ш}{\pi D_{cp}}. \qquad (3.183)$$

The number of blades $z_ш$, as a rule, is selected equal to 2. But at large diameters of the screw conveyor D_{cp} (heavy-gauge $D_ш$) for obtaining the necessary density τ_{cp} when $z_ш = 2$ long length of the blade $b_{л.cp}$ [see equation (3.183)], and, therefore,

the long axial length of the screw conveyor can be required. For a decrease in the axial length, it is possible to have an increase in the number of blades to $z_ш = 3$, in this case somewhat making the anticavitation qualities of the pump worse (see source [74]). Besides $b_{л.ср}$, the axial length of the screw conveyor depends also on a number of other parameters: the angles of taper of the screw conveyor θ_1 and θ_2 (see Fig. 3.91), the law of the change in the pitch of the screw conveyor along the length (for the screw conveyor of variable pitch, s = var).

Angles of Taper of the Screw Conveyor

For an improvement in anticavitation qualities the screw conveyor is made with an angle of taper at the inlet θ_1 (see Fig. 3.91), which is 90°-120°. In the presence of the angle of taper at the inlet θ_1, as a result of the action of centrifugal forces of the flow twisted by the root cross sections, the pressure at the inlet into the peripheral cross sections of the cascade of the screw conveyor increases. This facilitates operating conditions of the peripheral cross sections in cavitation conditions. Sometimes for an increase in the resistance of the blade of the screw conveyor to vibrations, a conicity at the outlet of θ_2 = 140-160° is introduced. Smaller values of θ_1 and θ_2 correspond to small diameters $D_ш$.

Trimming of the Inlet Part of the Blade of the Screw Conveyor

A favorable effect on anticavitation properties of the screw conveyor is had by the trimming of the inlet part of the blade with a radius of $R = (0.25\text{-}0.35)D_ш$ (see source [75]) (Fig. 3.94B).

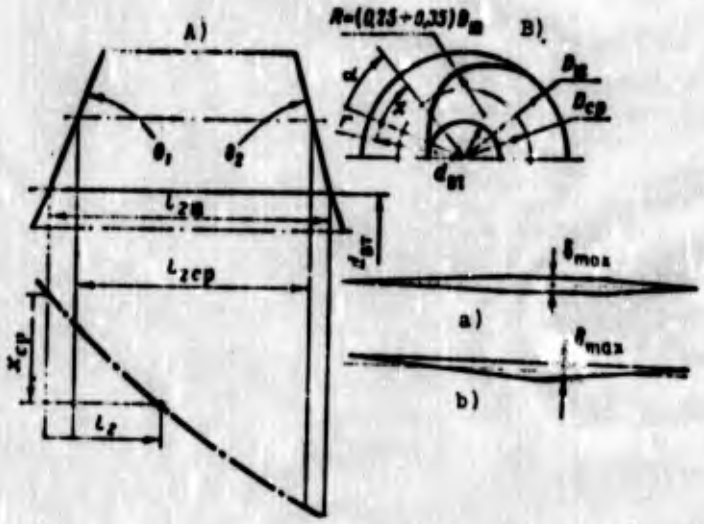

Fig. 3.94. Profiling of screw conveyor.

Thickness and Shape of the Blades

The shape of the blade of screw conveyor is made in the form of a cross section of straight (with s = const) or bent (when s = var) plate with pointed leading and trailing edges (Fig. 3.94a, see source [70]) or in the form of a triangle (Fig. 3.94b, see source [75]).

The thickness of the blade should be selected as less as possible for a decrease in the blocking of the cross section. From considerations of strength the root cross sections should have greater thickness than the peripheral do. Usually $(\delta_{max})_{вт}$ is equal to 0.015-0.02 of the length of the blade in the root cross section, and $(\delta_{max})_{п}$ is equal to 0.005-0.01 of the length of blade in the peripheral cross section (see source [70]).

The length of the sharpening of the leading edge should be 40-50% of the length of the blade, and the trailing edge - 20-30% of the length of the blade. For an improvement in the

anticavitation surface qualities the blade must be made with a finish of ∇6-∇7 (see source [86]).

Radial Clearance of the Screw Conveyor

For a decrease in the overflowing of the fluid from one side of the blade to the other and for the elimination of the possibility of the appearance of slot cavitation, the radial clearance must be maintained the smallest possible from design and technological considerations.

Axial Length of the Screw Conveyor

The axial length of the screw conveyor is determined by values of parameters $D_ш$, $d_{вт}$, s_1, s_2, θ_1, θ_2, $\tau_{ср}$ and $z_ш$, recommendations by choice of which were examined in this section.

Let us discuss the determination of the axial length of the screw conveyor of constant pitch ($s_1 = s_2 = s$).

a) Screw Conveyor of Constant Pitch

Let the cascade of the screw conveyor presented on Fig. 2.62 be the development of the cylindrical cross section of the screw conveyor according to mean diameter $D_{ср}$. Then the axial length of this diameter will be determined from the expression

$$l_{z\,ср} = b_{л.ср} \sin \beta_{л.ср}.$$

Let us express $b_{л.ср}$ in terms of the cascade density $\tau_{ср}$ from equation (3.182), and the angle $\beta_{л.ср}$ by the pitch of the screw conveyor $s = \pi D_{ср} \operatorname{tg} \beta_{л.ср}$. We will obtain

$$l_{z\,ср} = \frac{\pi D_{ср} \tau_{ср}}{z_ш} \sin \operatorname{arctg} \frac{s}{\pi D_{ср}}. \qquad (3.184)$$

From Fig. 3.94A, it is easy to establish the following relation between the length of the screw conveyor $l_{z\ ш}$ and $l_{z\ ср}$:

$$l_{z\,ш} = l_{z\,ср} \cdot \frac{D_{ср} - d_{вт}}{2^{\circ}} \left(\operatorname{ctg} \frac{\varphi_1}{2} + \operatorname{ctg} \frac{\varphi_2}{2} \right). \qquad (3.185)$$

After the substitution of expression (3.184) into equation (3.185) we obtain

$$l_{z\,ш} = \frac{D_{ср}}{2} \left[\frac{2\pi r_{ср} \sin \operatorname{arc\,tg} \frac{s}{D_{ср}}}{s_{ш}} + \left(1 - \frac{d_{вт}}{D_{ср}} \right) \left(\operatorname{ctg} \frac{\varphi_1}{2} + \operatorname{ctg} \frac{\varphi_2}{2} \right) \right]. \qquad (3.186)$$

b) Screw Conveyor of Variable Pitch

With a sufficient degree of accuracy it is possible to determine $l_{ср}$ for the screw conveyor of variable pitch by equation (3.184), utilizing a mean arithmetic value of the pitch of the screw conveyor:

$$l_{z\,ср} = \frac{\pi D_{ср} r_{ср}}{s_{ш}} \sin \operatorname{arc\,ctg} \frac{s_1 + s_2}{2\pi D_{ср}}.$$

Then the length of the screw conveyor $l_{z\ ш}$ will be found with the aid of equation (3.185):

$$l_{z\,ш} = \frac{D_{ср}}{2} \left[\frac{2\pi r_{ср} \sin \operatorname{arc\,tg} \frac{s_1 + s_2}{2\pi D_{ср}}}{s_{ш}} + \left(1 - \frac{d_{вт}}{D_{ср}} \right) \left(\operatorname{ctg} \frac{\varphi_1}{2} + \operatorname{ctg} \frac{\varphi_2}{2} \right) \right]. \qquad (3.187)$$

A comparison of equations (3.186) and (3.187) shows that for obtaining the identical density $\tau_{ср}$, the screw conveyor of variable pitch should have a longer length than does the screw conveyor of constant pitch with the same value of pitch at the inlet s_1.

Camber Line of the Blade Profile of the Screw Conveyor of Variable Pitch

When s = const the camber line of the blade is a straight line, and when s = var it is a bent line with a smoothly varying pitch from s_1 to s_2 (see Fig. 2.64). Let us find the expression for the center line of the blade of the screw conveyor of variable pitch.

For the helix the axial displacement of l_z is connected with the angular displacement α (see Fig. 3.94B) by expression

$$dl_z = (s/2\pi) \cdot d\alpha. \qquad (3.188)$$

Let us assign the law of the change in pitch s depending on angle α in the form

$$s = s_1 + (k\alpha)^n. \qquad (3.189)$$

The law taken of the change in s should satisfy two conditions. It should provide the assigned length of the screw conveyor $l_{z\,w}$ [see equation (3.187)] and a small change in the pitch and, consequently, the angle of the blade in the initial section. The latter is necessary in order that the trimming of the leading edge of the blade at angle θ_1 would not lead to a considerable increase in the angle of incidence (due to an increase in the angle of the blade) and a deterioration in the anticavitation qualities of the screw conveyor. When n = 5-7 the change in the angle in the initial section of the blade is quite small. It is inexpedient to accept larger values of n, since, although the camber of the initial section of the blade in this case is decreased, the camber of the outlet part of the blade increases, which can lead to an increase in the lag of flow from the blade and a drop in pressure of the screw conveyor.

Let us find the relation of coefficient k with $l_{z\,ш}$. Having substituted expression (3.189) into (3.188) and having integrated the obtained equation from s_1 to s_2, we obtain

$$l_{z\,ш} = \frac{(s_1 + ns_1)(s_2 - s_1)^{1/n}}{2\pi k(n+1)},$$

whence

$$k = \frac{(s_1 + ns_1)(s_2 - s_1)^{1/n}}{2\pi(n+1)l_{z\,ш}}. \qquad (3.190)$$

The equation of the development of the screw conveyor $l_z = f(\alpha)$ is found by the integration of equation (3.188), taking into account expression (3.189):

$$l_z = \frac{s_1}{2\pi}\alpha + \frac{k^n}{2\pi(n+1)}\alpha^{n+1}.$$

Then the equation for the camber line of the blade at diameter D, taking into account that $x = \alpha D/2$ (see Fig. 3.94), will have the form

$$l_{zD} = \frac{s_1}{\pi D}x + \frac{(2k)^n}{\pi(n+1)D^{n+1}}x^{n+1}. \qquad (3.191)$$

The plotting of the camber line for the mean diameter is shown on Fig. 3.94A.

3.3.7.4. Arrangement of the Cone in Front of the Centrifugal Wheel

A positive effect on anticavitation qualities of the pump is exerted by the arrangement of the fixed cone in front of the centrifugal wheel (Fig. 3.95, see source [79]). The favorable effect of the cone can be explained by the fact that the cone intercepts the return currents coming out of the centrifugal wheel (see source [99]), and weakens their harmful

effect on the operation of the screw conveyor. With the setting of the cone the expenditure of energy of the flow proceeding from the screw conveyor for the rotation of return currents and their direction into the wheel is decreased. The arrangement of the cone in front of the screw conveyor because of this can also be useful. Furthermore, the cone located in front of the centrifugal wheel directs along the flow leakages passing through the front seal. In this case the leakages do not disturb the flow coming out of the screw conveyor.

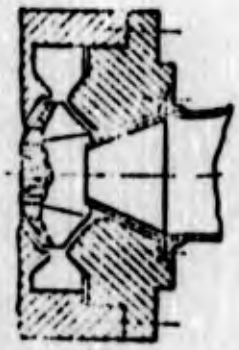

Fig. 3.95. Centrifugal wheel with the cone at the inlet.

3.3.7.5. Screw-Centrifugal Pump with Bilateral Inlet

The improvement of anticavitation qualities of a screw-centrifugal pump can be obtained by use of a two-sided inlet (Fig. 3.96). Through every inlet enters half of the entire fluid flow rate fed by the pump. Inlet velocity of the screw conveyor c_{1z} is decreased, which leads to a decrease in the cavitation pressure drop Δp^{*}_{cps} [see equation (3.156)].

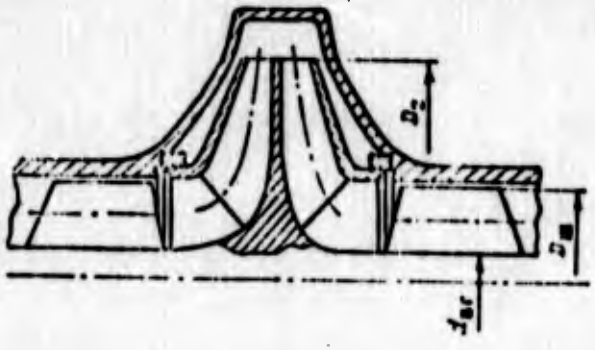

Fig. 3.96. Screw-centrifugal pump with two-sided inlet.

If there is no need for a decrease in Δp^*_{cps} or if this value is assigned, then with the two-sided inlet [see equation (3.163)] it is possible to increase the angular velocity ω by $\sqrt{2}$ times (with an invariable value of C_{cps}), since the flow rate through the screw conveyor is decreased by two times. In actuality an increase in the angular velocity will be somewhat less, since for a pump with a two-sided inlet the value C_{cps} will be less than that for a pump with a one-way inlet. This occurs both due to an increase in the coefficient $K_{d_{sr}} = \frac{2{,}13 d_{sr}}{\sqrt[3]{Q_{sr}}}$ (decrease in the flow rate through the screw conveyor) (see Fig. 3.90) and also because in the pump with the two-sided inlet, according to design considerations, it is not possible to utilize the axial feed, and in pump with the one-way inlet this can be done.

Let us note that the use of the bilateral inlet makes it possible not only to improve the anticavitation qualities of the pump, but also to increase somewhat its efficiency at large n^*_s and K_{D_0} (see Figs. 3.39 and 3.40). At the same time, the bilateral inlet complicates the design of the pump and increases its mass, and therefore the question of the advisability of the use of the two-sided inlet should be examined in every specific case separately.

3.3.8. THE USE OF BOOSTER PUMPS IN FEED SYSTEMS OF LIQUID-PROPELLANT ROCKET ENGINES

3.3.8.1. Vane Booster Pumps

For an increase in the anticavitation qualities of the feed system of LPRE, auxiliary (booster) pumps are used (see sources [31, 34]). The booster pump is installed in front of the main screw centrifugal pump of the turbopump unit of the engine

(Figs. 3.97 and 3.97a) and, as a rule, its shaft is rotated with less frequency than the shaft of the main pump.

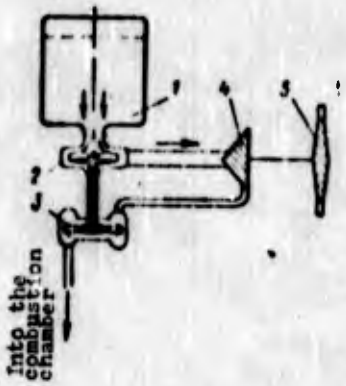

Fig. 3.97. Booster vane pump in the feed system: 1 - tank with fuel component; 2 - booster pump; 3 - hydraulic turbine of booster pump; 4 - main pump; 5 - turbine of main pump.

The purpose of the booster pump consists of a pressure increase from the inlet pressure of the feed system to the pressure necessary for nonstalling operation of the screw-centrifugal pump. The booster pump, in view of the less frequency of the rotation of its shaft, required for nonstalling operation less inlet pressure, and therefore its arrangement makes it possible to decrease the inlet pressure of the feed system, and, consequently, tank pressure. The frequency of rotation of the shaft of the main pump in the presence of a booster pump can be selected higher. Virtually in this case the anticavitation properties of the main pump are no longer limiting.

To establish the relation between the frequency of the rotation ω of the shaft of the main pump of the turbopump unit and the minimally permissible inlet pressure of the booster pump (the feed system), in the calculations the cavitation power-speed coefficient of the feed system is formally applied:

$$C_{\text{п}} = 298 \frac{\omega \sqrt{Q}}{(\Delta p_{\text{доп}}/\rho)^{3/4}}, \qquad (3.192)$$

where Q is the volumtric flow rate through the main pump in m^3/s.

As booster pumps it is possible to use vane pumps - both axial (screw conveyors) and centrifugal and screw-centrifugal, or jet pumps - ejectors (Fig. 3.98).

When using vane booster pumps the value of $C_{c.n}$ reaches 10,000-15,000, and when using jet pumps - 8000-10,000.

Booster pumps can be built into the turbopump unit (Fig. 3.99); it is accepted to call such pumps preliminary pumps. If a booster pump is made in the form of an individual unit, then it is called a booster pump (see Fig. 3.97).

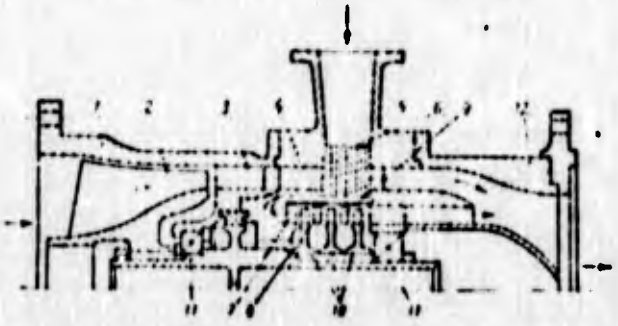

Fig. 3.97a. Structural diagram of a booster pump with a hydraulic turbine: 1 - feed of booster pump; 2 - wheel of booster pump; 3 - blades of the first guide device; 4 - blades of second guide device through which the feed of fluid to the hydraulic turbine is achieved; 5 - feed of the turbine; 6 - openings; 7 - nozzle box of the turbine; 8, 9 - guide vanes; 10 - turbine wheel; 11 - bearings; 12 - branch.

The active liquid for the jet booster pump is removed at the outlet from the main pump or from cavities of high pressure of the main pump. Vane preliminary pumps can be led from the shaft of the main pump through the reducer (hydraulic or mechanical), which decreases the frequency of rotation of the shaft of the booster pump. For driving the booster vane pumps, a hydraulic turbine which operates on fluid of high pressure

entering from the main pump can be used. The possible layout of the booster pump with a hydraulic turbine is given on Fig. 3.97a.

More frequently the drive of the booster pumps is achieved from the gas turbine, the gas for which is produced in a special gas generator, and it can also be taken from the main gas generator or at outlet of the main turbine. If a component is cryogenic, then the turbine can operate on vapors of this component (see source [112]). The gasification of the component in this case will occur either in the special heat exchanger, being heated by the gas coming out of the turbine, or in the cooling jacket of the combustion chamber (see source [112]). The gas after the turbine is ejected into the atmosphere, which leads to a certain decrease in the specific thrust of the engine. The latter fact causes the need for the design of booster vane pumps and their turbines with high efficiency.

Booster vane pumps are used in LPRE with autonomous and precombustion-chamber turbines. It is advantageous to use the jet pumps, which have considerably less efficiency, in LPRE with a precombustion chamber turbine. In LPRE with a precombustion chamber turbine an increase in the energy of the turbine as a result of the removal of the fluid to the jet pump does not lead to a decrease in the specific thrust, but only requires an increase in pressure and temperature in the gas generator.

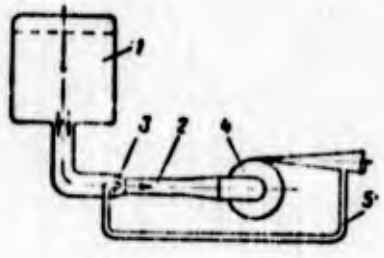

Fig. 3.98. Booster jet pump in the feed system: 1 - tank with fuel component; 2 - booster jet pump; 3 - nozzle of booster pump; 4 - main pump; 5 - main line of the component of high pressure leading to the nozzle 3.

The booster pumps are located in direct proximity to the tank of the component, and therefore the use of booster pumps makes it possible to operate at less tank pressure than in the case of the use of series-connected pumps by the magnitude of losses in the main line from tank to the inlet into the series-connected pump.

Inlet pressure of the booster pump, necessary for its operation without cavitation stalling, can be determined from the expression for the cavitation power-speed coefficient of the booster pump $C_{б.н}$ in the following way:

$$(p^*_{с(н)})_{б.н} = \frac{298 \rho_{ж.н} n_{б.н}^4 Q^{2/3}}{C_{б.ф}^{4/3}} + p_н. \qquad (3.193)$$

After the substitution of expression (3.193) into equation (3.192) let us record:

$$C_{с.н} = C_{б.н}(\omega/\omega_{б.н}). \qquad (3.194)$$

An increase in $C_{б.н}$ and decrease in the frequency of the rotation of the shaft of the booster pump $\omega_{б.н}$ lead to a decrease in the necessary inlet pressure of the feed system [see equation (3.193)] and to an improvement in its anticavitation qualities [see equation (3.192)].

The axial screw and screw-centrifugal pumps have larger values of the cavitation power-speed coefficient, and therefore the use of them as booster pumps is more preferable.

The required head of the booster pump $H_{б.н}$ is determined from the condition of the nonstalling operation of the main screw-centrifugal pump during acceleration of the rocket equal to zero:

$$(p^*_{cpв})_{б.н} + \rho g H_{б.н} + \rho g l - \rho L_{conp} \geq p^*_{cpв}; \qquad (3.195)$$

$$H_{б.н} \geq \frac{p^*_{cpв}}{\rho g} - \frac{(p^*_{cпв})_{б.н}}{\rho g} + L_{conp} - l, \qquad (3.196)$$

where ρL_{conp} - the pitot loss in main line from outlet of the booster pump to the inlet in the main screw-centrifugal pump; $p^*_{cpв}$ - the stall pressure of the main screw-centrifugal pump; l - the difference in levels of arrangement of the booster and main pumps.

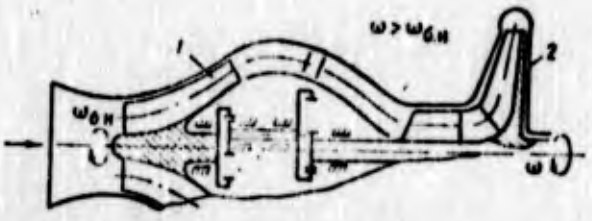

Fig. 3.99. Screw-centrifugal pump with a preliminary pump: 1 - preliminary pump; 2 - main screw-centrifugal pump.

With high required pressures of the booster pump high angles of incidences at the inlet into the screw conveyor of constant pitch are necessary, which makes the anticavitation qualities of the screw conveyor worse. In connection with this at high required pressures (usually higher than 50-100 J/kg) the booster pump should be made in the form of a screw conveyor of variable pitch, and at pressures exceeding 100-150 J/kg - a screw-centrifugal pump.

The calculation of geometric dimensions and characteristics of booster screw-centrifugal pumps is produced in the same way as the calculation of the basic screw-centrifugal pump. The energy characteristics of helical-type pump are determined with the aid of the relations given in section 3.2.3.3.

3.3.8.2. Jet Booster Pumps (Ejectors)

Used as booster pumps in LPRE are jet pumps, which we will call ejectors. In the feed systems of LPRE a pressure increases is required of the jet apparatus.

Constructively the ejector is simpler than the booster vane pump. However, for obtaining high pressure of the ejector a high flow rate of the active fluid is necessary and therefore the ejectors should be used when the required pressure is less than 150-200 J/kg. The required pressure of the ejector is defined just as the pressure of vane booster pump [see equation (3.196)].

Figure 3.100 gives a diagram of an ejector. An ejector consists of a converging nozzle section, cylindrical mixing chamber, diffuser and nozzle (or several nozzles) of active fluid. In the nozzle there occurs the energy conversion of the pressure of the active fluid into kinetic energy. In the mixing chamber, in the process of turbulent mixing there occurs the energy transfer from the active fluid to ejected, approaching the inlet into the ejector (cross section 0-0).

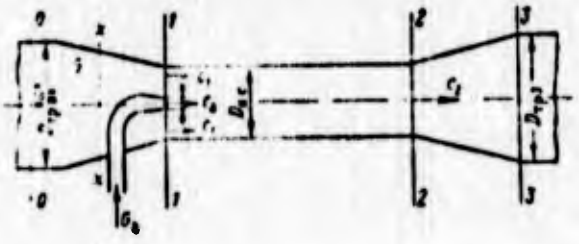

Fig. 3.100. Diagram of a jet pump (ejector) with one nozzle.

If the nozzle is located in the converging nozzle section, then the process of mixing begins in the converging nozzle

section. With the mixing of the active and ejected fluids the pressure of the ejected fluid increases, and the speed of the active flow is decreased (Fig. 3.101, see source [104]). The mixing of the jets is completed in the cross section 2-2, where the velocity field is virtually equalized. The diffuser is intended for the conversion of the kinetic energy of mixed flow into pressure energy. At the outlet of the diffuser the velocity reaches the value which must be had at the inlet into the main screw-centrifugal pump.

Let us examine first the ejector, the nozzle edge of which is located in the cross section of the chamber into the mixing inlet (see Fig. 3.100). For determining the pressure increase, in the ejector we use the theorem about the momentum for cross sections 1-1 and 2-2, assuming that the wall friction of the mixing chamber is absent (subsequently, let us consider the frictional effect with the aid of experimental coefficients):

$$G_a c_a + G c_1 - (G_a + G) c_2 = F_2 (p_2 - p_1), \qquad (3.197)$$

where G and G_a are mass flow rates of the ejected and active (ejecting) fluids, respectively; c_1 and c_a are the mean velocities of the ejected and active fluids; c_2 is the mean velocity of the mixed flow in cross section 2-2; p_1 and p_2 are, respectively, pressure of the fluid, respectively, in cross sections 1-1 and 2-2; $F_2 = F_1 = F_{к.с}$ is the area of the mixing chamber.

We will assume that the density of the fluid in all cross sections is constant (identical temperature); then it is possible to record

$$G = \rho Q; \quad G_a = \rho Q_a \quad \text{and} \quad G + G_a = \rho (Q + Q_a).$$

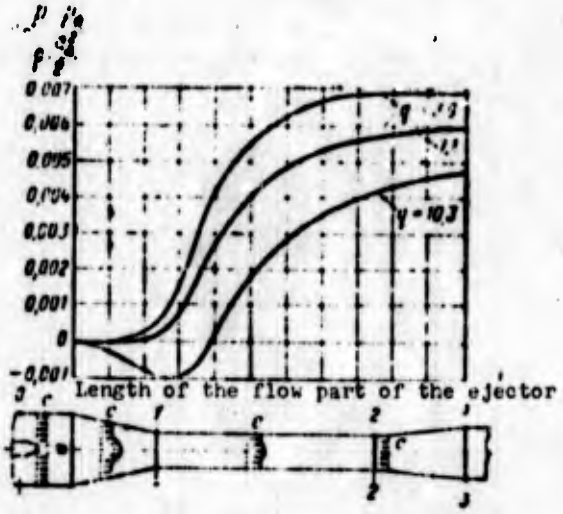

Fig. 3.101. Change in pressure and velocity along the length of the flow part of the ejector.

Velocities c_1, c_a and c_2 are expressed in terms of the volumetric flow rate in the following manner:

$$c_1=\frac{Q}{F_2-f_1};\quad c_a=\frac{Q_a}{f_1};\quad c_2=\frac{Q+Q_a}{F_2},$$

where f_1 is the area of the nozzle exit.

Let us substitute these relations into equation (3.197) and obtain the expression for the pressure difference $\Delta p_{1-2} = p_2-p_1$ in the form of

$$\Delta p_{1-2}=\frac{Q_a^2\rho}{f_1F_2}\left[1+\frac{q^2}{m-1}-\frac{(1+q)^2}{m}\right]. \qquad (3.198)$$

where $q = Q/Q_a$ is called the coefficient of ejection; $m = F_2/f_1$.

Let us attribute the pressure difference Δp_{1-2} to the kinetic energy of the active fluid at the nozzle exit; then we will obtain

$$\overline{\Delta p_{1-2}} = \frac{\Delta p_{1-2}}{\rho \frac{c_a^2}{2}} = \frac{2}{m}\left[1 + \frac{q^2}{m-1} - \frac{(1+q)^2}{m}\right]. \qquad (3.199)$$

A pressure increase in the ejector is a pressure difference of the fluid at the outlet from the ejector (cross section 3-3) and the ejected fluid at the inlet into the ejector (cross section 0-0). An increase in the total pressure in the ejector without losses $\Delta p^*_{эж} = p^*_3 - p^*_0$ can be expressed by Δp_{1-2} in the following way:

$$\Delta p^*_{эж} = \Delta p_{1-2} + \rho \frac{c_2^2}{2} - \rho \frac{c_1^2}{2}. \qquad (3.200)$$

An increase in the static pressure will be recorded in the form

$$\Delta p_{эж} = \Delta p_{1-0} = \Delta p^*_{эж} + \rho \frac{c_0^2}{2} - \rho \frac{c_3^2}{2}. \qquad (3.201)$$

Having divided expressions (3.200) and (3.201) by $\rho c_a^2/2$, we will obtain

$$\overline{\Delta p^*_{эж}} = \overline{\Delta p_{1-2}} + \frac{(1+q)^2}{m^2} - \frac{q^2}{(m-1)^2};$$

$$\overline{\Delta p^*_{эж}} = \frac{2}{m}\left[1 + \frac{q^2}{m-1} + \frac{(1+q)^2}{m}\right] + \frac{(1+q)^2}{m^2} - \frac{q^2}{(m-1)^2}; \qquad (3.202)$$

$$\overline{\Delta p_{эж}} = \overline{\Delta p^*_{эж}} - \frac{q^2}{(F_0/F_3)^2}\left[1 - \frac{(1+q)^2}{q^2(F_3/F_0)^2}\right], \qquad (3.203)$$

where F_0 and F_3 are, respectively, areas of the inlet into the ejector and outlet from it.

Usually the second term in the brackets of expression (3.203) is close to unity, and therefore an increase in the static pressure in the ejector is virtually equal to an increase in the total pressure.

In the actual case friction losses in the converging nozzle section of the ejector, losses to the mixing and friction in the mixing chamber and diffuser losses during the conversion of kinetic energy of the fluid into potential energy will take place. On the basis of the experimental data (see source [81]) the following empirical equation for determining the pressure increase in the ejector was proposed:

$$\overline{\Delta p}^{*}_{\text{эж}} = \frac{2m - 1.2(3q + 1)}{m^2} + \frac{(1 + q)^2}{m^2 (F_1 / F_2)^2}. \qquad (3.204)$$

The curves of the dependence of the pressure increased in the ejector on q and m, calculated from equation (3.204) are given on Fig. 3.102. It is evident that a relative pressure increase in the ejector $\overline{\Delta p}^{*}_{\text{эж}}$ increases with a decrease in the coefficient of ejection q (increase in the discharge of active fluid) and a decrease in the area ratio m (decrease in area of the mixing chamber). At the selected values of q and m, the absolute pressure increase in the ejector $\Delta p^{*}_{\text{эж}}$ will be the greater, the higher the rate of the active fluid c_a:

$$c_a = \varphi \sqrt{2 \frac{p_a - p_1}{\rho}}, \qquad (3.205)$$

where φ is the coefficient of discharge of the nozzle; p_a - pressure at the place of the removal of the active fluid (pressure behind the pump).

From equation (3.205) it follows that an increase in the pressure of the active fluid p_a leads to increase in c_a, and, therefore, to a pressure increase in the ejector.

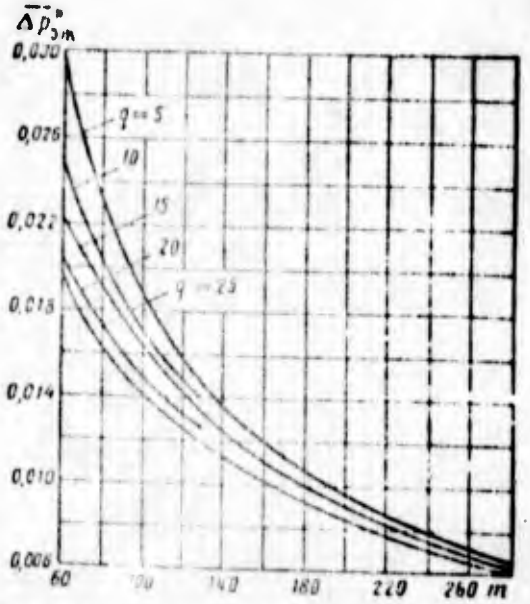

Fig. 3.102. Dependence of the relative increase in the total pressure in the ejector on q and m.

Let us determine the operating conditions of the ejector without cavitation stalling (see Fig. 3.100). If in a simplified way we consider that the mixing of the ejected and active fluids begins immediately after cross section 1-1, then the minimum pressure will take place in this cross section. Let us record the equation of the conservation of energy (we disregard the losses) for cross sections 0-0 and 1-1:

$$\frac{p_0}{\rho} + \frac{c_0^2}{2} = \frac{p_1}{\rho} + \frac{c_1^2}{2}. \qquad (3.206)$$

We will consider that the cavitation stalling of the ejector will begin at the minimum pressure equal to the pressure of the vapor pressure ($p_1 = p_п$). Then we can write:

$$\frac{p_0 + p_a}{\rho} + \frac{c_0^2}{2} = \frac{p_п}{\rho} + \frac{c_1^2}{2}; \qquad (3.207)$$

$$\frac{\Delta p_{кр}}{\rho} = \frac{p_0 + p_a - p_п}{\rho} = \frac{c_0^2}{2}\left[\left(\frac{c_1}{c_0}\right)^2 - 1\right]. \qquad (3.208)$$

Let us denote

$$\lambda'_{\text{эж}} = \left(\frac{c_1}{c_0}\right)^2 - 1 \qquad (3.209)$$

and let us call $\lambda'_{\text{эж}}$ the cavitation coefficient of the ejector in stalling conditions. After this let us record:

$$\frac{\Delta p_{\text{сро}}}{\varrho} = \lambda'_{\text{эж}} \frac{c_0^2}{2}; \qquad (3.210)$$

$$\frac{\Delta p^*_{\text{сро}}}{\varrho} = \frac{c_0^2}{2} + \lambda'_{\text{эж}} \frac{c_0^2}{2} = (1 + \lambda'_{\text{эж}}) \frac{c_0^2}{2}. \qquad (3.211)$$

Let us transform expression (3.209) and obtain

$$\lambda'_{\text{эж}} = \frac{m^2}{(m-1)^2}\left(\frac{F_0}{F_1}\right)^2 - 1,$$

or

$$\lambda'_{\text{эж}} = \left(\frac{c_a}{c_0}\right)^2 \frac{q^2}{(m-1)^2} - 1. \qquad (3.212)$$

The cavitation coefficient $\lambda'_{\text{эж}}$ at the given velocities c_a and c_0 and selected coefficient of ejection q is decreased with an increase in the area ratio $m = F_2/f_1$ [see formula (3.212)], since the rate of the ejected fluid in cross section 1-1 is decreased. However, an increase in m leads to a decrease in the pressure of the ejector (see Fig. 3.102), and therefore for an ejector with a nozzle located in the cross section of the mixing chamber inlet, an increase in the anticavitation qualities is connected with a decrease in its pressure quality.

For an improvement in the anticavitation qualities of the ejector, the cross section of the nozzle is located in the

converging nozzle in the cross section x-x (see Fig. 3.100) located at a certain distance from the mixing chamber inlet. This leads to a decrease in the velocity of the ejected fluid in the cross section corresponding to the minimum pressure (cross section x-x) and to a decrease in the stall pressure. The stall pressure will be the same as it would be in such a case when the nozzle was located in the cross section of the mixing chamber inlet with area F_x. The pressure quality of the ejector will be more, since basically the process of mixing occurs in the mixing chamber with an area of $F_2 = F_1$ less than F_x.

It is possible to determine approximately the pressure of such an ejector by the equivalent area:

$$F_{экв} = \frac{F_x + F_1}{2}.$$

Having recorded the equation (3.206) for cross sections 0-0 and x-x, it is possible to obtain the following expression for the cavitation coefficient $\lambda'_{эж}$ of the ejector with the nozzle located in the converging nozzle section:

$$\lambda'_{эж} = \frac{m^2}{\left(m\frac{F_x}{F_1} - 1\right)^2}\left(\frac{F_0}{F_1}\right)^2 - 1,$$

or

$$\lambda'_{эж} = \left(\frac{\sigma_x}{\sigma_0}\right)^2 \frac{q^2}{\left(m\frac{F_x}{F_1} - 1\right)^2} - 1. \qquad (3.213)$$

With a considerable difference in the rates of the active and ejected fluids their mixing begins not in the section of the nozzle edge but lower along the flow. Under the action of a great difference in the rates on the boundary between

the ejected and active fluids microvortices appear. In these vortices the pressure drops to a pressure of the vapor pressure. The active jet is covered with a vortical layer with the pressure of the vapor pressure preventing the mixing of the fluids and the energy transfer from the active fluid to that being ejected. The stagnation of the active flow on the boundary with vortical layer leads to a decrease in its average velocity and an increase in the cross section. The latter leads to a decrease in the flow area of the ejected flow and a pressure drop in it. The cross section with the minimum pressure proves to be displaced downstream relative to the cross section in which the nozzle is located.

The effect of the difference in rates on the anticavitation qualities of the ejector is not developed when $c_a/c_x < 3$-8 (see source [81]), and then the calculation of the cavitation coefficient can be carried out by equations (3.212) and (3.213). At larger values of ratio c_a/c_x the cavitation coefficient of the ejector increases in accordance with the equation proposed by A. S. Piskunov:

$$\lambda_{кр} = \lambda'_{кр} + k\left(\frac{c_x}{c_a}\right)^2, \qquad (3.214)$$

where

$$k = \left(\frac{c_a}{c_x} - 1\right)^2 \left(0{,}006 - 0{,}0073\sqrt{\lg\frac{c_a + c_x}{d_{1z}} - 4{,}8}\right);$$

d_{1z} is the diameter of the nozzle in m. Equation (3.214) is valid when $c_a/c_x \leq 35$; $5{,}12 \geqslant \lg\frac{c_a + c_x}{d_{1z}} \geqslant 4{,}8$.

For the completion of the process of the transmitting of energy from active fluid to that being ejected, the length of the mixing chamber should be equal to 8-10 of its diameters.

For a decrease in the length of the mixing chamber and, therefore, the entire length of the ejector, (see source [89]) multijet ejectors (Fig. 3.103) and ejectors with a ring nozzle are used (Fig. 3.104).

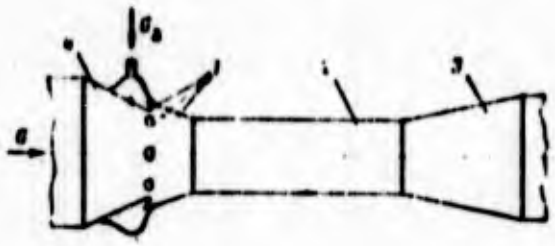

Fig. 3.103. Diagram of the multijet ejector:
1 - nozzle; 2 - mixing chamber; 3 - diffuser;
4 - converging nozzle.

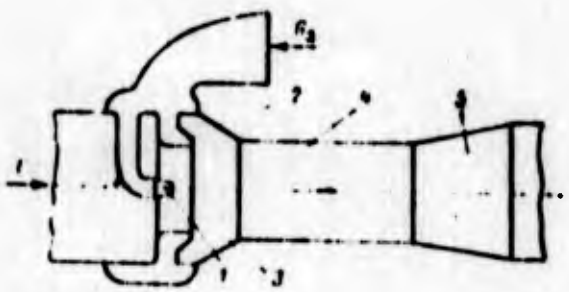

Fig. 3.104. Diagram of an ejector with a ring nozzle: 1 - nozzle; 2 - ring nozzle;
3 - converging nozzle; 4 - mixing chamber;
5 - diffuser.

A decrease in the length of such ejectors in comparison with the length of the ejector from one circular nozzle can be determined from the condition of the equality of the mixing surfaces. For example, for a multijet ejector it is possible to write:

$$z d_{1z} l'_{н.с} = \pi d_1 l_{к.с}, \tag{3.215}$$

where d_{1z}, z, $l'_{н.с}$ are the diameter of one nozzle, the number of

the nozzles and the length of the mixing chamber of the multijet ejector, respectively; d_1, $l_{к.с}$ are the diameter of the nozzle, and the length of the mixing chamber of the single-jet ejector respectively.

Since the sum of the areas of nozzles of the multijet ejector is equal to the area of the nozzle of the single-jet ejector, it is possible to write:

$$d_{1c} = d_1 / \sqrt{z}. \qquad (3.216)$$

By substituting expression (3.216) into (3.215), we finally obtain

$$l_{к.с} = l_{к.с} / \sqrt{z},$$

i.e., the length of the multijet ejector is $\sqrt{z}$ times less than the length of the single-jet ejector. Usually z = 10-15. The multijet ejector and ejector with a ring nozzle can be calculated approximately as a single-jet ejector with a circular nozzle, understanding by f_1 the sum of the areas of the nozzle exit.

In certain cases the use of a multistage ejector can prove to be advisable (see source [114]).

Calculation of the Ejector

The purpose of the calculation of an ejector is for determination of the required discharge of the active fluid and geometric dimensions of the ejector. The initial data are usually: Q, p. p_a, p_0, $p_п$, c_0, c_3 and the required increase in pressure in the ejector $\Delta p^*_{эж}$.

The calculation of the ejector is conducted in the following order. According to equation (3.205) the speed of the active flow c_a is determined. It is possible to assume in this case that φ = 0.92-0.97. Then the required relative pressure increase

$\overline{\Delta p}^{*}_{эж} = \frac{\Delta p^{*}_{эж}}{(\rho c_a^2/2)}$ is determined. With the aid of the graph (see Fig. 3.102) determine the values q and values m corresponding to them at which the pressure $\overline{\Delta p}^{*}_{эж}$ is provided. For several of the obtained values q determines the flow rate of the active fluid $Q_a = Q/q$ and area of the nozzle $f_1 = Q_a/c_a$; by m and f_1 we find the equivalent area of the mixing chamber $F_{эжв} = mf_1$.

Being assigned several values of the ratio F_x/F_1 in the range 1-2, we determine the cross-sectional area of the mixing chamber from the relation $F_{эж} = \frac{F_1}{2}\left(1 + \frac{F_x}{F_1}\right)$. For each value F_x/F_1 at the selected values of q, we determine the ratio of the velocities $\frac{c_a}{c_x} = \frac{m(F_x/F_1) - 1}{q}$, and then $\lambda_{эж}$ according to equation (3.214) (in this case the number of the nozzles is assinged). The value $\lambda_{эж}$ is used for determining the cavitation pressure drop $\Delta p_{срв}/\rho$ according to equation (3.210). We plot curves of the dependence $\Delta p_{срв}/\rho$ on q at the selected values of F_x/F_1. The permissible value of the cavitation pressure drop is determined from the initial data:

$$\left(\frac{\Delta p_{срв}}{\rho}\right)_{доп} = \frac{p_0 - p_н - \Delta p_{зап}}{g},$$

where $\Delta p_{срв}/\rho$ = 10-20 J/kg - pressure reserve, i.e., the excess in the assigned pressure p_0 above the stall pressure $p_{срв}$.

According to value $(\Delta p_{срв}/\rho)_{доп}$ and the plotted graph $\Delta p_{срв}/\rho = f(q, F_x/F_1)$, we determine the values of q corresponding to each of the selected ratios F_x/F_1. One should finally accept that value of F_x/F_1 at which q will be smallest. According to this value of q and the values of m and F_x/F_1 corresponding to it we determine the following parameters of the calculated ejector: Q_a, f_1, F_1, F_x, F_3 and $\Delta p^{*}_{эж}$.

If $\Delta p^*_{эж}$ considerably differs from that necessary, then one must repeat the calculation, having plotted the graph similar to that given on Fig. 3.102 for ratio F_3/F_2 close to that obtained during the calculation.

The length of the mixing chamber is determined depending on the design of the ejector. The lengths of converging nozzle and diffuser are determined by their expansion angles. For the converging nozzle the expansion angle should not exceed 25-30°, and for the diffuser - 6°-10°.

3.4. SELECTION OF PARAMETERS AND THE ORDER OF CALCULATION OF PUMPS OF LIQUID-PROPELLANT ROCKET ENGINES

3.4.1. INITIAL DATA FOR THE CALCULATION

The initial data for claculating a pump are:

1) the fundamental characteristics of the component of fuel being pumped by the pump - its density, pressure of the vapor pressure, and so on. These characteristics are given in the appropriate handbooks and books (the pressure of vapor pressure of some fuel components of LPRE can be determined in the temperature dependence on Fig. 3.84);

2) the minimum pressure and maximum temperature of the component at the inlet into the feed system (these data are assigned in the designing of the LPRE);

3) volumetric flow rate of the component;

4) required outlet pressure from the pump.

The volumetric flow rate is determined from the thrust, specific thrust and the relationship of components of the engine with the aid of equations given in section 1.1. The necessary pressure of the pump is determined depending on the selected design of the feed system (see section 5.1).

The purpose of the calculation is the determination of the frequency of the rotation of the shaft and dimensions of the basic elements: feed, screw conveyor, centrifugal wheel and branch which satisfy the initial data and are necessary for the design of the pump.

3.4.2. CALCULATION OF THE OXIDIZER PUMP

3.4.2.1. Determination of the Rotation Frequency

The oxidizer pump, as a rule, is associated with a considerably higher volumetric flow rate of the working medium than that of the fuel pump. Therefore, [see equation (3.165)], other conditions being equal, (identical values of C_{cps} and $\Delta p^*_{cpз}/\rho$) the oxidizer pump is able to operate without cavitation stalling at less rotation frequency than is the fuel pump. Hence it follows that the rotation frequency of a single-shaft turbopump unit should be determined by the oxidizer pump.

For an increase in the rotation frequency of the shaft of turbopump unit, the oxidizer pump must have higher anticavitation qualities than those of the fuel pump. Therefore, in the calculation of the oxidizer pump it is attempted to insure as high a value of the cavitation power-speed coefficient C_{cps}. For an increase in C_{cps} it is necessary to strive for the use of the axial feed and the reducing of the hub diameter of the screw conveyor. From this viewpoint, it is advantageous in the turbopump unit to position the oxidizer pump cantilever-wise (Fig. 3.105). The feed will be axial, and the diameter of the hub of the screw conveyor will be minimum, since the screw conveyor shaft does not transfer the considerable torsional moments, and its diameter is determined from design considerations.

If it is not possible to arrange the oxidizer pump cantilever-wise (for example, in the case of the cantilever precombustion-chamber turbine, which operates on oxidizing gas), then the radial feed of the fluid to the oxidizer pump should be achieved from the side of the fuel pump (Fig. 3.106). In this case the screw-conveyor shaft of the oxidizer pump will transfer only the torsional moment coresponding to the power of fuel pump. If the feed is achieved from the side of turbine, then the moment being transferred by the screw-conveyor shaft of the oxidizer is increased by the magnitude of the moment which corresponds to the oxidizer pump.

Both of the examined layout designs of the oxidizer pump in the turbopump unit (see Fig. 3.105 and 3.106) are most characteristic. Depending on the taken design, the order of the determination of the frequency of rotation of the pump is changed. It is logical that in the case of the cantilever arrangement of the oxidizer pump, the possible frequency of rotation will be more.

Fig. 3.105. Diagram of the turbopump unit with the cantilever arrangement of the oxidizer pump: 1 - oxidizer pump; 2 - fuel pump; 3 - turbine.

Fig. 3.106. Diagram of a turbopump unit with the cantilever arrangement of the fuel pump: 1 - oxidizer pump; 2 - fuel pump; 3 - turbine.

Let us discuss the determination of the rotation frequency of the shaft of the oxidizer pump with its cantilever arrangement. In this case the diameter of the hub of the screw conveyor is determined by design considerations, and usually its relative

value $\bar{d}_{вт} = d_{вт}/D_ш$ is equal to 0.15-0.25. By assigning the value $\bar{d}_{вт}$ within these limits, according to the graph given on Fig. 3.90, for the axial feed, we determine the maximally possible value of the cavitation power-speed coefficient $(C_{срв})_{max}$ of the screw-centrifugal oxidizer pump. Then the frequency of rotation of the shaft of the oxidizer pump is determined on the basis of equation (3.163):

$$\omega = \frac{(C_{срв})_{max}\left(\frac{p_{вх}}{\rho}\right)^{3/4}}{Q^{1/2}}. \qquad (3.217)$$

where $\frac{p_{вх}}{\rho}$ corresponds to the minimum inlet pressure of the pump and the maximum temperature of the oxidizer ($\Delta p_{зап}$ - the value of cavitation reserve), and Q corresponds to conditions of the maximum thrust of the engine.

Simultaneously with ω, according to the selected value $\bar{d}_{вт}$ we determine values $K_{D_э}$ and $K_{d_{вт}}$ with the aid of the graph given on Fig. 3.90. According to these values of $K_{D_э}$ and $K_{d_{вт}}$ and according to the rotation frequency ω, we calculate the geometric dimensions of the screw conveyor $D_э$, $d_{вт}$ and $D_ш$:

$$D_э = 0{,}47K_{D_э}\frac{\sqrt{Q}}{\omega^{1/3}}; \quad d_{вт} = 0{,}47K_{d_{вт}}\frac{\sqrt{Q}}{\omega^{1/3}}; \quad D_ш = D_э - d_{вт}.$$

Let us examine the case of a noncantilever arrangement of the oxidizer pump (see Fig. 3.106). Here the diameter of the hub of the screw conveyor of the oxidizer pump will be determined with sufficient accuracy by the power being transferred by the screw conveyor shaft equal to the power of the fuel pump $N_{н.гор}$. The power $N_{н.гор}$ is usually known from the calculation of the balance of turbopump unit of the powers (this question will be examined further in detail in Section 5.1).

For determining the rotation frequency of the shaft of the oxidizer pump, we need the value of the coefficient of the hub of the screw conveyor of the pump $K_{d_{вт}}$. Let us determine this value. Let us write

$$K_{d_{вт}} = 2{,}13\frac{d_{вт}}{\sqrt[3]{Q/\omega}}, \qquad (3.218)$$

where $d_{вт}$ is usually 1-1.2 of the diameter of the shaft $d_в$:

$$d_{вт} = (1 \div 1{,}2)d_в. \qquad (3.219)$$

The diameter of shaft is determined according to the power $N_{н.гор}$:

$$d_в = \sqrt[3]{\frac{5{,}1N_{н.гор}}{\omega\tau_{доп}}}. \qquad (3.220)$$

where $\tau_{доп}$ is the allowable torsional stress. For alloy steels $\tau_{доп} = (10\text{-}30)\cdot 10^7$ N/m^2.

By substituting expression (3.220) into equation (3.218), we obtain

$$K_{d_{вт}} = (2{,}13 \div 2{,}56)\sqrt[3]{\frac{5{,}1N_{н.гор}}{Q\tau_{доп}\omega}}. \qquad (3.221)$$

By knowing the value $K_{d_{вт}}$, according to the graph given on Fig. 3.90, we determine $(C_{cps})_{max}$ for the case of the nonaxial feed, and then according to formula (3.217) we find the rotation frequency of the shaft of the oxidizer pump ω.

Simultaneously with the determination of the rotation frequency ω, in terms of the value $K_{d_{вт}}$ let us determine the value $K_{D_э}$ (see Fig. 3.90), and then, by knowing ω, we find $D_э$ and $D_ш$.

3.4.2.2. The Use of the Oxidizer Pump with a Double Inlet

The rotation frequency ω, determined according to equation (3.127), is the rotation frequency of a single-shaft turbopump unit. According to the value of this rotation frequency one should estimate the mass of the turbopump unit (see Section 5.4). If the mass of the turbopump unit proves to be above that permissible, then for its decrease one should increase the rotation frequency of the shaft of the turbopump unit. For this purpose one should evaluate the advisability of the use of a wheel with a two-way inlet in the oxidizer pump (see Fig 3.96).

In the oxidizer pump with a two-way inlet (Figs. 3.107 and 3.108) the greatest diameter of the hub should be had by a screw conveyor located nearer to the turbine. If oxidizer and fuel pumps are located along one side of the turbine (see Fig. 3.107), then the shaft of this screw conveyor transmits the power equal to the total pump power (power of the turbine). If the pumps are arranged on different sides of the turbine (see Fig. 3.108), then through the screw-conveyor shaft the power of the oxidizer pump is transferred. The feed to the screw conveyor will be radial.

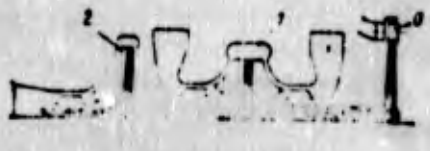

Fig. 3.107. Diagram of a turbopump unit with the oxidizer pump of two-way inlet (oxidizer and fuel pumps are located along one side of the turbine): 1 - oxidizer pump; 2 - fuel pump; 3 - turbine.

Fig. 3.108. Diagram of a turbopump unit with an oxidizer pump of two-way inlet (oxidizer and fuel pumps are located along different sides of the turbine): 1 - oxidizer pump; 2 - fuel pump; 3 - turbine.

The value $(C_{спв})_{max}$ of the oxidizer pump with a two-way inlet is determined according to value $K_{d_{вт}}$ with substitution of the appropriate power and of the volumetric flow rate equal to half of the flow rate through the pump [see equation (3.221)].

The rotation frequency ω is found by equation (3.217), in which the volumetric flow rate Q is also equal to half of the flow rate through the pump. As a rule, the diameters of the hubs of both screw conveyors are made identical.

3.4.2.3. The Use of a Booster Pump

In such a case when the use of a pump with a two-way inlet does not give the desired reduction in the mass of the turbopump unit, it is necessary to use a booster pump in the feed system of an engine with an oxidizer. Then the rotation frequency of the main shaft of the turbopump unit will be determined from expression (3.192), in which the cavitation power-speed coefficient of the feed system C_c is selected depending on the type of the booster pump (see Section 3.3.8.1) within limits of 8000-15,000.

The cavitation power-speed coefficient of the main oxidizer pump $(C_{спв})_{max}$ and the values $K_{D_э}$ and $K_{d_{вт}}$ corresponding to it are defined just as it was stated above for the case of the absence of a booster pump. It is necessary only to bear in mind that if the ejector is used as a booster pump, then the discharge through the oxidizer pump will increase by the rate of the discharge of the active fluid for the ejector (usually 8-12%).

According to the values ω, $K_{D_э}$ and $K_{d_{вт}}$ the dimensions of the screw conveyor $D_э$, $d_{вт}$, $D_ш$ are determined. According to the value $(C_{спв})_{max}$ the necessary inlet pressure of the main pump is determined [see equations (3.141) and (3.163)], and

then the necessary pressure of the booster pump - according to equation (3.196).

In the case of the use of a booster pump, for the purpose of the simplification in the design and decrease in the mass of the turbopump unit, the main pump is made with a one-way inlet.

3.4.2.4. Calculation of the Screw Conveyor

In the determination of the frequency of the rotation of the shaft of the oxidizer pump ω the outside diameter of the screw conveyor $D_ш$ and the diameter of the hub of the screw conveyor $d_{вт}$ became known. Let us explain whether or not one should make screw conveyor exposed.

The exposed screw conveyor ($D_ш > D_0$) (see Fig. 3.91) is advantageously used when with a nonexposed screw conveyor the ratio of the diameters of the centrifugal wheel D_1/D_2 exceeds 0.55. The use of an exposed screw conveyor will make it possible to lower the value of the ratio D_1/I_2 of the centrifugal wheel and thus make possible to raise the efficiency of the pump (see Section 3.1.1.5).

Let us determine the ratio D_1/D_2 by means of equations (3.5) and (3.59) by means of several approximations. Let us find the power-speed coefficient of the pump n_s^* from equation (2.179). The value φ can be taken equal to 0.85, and $q = 0.02$. If we obtain $D_1/D_2 > 0.55$, then we will discuss the exposed screw conveyor.

On the basis of the design considerations it can prove to be unsuitable to use the exposed screw conveyor. Then for the purpose of a decrease in ratio D_1/D_2, one should examine the possibility of reducing the diameter of screw conveyor $D_ш$. Here in the case of the absence of a booster preliminary

pump, in order not to decrease the rotation frequency ω, it is necessary to attempt to leave the same value $(C_{cpв})_{max}$ by means of a decrease in the angle of incidence and increase in the pitch of the screw conveyor at the outlet. If in the system the arrangement of the booster pump is provided for, then the drop in coefficient $C_{cpв}$, caused by a decrease in $D_ш$, does not lead to a decrease in the rotation frequency ω, but will increase the required head of the booster pump and increase the expenditure of energy for its drive.

In the exposed screw conveyor the coefficient of the diameter of the inlet into the wheel K_{D_0} is determined from expression (3.59), assuming that $D_1/D_2 = 0.5\text{-}0.55$. If the inlet into the wheel proves to be greatly narrowed, one should accept a somewhat larger value D_1/D_2. From K_{D_0} let us find the diameter of the inlet into the wheel D_0. The mean diameter of the leading edges of the impeller vanes $D_1 = \varphi D_0$.

Having assigned the area ratio of the outlet from the screw conveyor and the inlet into the wheel χ [see equation (3.172)] in the range of 0.65-0.8, let us determine the width of the wheel at the inlet

$$b_1 = \frac{D^2_{э.кол}}{4D_1 t}, \qquad (3.222)$$

where $D_{э.кол} = D_0^2 - d_{вт}^2$ - the equivalent diameter of the inlet into the wheel.

According to equation (3.173) let us determine the cavitation coefficient $\lambda_{cpв}$ of the centrifugal wheel, and then from condition (3.175) of the operation of the centrifugal wheel without cavitation stalling let us find the pitch of the screw conveyor at the outlet, whereupon let us determine the pitch of the screw conveyor at inlet (see Section 3.3.7).

After the determination of the pitch of the screw conveyor it is necessary to check whether or not the designed screw conveyor has necessary anticavitation qualities, i.e., it is necessary to be convinced of the fact that the value of the cavitation power-speed coefficient C_{cps} provided by the screw conveyor is not less than $(C_{cps})_{max}$, placed into the calculation of the rotation frequency of the pump shaft. For this purpose it is necessary to determine the angle of attack at the inlet into the screw conveyor on the outside diameter and then the cavitation coefficient of the screw conveyor λ_{1cps} in the equation (3.152) (if $c_{1z}/u_n < 0.06\text{-}0.08$, then λ_{1cps} is determined from Fig. 3.87). With respect to λ_{1cps} let us determine the value $\Delta p^*_{cps}/\rho$ [see equation (3.157)] which we use for determining the values of C_{cps} from equation (3.163).

If C_{cps} proves to be less than $(C_{cps})_{max}$ by more than 5%, then one should decrease the angle of attack at the inlet into the screw conveyor by means of decreasing the inlet pitch of the screw conveyor s_1; and in order that there is no disturbance in the condition of the nonstalling operation of the centrifugal wheel the pitch at outlet s_2 must be increased. It is possible to manage without a decrease in value χ [see equation (3.172)], leaving the pitch at the outlet constant with a decrease in the pitch at the inlet.

After the determination of the pitch of the screw conveyors s_1 and s_2 the number of blades is selected, and the axial length of the screw conveyor is determined (see Section 3.3.7). In this case the angles of the trimming of the screw conveyor θ_1 and θ_2 (see Section 3.91) are assigned within the limits indicated in Section 3.3.7. The profiling of the leading edge of the blade of the screw conveyor and the profiling of the cross section of the blade is carried out from recommendations given in Section 3.3.7.

3.4.2.5. Calculation of the Centrifugal Wheel

Dimensions of the wheel D_0, D_1 and b_1 were determined in the calculation of the screw conveyor. The angle of the impeller vanes at the inlet $\beta_{1л}$ can be determined by the angle of the flow β_1:

$$\beta_{1л} = \beta_1 + i_{кол},$$

where $i_{кол}$ is the angle of attack at the inlet into the wheel at diameter D_1. Experience shows (see sources [87, 102]) that the angle of attack can be accepted equal to 10-15°:

$$\operatorname{tg}\beta_1 = \frac{c_{1м}}{u_1}; \quad c_{1м} = \frac{Q}{\pi D_1 b_1}; \quad u_1 = \omega \frac{D_1}{2}.$$

In the first approximation, let us determine the outside diameter of the wheel D_2. The required pump pressure H is determined according to equation (1.10). Depending on the required form of the pressure and power pump characteristic (see Figs. 3.54 and 3.60), let us select the value of the flow parameter of the pump q_p. Having selected q_p, let us determine the coefficient of pressure $\bar{H}$ in equation (3.3); ratio D_1/D_2 is taken close to that accepted in the process of the calculation of the screw conveyor. By knowing H and $\bar{H}$, let us find D_2 from equation

$$D_2 = \frac{2}{\omega}\sqrt{\frac{gH}{\bar{H}}}. \qquad (3.223)$$

At the found value of D_2 it is possible to proceed to the determination of the angle of the impeller vanes at the outlet $\beta_{2л}$ and the width of the wheel b_2. Experience shows that the width of wheel b_2 must be selected sufficiently large in order that at the outlet from the wheel the joining of boundary layers on internal surfaces of the wheel disks would not occur. For this purpose one should accept the area ratio

$$\frac{F_1}{F_2} = \frac{D_1 b_1 \sin\beta_{1л}}{D_2 b_2 \sin\beta_{2л}} = 0{,}8 \div 1. \qquad (3.224)$$

From equation (3.224) we have the following ratio between b_2 and $\beta_{2л}$:

$$b_2 = \frac{D_1 b_1 \sin\beta_{1л}}{D_2 F_1 / F_2} \cdot \frac{1}{\sin\beta_{2л}}. \qquad (3.225)$$

Another relation between b_2 and $\beta_{2л}$ can be found from the expression for the flow parameter q_p:

$$b_2 = \frac{Q}{\pi D_2 \varepsilon_2 q_p \sin\beta_{2л}}. \qquad (3.226)$$

By equating the right sides of equations (3.225) and (3.226), we obtain the equation for determining the angle $\beta_{2л}$:

$$\sin\beta_{2л} = \frac{\pi D_1 b_1 \varepsilon_2 q_p \sin\beta_{1л}}{F_1 / F_2}. \qquad (3.227)$$

The value $\beta_{2л}$ obtained from equation (3.227) is rounded off up to the whole degrees. The width b_2 is determined from equation (3.225). If $\beta_{2л}$ is taken equal to 90°, then in the determination of b_2 from equation (3.225) one should accept the ratio F_1/F_2 on the lower recommended limit. The number of impeller vanes of the wheel is taken equal to 6-12. If in the tracing of the intervane channel of the wheel it is explained that the inlet is greatly blocked, then one should decrease the number of blades by introducing additional short blades, beginning at diameter $D_{1\text{коорот.лоп}} > D_1$.

After the conducting of the indicated calculations one should finally refine the outside diameter of the wheel. In terms of the value D_2 found in the first approximation, we find the ratio D_1/D_2 and determine the hydraulic efficiency of

the pump $\eta_г$ according to equation (3.31). Then we compute the theoretical pump pressure $H_т = H/\eta_г$. By knowing D_1/D_2, z and $\beta_{2л}$, according to the graph given in Figs. 3.11-3.13 we determine the coefficient of the effect of the finite number of blades k_z. With respect to k_z we find theoretical pressure at the infinite number of blades:

$$H_{т\infty} = H_т k_z.$$

With equation (3.2) as a basis, it is possible to find the circular velocity on the outside diameter of the wheel:

$$u_2 = \sqrt{\frac{H_{т\infty}}{\psi_т}} \qquad (3.228)$$

and

$$D_2 = \frac{2u_2}{\omega}. \qquad (3.229)$$

From considerations of strength the value u_2 should not exceed 400-450 m/s. Usually in pumps of LPRE (except hydrogen) the circular velocity is noticeably less than the limiting value. If from the calculation the value $u_2 > 400$-450 m/s was obtained, then the pump should be multilevel (see source [107]). The number of stages is determined from the condition that the circular velocity of the stage $u_{2ступ}$ would not exceed the indicated limit.

The maximum permissible pressure of the stage can be found on the basis of equation (3.3). When $q_p = 0$ and $D_1/D_2 \leq 0.55$ it is

$$H_{ступ max} = (10 \div 15) \cdot 10^3 \text{ [J/kg]}. \qquad (3.230)$$

The value D_2 obtained from equations (3.228)-(3.229) should be compared with the initial quantity; if the difference

exceeds 2-5%, then one should make one additional approximation. In terms of the finally obtained value D_2, it is necessary to refine the width b_2.

3.4.2.6. Calculation of the Branch

The spiral branch (see Fig. 3.18) and branch with a circular vane diffuser (see Fig. 3.19) are calculated with the aid of relations given in Section 3.1.1.4.

At moderate pressures the pumps are made with spiral branches. The spiral branch can be selected with a rectangular cross section (see Section 3.1.1.4). As a result of the calculation of the spiral branch the width of the spiral collector, the intake area into the conical diffuser [see equation (3.23)], the cross-sectional area [see equation (3.24)] and radii of the spiral [see equation (3.26)] are determined. According to the allowable velocity at the outlet from the pump, the area and the diameter of the outlet from the conical diffuser are determined.

The branch with a circular vane diffuser is selected at high pressures - for increasing the strength of the branch. In the calculation the width of the vane diffuser, its outside diameter, and angles of the blades at the inlet and outlet are determined. Then the blades of branch are profiled. The spiral collector of the branch with a circular vane diffuser is calculated from the same relations which are used in the case of the spiral branch, but from parameters of flow at the outlet from the vane diffuser [for example, instead of c_{2u} one should substitute into equation (3.23) the twist of flow at the outlet from the vane diffuser and so on].

3.4.2.7. Calculation of the Energy Characteristics of the Pump

The universal energy pump characteristics H/ω^2, N_H/ω^3, $\eta_H = f(Q/\omega)$ is calculated by means of equations (3.82), (3.63) and (3.90) according to pressure, efficiency, characteristics and frequency of rotation corresponding to the design conditions.

The field of characteristics H, $\eta_H = f(Q)$ when $\omega = \text{const}$ are determined according to equations (3.83) and (3.91). The calculated relations are valid for $\omega \geq 0.5\ \omega_p$ (see Section 3.1.4.3). If the pump is designed with a spiral branch, then according to the indicated equations it is possible to calculate the energy characteristics in a wide range of the change in discharge $Q/\omega = (0\text{-}1.4)(Q/\omega)_p$. For a pump with a branch which has a circular vane diffuser, equations (3.82), (3.83), (3.90) and (3.91) should be used in the narrow range of $Q/\omega = (0.7\text{-}1.2)(Q/\omega)_p$.

3.4.3. CALCULATION OF THE FUEL PUMP

3.4.3.1. Selection of the Type of Pump

When the turbopump unit is not single-shaft or if the fuel pump has its drive, the rotation frequency of the shaft of the fuel pump is determined in the same way as the rotation frequency of the shaft of the oxidizer pump (see Section 3.4.2.1).

In the calculation of the single-shaft turbopump unit, the rotation frequency of the shaft of the fuel pump is known from the calculation of the oxidizer pump. Then the required value of the cavitation power-speed coefficient for the fuel pump $(C_{cps})_{\text{потр}}$ is determined according to the rotation frequency.

For a pump with a one-way inlet this value is determined by equation (3.163). If it appears that $(C_{срв})_{потр}$ does not exceed 3500-4000, then the pump can be designed with a one-way inlet. In such a case, when $(C_{срв})_{потр}$ exceeds the indicated value, one should discuss the calculation of the pump with a two-way inlet.

With the two-way the discharge, decreased two times, is substituted inlet to equation (3.163). If it appears that $(C_{срв})_{потр.двухст}$ exceeds 3500-4000, then it is necessary to use in the fuel feed system of the engine a booster pump, and the main fuel pump for the sake of simplicity in the design is made with a one-way inlet. Depending on which of these three cases is examined, the order of calculation of the screw conveyor is changed.

3.4.3.2. Calculation of the Screw Conveyor of a Pump with a One-way Inlet

Just as in the case of the oxidizer pump (see Section 3.4.2), depending on the arrangement of the fuel pump in the turbopump unit, the type of feed is changed. Furthermore, the diameter of the screw conveyor can either be determined by the transmitted moment or be selected from design considerations. In the first case, according to equations (3.219)-(3.220), the diameter of the hub of the screw conveyor is estimated, and according to equation (3.218) - the coefficient $K_{d_{вт}}$. According to value $(C_{срв})_{потр}$ and $K_{d_{вт}}$ with the aid of Fig. 3.89 the coefficient $K_{D_э}$ and then $D_э$ and $D_ш$ are determined.

In the second case when the diameter of the hub is selected from design considerations, it is possible to assume that $\bar{d}_{вт} = 0.15\text{-}0.25$. From Fig. 3.89, using value $(C_{срв})_{потр}$, one

should find values $K_{D_э}$, which correspond to $K_{d_{вт}} = 0, 2, 4$, and determine the appropriate values of $\bar{d}_{вт} = \frac{K_{d_{вт}}}{\sqrt{K^2_{D_э} + K^2_{d_{вт}}}}$.

For value $\bar{d}_{вт}$, selected in the range of 0.15-0.25 we determine $K_{d_{вт}}$, $K_{D_э}$, and then $D_э$, $D_ш$, $d_{вт}$. After determining the basic geometric dimensions of the screw conveyor ($D_ш$, $d_{вт}$) the calculation of the screw conveyor of the fuel pump is produced just as the calculation of the screw conveyor of the oxidizer pump (see Section 3.4.2.4).

3.4.3.3. Calculation of the Screw Conveyor of a Pump with a Double Inlet

Depending on the location of the fuel pump with a two-way inlet, just as in the case of the oxidizer pump, the power transmitted by the screw conveyor shaft is determined. According to power with the aid of relations (3.218), (3.219) and (3.220), value $K_{d_{вт}}$ is determined. According to Fig. 3.89, by knowing $(C_{срв})_{потр.двухст}$ and $K_{d_{вт}}$; $K_{D_э}$, and then $D_э$ and $D_ш$ are determined. Further calculation of the screw conveyor is conducted in the same way as the calculation of the screw conveyor of the oxidizer pump (see Section 3.4.2.4).

3.4.3.4. Calculation of the Screw Conveyor of a Fuel Pump in the Use of a Booster Pump in the Feed System

In order to decrease the necessary pressure of the booster pump and thus to reduce the expenditure of energy necessary for its drive, one should design a main screw-centrifugal pump with the best anticavitation qualities [see equation (3.196)].

Depending on whether or not the screw conveyor of the fuel pump transmits considerable power, we determine $K_{d_{вт}}$ according to equations (3.218)-(3.219) or select $\bar{d}_{вт}$ in the range of 0.15-0.25.

With respect to $K_{d_{вт}}$ or $\bar{d}_{вт}$ with the aid of Fig. 3.89, we determine $(C_{cpв})_{max}$ and the corresponding value $K_{D_э}$. Then according to the known value ω and according to $K_{D_э}$, we determine $D_э$, $D_ш$, $d_{вт}$. Further the calculation of the screw conveyor of the fuel pump is conducted in the same way as the calculation of the screw conveyor of the oxidizer pump.

3.4.3.5. Calculation of the Centrifugal Wheel, Branch and Energy Characteristics of the Fuel Pump

The calculation of the centrifugal wheel of the fuel pump and branch and the calculation of its energy characteristics are conducted in the same way as for the oxidizer pump (see Sections 3.4.2.5-3.4.2.7).

3.4.3.6. Features of the Calculation of Hydrogen Pumps

The low density of hydrogen and its noticeable dependence on pressure and temperature condition the features of the calculation of hydrogen pumps. At outlet pressures from the pump of 200-300 bar, the required pump heads are $(300\text{-}400)\cdot10^3$ J/kg. Therefore, hydrogen pumps for LPRE, as a rule, must be made centrifugal and multistage. For the sake of simplicity in the design, the first stages are made with a one-way inlet. With high thrusts the volumetric flow rate of hydrogen through the pump increases, and the use of centrifugal pumps can prove to be unsuitable, since they are very bulky. In view of this, with high volumetric flow rates of the liquid hydrogen, the use of axial multistage pumps can prove to be advisable.

To decrease the number of stages of the hydrogen pump the rotation frequency of the pump shaft should be as large as

possible. An increase in the rotation frequency is limited by the strength of the wheel. According to conditions of strength, the circular velocity on the outside diameter of the wheel should not exceed 400-450 m/s. For a decrease in the tank pressure of the rocket or a decrease in the value of the required pressure of the booster pump (if in system installation of the booster pump is provided for) the first stage of the pump should be made with a screw conveyor.

The initial data for calculating the hydrogen pump are the same as for the calculation of pumps which operate on ordinary components of fuel (see Section 3.4.1); the same is true for the purpose of the calculation. Only in the calculation of the hydrogen pump does there appear the need for the determination of the temperature and density of hydrogen at the outlet from the pump for calculating the subsequent engine units. Since hydrogen is a liquid with noticeable compressibility, the temperature and density of hydrogen at the outlet from the pump can considerably differ from their values at the inlet.

In connection with the insignificant change in pressure and temperature at the inlet part of the pump, in the calculation for cavitation the density and temperature are taken equal to those assigned at the inlet into the pump. At the present time there are no reliable methods of calculating the positive effect of thermodynamic properties of liquid hydrogen on the anti-cavitation qualities of the pump. Therefore, the calculation for cavitation is conducted without allowing for this effect - the expected improvement in the anticavitation properties goes into a reserve.

The feature of the calculation of a hydrogen pump consists in an account of the compressibility of hydrogen in the determination of the pump head necessary for providing the assigned outlet pressure of the pump.

The pressure of the hydrogen pump (when $c_{вх} = c_{вых}$), just as that of the pump which operates on the working substance being compressed (see Section 2.14), is determined from the equation

$$H_{н.д} = H = \int_{p_{вх}}^{p_{вых}} v\,dp = \int_{p_{вх}}^{p_{вых}} \frac{dp}{\rho}. \qquad (3.231)$$

If losses in pump are absent, then the process in the pump would be adiabatic (we examine the pump which is heat-insulated from the environment). The adiabatic process is depicted in p-v coordinates by line $1\text{-}2_{ад}$ (see Fig. 2.93). In the presence of losses the process of compression will be polytropic, i.e., line 1-2 in Fig. 2.93 (line 1-2 in Fig. 2.92 characterizes the process of the pressure increase of an incompressible fluid). The nature of the course of the polytropic compression curve depends on the magnitude of losses in the pump. With a decrease in the losses the polytropic curve approaches an adiabatic curve (with an increase in the losses the specific volume increases).

Thus, an increase in the specific volume of hydrogen in connection with the heat feed of losses is compensated by a decrease in the volume as a result of its compressibility. Therefore, even with a considerable increase in the pressure the density of the fluid hydrogen can be changed insignificantly. On the basis of the fact that the specific volume and density are not greatly changed, for determining the pressure it is possible to use equation (1.11), which is intended for determining the pressure of the incompressible fluid:

$$H = \frac{p_{вых} - p_{вх}}{\rho_{ср}}, \qquad (3.232)$$

where $\rho_{ср} = \frac{\rho_{вых} + \rho_{вх}}{2}$ is the mean mass density.

We will use equation (3.232) in determining the pressure of the hydrogen pump.

The number of stages of the pump z is determined by the required pump head H and permissible magnitude of pressure of the stage $(H_{ступ})_{max}$ [see equation (3.230)]:

$$z = H/(H_{ступ})_{max},$$

where z is rounded off to integer. Since in this case the parameters of hydrogen at the outlet are not known, then, assuming in the first approximation $\rho_{ср} = \rho_{вх}$ from equation (3.232) we obtain

$$H = \frac{p_{вых} - p_{вх}}{\rho_{вх}}. \qquad (3.233)$$

The pressure of the stage according to the accepted z is determined in the following manner:

$$H_{ступ} = \frac{H}{z}. \qquad (3.234)$$

According to the pressure of the stage $H_{ступ}$ and the value of the rotation ω frequency known from the calculation for cavitation, let us determine the power-speed coefficient of the stage:

$$n_s^* = 193{,}3\omega \frac{\sqrt{Q}}{H_{ступ}^{3/4}}, \qquad (3.235)$$

where we assume that

$$Q = G/\rho_{вх}. \qquad (3.236)$$

According to the power-speed coefficient n_s^*, assuming that K_{D_0} = 5.2-6.5, with the aid of the dependences given on

Figs. 3.38 and 3.39 and equation (3.62), let us estimate the efficiency of the pump $\eta_н = \eta_{ступ}$ and determine the pump power:

$$N_н = \frac{GH}{\eta_н}.$$

The pump power determines an increase in the enthalpy of the fluid in the pump:

$$\Delta i = i_{вых} - i_{вх} = \frac{N_н}{G} = \frac{H}{\eta_н}. \qquad (3.237)$$

Let us plot in the i-s-diagram [i-s-diagram of liquid hydrogen (parahydrogen) the value Δi borrowed from work [111], depicts on Fig. 3.109, see insert] from point 1 (Fig. 3.110) which characterizes the hydrogen parameters at the inlet into the pump. The intersection of the straight line $i_{вых}$ = const with isobar $p_{вых}$ = const gives point 2, which determines the parameters at the outlet from the pump. By knowing $p_{вых}$, it is possible to refine the pump head according to equation (3.232) and then the number of stages and the pressure which is necessary for one stage.

The calculation of the first stage of the hydrogen pump is performed just as it is done for ordinary pumps (see section 3.4.3). Dimensions of the subsequent stages are taken in the same way as dimensions of the first stage, with the exception of the diameter of the inlet into the wheel. Since the diameter of the inlet into the wheel of the first stage is determined on the basis of conditions of the provision for the necessary anticavitation qualities, then the diameter of subsequent stages can be taken less (K_{D_0} = 3.5-4.5). This somewhat decreases losses in subsequent stages basically because of flow losses. Remaining losses and pressure should not be changed, since the

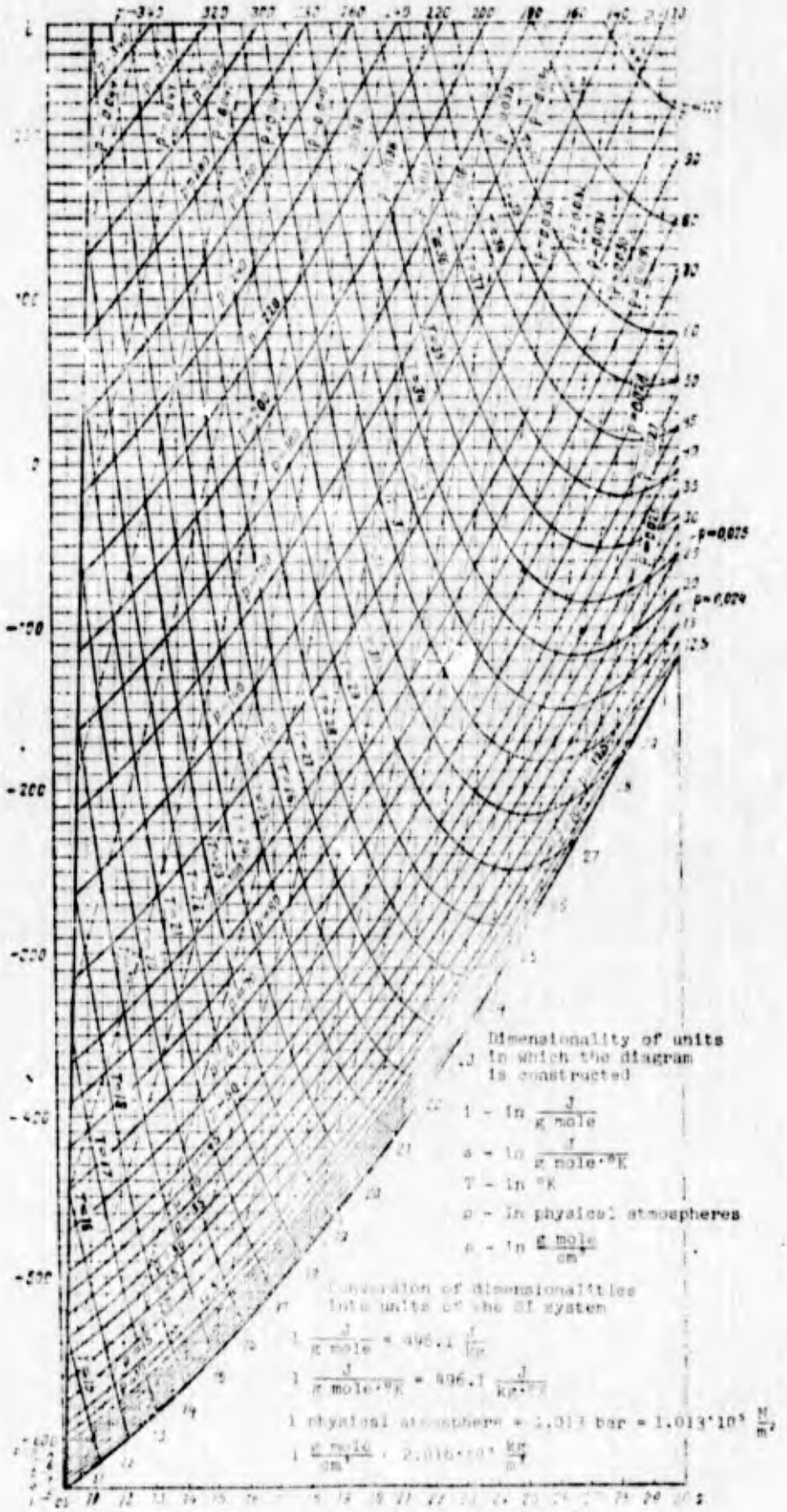

Fig. 3.109. An l-s diagram of liquid hydrogen (parahydrogen). Molecular mass of hydrogen is equal to 2.0158.

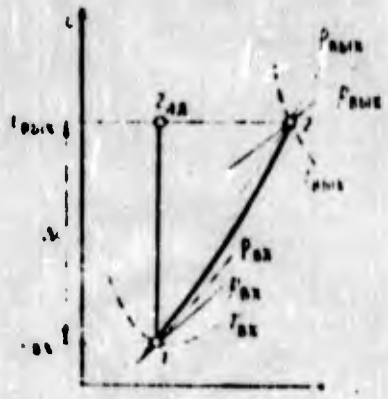

Fig. 3.110. Graph of the process in the hydrogen pump in the i-s-diagram.

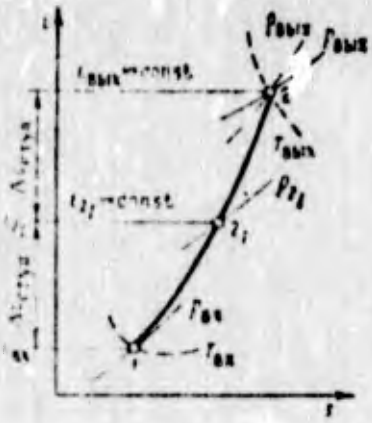

Fig. 3.111. Graph of the process in a two-stage hydrogen pump in i-s-diagram.

relative diameter $\bar{D}_1$ of the first stage of the hydrogen pump does not exceed the values, after which the hydraulic efficiency and coefficient K_z decrease. With a sufficient degree of accuracy it is possible to assume that the efficiency and pressure for the subsequent stages of the pump will be the same as those of corresponding values for the first stage.

In summation of the calculation it follows to check to see if the pump provides the assigned pressure and what the temperature and density of the hydrogen are at the outlet from the pump. For this it is necessary to calculate an increase in the enthalpy of hydrogen in the stage:

$$\Delta i_{ст} = i_{вых} - i_{вх}$$

Let us plot this value from point 1 (inlet into the pump, inlet into the first stage) (Fig. 3.111). The point which corresponds to the state of hydrogen at the outlet from the first stage must be located on line $i_{2_I} = \text{const}$. Being assigned several values of pressure on this line, we find such pressure p_{2_I} at which the equality (3.232) recorded for stage

is satisfied. This will be the pressure at the outlet from the first stage. Curve $1\text{-}2_I$ is the polytropic curve of compression of hydrogen in the first stage with uniform heat feed of losses in the compression process.

Parameters of hydrogen at the outlet from subsequent stages are determined analogously. The point which corresponds to the outlet from the last stage will determine the pressure $p_{вых}$ temperature and density of the hydrogen at the outlet from the pump (on Fig. 3.111, plotted for the two-stage pump, this will be point 2). If the pressure $p_{вых}$ differs from that assigned by more than 5%, the calculation of the hydrogen pump should be repeated, utilizing the obtained value of the density of hydrogen at the outlet from the pump.

3.4.4. AN EXAMPLE OF THE CALCULATION OF THE PUMP

Let us examine the calculation of the pump of LPRE in the example of a pump of a screw-centrifugal oxidizer. Let us assume that the oxidizer pump is designed for the turbopump unit with the precombustion-chamber turbine operating on an oxidizing gas. Then the oxidizer pump should be placed on the diagram shown on Fig. 3.107 nearer to the turbine.

In such a circuit the feed of the component to the pump is impossible to make in an axial way. Let us select circular input branch. In connection with the fact that the required pump head (see item 10 in Table 3.2) is less than the maximum permissible for one stage [see equation (3.230)], the pump can be made single-stage.

From considerations of the simplicity of design and decrease in mass, let us select the pump with a one-way inlet.

Table 3.2 gives the initial data for calculating and the calculating values. Figure 3.112 shows the flow part of the calculated pump traced on the basis of the obtained calculating values. On the same figure, for the calculated pump, velocity triangles and energy characteristics are given.

Table 3.2

No.	Name of Quantity	Notation	Number of equation	Dimension	Numerical value	Remark
1	2	3	4	5	6	7
	I. Initial data					
1	Working medium of pump - nitrogen tetroxide (oxidizer)	-	-	-	-	-
2	Mass flow rate of component through pump	G	-	kg/s	42	-
3	Total pressure of feed	$p^{s}_{вых}$	-	bar	240	-
4	Minimum total pressure at inlet into pump	$p^{s}_{вх}$	-	bar	4	-

1	2	3	4	5	6	7
5	Maximum temperature of component at inlet	$T_{ex\ max}$	-	°K	333	-
6	Density of component	ρ	-	kg/m^3	1400	-
7	Pressure of vapors at T = 333°K	p_n	-	bar	2.28	-
8	Kinematic viscosity of component	v	-	m^2/s^2	$5 \cdot 10^{-6}$	-
	II. Calculation values					
9	Volume flow rate of component	Q	(1.6)	m^3/s^3	0.03	-
10	Required pump heads	H	(1.9)	J/kg	16,800	-

1	2	3	4	5	6	7
	a) Determination of rotation frequency and the calculation of the screw conveyor					
11	Cavitation reserve of pressure at inlet into pump	$\Delta p_{зад}$	-	bar	0.28	Is assigned
12	Permissible cavitation drop in total pressure	$\Delta p^{*}_{срв}$	(3.142)	bar	1.44	-
13	Power of fuel pump	$N_{н.г\ р}$	-	W	$1000 \cdot 10^3$	Is determined in calculation of the turbopump unit (see Section 5.1)
14	Coefficient of hub of screw conveyor	$K_{d_{вт}}$	(3.221)	-	2.67	Is assigned $\frac{d_{вт}}{d_в} = 1.2$

1	2	3	4	5	6	7
15	Maximally attainable value of cavitation power-speed coefficient	$(C_{cpe})_{max}$	-	-	3840	Determined from Fig. 3.90
16	Coefficient of equivalent diameter of screw conveyor	K_{D_e}	-	-	7.5	Determined from Fig. 3.90
17	Rotation frequency of pump	ω	(3.217)	s^{-1}	2410	-
18	Power-speed coefficient	n_s	(2.179)	-	54	-
19	Flow parameter of pump	q_p	-	-	0.05	Is assigned proceeding from form of head characteristic (see Fig. 3.54). Usually $0 < q_p < 0.2$

1	2	3	4	5	6	7
20	Diameter of hub of screw conveyor	d_{BT}	(3.218)	m	0.03	-
21	Equivalent diameter of screw conveyor	D_e	-	m	0.0816	See equations in Section 3.3.7
22	Outside diameter of screw conveyor	D_w	-	m	0.086	The same
23	Coefficient of outside diameter of screw conveyor	K_{D_w}	-	-	8	"
24	Mean diameter of screw conveyor	D_{cp}	-	m	0.058	See items 20 and 22
25	Inlet velocity of screw conveyor	c_{1z}	(2.3)	m/s	5.9	Determined approximately η_p from Fig. 3.35. Calculation of velocities is

1	2	3	4	5	6	7
						conducted on Q' [see equation (2.255')]: $\eta_p = 0.97$
26	Circular velocity on periphery of screw conveyor	u_n	(2.1)	m/s	108	-
27	Ratio of velocities	$c_{1z}u$	-	-	0.054	-
28	Coefficient of diameter of inlet into centrifugal wheel	K_{D_0}	-	-	8	Is assigned $L_{D_0} = K_{D_w}$ ($D_0 = D_w$)
29	Ratio of diameters of centrifugal wheel (in first approximation)	D_1/D_2	(3.5) and (3.59)	-	0.52	Is assigned $\varphi = 0.85$

1	2	3	4	5	6	7
30	Form of screw conveyor insert ($D_0 = D_w$)	-	-	-	-	$D_1/D_2 < 0.55$ (see Section 3.4.2.4)
31	Losses in underwater branch	$\frac{\Delta p^*_{\text{пов}}}{\rho}$	(2.199)	J/kg	21	Is assigned $\xi_{\text{пов}} = 1.3$
32	Permissible cavitation drop in total pressure at inlet into screw conveyor	Δp^*_{1cps}	(3.155)	bar	1.15	We assume m = 1
33	Cavitation coefficient of centrifugal wheel	$\lambda_{\text{cps.u}}$	(3.173)	-	0.117	Is assigned $\delta/\delta_0 = 0.615$ $\chi = 0.75$
34	Ratio of velocities at outlet from screw conveyor on periphery	$\frac{c_{2u_n}}{u_n}$	(3.175)	-	0.16	Is assigned $\eta_{\text{s.w.n}} = 0.4$; $D_1/D_w = 1$

1	2	3	4	5	6	7
35	Angle of blades on periphery of screw conveyor (in first approximation)	$\beta_{л.л}$	(3.176)	-	3°39'	We assume $s_1 = s_2 = s$
36	Angle of flow entry on periphery	$\beta_{1л}$	-	-	3°02'	From input velocity triangle
37	Angle of attack	$i_л$	-	-	2°	Is assigned, since by calculation the angle is too small, $i_л$ = 37' (see equation (3.179)]
38	Angle of blades of screw conveyor on periphery (refined)	$\beta_{л.л}$	(3.179)	-	5°02'	-
39	Pitch of the screw conveyor	s	(3.181)	m	0.024	-

1	2	3	4	5	6	7
40	Cavitation coefficient of screw conveyor	λ_{1cps}	-	-	0.012	We determine from Fig. 3.87 ($c_{1z}u_n < 0.06$--0.08)
41	Obtained value of cavitation pressure drop at inlet into screw conveyor	Δ_{1cps}	(3.132)	bar	0.98	We determine w_1 from the velocity triangle
42	Obtained value of cavitation drop in total pressure	Δp^*_{cps}	(3.155)	bar	1.5	Difference between obtained and allowed values does not exceed 5% (see item 12)
43	Angle of taper of screw conveyor at inlet	θ_1	-	-	120°	Is assigned taking into account recommendations given in Section 3.3.7
44	Angle of taper at outlet	θ_2	-	-	160°	Is assigned taking into account recommendations given in Section 3.3.7

1	2	3	4	5	6	7
45	Cascade density of screw conveyor	τ_{cp}	-	-	2.5	Is assigned taking into account recommendations given in Section 3.3.7
46	Number of blades of screw conveyor	z_w	-	-	2	The same
47	Axial length of screw conveyor	$l_{z\ w}$	(3.186)	-	0.045	-
48	Length of blade of screw conveyor on mean diameter	$b_{л.cp}$	(3.183)	m	0.224	-
49	Angle of blades at mean diameter	$\beta_{л.cp}$	(2.150)	-	7°	-
50	Sharpening of leading edge of profile	$b'_{cp}/b_{л.cp}$	-	-	0.4	Is assigned

1	2	3	4	5	6	7
51	Sharpening of trailing edge of profile	$b''_{ср}/b_{л.ср}$	-	-	0.2	Is assigned
52	Maximum relative thickness of profile b) Circular intake pipe	$\frac{\delta_{ср\ max}}{b_{л.ср}}$	-	-	0.015	Is assigned
53	Inlet velocity of inlet branch	$c_{вх}$	-	m/s	4.7	Is assigned $c_{1z}/c_{вх} = 1.22$
54	Intake area of branch	$F_{вх}$	(2.3)	m^2	$6.36 \cdot 10^{-3}$	-
55	Diameter of inlet	$D_{вх}$	-	m	0.09	-
56	Diameter of outlet from branch	D	-	m	0.088	Is assigned $D/D_{ш}$-1.022

1	2	3	4	5	6	7
	c) Centrifugal wheel					
57	Mean diameter of leading edges of the impeller vanes	D_1	-	m	0.073	Is assigned $D_1/D_w = 0.85$ (see items 22 and 29)
58	Width of blades at inlet	b_1	(3.222)	m	0.029	See items 20, 28 and 57
59	Meridian velocity at inlet into wheel	c_{1m_n}	(2.3)	m/s	7.9	-
60	Flow angle at the inlet into wheel	β_1	-	-	5°10'	From velocity triangle, assuming $(c_{2u}')_w = (c_{1u}')_n$
61	Angle of blades at inlet	β_{1n}	-	-	15°	Is assigned by angle of attack $i_n = 9°50'$

1	2	3	4	5	6	7
62	Outside diameter of wheel	D_2	-	m	0.140	Is determined from value D_1/D_2 (see item 29)
63	Angle of blades at outlet	$\beta_{2л}$	(3.227)	-	38°	Is assigned $F_1F_2 = 0.6$ [see equation (3.224)]
64	Width of blades at outlet	b_2	(3.225)	m	0.0105	-
65	Meridian velocity	c_{2m}	(2.19)	m/s	6.55	-
66	Ratio of speeds	c_{2m}/u_2	-	-	0.039	We refine q_p(q_p = 0.05)
67	Quantity of impeller vanes	z	-	-	6	Is assigned
68	Coefficient of the effect of number of blades	k_z	-	-	0.767	Determined from Figs. 3.11-3.13

1	2	3	4	5	6	7
69	Hydraulic efficiency of pump	η_r	(3.31)	-	0.83	-
70	Theoretical pressure	H_T	(3.1)	J/kg	20,250	-
71	Theoretical pressure with infinitely large number of blades	$H_{T\infty}$	(2.130)	J/kg	26,400	-
72	Circular velocity	u_2	(3.228)	m/s	167.5	-
73	Outside diameter of wheel	D_2	(3.229)	m	0.140	-
74	Circular velocity component at outlet from wheel at infinitely large number of blades	c_{2u}^{∞}	(3.65)	m/s	159	-
75	Circular velocity component	c_{2u}	(3.7)	m/s	122	-

1	2	3	4	5	6	7
76	Flow angle at outlet d) Spiral branch	α_2	-	-	3°04'	From velocity triangle
77	Radius of inlet into branch	R_2	-	m	0.0735	Is assigned $R_2/r_2 = 1.05$
78	Width of branch	b	-	m	0.020	Is assigned taking into account width b_2
79	Area of inlet into conical diffuser	f_3	(3.23)	m^2	$2.8 \cdot 10^{-4}$	-
80	Height of inlet into diffuser	$h_д$	-	m	0.014	See items 78 and 79
81	Equivalent diameter of inlet into diffuser	d_3	-	m	0.0188	See Section 3.1.1.4

1	2	3	4	5	6	7
82	Outlet velocity of diffuser (outlet from pump)	$c_{вых}$	-	m/s	20	Is assigned
83	Area of outlet of diffuser	$F_{вых}$	-	m^2	$15 \cdot 10^{-4}$	-
84	Diameter of outlet of diffuser	$D_{вых}$	-	m	0.045	-
85	Length of diffuser	$l_д$	-	m	0.085	Is assigned $l_д/d_3 = 4.5$
86	Length of section of diffuser with constant cross section	$l'_д$	-	m	0.025	Is assigned $l'_д/l_д = 0.3$
	e) Losses, power and efficiency of pump					

1	2	3	4	5	6	7
87	Losses in branch	$L_{отв}$	(3.28)	J/kg	1640	Is assigned $\xi_{отв} = 0.22$
88	Hydraulic efficiency of screw-centrifugal wheel	$\eta_{г.к}$	-	-	0.911	See equations in Section 3.1.1.5
89	Efficiency of branch	$\eta_{отв}$	-	-	0.91	The same
90	Static head of wheel	$H_{ст}$	(3.39)	J/kg	10930	-
91	Pressure lost in seal of centrifugal wheel	L_y	(3.38)	J/kg	9100	Is assigned R_y 0.045 m
92	Radial clearance in seal	δ_y	-	m	$0.1 \cdot 10^{-3}$	Is assigned
93	Width of seal	l_y	-	m	0.01	Is assigned $l/\delta = 100$

1	2	3	4	5	6	7
94	Leakage through front seal	Q_{y1}	(3.32)	m^3/s	0.0016	We assume $\mu = 0.4$
95	Leakage of pump	Q_y	-	m^3/s	0.0024	We assume $Q_{y2} = 0.5Q_{y1}$
96	Flow efficiency	η_p	(3.53)	-	0.98	Divergence with previously found value less than 5%
97	Circular energy	N_u	(2.233)	W	$940 \cdot 10^3$	-
98	Reynolds number of centrifugal wheel	Re	(2.202b)	-	$2.35 \cdot 10^6$	-
99	Coefficient of friction of wheel disks against the fluid	$C_{тр.д}$	(2.202a)	-	$2.07 \cdot 10^{-3}$	-
100	Power of disk friction	$N_{тр.д}$	(2.202)	W	$128 \cdot 10^3$	-

1	2	3	4	5	6	7
101	Internal power of pump	$N_{вн}$	(2.244)	W	$1040 \cdot 10^3$	-
102	Disk efficiency	$\eta_д$	(2.239)	-	0.88	-
103	Internal power efficiency	$\eta_{вн\ N}$	(2.256)	-	0.68	-
104	Mechanical efficiency	$\eta_{мех}$	-	-	0.95	Is assigned
105	Overall efficiencies of pump	η_1	(3.62)	-	0.645	-
106	Net power of pump	$N_{н.пол}$	(2.223)	W	$750\ 10^3$	-
107	Power input of pump	$N_н$	(2.247)	W	$1167 \cdot 10^3$	

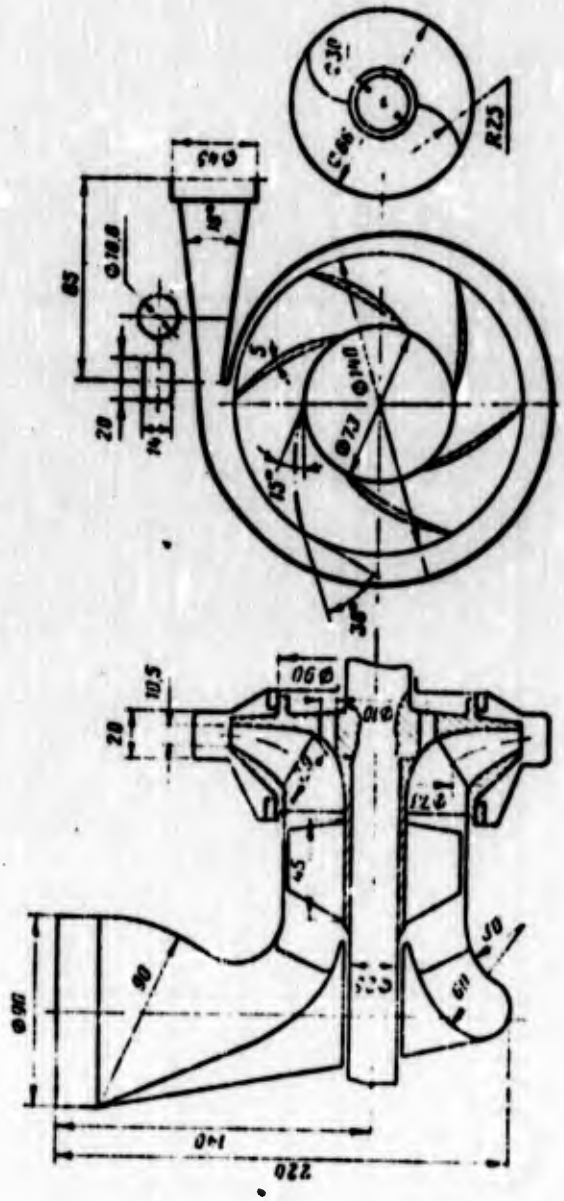
R25
220
140

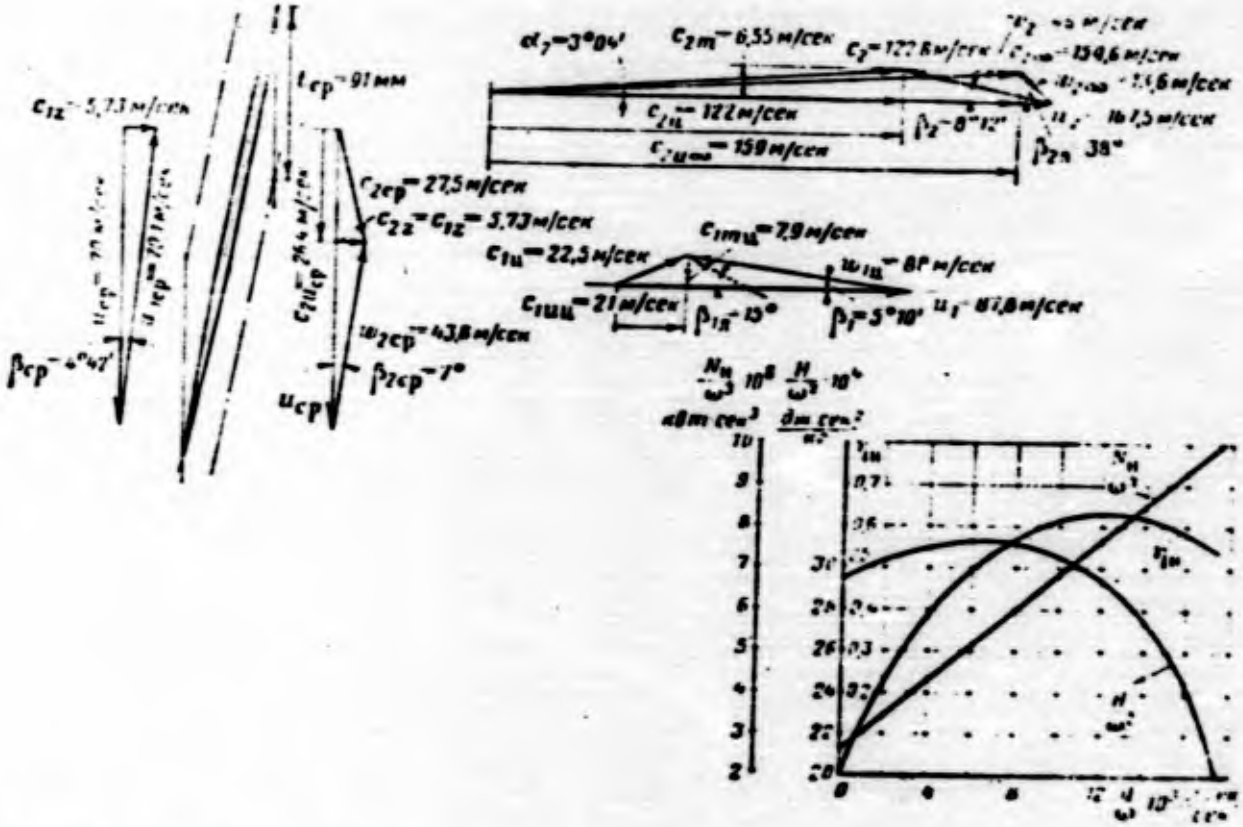

Fig. 3.112. Example of calculation of a pump.
Designations: м/сек = m/s, мм = mm,
квт·сек³ = kW·s³, $\frac{\text{л·сек}}{\text{сек}} = \frac{\text{l·s}}{\text{s}}$, $\frac{\text{дж·сек}^2}{\text{кг}} = \frac{\text{J·s}^2}{\text{kg}}$.

CHAPTER 4

TURBINES OF LIQUID-PROPELLANT ROCKET ENGINES

4.1. BASIC FEATURES OF TURBINES OF LIQUID-PROPELLANT ROCKET ENGINES

In liquid-propellant rocket engines autonomous or precombustion-chamber turbines are used (see Section 1.4). We will discuss the features of these turbines.

4.1.1. FEATURES OF AUTONOMOUS TURBINES

The value of the required power of the turbine of the turbopump unit [TU] (ТНА) of the rocket engines [LPRE] (ЖРД) is determined by the necessary power for the pump drive:

$$N_т = \sum N_н.$$

The greater the thrust of the engine plant, the more the required power of the turbine. The fulfilled engines have turbines with a power of tens to hundreds and thousands of kilowatts.

With the assigned magnitude of the power $N_т$ parameters of the autonomous turbine should be selected with such that the flow-rate of the working medium through the turbine would be minimum (see Section 1.4.1.).

The requirement for the minimum flow-rate of the working medium (at the assigned energy) denotes the need for the obtaining of the maximum value of specific work of the turbine (or, in other words, the power which is necessary for the gas flow rate equal to 1 kg/s):

$$L_т = \frac{N_т}{G_т}\left[\frac{кг}{(кг/с)} : \frac{Дж}{кг}\right]. \qquad (4.1)$$

With $G_т \to \min$, $L_т \to \max$;

$$L_т = L^*_{aт}\eta_т. \qquad (4.2)$$

In turbines of LPRE the specific work $L_т$ is 400-800 kJ/kg.

Since the value of efficiency of the turbine is limited ($\eta_т < 1$), the maximum value of the specific work $L_т$ [see equation (4.2)] can be obtained with an increase in the adiabatic work $L^*_{aт}$, although the efficiency of the turbine is lowered with increase in $L^*_{aт}$. Hence there ensues the feature of autonomous turbines of LPRE consisting in the fact that because of the need for the operation of these turbines with the low flow-rate of the working medium it is important to obtain not the maximum value of the efficiency of the turbine, but a high value of the specific work $L_т$, which is provided by the high adiabatic work $L^*_{aд}$. However, at the assigned adiabatic work $L^*_{aд}$ an increase in the value of the efficiency of the turbine increases the specific work of the turbine $L_т$ [see equation (4.2)] and decreases the required flow rate of the working medium $G_т$ [see equation (4.1)].

The requirement for the maximum capacity $L_т$, obtained from 1 kg of mass of the working medium, means that with the assigned magnitude of circular velocity, which is determined by the diameter of the turbine and frequency of its rotation, usually equal to the frequency of rotation of the pumps, the operating factor

$$\bar{L}_т = L_т/u^2 \qquad (4.2a)$$

should be maximum. The diameter of the turbine is selected taking into account the layout and provision for the minimum overall dimensions or is limited by strength of the turbine rotor.

Since greater adiabatic work makes it possible to obtain greater specific work $L_т$, then parameters of the turbine should be selected such that the value of the adiabatic work is as large as possible.

From the equation for adiabatic work

$$L_{ад} = \frac{k}{k-1} RT_0^* \left(1 - \frac{1}{\delta^{\frac{k-1}{k}}}\right), \qquad (4.3)$$

where $\delta = p_0^*/p_2$ is the pressure ratio in the turbine, it follows that with the selected working medium (assigned values k and R) large values of the adiabatic work can be achieved with the use of high temperatures of the working medium and high pressure ratios.

In autonomous turbines a reducing gas is more frequently used, i.e., the gas generator operates on an excess of fuel (see Section 1.4.1), since the product RT_0^* for such a gas is more than the corresponding value for the oxidizing gas. The use of high temperatures is restricted to the work of the design. In LPRE uncooled turbines, simpler and lighter, are used. The temperature in front of the uncooled turbine is limited to the value of 1000-1200°K.

High pressure ratios are reached by an increase in the initial pressure p_0^*, since the value of the counterpressure p_2 is selected depending on the pressure of the medium, where the gas is ejected, or depending on the pressure at the inlet into the control nozzles of the engine, if the gas after the turbine enters into the nozzles, or depending on the pressure in the tank, if the gas pressurizes the tank.

In the first case, in order to eliminate the effect of the change in atmospheric pressure $p_{атм}$ on the work of the turbine,

the pressure p_2 at the turbine exhaust is selected such that it is more than the critical pressure determined by $p_{атм}$:

$$p_2 \geqslant \delta_{кр} p_{атм},$$

where

$$\delta_{кр} = \left(\frac{k+1}{2}\right)^{\frac{k}{k-1}} \qquad (4.4)$$

is the critical pressure ratio. Here in the minimum cross section of the outlet device of the turbine the speed of sound is established, and a change in the pressure of the external medium will not affect the operation of the turbine. In the case of the feed with gas of the control nozzles, the speed of sound is established in the minimum cross section of the control nozzle.

At the assigned outlet pressure, the pressure ratio of the turbine is determined by the selection of inlet pressure of the turbine. With an increase in δ $L^*_{ад}$ increases, but the efficiency of the turbine decreases. For the obtaining of the maximum operation of the turbine, there is an optimum value of the pressure ratio in the turbine δ. The optimum pressure ratios δ are usually greater than those which are selected in practice. The value of the initial pressure in front of the turbine (pressure in the gas generator) is determined by pressure after the pumps with the subtraction of the resistance of the main lines of the gas generator. Usually the initial pressure in front of the turbine is limited by the value of 6-10 MN/m^2. The pressure ratio in this case reaches values of 20-50. Consequently, the autonomous turbines of LPRE are high-pressure differential turbines. This is one of the basic features of autonomous turbines of LPRE.

From considerations of simplicity of design and decrease in mass, autonomous turbines are made single-stage and seldom two-stage. During function in the small number of stages of high pressure differentials, the rates of the flow of the gas become supersonic. The supersonic rates of flow are also a feature of autonomous turbines of LPRE.

One additional feature of autonomous turbines of LPRE is the fact that they are frequently made with the gas feed to the blade row of the rotor not over the entire circumference but over part of it. With the low gas flow rate the feeding of gas to the rotor wheel over the entire circumference is possible only at a low height of the nozzle channels and rotor blades. An experiment showed that at the low height of the blades the efficiency of the turbine sharply falls. At the assigned height of the nozzle, with low flow rates of the working medium, the nozzle must be located not on the entire circumference but along part of it - in the form of segments or separate nozzles. Such a method of gas feed is called partial. The presence of partial admission is characteristic for many turbines of TU of LPRE.

A partial-admission turbine is always made impulse, since with partial admission, as a result of the spreading of the gas and its overflowing from the inlet into the wheel to the outlet on the arc not occupied with nozzles, it is not possible to maintain the pressure differential necessary for providing the reaction of the wheel, and with the introduction of the reaction losses to overflowing increase. The autonomous turbine of LPRE are always made impulse - even in the case of the gas feed over the entire circumference - as a result of the fact that for impulse turbines high operating factors $\bar{L}_т$ are characteristic.

4.1.2. FEATURES OF PRECOMBUSTION-CHAMBER TURBINES

For the turbine of the rocket engine made by the design with the gas feed from the turbine into the chamber, the assigned parameters, determined by parameters of the engine plant, are the outlet pressure of the turbine p_2 and gas flow rate through the precombustion chamber turbine at the selected gas temperature in front of the turbine T_0^*. Then from the condition of the equality of powers of the pump and turbine, the inlet pressure p_0^* is determined (see Chapter 5).

The outlet pressure of the turbine p_2 should be more than the pressure in the chamber by the value of resistances of the gas channel between the turbine and chamber.

The gas temperature in front of the turbine T_0^* is assigned on the basis of conditions of reliable working capacity of the design of the turbine and selected materials. The rated temperature is provided by appropriate conditions of the gas generator, i.e., by the specific relationship of the components $\kappa_{гг}$. Consequently, by assigning temperature, thereby the physical constants of the producer gas (R and k) are established.

The greater the temperature that can be allowed in front of the turbine, the less the pressure should be in front of the turbine. The determining consideration when selecting the temperature in front of the turbine is the reliability of the structural elements operating at high temperature. As a rule, the permissible temperature for the reducing gas T_0^* = 1000-1200°K and for the oxidizing gas, T_0^* = 700-800°K.

The gas flow rate through the precombustion-chamber turbine at the known temperature in front of the turbine is assigned. The quantity of component being passed entirely through the turbine is determined by the thrust and relationship of the components in the chamber, but the quantity of the component being added is determined by the relationship of components in the gas generator, i.e., in the last analysis by the temperature in front of the turbine (see Section 5.1.2.).

Usually in precombustion-chamber turbines the ratio of the initial pressure to the outlet pressure of the turbine is 1.2-1.8. The absolute value of the pressure in front of the turbine can reach dozens and hundreds of bars. Consequently, the precombustion-chamber turbines of LPRE are low-pressure (subsonic) and high-flow. The parameters of these turbines very substantially differ from parameters of turbines used for designs of LPRE with the ejection of the gas into the atmosphere.

In view of the high flow-rates through the precombustion-chamber turbine the specific work of the turbine at the assigned power is low, and therefore the operating factor of the turbine $\bar{L}_т$ is low - it is considerably less than that of autonomous turbines.

Usually in precombustion-chamber turbines the gas is fed over the entire circumference, but sometimes (in spite of the high gas flow rates), in connection with the high gas density, it is necessary to use the partial admission.

The efficiency of the turbine and pumps does not affect the outlet energy indices ($R_{уд}$) of the power plant as a whole, since the enthalpy of the gas coming out of the turbine and the enthalpy of components of fuel coming out of the pumps are used in the chamber; but as has already been indicated (see Section 1.4.2), the value of the efficiency plays a significant role for obtaining the minimum mass of the TU and the pipelines connected with it.

The higher the efficiency, the less the initial pressure in front of the turbine can be selected, thereby making the entire apparatus lighter. With low efficiencies of the pumps and turbine high pressures in front of the turbine are necessary, and this in turn requires high pressures after the pumps. There is (as will be shown in Section 5.1) a maximum pressure in front of the turbine, with the excess of which the energy of the turbine will be less than that necessary for driving the pump. Therefore, the precombustion-chamber turbines, just as the pumps, have the requirement that they should have high efficiency with minimum mass and sufficient simplicity and reliability of design. For an increase in efficiency, the precombustion-chamber turbines can be made with the degree of reaction 0.2-0.3. However, for a decrease in the axial force, we assign a lower degree of reaction, and frequently such turbines are even made impulse.

4.2. THE STAGE OF THE TURBINE (SINGLE-STAGE TURBINE). BASIC CONCEPTS AND RELATIONS

4.2.1. THE STAGE OF AN AXIAL-FLOW TURBINE

4.2.1.1. Change in the Parameters Along the Length of the Flow Area

Figure 4.1 schematically depicts a change in the pressure, velocity and temperature along the length of the flow area of the axial reactive stage (single-stage turbine). In the upper part of the figure a change in stagnation parameters is shown. Shown by a dashed line is a change in the stagnation pressure without losses (in the ideal case). The stagnation temperature and stagnation pressure in relative motion are less than they are in absolute motion.

From expressions for the stagnation enthalpies

$$i_{1}^{*}=i_{1}+\frac{c_{1}^{2}}{2} \tag{4.5}$$

and

$$i_{w_1}^{*}=i_{1}+\frac{w_{1}^{2}}{2} \tag{4.6}$$

the relationship between the stagnation temperatures in relative and absolute motions is derived:

$$T_{w_1}^{*}=T_{1}^{*}\left[1-\frac{k-1}{k+1}\left(2\lambda_{1}\lambda_{1w}\cos\alpha_{1}-\lambda_{1}^{2}\right)\right]. \tag{4.7}$$

Correspondingly, the stagnation pressure in the relative motion is thus expressed:

$$p_{w_1}^{*}=p_{1}^{*}\frac{\tau(\lambda_{1})}{\tau(\lambda_{w_1})}. \tag{4.8}$$

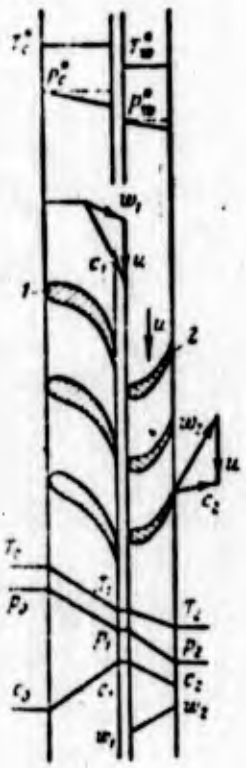

Fig. 4.1. Development of the cylindrical cross section of the flow area of the reactive stage of the turbine and a change in parameters of the gas along the length of the flow area: 1 - nozzle cascade; 2 - rotor cascade.

For the purpose of simplification in the recording subsequently in the index, which refers to the pressure of flow in absolute motion, the sign of the velocity c will be withdrawn; for example, instead of $p^*_{c_1}$ we will write p_1^*.

The reactive axial stage of the turbine is characterized by a change in the kinetic energy in relative motion on the basis of the general determination of the kinematic degree of reaction of the vane machine:

$$\rho_к = \frac{(w_2^2 - w_1^2)/2}{L_a} > 0.$$

Thus, for reaction turbine $w_2 > w_1$; corresponding to this, Fig. 4.1 shows a change in the relative velocity along the length of the flow area of the rotor wheel blades. The nature of the change in the flow areas of the vane channel is shown on Fig. 2.11.

A diagram of the flow area of the active stage of the turbine (single-stage turbine) is shown on Fig. 4.2. The meridian cross section and end view drawing can be the same as that of the reaction turbine (see Fig. 2.21). Figure 4.2 also gives a change in the parameters along the length of the flow area of the impulse turbine.

Fig. 4.2. Development of the cylindrical cross section of the flow area of the impulse stage of a turbine and a change in the parameters of gas along the length of the flow area: 1 - nozzle cascade; 2 - rotor cascade.

The impulse turbine is characterized by the equality of pressures of the inlet into the blades and at the outlet from the blades ($p_1 = p_2$) and by the equality of the relative inlet velocities and at the outlet ($w_1 = w_2$) (not allowing for losses). In impulse turbines the area of the inlet section of the vane channel differs little from the outlet area.

4.2.1.2. Thermal Degree of Reaction

Unlike the degree of reaction which in Chapter 2 we called kinematic, in turbines the concept of the thermal degree of reaction is used:

$$\rho_t = \frac{L_{0\,2}}{L_{0\,1}^{*}}, \qquad (4.9)$$

where $L_{ад2} = i_1 - i_2$ - the available adiabatic work on the impeller blades;

$L^*_{ад} = i^*_0 - i_2$ - the available adiabatic work of an entire stage of the turbine [see equation (4.3)].

If we express the kinematic degree of reaction by the ratio of heat differentials, then, taking into account that without allowing for losses and when $c_0 = 0$ heat differential of the nozzle box $L^*_{ад1}$ will be expressed as

$$l^*_{ад1} = \frac{c_1^2}{2} \quad \text{and} \quad l_{ад2} = \frac{w_2^2 - w_1^2}{2},$$

the expression for $\rho_к$ will be written in the form [see equation (2.102)]

$$\rho_к = \frac{l_{ад2}}{L_д} = \frac{l_{ад2}}{l^*_{ад1} + l_{ад2} - \frac{c_2^2}{2}} = \frac{l_{ад2}}{L^*_{ад} - \frac{c_2^2}{2}}. \qquad (4.10)$$

Let us establish the relationship between the kinematic and thermal degrees of reaction. The expression for $\rho_т$ (for an ideal turbine) can be written in the form [see equation (4.9)]

$$\rho_т = \frac{l_{ад2}}{L_д + \frac{c_2^2}{2}}; \qquad (4.11)$$

having divided expression (4.10) by (4.11), we obtain

$$\frac{\rho_к}{\rho_т} = 1 + \frac{c_2^2}{2L_д}. \qquad (4.12)$$

The thermal and kinematic degrees of reaction will be equal with each other when $c_2 = 0$, i.e., in the absence of energy losses with the outlet velocity. The thermal degree of reaction in essence determines the ratio of the available heat differentials, i.e., the available adiabatic work of the rotor wheel to the total available adiabatic work of the turbine. The kinematic degree of

reaction is greater in value than is the thermal. For the impulse stage of the turbine with the equality to zero of kinematic degree of reaction ($\rho_к = 0$), the thermal degree of reaction is equal to zero ($\rho_т = 0$). The thermal degree of reaction is widely applied in the analysis of the operation of turbines, because it is easy to determine, even without calculating the turbine and without determining the rates of gas flow.

For determining the thermal degree of reaction, it suffices to know the pressure ratio in front of the rotor wheel and after the rotor wheel to the full initial gas pressure. When c_p = const, from equation (4.9) we obtain

$$\rho_т = \frac{T_1 - T_{2t}}{T_0^* - T_{2t}}.$$

Passing over to the gas-dynamic functions, we obtain

$$\rho_т = \frac{\tau(\lambda_{c_{1t}}) - \tau(\lambda_{c_{2t}})}{1 - \tau(\lambda_{c_{2t}})}, \qquad (4.13)$$

where $\lambda_{c_{1t}} = f\left(\pi_1 = \frac{p_1}{p_0^*}\right)$; $\lambda_{c_{2t}} = f\left(\pi = \frac{p_2}{p_0^*}\right)$.

It is especially convenient to determine the thermal degree of reaction by using the graph of the process in the turbine in i-s coordinates.

Figure 4.3 depicts the i-s-diagram of an ideal (without hydraulic losses) reactive stage of a turbine. The available adiabatic work of the nozzle cascade is depicted by the segment 0-1, the available adiabatic work of the rotor wheel - by segment 1-2, and the adiabatic work of the entire turbine - by the segment 0-2. The ratio of the segment 1-2 to the segment 0-2 determines the thermal degree of reaction of the turbine.

The circular efficiency of the ideal turbine considers only losses with the outlet velocity:

$$\eta_u = \frac{L_u}{L_{ad}} = \frac{i_0^* - i_2^*}{i_0^* - i_2}.$$

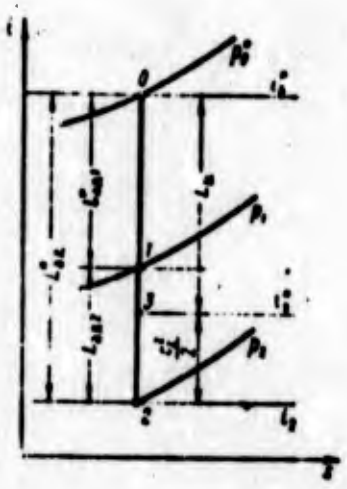

Fig. 4.3. Graph of the process of an ideal reactive stage of a turbine in i-s coordinates.

For an ideal active stage of the turbine, the i-s-diagram is represented on Fig. 4.4. Segment 0-1 corresponds to the adiabatic work of the nozzle cascade and simultaneously to the adiabatic work of the entire turbine, since they are equal. Segment 2-3 depicts losses with the outlet velocity, and segment 0-3 - the work of the circumference of the wheel. The circular efficiency of an ideal active stage of the turbine η_u is determined by the ratio of segments 0-3 and 0-1.

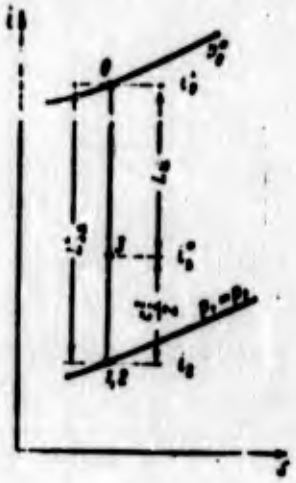

Fig. 4.4. Graph of the process of an ideal active stage of a turbine in i-s coordinates.

4.2.1.3. Representation of Real Processes of the Turbine in Thermal Diagrams

We will discuss primarily the process of the gas flow with expansion in the vane channels on the cascades, i.e., the flow in nozzle cascades.

The irreversible loss of mechanical energy in the nozzle cascade can be designated L_ϕ. It is obvious that

$$L_\phi = \frac{c_{1t}^2}{2} - \frac{c_1^2}{2}. \qquad (4.14)$$

Then having expressed L_ϕ by the speed factor ϕ (see Section 2.13.2.1), we obtain

$$L_\phi = (1-\varphi^2)\frac{c_{1t}^2}{2}, \qquad (4.15)$$

or

$$L_\phi = (1-\varphi^2)L_{ad}^*. \qquad (4.16)$$

The calculation of the flow in turbine cascades is expediently conducted with the aid of gas-dynamic functions:

$$\lambda_{c_{1t}} = \frac{c_{1t}}{a_{1cp}}; \quad a_{1cp} = \sqrt{2\frac{k}{k+1}RT_1^*} = \sqrt{2\frac{k}{k+1}RT_0^*} = a_{kp};$$

$$\lambda_{c_{1t}} = f(\pi_1); \quad \pi_1 = 1/\lambda_1 = p_1/p_0^*.$$

The real normalized velocity

$$\lambda_{c_1} = \varphi\lambda_{c_{1t}}. \qquad (4.17)$$

The energy loss being defined by the value L_ϕ is not equal to the entire work of friction, but is only a part of it, as was shown in Section 2.14.

Losses during flow in the rotor cascade are estimated in a similar way with losses in the nozzle cascade. The irreversible energy loss during the flow in the rotor cascade will be found from the expression

$$L_2 = \frac{w_{2ад}^2}{2} - \frac{w_2^2}{2}. \qquad (4.18)$$

where

$$w_{2ад} = \sqrt{2L_{2ад} + w_1^2} \qquad (4.19)$$

$w_{2ад}$ and w_2 are the adiabatic and real velocity, respectively, at the outlet from the rotor cascade.

The velocity factor of the rotor cascade is found as the ratio of the real discharge velocity from the cascade to the adiabatic velocity:

$$\psi = \frac{w_2}{w_{2ад}} = \frac{\lambda_{w_2}}{\lambda_{w_{2ад}}}; \qquad (4.20)$$

$$\lambda_{w_2} = \frac{w_2}{a_{кр\,w}}; \quad a_{кр\,w} = \sqrt{2\frac{k}{k+1}RT^*_{w_1}}. \qquad (4.21)$$

Having expressed L_ψ by ψ, we obtain

$$L_2 = (1-\psi^2)\frac{w_{2ад}^2}{2}. \qquad (4.22)$$

Let us represent in i-s-diagram the real process of the expansion of gas in the reactive stage of the turbine (Fig. 4.5). Line 0-1 corresponds to the real process of the expansion in nozzle

cascade, and line 1-2 - to the process in the rotor cascade.

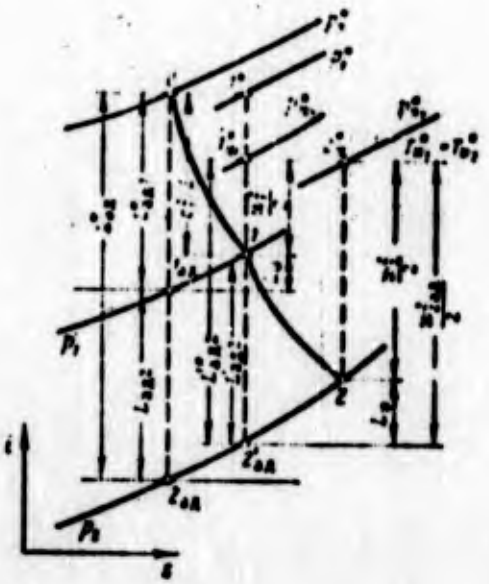

Fig. 4.5. Representation in i-s coordinates of the real process in the cascades of the reactive stage of the turbine.

Quantity L_ϕ is expressed by a difference in enthalpies $i_1-i_{1\text{д}}$ [see equation (4.14)]:

$$L_\phi=(i_0^*-i_{1\text{д}})-(i_0^*-i_1)=i_1-i_{1\text{д}}. \qquad (4.23)$$

The coefficient of the total pressure of the cascade σ_1 is found [see equation (2.192)] with respect to the ratio of the total pressure p_1^* to the total pressure p_0^* (see Fig. 4.5). In the absence of the external heat feed the increase in the entropy of gas during flow over a nozzle cascade is determined by the coefficient of the total pressure. For the isobaric process

$$s_1-s_{1\text{д}}=-R\ln\frac{p_1^*}{p_0^*}=-R\ln\sigma_1. \qquad (4.24)$$

The adiabatic heat differential of the rotor cascade can be somewhat increased in comparison with the adiabatic heat differential of the rotor cascade of an ideal turbine ($L'_{2ад} > L_{2ад}$, see Fig. 4.5), since the process in the rotor cascade, taking into account losses in the nozzle cascade, is accomplished in the area of high temperatures, and the heat capacity, determining the enthalpy ($i = c_p T$), increases with an increase in the temperature. Virtually the difference between $L'_{2ад}$ and $L_{2ад}$ is small. (For clarity the isotherms are drawn so that they coincide with lines of constant enthalpy).

In accordance with equation (4.18) L_ψ is found as a difference in segments 1^*_w-$2'_{ад}$ and 2^*_w-2. As follows from Fig. 4.5, $L_\psi = i_2 - i_{2ад}$.

The coefficient of total pressure of the rotor cascade σ_2 is found by the ratio of the pressure at point 2^*_w to the pressure at point 1^*_w. Since $T^*_{w_1} = T^*_{w_2}$, then the increase in entropy with the gas flow over the cascade will be equal to

$$s_2 - s_1 = -R \ln \frac{p^*_{w_2}}{p^*_{w_1}} = -R \ln \sigma_2. \qquad (4.25)$$

For the impulse stage of the turbine ($L_{2ад} = 0$), the energy loss with flow in the rotor cascade is determined from equation

$$L_r = \frac{w_1^2}{2} - \frac{w_2^2}{2}. \qquad (4.26)$$

which results from the general equation (4.18). By introducing the coefficient ψ, which in this case will be expressed thus:

$$\psi = \frac{w_2}{w_1} = \frac{\lambda_{w_2}}{\lambda_{w_1}}. \qquad (4.27)$$

we will obtain equation (4.26) in the form

$$L_r = (1 - \psi^2)\frac{w_1^2}{2}. \qquad (4.28)$$

Operating conditions of the cascade flow of the axial impulse stage of the turbine is depicted on the i-s-diagram (Fig. 4.6). The process in the running cascade occurs at a constant pressure - segment 1-2 on isobar $p_1 = p_2$. The energy losses with flow on the rotor cascade is found in accordance with equation (4.28) as a difference in the enthalpy:

$$l_{\text{т}} = l_2 - l_1. \qquad (4.29)$$

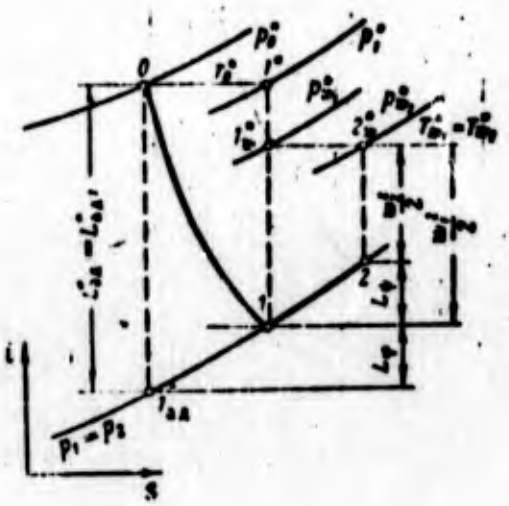

Fig. 4.6. Representation in i-s coordinates of operating conditions in cascades of the impulse stage of the turbine.

The total pressure loss factor is determined by the pressure ratio at points 2^*_w and 1^*_w.

Figure 4.7 gives diagrammatic representations of the process in cascades of the reactive stage of the turbine in T-s coordinates. Line 0-1-2 characterizes operating conditions in the nozzle cascade and in the rotor wheel. The shaded areas 0-а-б-в and 1-г-д-е correspond to the adiabatic heat differentials $L^*_{1ад}$ and $L_{2ад}$. The additional work of the volumetric expansion as a result of the heat feed of friction is characteristic both for the expansion in the nozzles and for the expansion in channels of rotor blades.

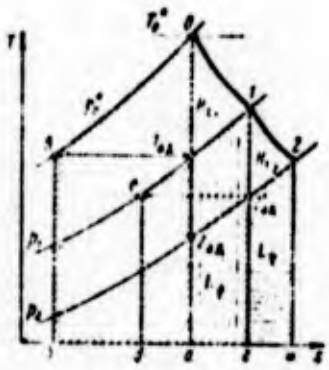

Fig. 4.7. Representation in T-s coordinates of the process in cascades of the reactive stage of the turbine.

The lost portions of mechanical energy L_ϕ and L_ψ are obtained if we subtract from the works of friction the returned works $H_{v_1}(0\text{-}1_{ад}\text{-}1)$ and $H_{v_2}(1\text{-}2'_{ад}\text{-}2)$. Correspondingly, L_ψ is characterized by the area $1_{ад}\text{-}1\text{-}в\text{-}а$, and L_ψ by the area $2'_{ад}\text{-}2\text{-}н\text{-}в$.

Figure 4.8 gives a diagrammatic representation in T-s coordinates of process in the impulse stage of the turbine. Line 0-1-2 characterizes the operating conditions; area 0-а-б-в is proportional to the adiabatic available work of the turbine. The additional work of the volumetric expansion as a result of the feed to the gas of heat of friction is realized only in the case of the expansion of the gas. Therefore, it can be revealed only for the process in the nozzle cascade (see H_{v_1} on Fig. 4.8). The entire work of friction with the gas flow in the rotor cascade at constant pressure (impulse lattice) turns into heat and is the irreversible loss of mechanical energy L_ψ.

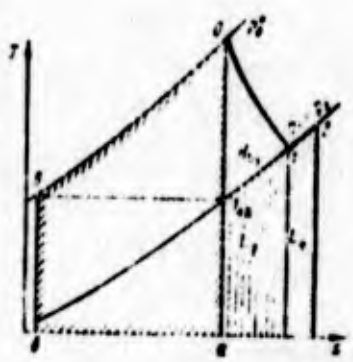

Fig. 4.8. Representation in T-s coordinates of the process in cascades of the reactive stage of the turbine.

It is necessary to keep in mind that for the supersonic flow the expansion ratios of nozzles, for the obtaining of the same pressure at the end of the expansion in the presence of losses and not allowing for losses, should be different. The heat feed of friction leads to the stagnation of supersonic flow, and for the achievement of the assigned outlet pressure the nozzle expansion ratio during the process with friction should be more than that during an ideal process. With an ideal adiabatic process in this nozzle it would be possible to obtain less pressure $p'_{1ад}$.

For the same nozzle (supersonic flow) the adiabatic and polytropic processes will be depicted in p-v and T-s-coordinates in the manner which it is shown on Fig. 4.9 and 4.10, respectively.

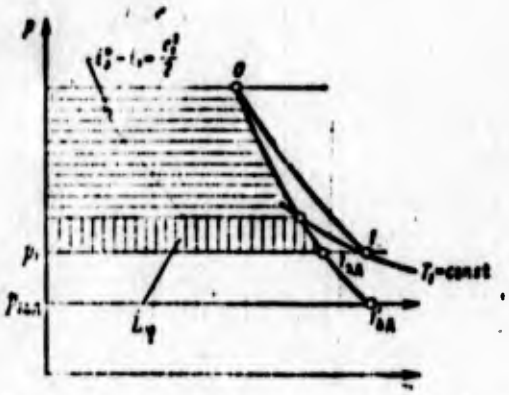

Fig. 4.9. Representation in p-v coordinates of adiabatic and polytropic processes for the same nozzle.

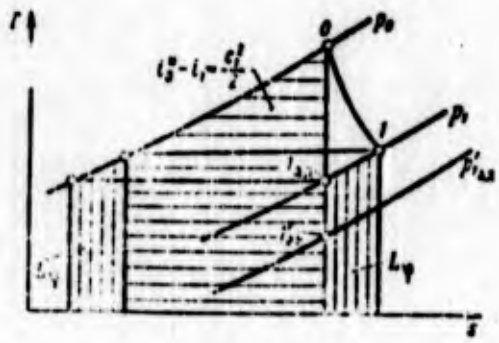

Fig. 4.10. Representation in T-s coordinates of adiabatic and polytropic processes for the same nozzle.

4.2.2. SINGLE-STAGE RADIAL-FLOW TURBINE. A CHANGE IN THE PARAMETERS IN THE LENGTH OF THE FLOW AREA. REPRESENTATION OF PROCESSES IN THE i-s-DIAGRAM

Figure 4.11 shows a diagram of a radial inward-flow turbine. In the LPRE radial-flow turbines are used as precombustion-chamber turbines; in this case the rotor wheel is made radial-axial so that

In essence the inward-flow turbines used in the LPRE are radial-axial turbines. Subsequently, however, we will call them radial-flow turbines. Purely the radial-flow turbine (see Fig. 2.23) is used in LPRE rarely, since it is poorly arranged with the combustion chamber.

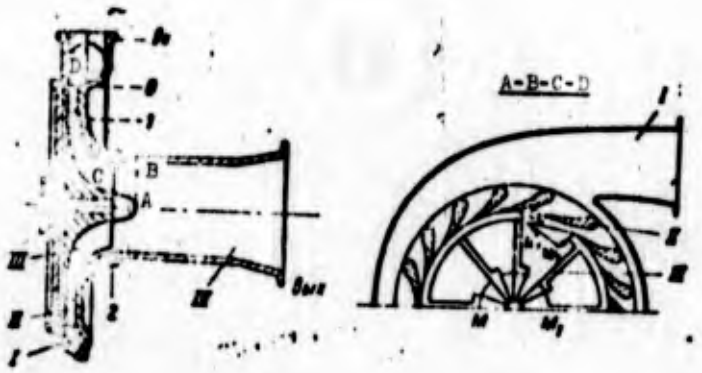

Development in mm_1

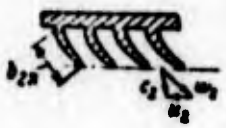

Fig. 4.11. The diagram of the radial inward-flow turbine: I - feed; II - nozzle cascade; III - rotor wheel; IV - branch.

With respect to the overall dimensions and mass of the design, the radial-flow turbine is inferior to the axial-flow turbine; furthermore, for the wheel of the radial-flow turbine greater axial thrust is characteristic. High axial thrust impedes the designing of the turbopump unit. According to conditions of the strength of the wheel, the design of the radial-flow turbine also presents definite difficulties, but in manufacture the wheel of the radial-flow turbine is simpler than that of the axial-flow turbine.

From Fig. 4.11, where shown is a structural diagram of the single-stage radial-flow turbine, which provides the output of the gas close to axial, numeral I denotes the feed device, which

is the circular feed, which most frequently is made as helical with a gradual decrease in the flow area. This makes it possible to equalize the feeds and provide a more uniform gas feed to the nozzles. Numeral II denotes the nozzle cascade, which is made in the form of a circular cascade; in principle, the role of the nozzle cascade can fulfill the spiral feed. Numeral III denotes the rotor wheel; the outlet device (branch) IV is usually made in the form of a straight diffuser.

Let us observe the change in the gas parameters along the length of the flow area of the radial inward-flow turbine (Fig. 4.12). Conditionally plotted along the axis of the abscissae is the length of the flow area of the turbine, and characteristic cross sections are noted. In the feed collector, which is usually made convergent, the pressure somewhat falls; correspondingly the temperature decreases and the velocity increases. Such a change is characteristic for the averaged parameters, since the velocity distribution over the cross section of the feed collector is substantially uneven.

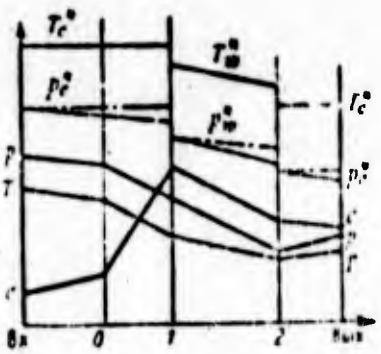

Fig. 4.12. Change in the gas parameters along the length of the flow area of the radial inward-flow turbine.

Cross sections 0 and 1 separated the nozzle box, in which the expansion of gas and acceleration of the gas flow occurs. The pressure and temperature of the gas decrease, and the velocity increases. The stagnation pressure in an ideal case (dot-dash line) remains constant, and in the actual case it decreases as a result of losses. The stagnation temperature remains constant.

Figure 4.11 gives velocity triangles at the inlet into the rotor wheel and at the outlet from it. They are located in different planes.

The velocity triangle at the inlet into the rotor wheel lies in the plane of rotation, and the velocity triangle at the outlet from the wheel lies in the plane tangential to the cylindrical surface with the axis coinciding with the axis of rotation. The combined velocity triangles are given separately on Fig. 4.13.

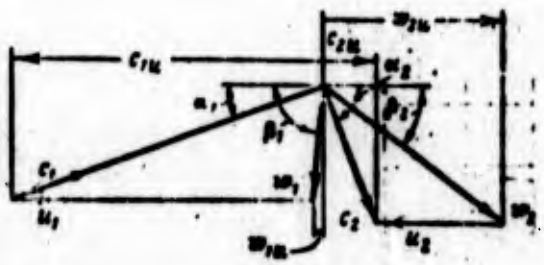

Fig. 4.13. Velocity triangles at the inlet into the rotor wheel and at the outlet from it for the radial inward-flow turbine.

The trailing edges of the nozzle blades are tilted at a small angle toward the circumference. The angle of inclination is usually 15-20°. The velocity is determined by the ratio of pressures at the inlet into the nozzle cascade and at outlet from it and also by the initial temperature.

The circular velocity at the assigned angular velocity ω is determined by the outside diameter of the wheel. The maximum value of the circular inlet velocity is limited by the strength of the wheel ($u_1 \leq$ 250-300 m/s). Single shrouded (see Fig. 4.11) and double shrouded (see further Fig. 4.52) wheels are used. On the basis of considerations of strength it is most advantageous to use radial blades at the inlet. Therefore, one attempts to insure such a relationship of velocities u_1 and c_1 so that the direction w_1 is close to the radial (see Fig. 4.11). If such a relationship of

velocities is not possible, then it is necessary to use blades having an inlet angle different from the radial (see Fig. 2.23).

In the rotor wheel, i.e., between cross sections 1-2 (see Fig. 4.12), there occurs the selection of mechanical energy, as a result of which the absolute gas velocity is decreased. In this case the gas flow occurs in the field of inertial forces of rotary motion, and with transition to less radii the gas pressure is reduced [see equation (2.85)]. An additional decrease in pressure on the wheel takes place when vane channels are made convergent, and in them a velocity increase relative to the wheel (relative velocity) occurs.

Figure 4.12 depicts such a flow ($w_2 > w_1$). The additional pressure drop on the wheel as a result of the acceleration of the gas is not the necessary condition of the course of operating conditions in a radial inward-flow turbine, but such a change in the parameters is most favorable, since it eliminates the diffuser gas flow along the vane channels which is accompanied by great losses.

Let us say that by artificially providing the diffuser flow in its channels by a change of flow areas of the wheel, it is possible to obtain a less pressure drop on the wheel than the unavoidable pressure drop connected with the flow directed toward the center of the rotating wheel. In this case the relative velocity of motion of the gas on the wheel will be decreased. Such a course of the process will be disadvantageous, since the diffuser flow is accompanied by great hydraulic losses.

The temperature T_w^* and stagnation enthalpy in the wheel will be changed with a decrease in the radius, since the flow occurs with a change in the inertial forces of rotary motion (see Section 2.8):

$$i_{w_1}^* = i_{w_2}^* - \frac{u_1^2 - u_2^2}{2}; \qquad (4.30)$$

correspondingly

$$T^*_{w_1} = T^*_{w_2} - \frac{k-1}{2kR}(c_1^2 - c_2^2). \qquad (4.31)$$

Value $T^*_{w_1}$ is found from relation (4.7):

$$T^*_{w_1} = T^*_0 - \frac{k-1}{2kR}(c_1^2 - w_1^2). \qquad (4.32)$$

Similarly the stagnation pressure even in an ideal case will be changed (see Fig. 4.12).

The temperature in the wheel T will be reduced because of a decrease in stagnation temperature and as a result of the flow expansion if $w_2 > w_1$.

This property of radial inward-flow turbines is used for obtaining low temperatures. The radial inward-flow turbines used in refrigeration technology are called turboexpanders.

At the outlet from the wheel of a radial-flow turbine an outlet device is placed (see position IV on Fig. 4.11), which it is advantageous to make in the form of a diffuser in order to convert the kinetic energy of the flow coming out of the turbine into potential energy - pressure energy. This makes it possible at the assigned counterpressure (outlet pressure from the diffuser) to increase the pressure ratio for the wheel. Furthermore it is difficult to use the energy directly in high-speed form in gas injectors or in the combustion chamber. A decrease in velocity in the diffuser after the turbine is advantageous, since the pressure of high velocities in the adapter, which connects the turbine and the chamber, will be associated with high hydraulic losses. In general let us assume that in the outlet section of the turbine the pressure increases, and the velocity decreases.

To obtain, in the absolute motion of the direction, an outlet velocity close to the axial, the impeller vane must be bent to the side opposite to the rotation (see Fig. 4.11). The presence of great twist of the flow in the turbine exhaust can lead to great hydraulic losses in the device feeding gas to the combustion chamber.

Let us emphasize again that the total pressure ratio at the inlet into the wheel and at the outlet of it should be more than is necessary for the expansion of gas, if we proceed from the geometric relationships of the channel. The considerable portion of pressure drop on the wheel is connected with the movement of gas from larger radii to smaller. Thus, the wheel of the inward-flow turbine is always reactive. The kinematic degree of reaction of the wheel is found from the general relation (2.102).

The expression for the thermal degree of reaction is recorded in the same form as that for the axial-flow turbine [see equation (4.9)].

The process of an ideal radial turbine in an i-s-diagram is depicted in the same way as for a reactive axial-flow turbine (see Fig. 4.3), but the segment 1-2 in this case will be the sum of two terms:

$$\frac{w_2^2 - w_1^2}{2} + \frac{u_1^2 - u_2^2}{2}.$$

For the real stage of the radial reaction turbine, which is the total form of the stage of the turbine, the process of cascade flow in i-s coordinates in a simplified way is depicted on Fig. 4.14. We focus attention to the fact that the stagnation temperature in relative motion at the outlet of the wheel is less than the stagnation temperature in relative motion at the inlet into the wheel in connection with a decrease in the potential energy of the gas upon the transition to smaller radii.

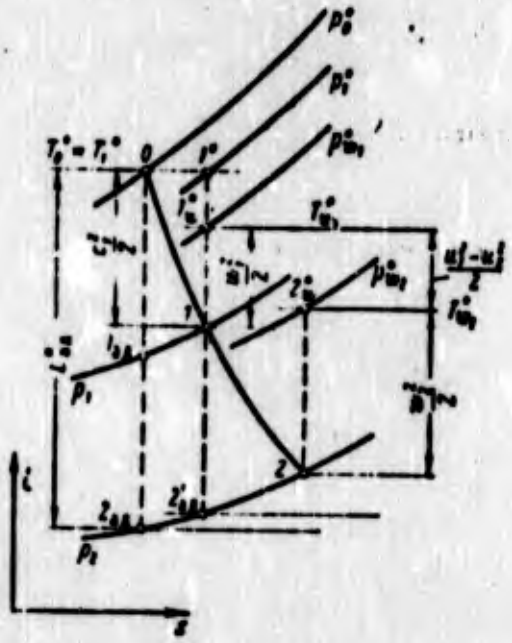

Fig. 4.14. Representation in i-s coordinates of the process in the cascades of the stage of the radial inward-flow turbine.

4.3. FLOW IN TURBINE CASCADES. THE SELECTION OF DESIGN PARAMETERS OF CASCADES

The expansion of gas in general occurs both in the nozzle and the rotor cascades (reactive stage). In the active stage the gas is expanded only in the nozzle cascade. Turbines of LPRE are made with a small or zero (impulse turbines) degree of reaction. Therefore, in turbines of LPRE the process of expansion occurs basically in multinozzle grids.

The streamline flow of cascades and losses in them were examined in detail in Section 2.13.2.1. In this section we discuss the process of the expansion of gas in cascades and features of the flow around the cascades with transonic and supersonic velocity.

4.3.1. EXPANSION OF GAS IN CASCADES

4.3.1.1. Expansion of Gas in Convergent Cascades

Let us examine flow in convergent cascades. For concreteness we will examine the nozzle cascade. All the relations will be valid for the cascade of the rotor wheel in the replacement of the absolute velocity by the relative velocity and upon the consideration of the initial velocity. The geometric shape of the cascade is shown on Fig. 4.15.

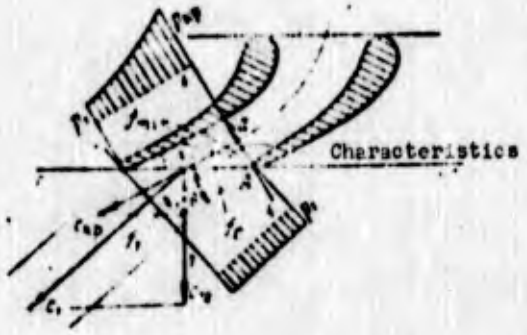

Fig. 4.15. Determination of the angle of deflection of the flow in the oblique section of a convergent nozzle cascade.

The work of expansion of such a cascade depends on the pressure ratio at the inlet into the cascade and at the outlet from it ($\delta_1 = p_0^*/p_1$). The flow pattern will be different for conditions $\delta_1 < \delta_{кр}$ and $\delta_1 \geq \delta_{кр}$, where $\delta_{кр}$ is the critical pressure ratio [see equation (4.4)].

Let us examine which parameters will be at the outlet from the convergent cascade when $\delta_1 < \delta_{кр}$ (such pressure ratios are characteristic for the precombustion-chamber turbines).

Let us find the real discharge velocity from the relationship

$$c_1 = \varphi c_{1a}, \qquad (4.33)$$

where ϕ is the velocity factor for the averaged velocity. Averaging can be carried out from the equations of conservation, continuity, momentum and energy (see Section 2.13.2.1), depending on the problem being solved.

Usually the coefficient ϕ of the convergent nozzles is equal to:

$$\varphi = 0{,}97 \div 0{,}98.$$

We find the gas flow rate with the aid of gas-dynamic tables in terms of the given flow rate

$$q(\lambda_{c_1}) = \frac{\rho_1 c_1}{\rho_{1\,sp} a_{1\,sp}}; \qquad (4.34)$$

Let us find the flow rate through the cascade from the equation

$$G = z_c f_{min} \rho_1 c_1, \qquad (4.35)$$

or, taking into account equation (4.34), after conversions we obtain

$$G = z_c f_{min} \frac{p_1^*}{\sqrt{RT_1^*}} q(\lambda_{c_1}) m, \qquad (4.36)$$

where

$$m = \sqrt{k\left(\frac{2}{k+1}\right)^{\frac{k+1}{k-1}}}.$$

is denoted.

Let us express pressure p_1^* by the initial stagnation pressure with the aid of the coefficient or total pressure:

$$p_1^* = \sigma_1 p_0^*; \qquad (4.36a)$$

then

$$G = \varepsilon_c f_{min} m \frac{P_0^*}{\sqrt{RT_0^*}} q(\lambda_{c_1}), \qquad (4.37)$$

since $T_0^* = T_1^*$.

For determining the flow direction at the outlet from the cascade at subsonic velocities, in the practice of turbine construction we have the common formula

$$\sin \alpha_1 (\beta_2) = m \frac{a}{t}, \qquad (4.38)$$

where m is experimental coefficient; a is the dimension of the throat of the vane channel.

This equation agrees well with the experiment (when coefficient m = 1) for escape velocities close to sonic. At lower velocities (M < 0.4-0.5) it is recommended (see source [6]) to accept the coefficient m equal to 1.08.

Let us examine the fundamental relations for flow in a convergent cascade when $\delta_1 = \delta_{1кр}$. We will accept approximately that in the minimum cross section the critical velocity is established:

$$c_{1кр} = w_{1кр} = \varphi \sqrt{2 \frac{k}{k+1} RT_0^*}, \qquad (4.39)$$

which determines the gas flow rate through the nozzle.

The flow rate is equal to the maximum (critical) flow rate:

$$G = G_{кр} = \varepsilon_c f_{min} m \frac{P_0^*}{\sqrt{RT_0^*}} q(\lambda_{c_{1кр}}). \qquad (4.40)$$

By f_{min} in equations (4.37) and (4.40) one should understand as the effective cross section, which can be less than the geometric in view of the jet narrowing:

$$f_{min} = \alpha f_{min\ geom},$$

where α is the coefficient of the jet narrowing; in the first approximation, it is possible to assume that $\alpha = 1$; value $\sigma_{1кр}$ in equation (4.40): $\sigma_{1кр} = p^*_{1кр}/p^*_0$ - the coefficient of total pressure from the inlet to the critical cross section.

When $\delta_1 > \delta_{1кр}$ the expansion of the gas is continued within limits of the oblique section of the vane channel, i.e., from cross section k-k up to the cross section c-c (see Fig. 4.15). Let us examine this question in more detail.

4.3.1.2. Expansion of Gas in the Oblique Section of the Converging Cascade

Vane cascades almost always have an oblique shear, since the angle of inclination of the blades at the outlet is usually considerably less than 90°. At a pressure after the multinozzle grid p_1 less than $p_{кр}$, in the space between the critical cross section and the shear the expansion of the gas occurs. The pressure along the wall falls gradually and at point A immediately (see Fig. 4.15). Around point A there appears the Prandtl-Meyer flow (flow with the flow around an obtuse angle), which leads to a velocity increase of the gas from sonic ($\lambda_{кр} = 1$) to supersonic ($\lambda > 1$) and rotation of the flow to the side of less pressure.

In a plane oblique section constant pressure is established along the characteristic, i.e., along the ray coming out from point A (see Fig. 4.15). The pressure which corresponds to the output can be established within limits of the oblique section. In this case there will be an incomplete use of the oblique section.

When the characteristic which corresponds to outlet pressure is established on the nozzle edge, then the expansion ability of the oblique section will be used completely. The velocity is determined by the pressure ratio δ_1 and losses in the nozzle and is found from equation (4.33). The gas flow rate remains equal to the critical, since in the critical section we have minimum flow area, and the velocity in this section in the oblique section is not affected by the expansion. Expansion in the oblique section is accompanied by a deviation in the flow to the side of an increase in the angle at which the flow emerges.

From the diagrams of pressure shown on Fig. 4.15, it follows that acting on the gas jet flowing along the oblique section is the pressure impulse in a circular direction. Under the action of this pressure impulse the jet is deflected from the nozzle axis (see Fig. 4.15).

The deflection angle in the oblique shear can be found by calculation. Precise equations for determining the angle of deflection of the flow in the oblique shear are given in the courses of gas dynamics (see source [37]).

The approximation equation for determining the angle of deflection of flow in an oblique section is obtained from the continuity equation, written for the sections k-k and 1-1, not allowing for the possible detached flow (see Fig. 4.15):

$$q_{\lambda_{np}} r_{np} f_{min} = q_{\lambda_1} r_1 f_1, \qquad (4.41)$$

where f_1 is the jet cross-sectional area of the nozzle exit.

Considering that the height of the cascade (the dimension perpendicular to the plane of the drawing, see Fig. 4.15) remains constant within limits of the oblique section, and that in the jet up to cross section 1-1 this dimension is retained, we will obtain

the relations between sections f_{min}, f_1 and the section in the shear plane f_c:

$$f_1 = f_c \sin(\alpha_1 + \theta) \quad \text{and} \quad f_{min} = f_c \sin \alpha_1.$$

Having substituted these relations into equation (4.41) and having produced cancellations, we obtain

$$\rho_{кр} c_{кр} \sin \alpha_1 = \rho_1 c_1 \sin(\alpha_1 + \theta),$$

whence

$$\sin(\alpha_1 + \theta) = \sin \alpha_1 \frac{\rho_{кр} c_{кр}}{\rho_1 c_1}. \qquad (4.42)$$

Disregarding the losses, i.e., assuming that $\rho_{кр} = \rho_{кр,зд}$ and $c_{кр} = a_{кр}$ from equation (4.42) we obtain

$$\sin(\alpha_1 + \theta) = \sin \alpha_1 \frac{\rho_{кр} a_{кр}}{\rho_{1ст} c_{1ст}}. \qquad (4.43)$$

Taking into account the fact that

$$\frac{\rho_{1ст} c_{1ст}}{\rho_{1кр} a_{1кр}} = q(\lambda_{c_{1ст}}) \qquad (4.44)$$

($a_{кр} = a_{1кр}$, since $T_0^* = T_1^* = \text{const}$), we will obtain the equation known by the name of the Baire equation:

$$\sin(\alpha_1 + \theta) = \sin \alpha_1 \frac{1}{q(\lambda_{c_{1ст}})}. \qquad (4.45)$$

The calculations according to this equation give somewhat decreased values of the angles of deflection of the flow, especially when $\lambda > 4$ (see source [137]).

Let us derive the quantitative ratios for determining the expansion ability of the oblique shear. The velocity component of the gas, perpendicular to the isobaric surface (characteristic), is equal to the speed of sound. Then for the maximum expansion in

the oblique shear (the characteristic coincides with the nozzle edge), the axial component of outlet velocity (perpendicular to the front of the cascade) should be the speed of sound at this temperature (Fig. 4.16). For the limiting case of expansion (not allowing for losses) it is possible to write (see Fig. 4.16):

$$\sin(\alpha_1 + \vartheta_{np}) = \frac{a_{1np}}{c_{1np.a1}}. \qquad (4.46)$$

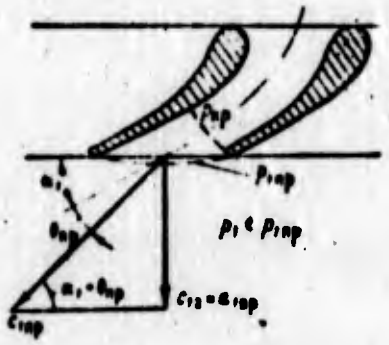

Fig. 4.16. Determination of maximum expansion in the oblique section of the cascade.

Let us write equation (4.45) in the form

$$\sin(\alpha_1 + \vartheta_{np}) = \sin\alpha_1 \frac{1}{q(\lambda_{c_{1np.a1}})}. \qquad (4.47)$$

Having equated the right sides of equations (4.46) and (4.47) and transforming them, we obtain

$$\lambda_{1np} = \delta_{np} \frac{1}{(\sin\alpha_1)^{2k/(k+1)}}. \qquad (4.48)$$

The asymptotic relation of pressures depends on the slope angle of the nozzle by which the ratio of areas f_{min}/f_c is determined.

Table 4.1 gives values of the maximum expansion ratio of the converging nozzle with oblique shear for $k = 1.33$ and for three values of angle α_1.

Table 4.1. Dependence of the asymptotic ratio of pressures $\delta_{1кр}$ for the converging nozzles on the slope angle of the nozzle α_1.

α_1°	15	20	25
$\delta_{1кр}$	8,4	6,2	4,9

The larger expansion ratio in the converging nozzle with oblique section can be obtained with the smaller slope angles of nozzle α_1 (the more the increase of area in the oblique shear) and less pitot losses (the less the specific volume of gas, and, therefore, the less the required area). But finally the question of the selection of the expansion ratio in the converging nozzle can be solved, having estimated the value of angles of deflection in the case of the maximum expansion.

Having substituted (4.47) the value $\lambda_{c1кр.зд}$ for the maximum degree of pressure drop into equation [see equation (4.48)], let us find the value of the angle of deflection corresponding to the full use of the expansion ability of the oblique shear of the converging nozzle.

Table 4.2 gives values of the angles of deflection which correspond to the maximum expansion in the oblique shear.

Table 4.2. Dependence of angles of deflection of the flow in the oblique section $\theta_{кр}$ which correspond to the asymptotic ratio of pressures on the slope angle of the nozzle α_1.

α_1°	15	20	25
$\theta_{кр}^\circ$	14°	12°10'	10°30'

Usually the calculated value of the angle of deflection of the flow with expansion in the oblique shear is limited by values of 3-5°. The larger angles of deflection in the flow at the outlet from the multinozzle grid lead to larger angles of inleakage to blades of the rotor wheel, which is disadvantageous, since losses with the outlet velocity from the rotor wheel increase. The outlet velocity increases due to an increase in the axial component of velocity. It is also inexpedient to pass over to small output angles of the multinozzle grid, since this will increase the losses in connection with an increase in the friction surface and value of the edges and also in connection with an increase in the angle of rotation at the inlet. In connection with this the nozzle cascade is never calculated for the asymptotic ratio of pressures. The maximum calculated pressure ratio for the converging nozzles, proceeding from angles of deflection in the oblique section θ = = 3-5°, is δ_1 = 3-4.

4.3.1.3. Expansion Gas in Cascades and Nozzles with Expanding Ducts

For large expansion ratios (δ_1 > 3-4) in nozzle cascades, profiles which form vane channels in the form of Laval nozzles (Fig. 4.17) are used. In turbines with a low gas flow rate, separate nozzles made in the form of the Naval nozzles (see further Fig. 4.23) are frequently used. Nozzle cascades which form the converging-expansion channels make it possible to obtain high supersonic velocities of outflow.

Figure 4.17 depicts the element of the cascade with vane channels made in the form of Laval nozzles. Shown on the left is a change in the flow parameters. Two characteristic cross sections - the minimum cross section k-k (critical) and cross section 1'-1' at the end of divergent section perpendicular to the axis of the nozzle, are distinguished. The parameters in cross section 1'-1' will be designated by the numeral "1" with a prime. The flow areas f_{min} and f_1' are the calculated cross sections. The value of the

critical cross section will determine the flow rate through the cascade [see equation (4.40)]. If the flow rate is assigned, then from equation (4.40) it is possible to determine the required value of the minimum (critical) cross section f_{min}.

Fig. 4.17. Examination of the gas flow through the cascade with vane channels made in the form of Laval nozzles.

The flow area f_1' determines the nozzle expansion ratio and the velocity c_1'. Let us find the connection of the nozzle expansion ratio with gas parameters.

Let us use the continuity equation for cross sections k-k and 1'-1':

$$G = \frac{p_0^*}{\sqrt{RT_0^*}} m z_1 q(\lambda_{c_1'}) = \frac{p_0^*}{\sqrt{RT_0^*}} m z_1 f_1 q(\lambda_{c_1'})$$

where

$$\bar{f}_1 = \frac{f_1'}{f_{min}} = \frac{z_1 q(\lambda_{c_1'})}{z_1 q(\lambda_{c_1'})}. \qquad (4.49)$$

Losses in the subcritical part of the nozzle will be disregarded. Let us assume that $\sigma_{кр} = 1$ and $q(\lambda_{c_{кр}}) = 1$; then from equation (4.49) we obtain

$$\bar{f}_1 = \frac{1}{z_1 q(\lambda_{c_1'})}. \qquad (4.50)$$

Since

$$\pi_1' = \frac{(p_1)^*}{p_0^*},$$

then

$$\overline{f_1'} = \frac{p_0^*}{(p_1')^* q(\lambda_{c_1'})}. \qquad (4.51)$$

Let us express $\overline{f_1'}$ by the static pressure p_1' and the velocity coefficient $\varphi' = \frac{c_1'}{c_{1ад}}$:

$$\lambda_{c_1'} = \varphi'(\lambda_{c_{1ад}}) \quad \text{and} \quad (p_1')^* = \frac{p_1'}{\left[1 - \frac{k-1}{k+1}(\varphi')^2 \lambda^2_{c_{1ад}}\right]^{\frac{k}{k-1}}}.$$

Correspondingly,

$$\overline{f_1'} = \frac{\pi_1' \left[1 - \frac{k-1}{k+1}(\varphi')^2 \lambda^2_{c_{1ад}}\right]^{\frac{k}{k-1}}}{q(\lambda_{c_1'})}, \qquad (4.52)$$

where

$$\pi_1' = \frac{p_0^*}{p_1'}.$$

Having substituted the expanded expression for $q(\lambda_{c_1'})$ into equation (4.52), after simplifications we obtain

$$\overline{f_1'} = \pi_1' \left(\frac{2}{k+1}\right)^{1/(k-1)} \frac{1 - \frac{k-1}{k+1}(\varphi')^2 \lambda^2_{c_{1ад}}}{\varphi' \lambda_{c_{1ад}}}. \qquad (4.53)$$

Being assigned the desired degree of the lowering of pressure δ_1' from the nozzle inlet to cross section 1'-1' (see Fig. 4.17) and the velocity factor ϕ', considering losses in this section, we determine according to the table of gas-dynamic functions $\lambda_{c_{1ад}'} = f(\pi_1' = 1/\delta_1')$ and calculate the nozzle expansion ratio $\overline{f_1'}$.

Equation (4.53) includes only one experimental coefficient, namely, the velocity factor ϕ'. According to experimental data

the value ϕ' can be accepted within limits of 0.94-0.98.

Figure 4.18 depicts the dependence of the nozzle expansion ratio on the pressure ratio δ_1', calculated at different values of the velocity factor of the nozzle ϕ'. Value ϕ' affects the broadening of the nozzle. Being assigned during the calculation of nozzle with the decreased value ϕ', it is possible to obtain the excessive broadening of the nozzle for rated value δ_1'. Such a nozzle will operate in the system of overexpansion, which can cause added losses.

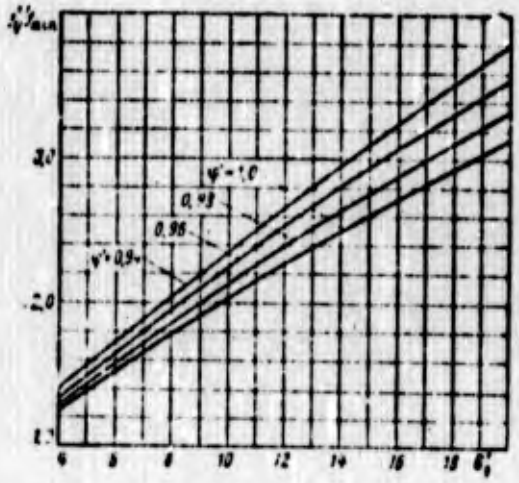

Fig. 4.18. Dependence of the nozzle expansion ratio on the pressure ratio δ_1' at different values of velocity factor ϕ' ($k = 1.33$).

In the calculation of nozzles it is better to select the excessive values of ϕ', since in operation of the nozzle in conjunction with the rotor cascade, it is more preferable to have conditions of underexpansion. The velocity at the end of the divergent section is found as the velocity of the full expansion:

$$c_1' = \varphi' \lambda_{c_{1a}} a_{*p},$$

where

$$\lambda_{c'_{1ad}} = f(\pi'_1 = 1/\delta'_1).$$

If the pressure ratio δ_1, calculated according to the total pressure in front of the cascade and the static pressure at the outlet from the cascade, is equal to the calculated degree of lowering of pressure in the nozzle ($\delta_1 = \delta'_1$), then the outlet velocity c_1 will be equal to the velocity in the cross section 1'-1' (see Fig. 4.17) if we disregard the losses in the oblique section:

$$c_1 = c'_1; \quad \lambda_{c_1} = \lambda_{c'_1}.$$

4.3.1.4. Gas Expansion in the Oblique Section of the Expanded Cascades and Nozzles

If the pressure ratio δ_1 will be more than δ'_1, then in the oblique shear further expansion of gas can occur. The gas flow in this case will be deflected to the side of an increase in the angle of discharge. The change in the gas parameters, taking into account expansion in the oblique section, is shown by dashed lines on Fig. 4.17. In this case $\lambda_{c_1} > \lambda_{c'_1}$.

Expansion in the oblique shear begins not from the cross section 1'-1' but only from the characteristic a-a displaced relative to the cross section 1'-1' (see Fig. 4.17). The rarefaction wave from point A will not reach cross section 1'-1', since the gas is carried away at the velocity exceeding the speed of sound ($c'_1 > a$), i.e., exceeding the propagation velocity of the rarefaction wave. The angle ε at which characteristic a-a is located with respect to the axis is determined from the known relation:

$$\sin\varepsilon = \frac{a'_1}{c'_1} = \frac{1}{M'_1}. \qquad (4.54)$$

At high supersonic velocities the expansion in the oblique section can not generally occur. In this case the characteristic which corresponds to pressure p_1' coincides with the nozzle edge. For this case it is possible to write the relation

$$\sin\varepsilon = \sin\alpha_1 = \frac{1}{M_{1пр}'}. \qquad (4.55)$$

Thus, for instance, when $\alpha_1 = 20°$ value $M_{1пр} = 2.9$. When $M_1' < M_{1пр}'$ the expansion in the oblique section can take place, but it virtually leads to a small increase in the velocity in comparison with that which is observed during expansion in the oblique section of the convergent nozzle. This is explained by the fact that in the supercritical region, in connection with a sharp increase in the specific volumes of gas, the necessary increase in the area during the gas expansion is also great.

It is possible to obtain the approximate relations for the angle of deflection of the flow, having used the continuity equation. Having written the continuity equation for the two cross sections k-k and 1'-1' (see Fig. 4.17), we obtain after conversions similar to those which were used in the solution of equation (4.45) for the adiabatic flow:

$$\sin(\alpha_1 + \delta) = \sin\alpha_1 \frac{q(\lambda_{c_{1ад}})}{q(\lambda_{c_{1ад}})}. \qquad (4.56)$$

Figure 4.19 (see source [146]) shows the spectrum of flow in the divergent nozzle cascade. The pressure ratio is such that gas expansion in the oblique section occurs. The rarefaction wave in the oblique shear, the boundary of the flow which leaves the cascade, the reflected rarefaction waves, and rarefaction waves on trailing edges are evident.

Fig. 4.19. Spectrum of flow in expanded multinozzle grid. Setting angles of the profile χ: 1-18°; 2-16° (calculated); 3-14°; 4-12°; 5-10°.

4.3.1.5. Profiling of Nozzle Cascades and Nozzles

The nozzle cascade should be profiled in such a way that it provides the necessary direction and magnitude of the flow velocity at the outlet and have minimum losses.

The gas is fed to the multinozzle grid from the gas generator in an axial direction. Therefore, usually $\alpha_0 = 90°$. The outlet angle α_1 is selected within limits of 15-20°. The less the angle

of departure, the more the span of the blade will be, and the more the camber of the nozzle and rotor blades. Profile losses (especially edge and secondary) will increase. At large angles of α_1 will increase the losses with the outlet velocity as a result of an increase in the axial component of velocity at the outlet from the wheel, which is close in value to the axial component of velocity at the inlet into the wheel. The axial component of the inlet velocity increases with an increase in α_1.

When designing turbines of LPRE as profiles of nozzle cascades one should select profiles with known characteristics and possessing minimum losses. The profiles developed at the Moscow-Power Institute on the basis of theoretical and experimental studies are given in the atlas of profiles (see source [4]).

The profiles of nozzle cascades are divided into three groups: A, B, and C (Fig. 4.20). The cascades of groups A and B are converging, and the cascades of group C are converging-diverging. The profiles of group A are designed for nozzle cascades with subsonic velocity at the outlet (M_1 = 0.4-0.9). In transonic velocities ($0.9 < M_1 < 1.2$) cascades of group B are used. In these cascades supersonic velocity is reached as a result of the gas expansion in the oblique section (pressure ratio $\delta_1 \leq 2.5$). The cascades of group C are designed for high supersonic velocities ($M_1 > 1.2$).

Cascades for subsonic velocities (group A) have profiles with smoothly varying curvature of the back and face, which provides a sufficiently uniform, without diffuser sections, profile pressure distribution (see, for example, Fig. 2.50, α_0 = 60°-90°) with which losses in the cascade are minimum.

In cascades of group B ($M_1 < 1.2$) the back in the oblique shear, where there occurs a velocity increase in the flow up to supersonic, is made rectilinear. This is done because the convex back (great curvature) would lead to a local increase in velocity at the surface of the blade up to a considerable supersonic velocity

(local flow around an obtuse angle) with the subsequent stagnation in the shock wave, which is accompanied by energy losses (wave losses).

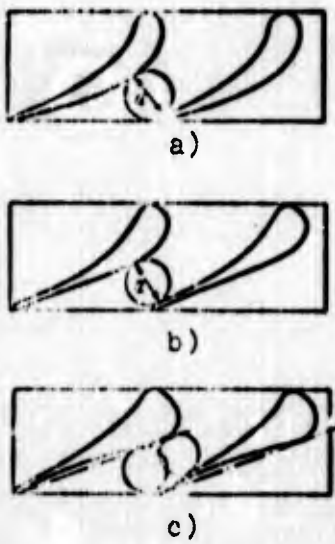

Fig. 4.20. Profiles of nozzle cascades: a) subsonic profile (group A); b) transonic profile (group B); c) supersonic profile (group C).

After the minimum cross section the nozzle cascades of group C have a concave back, forming the expanding duct.

Nozzle cascades correspond to losses which are found at a level of the minimum and at computed values of M_1 (Fig. 4.21). Basically they are determined by losses of friction. With deviation from the computed value M_1, in connection with the off-design flow, the losses increase. At high values of M_1 (the pressure ratio δ_1 is more than calculated δ_p) the gas expansion occurs beyond limits of the cascade. It is accompanied by shock waves, which increase the losses (see source [37]).

If values M_1 are less than those calculated, then in the converging cascade (group A and B) the boundary layer thickness increases, in consequence of which the profile and tip losses increase. An increase in losses in the expanding cascades at values of M_1 less than the calculated (pressure ratio $\delta_1 < \delta_p$) is basically explained by an increase in the wave losses caused

by shock waves in the expanding section of the channel (see source [37]).

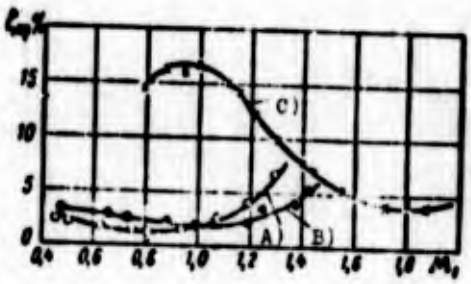

Fig 4.21. Dependence of the loss factor of a multinozzle grid on the M number at the outlet; A) subsonic cascade (group A); B) transonic cascade (group B); C) supersonic cascade (group C).

After the selection according to values M_1, α_0 and α_1, the profiles of the nozzle cascade determine the relative pitch $\bar{t} = t/b_л$ (where $b_л$ - the airfoil chord) and the loss factor of the cascade. For this the graphic characteristics of the air foil given in an atlas are used [4].

There is an optimum value of the relative pitch $\bar{t}$ at which losses in the cascade are minimum. This is caused by the fact that with an increase in the pitch the frictional surface is decreased and profile losses are lowered. But, together with this, an increase in the pitch as a result of the less interaction of adjacent profiles leads to a pressure drop on the back and pressure rise on the face (Fig. 4.22). In this case secondary losses are increased, and the possibility for the flow separation is created. With an increase in the pitch the deflecting properties of the cascades deteriorate. For the nozzle cascades $\bar{t}_{opt} = 0.7\text{-}0.9$.

Precombustion-chamber turbines of LPRE correspond to small pressure ratios δ_1 (see Section 4.1.2) at which $M_1 < 1.2$, and therefore in the precombustion-chamber turbines the cascades of groups A and B can be used as nozzle cascades. Values of $M_1 > 1.2$ correspond to autonomous turbines of LPRE with a high pressure ratio δ_1; and therefore for autonomous turbines nozzle cascades of group C can be used. However, in the autonomous turbines, which, as a

rule, are made partial (with the gas feed not over the entire circumference of the wheel), conical nozzles are used extensively (Fig. 4.23). As experiments showed (see source [139]), the efficiency of the turbine with conical nozzles is equal or somewhat more than the efficiency of the turbine with a blade nozzle cascade.

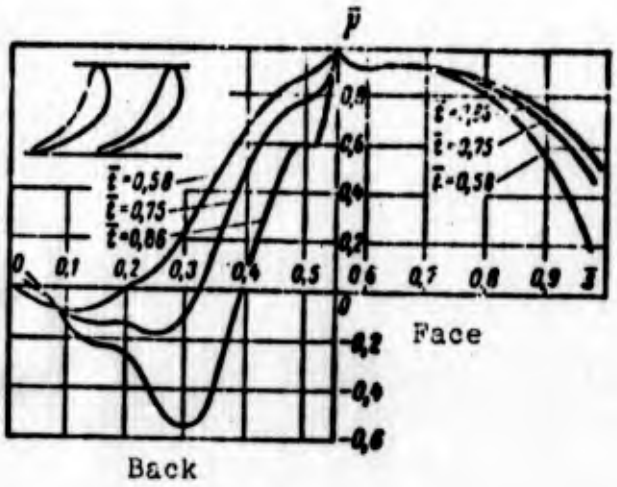

Fig. 4.22. Pressure distribution along the reactive profile at different values of the relative cascade pitch.

Fig. 4.23. Separate conical divergent nozzle.

Let us note that the conical nozzles are simple in a technological respect. In the conical nozzle the flow reaches the speed of sound in a cross section with a diameter of d_{min}. The

subsonic part of the nozzle is made with smooth contours. It is advantageous to design the divergent section of the nozzle of cross section d_{min} up to cross section 1'-1' with an angle of conicity not exceeding 12°-15°. Within limits of the oblique shear the conical surface of the nozzle usually passes over to a cylindrical section.

The inclination of the nozzle axis is made such that by taking into account the deviation in the flow in the oblique section, angle α_1 would be equal to 15°-20°. The determining of dimensions of the conical nozzle d_{min}, d' and the number of nozzles z_c will be examined further in Section 4.3.3.2.

4.3.2. FLOW OF GAS ABOUT THE CASCADES

4.3.2.1. Streamline Flow and Profiling of the Cascades at Subsonic Speeds

With a change in the flow velocity at the inlet into the cascade in the region $M_{w_1} < 0.3$-0.4 the nature of the flow in the cascade is not changed: the pressure distribution and loss factors remain constant. The gas is conducted basically as an incompressible liquid.

With M_{w_1} numbers which exceed 0.3-0.4, there appears the compressibility of the gas - the distribution pressure (see Fig. 2.49) and velocities on the cascade profile is changed, and the loss factors are changed.

At high subsonic speeds at the inlet into the cascade (M_{w_1} = 0.7-0.9), the velocity, increasing on the blade back, can become sonic and supersonic. If below along the flow the velocity is subsonic, then the translation of flow from supersonic velocity to subsonic occurs in the shock wave and is accompanied by an increase in losses in the cascade (wave losses). The supersonic

zones and shock waves appear at the trailing edge of the blade on the back side. They are connected with a velocity increase of the flow in the trailing edge, caused by the curvature of the trailing edge of the profile. A decrease in the curvature facilitates a decrease in the shock-wave intensity. This also facilitates a decrease in the thickness of the trailing edge.

With increase in M_{w_1} from low subsonic speeds ($M_{w_1} < 0.3$-0.4) to high subsonic speeds, losses in the subsonic cascade are first decreased and then increased (see curves A and B on Fig. 4.24). A decrease in losses is connected with a decrease in the boundary-layer thickness with an increase in M_{w_1}, which leads to a decrease in the profile and tip losses.

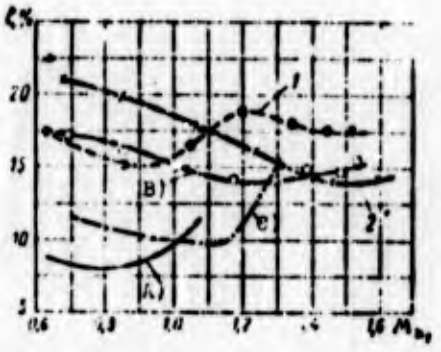

Fig. 4.24. Dependence of the loss factor in the rotor cascade on M number: A) subsonic cascade; B) transonic cascade; C) supersonic cascade with converging-expansion channels designed according to the method of the normal shock; 1 - supersonic cascade with a channel of constant section designed according to the method of normal shock; 2 - supersonic cascade designed according to the method of stepped braking.

The number $M^*_{w_1}$, at which in the vane channel the speed of sound is reached, is called critical. An increase in losses in the cascade begins after the achievement of critical value $M^*_{w_1}$ and is connected with wave losses and the flow separation caused by shock waves.

The rotor cascades designed for subsonic speeds of flow, just as the subsonic nozzle cascades (see Section 4.3.1.5), are made with a smoothly changing curvature of the back and face with a rounded leading edge. The greater the radius of rounding, the

less sensitive the cascade is to a change in the operating mode (angle of incidence).

Subsonic velocities at the inlet into the rotor cascade correspond to precombustion-chamber turbines of the LPRE made reactive (with a small degree of reaction) or impulse. Subsonic is usually also the flow at the inlet into the second stage of the autonomous double-staged turbine with the velocity stages.

Used as a rotor cascade of the reactive precombustion-chamber turbine are cascades of group A (see Fig. 4.20a), which are used as nozzle (see Section 4.3.1.5). Subsonic impulse cascades are selected from cascades of group A (see further Fig. 4.27), given in an atlas [4].

The cascades of group A have a smoothly convergent channel. The profile of these cascades is designed so that the working values M_{w_1} would be less than the critical number $M^*_{w_1}$.

As impulse cascades and cascades with small reaction, which have small span ($h_л/b_л$ < 1.5-1.7), in which losses to the vortex pair are great, it is recommended to use cascades of group $A_к$ (Fig. 4.25). The cascades of this group have an inlet nozzle divergent section ($a_m > a_1$) and an outlet convergent section ($a_m > a_2$). The entire vane channel acquires the diverging-converging shape. In the initial section of such a channel the rotation of the flow occurs at the reduced velocity, and, therefore, the transverse gradient of pressure is decreased. This leads to a decrease in the secondary losses (losses to the vortex pair). The convergent outlet section of the channel provides convergent flow on the back in the oblique shear, which prevents flow separation. Therefore, cascades $A_к$ make it possible to increase the angle of rotation of the flow (decrease the angles ($\beta_{1л}$ and $\beta_{2л}$), without fearing flow separation and increasing the losses. With the small span of the blade cascades of group $A_к$

have less than 1.3-1.5 times the losses than the cascades of group A over a wide range of subsonic velocities (Fig. 4.26).

Fig. 4.25. Rotor impulse cascade with diverging-converging channels (group A).

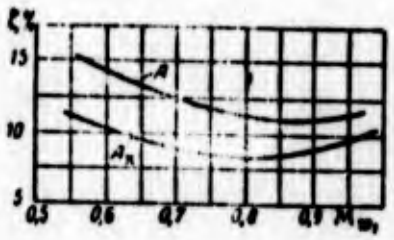

Fig. 4.26. Dependence of the loss factor on M number for the cascade of group A and cascade of group $A_н$ when $h_л/b_л = 0.9$.

Fig. 4.27. Spectrum of the flow in the subsonic rotor cascade (group A) at supersonic flow velocity at the inlet: 1, 2, 3, 4, 5 - shock waves.

The rotor cascade pitch and losses are determined in a similar way as the determination of corresponding values for nozzle cascades (see Section 4.3.1.5) - according to characteristics of the cascades given in atlas [4].

The angle of the blade at the inlet $\beta_{1л}$ is determined by the angle of the flow and angle of the attack:

$$\beta_{1л} = \beta_1 + i.$$

From the velocity triangle (see Fig. 2.22) we have

$$\beta_1 = \operatorname{arctg} \frac{\sin \alpha_1}{\cos \alpha_1 - (u/c_1)}.$$

The angle of attack is selected depending on the shape of the blade. For subsonic speeds the small negative angles of attack $i = -2° - -6°$ correspond to the minimum profile losses. The more the positive angle of attack, the more considerable falls the pressure on the blade back, and total magnitude of the circumferential force increases (see Fig. 2.49). The flow at large positive angles of attack at subsonic speeds leads to great losses, since regions of the diffuser flow are increased (see points 1-6 for $\beta_1 = 18°$ on Fig. 2.49).

Thus, losses with the flow around the profiles greatly depend on the angle of attack. Profiles with blunt rounded leading edges and dense cascades are less sensitive to a change in the angle of attack. Calculation of the effect of the angle of attack to losses in the cascade can be produced according to the approximate empirical dependence. Similar dependences are given in the atlas of profiles [4].

For the tentative calculations in the presence of the impulse profile, the following equation for determining the decrease in the efficiency of cascade can be used (see source [136]):

$$\frac{\Delta\eta}{\eta_p} = \left(\frac{\beta_{1p} - \beta_1}{\beta_{1p}}\right)^2 \text{ when } i > 0;$$

$$\frac{\Delta\eta}{\eta_p} = 0{,}15\left(\frac{\beta_{1p} - \beta_1}{\beta_{1p}}\right)^2 \text{ when } i < 0,$$

where β_1 and β_{1p} - the current and calculated flow angles, respectively; η_p - the calculated efficiency of the cascade.

The outlet angle $\beta_{2л}$ is selected depending on the degree of reaction of the cascade. In profiles of reaction cascades it is always less than $\beta_{1л}$, and it is determined by the necessary values of β_2. In impulse cascades it is also advantageous to make the outlet angle somewhat less than that of the input; this will insure the small convergence of the vane channel and will favorably be reflected on the reduction in the magnitude of losses:

$$\beta_{2л}=\beta_{1л}-(2^\circ \div 4^\circ).$$

4.3.2.2. Streamline Flow and Profiling of Cascades at Supersonic Velocities

The nature of the flow in the cascade is changed upon the reaching by the flow in front of the cascade of supersonic velocity. Figure 4.27 (see source [118]) shows the pattern of flow by the supersonic flow around the airfoil cascade adapted for the operation at subsonic velocities (group A). The profile has a rounded-off leading edge and the back in the intake and in the oblique shear is curvilinear.

In front of the leading edge there appears a bow shock wave 1, which in intensity is close to a straight line. After the shock wave the flow remains supersonic. In flowing past the convex intake of the back, the flow is accelerated in the beam of the characteristics (dashed line) just as with the flow around an obtuse angle. In the interaction of supersonic flow with the flow of less velocity, which passed through the bow wave of the adjacent blade, the supersonic flow is braked. There appears the shock wave 2, after which the boundary-layer separation is observed. Shock waves 1 and 2 form a Λ-shaped bow wave, after which the velocity drops to subsonic.

If pressure is sufficiently great, then in the oblique shear of the cascade the acceleration of flow will occur. As

a result of the great curvature of the outlet part of the back, the flow on the back will be accelerated in the beam of the characteristics (flow of an obtuse angle).

In flowing around the trailing edge of great curvature (thick edge) the supersonic flow is detached and braked. An edge shock 3 appears. The disturbance from this shock leads to the appearance of a shock 4 on the edge of the concave side. At the place of incidence in this shock on the adjacent blade shock 5 is formed. After shock 5, due to the great curvature of the back, the flow will be accelerated, being braked then in shock 3.

Thus, in the cascade designed for subsonic velocities, at supersonic velocities there appear additional losses in shock waves (wave losses) and losses in connection with the boundary-layer separation. With a velocity increase of the incident flow these losses rapidly increase. Hence there follows the need for the special profiling of blades for the supersonic flow of velocities.

The examined pattern of flow (see Fig. 4.27) makes it possible to conclude that the outlet and outlet sections of the back should be made rectilinear for the elimination of the acceleration of flow with its subsequent stagnation in the shocks. The leading and trailing edges are made sharp.

In the atlas [4] for transonic speeds the cascades of group B ($0.9 < M_{w_1} < 1.2$) are recommended (Fig. 4.28), and for supersonic velocities ($M_{w_1} = 1.2\text{-}1.8$) - the cascade of group C (see further Fig. 4.30a). The supersonic velocities of the flow of the rotor cascade correspond to autonomous turbines of LPRE. These turbines are made impulse.

The cascades of group B (see Fig. 4.28) are characterized by leading and trailing edges with small radii of rounding off and

Fig. 4.28. Rotor impulse cascade designed for transonic and low supersonic flow velocities (group B).

smoothly converging vane channels. The cascades of group B are designed according to the method of the normal shock. When $M_{w_1} > 1$ in front of the cascade the flow is braked in a normal shock (Fig. 4.29) and then is accelerated up to the sonic speed in the throat and supersonic speed in the oblique shear. In the region of the trailing edge shocks appear (similar to the profile of group A, see Fig. 4.27). However, the intensity of the shocks is less here, since the curvature of the back in the oblique shear is less than that in the cascade of group A. Losses in the cascades of group B are small. When $M_{w_1} > 1$ losses in the cascade of group B are considerably less than those in the cascade of group A, and at subsonic velocities - it is the opposite (see Fig. 4.24).

For high supersonic velocities ($M_{w_1} = 1.2\text{-}1.8$) in the atlas [4] cascades of group C, designed just as the cascade of group B, according to the method of the normal shock, are recommended.

The supersonic flow (Fig. 4.30a) is braked in the oblique shock 1 and then in the normal shock 2. The vane channel is convergent-divergent. In the initial convergent part the rotation of the flow at low subsonic velocities occurs. In the minimum cross section the speed of sound is reached. Then the flow is accelerated to the supersonic velocity in the divergent section of the channel and in the oblique section. The inlet and outlet parts of the back of the profile are made rectilinear. The contraction ratio of the channel and the expansion ratio of the channel

Fig. 4.29. Spectrum of cascade flow of group B at the supersonic inlet velocity.

a) b) c)

Fig. 4.30. Rotor impulse cascades designed for high supersonic flow velocities: a) cascade designed from the method of the normal shock (group C); b) cascade designed from the method of stepped stagnation; c) cascade designed from the method of smooth stagnation along the concave initial section of the back.

are selected at $M_{w_1} = 1.5\text{-}1.8$ within the following limits: $a_1/a_m = 1.1\text{-}1.2$; $a_2/a_m = 1.15\text{-}1.25$.

In previous designs of supersonic turbines cascades with channels of constant section were used. In this case after the normal shock prior to the beginning of the oblique section, the subsonic flow is braked because of friction, and only in the oblique section is the flow accelerated to supersonic velocity. However, experience shows that such an organization of the flow is accompanied by greater losses than in the convergent-divergent cascades (see Fig. 4.24). The use of convergent-divergent cascades of group C in turbines of LPRE is more preferable.

Besides the method of the normal shock, on the basis of which designed are the cascades of groups B and C, included in the atlas of the profiles [4], for calculating supersonic cascades (M_{w_1} > > 1.2) there are the method of stepped braking in the system of shocks (see Fig. 4.30b) and the method of smooth stagnation along the concave initial section of the back (see Fig. 4.30c) (see source [4, 118]). During the calculation, according to these methods the stagnation of flow is organized in the system of shocks consisting of several oblique shocks closed by a normal shock. After the normal shock, just as in the case of cascades of group C, the subsonic flow is accelerated in the convergent-divergent channel up to supersonic velocity. Thus, in the channel mixed flow takes place: first subsonic and then supersonic.

The cascade can be designed in such a way that the flow over the entire length of the vane channel is supersonic (see sources [4, 37]). Figure 4.31 (see source [146]) shows the spectrum of flow in such a cascade. At the inlet into the cascade an oblique shock wave is formed, after which the supersonic flow is turned by the vane channel to a preset angle. In the channel the supersonic flow is accompanied by the compression and rarefaction waves, which are seen on Fig. 4.31.

The methods of stepped braking, smooth stagnation and the method of supersonic flow in the channel make it possible to design cascades having less losses at M_{w_1} > 1.4-1.5 than those of cascades calculated in the method of the normal shock (see Fig. 4.24). However, such cascades are more sensitive to a change in the operating mode. With a change in M_{w_1} and the incidence the calculated system of shocks is disturbed, and the losses increase sharply.

GRAPHIC NOT REPRODUCIBLE

Fig. 4.31. Spectrum of supersonic flow in the channel of the impulse rotor cascade: 1 - arrangement of the edge of the blade of the shadow instrument.

4.3.2.3. Determination of tne Angle of Departure from the Cascade with the Flow of Gas about it at Supersonic Speed

With the flow around the cascade of impulse profiles by supersonic flow, the outlet angle from cascade (Fig. 4.32) can be accurately determined by experimental means (see source [4]). For its approximate computations it can be found from the continuity equation recorded for the averaged parameters.

For the cross Section 1-1 (see Fig. 4.32) and cross section 2-2 behind cascade (theoretically at infinity), it is possible to write (at the constant height of the cascade):

$$q(\lambda_{w_1})\varepsilon_1 \sin\beta_1 = q(\lambda_{w_2})\varepsilon_2 \sin\beta_2. \qquad (4.57)$$

From expression (4.57) we will obtain

$$\sin\beta_2 = \frac{\varepsilon_1}{\varepsilon_2}\sin\beta_1 \frac{q(\lambda_{w_1})}{q(\lambda_{w_2})}. \qquad (4.58)$$

4.3.2.4. Conditions of "Blocking" of the Rotor Cascade

As was noted in Section 4.3.2.1, in the minimum cross section of the nozzle cascade with the critical pressure ratio ($\delta_1 = \delta_{кр}$) the speed of sound is established; in this case the flow rate reaches the maximum value at the assigned parameters at the inlet p_0^* and T_0^*. An increase in the pressure ratio ($\delta_1 > \delta_{кр}$) leads to expansion of the gas in the oblique section without a change in the flow rate through the cascade, i.e., the cascade is "blocked" without passing the flow rate more than the maximum. Conditions of "blocking" can also take place in the rotor cascade.

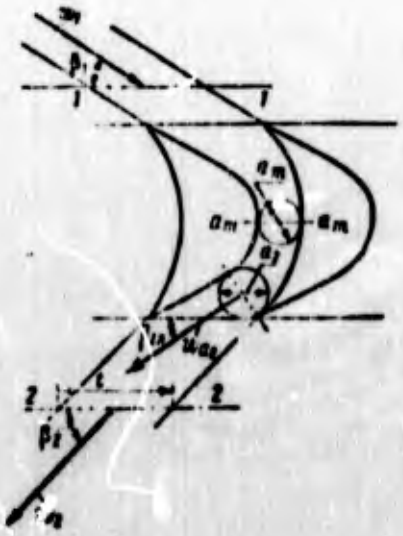

Fig. 4.32. Determination of the angle of departure of the flow form the impulse cascade.

Let us find the condition determining the conditions of "blocking" with constant initial pressure $p^*_{w_1}$ and temperature $T^*_{w_1}$, considering the cross section a_m-a_m (see Fig. 4.32) as the minimum cross section of the vane channel. From the continuity equation let us determine the dependence of the current density in cross section a_m-a_m from the initial parameters:

$$q(\lambda_{w_1}) f \sin\beta_1 = \sigma_{a_m} q(\lambda_{w_m}) a_m;$$
$$q(\lambda_{w_m}) = \frac{q(\lambda_{w_1}) f \sin\beta_1}{\sigma_{a_m} a_m}, \tag{4.59}$$

where σ_{a_m} is the coefficient of total pressure for the flow from inlet to the cross section a_m-a_m.

The relation

$$q(\lambda_{w_m}) \leqslant 1 \tag{4.60}$$

corresponds to the possible (including sonic) flows in the minimum cross section of the cascade, i.e., with the maintaining of this relation the cascade is flowed around without "blocking."

The relation

$$q(\lambda_{w_m}) > 1 \tag{4.61}$$

determines conditions which cannot be realized, i.e., it is the condition of "blocking" of the rotor cascade. The assigned flow rate in this case cannot be passed through the cascade. With "blocking" in the case of supersonic flow the reference system of shocks is disturbed, and, as a rule, in front of the cascade a normal shock appears.

Conditions of "blocking" [$q(\lambda_{w_{a_m}}) > 1$] is undesirable, since it leads to added losses. In the designing of its stage it is possible to avoid, in selecting the angle β_1, the area of the minimum cross section and the cascade pitch in order to insure the relation (4.60).

Let us note that conditions of "blocking" can appear also in the off-design operating modes.

4.3.3. HEIGHT AND WIDTH OF CASCADE AXIAL CLEARANCE

4.3.3.1. Height and the Width of Nozzle Cascade. Degree of Admission

The height of the nozzle blades is determined by the flow rate of the gas which must be passed through the cascade.

Let us write equation (4.37) for parameters in the cross section after the cascade where the flow was equalized:

$$G_1 = \pi D_{cp} h_c \frac{p_1^* m}{\sqrt{RT_1^*}} q(\lambda_{c_1}) \sin \alpha_1. \qquad (4.62)$$

From equation (4.62) h_c is determined:

$$h_c = \frac{G_1 \sqrt{RT_1^*}}{\pi D_{cp} \sigma_1^* p_1^* q(\lambda_{c_1}) m \sin \alpha_1}, \qquad (4.63)$$

where σ_1^* is the coefficient of total pressure from the inlet to the calculated cross section.

The coefficient of total pressure is determined according to wind-tunnel tests directly or in terms of the speed factor ϕ. The coefficient ϕ is determined from the loss factor ζ, the value of which is found by the characteristics of the selected nozzle cascade (see source [4]).

It is desirable to have a great height of the nozzle, since secondary losses will be less at greater height of the nozzle.

The dependence of the speed factor of the cascade (taking into account secondary losses) on the relative height of the nozzle is represented by the graph given on Fig. 4.33. If the height of the nozzles is less than 8-12 mm, then usually one should turn to the gas feed not over the entire circumference but over part of it (partial admission); in this case the stage should be made impulse. Turbines with partial admission are usually autonomous turbines of the [LPRE] (ЖРД).

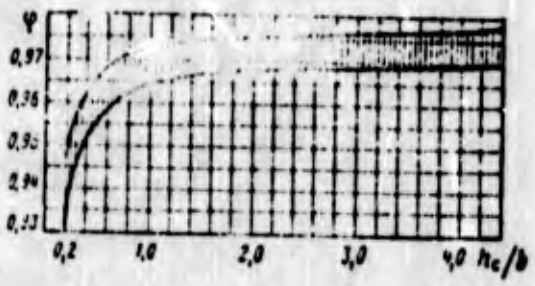

Fig. 4.33. Approximate dependence of the velocity factor of the converging cascade on the relative height of the nozzle.

Let us introduce the concept about the degree of admission for the nozzle cascade. Let us define the degree of admission as the ratio of the arc occupied by the nozzle cascade to the length of the circumference according to the mean diameter:

$$\varepsilon = \frac{t_c z_c}{\pi D_{cp}}. \qquad (4.64)$$

For $\varepsilon < 1$ equation (4.63) takes the following form:

$$h = \frac{G\sqrt{RT_0^*}}{\sigma_{cp} D_{cp} P_0^* q(\lambda_{c_1}) m \sin\alpha_1}; \qquad (4.65)$$

hence

$$s = \frac{G\sqrt{RT_0^*}}{h_c \sigma_{cp} D_{cp} P_0^* q(\lambda_{c_1}) m \sin\alpha_1}. \qquad (4.66)$$

It is necessary to keep in mind that with the assigned flow rate through the turbine there is an optimum, with respect to efficiency, degree of admission (height of the nozzle blades) (see further Section 4.5.4.2).

For the converging nozzle cascades of small height, it is advantageous to shape specially the meridian section (Fig. 4.34). In cascades with the compression of the outlet section in the meridian plane, the convergent flow on the back in the oblique section is provided, and the point of the minimum of pressure is shifted to the trailing edge. A pressure difference between the face and the back in the region of the maximum curvature is decreased, and the intensity of the secondary flows is reduced. The efficiency of the turbine is usually increased in this case by 1-1.5% (see source [3]).

The optimum value of compression $\frac{h_0 - h_c}{h_c} = 0.3\text{-}0.6$ at $h_c/b_c = 0.2\text{-}0.5$ (where b_c is the airfoil chord).

At the low height of the nozzle cascade for a decrease in losses to the vortex pair, one should decrease the blade chord (see source [17]), striving to insure $h_c/b_c > 1$ (see Fig. 4.33).

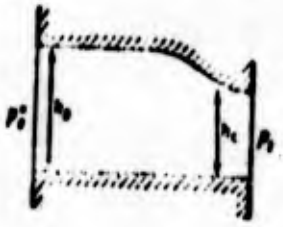

Fig. 4.34. Profiling of the meridian section of the nozzle cascade of low height.

In this case the blade chord is selected at a minimum from technological considerations ($b_c \geq$ 8-15 mm).

Nozzle blades of the precombustion-chamber turbines have a sufficiently high height, and therefore their chord is accepted usually larger than that of autonomous turbines ($b_c \geq$ 15-30 mm).

4.3.3.2. Height of Conical Nozzles. Quantity of Nozzles

In autonomous partial-admission turbine of LPRE, as a rule, nozzle cascades consisting of separate conical nozzles are used (see Fig. 4.23). It is advantageous to begin the calculation of such nozzle cascades from the determination of the total area of the minimum (critical) cross section $F_{min} = z_c f_{min}$ [see equation (4.40)].

After the determination of F_{min} we determine the nozzle expansion ratio $\bar{f}_1'$ according to equation (4.53). For design conditions we usually assume that $\delta_1' = \delta_1$, i.e., in the design conditions expansion in the oblique section is not provided for in view of the small expansion ability of the section.

For multimode turbines of the LPRE operating in off-design conditions, with the degrees of the pressure drop which exceed

those calculated it is advantageous to select the expansion ratio of the nozzles at 15-20% less than that which is obtained as a result of the calculation according to equation (4.53).

The cross-sectional area of the nozzles 1'-1' (see Fig. 4.23) is determined according to the found expansion ratio:

$$F_1' = \bar{f}_1 F_{min}; \qquad (4.67)$$

The area of the nozzle outlet $F_c = F_1'/\sin \alpha_{1r}$ (where α_{1r} is the angle of inclination of the nozzle axis).

Height of nozzle cascade h_c is the dimension of the radial axis of the ellipse in the nozzle outlet section (Fig. 4.35). The major axis of the ellipse is connected with h_c by the relation

$$a_c = h_c/\sin \alpha_{1r},$$

and the area of the nozzle outlet is determined according to equation

$$f_c = \frac{\pi}{4} h_c a_c = \frac{\pi}{4} \frac{h_c^2}{\sin \alpha_{1r}}. \qquad (4.68)$$

the optimum height of the nozzle $(h_c)_{opt}$ at which the degree of admission is optimum and the efficiency of the turbine reaches a maximum is determined according to equation (4.132), assuming that $h_c = h_{1n}$ (see further Section 4.5.4.2). Then the optimum quantity of the nozzles will be determined by the expression

$$(z_c)_{opt} = F_c/(f_c)_{opt};$$

or, having substituted expressions (4.67) and (4.68), we obtain

$$(h_c)_{1,4} = \frac{\Delta P_1'}{\pi (h_c)_{opt}^2}. \qquad (4.69)$$

By rounding off the number of the nozzles to the smaller integer, let us refine the height of the nozzles h_c.

For nozzle cascades comprised of conical nozzles, the degree of admission is the ratio of the total area of the nozzle outlet to the area of the ring with width of h_c:

$$\varepsilon = \frac{z_c f_c}{\pi D_{cp} h_c} = \frac{F_c}{\pi D_{cp} h_c}. \qquad (4.70)$$

The diameter of the cone in cross section 1'-1' (see Fig. 4.23) is equal to h_c. Let us find the diameter of the minimum cross section from value F_{min} and the number of the nozzles:

$$d_{min} = \sqrt{\frac{\Delta P_{min}}{\pi a_c}}.$$

Sometimes, for purposes of decreasing the area between the nozzles (see Section 4.5.2.2), the nozzles are arranged so that their outlet sections would partially overlap (see Fig. 4.35). With considerable overlap the losses will increase in connection with the intersection of the jets escaping from the adjacent nozzles. Therefore, the relative overlap

$$\eta = \frac{a_c - l_c}{a_c}$$

should not exceed 0.02 (see source [145]).

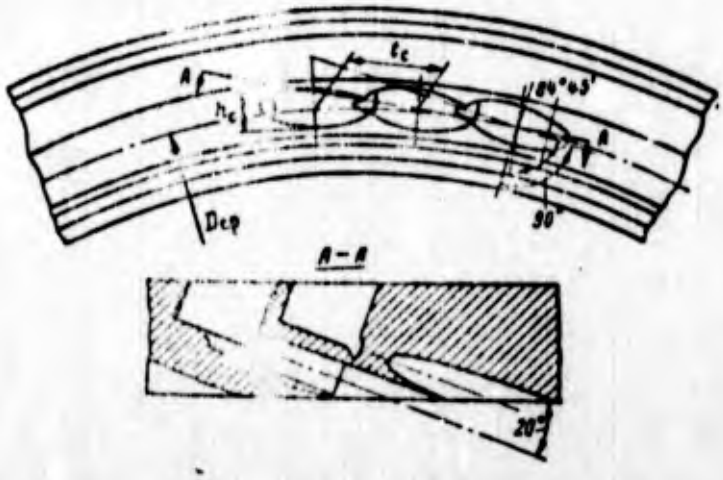

Fig. 4.35. Segment of conical nozzles with the overlap of the outlet sections.

4.3.3.3. Height and Width of the Rotor Cascade

The height of the rotor blade at the inlet is determined according to value of the height of the nozzle cascade (conical nozzle), increased by the dimension of the overlaps, (Fig. 4.36):

$$h_{1л} = h_c + \Delta h_п + \Delta h_{вт}, \qquad (4.71)$$

where $\Delta h_п$ and $\Delta h_{вт}$ are the overlaps of the rotor blade, in comparison with the nozzle, on the periphery and near the hub, respectively.

The overlaps $\Delta h_п$ and $\Delta h_{вт}$ are introduced in order, with technological errors in the relative location of the nozzle cascade and wheel and with shaft deflections, to insure the unimpeded gas flow from the nozzle cascade into the wheel.

An experiment shows (see source [2]) that for a decrease in losses in the impulse subsonic and supersonic stages the

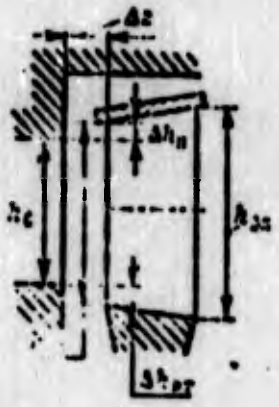

Fig. 4.36. Meridian section of the rotor wheel.

overlaps should be a minimum. It is possible to accept an overlap on the periphery of 1-2 mm and at the hub - 0.1 mm.

In reaction turbines it is also advantageous to introduce overlaps (see source [120]). On the periphery the overlap should be made more, the higher the degree of reaction and the axial clearance: usually $\Delta h_п$ = 2-4 mm; $\Delta h_{вт}$ = 1-2 mm.

The height at outlet from the rotor cascade is calculated on the basis of the continuity equation:

$$h_{2a} = \frac{G' \sqrt{RT^*_{0_1}}}{m z \lambda_{2p} p^*_{0_1} \varepsilon(\lambda_{0_2}) \sin\beta_2}. \qquad (4.72)$$

where G' - flow rate, taking into account leakages or inleakage.

From the conservation equation, recorded for cross sections at the inlet into the blades and at the outlet from them, we have the ratio

$$\frac{h_{2a}}{h_{1p}} = \frac{q_1}{q_2} \frac{c_{1a}}{c_{2a}}.$$

Consequently, the greater ρ_1 will be than ρ_2, the less c_{2z} will be than c_{1z} and the greater $h_{2л}$ will be than $h_{1л}$. For reaction blades, as a result of the expansion of gas, always $\rho_1 > \rho_2$. For impulse blades, as a result of preheating because of the heat of friction, we also have $\rho_1 > \rho_2$. The axial velocity at the outlet for impulse turbines is less than that at the inlet, as a result of a decrease in the velocity w ($w_2 < w_1$ and $c_{2z} < c_{1z}$).

For reactive blades a decrease in the angle $\beta_{2л}$ leads to reduction in c_{2z}, and an increase in velocity w_2 increases the value c_{2z}.

When $h_{2л} > h_{1л}$ (which is especially characteristic for impulse blades) the meridian section is made expanded. It is advantageous to limit the angle of expansion as was shown in Section 2.13.2.1 ($\lambda \leq 15°-20°$, see Fig. 2.86). Sometimes, taking into account the overlaps, the span of the blade at the inlet is equal to its span at the outlet: $h_{1л} = h_{2л}$. If too large an overlap is taken, then according to the calculation $h_{2л} < h_{1л}$ can be obtained. Virtually in this case the overlap is decreased, and $h_{2л} = h_{1л}$ is accepted.

With short and wide blades the profiling of their meridian section should be made with a narrowed average section (Fig. 4.37). The introduced convergence in the initial section can reduce the secondary losses as a result of the thinning of the boundary layer on limiting surfaces.

With short blades the secondary losses will be more. The velocity factor, which considers profile losses and secondary

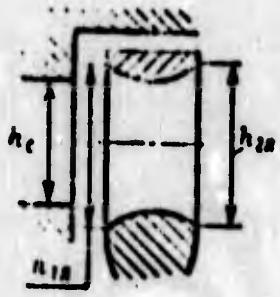

Fig. 4.37. Profiling of the meridian section of the rotor cascade of low height.

losses, will be lowered noticeably with a decrease in the height of the blades (see Fig. 4.38, taken from work [17], where data on velocity factors ψ are given).

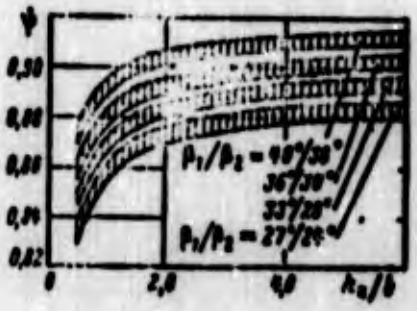

Fig. 4.38. Approximate dependence of velocity factor ψ for impulse profiles on the relative height of the blade.

Short rotor blades, just as the nozzle blades, should be made narrow, providing ratios $b_{1л}/b_л > 1$. The width of the short blades should be selected at a minimum from technological considerations (8-15 mm).

Losses connected with the finite length of the blade - mainly losses to the vortex pair - can be taken into account by a decrease in the efficiency of the rotor cascade ($0.7 < M_{w_1} < 1.5$) (see source [138]):

$$\Delta\eta_{\text{вн}} = 0{,}13 \frac{h'/b_{1л}}{1 + M_{w_1}}, \qquad (4.72a)$$

where b is the width of the blade.

With an increase in the M_{w_1} number, losses to the vortex pair are decreased, since the boundary-layer thickness on the limiting surfaces and blades is decreased.

For short blades it is advantageous to have a closed radial clearance, i.e., to use shrouds for the overlap of the vane channel on the periphery (see Fig. 4.36) and the prevention of gas overflow from the face to the back. The efficiency of the turbine from the use of a shroud can be raised by 5-10% (see source [129]). Limitation for the use of blades with a shroud is the fact that the shroud increases the inertia mass, and forces from the centrifugal forces of inertia sharply increase.

In turbines of LPRE which have comparatively short blades (which is explained by the low volumetric gas flow rate), it is advantageous to use shrouds. The use of shrouds with long blades and also during partial admission is advantageous for the prevention of vibrations of the blades, since the shroud increases the rigidity of the wheel.

In rotor blades the shroud, of course, does not remove overflowing through the radial clearance above the shroud in an axial direction under the action of a pressure difference at the inlet into the cascade and at the outlet from it.

If the shroud cannot be used according to the conditions of strength, then radial clearance should be made as minimum as permissible. Usually it is selected in order that in the heated state a clearance of 0.4-0.6 mm would be guaranteed.

The expression for the velocity coefficient of rotor blades with a shroud at supersonic velocities can approximately be presented in the form (see source [135])

$$\varphi = \left[1 - 0{,}03\left(1 - \frac{b_1 + b_2}{a}\right)^2\right]\left[1 - 0{,}05(M_{w_1} - 1)^2\right]\left[1 - 0{,}06\frac{\delta}{\Delta_{1,2}}\right]. \qquad (4.73)$$

The first term in equation (4.73) considers friction losses and vortex formation during the flow around the blade, the second term - the wave losses (when $M_{w_1} \leq 1$ this term should be taken equal to unity) and the third term - tip losses in the cascade. The first two terms together characterize profile losses of the cascade with the supersonic flow of the rotor-wheel blades.

Let us recall that the blades of autonomous turbines of LPRE are relatively short ($D_{cp}/h_л > 10$). Therefore, they are made with respect to height. Blades of the precombustion-chamber turbines when $D_{cp}/h_л < 5$-8 should be shaped over the radius (see Section 2.11.2).

4.3.3.4. Determination of Axial Clearance

An increase in the axial clearance Δz (see Fig. 4.36) between the nozzle cascade and the rotor cascade leads to the equalizing of the flow velocities at the inlet into the wheel. However, an increase in the axial clearance increases friction losses in the clearance and also the inleakage or leakage of the gas. The latter fact proves to be the determining one for autonomous

turbines of LPRE where the seal on the axial clearance is absent. With partial feed the gas through the axial clearance overflows on the arc not occupied with nozzles to the turbine exhaust. This leads to a drop in the efficiency of the turbine.

Figure 4.39 gives the experimental dependence of the efficiency for the autonomous turbine with partial admission from the axial clearance. It is evident that with an increase in the clearance the efficiency falls. Therefore, in partial-admission turbines the axial clearance is made as minimum as permissible in order to provide a reliable operation in a hot state, i.e., under conditions when temperature strains are developed. In a cold state this clearance is 2-3 mm.

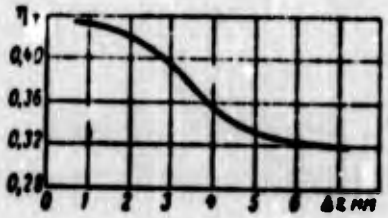

Fig. 4.39. Dependence of efficiency on axial clearance for a high-pressure turbine with partial admission ($\varepsilon = 0.3$).

Figure 4.40 gives results of experiments which reveal the effect of the axial clearance on the efficiency of the turbine with a full feed (precombustion-chamber turbine). The calculated reaction of the turbine at the mean diameter was 0.25. The radial clearance between the shroud of the blade and housing was 2 mm. The effect of the axial clearance on the efficiency of the turbine is considerable; the optimum amount of the clearance is clearly revealed. Usually for precombustion-chamber turbines the axial clearance is selected from design considerations in the range of 4-6 mm.

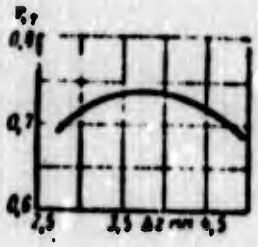

Fig. 4.40. Dependence of efficiency on the axial clearance for low-pressure turbine.

4.3.4. FEATURES OF THE CASCADE FLOW OF RADIAL-AXIAL INWARD-FLOW TURBINES AND METHODS OF THEIR DESIGN

4.3.4.1. Fixed Circular Cascades (Nozzle)

In circular turbine cascades (Fig. 4.41) the flow lines in front of the cascade and after the cascade will be spirals, and therefore trailing edge of the blade back is delineated on a curve close to the logarithmic spiral (see Fig. 4.41b). Profiles simpler in a technological respect, formed with the aid of three straight lines connected by circular arcs (see Fig. 4.41a), are used. A turbine with a nozzle cascade composed of such profiles has a sufficiently high efficiency with pressure ratios $\delta < 2$.

In the nozzle cascade of a radial-flow turbine it is advantageous to use profiles which are well recommended in an axial-flow turbine with reconstruction of them by the method of conformal mappings from the cascade into the circular. Reconstruction is produced with the aid of equations given in work [7]:

$$\bar{r} = \bar{r}_0 e^{\bar{y}}; \quad \bar{y} = \bar{x} \ln \bar{r}_0,$$

where $\bar{r} = \frac{r}{r_1}$; $\bar{r}_0 = \frac{r_0}{r_1}$; $\bar{y} = \frac{y}{b}$; $\bar{x} = \frac{x}{b}$;

Fig. 4.41. Different forms of circular cascades: a) with the profile of the blades formed by straight lines and circular arcs; b) with the profile of the blades the trailing edge of the back of which is outlined by the logarithmic curve; c) with the profile of blades obtained by the conformal mapping of the profile of the cascade on the circular region (profile from those presented in work [7]).

x, y - coordinates of the initial profile; r_0 - maximum radius of the circular cascade; r_1 - the minimum radius of the circular cascade; r - the current radius of circular grating; b is the width of cascade.

For an example Fig. 4.41c depicts the cascade changed over from a straight cascade. The information necessary for the construction of such profiles and data on the results of the testings are given in work [7]. Used an initial profile was the profile for the axial-flow turbine TS-2A. Cascades with profiles of such type operate well in varying conditions and make it possible without a noticeable change in magnitudes of losses to pass over from subsonic to supersonic conditions. The optimum value of the relative pitch according to the outside diameter for such profiles lies within limits of $\bar{t}_1 = 0.5\text{-}0.7$.

In connection with the natural convergence during the flow to less radii, the angle of departure from the nozzles can be

large. Secondary losses in this case should be less than those of axial-flow turbines, since the turn of the flow will be not so steep. Their value will be changed inversely proportional to the parameter h_c/b. As a rule, in radial-flow turbines it is possible to use the lower heights (widths) of the nozzle blades h_c than in axial-flow turbines, without fearing very great losses.

At low heights of the nozzle blades ($h_c/b < 0.3$) the meridian profiling of the blades, similar to the meridian profiling of the nozzle cascades of axial-flow turbines (see Fig. 4.34), can prove to be advisable.

The relationships used for determining the angle of departure of the flow from the cascade are valid also for the circular cascade.

4.3.4.2. Rotor Wheels of Radial-Axial Inward-Flow Turbines

General Considerations

The form of the interblade impeller channels depends on the relationship of diameters of the inlet and outlet and on the direction of blades at inlet and outlet. The basic requirement which must be made for obtaining minimum losses in the flow along the vane channels is the absence of diffuser flows.

In comparison with the relative velocity in channels of the wheel of the axial-flow turbine, the relative velocity in channels of the wheel of the radial-axial turbine, with the identical ratio of pressures for rotor wheels of both turbines, will be less. This is explained by the fact that only part of

the potential energy turns into kinetic energy, and its remaining part is transferred to the wheel with the moving of the gas to smaller radii in the field of inertial forces. Because of the fact that the surface of the blades will be more, the pressure differential appearing per unit length of the blades cannot be very large. Therefore, secondary losses are decreased, which makes it possible to use radial wheels with a small width of the meridian section. This circumstance is important for the turbine of the LPRE, since the gas enters from the gas generator into the turbine with a low volume flow rate and, as a rule, the calculated width of the wheel at the inlet is small.

Number of Blades and Blade Pitch

Radial-axial wheels have a smaller number of blades than do the axial, since the number of blades is determined from the value of the optimum blade pitch at the outlet, i.e., where there occurs rotation of the flow. The outlet diameters of radial-axial wheels are small, and even with the small numbers of the blades there is provided great cascade density in the region of the outlet from the wheel, in the zone of the sharp turn of the flow. On the average outlet diameter the relative blade pitch can be selected from the smallest value for the axial-flow turbines: $\bar{t} = 0.45\text{-}0.65$.

Profiling of the Meridian Section

The width of the wheel at the inlet is determined by the value and angle of the inclination of the absolute outlet velocity from the nozzles. With the high densities of the working medium and moderate flow rates (low values of $n_{s\ T}$), it is desirable to increase the width of the wheel at the inlet.

This can be achieved, having decreased the velocity c_{1m}, selecting smaller angles of α_1 (up to 12°-15°). If the width of the wheel in this case is less than 4-6 mm, then partial admission is used. The width of the nozzle cascade is found from the equation of the flow rate according to the equation similar to equation (4.65):

$$b_c = \frac{G\sqrt{RT_0^*}}{m\pi D_1 p_0^* q(\lambda_{c_1}) \sin\alpha_1}. \qquad (4.74)$$

The width of the wheel on the outside diameter

$$b_{1a} = b_c + \Delta b, \qquad (4.74a)$$

where Δb is the overlap equal to 0.5-1.5 mm.

For a smooth change in the meridian section the relation of the meridian velocity is assigned (see source [7]):

$$\frac{c_{2m}}{c_{1m}} = 0{,}7 \dots 1{,}2$$

with the assigned value c_{2m}, the flow angle at the outlet from the wheel will be found from relation

$$\sin\beta_2 = \frac{c_{2m}}{w_2}.$$

The height of the trailing edges is found by the equation similar to equation (4.72):

$$b_{2a} = \frac{G\sqrt{RT_{w_2}^*}}{m\pi D_{2cp} p_{w_2}^* q(\lambda_{w_2}) \sin\beta_{2cp}}. \qquad (4.75)$$

The width of the impeller vanes at the outlet b_{2n} (on diameter D_2, see Fig. 4.42) is usually selected within limits $(0.1\text{-}0.2)D_1$.

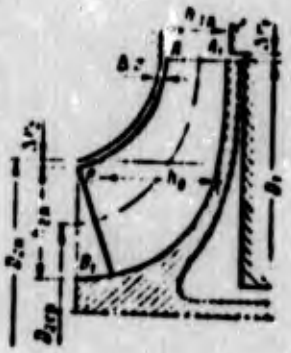

Fig. 4.42. Meridian section of the wheel of a radial inward-flow turbine.

The contours of side surfaces of the rotor wheel are selected arbitrarily, but they should insure a smooth change in the flow areas. It is desirable to have at extreme points A and A_1 and B and B_1 (Fig. 4.42) a zero or small curvature.

Profiling of the Blades

The optimum angle of attack for blades of the radial wheels is negative and consists of -10°to-20°.

In the rotating wheel the flow undergoes the effect of the Coriolis forces of inertia, deviating the flow relative to the wheel to the side of the rotation (see Fig. 2.58). Therefore, at the inlet into the wheel it is advantageous to have a direction of relative velocity different from the direction of the blade, i.e., the vector of relative inlet velocity w_1 should be displaced relative to the blades to the side opposite to the rotation.

By knowing from the inlet velocity triangle the flow direction in the relative motion - the flow angle β_1, let us find the angle of the blade from the relation

$$\beta_{1л} = \beta_1 - (10° + 20°). \qquad (4.76)$$

In practice (basically, this is dictated by considerations of strength) blades radial at the inlet ($\beta_{1л} = 90°$) are most frequently used. The radial inlet ($\beta_{1л} = 90°$) requires a completely specific relationship of velocities u_1/c_1, taking into account the incidence [see equation (4.76) and Fig. 2.24)]:

$$\frac{u_1}{c_1} = \cos\alpha_1 - \sin\alpha_1 \cdot \operatorname{ctg}\beta_{1л}. \qquad (4.76a)$$

With the assigned magnitude of the circular velocity the absolute velocity c_1, and correspondingly, the pressure ratio, acquire a quite definite value. When u_1 = 300 m/s and RT_0^* = $= (3\text{-}5)\cdot 10^5$ J/kg the value δ should be equal to 1.15-1.35. Such values of the pressure ratio δ are characteristic for the turbine with the gas feed into the combustion chamber. For turbines of the uncovered design such low pressure ratios are disadvantageous. This is one of the reasons why radial autonomous turbines are not usually used in LPRE.

The trailing edge of the blade is made with the angle of bending back to the side opposite to the rotation. For obtaining a purely axial velocity (without the circular component) the angle of bending back at the mean diameter is found from the relation

$$\cos\beta_{2л.ср} = \frac{u_2}{w_2}. \qquad (4.76b)$$

Angles $\beta_{2л}$ on different radii are found from the relation

$$\operatorname{ctg}\beta_{2л} = \operatorname{ctg}\beta_{2л.ср}. \qquad (4.77)$$

which corresponds to $c_{2u} = 0$ and $c_{2z} = \text{const}$. Experience shows that it is possible to use successfully radial-axial wheels made with a constant angle of bending back of the blades (see source [7]).

The value $D_{2ср}$ is determined from design considerations, and frequently we select $D_{2ср} = (0.3\text{-}0.6)D_1$.

The relative outlet velocity w_2 will be found from the relation

$$L_{вн} = \frac{\left(\frac{w_2}{2}\right)^2 - w_1^2}{2} + \frac{w_1^2 - w_2^2}{2}, \qquad (4.78)$$

where

$$L_{вн} = \frac{k}{k-1} RT^*_{w_1}\left[1 - \left(\frac{p_2}{p_1}\right)^{\frac{k-1}{k}}\right]; \qquad (4.79)$$

$T^*_{w_1}$ is determined from equation (4.32).

From equation (4.78) we have

$$w_2 = 2\sqrt{2L_{вн} + w_1^2 - (u_1^2 - u_2^2)}; \qquad (4.80)$$

$$\lambda_{w_0} = \frac{w_1}{\sqrt{2\frac{k}{k+1}RT^*_{w_0}}}. \qquad (4.81)$$

The stagnation temperature in the process of flow over the wheel is decreased. The energy of the gas is lowered by the value of the potential energy corresponding to the transition of particles of gas on smaller radii in the field of inertial forces of the rotary motion:

$$T^*_{w_1} = T^*_{w_0} - \frac{k-1}{kR}\frac{u_1^2 - u_0^2}{2} \qquad (4.82)$$

(see the representation of the process in the radial-flow turbine in i-s-diagram shown on Fig. 4.14).

For precomputations of radial-axial turbines, it is possible to assume that $\psi = 0.86\text{-}0.92$.

Selection of Clearances

The selection of clearances for radial-axial turbines is based on experimental data. Experiments (see source [131]) showed the weak dependence of the effectiveness of the turbine on the value of the axial clearance. This is one of the advantages of a radial-flow turbine. The clearance can be selected within limits of $\Delta z = (0.5\text{-}0.15)\ h_{1л}$, but it should always be more than 0.5-1 mm.

The weak effect of the axial clearance on the effectiveness of the turbine can be explained by the fact that in the clearance

the static pressure of the gas is greater than that in the wheel, since in the wheel with motion toward the center the static pressure rapidly falls. Therefore, the gas overflow through the top of blade and the gas escape along the radial part of the wall of the housing are restricted. The gas escape in this case will be determined by the clearance at the outlet from the wheel.

Experiments show that the radial clearance at the outlet from the wheel Δr_2 (see Fig. 4.42) has a more considerable effect on the effectiveness of the turbine. The great effect Δr_2 on the effectiveness of the radial wheels is explained by the fact that in the region of the outlet there appear secondary flows connected with the radial clearance similar to flows in the axial-flow turbine. The radial clearance Δr_2 can be selected within limits of $\Delta r_2 = (0.015\text{-}0.03)h_0$ (see Fig. 4.42), but it is not less than 0.5-1 mm.

The effect of the radial clearance Δr_1 (see Fig. 4.42) is analogous to the effect of the axial clearance in axial-flow turbines; basically it is selected from design considerations and should be not less than 0.5-1 mm.

On the basis of the effect of clearances established above, it can prove to be advisable to cover the blades with a shroud (double shrouded wheels, see further Fig. 4.52).

4.4. CIRCULAR EFFICIENCY AND OPERATING FACTOR OF THE STAGE OF THE TURBINE

4.4.1. Derivation of the Equation for Circular Efficiency

In Section 2.15 the concept about the circular efficiency of the turbine was introduced.

Work on the circumference of the wheel L_u is less than the available energy $L^*_{ад}$ by the value of losses of energy in the nozzle cascade L_ϕ [see equation (4.16)], losses in the rotor cascade L_ψ [see equation (4.22)] and losses with the outlet velocity $L_c = c_2^2/2$:

$$L_u = L^*_{ад} - L_\phi - L_\psi - L_c. \qquad (4.83)$$

We determine the circular efficiency of the stage of the turbine in the same way as we defined it in Section 2.15.1, i.e., as the ratio of the circular work of the wheel to the available adiabatic work:

$$\eta_u = \frac{L_u}{L^*_{ад}} = 1 - \frac{L_\phi + L_\psi + L_c}{L^*_{ад}}. \qquad (4.84)$$

The efficiency on the circumference of the wheel estimates the degree of utilization of the available work being converted into the useful work of the wheel, and considers the losses with the outlet velocity and hydraulic losses in flow area, including the profile, secondary and additional losses. Losses in the flow area of the turbine are estimated by values L_ϕ and L_ψ.

The hydraulic perfection of the flow area is determined by the hydraulic efficiency of the turbine (see Section 2.15.1), which is the ratio of the full circular work to the available adiabatic work:

$$\eta_г = \frac{L^*_u}{L^*_{ад}} = \frac{L_u + \frac{c_2^2}{2}}{L^*_{ад}} = \eta_u + \frac{L_c}{L^*_{ад}}. \qquad (4.85)$$

The value of the circular efficiency η_u largely defines the effective efficiency of the turbine $\eta_т$ characterizing the perfection of the turbine as a drive engine (see Section 2.15.4). The circular efficiency is especially similar to the effective for the precombustion-chamber turbines of the LPRE, which, as a rule, are made with a full gas feed in the circumference of the wheel ($\varepsilon = 1$) and therefore do not have the additional disk losses connected with the partiality (see further Section 4.5.2.2).

Let us derive the dependence of the circular efficiency from parameters of the conditions and from design parameters for the stage of the turbine. They naturally will also refer to the single-stage turbine. Let us conduct the derivation in general form in order to obtain the dependence valid also for the radial and the axial-flow turbine with any degree of reactivity.

In accordance with equation (2.28) and the velocity triangle given on Fig. 4.13, we can write:

$$L_u = u_1 c_1 \cos\alpha_1 + u_2 c_2 \cos\alpha_2; \tag{4.86}$$

$$\eta_u = \frac{u_1 c_1 \cos\alpha_1 + u_2 c_2 \cos\alpha_2}{L_{ad}^*}. \tag{4.87}$$

We transform equation (4.9) for $\rho_т$:

$$\rho_т = \frac{L_{ad2}}{L_{ad}^*} = \frac{L_{ad}^* - L_{ad1}}{L_{ad}^*} = 1 - \frac{L_{ad1}}{L_{ad}^*} = 1 - \frac{c_1^2}{2\varphi^2 L_{ad}^*}; \tag{4.88}$$

hence

$$L_{01}^{*}=\frac{c_1^2}{2\varphi^2(1-\varrho_1)}. \qquad (4.89)$$

Having substituted the expression (4.89) into (4.87), we obtain

$$\eta_u=\frac{2\varphi^2(1-\varrho_1)(u_1c_1\cos\alpha_1+u_2c_2\cos\alpha_2)}{c_1^2}. \qquad (4.90)$$

From the outlet velocity triangle we have

$$c_2\cos\alpha_2=w_2\cos\beta_2-u_2. \qquad (4.91)$$

Having substituted the expression (4.91) into (4.90), we obtain

$$\eta_u=2\varphi^2(1-\varrho_1)\left[\frac{u_1}{c_1}\cos\alpha_1+\frac{u_2}{c_1}\frac{w_2}{c_1}\cos\beta_2-\left(\frac{u_2}{c_1}\right)^2\right]. \qquad (4.92)$$

Bearing in mind equation (4.80), we obtain when using the relation $w_1^2=c_1^2+u_1^2-2u_1c_1\cos\alpha_1$:

$$\frac{w_2}{c_1}=\frac{1}{\varphi}\sqrt{1+\frac{\varrho_1}{\varphi^2(1-\varrho_1)}-2\frac{u_1}{c_1}\cos\alpha_1+\left(\frac{u_2}{u_1}\right)^2\left(\frac{u_1}{c_1}\right)^2}. \qquad (4.93)$$

Having substituted expression (4.93) into (4.92), we obtain the resultant expression for η_u:

$$\eta_u=2\varphi^2\frac{u_1}{c_1}(1-\varrho_1)\left[\cos\alpha_1+\frac{1}{\varphi}\frac{u_2}{u_1}\cos\beta_2\times\right.$$
$$\left.\times\sqrt{1+\frac{\varrho_1}{\varphi^2(1-\varrho_1)}-\left(\frac{u_2}{u_1}\right)^2\left(\frac{u_1}{c_1}\right)^2-2\frac{u_1}{c_1}\cos\alpha_1}-\left(\frac{u_2}{c_1}\right)^2\left(\frac{u_2}{u_1}\right)^2\right]. \qquad (4.94)$$

This expression for the circular efficiency is universal - it is correct for any form of the stage of the turbine and contains all parameters in dimensionless form. In accordance with equation (4.94) it can be concluded that the circular efficiency depends on the loss factor in the flow area ϕ and ψ, on design parameters, angles α_1, and β_2, ratio u_2/u_1, the degree of the reaction ρ_T and on the parameter of conditions u_1/c_1.

The less the outlet flow angles α_1 and β_2, the higher the efficiency, since the less the value of the outlet velocity will be and the less the losses with the outlet velocity. In practice the minimum values of these angles are limited by the fact that with a strong reduction in their values the hydraulic losses increase. At small angles α_1 and β_2 the profile, secondary and edge losses are increased, since the length of the profile, the angle of turn and the thickness of the trailing edges in the plane of rotation are increased.

Figure 4.43 gives graphs of the change in η_u, depending on u_1/c_1, at different ratios of the circular velocities u_2/u_1 and different degrees of reaction ρ_T (other parameters are accepted as being constant). It is necessary to keep in mind that these graphic representations have a conditional quantitative nature, since the velocity factors ϕ and ψ and angles α_1 are connected with values u_1/c_1; u_2/u_1 and ρ_T, and in the plotting of the graphs they are taken as being constant. Furthermore, ρ_T and u_2/u_1 are also connected with each other. A change in ρ_T at constant u_2/u_1 means that the degree of reaction is changed only as a result of a change in relative velocity w_2.

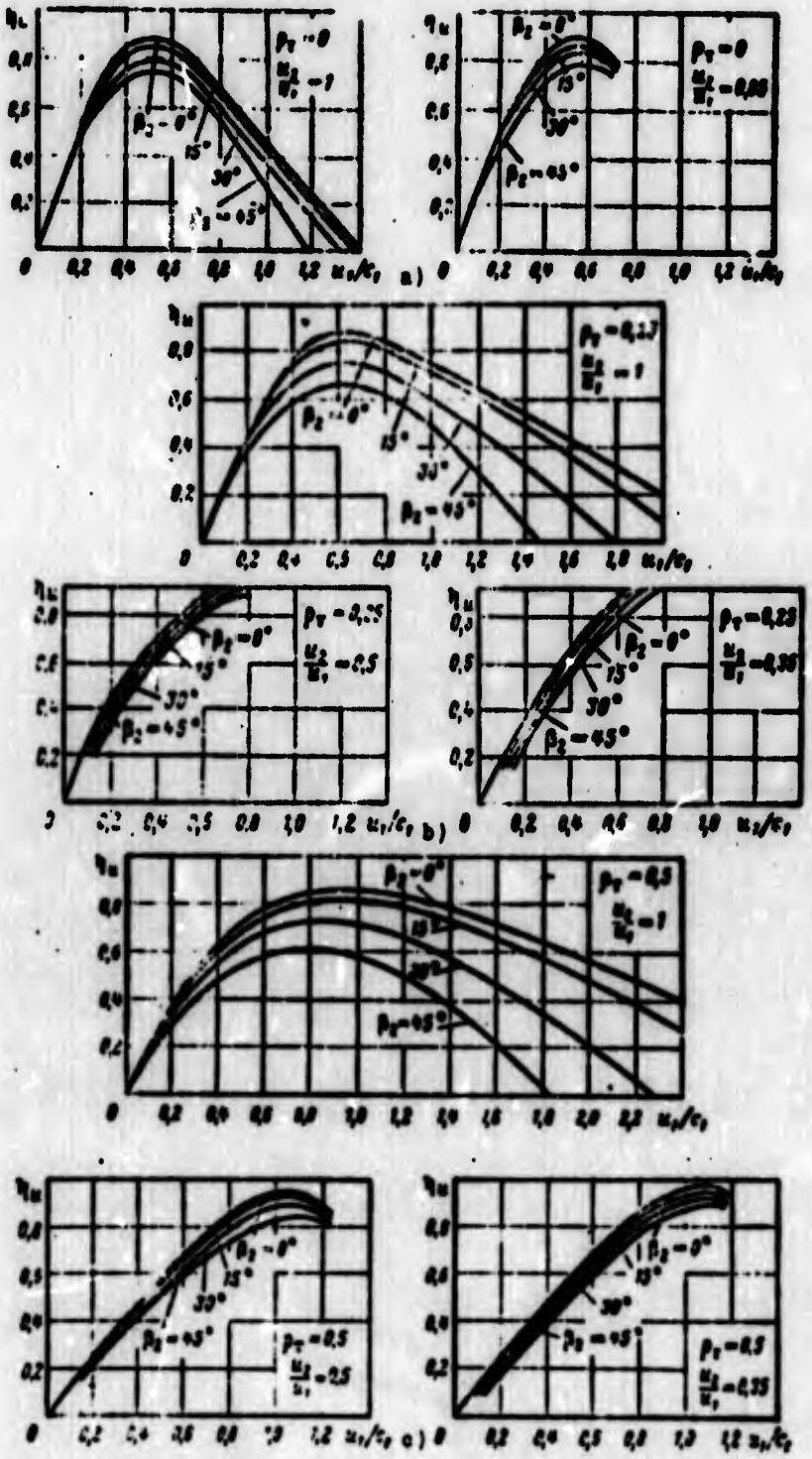

Fig. 4.43. Dependence of the circular efficiency η_u on u_1/c_1 for different ratios of circular velocity u_2/u_1 and different degrees of reaction of the turbine ρ_T ($\phi = 0.95$; $\psi = 0.9$; $\alpha_1 = 20°$ - from source [123]): a) $\rho_T = 0$; b) $\rho_T = 0.25$; c) $\rho_T = 0.5$.

Although the graphs given on Fig. 4.43 have a conditional nature, all the same they make it possible to explain the quantitative effect of the parameter u_1/c_1 on η_u and the basic tendencies of the change in η_u with a change in $\rho_т$.

At low values of u_2/u_1 not at any value of u_1/c_1 is it possible to obtain the rational value η_u. This means that work of the inward-flow turbine ($w_2 > 0$) is possible only in such a case when the available energy of the flow in relative motion will be more than a decrease in the energy with the flow against the direction of the centrifugal forces:

$$\text{[illegible]} \frac{w_1^2}{2} > \frac{w_1^2 - w_2^2}{2}.$$

The graphs given on Fig. 4.43 show that there is always an optimum value of u_1/c_1, since the efficiency passes through the maximum. The less the value of u_2/u_1 at the assigned degree of reaction $\rho_т$ (and vice versa, the more $\rho_т$ at $u_2/u_1 = \text{const}$), then at a large value of u_1/c_1 the minimum of losses and the maximum η_u take place. Consequently, radial, and generally reactive, turbines are used advantageously at large values of u_1/c_1.

The expression for η_u with the independent selection of $\rho_т$ and β_2 has an approximate nature, since $\rho_т$ and β_2 should be connected with each other with a change in u_1/c_1.

When $u_2/u_1 = 1$ we obtain the following expression for the circular efficiency of the axial stage of the turbine:

$$\eta_u = 2\varphi^2 \frac{u}{c_1}(1-\rho_T)\left(\cos\alpha_1 + \psi\cos\beta_2 \times \right.$$
$$\left. \times \sqrt{1+\frac{c_1^2}{\varphi^2(1-\rho_T)}+\left(\frac{u}{c_1}\right)^2-2\frac{u}{c_1}\cos\alpha_1}-\frac{u}{c_1}\right). \qquad (4.95)$$

From an examination of the graphs given on Fig. 4.43, plotted for $u_2/u_1 = 1$, it follows that the maximum efficiency with an increase in ρ_T is shifted to the side of larger values u_1/c_1 (nearer to unity). For real turbines a growth in η_u with an increase in ρ_T will be observed, since coefficients ϕ and ψ for reaction turbines are higher than those for the impulse due to less outlet velocities from the nozzle cascade and at the inlet into the wheel.

4.4.2. CIRCULAR EFFICIENCY OF THE ACTIVE STAGE OF THE TURBINE

The expression for the impulse axial stage of the turbine ($\rho_T = 0$, $u_2/u_1 = 1$):

$$\eta_u = 2\frac{u}{c_1}\varphi^2\left(\cos\alpha_1 + \psi\cos\beta_2 \sqrt{1+\left(\frac{u}{c_1}\right)^2-2\frac{u}{c_1}\cos\alpha_1}-\frac{u}{c_1}\right). \qquad (4.96)$$

Let us derive the equation η_u in another form, for which in equation (4.92) let us assume that $\rho_T = 0$; let us replace $u_1 = u_2 = u$ and w_2 with the product ψw_1. In turn, let us present w_1 as $w_{1u}/\cos\beta_1$.

From the velocity triangle (see Fig. 2.22) we have

$$w_1 = c_1 \cos\alpha_1 - u.$$

taking into account these relations, we obtain

$$\eta_u = 2\varphi^2 \frac{u}{c_1}\left(\cos\alpha_1 - \frac{u}{c_1}\right)\left(1 + \psi\frac{\cos\beta_2}{\cos\beta_1}\right). \qquad (4.97)$$

This equation is called the equation of Banki [Translator's note: name not verified]. In such a form the expression for η_u is more convenient for analysis, since the ratio $\cos\beta_2/\cos\beta_1$ for impulse turbines virtually does not depend on u/c_1, and it is close to unity. The outlet angle β_2 in the first approximation is determined by the blade angle $\beta_{2л}$, which is selected depending on $\beta_{1л}$. The angle $\beta_{1л}$, in turn, is determined by the angle of the flow β_1 and the angle of attack. The relationship between $\beta_{2л}$ and $\beta_{1л}$, and also between $\beta_{1л}$ and β_1 is selected independently of the value u/c_1.

The value η_u takes a zero value when $u/c_1 = 0$ and when $u/c_1 = \cos\alpha_1$.

Assuming φ and ψ to be independent of u/c_1, and also considering that $\beta_2 = \beta_1$, by differentiation let us determine the value u/c_1 at which the maximum η_u takes place.

From the relation

$$\frac{d\eta_u}{d(u/c_1)}=0$$

we obtain

$$\cos\alpha_1-2(u/c_1)_{\text{опт}}=0;$$

$$(u/c_1)_{\text{опт}}=\frac{\cos\alpha_1}{2}. \qquad (4.98)$$

The maximum efficiency of the active single-stage turbine takes place when $u/c_1 = \cos\alpha_1/2$. In this case its value, which we will obtain, having substituted into equation (4.97) $\cos\alpha_1/2$ instead of u/c_1, is equal to

$$\eta_{u\,\max}=\varphi^2\left(1-\varphi^2\frac{\cos^2\alpha_1}{2}\right). \qquad (4.99)$$

Figure 4.44 shows the approximate form of the dependence $\eta_u = f(u/c_1)$ for the impulse single-stage turbine when $L^*_{ад}$ = const. For clarity plotted there are the relative portions of power losses with flow in the nozzle cascade $L_\phi/L^*_{ад}$ and with the flow around the blades $L/L^*_{ад}$.

Losses in the nozzle cascade do not depend on ratio u/c_1 $\left(\frac{L_\varphi}{L^*_{ад}}=1-\varphi^2\right)$, but losses in the rotor wheel depend on it:

$$\frac{L_л}{L^*_{ад}}=(1-\varphi^2)\varphi^2\frac{w_1^2}{c_1^2}.$$

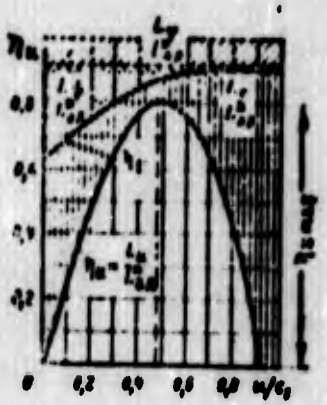

Fig. 4.44. Dependence of losses and circular efficiency of the impulse turbine on u_1/c_1.

Having replaced w_1 with the value $w_{1u}/\cos\beta_1$, and $w_{1u} = c_1\cos\alpha_1 - u_1$, we obtain

$$\frac{L_u}{L_{0a}^*} = (1-\varphi^2)+\varphi^2\frac{(\cos\alpha_1-(u/c_1))^2}{\cos^2\beta_1}. \qquad (4.100)$$

The value $\eta_u = (L_u/L_{0a}^*)$ determines the hydraulic efficiency of the turbine. The dependence $\eta_u = f(u/c_1)$ affects the nature of change in $L_\varphi L_{0a}^*$ and L_φ/L_{0a}^* from u/c_1.

The value $\eta_{u\ max}$ is reached when $u/c_1 = \cos\alpha_1/2$, and the minimum of losses with the outlet velocity lies somewhat more to the left, but it is virtually very close to this value u/c_1.

For an ideal impulse turbine, i.e., on the assumption that the hydraulic losses are absent ($\phi = \psi = 1$), the optimum with respect to u/c_1 will remain the following:

$$\left(\frac{u}{c_1}\right)_{\eta_{u\ max}} = \frac{\cos\alpha_1}{2}, \qquad (4.101)$$

i.e., it does not depend on the magnitude of the losses.

Let us note that the relation (4.101) directly results from the velocity triangle constructed on Fig. 4.45. With an axial outlet ($c_{2u} = 0$) the relation $2(u/c_1) = \cos \alpha_1$ is obtained, i.e., relation (4.101).

Fig. 4.45. Velocity triangle for an ideal impulse turbine.

Conditions with respect to u_1/c_1 for the maximum of the efficiency η_u and for the minimum of losses with the outlet velocity for an ideal turbine coincide. The maximum circular efficiency of such a turbine in value will be equal to $\cos^2\alpha_1$ [see equation (4.99)]. Correspondingly, the relative value of velocity losses in this case will be

$$\frac{L_c}{L_{0a}} = \frac{c_2^2}{c_1^2}\frac{2}{2} = 1 - \eta_{u\,max} = 1 - \cos^2\alpha_1 = \sin^2\alpha_1.$$

From equation (4.97) it follows that the value η_u of the impulse stage is greatly affected by α_1 - the angle of inclination of the vector of absolute velocity c_1. The less α_1, then (at constant ϕ and ψ) the higher the efficiency η_u. But, taking into account the losses, in cascades the optimum value of the angle is found with limits of 15°-20°.

Figure 4.46 gives the dependence $\eta_u = f(u/c_1)$ obtained by calculation at different angles of α_1 for the impulse turbine

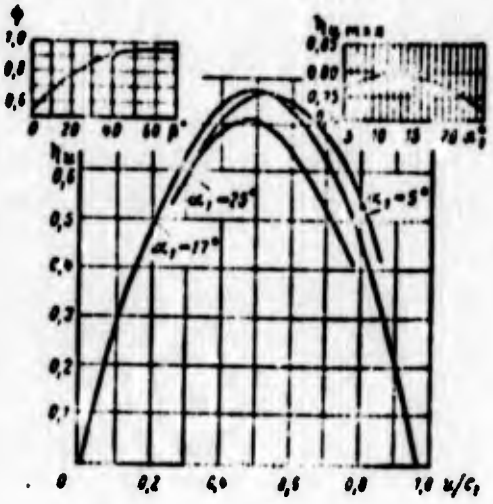

Fig. 4.46. Dependence of circular efficiency on u_1/c_1 for the impulse turbine at different angles of α_1.

with a variable value $\beta_1 = f(u/c_1)$; in this case $\beta_1 = \beta_2 = \beta$. Value ψ is taken not as constant but dependent on the angle β (actually, according to the sum of the angles $\beta_1 + \beta_2$, see the graph in the left corner of (Fig. 4.46). For greater clarity the dependence of $\eta_{u\ max}$ on α_1 is shown separately in the right corner of Fig. 4.46.

Let us discuss the question of the determination of the optimum u/c_1 for the reaction turbine. From the graph given on Fig. 4.43, it follows that the greater the degree of reaction for the axial-flow turbine, the larger the value the optimum value u/c_1 is (corresponding to $\eta_{u\ max}$). For clarity let us determine the optimum value u/c_1 for the special case $\rho_T = 0.5$ ($c_{1z} = c_0 = w_1$). Let us construct the velocity triangle for this case, disregarding the hydraulic losses (Fig. 4.47). From the construction it follows that when $c_{2u} = 0$

$$\left(\frac{u}{c_1}\right)_{\eta_{u\ max}} = \cos\alpha_1. \qquad (4.102)$$

Fig. 4.47. Velocity triangle for an ideal reaction turbine: $\rho_T = 0.5$; $c_0 = w_1$.

For the precomputations and selection of the optimum mode with respect to efficiency for the different degrees of reaction of the turbine, it is convenient to use the dependences

$$\eta_u = f(u/c_{ад}),$$

where

$$c_{ад} = \sqrt{2L_{ад}^*}; \qquad (4.102a)$$

$c_{ад}$ for the reaction turbine is the fictitious velocity determined with respect to the whole value of the available adiabatic work:

$$c_{ад} = c_{1ад}\sqrt{1-\rho_T}, \qquad (4.103)$$

for the impulse turbine

$$c_{ад} = c_{1ад}. \qquad (4.104)$$

Then from expressions (4.98) and (4.102) we obtain:

<u>for the impulse stage</u>

$$\left(\frac{u}{c_{ад}}\right)_{\eta_u\,max} = \frac{\varphi\cos\alpha_1}{2}; \qquad (4.105)$$

for the reactive stage ($\rho_т$ = 0.5)

$$\left(\frac{u}{c_{ад}}\right)_{\eta_u\max} = \frac{\varphi\cos\alpha_1}{\sqrt{2}}. \qquad (4.106)$$

Figure 4.48 gives the calculated dependences $\eta_u = f(u/c_{ад})$. With the calculations it is accepted that α_1 = 24° as well as increase in φ and ψ with an increase in $\rho_т$. From the course of the curves given on Fig. 4.48 it follows that the greater the degree of reaction $\rho_т$, the more optimum the value $u/c_{ад}$ for the efficiency η_u. The displacement of the optimum $u/c_{ад}$ η_u with a change in $u/c_{ад}$ is determined by the fact that with an increase in the degree of reaction conditions of the minimum of losses with the outlet velocity corresponds to larger values of $u/c_{ад}$ [compare relation (4.105) and (4.106)].

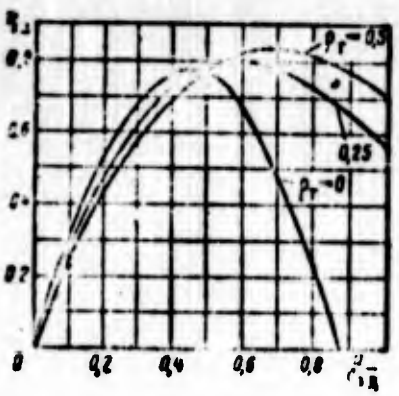

Fig. 4.48. Dependence of the circular efficiency η_u on $u/c_{ад}$ for stages of the turbine with a different degree of reaction $\rho_т$ (α_1 = 24°).

4.4.3. COEFFICIENT OF CIRCULAR WORK OF THE TURBINE STAGE

An important parameter for the turbines is the coefficient of circular work:

$$L_u = \frac{L_u}{u^2} = \frac{c_{1u} \pm c_{2u}}{u}. \qquad (4.107)$$

It characterizes the degree of the use of the permissible circular velocity. The permissible value of the circular velocity of turbines of the LPRE is defined by the overall dimensions, since the angular velocity is already assigned by the angular velocity of the pump. Usually u = 250-300 m/s, i.e., it does not reach the limiting value determined by the reserve of the strength and equal to u = 350-400 m/s.

For a decrease in the mass of the construction and reduction in the flow rate of the working medium, it is necessary to have high coefficients of circular work. This is especially important for autonomous turbines of LPRE (see Section 4.1.1).

From equation (4.107) it follows that

$$L_u = \frac{\eta_u L_{ad}^*}{u^2} = \frac{\eta_u}{2(u/c_{ad})^2}. \qquad (4.108)$$

having substituted here the expression (4.97) for η_u, we obtain for the impulse turbine

$$L_u = \left(\frac{\varphi \cos \alpha_1}{(u/c_{ad})} - 1\right)\left(1 + \psi \frac{\cos \beta_2}{\cos \beta_1}\right). \qquad (4.109)$$

In the conditions $\eta_u = \eta_{u\,max}$ we have $(u/c_{ad})_{\eta_{u\,max}} = \frac{\varphi \cos \alpha_1}{2}$; then for the impulse stage when $\psi = 1$ we obtain

$$(L_u)_{\eta_{u\,max}} = 2.$$

From equation (4.109) it is evident that with a decrease in $u/c_{ад}$, in spite of the incidence η_u in the region $u/c_{ад} < \varphi \cos \alpha_1/2$ (see Fig. 4.44), due to an increase in losses with an outlet velocity and losses in the rotor wheel, the coefficient of circular work increases, since a decrease in $u/c_{ад}$ is connected with an increase in $L^*_{ад}$ (u = const). When $u/c_{ад} \to 0$, $\bar{L}_u \to \infty$.

The dependence of $\bar{L}_u$ on $u/c_{ад}$ at different $\rho_т$ is represented on Fig. 4.49. The dependence is obtained by the calculation according to equation (4.108) with the use of graphs given on Fig. 4.48. From Fig. 4.49 it follows that the nature of the change in $\bar{L}_u$ is identical for impulse and reactive stages.

In autonomous turbines of LPRE for the purpose of decreasing the gas flow rate, it is attempted to insure the large values of the adiabatic work ($L^*_{ад} \to \max$) (see Section 4.1.1). With the limited circular velocity small values of $u/c_{ад} = 0.05$-0.3 correspond to this requirement.

Figure 4.49 shows that at small values of $u/c_{ад}$ the impulse single-stage turbine has larger values of the operating factor $\bar{L}_u$ and efficiency η_u (see Fig. 4.48) than do the reactive single-stage turbine. Therefore, impulse turbines are used as autonomous turbines.

The precombustion-chamber turbines of LPRE, in connection with the high flow rates of the working medium, correspond to small adiabatic works (see Section 4.1.2). Therefore, these turbines have large values $u/c_{ад}$, which exceed 0.5-0.6. Then (see Fig. 4.49) the use of reaction turbines as the precombustion-chamber becomes advisable: they have at large values of

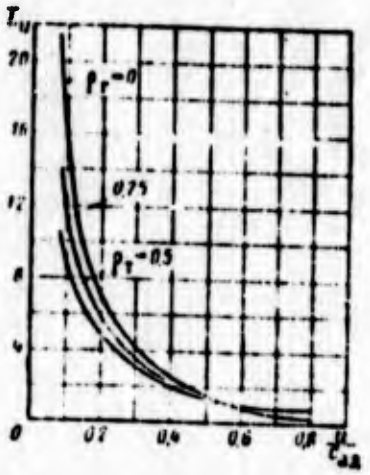

Fig. 4.49. Dependence of the coefficient of circular work $\bar{L}_u$ on $u/c_{ад}$ for stages of the turbine with a different degree of reaction $\rho_т$ (α_1 = 24°).

$u/c_{ад}$ values of $\bar{L}_u$ exceeding values of the operating factor for the impulse turbine.

However, for a decrease in axial thrust (see further Section 5.3.1.2) the precombustion-chamber turbines are frequently made impulse. In this case for an increase in $\bar{L}_u$ the ratio $u/c_{ад}$ is decreased by means of a decrease in the circular velocity (decrease in $D_{ср}$ when ω = const).

4.5. LOSSES OF THE STAGE OF THE TURBINE

Let us examine the losses connected with work of the stage as a whole. We will conditionally call these losses of the stage of the turbine. These losses include the losses connected with the leakage of the working medium from the flow area, disk losses (losses to friction against the gas of the disk and shroud and losses connected with partial admission) and mechanical losses.

4.5.1. Losses Conncected with Leakage of the Working Medium from the Flow Area of the Stage of the Turbine (Expenditure Losses)

The leakage of the working medium through clearances between the housing and the rotor wheel leads to a reduction in the work of the turbine. Passing through the nozzle cascade is greater working medium than through the vane cascade of the rotor wheel. Since with calculation of the efficiency the work of the wheel refers to the adiabatic work of 1 kg of the mass of the working medium, calculated from parameters at the inlet into the nozzle cascade, the value of leakage has an effect on the value of the effective efficiency (see Section 2.15.4).

Figure 4.50 gives a diagram of the axial stage of the turbine, and the possible directions of leakages in it are shown. The leakage above the shroud determines that one of the clearances $\Delta z_1 = \Delta r$ (axial or radial) which has a larger value (we will designate it Δ).

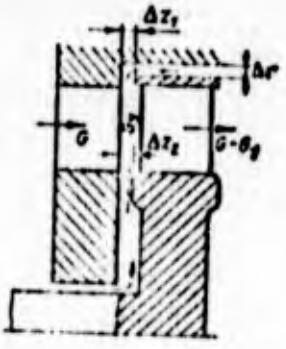

Fig. 4.50. Diagram of the axial stage of a turbine and the possible directions of leakages in it.

With a reduction in the axial clearance Δz_2 the inleakage of the gas on the side of the shaft will be decreased. Located on

the shaft is a seal system, which prevents the penetration of the fuel component from the cavity of the pump into the cavity of the turbine. However, a certain quantity of the component penetrates through the seals, and in the form of gas it enters into the flow area of the turbine through the clearance Δz_2.

In the turbine without a shroud the losses connected with leakages are determined by the radial clearance Δr. These losses, other conditions being equal, will be more for a turbine without a shroud than for a turbine with a shroud, since, apart from a decrease in the flow rate through the cascade of the wheel, leakages through the radial clearance disturb the flow pattern in the peripheral cross sections of the impeller vanes, making the effectiveness of their work worse (see Section 2.13.3).

The leakages above the shroud of the axial stage are determined by the clearance area, by a pressure differential in the peripheral cross section of the impeller vanes (the degree of reaction on the periphery $\rho_{т.п}$), by the density of the gas on the periphery $\rho_п$ and by its outlet velocity from the nozzle cascade (see source [130]):

$$G_y = \mu_{заз} \pi D_{ср.п} \Delta \sin \alpha_{1п} \times \sqrt{\rho_{т.п}\left(1 - \frac{\rho_п}{\rho_{т.п}} \sin^2 \alpha_{1п}\right) - \frac{\rho_п}{\rho_{т.п}} \sin^2 \alpha_{1п}}, \quad (4.110)$$

where $\mu_{заз}$ is the coefficient of flow rate of the clearance leakages (Fig. 4.51); Δ - clearance which is minimum of clearances Δz_1 and Δr.

Disregarding the change of the parameters with respect to height and the overlaps of the blades, and bearing in mind that

$$G = \rho_{1п} \pi D_{ср.п} h_{1п} \sin \alpha_{1п},$$

we obtain on the basis of expression (4.110) the following simple equation for calculating the leakages ($\varepsilon \leq 1$):

$$\frac{c_{1z}}{c_1} = \mu_{заз}\sqrt{1+\rho_1\left(\frac{1}{\varphi^2\sin^2\alpha_1}-1\right)}\left(1+\frac{b_{1a}}{D_{cp}}\right)\frac{\delta}{b_{1a}}. \qquad (4.111)$$

The losses connected with leakages for the axial stage of the turbine without a shroud with a full gas feed ($\varepsilon = 1$) are estimated by a decrease in the full efficiency of the stage (see source [125]):

$$\frac{\eta_{т(\Delta=0)}-\eta_т}{\eta_{т(\Delta=0)}} = \frac{\Delta\eta_т}{\eta_{т(\Delta=0)}} = 1{,}37(1+1{,}6\rho_1)\left(1+\frac{b_{1a}}{D_{cp}}\right)\frac{\Delta r}{b_{1a}}. \qquad (4.112)$$

where $\eta_{т(\Delta=0)}$ and $\eta_т$ are complete efficiencies, respectively, with zero clearance and fixed clearance. The structure of equations (4.111) and (4.112) is identical.

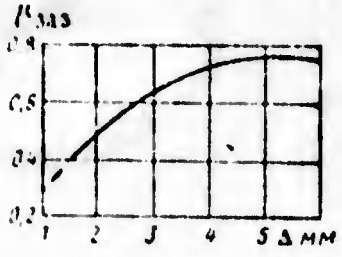

Fig. 4.51. Dependence of the coefficient of flow rate of leakages through the clearance $\mu_{заз}$ on the magnitude of the clearance for an axial-flow turbine with a shroud.

In turbines with the full feed ($\varepsilon = 1$) losses of the stage consist only of friction losses of the disk. Their relative magnitude is small with $\varepsilon = 1$, and therefore the correction given by the equation (4.112) can be considered as a correction to the circular efficiency:

$$\frac{\eta_{u(\Delta=0)}-\eta_u}{\eta_{u(\Delta=0)}}=\frac{\Delta\eta_u}{\eta_{u(\Delta=0)}}=1{,}37(1+1{,}6\varepsilon_t)\left(1+\frac{h_{1a}}{D_{cp}}\right)\frac{\Delta r}{h_{1a}}. \qquad (4.113)$$

where $\eta_{u(\Delta-0)}$ and η_u are circular efficiencies, respectively, with zero clearance and with the fixed clearance.

Equation (4.113) can be used for estimating the losses connected with leakages in the axial stages without a shroud with partial admission ($\varepsilon < 1$).

In the radial-axial turbine of the turbopump unit the gas leakage occurs through the front axial clearance (see Fig. 4.42). Into the axial clearance between the rear disk and the housing can enter a certain quantity of the fuel component, which penetrates from the cavity of the pump through the seal system to the shaft (pump leakages).

For a radial-axial turbine with a half unshrouded wheel (see Fig. 4.42) the effect of the axial clearance is estimated by a decrease in the overall efficiency of the turbine (see source [142]):

$$\frac{\Delta\eta_t}{\eta_{t(\Delta=0)}}=1{,}3\frac{\Delta z_{cp}}{h_{л.cp}}, \qquad (4.114)$$

where Δz_{cp} and $h_{л.cp}$ are mean values of the axial clearance and span of the blade, respectively.

For turbines with a double shrouded wheel a decrease in the gas leakage is reached by means of the seal of radial clearance (Fig. 4.52).

With the subcritical pressure ratio corresponding to precombustion-chamber turbines of LPRE on the seal $\delta_y = p_y/p_2$

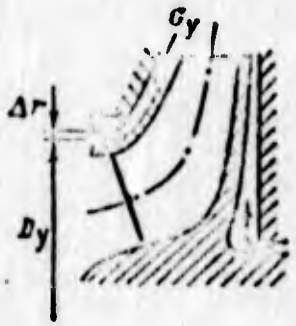

Fig. 4.52. Diagram of leakages in the stage of a radial inward-flow turbine with a double shrouded wheel.

(where p_y is pressure in front of the seal; p_2 - outlet pressure from the wheel) the leakages through the seal are calculated from equation (2.188).

In connection with the low gas velocities in the clearance, the gas can be considered incompressible, and the pressure p_y can be estimated with the aid of the relations given in Section 3.1.2.1, by substituting into equations instead of p_2 the pressure in front of the turbine wheel p_1 and understanding by the density ρ the average density of the gas in the axial clearance. The stagnation temperature in the clearance can be taken equal to the static temperature at the inlet into the wheel. With the approximate computations, in connection with the low density of the gas and the usually small difference between the outside diameter of the wheel and the diameter of the seal, it is possible to take the pressure p_y equal to p_1.

The coefficient of the flow rate of the seal can be estimated according to equation (see source [149])

$$\mu = \sqrt{\frac{\lambda_y}{\lambda z_y}}, \qquad (4.115)$$

where λ is the coefficient dependent on the type of labyrinth seal (Fig. 4.53).

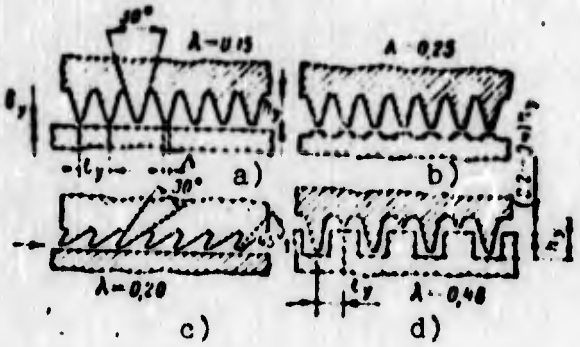

Fig. 4.53. Forms of labyrinth seals; a) with triangular straight flanges; b) with inclined flanges; c and d) complex labyrinths.

The clearance δ_y is selected from design considerations. Its magnitude should guarantee the absence of the interference of the wheel against the housing with the heating of the wheel and deflections of the shaft. Usually at operating temperatures of the wheel and housings, we take δ_y = 2-4 mm. The pitch of the flanges t_y is taken at $t_y > (10\text{-}15)\delta_y$. The height of the flanges h_y is taken within limits of $(1\text{-}17)\delta_y$; it weakly affects the coefficient of the flow rate μ (see source [148]). The edges of the flanges should be made sharp. The thickness of the flange Δ is selected at the smallest possible.

4.5.2. DISK LOSSES

4.5.2.1. Friction Losses of the Disk and Shroud

Friction losses of disk $N_{тр.д}$ in turbines are less in absolute value than those in pumps, since the density of the medium in the flow area and in the cavity between the housing and rotary disk of the turbines is less than that of the pumps.

The friction power of the disk is calculated according to equation (2.202), where understood by diameter D_2 is the outside diameter of the wheel disk: for the axial-flow turbine $D_{диска} = D_{ср} - h_{1л}$, and for the inward-flow turbine with a double shrouded wheel $D_{диска} = D_1$.

For axial-flow turbines with a large ratio $D_{ср}/h_{1л}$ the friction power over the external surface of the shroud can comprise a noticeable magnitude. This power is the power of the rotational resistance of the cylinder in the cylinder, which can be calculated by utilizing the data given in work [42].

The expression for the friction power of the shroud is written thus:

$$N_{тр.б} = C_{банд} \rho_{ср} \omega^3 b_{банд} D^4_{банд} \text{ [W]}. \qquad (4.116)$$

where $b_{банд}$ is the width of the shroud; $D_{банд} = D_{ср} + h_{1л}$ is the outside diameter of the shrouded wheel; $C_{банд}$ is the coefficient of friction of the shroud.

When $2\Delta r/D_{банд} = 0.017$-$0.21$ (where Δr is the radial clearance between the wheel and housing) $C_{банд}$ can be presented in the form

$$C_{банд} = \frac{0.1}{\sqrt{Re_{банд}}}; \quad Re_{банд} = \frac{D_{банд} \Delta r}{2\nu}.$$

4.5.2.2. Losses Connected with Partial Admission

In turbines of IPHE partial admission is frequently used. In autonomous turbines partial admission is used especially

frequently, since with the low flow rate of the working medium in the case of the gas feed over the entire circumference the height of the nozzle and rotor blades would be very small and the gas flow in vane channels would be accompanied by great losses (great tip losses).

In precombustion-chamber turbines the partial admission can also be used, since as a result of the high density of the working medium ($p_0^* > 12\text{-}15$ MN/m^2) the low volume flow rate does not manage to pass over the entire circumference of the turbine with the acceptable height of the blades.

Although the partial admission is undesirable, since it causes additional energy losses, sometimes its use is unavoidable, since the low height of the blades leads to even greater losses. Let us examine which energy losses are connected with the partial admission.

The gas flow through the vane cascade with partial admission has a complex nature. With motion of the blades on the arc not occupied with nozzles, the mixing of the gas by the blades takes place; in this case friction of edges of the blades against the gas occurs.

The flow pattern in the inoperative blades depends on the velocity of the gas coming out of the nozzles. At subsonic velocities the reverse gas flow can exist along the vane channels during their movement along the dead-end wall. The reverse gas flow can be explained to any degree by the dissymmetry of the blade shape, but mainly it is associated with the fact that in impulse turbines in the clearance between the wheel and the nozzle cascade there can be uniform pressure p_1, which is lower than the outlet pressure p_2 (Fig. 4.54) as a result of the ejecting action

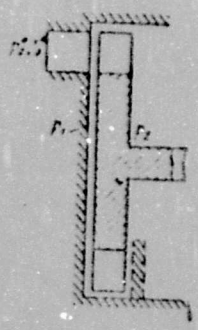

Fig. 4.54. Diagram of the stage of the turbine with the partial gas feed.

of the jet escaping from the nozzle. In connection with this in impulse subsonic turbines it is advantageous to have the introduction of the small reaction ρ_T = 0.02-0.05, at which pressures p_1 and p_2 can be equalized in spite of the ejecting action of the jet.

Let us note that the use of axial-flow turbines with the reaction $\rho_T > 0.05$ with partial admission is not justified, since the gas will spread over the axial clearance, and the flow around the rotor blades on the arc not occupied with nozzles will be off-design, i.e., it will be accompanied by great losses.

At the subsonic velocities of outflow from nozzle, for a decrease in the backflow of the gas from the nonoperative side over an arc not occupied with nozzles, we place a deflector (on Fig. 4.54 it is shown by a dashed line).

The flow pattern in the partial stage becomes complicated by the fact that the gas escaping from the nozzles, in being encountered with the blades which came from the nonoperative zone, the vane channels of which are filled by the stagnation gas (in any case, moving at low velocities, - on Fig. 4.55 these channels are shaded into cage), transfers part of its energy to this stagnation gas.

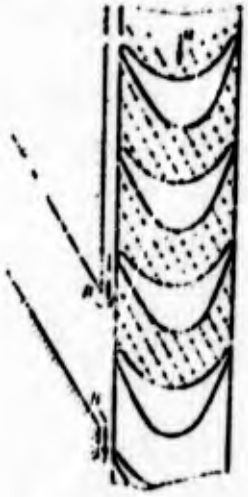

Fig. 4.55. Diagram of the gas flow with the partial admission.

It is obvious that the process of "filling" of the vane channels and "ejection" will periodically be repeated if the gas feed is achieved by several groups of nozzles. Hence, for the reduction in losses on boundaries of the feed, it is advantageous to place the nozzles in the partial-admission turbine in one segment and not scatter them on the circumference. True, the unsymmetric arrangement of the nozzles leads to the uneven distribution of the forces acting on the rotor wheel and the emergence of the radial stress (see Section 5.3.2.2).

An especially complex flow pattern appears on boundaries of the arc of the intake. On the boundaries the jet which escapes from the nozzle undergoes a sudden expansion. In the region of point A (see Fig. 4.55) the jet exerts an ejecting action on the gas in the clearance (see dashed arrow). In the region of point A the gas escape always takes place.

At supersonic velocities of the outflow the flow pattern in the partial stage is changed. In practice the rotor wheel impulse in calculation will operate as a reaction wheel - the static pressure in the clearance will exceed the outlet pressure.

The leakages in the circular direction acquire a great value. It is obvious that at supersonic velocity the leakage also in the region of point B will occur (see Fig. 4.55, solid arrow). The axial clearance for the partial supersonic turbine whould be selected as minimum as permissible according to conditions of assembly and operation.

On the basis of the physical flow pattern in the partial stage, conditionally the losses connected with the partiality can be divided into four groups:

1) windage losses (i.e., losses connected with the emergence of the braking wheel of the moment from backflows, mixing and turbulence of the gas and friction of edges of the blades with motion of the wheel along the dead-end wall);

2) losses to "ejection" (i.e., losses connected with the expenditure of energy for the acceleration of the stagnation gas flow in the vane channels which came from the nonoperative zone);

3) losses from sudden expansion on boundaries of the arc of the intake;

4) losses connected with the gas overflow in a circular direction.

It is very difficult to evaluate the effect of each of the losses experimentally, since they are interconnected. But in a number of studies equations are proposed for evaluating the individual forms of losses connected with the partiality.

Thus, in work [135] the losses connected with the gas overflow in a circular direction are considered by the decrease in the velocity factor ψ of the rotor blades:

$$\psi_0 = \psi_{0-1}\left(1 - \frac{t}{2\pi l_{cp}}\right). \qquad (4.117)$$

It is recommended to estimate the first three groups of losses - windage losses, losses, to "ejection" and losses from sudden expansion - totally according to the equation

$$N_{\text{в}} = 0{,}03 k_1 \frac{b_{\text{а}}}{D_{cp}}\left(1 + 10\frac{\delta}{D_{cp}}\right)(1-\varepsilon)\omega^3 D_{cp}^5. \qquad (4.118)$$

Equation (4.118) is empirical, and it corresponds to impulse single-stage turbines with the Mach number $M_{c_1} = 1.7\text{-}1.8$ with one group of nozzles. With an increase in the groups of nozzles the losses to "ejection" and losses from the sudden expansion will increase approximately in proportion to the number of groups of the nozzles, and windage losses virtually will not be changed.

Since windage losses and losses to "ejection" and sudden expansion are commensurable, it is possible to consider that with an increase in the groups of nozzles the total power of the losses from partiality will increase $(i_c\text{-}1)/2$ times (where i_c - the number of groups of the nozzles). In two-stage partial-admission turbines, the losses from partiality are defined as the sum of losses in each stage.

The introduction of partial admission is possible in radial-flow turbines. In this case noticeably the efficiency falls.

According to experimental data (see source [7]) the dependence of the maximum efficiency on ε is close to being linear and can be estimated by equation

$$\eta = \eta_{\tau}(\varepsilon = 1) - 0{,}24(1-\varepsilon). \qquad (4.119)$$

The optimum of $u/c_{ад}$ is decreased with the introduction of partiality (Fig. 4.56, taken from work [45]). In one of the experiments with a radial-flow turbine (see source [7]) for ε = 1 the value $(u/c_{1ад})_{\eta_{т\ max}} = 0.65$, for ε = 0.5 the value $(u/c_{1ад})_{\eta_{т\ max}} = 0.55$, and for ε = 0.12 the value $(u/c_{1ад})_{\eta_{т\ max}} = 0.53$.

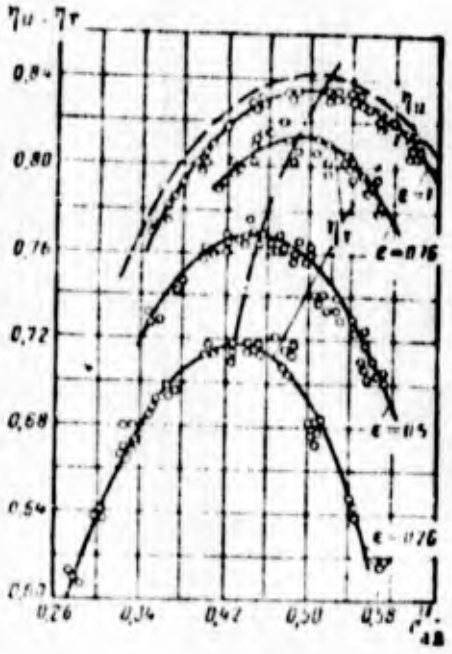

Fig. 4.56. Experimental dependence of the efficiency of the single-stage turbine on $u/c_{ад}$ at different values of the degree of the admission ε.

4.5.3. MECHANICAL LOSSES

Mechanical losses include losses in seals of the shaft and bearings of the turbine. In turbopump units losses in the

seals of the shaft and bearings refer to mechanical losses of the pumps. Therefore, for turbines of the turbopump unit the mechanical efficiency η_{mex} is taken equal to unity.

4.5.4. OVERALL (FULL) EFFICIENCY

4.5.4.1. Dependence of Overall Efficiency of a Turbine on $u/c_{ад}$

The power of a turbine being transferred to the shaft, i.e., the effective power of the turbine $N_т$, is determined by a difference in the circular power and losses of the stage. Since the mechanical efficiency of the turbine of the turbopump unit can be taken equal to unity, we will assume that the effective and internal power will be identical. For the axial-flow turbine, which has blades with a shroud, the expression for $N_т$ will be written in the form

$$N_т = GL_u - G_у L_u - N_{тр.д} - N_{тр.б} - N_с = \\ = (G - G_у) L_u - N_{тр.д} - N_{тр.б} - N_с. \qquad (4.120)$$

From equation (4.120) let us find the effective work of the turbine $L_т = N_т/G$:

$$L_т = \eta_у L_u - L_{тр.д} - L_{тр.б} - L_с, \qquad (4.121)$$

where

$$L_{тр.д} = \frac{N_{тр.д}}{G}; \quad L_{тр.б} = \frac{N_{тр.б}}{G}; \quad L_с = \frac{N_с}{G}$$

are the work of friction of the disk, the work of friction of the shroud, and the work of losses connected with admission, respectively.

Having divided $L_т$ by $L^*_{ад}$, let us determine the overall (fuel) efficiency of the turbine:

$$\eta_т = \eta_у \varphi_u - \zeta_{тр.д} - \zeta_{тр.б} - \zeta_с, \qquad (4.122)$$

where

$$\zeta_{тр.д} = \frac{L_{тр.д}}{L^*_{ад}}; \ \zeta_{тр.б} = \frac{L_{тр.б}}{L^*_{ад}}; \quad \zeta_с = \frac{L_с}{L^*_{ад}} \qquad (4.123)$$

is the loss factor of the stage.

With the aid of relations (2.202), (4.116), (4.118) and (4.123), we obtain the expressions for the loss factor $\zeta_{тр.д}$, $\zeta_{тр.б}$ and ζ_{ε}. For this the flow rate (in the absence of overlap of the impeller vanes) is expressed by the area covered by the impeller vanes ($\rho_т = 0$):

$$G = \varepsilon_1 \pi D_{ср} h_{1,2} \varphi c_{a1} \sin \alpha_1. \tag{4.124}$$

Then we obtain

$$\zeta_{тр.д} = 0{,}32 \frac{C_{тр.1}[1 - (h_{1,1}/D_{ср})]^3}{\varepsilon (h_{1,2}/D_{ср}) \varphi \sin \alpha_1} \left(\frac{u}{c_{a1}}\right)^3; \tag{4.125}$$

$$\zeta_{тр.б} = 5{,}1 \frac{C_{тр.1}(b_{сан}/D_{ср})[1 + (h_{1,1}/D_{ср})]^4}{(h_{1,2}/D_{ср}) \varepsilon \varphi \sin \alpha_1} \left(\frac{u}{c_{a1}}\right)^3; \tag{4.126}$$

$$\zeta_{\varepsilon} = 0{,}175 \frac{[1 + 10(b'/D_{ср})]}{\varphi \sin \alpha_1} \frac{1 - \varepsilon}{\varepsilon} \left(\frac{u}{c_{a1}}\right)^3. \tag{4.127}$$

With a decrease in the degree of admission ε, the loss factors $\zeta_{тр.д}$, $\zeta_{тр.б}$ and ζ_{ε} increase. With an increase in $u/c_{ад}$ these coefficients grow according to a cubic dependence (Fig. 4.57). Figure 4.57 depicts also the dependences η_u and $\eta_т$ on $u/c_{ад}$. It is evident that the maximum $\eta_т$ is located more to the left with respect to $u/c_{ад}$ than is the maximum η_u. The displacement of the maximum $\eta_т$ with respect to the maximum η_u is insignificant for turbines with full admission ($\varepsilon = 1$). For partial-admission turbines the displacement is substantial, and the more it is, the less the degree of the admission ε (see Fig. 4.56), i.e., the more the losses $\zeta_{тр.д}$, $\zeta_{тр.б}$ and ζ_{ε}.

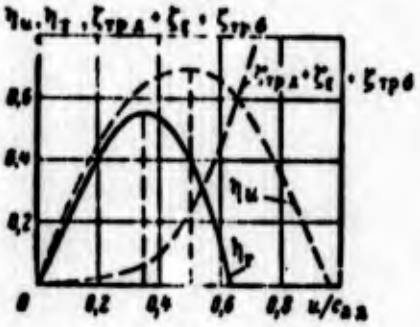

Fig. 4.57. Dependences of the circumferential efficiency of the sum of loss factors of the stage and overall efficiency on $u/c_{ад}$ for a single-stage impulse turbine.

Figure 4.56 shows that the partial admission caused by the small volume flow rate of gas (autonomous turbines of [LPRE] (ЖРД)) leads to a drop in the efficiency of the turbine commensurable with a drop in the efficiency connected with hydraulic losses and losses with discharge velocity considered by the circumferential efficiency η_u.

4.5.4.2. Determination of the Optimum Degree of Admission and Optimum Ratio $u/c_{ад}$ of Single-Stage Impulse Turbines

The autonomous turbines and at high pressure at the inlet the precombustion-chamber turbines of the LPRE must be made partial-admission ($\varepsilon < 1$). The introduction of the degree of admission ($\varepsilon < 1$) increases the span of the blade of the rotor wheel [see equations (4.65) and (4.71)], and this leads to a decrease in tip losses in the cascade [see equation (4.72a)], losses produced by leakages [see equations (4.111), (4.112)], and disk losses [see equation (4.125)]. However, at the same time, a decrease in ε leads to an increase in losses connected with admission [see equation (4.127)]. Therefore, there is such a value ε at which losses in the turbine reach the minimum, and the effective efficiency - the maximum. The value ε is called the optimum.

In designing a partial-admission turbine one should select the optimum magnitude of the degree of the admission ε_{opt}. Let us determine ε_{opt} for a single-stage impulse turbine. It is more convenient to search for not ε_{opt} but the value $(h_{1л})_{opt}$, according to which then it is possible to determine ε_{opt}. Let us express ε in terms of $h_{1л} = h_c$ and the volume flow rate; from equation (4.124) it follows that

$$\varepsilon = \frac{Q_1}{\pi D_{cp} h_{1л} \bar{c}_{a1} \sin \alpha_1} = \frac{Q_{1л} \bar{\tau}}{\pi D_{cp} h_{1л} \bar{c}_{a1} \sin \alpha_1}. \qquad (4.128)$$

where

$$\bar{\tau} = \frac{c_{1a1}}{c_1} = \frac{\tau(\bar{\tau}\lambda_{c_{a2}})}{\tau(\lambda_{c_{a2}})}. \qquad (4.129)$$

Having expressed the adiabatic volume flow rate $Q_{1ад}$ by $n_{s\,т}$ [see equation (2.185)], let us write equation (4.128) in the following form:

$$\varepsilon = 0{,}75 \cdot 10^{-6} \frac{\bar{\tau} n_{s\,т}^2}{\tau(\lambda_{c_{a2}}) \cdot (h_{1л}/D_{ср}) \cdot \ln a_1}. \qquad (4.130)$$

Converting expression (4.122) for the overall efficiency with the aid of relations (4.125)-(4.127) and assuming $\beta_1 = \beta_2$, we obtain the dependence which takes the following functional form:

$$\eta_т = f\left(\frac{h_{1л}}{D_{ср}}, \frac{u}{c_{a1}}, \bar{\tau}, a_1, \frac{b}{D_{ср}}, \frac{t}{b}, C_{тр.л}, C_{тр.б}, \frac{\Delta}{D_{ср}}\right) \qquad (4.131)$$

After linearization of the dependence $\zeta_{тр.д}$, $\zeta_{тр.б}$ in the range $h_{1д}/D_{ср} \leq 0.15$, it is possible to find the optimum value $\partial\eta_т/\partial(h_{1л}/D_{ср}) = 0$. The derivative is the polynomial of the cube relative to $h_{1л}/D_{ср}$. Therefore, in order to find the expression for $h_{1л}/D_{ср}$, it is necessary to solve the cubic equation. The solution can be obtained in the following way (when $n_{s\,т} > 6$):

$$\left(\frac{h_{1л}}{D_{ср}}\right)_{опт} = \sqrt{\frac{[\varphi\cos\alpha_1 - (u/c_{a1})]\,[0{,}4k_3/k_1 + k_3]\,[1 + k_1 - 0{,}4k_3\bar{b}(1-k_1)]}{k_1k_2[\bar{\tau}\cos\alpha_1 - (u/c_{a1})](1 - k_2\bar{\Delta}) + (k_4 + k_5 - k_6)(u/c_{a1})^2}}. \qquad (4.132)$$

where

$$k_3 = \left[1 - 0{,}23\left(1 - \frac{\bar{h}_1 + \bar{h}_2}{2}\right)^3\right][1 - 0{,}05(M_{w1} - 1)^2];$$

$k_2 = \mu_{зав}$ - for the turbine with the shroud;

$k_2 = 1.37$ - for the turbine without the shroud;

$$k_5 = 1{,}9 \cdot 10^{-6}\bar{\tau}\bar{t}\frac{(u/c_{a1})^2}{n_{s\,т}^2\bar{\tau}}\varphi\sin\alpha_1;$$

$$k_6 = 0{,}31 \cdot 10^{-6}(1 + 10\bar{b})\frac{\bar{\tau}(u/c_{a1})^2}{\bar{\tau}n_{s\,т}^2};$$

$k_5 = 11C_{банд}\bar{b}_{банд}\bar{b}$ - for the turbine with the shroud;

$k_5 = 0$ - for the turbine without the shroud;

$k_6 = 2.7C_{тр.д}$;

$$\bar{b} = \frac{b}{D_{ср}}; \quad \bar{\lambda} = \frac{\lambda}{D_{ср}}; \quad \bar{t} = \frac{t}{b}; \quad \bar{b}_{банд} = \frac{b_{банд}}{b};$$

$$\beta_1 - \beta_2 = \operatorname{arctg} \frac{\varphi \sin \alpha_1}{\varphi \cos \alpha_1 - (u/c_{ад})}.$$

From equations (4.130) and (4.132) let us find the optimum degree of admission ε_{opt} and for circular nozzles - the optimum number of nozzles (see Section 1.3.3.2).

Let us discuss the determination of the optimum value of the ratio $(u/c_{ад})_{opt}$ at which $\eta_т$ reaches a maximum. It is useful to know this value in the calculation of the autonomous turbine of the LPRE although, as a rule, the computed value $u/c_{ад}$ of the autonomous turbines is less than the optimum value.

If we substitute the expression for the optimum length of the blade and the corresponding optimum degree of admission into equation (4.122), then we will obtain the expression for the optimum (maximum) efficiency of the turbine with the optimum degree of admission. This efficiency will depend on ratio $u/c_{ад}$. At the specific value of $u/c_{ад}$ the optimum efficiency will reach a maximum. This value will be optimum $[(u/c_{ад})_{opt}]$ with the optimum degree of admission ε_{opt}.

In connection with the complexity of the bonds it is difficult to find an analytical expression for $(u/c_{ад})_{opt}$. Therefore, the value $(u/c_{ад})_{opt}$ is determined graphically: for a number of values of $u/c_{ад}$ the optimum height of the blade is calculated according to equation (4.132), and then the optimum value of the efficiency is calculated. According to the maximum of the optimum efficiency, $(u/c_{ад})_{opt}$ is determined.

Figure 4.58 depicts the thus calculated value $(u/c_{ад})_{opt}$ for the impulse single-stage turbine with a shroud. Given there are values of the optimum efficiency $\eta_{т\ opt}$ (at ε_{opt}) and of the maximum efficiency $\eta_{т\ max}$ [at ε_{opt} and $(u/c_{ад})_{opt}$]. These dependences can be used in the approximation calculations of the impulse single-stage turbines with a shroud which have the parameters: $\alpha_1 = 15°\text{-}20°$; $M_{w_1} \leq 1.5$; $Re \approx 5\cdot10^5$; $\phi = 0.93\text{-}0.95$; $\bar{б} = 0.03\text{-}0.05$; $\mu_{зав} = 0.4\text{-}0.6$; $\bar{t} = 0.55\text{-}0.65$; $b_{банд}/b = 1.1\text{-}1.3$.

Let us discuss the analysis of dependences given on Fig. 4.58. It is evident that parameters of the turbine and its effectiveness are substantially affected by the power-speed coefficient of the turbine $n_{s\ т}$. With an increase in $n_{s\ т}$, the efficiency of turbine, the optimum degree of admission (Fig. 4.59) and $(u/c_{ад})_{opt}$ (Figs. 4.58 and 4.60) increase.

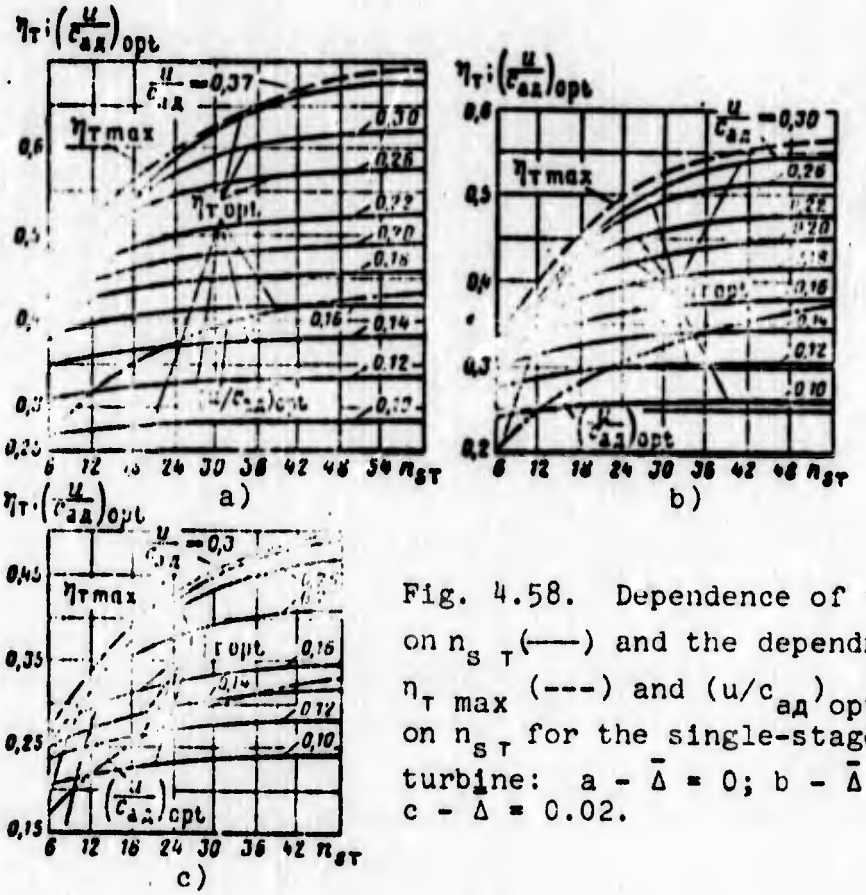

Fig. 4.58. Dependence of $\eta_{т\ opt}$ on $n_{s\ т}$ (——) and the dependnece of $\eta_{т\ max}$ (---) and $(u/c_{ад})_{opt}$ (-·-·-) on $n_{s\ т}$ for the single-stage impulse turbine: a - $\bar{\Delta} = 0$; b - $\bar{\Delta} = 0.01$; c - $\Delta = 0.02$.

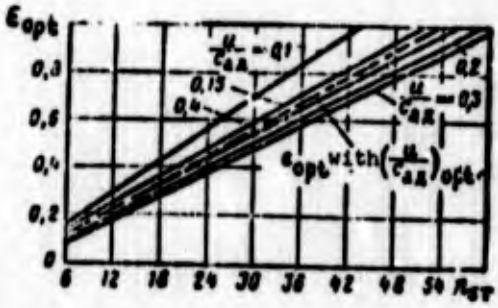

Fig. 4.59. Dependence of the optimum degree of admission ε_{opt} on the power-speed coefficient $n_{s\,т}$ and $u/c_{ад}$ for the single-stage impulse turbine when $b = 0.04$ and $\Delta = 0$.

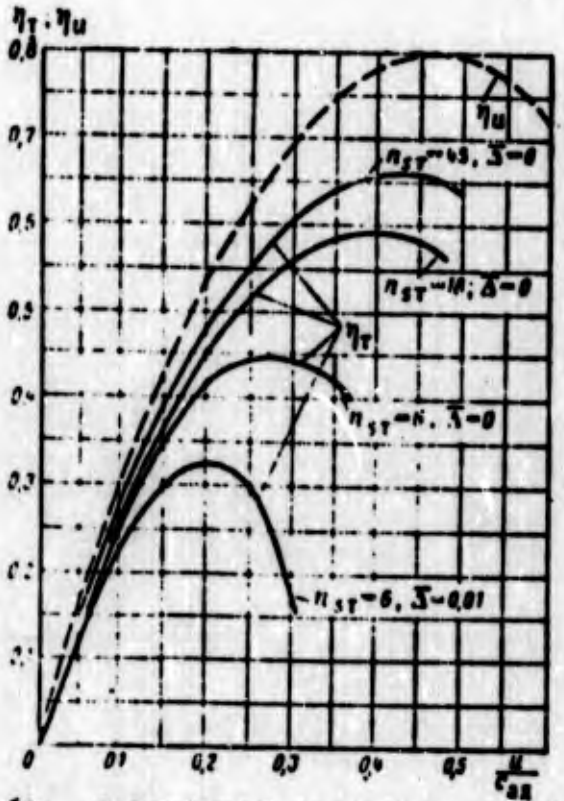

Fig. 4.60. Calculated dependence of the overall efficiency of the single-stage impulse turbine on $u/c_{ад}$ at different values of the power-speed coefficient $n_{s\,т}$ and the relative clearance $\bar{\Delta}(\alpha_1 = 17°)$

With a small clearance between the wheel and housing, beginning with $n_{s\,т} = 50$-60, the optimum degree of admission becomes equal to unity (see Fig. 4.59). Such an effect of $n_{s\,т}$ is the consequence of the fact that an increase in $n_{s\,т}$ is

connected with an increase in the volumetric flow rate of the gas and a drop in the adiabatic velocity [see equation (2.185)]. But since for the feed of gas of larger volumetric flow rate with lower velocity a larger area is required, then this leads to an increase in the degree of admission and a decrease in the losses produced by the partial admission.

An increase in $n_{s\ т}$ can be caused by an increase in the angular velocity of the wheel ω. And this means that, other conditions being equal, (u = const; $c_{ад}$ = const) the diameter of the wheel $D_{ср}$ should be decreased, and, therefore, the degree of admission, furthermore, will increase.

It should be noted that at small values of $u/c_{ад}$ the effect of $n_{s\ т}$ on the value of the optimum efficiency is less substantial. This is explained by the fact that at small values of $u/c_{ад}$ losses with discharge velocity and profile losses of the impeller vanes (large angle of the flow rotation) play the dominant role.

As one would expect, with an increase in the clearance the efficiency decreases (see Fig. 4.60). A decrease in efficiency will be the result of an increase in the width of the impeller vanes basically because of an increase in the secondary losses in the cascade and losses connected with the admission. With an increase in $\bar{b}$ and $\bar{\Delta}$ the optimum height of the blade increases. In turbines without a shroud, because of the greater effect of the clearance on the losses, the optimum length of the blade will be more, and the efficiency is less than that in turbines with a shroud. In the designing of a turbine (see further Section 4.8.2) the dependences given on Fig. 4.58 make it possible to estimate without the conducting of detailed calculations the efficiency of the turbine with the absolute width of the blade b and absloute value of the clearance Δ selected from conditions of the technology and operating conditions of the design.

4.6. MULTISTAGE TURBINES

In technology multistage turbines are widely used. In LPRE, for the purpose of obtaining light and simple constructions, it is attempted to use single-stage turbines, but in a number of cases here it proves to be expedient to use multistage turbines. Let us examine the basic forms of multistage turbines.

4.6.1. MULTISTAGE REACTION TURBINE

The multistage reaction turbine is a number of consecutively installed reaction stages. Figure 4.61 schematically shows the meridian section of a three-stage reaction turbine, and the development of the cylindrical section which reveals the form of the blades is given. Above the meridian sections a change in the gas pressure p and velocity c along the length of flow area is shown.

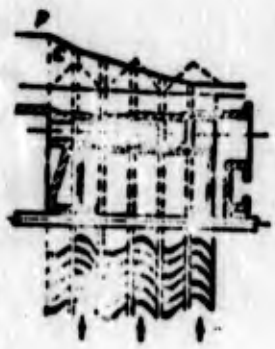

Fig. 4.61. Diagram of a three-stage reaction turbine.

The total pressure differential is divided between the stages. In each stage it is possible to insure the comparatively low flow rates along the flow area. This decreases the hydraulic losses and makes it possible to obtain a high efficiency. In accordance with the degree of reaction the relative velocity in the impeller channels is changed. The high efficiency is the major advantage of such turbines. The output kinetic energy of the first and intermediate stages is used in the subsequent stage.

The energy calculated from the discharge velocity of the last stage represents losses in the turbine with discharge velocity.

Figure 4.62 depicts the process in the i-s-diagram for a three-stage reaction turbine. Noted on Fig. 4.62 are adiabatic and circumferential works of the entire turbine and each of the stages. For the intermediate stage of the initial enthalpy, one should consider the gas enthalpy at the outlet from the previous stage calculated from the stagnation parameters.

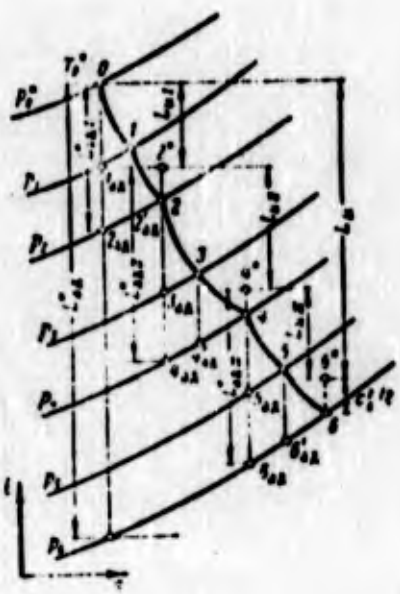

Fig. 4.62. Representation in i-s coordinates of the process in a three-stage reaction turbine.

Assuming that adiabatic works of each stage are identical ($L^*_{ад\ i} = L^*_{ад}/z$), then all the stages will operate with the identical ratio $u/c_{ад\ i}$, where $c_{ад\ i} = \sqrt{2L^*_{ад\ i}}$. Then with the identical degrees of reaction the circumferential efficiencies of the stages will be identical, and, therefore, the circumferential works ($L_{ui} = L^*_{ад\ i}\eta_u$) will be identical. The circumferential work of the turbine, defined as the sum of works of the stages will be equal to: $L_u = zL_{ui}$, and the operating factor

$$\bar{L}_u = \bar{L}_{ul}. \qquad (4.133)$$

For the stage with the reaction $\rho_т = 0.5$, in the conditions $(u/c_{ад\ i})_{\eta_{u\ max}}$ (when $c_{2u} = 0$) the value $c_{1u} = u$ (see Fig. 4.47), and therefore in accordance with equation (4.107) $L_{un_{u\ max}} = 1$. Then for the multistage reaction turbine with such stages, the coefficient of circumferential work will be equal to the number of the stages:

$$\bar{L}_{u_{max}} = z. \qquad (4.134)$$

In general, at ratio $u/c_{ад\ i}$, equal to ratio $u/c_{ад}$ of the single-stage turbine with the same degree of reaction, the coefficient of circumferential work of the multistage turbine will be z times more than that for the single-stage turbine. However, it will correspond to a smaller ratio $u/c_{ад}$ than of single-stage turbine, calculated from the entire adiabatic work of the multistage turbine ($c_{ад} = \sqrt{2L^{*}_{ад}}$):

$$\frac{u}{c_{ад}} = \frac{1}{\sqrt{z}} \frac{u}{c_{ад\,i}}. \qquad (4.135)$$

Figure 4.63 shows the dependence of the coefficient of circumferential work $\bar{L}_u$ on $u/c_{ад}$ for two- and four-stage reaction turbines ($\rho_т = 0.5$), obtained by conversion with the aid of equations (4.133) and (4.135) corresponding to the dependence for the single-stage turbine (see Fig. 4.49).

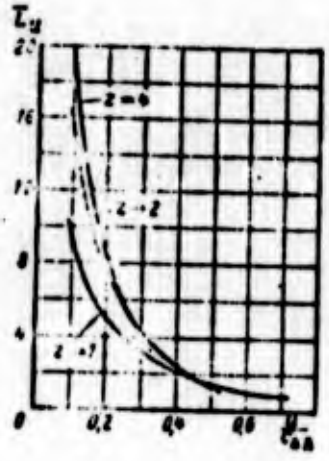

Fig. 4.63. Dependences of the coefficient of circumferential work $\bar{L}_u$ on $u/c_{ад}$ for reaction turbines ($\rho_т = 0.5$) with a different number of stages.

Figure 4.63 shows that with a larger number of stages the multistage reaction turbine makes it possible to obtain greater circumferential work, in particular, in the region of small ratios $u/c_{ад}$, which is necessary in the case of the autonomous turbines of the LPRE. However, an increase in the number of stages complicates the construction and increases the mass of the turbine, which is undesirable. Besides this, the multistage reaction turbine has high axial force acting on the rotor. The indicated deficiencies led to the fact that the multistage reaction turbines found no use in the LPRE.

4.6.2. MULTISTAGE IMPULSE TURBINES

Considerably greater interest for the use in LPRE is in multistage impulse turbines. Multistage impulse turbines can be subdivided into two forms: impulse turbines with pressure stages and impulse turbines with velocity stages.

4.6.2.1. Multistage Impulse Turbines

Let us examine the layout scheme of a multistage impulse turbine and the flow of the process in it. Figure 4.64 gives a diagram of the impulse turbine with two pressure stages. Such a turbine is formed by the sequential combination of two impulse stages.

Fig. 4.64. Diagram of an impulse turbine with two pressure stages.

Representation of the process in the i-s-diagram for such a turbine is given on Fig. 4.65. Sections which correspond to adiabatic and circumferential work of the entire turbine and its individual stages are noted.

The circumferential efficiency of such a turbine is determined by the relation

$$\eta_u = \frac{L_u}{L_{ad}} = \frac{L_{u1} + L_{u2}}{L_{ad}}. \qquad (4.136)$$

The efficiency of such a turbine can be higher than the efficiency of a single-stage impulse turbine, since the flow velocities in the flow area of the double-stage turbine will be less. The use of the discharge velocity of the first stage also increases the efficiency of the turbine.

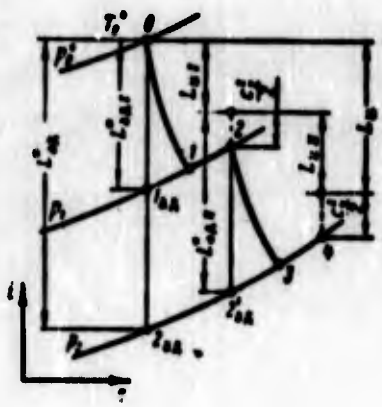

Fig. 4.65. Representation in coordinates of the i-s process in an impulse turbine with two pressure stages.

Hydraulic losses in the impulse turbine with pressure stages will be more than in the reaction turbine calculated for the same pressure differential, since in the reaction turbine the flow rates will be less. In the impulse pressure stages the rotor wheel does not undergo great axial force. In comparison with the design of the single-stage impulse turbine, the design of the double-staged turbine is more complex, and such a turbine has larger mass. A shortcoming in such turbines is the possibility of leakage between the stages.

With the equality of operation of every stage, bearing in mind that the coefficient of circumferential work for the stage $\bar{L}_{u\eta_{u\ max}} = 2$ (when $c_{2u} = 0$), we will obtain that the coefficient of circumferential work of the impulse turbine with pressure stages in conditions of the axial outlet from every stage is equal to the doubled number of the stages:

$$\bar{L}_{u\eta_{u\ max}} = 2z. \qquad (4.137)$$

The coefficient of circumferential work for the impulse turbines with pressure stages increases in proportion to the number of stages in the first degree and exceeds two times the coefficient of circumferential work for the turbine with reaction stages in conditions $c_{2u} = 0$ [see equation (4.134)].

For other conditions the coefficient of circumferential work for the impulse turbine with pressure stages can be estimated according to the value L_u for the impulse stage ($\rho_т = 0$) (see Fig. 4.49), using relations (4.133) and (4.135) for the reactive multistage turbine, since the impulse turbine with pressure stages is its special case ($\rho_т = 0$).

Figure 4.66 gives the dependences of $\bar{L}_u$ on $u/c_{ад}$ for the two-stage impulse turbine with pressure stages and for the two-stage reaction turbine. It is evident that in the range of small ratios $u/c_{ад}$ the impulse turbine with pressure stages makes it possible to obtain larger values of the operating factor than does the mulistage reaction turbine with the same number of stages.

Of the multistage turbines the most widespread in LPRE are the impulse turbines with velocity stages. As will be shown below, these turbines make it possible to obtain with the same number of stages larger values of operating factors in the region of low values of $u/c_{ад}$ than do the multistage reaction turbines and impulse turbines with pressure stages. Low values of $u/c_{ад}$, as was already repeatedly noted, correspond to autonomous turbines of LPRE.

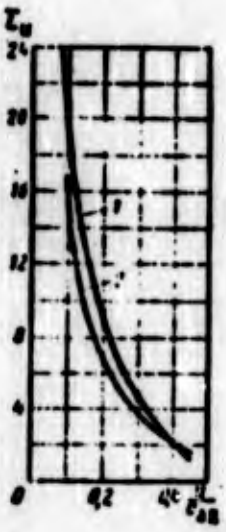

Fig. 4.66. Dependences of the coefficient of circumferential work L_u on $u/c_{ад}$: 1 - two-stage impulse turbine with pressure stages; 2 - two-stage reaction turbine ($\rho_T = 0.5$).

Let us examine the impulse turbines with velocity stages in more detail.

4.6.2.2. Impulse Turbines with Velocity Stages

A. REPRESENTATION OF THE PROCESS OF THE VELOCITY TRIANGLE IN THE i-s-DIAGRAM. CIRCUMFERENTIAL WORK

A diagram of an impulse turbine with two velocity stages is given on Fig. 4.67. The expansion of gas occurs only in one nozzle cascade. Standing after the blades of the first row are the stationary blades (guide vanes), which turn the gas current so that it would flow without a shock around the next row of rotor blades. Both rows of rotor cascades, for facilitating the design of the turbine are usually fastened on the rim of one wheel (see Fig. 4.67). All cascades except the cascade of nozzle cascade are of impulse action. For an ideal case $w_{1I} = w_{2I}$ and $W_{1II} = w_{2II}$.

In the second stage the kinetic energy of the gas emerging from the first stage is used. Hydraulic losses in such a turbine

are great, since the flow rates of the gas on cascades are high, but losses with the discharge velocity are lowered in comparison with losses in the single-stage turbine.

Figure 4.68 depicts in the i-s-diagram the process in the impulse turbine with two velocity stages. The real process is shown by a line which unites points 0-1-2-3-4. Line 0-1 corresponds to the process in the nozzle cascade; L_ϕ is energy losses in the nozzle cascade. Just as for the single-stage turbine,

$$L_\phi = (1-\varphi^2)L_{ad}. \qquad (4.138)$$

The process in the vane channels of the first row of rotor blades is depicted by line 1-2. An increase in enthalpy $i_1 - i_2 = L_{\psi I}$, where $L_{\psi I}$ is the energy losses during flow in the first row of the rotor blades:

$$L_{\psi 1} = (1-\psi_1^2)\frac{w_{2ad}^2}{2}. \qquad (4.139)$$

Fig. 4.67. Diagram of an impulse turbine with two velocity stages.

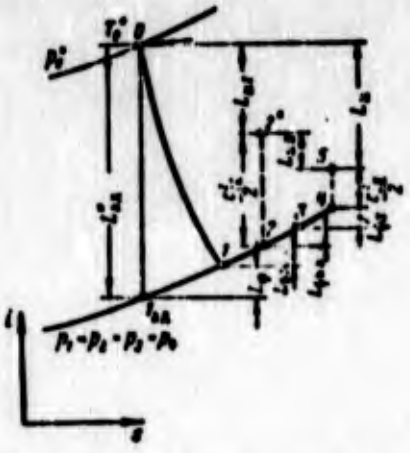

Fig. 4.68. Representation in i-s coordinate of the process in an impulse turbine with two velocity stages.

Line 2-3 corresponds to the process in guide vane, i.e., the process of the gas flow at constant pressure with an increase

in the entropy and enthalpy because of the work of friction. In the channel of constant section the rotation of flow is achieved. Let us introduce the concept of the velocity factor of the guide vane $\psi_{н.а}$:

$$\psi_{н.а}=\frac{c_1}{c_{1ад}}. \tag{4.140}$$

We will obtain that the energy losses with flow in vane channels of the guide vane

$$L_{н.а}=(1-\psi^2_{н.а})\frac{c^2_{1ад}}{2}. \tag{4.141}$$

The process of flow along the vane channels of the second row of rotor blades at constant pressure is depicted in the i-s-diagram as line 3-4. The corresponding loss of energy in the second row of the rotor blades is designated by $L_{\psi II}$:

$$L_{\psi II}=(1-\psi^2_{рII})\frac{w^2_{2ад\,II}}{2}. \tag{4.142}$$

The circumferential work of the entire turbine L_u will be found as a difference in the initial enthalpy i_0^* and the enthalpy at point 5, which corresponds to the stagnation state of the gas, after the rotor blades of the second stage:

$$L_u=i_0^*-i_5.$$

The difference in enthalpies of $i_5 - i_4$ corresponds to the outlet high-speed energy, which determines the losses with the discharge velocity of the entire turbine.

The work of the first stage is determined from the difference in the initial enthalpy and stagnation gas enthalpy at the outlet from the first stage. The outlet high-speed energy $c^2_{2I}/2$, being losses for the first stage, is the available energy for the second stage.

The work of the second stage is found as the difference in enthalpies at point 2* and at point 5. Actually, the installation

of the second stage is one of the methods of the use of energy losses with discharge velocity. If the outlet velocity from the second stage is sufficiently great, then it is possible to install another row of guide vanes and a row of rotor blades. Such a turbine will be three-stage with three velocity stages (Fig. 4.69).

In the LPRE the three-stage turbines are usually not used because of the noticeable complication of the design and increase in the mass of the turbine, although the coefficient $\bar{L}_u$ of the circumferential work of such a turbine, as will be subsequently shown, is great.

Let us observe the plotting of velocity triangles for turbines with tvelocity stages in the example of the impulse turbine with two velocity stages (Fig. 4.70). Angle α_1 - the angle of inclination of the jet which escapes from the nozzle cascade - is assigned. The velocity c_{1I} is determined from the assigned magnitude of the adiabatic work and velocity factor of the nozzles:

$$c_{1I} = \varphi \sqrt{2L_{ad}}. \qquad (4.143)$$

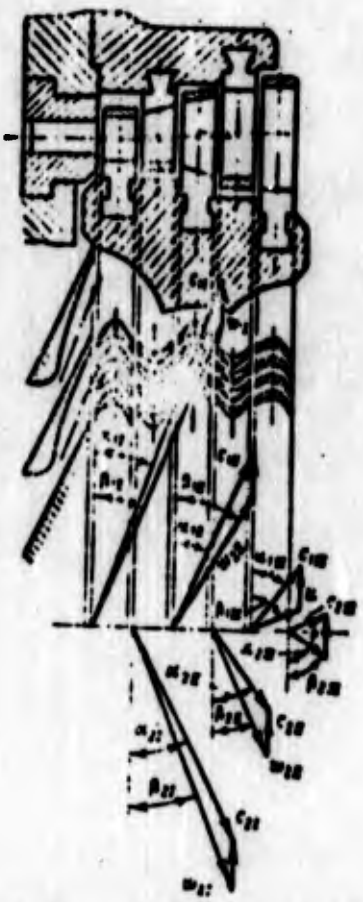

Fig. 4.69. Diagram of an impulse turbine with three velocity stages.

In subtracting vectorialy from c_{1I} the circular velocity u, we find the value and direction of velocity w_{1I}. Leading edges of the blades should be oriented in accordance with the angle β_1. In rotor blades of the first row the rotation of the flow occurs. The outlet angle of the blades is equal to

inlet angles or somewhat less than it. The velocity w_{2I} is less than w_{1I} due to the presence of losses:

$$w_{2I} = \psi_I w_{2ad}; \tag{4.144}$$

$$w_{1II} = w_{2ad}. \tag{4.145}$$

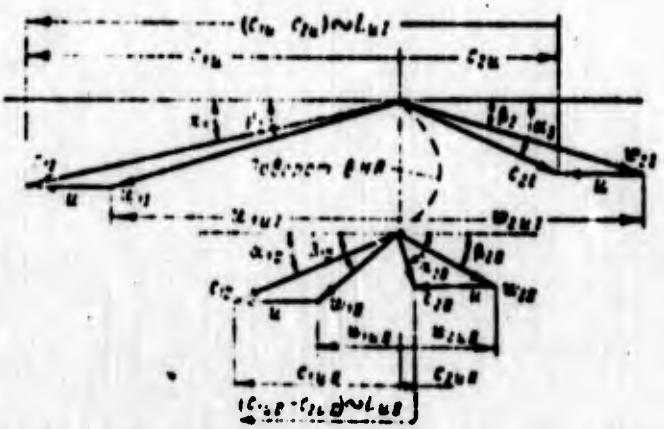

Fig. 4.70. Velocity triangles for an impulse turbine with two velocity stages.

The outlet velocity from the first stage c_{2I} is found by the vector subtraction of the circular velocity u from w_{2I}.

The guide vane carries out rotation of the flow. The angles of the stator blade are determined by angle α_{2I}, where α_{2I} is the angle of inclination of vector c_{2I}. The outlet angle of the guide vane is made equal to the inlet angle or less than it for eliminating the diffusivity of the flow. In value c_{1II} is less than c_{2I} due to the presence of losses:

$$c_{1II} = \psi_{н.а} c_{2I}. \tag{4.146}$$

For the second stage c_{1II} will be the absolute flow velocity at the inlet. The plotting of the velocity triangle for the second stage is produced in a way similar to the plotting of the velocity triangle for the first stage. Profiles of blades of the second stage are less bent, since they achieve less rotation of the flow.

The work of the first stage will be proportional to the section ($c_{1uI} = c_{2uI}$):

$$l_{uI} = u(c_{1uI} - c_{2uI}); \tag{4.147}$$

$$l_{uII} = u(c_{1uII} - c_{2uII}). \tag{4.148}$$

Correspondingly the circular work of the stages can be calculated according to the circular projections of the relative velocities:

$$l_{uI} = u(w_{1uI} - w_{2uI}); \tag{4.149}$$

$$l_{uII} = u(w_{1uII} - w_{2uII}). \tag{4.150}$$

The work of the entire turbine will correspondingly be equal to:

$$l_u = l_{uI} + l_{uII} = u(c_{1uI} - c_{2uI} + c_{1uII} - c_{2uII}). \tag{4.151}$$

or

$$l_u = u(w_{1uI} - w_{2uI} + w_{1uII} - w_{2uII}). \tag{4.152}$$

All the circular projections of the velocities are considered as vectors.

B. CIRCULAR EFFICIENCY

The circular efficiency is determined by the relation (4.136). By conducting the derivation similar to the derivation of equation (4.97), and assuming that $\psi_I = \psi_{II.a} = \psi_{II} = \psi$ for the symmetrical blades, we will obtain

$$\eta_u = 2\frac{u}{c_{aI}}(1+\psi)\left[(1-\psi)\left(\cos\alpha_1 - \frac{u}{c_{aI}}\right) - (1+\psi)\frac{u}{c_{aII}}\right]. \tag{4.153}$$

Having taken the first-order derivative from expression (4.153) and having equated it to zero, when $\psi = 1$ we will obtain

$$\left(\frac{u}{c_1}\right)_{\eta_u \max} = \frac{\cos\alpha_1}{4}. \tag{4.154}$$

This relation can be obtained visually from an examination of the velocity triangles, which are plotted not allowing for losses in the blades and symmetrical profiles.

For the turbine with two velocity stages such a velocity triangle is given on Fig. 4.71.

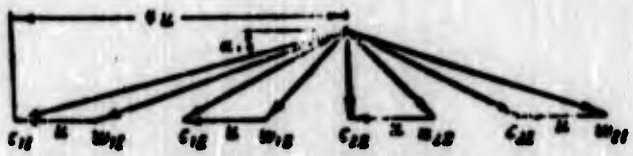

Fig. 4.71. Velocity triangles for the impulse turbine with two velocity stages, with symmetrical blades, in the absence of losses.

Under the selected conditions: $w_{1II} = w_{2I}$; $c_{1III} = c_{2I}$; $w_{1III} = w_{2II}$; $c_{2uII} = 0$, from the velocity triangles we obtain

$$c_{1I}\cos\alpha_1 = 4u,$$

or

$$\left(\frac{u}{c_1}\right)_{\eta_u \max} = \frac{\cos\alpha_1}{4}.$$

For z stages we will respectively obtain

$$\left(\frac{u}{c_1}\right)_{\eta_u \max} = \frac{\cos\alpha_1}{2z}. \qquad (4.155)$$

Figure 4.72 gives the calculated curves of the circular efficiency for the single-stage impulse turbine (I), impulse turbine with two velocity stages (II) and impulse turbine with three velocity stages (III). The curves are calculated for the different slope angles of the nozzle blades α_1. Coefficient ϕ is taken equal to 0.95; coefficient ψ is taken as being variable depending on the bending of the profile. (Values of ψ are taken somewhat understated; contemporary turbines frequently have

larger values of efficiency than those which are given on the graph). The optimum of efficiency with respect to u/c_1, with an increase in the number of the stages, is shifted to the left.

The greater the number of the stages, the larger angle α_1 can be selected. This is explained by the fact that the portion of losses with the outlet velocity (determined by the axial component of velocity, depending on angle α_1) is reduced with an increase in the number of the stages, and the bending of the profiles is decreased with an increase in angle α_1, and, therefore, the value ψ of the blades increases, which is especially noticeable in multistage turbines.

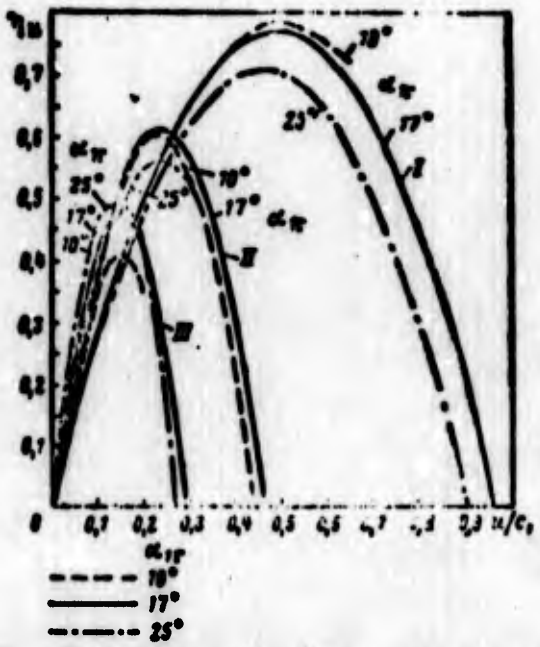

Fig. 4.72. Dependences of the circular efficienty η_u on u/c_1 and angle α_1 for impulse turbines with a different number of velocity stages.

C. COEFFICIENT OF CIRCULAR WORK

Figure 4.73 gives dependences of the coefficient of circular work $\bar{L}_u$ on $u/c_{ад}$ for impulse turbines with one, two

and three velocity stages, calculated with the aid of equation (4.108), according to data given on Fig. 4.72 ($\alpha_1 = 25°$).

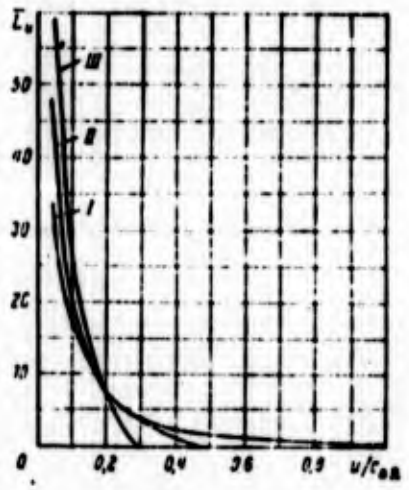

Fig. 4.73. Dependences of the coefficient of circular work L_u on $u/c_{ад}$ for turbines with a different number of velocity stages: I - single-stage turbine; II - turbine with two velocity stages; III - turbine with three velocity stages.

In the region of small values $u/c_{ад}$, i.e., in the region of the operational conditions of autonomous turbines of turbopump units of LPRE, values of the coefficients of circular work for multistage turbines with velocity stages considerably exceed the value of the operating factor for a single-stage impulse turbine. This excess increases with an increase in the number of stages. However, from considerations of the minimum complication of the design and minimum increase in the mass, the number of stages made is not more than two.

Figure 4.74 gives a comparison of the coefficients of circular work of a double-stage turbine with the velocity stages (1), with the two-stage reaction turbine ($\rho_т = 0.5$) (3), and with the two-stage impulse turbine with pressure stages (2). It is evident that at small values of $u/c_{ад}$, inherent to autonomous turbines, the turbine with velocity stages has an advantage; therefore, this type of double-stage turbine found use in the turbopump unit.

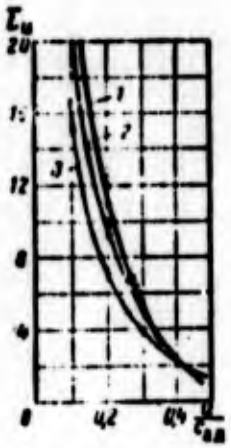

Fig. 4.74. Dependences of the coefficient of the circular work L_u on $u/c_{ад}$ for double-stage turbines: 1 - impulse stage turbine with velocity stages; 2 - impulse turbine with pressure stages; 3 - reaction turbine ($\rho_т = 0.5$).

D. OVERALL EFFICIENCY OF AN IMPULSE TURBINE WITH TWO VELOCITY STAGES

The effective power of the impulse turbine with two velocity stages can be presented as the sum of the effective powers of the first (N_I) and second (N_{II}) stages:

$$N_e = N_I + N_{II}. \tag{4.156}$$

The powers N_I and N_{II} can be expressed in the following manner:

$$N_I = GL_{uI} - G_{yI}L_{uI} - N_{тр.дI} - N_{тр.бI} - N_{εI} =$$
$$= (G - G_{yI})L_{uI} - N_{тр.дI} - N_{тр.бI} - N_{εI}; \tag{4.157}$$
$$N_{II} = (G - G_{yII})L_{uII} - N_{тр.дII} - N_{тр.бII} - N_{εII}. \tag{4.158}$$

If the stages are made with an identical degree of admission ε and have an identical mean diameter, width and span of the blade of the wheel and width of the shroud, then, by disregarding the distinction in the gas densities, it is possible to write (with two disks) that $N_{тр.дI} = N_{тр.дII} = N_{тр.д}$; $N_{тр.бI} = N_{тр.бII} = N_{тр.б}$; $N_{εI} = N_{εII} = N_ε$.

Then, accepting the leakages in the first and second stages to be identical, we obtain

$$N_i = (G - G_y) L_a - 2N_{тр.л} - 2N_{тр.д} - 2N_в, \qquad (4.159)$$

where $L_a = L_{a1} + L_{a11}$.

Having divided the relation (4.159) by $GL_{ад}$, we obtain the expression for the overall efficiency of the double-stage turbine with velocity stages:

$$\eta_i = \eta_p \eta_u - \zeta_{тр.л} - \zeta_{тр.д} - \zeta_в, \qquad (4.160)$$

where η_p - the flow efficiency determined with the aid of equation (4.111);

η_u - the circular efficiency of the turbine determined according to equation (4.153);

ζ - loss factors calculated by equations (4.125), (4.126) and (4.127).

Expression (4.160) is similar to equation (4.122) for the overall efficiency of the single-stage impulse turbine. Just as in the case of the single-stage turbine, the flow losses and disk losses (friction losses of the disk and shroud and losses connected with admission) displace the maximum of the overall efficiency from the maximum of the circular efficiency to the side of smaller values of $u/c_{ад}$; the greater the displacement, the less the degree of admission ε.

With an increase in the span of the blade the efficiency of the cascade (as a result of a reduction in secondary losses) and the flow efficiency of the turbine η_p will increase, but the losses to admission will increase, since ε is decreased. Therefore, just as in the case of the single-stage turbine (see Section 4.5.4.2), the optimum degree of admission should exist at which the overall efficiency will be maximum.

The power of the second stage comprises a smaller part of the power of the turbine. The larger part of the power occurs in the first stage. Thus, the optimum span of the blade (optimum degree of admission) will be determined according to first stage, taking the spans of the blades of the first and second stages identical. Then, depending on the power-speed coefficient of the turbine with velocity stages (it is numerically equal to the power-speed coefficient of the first stage), depending on the ratio $u/c_{ад}$ and other parameters, the optimum span of the impeller vanes will be determined according to equation (4.132).

Figure 4.75 depicts values of the optimum efficiency $\eta_{т\ opt}$ (with ε_{opt}), the maximum efficiency $\eta_{т\ max}$[with ε_{opt} and $(u/c_{ад})_{opt}$] and the optimum ratio $u/c_{ад}$ for the active double-stage turbine with velocity stages calculated with the aid of equations (4.160) and (4.132). These dependences can be utilized in the approximate computations (α_1 = 13°-20°; $M_{w_1 I} \leq 1.5$; Re ≈ $5 \cdot 10^5$; ϕ = 0.93-0.95; $\bar{b}$ = 0.03-0.05; $\mu_{заз}$ = 0.4-0.6; $\bar{t}$ = 0.55-0.65).

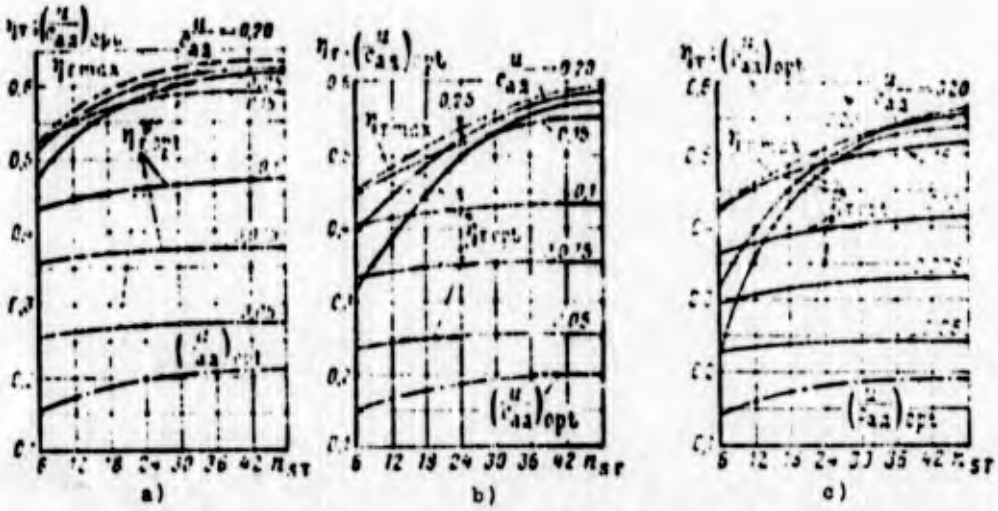

Fig. 4.75. Dependence of the optimum efficiency (solid lines) on the power-speed coefficient $n_{s\ т}$ and $u/c_{ад}$ and dependences of the maximum efficiency (dashed line) and optimum ratio $u/c_{ад}$ (dot-dashed line) on the power-speed coefficient $n_{s\ т}$ for the two-stage impulse turbine with velocity stages: a)- $\bar{\Delta}$ = 0; b)- $\bar{\Delta}$ = 0.01; c)- $\bar{\Delta}$ = 0.02.

Figure 4.75 shows that an increase in $n_{s\ т}$ leads to an increase the efficiency of the turbine. Moreover, an increase in the efficiency is more at large values of $u/c_{ад}$. Thus, the effect of $n_{s\ т}$ in this case is similar to its effect for the single-stage impulse turbine (see Section 4.5.4.2).

Figure 4.76 depicts the calculated dependences of the circular efficiency η_u, the overall efficiency $\eta_т$, and the coefficient of the effective work $\bar{L}_т$ (with ε_{opt}) for the single-stage impulse turbine (subscript "I") and the two-stage impulse turbine with velocity stages (subscript "II") when $n_{s\ т} = 48$.

The maximum value of the overall efficiency of the partial double-stage turbine with velocity stages with low $n_{s\ т}$ can be close to the value of the maximum overall efficiency of the partial-admission single-stage impulse turbine (or even more than it). This is explained by the fact that the loss factors ζ_ε, $\zeta_{тр.д}$ and $\zeta_{тр.б}$ (disk losses) in the optimum mode of the double-stage turbine are less than those in the optimum mode of the single-stage turbine. The coefficients ζ_ε, $\zeta_{тр.д}$ and $\zeta_{тр.б}$ are decreased in proportion to the cube of the ratio $u/c_{ад}$ [see equations (4.125), (4.126) and (4.127)].

The optimum modes of the two-stage and single-stage turbines differ in $u/c_{ад}$ by approximately two times. Thus, the values of the coefficients ζ_ε, $\zeta_{тр.д}$ and $\zeta_{тр.б}$ in the optimum mode for the double-stage turbine will be approximately eight times less than those for the single-stage. Taking into consideration that the double-stage turbine has two blade rims, we will obtain that the relative value of the disk losses in the double-stage turbine in the optimum mode will be approximately four times less than that in the single-stage.

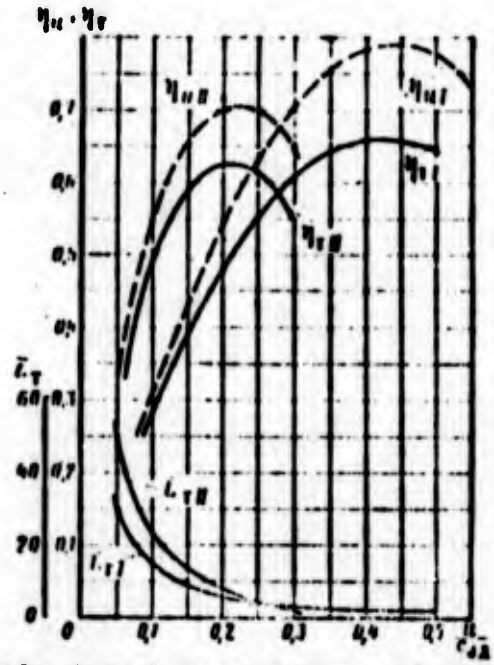

Fig. 4.76. Calculated dependences of the circular efficiency η_u, overall efficiency $\eta_т$ and the coefficient of effective work $\bar{L}_т$ on $u/c_{ад}$ for the single-stage impulse turbine (subscript "I") and the two-stage impulse turbine with velocity stages (subscript "II") when $n_{s\ т} = 48$.

A decrease in the disk losses can compensate for a decrease in the circular efficiency of the double-stage turbine in comparison with its value for the single-stage turbine. This leads to the fact that between the maximum efficiency of the two-stage and single-stage turbines there will be only a small difference, or even the maximum efficiency of the double-stage turbine will exceed the maximum efficiency of the single-stage turbine. This is especially developed at small values of $n_{s\ т}$, when the degree of admission ε is low [see equation (4.130)], and therefore the relative value of the disk losses is great.

From Fig. 4.76 it follows that at low values of $u/c_{ад}$ the double-stage turbine with the velocity stages has a larger coefficient of effective work than does the single-stage impulse

turbine. Calculations show that the advantages of the double-stage turbine appear when $u/c_{ад} < 0.2\text{-}0.25$ (smaller values correspond to smaller $n_{s\ т}$ and larger $\bar{\Delta}$). Thus, in the indicated range of values $u/c_{ад}$ more preferable is the use of the double-stage turbines with velocity stages as autonomous turbines of LPRE than the use of active single-stage turbines.

4.6.2.3. Single-Rim Multistage Impulse Partial-Admission Turbines

Single-rim impulse turbines with a small degree of admission can be made in the form of turbines with velocity stages and pressure stages. Single-rim impulse turbines with velocity stages were used for turbopump unit in some of the first LPRE (see source [143]).

A structural diagram of a single-rim impulse turbine with two velocity stages is given on Fig. 4.77. The role of the guide vane in such a turbine is played by the rotary channel. The use of such turbines showed that their efficiency is low due to the great hydraulic losses in the rotary channel and leakages in the axial clearances. With low degrees of admission such a turbine can still have an advantage over the common turbine with two velocity stages, since the losses connected with partial admission in it will be less; furthermore, such a turbine has less mass of construction.

With an especially low degree of admission the single-rim turbine can be made with the triple gas feed, i.e., actually, in the form of a turbine with three velocity stages.

With high pressure ratios ($\delta > 100$) and a low degree of admission, single-rim stage turbines with pressure stages can be used. Such turbines are used as auxiliary turbines for aircraft and rockets (see source [135]).

Fig. 4.77. Diagram of a single-rim impulse turbine with two velocity stages.

A structural diagram of such a turbine is given on Fig. 4.78. The dashed lines with arrows denote the possible directions of leakages. A considerable operation shortcoming in such a turbine is the great leakage of the working medium through the axial and radial clearances. The clearances must be made extremely small, which is associated with considerable design difficulties.

Fig. 4.78. Diagram of a single-rim impulse turbine with two pressure stages.

4.6.3. BIROTARY TURBINES

4.6.3.1. Impulse Birotary Turbine with Two Velocity Stages

Examined in Sections 4.6.1 and 4.6.2 were multistage turbines in which rotor blades of all the stages are rotated with identical

(in magnitude and direction) angular velocity. But in turbopump units of LPRE it is inexpedient to have different angular velocities for pumps which pump the oxidizer and for pumps which pump the fuel. For the pumping of oxidizers, in connection with the cavitation, usually it is possible to assign less angular velocities of the pump than for the fuel transfer (see Section 3.4.2.1). The accomplishing of a fuel pump with greater angular velocity than the angular velocity of the oxidizer pump makes it possible to decrease the dimensions of the fuel pump and its mass.

It is especially advantageous to design the fuel pump with greater angular velocity in the case of the use of liquid hydrogen as the fuel. In connection with the low density of the hydrogen at low angular velocity, the dimensions of the pump are considerable.

The thermodynamic properties of hydrogen favorably affect the anticavitation qualities of the fuel pump, allowing an increase in its angular velocity.

If the oxidizer and fuel pumps have different angular velocities, then the drive of each of them can be carried out from an individual turbine, i.e., in the turbopump unit there will be two turbines. However, it is possible to drive the pumps from the different stages of the same turbine of the LPRE. The impulse turbine with velocity stages can easily be made as a turbine with different angular velocities of the rotor wheels. The rotor wheels of the first and second stages in such a turbine will have different shafts. The connection between the stages will be achieved only by hydraulic means, since in both stages the same working medium is utilized. Having virtually allowed the different angular velocities of rotor blades of the first and second stages, it is advantageous to allow their rotation

in different directions. In such a kinematic scheme there is no need for a guide vane between the stages.

Turbines with the reverse direction of rotation of rotor blades of different stages without an intermediate guide vane will be called birotary. Figure 4.79 gives a diagram of an impulse birotary turbine with two velocity stages. The combined velocity triangles for such a turbine are given on Fig. 4.80. The relative velocity at the inlet into the second row of rotor blades w_{1II} is determined by subtraction from vector w_{2I} of the sum of vectors u_I and u_{II}. The dashed line shows the absolute gas velocity in the clearance. The work of the first stage will be found from equation

$$l_{uI} = u_I(w_{1uI} - w_{2uI}). \qquad (4.161)$$

and the work of the second stage from equation

$$l_{uII} = u_{II}(w_{1uII} - w_{2uII}). \qquad (4.162)$$

Sections $(w_{1uI}-w_{2uII})$ and $(w_{1uII}-w_{2uII})$ are shown on Fig. 4.80.

At equal circular velocities u_I and u_{II}, with symmetrical profiles of the blades, disregarding the losses with flow in the interblade impeller channels, for the case $c_{2uII} = 0$ we will obtain from the velocity triangles (Fig. 4.81) the relation $(u/c_I)\eta_{u\ max} = \frac{\cos \alpha_1}{4}$; a similar relation was obtained earlier for an impulse turbine with two velocity stages. This was to be expected, since the birotary turbine with two rows of rotor blades is also a turbine with two velocity stages. From the birotary turbine it is possible to obtain a somewhat greater efficiency, since the absence of the intermediate guide vane has a favorable effect on the decrease in hydraulic losses (see further Fig. 4.88).

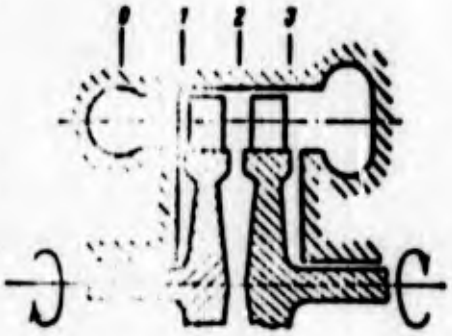

Fig. 4.79. Diagram of an impulse birotary turbine with two velocity stages.

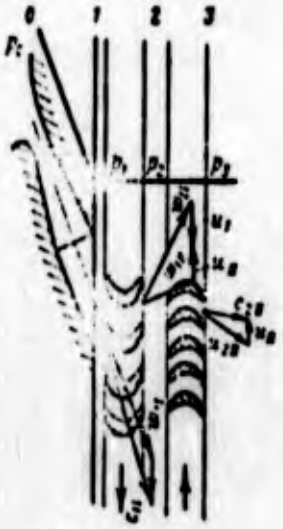

Fig. 4.80. Combined velocity triangles for an impulse birotary turbine with two velocity stages.

Fig. 4.81. Velocity triangles for an impulse birotary turbine with two velocity stages, when $c_{2uII} = 0$ (symmetrical blades, $u_I = u_{II}$, not allowing for losses in the rotor wheels).

The work of the second stage under conditions formulated above ($u_I = u_{II} = u$, etc.) is three times less than the work of the first stage: $L_{uI} = 6u^2$; $L_{uII} = 2u^2$ (see Fig. 4.81).

Values of the coefficients of circular work will be the same as those for the common turbine with two velocity stages.

The main disadvantage of a turbine of this design is that in the turbine it is difficult to provide the required balance of energy in off-design conditions. The energy of the second stage depends on parameters of the first stage, and it is not always possible to achieve the matched change in the available powers and loads on the stages.

Let us find the relationship of powers for the first and second stages with symmetrical blades but at different circular velocities. Disregarding the losses in the blades, considering losses in the stages equal, assuming $c_{2uII} = 0$ (Fig. 4.82) and passing over to scalar quantities, we obtain

$$\frac{N_{uI}}{N_{uII}} = \frac{L_{uI}}{L_{uII}} = \frac{u_I(x_{uI} + x_{uI})}{u_{II}(x_{uII} - x_{uII})} = \frac{u_I(2u_I + 4u_{II})}{u_{II}2u_{II}}; \tag{4.163}$$

$$\frac{N_{uI}}{N_{uII}} = \frac{u_I^2}{u_{II}^2} + 2\frac{u_I}{u_{II}}. \tag{4.164}$$

With identical mean diameters

$$\frac{N_{uI}}{N_{uII}} = \left(\frac{\omega_I}{\omega_{II}}\right)^2 + 2\frac{\omega_I}{\omega_{II}}. \tag{4.165}$$

The greater the angular velocity of the first stage, the greater its power. This property of the birotary turbine is very profitable for its use in the turbopump unit of the engine which operates on hydrogen: given from the first stage is the hydrogen pump, the power of which is considerably more than the pump power of the oxidizer.

However, the optimum relationship of angular velocities cannot be obtained, since with an increase in the ratio ω_I/ω_{II} the ratio of the powers rapidly increases, and it is not possible to insure sufficient pump power of the oxidizer. With the use of pumps with bladed preliminary pumps (see Section 3.3.8.1),

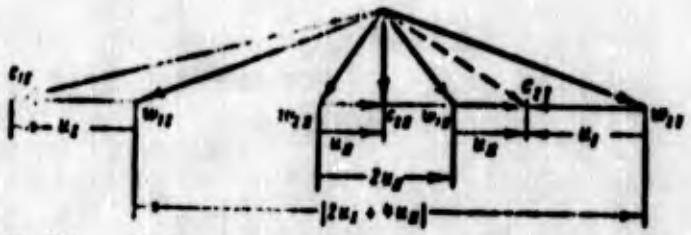

Fig. 4.82. Velocity triangles for the impulse birotary turbine with two velocity stages when $c_{2uII} = 0$ (symmetrical blades not allowing for losses in the rotor wheels).

it is possible to use a version of the turbopump unit in which the hydrogen pump and oxidizer pump will be driven from the first stage of the turbine possessing high angular velocity and the bladed preliminary pump - from the second stage having low angular velocity.

On the basis of the general expression for circular efficiency (4.136), and utilizing relations (4.161) and (4.162), it is possible to obtain an expanded expression for the circular efficiency of the birotary turbine:

$$\eta_u = 2\left\{\cos\alpha_1\left[\frac{u_1}{c_{11}}(\psi_1'+1) - \psi_1'\frac{u_{11}}{c_{111}}(\psi_{11}'+1)\right] - \left(\frac{u_1}{c_{11}}\right)^2(1+\psi_1') - \frac{u_1}{c_{11}}\frac{u_{11}}{c_{111}}(\psi_1'+1)(\psi_{11}'+1) - \left(\frac{u_{111}}{c_{111}}\right)^2(\psi_{11}'+1)\right\}. \quad (4.166)$$

where

$$\psi_1' = \psi_1\frac{\cos\beta_{21}}{\cos\beta_{11}}; \quad \psi_1 = \frac{w_{21}}{w_{11}};$$
$$\psi_{11}' = \psi_{11}\frac{\cos\beta_{211}}{\cos\beta_{111}}; \quad \psi_{11} = \frac{w_{211}}{w_{111}}.$$

The relation of the powers in the expanded form is

$$\frac{N_{u1}}{N_{u11}} = \frac{L_{u1}}{L_{u11}} = \frac{(c_{11}\cos\alpha_1 - u_1)(1+\psi_1')\frac{u_1}{u_{11}}}{\left[\psi_1 c_{11}\cos\alpha_1 - u_1(1+\psi_1') - u_{11}\right](1+\psi_{11}')}. \quad (4.167)$$

Having introduced the notations

$$\frac{N_{u1}}{N_{u11}} = \bar{N} \quad \text{and} \quad \frac{u_1}{u_{11}} = \bar{u},$$

and also

$$a = 1 + \psi_I' \quad \text{and} \quad b = 1 + \psi_{II}',$$

from formula (4.167) we obtain the relation

$$\frac{u_1}{c_{II}} = \frac{\cos\alpha_1\left(\varphi_1 - \frac{d\bar{N}}{b\bar{N}}\right)}{a + \frac{1}{\bar{u}} - \frac{d\bar{N}}{b\bar{N}}}. \qquad (4.168)$$

To establish the connection between the ratio of powers $\bar{N}$ and the efficiency η_u, calculations were conducted with the following initial data: $\alpha_I = 20°$; $\phi = 0.95$; $\psi_I' = 0.83$; $\psi_{II}' = 0.93$.

The results of the calculation are given in graphs which can be used for the approximate computations (Fig. 4.83 and 4.84).

Fig. 4.83. Dependence of u_I/c_{II} on the ratio of circular velocities $\bar{u}$ at different ratios of powers $\bar{N}$ for a birotary impulse turbine.

The dependences of η_u on the coefficient of circular velocity $\bar{u}$ at different $\bar{N} > 1$ (see Fig. 4.84) are sufficiently slanting, which makes it possible to select the ratio of circular velocities with the assigned ratio of powers in a sufficiently wide range. (Approximately the ratio of the powers on the circumference of the wheel can be replaced with the ratio of the available powers).

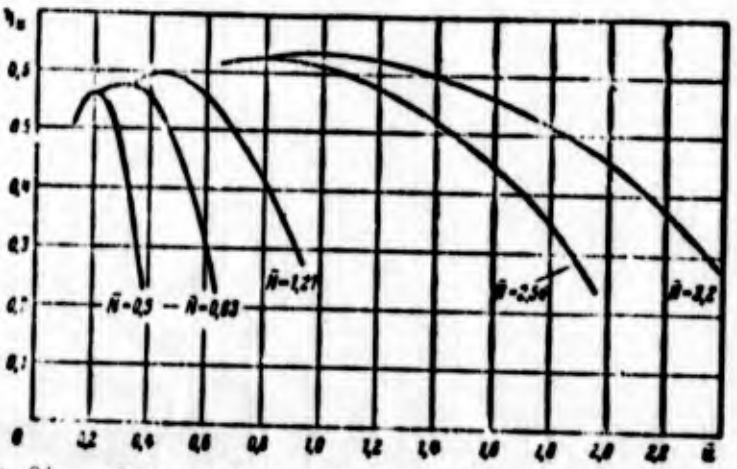

Fig. 4.84. Dependence of the circular efficiency η_u on the ratio of the circular velocities $\bar{u}$ at different power ratios $\bar{N}$ for the birotary impulse turbine.

Having selected the values of $\bar{N}$ and $\bar{u}$, which satisfy the specified conditions with as high an efficiency as possible (see Fig. 4.84), according to Fig. 4.83 we fing the ratio u_I/c_{1I}, and, by knowing the value u_I, we find the necessary value of c_{1I}. According to value c_{1I} it is possible to select the necessary parameters p_0^*, T_0^* and p_2. At the assigned parameters p_0^*, T_0^* and p_2 the diameter of the wheel of the first stage can be selected on the basis of value u_I. The value η_u determined according to Fig. 4.84, after the calculation of flow disk losses (see Section 4.5), makes it possible to assign the efficiency of the turbine in the calculation of the required gas flow rate.

4.6.3.2. Reaction-Impulse Birotary Turbine

Having allowed the possibility of driving the pumps from different shafts, it is possible to use the turbine for which the nozzle cascade will be rotated and develop a torsional moment. The diagram of such a turbine is given on Fig. 4.85. This turbine is formed from the impulse single-stage turbine by means

of setting the nozzle cascade on the rotating wheel. According to operating principle the turbine, depicted on Fig. 4.85, is a reaction-impulse and two-stage, since it has two rotor wheels. The change in gas pressure along the length of flow area is also shown on Fig. 4.85, where the velocity triangles are plotted. The combined velocity triangles are given on Fig. 4.86. The gas at the inlet into the first cascade has an absolute velocity c_0 and relative velocity w_0. In the channels of this cascade the conversion of the potential energy and the acceleration of flow up to the velocity w_{1I} occur.

Fig. 4.85. Diagram of a reaction-impulse birotary turbine.

The gas enters into the second rotor cascade with considerably lower velocity w_{1III}, since it is the vector difference $\vec{w}_{1I}$ and $(\vec{u}_I - \vec{u}_{II})$. Incidentally this is one of the important positive characteristics of this turbine. At supersonic velocities of outflow from the first row of the blades at the inlet into the second row there can be subsonic velocities. In this case wave losses during the flow around the second row of blades will be absent.

The work of the wheel of the first stage is determined from the equation

$$L_{u1} = u_1(w_{u1} - w_{u2}) = u_1 \Delta w_{u1}. \qquad (4.169)$$

and the work of the wheel of the second stage - from the equation

$$L_{uII} = u_{II}(w_{1uII} - w_{2uII}) = u_{II}\Delta w_{uII}. \qquad (4.170)$$

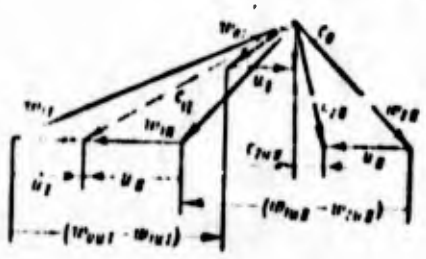

Fig. 4.86. Combined velocity triangles for a reaction-impulse birotary turbine.

For the symmetrical blades of the second row, if we disregard losses in them, we will have with axial outlet $c_{2uII} = 0$. From an examination of the velocity triangles, plotted for this case on Fig. 4.87, it is easy to establish the ratio of the powers and angular velocities of the stages. With the adopted assumptions we will obtain

$$L_{uI} = 2u_I u_{II} \quad \text{and} \quad L_{uII} = 2u_{II}^2.$$

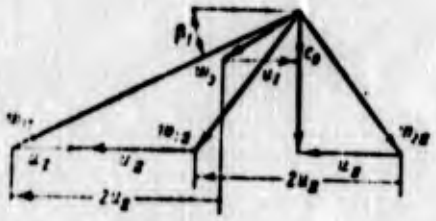

Fig. 4.87. Velocity triangles for a reaction-impulse turbine when $\beta_{1II} = \beta_{2II}$, not allowing for losses in the impulse blades, when $c_{2uII} = 0$.

Hence it follows that the ratio of the powers is directly proportional to the ratio of angular velocities:

$$\frac{N_{uI}}{N_{uII}} = \frac{L_{uI}}{L_{uII}} = \frac{u_I}{u_{II}} = \frac{\omega_I}{\omega_{II}}. \qquad (4.171)$$

Calculations showed that by taking the losses into account this relation is somewhat changed:

$$\frac{N_I}{N_{II}} = k\frac{\omega_I}{\omega_{II}}, \text{ where } k = 1.25\text{-}1.4.$$

In the presence of twist at the outlet from the second wheel in the direction opposite to the rotation, for symmetrical blades the power of the second wheel even at equal angular velocities will be more than the power of the first wheel.

From Fig. 4.86 it follows that

$$\Delta w_{uI} = 2u_{II} + c_{2uII}; \quad \Delta w_{uII} = 2u_{II} + 2c_{2uII}; \quad \Delta w_{uII} > \Delta w_{uI}. \tag{4.172}$$

With the assigned ratio of velocities $u_I/u_{II} = \bar{u}$ and the assigned ratio of powers $N_{uI}/N_{uII} = \bar{N}$ it is possible to obtain the ratio between the relative twist $c_{2uII}/u_{II} = \bar{c}_{2uII}$, $\bar{N}$ and $\bar{u}$.

Let us write with the aid of equations (4.169), (4.170), (4.172) the following relationship:

$$\bar{N} = \frac{(2 + \bar{c}_{2uII})\bar{u}}{2 + 2\bar{c}_{2uII}}, \tag{4.173}$$

whence it is easy to obtain

$$\bar{c}_{2uII} = \frac{\bar{u}/\bar{N}}{2 - \frac{\bar{u}}{\bar{N}}} - 1 \tag{4.174}$$

(with symmetrical blades and when we disregard losses in them).

When $\bar{c}_{2uII} = 0$ we obtain the already known relation (4.171).

The relation (4.174) is useful, since it makes it possible, having the assigned values $\bar{N}$ and $\bar{u}$ (from the calculation of pumps), to estimate which velocity triangle corresponds to the assigned magnitudes $\bar{u}$ and $\bar{N}$. The velocity triangle can be obtained in an unreal manner. This will mean that the turbine with the assigned relations $\bar{u}$ and $\bar{N}$ cannot be made. Then one should assign the advisable value of twist at the outlet c_{2uII} and from the assigned magnitude $\bar{N}$ find which relations of angular velocities can be relaized.

For determining $\bar{u}$ we convert the formula (4.174):

$$\bar{u} = 2N\frac{\bar{c}_{2uII}+1}{\bar{c}_{2uII}+2}. \qquad (4.175)$$

The coefficient of circular work $(\bar{L}_u)_{\eta_u \max}$ for the birotary reaction turbine at equal velocities $u_I = u_{II}$ and $c_{2uII} = 0$ (with nonsymmetric blades, not allowing for losses, see (Fig. 4.87) will be equal to $(\bar{L}_u)_{\eta_u \max} = 4$. The coefficient of circular work of such a turbine is two times more than the coefficient of circular work of a single-stage impulse turbine with the same number of vane cascades.

In comparison with the impulse turbine with two velocity stages, the maximum of efficiency here is shifted to the right with respect to u/c_1 (for a birotary reaction turbine - with respect to u/w_{1I}). One should expect that for such a turbine the absolute value of the efficiency will be more than that for the impulse turbine with two velocity stages, including that for the birotary, since the number of rows of the vane cascades is minimum and the velocity at the inlet into impulse cascade is minimum (on Fig. 4.88 the curve of the change in efficiency of the birotary reaction-impulse turbine is designated by number III).

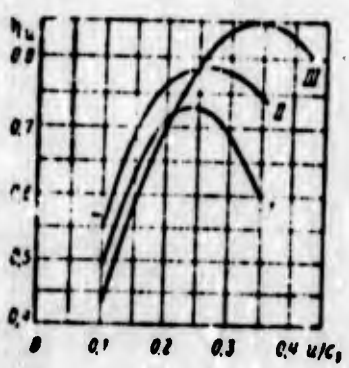

Fig. 4.88. Dependences of the circular efficiency η_u on u/c_1 for the impulse turbine with two velocity stages (I), the birotary impulse turbine (II) and the birotary reaction-impulse turbine (III).

The use of the reaction-impulse turbine is limited by the fact that such a turbine just as any reaction turbine, will effectively work only with a full gas feed, i.e., when $\varepsilon = 1$. This means that such a turbine can be used only for high flow rates. For turbines with the high pressure ratio, the flow rate causes high power, and, therefore, such turbines can be used in turbopump units of high-thrust engines.

4.6.3.3. Multistage Birotary Reaction-Impulse Birotary Turbine with Two Velocity Stages

The reaction-impulse birotary turbine can be made with any number of stages, in particular with any number of velocity stages.

Figure 4.89 gives a diagram of a reaction-impulse birotary turbine with two velocity stages.

Fig. 4.89. Diagram of the reaction-impulse birotary turbine with two velocity stages.

Velocity triangles for the reaction-impulse birotary turbine with two velocity stages with symmetrical blades of the second and third rows not allowing for losses in them, when $c_{2uIII} = 0$ and $u_I = u_{II} = u_{III} = u$, are given on Fig. 4.90.

Works of rows of the rotor blades are, respectively, equal to:

$$L_{u1} = 4u^2; \quad L_{uII} = 6u^2; \quad L_{uIII} = 2u^2.$$

The most loaded is the second row of the rotor blades. The power between the rotor wheels is distributed equally, since the first and third rows of the blades operate on one shaft.

The operating factor of the entire turbine under conditions of $\eta_{u\ max}$:

$$(\bar{L}_u)_{\eta_{u\ max}} = 12;$$

the optimum relation

$$\left(\frac{u}{c_{1I}}\right)_{\eta_{u\ max}} = \frac{\cos\alpha_1}{5}. \qquad (4.176)$$

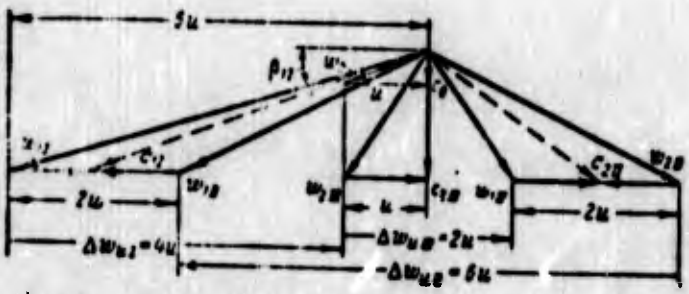

Fig. 4.90. Velocity triangles for the reaction-impulse birotary turbine with two velocity stages with symmetrical blades, not allowing for losses, when $c_{2uIII} = 0$ and $u_I = u_{II} = u_{III} = u$.

Turbines of this design are characterized by the high values of the coefficient of circular work with a small number of rims.

4.7. ENERGY TURBINE CHARACTERISTICS

4.7.1. FORMS OF TURBINE CHARACTERISTICS

Dependences of the work, efficiency, power of the turbine or the values derived from them on any independent parameter, which determines conditions of the turbine, are called the power turbine characteristics.

Selected as an independent variable is the parameter sharply changing conditions of the turbine (as, for instance, $u/c_{ад}$) or the parameter which affects the control element (for example, the initial pressure, the frequency of rotation, etc.)

The dependence $\eta_т = f(u/c_{ад})$ examined earlier (see Fig. 4.60) for impulse single-stage turbines is the characteristic of a series of turbines having different computed values of $u/c_{ад}$, since at each value $u/c_{ад}$ we assume that the degree of admission is optimum, and the flow angles are equal to the angles of the blade, and that the angles of the blades are changed in accordance with the conditions. For this turbine the angles $\beta_{1л}$ and $\beta_{2л}$ remain constant, and the angle of attack, which increases losses in the cascade is changed. Therefore, the characteristic $\eta_т = f(u/c_{ад})$ for this turbine will not coincide with the dependence $\eta_т = f(u/c_{ад})$ for a series of turbines. Dependences constructed in criterial form have a common nature.

In Section 2.12.4 it is shown that for geometrically similar turbines with the self-similar Reynold's criterion $Re > 10^5$–10^6, there is the relation between the criteria characterizing the effectiveness of the turbine and the mode criteria:

$$\bar{G},\ \bar{N}_т(\text{или } \eta_т) = f(u/c_{ад},\ \lambda_{c_{ад}},\ k). \qquad (4.177)$$

For turbines of turbopump units the mechanical efficiency is taken equal to unity (see Section 4.5.3); and therefore values

of the internal efficiency and internal power for which there were obtained dependences (4.177) will be respectively equal to the effective values of the efficiency and power. From expression (4.177) for the same turbine, let us find the relation of the flow rate, power and efficiency with the operating mode.

Expressions for the criteria can be simplified. Since the criteria can be multiplied (divided) by each other, in the obtaining of new criteria, then having multiplied $\bar{G}$ and $\bar{N}_т$ by $u/c_{ад}$ and $\lambda_{c_{ад}} = c_{ад}/a_{кр}$ and bearing in mind that $\rho_0^* = p_0^* RT_0^*$, we will obtain instead of $\bar{G}$ and $\bar{N}_т$ the following criteria:

$$\bar{G}' = \frac{G\sqrt{RT_0^*}}{2\sqrt{2\frac{k}{k+1}p_1^* p_{1cp}^*}}; \quad \bar{N}_т' = \frac{N_т\sqrt{RT_0^*}}{2\sqrt{2\frac{k}{k+1}p_1^* p_{1cp}^*}}.$$

For the same gas (k = const, R = const) and the same turbine (D_{cp} = const) it is possible to write:

$$\bar{G}' \sim \frac{G\sqrt{T_0^*}}{p_0^*} \text{ and } \bar{N}_т' \sim \frac{N_т\sqrt{T_0^*}}{p_0^{*2}}.$$

Criterion $\lambda_{c_{ад}}$ can be presented in the form

$$\lambda_{c_{ад}} = \frac{c_{ад}}{a_{кр}} = \sqrt{\frac{k+1}{k-1}\left(1 - \frac{1}{\delta^{\frac{k-1}{k}}}\right)}. \qquad (4.178)$$

From expression (4.178) it follows that when k = const, instead of $\lambda_{c_{ад}}$ it is possible to use the pressure ratio in the turbine δ.

The criterion of kinematic similarity

$$\frac{u}{c_{ад}} = \frac{\omega D_{cp}}{2\sqrt{2\frac{k}{k-1}RT_0^*\left[1 - \left(1/\delta^{\frac{k-1}{k}}\right)\right]}}. \qquad (4.179)$$

By eliminating constants k, R and D_{cp}, we obtain

$$\frac{u}{c_{ад}} \sim \frac{u}{\sqrt{T_0^*\left[1-\left(1/\delta^{\frac{k-1}{k}}\right)\right]}}. \qquad (4.180)$$

When δ = const, $u/c_{ад} \sim \omega/\sqrt{T_0^*}$. The criterion $\omega/\sqrt{T_0^*}$ is called the normalized frequency of rotation.

After simplification in the criteria, expression (4.177) for this turbine, which operates on definite gas (k = const, R = const), takes the following form:

$$\frac{G\sqrt{T_0^*}}{p_0^*} = f\left(\frac{\omega}{\sqrt{T_0^*}}, \delta\right); \quad \frac{N_т}{p_0^* \omega^2}\sqrt{T_0^*} \ (\text{or } \eta_т) = f\left(\frac{\omega}{\sqrt{T_0^*}}, \delta\right). \qquad (4.181)$$

Dependences of the normalized flow rate $G\sqrt{T_0^*}/p_0^*$ and normalized power $N_т\sqrt{T_0^*}/p_0^*\omega^2$ on the normalized frequency of rotation with the number of constant values δ are called, respectively, the flow and power characteristics of the turbine. The dependnece of the efficiency of the turbine on the normalized frequency of rotation at different δ characterizes the economy of the turbine.

Figure 4.91a gives the experimental energy characteristics of an impulse turbine with the calculated pressure ratio δ_p = 11. The given flow rate $G\sqrt{T_0^*}/p_0^*$ does not depend on the pressure ratio δ and the normalized frequency of rotation, since with a supersonic pressure differential the flow rate G is determined only by the pressure p_0^* and temperature T_0^*. In this case the effect of p_0^* and T_0^* is such that the complex $G\sqrt{T_0^*}/p_0^*$ should remain constant [see equation (4.40)].

The efficiency of the turbine $\eta_т$ increases with an increase in $\omega/\sqrt{T_0^*}$ (experimental values of $\omega/\sqrt{T_0^*}$ correspond to the range of values $u/c_{ад}$ less than the optimum), since in this case losses with the outlet velocity are decreased. The maximum efficiency level corresponds to the computed value δ. With a difference in

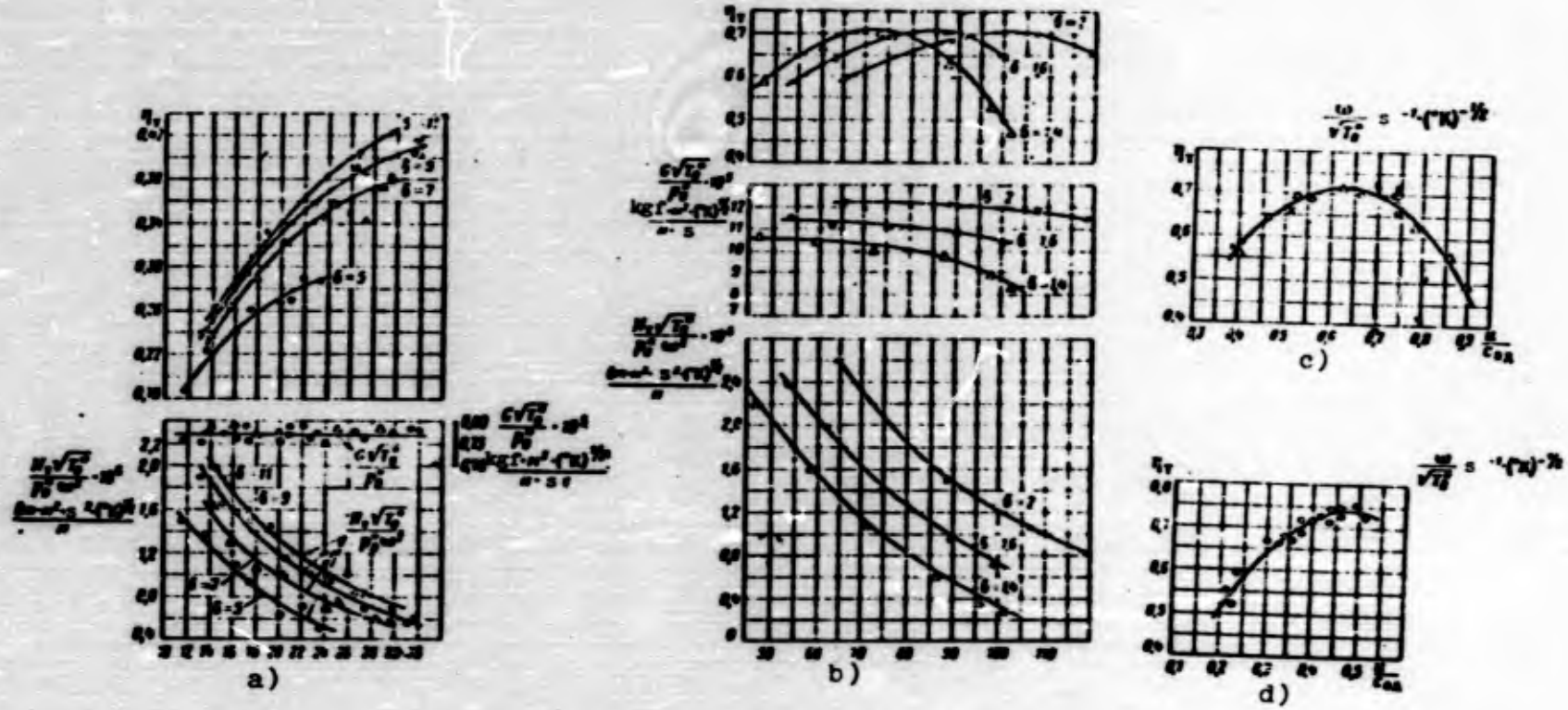

Fig. 4.91. Experimental energy characteristics of turbines: a) energy characteristics of a high-pressure impulse single-stage turbine, (ε = 0.3; model gas - dichlormethane); b) energy characteristics of a low-pressure radial-axial turbine (model gas - air); c) dependence of the efficiency of a low-pressure radial-axial turbine on $u/c_{ад}$ (model air - gas), x - δ = 2; 0 - δ = 1.6; Δ - δ = 1.4; d) dependence of the efficiency on $u/c_{ад}$ for a low-pressure axial-flow turbine with a low degree of reaction (model gas - dichlormethane), o - δ = 1.8; ● - δ = 1.4.

δ from the calculated value, the value of efficiency decreases, since losses in the nozzle cascade increase (because of the fact that the flow becomes off-design), and losses due to a difference in the incidence from the calculated increase.

With an increase in $\omega/\sqrt{T_0^*}$ a decrease in normalized power $N\sqrt{T_0^*}/p_0^*\omega^2$ occurs as a result of a decrease in the coefficient of the adiabatic work $\bar{L}_{ад}^* = L_{ад}^*/u^2$, in spite of an increase in efficiency. Let us explain this in more detail.

On the basis of equation

$$N_т = G L_{ад}^* \eta_т$$

let us write

$$\frac{N_т \sqrt{T_0^*}}{p_0^* \omega^2} = \frac{G \sqrt{T_0^*} R_{ср} \bar{L}_{ад}^* \eta_т}{2 p_0^*} = \text{const} \cdot \bar{L}_{ад}^* \eta_т \qquad (4.182)$$

where $$\bar{L}_{ад}^* = \frac{L_{ад}^*}{u^2} = \frac{c_{ад}^2}{2u^2} = \frac{1}{2(u/c_{ад})^2} \sim \frac{1}{(\omega/\sqrt{T_0^*})^2}.$$

The effect of δ on the normalized power corresponds to the effect of δ on the efficiency, since $G\sqrt{T_0^*}/p_0^* = \text{const}$.

The energy characteristics of a low-pressure turbine (see Fig. 4.91b) are similar to characteristics of a high-pressure turbine, with the exception of the dependence of the normalized flow rate $G\sqrt{T_0^*}/p_0^*$ on δ and $\omega/\sqrt{T_0^*}$. Since the low-pressure turbines have a subcritical pressure differential, with an increase in δ the normalized flow rate will increase [see equation (4.37)]. With an increase in $\omega/\sqrt{T_0^*}$ (an increase in $u/c_{ад}$) the normalized flow rate is somewhat decreased, since the throughput capacity of the wheel is decreased.

The dependence of the efficiency of low-pressure turbines on $u/c_{ад}$ (see Fig. 4.91c and 4.91d) is not affected by the pressure ratio δ (in the region of subsonic velocities).

4.7.2. METHODS OF THE OBTAINING OF TURBINE CHARACTERISTICS

4.7.2.1. Full-Scale Tests

For the obtaining of experimental turbine characteristics, it is necessary to conduct its bench tests. The test stand should be equipped with a brake, instruments for determining parameters of the turbine and regulating devices which make it possible to change the operating mode of the turbine. Similar test stands for turbines of considerable power are quite bulky and complex in construction and operation.

In practice for obtaining the necessary experimental data on the operation of the turbine, full-scale tests of the turbopump unit with the feed of natural gas to the turbine are carried out. In this case the pump performance should be known. This method is good in that operating conditions of the turbine during testing are maximally close to the conditions of normal operation. But the possibilities for obtaining data in the wide range of a change in the conditions are limited by the service life of the turbopump unit, the reliability of the installations, and the complexity of the experiments.

In connection with an increase in the required powers, frequencies of rotation and agressiveness of the components, are ever greater importance is acquired by model tests of turbines of turbopump units.

4.7.2.2. Model Tests

Model tests can be subdivided into two forms:

1) model tests of turbines (i.e., geometrically reduced or increased models);

2) model tests of natural turbines (tests on model gas).

In the testing of turbines of the turbopump unit of the LPRE of high thrusts, we resort to the modeling of turbines of less dimensions; when the dimensions of turbines are small, the use of the reduced models does not lead to a simplification in the tests. With wind-tunnel tests of elements of the turbine, it is frequently necessary to use enlarged models. For the testing of turbines of LPRE model tests of natural full-scale turbines are extensively used also.

With model tests of the turbines, when selecting the conditions, it is necessary to maintain the similarity criterion and process the results of the experiments in criterial form, disregarding the difference in k:

$$\bar{i},\ \bar{N}_T\ (\text{or } \eta_T) = f(u/c_{ad},\ \lambda_{c_{a1}}). \qquad (4.183)$$

Model conditions are selected so that the test conditions would be facilitated. For example, the lowerings of power, frequencies of rotation, temperatures, simplifications in the diagram of the test stand, reductions in prices, ect. are attained.

Widespread use was obtained in model tests in which as a model of the working medium air with low temperature is used. Let us explain what in this case the parameters of air and conditions of the tests should be.

Conditions of modeling (similarity)

$$\frac{u}{c_{a1}} = \text{idem and } \lambda_{c_{a1}} = \text{idem}$$

can be replaced with conditions

$$\frac{u}{c_{ad}} = \frac{u}{c_{a1}}\,\lambda_{c_{a1}} = \text{idem and } \lambda_{c_{a1}} = \text{idem}.$$

Then we will obtain for the model and natural conditions:

$$\frac{a_{\text{м}}}{a_{0\,\text{м}}} = \frac{a}{a_0}; \quad \frac{a_{\text{м}}}{\sqrt{2\frac{k_{\text{м}}}{k_{\text{м}}+1}RT^*_{0\,\text{м}}}} = \frac{a}{\sqrt{2\frac{k}{k+1}RT^*_0}}. \tag{4.184}$$

Bearing in mind that for natural and model gases complexes $\frac{k}{k+1}R$ are close to each other, it may be concluded that the circular velocities and, therefore, ω, with modeling on air should be lowered, since $T^*_{0\text{м}} \ll T^*_0$. A reduction in the frequency of rotation has a favorable effect on the reliability of the test stand, simplification in the measurements, lowering of the powers and so on.

It is possible to attain a reduction in the flow rate through the turbine by means of a reduction in the initial pressure. The limit of reduction in the initial pressure is the reduction in the Re criterion by means of a decrease in ν. The initial pressure can be lowered until according to the Re number the zone of self-similarity will take place, i.e., when $\text{Re} > 10^5$. The initial temperature must be selected in order that with the air expansion in the turbine there is no moisture condensation contained in the air (which will disturb the similarity during the modeling). Usually for this the air must be heated up to 400°-500°K.

Great possibilities are included in the modeling of turbines during tests on working media with great molecular weight (low R) (see source [58]).

For maintaining

$$u_{\text{м}}/a_{0\,\text{м}} = \text{idem} \tag{4.184a}$$

with modeling on heavy work media the circular velocity u and, consequently, the frequency of rotation ω can be greatly lowered, since the value $R_{\text{м}} \ll R$, and usually the temperature of the model working medium can also be selected at less than natural [see

relation (4.184)]. With such a test method the power of the turbine is considerably decreased, since value $L^*_{ад}$ is lowered because of less values of R and T^*_0. It is also possible to decrease the gas flow rate by lowering the initial pressure. In modeling with the use of gas with a low value of R, the power is lowered by dozens and hundreds of times.

The model working media with this test method are freon, for example:

dichlormethane .....k = 1.16; $R = 98 \frac{J}{kg \cdot ^\circ K}$

freon-22 ..... k = 1.18; $R = 99 \frac{J}{kg \cdot ^\circ K}$

freon-12 ..... k = 1.12; $R = 69 \frac{J}{kg \cdot ^\circ K}$.

Test data of the turbine on model gas for the purpose of the further conversion to natural gas, in accordance with the theory of similitude, should be represented in the form of rleations (4.183). Having eliminated the constant value $D_{ср}$ from the criteria $\bar{G}$ and $\bar{N}$, we obtain

$$\bar{G} \sim \frac{G}{\dots}; \quad \bar{N}_т \sim \frac{N_т}{\dots}.$$

Then the test data of the turbine on model gas can be presented in the form

$$\frac{G}{\dots} \cdot \frac{N_т}{\dots} \text{ (or } \eta_т) = f\left(\frac{n}{\dots}, \dots\right). \qquad (4.185)$$

Dependences (4.185) for the model gas will not be identical to the corresponding dependences for natural gas, since values of the criterion k for the model and natural gases are different ($k_м \neq k$), i.e., the full similarity of the processes is not observed. However, experience shows that with a difference in values $k_м$ and k of 10-15%, it is possible to take the relations (4.185) identical for the model and natural gases.

Then when necessary it is possible to convert the relations (4.185), obtained on model gas, into energy characteristics of the turbine which operates on natural gas:

$$\frac{G\sqrt{T_0^*}}{P_0^*}, \quad \frac{N_т\sqrt{T_0^*}}{P_0^*n^2} \quad (\text{or } \eta_т = f\left(\frac{n}{\sqrt{T_0^*}}, \pi\right).$$

An example of the characteristics obtained during model tests of turbines are the dependences given on Fig. 4.91.

4.7.2.3. Calculation of Characteristics of the Turbine

The third way to obtain characteristics of the turbine is calculation way. The characteristics of the designed turbine can be designed with a known approximation. The calculation of characteristics of the turbine is used to evaluate the parameters which can be obtained from the turbine designed. This is especially important in the calculation of the control system of the turbo-pump unit. These calculations, as a rule, have a tentative nature. With the storage of the experimental data according to the loss factors and with the perfection of the method of calculation, the reliability of characteristics by means of calculation, will increase.

For an example, let us examine the calculation of the characteristic of a single-stage turbine according to the frequency of rotation ω in the form of dependences of the moment and power on the frequency of rotation. This characteristic is of interest for an examination of the joint operation of the turbine and pumps; it is the external turbine characteristic, which shows which power can be developed by the turbine under given conditions depending on the frequency of rotation. Let us take the pressure ratio as being constant:

$$\delta = \frac{p_2^*}{p_1^*} = \text{const.}$$

We will examine the characteristic under the assigned initial conditions p_0^* and T_0^*. Let us first determine which form the characteristic will take under certain simplifying assumptions. Let us assume that $c_1 = c_{1p}$ (ϕ = const). Furthermore, let us assume that $w_2 = w_{2p}$ = const. This assumption means that conditions at the inlet into the vane channel with a change in the frequency of rotation do not affect the outlet velocity w_2. (The latter assumption is rough, and it will subsequently be shown that it can be rejected.)

Under these conditions the velocity triangle will be depicted in the manner that it is shown in Fig. 4.92. In this case the expression for the moment on the circumference of the wheel is recorded in scalar quantities in the following form:

$$M_u = Gr(c_{1u} + c_{2u}), \tag{4.186}$$

and in terms of the calculating values the moment is expressed thus:

$$M_u = Gr[c_{1u\,p} - c_{2u\,p} + (u_p - u)], \tag{4.187}$$

since

$$c_{2u} = c_{2u\,p} - (u_p - u).$$

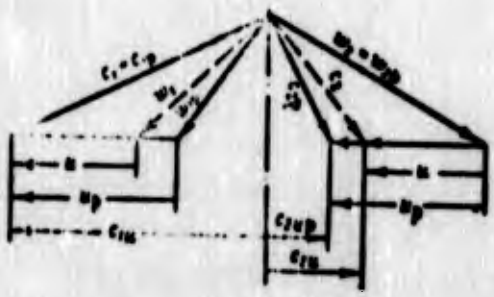

Fig. 4.92. Approximate velocity triangles with a variable frequency of rotation.

Since the values G, $c_{1u\,p}$, $c_{2u\,p}$, and u_p are constant, then the moment linearly depends on the frequency of rotation ω (Fig. 4.93). The maximum moment takes place when $\omega = 0$:

$$M_{u\,max} = (M_u)_{\omega=0}.$$

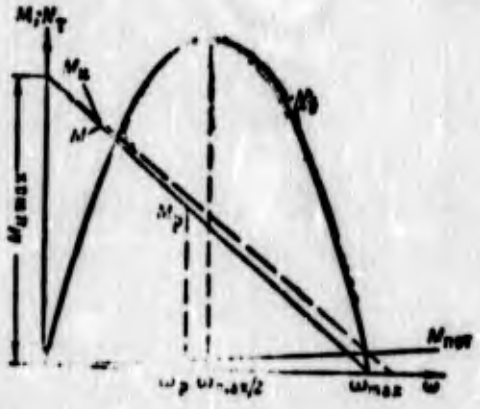

Fig. 4.93. A change in the power and torsional moment of the turbine depending on a change in the frequency of rotation.

The moment on the shaft M will be less than M_u by the value of the moment of the losses. Let us assume that $M_{пот}$ linearly increases with an increase in the frequency of rotation, which is usually confirmed by an experiment:

$$M_{пот} = a\omega,$$

where it is possible to assume that

$$a = (5 \div 6) \cdot 10^{-4}.$$

Having designated

$$Gr(c_{1u_p} + c_{2u_p} + u_p) = M_{нас} \qquad (4.188)$$

and having designated the moment at the calculated frequency of rotation (taking into account the moment of losses) M_p, we obtain the equation for the instantaneous value of the moment (see Fig. 4.93):

$$M = M_{нас} - (M_{нас} - M_p)\frac{\omega}{\omega_p}. \qquad (4.189)$$

Thus, the dependence of the torsional moment of the turbine on the frequency of rotation is depicted as a straight line. The experimental dependence of the torsional moment on the frequency of rotation also is usually close to a straight line.

From equation (4.189) it is possible to find the maximum frequency of the rotation ω_{max} which can be developed by the turbine rotor, having assumed in the equation M = 0:

$$\omega_{нас} = \frac{M_{нас}}{M_{нас} - M_p}\omega_p. \qquad (4.190)$$

It is important not to allow the acceleration of the rotor up to the maximum according to conditions of strength of the frequency of rotation in order to avoid its breakage; therefore it is attempted always to work with filled pumps or design a special counter acceleration device.

The less M_p, the less the value of the maximum frequency of rotation with the acceleration of the rotor. An increase in $M_{пот}$ leads to a reduction in M_p and to a reduction in ω_{max}.

The power of the turbine

$$N_т = M_т \omega = \omega \left[M_{max} - (M_{max} - M_p) \frac{\omega}{\omega_p} \right] \qquad (4.191)$$

in view of the linear dependence $M = f(\omega)$ will be depicted as a parabola with the maximum when $\omega = \omega_{max}/2$ (see Fig. 4.93).

Using the assigned initial and calculated parameters, the dependence of the power on the frequency of rotation will be expressed by the equation

$$N_т = A\omega - B\omega^2, \qquad (4.192)$$

where

$$A = M_{max}; \quad B = \frac{M_{max} - M_p}{\omega_p}.$$

Equation (4.192) is used in the calculation of the control and adjustment of the engine.

The maximum power is developed at a frequency of rotation somewhat greater than that calculated.

For a more precise calculation of the characteristic according to the frequency of rotation, one should consider the change in w_2 with a change in the frequency of rotation. A change in the frequency of rotation (see the velocity triangles given in Fig. 4.94) leads to a change in w_1 in value and direction. Let us find value w_2 from the relation

$$w_2 = \varphi w_{2a}. \qquad (4.193)$$

Fig. 4.94. Velocity triangles for the assigned impulse turbine at two values of u/c_1.

Value ψ will be variable and will depend on the incidence (see Section 4.3.2.1). According to value w_2 we construct the outlet velocity triangle, and, having determined value c_{2u}, we find L_u according to equation (2.29).

By conducting such calculations and plottings for several values of the frequency of rotation, we will obtain curves for L_u and η_u. After this it is possible to determine the efficiency of the turbine, having used equation (4.122). Losses connected with leakages, friction of the disk, shroud and admission are calculated from equations (4.111), (4.125), (4.126) and (4.127). The power of the turbine is found from the expression

$$N_т = G_т L_{ад.т} \eta_т.$$

We will now discuss the case of $\delta \neq \delta_p$. Let us assume, for example, that $\delta > \delta_p$. To facilitate the calculations, let us assume that a change in δ occurs in connection with a change in p_2. At the selected value of δ we determine the velocities $c_{ад}$ and c_1, assuming approximately that $\phi = \phi_p$. We find angle α_1 by taking into account the deviation in the flow in the oblique section (see Section 4.3.1).

Let us assign, as before, several values of u. For each of them we plot the velocity triangle at the inlet (Fig. 4.95), from which we determine c_{1u}. The outlet velocity w_2 is directed at angle β_{2p} which corresponds to the angle of the blades at the outlet. The velocity w_2 is determined with the aid of the relation (4.193). By knowing the velocity w_2, we plot the outlet velocity

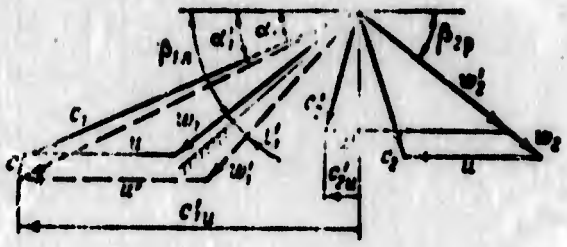

Fig. 4.95. Velocity triangles for the assigned impulse turbine at different circular velocities and pressure ratios.

triangle, from which we find c_{2u}. Then according to expression (4.107) we determine $\bar{L}_u$, according to equation (4.122) we determine η_T, whereupon we find $N_T = GL_{ад}\eta_T$.

The data obtained as a result of the calculation are represented in the criterial form:

$$\frac{n\sqrt{T_0^*}}{p_0^*} \quad \frac{N_T}{p_0^* \sqrt{T_0^*}} \quad \text{or} \quad \eta_T = f\left(\frac{u}{\sqrt{T_0^*}}, k\right)$$

(the energy turbine characteristic).

4.8. SELECTION OF PARAMETERS AND ORDER OF CALCULATION OF TURBINES OF LIQUID-PROPELLANT ROCKET ENGINES

4.8.1. SELECTION OF THE FORM OF THE TURBINE

4.8.1.1. Selection of the Form of the Autonomous Turbine

In LPRE with an autonomous turbine (see Fig. 1.14) gases from the turbine are either ejected into the atmosphere (for example, through the control nozzles) or are utilized for any auxiliary purposes (for example, for tank pressurization or as a heat source in heat-exchange or evaporative apparatuses).

In all these cases the gas flow rate through the turbine should be a minimum, since the gas of the turbine does not participate in the thrust creation by the main chamber. With the assigned magnitude of peripheral velocity, the condition

$$G_т = \frac{N_т}{L_т} = \frac{N_т}{\bar{L}_т u^2} \to \min$$

corresponds to the maximum work factor. Consequently, as an autonomous turbine there should be selected the turbine in which for 1 kg of mass of the working medium there is the maximum work, i.e., the turbine with the maximum operating factor $\bar{L}_т$ at the assigned peripheral velocity. Such turbines are impulse turbines.

In many instances autonomous turbines have a small flow rate of the working medium. With the low flow rate of the working medium the partial admission of the gas to the turbine wheel is achieved. The effectiveness of the reaction turbine with partial admission is substantially lowered. This is an additional circumstance which prevents the use of reaction turbines as autonomous turbines.

With calculation of the autonomous turbine of LPRE the value $u/c_{ад}$ is often assigned. The peripheral velocity u is selected from considerations of strength (it should not exceed 350-400 m/s), or it is conditioned by the frequency of rotation of the pump spindle and by permissible dimensions of the turbine; the adiabatic discharge velocity from the nozzles $c_{ад}$ is assigned by the available pressure ratio $\delta = p_0^*/p_2$. The initial pressure p_0^* is selected at as maximum as possible, i.e., it is determined by the pressure created by the pumps with deduction in the drop in pressures on gas-generator injectors and resistances of the main feed line of the gas generator.

The outlet pressure p_2 is determined by the scheme of the use of reaction gases of the turbine. The outlet pressure is greater than the calculated pressure of the environment (the pressure ratio should be more than the critical).

With the assigned magnitude $u/c_{ад}$ the operating factor $\bar{L}_т = L_т/u^2$ is uniquely connected with the efficiency of the turbine:

$$\bar{L}_т = \eta_т/2\left(\frac{\varepsilon}{\varepsilon_{кр}}\right)^{\frac{k-1}{k}}.$$

The less $u/c_{ад}$ (when $u/c_{ад} < 0.2$-0.25) (see Fig. 4.76), the more the basis for using a turbine with two velocity stages. (Let us recall that these turbines in the region of small values of $u/c_{ад}$ have the greatest values of the operating factor of all forms of multistage turbines, see Section 4.6.2.2.) The assigned magnitudes of $u/c_{ад}$ frequently lie within limits of 0.05-0.15. At such values of $u/c_{ад}$ the efficiency and the operating factor are noticeably more for a turbine with two velocity stages than for an impulse single-stage turbine. Consequently, it is advantageous to use turbines with two velocity stages with small values of u and large values of $c_{ад}$ (large δ).

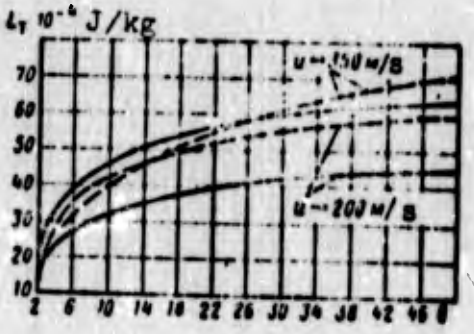

Fig. 4.96. Dependences of the effective work on the pressure ratio and peripheral velocity for the single-stage impulse turbine (solid lines) and for the two-stage impulse turbine with velocity stages (dashed lines).

Figure 4.96 gives the calculated dependences of the specific work $L_т$ on u and δ plotted on the basis of graphs given in Fig. 4.76. In the calculation the following were accepted: $RT_0^* = 40 \cdot 10^4$ J/kg; $k = 1.28$.

From an analysis of the graphs given in Fig. 4.96, it follows that for obtaining the maximum specific work (minimum gas flow rate) it is more preferable to use the impulse turbine with two velocity stages rather than the single-stage impulse

turbine, at peripheral velocities of $u \leq 200$ m/s for any pressure ratios in the turbine. When $u \geq 300$ m/s the advantage of the impulse turbine with two velocity stages is observed only with large pressure ratios ($\delta > 25$ when $u = 350$ m/s).

In practice turbines with two velocity stages are used only for engine installations with high thrusts. The turbine with two velocity stages is constructively more complex (it has a larger number of blades, possesses larger mass, and the cost of its production is higher than that of a single-stage impulse turbine). The final conclusion about the expediency of the use of a turbine in the form of one impulse stage or in the form of two velocity stages should be solved by taking into account the full economic analysis and mass analysis of the design.

For engines in which hydrogen is used as the fuel, the use of birotary turbines and, primarily, a birotary turbine with two velocity stages can be of interest (see Section 4.6.3.1). For high-powered engines with high flow rates of the working medium, it is possible to use a reaction-impulse birotary turbine (see Section 4.6.3.2).

4.8.1.2. Selection of the Form of Precombustion-Chamber Turbine

For designs of engine installations with gas feed into the combustion chamber, it is advantageous to use single-stage turbines, since the available pressure ratios in these designs are small. The determining requirement for this design is the effectiveness of the turbine, its efficiency, which, as the final result, determines the feed system characteristics throughout the mass of the construction (see Section 1.4.2).

In connection with the small pressure ratio, small values of $c_{ад}$, and, therefore, large ratios of $u/c_{ад} > 0.5$-0.6 correspond to precombustion-chamber turbines. Under these conditions the

greatest efficiency corresponds to reaction turbine (see Fig. 4.48).

However, the use of a reaction turbine leads to a number of design difficulties primarily because of the presence of a great axial force on the rotor wheel and increased gas overflow. Reaction turbines should be made with the full gas feed ($\varepsilon = 1$).

In practice precombustion-chamber turbines of the LPRE designed as turbines with a small degree of reaction or as impulse (according to the mean diameter $\rho_т = 0$-0.3). At high combustion-chamber pressures of the engine, and, therefore, in the gas generator feeding the turbine, and also with a low mass flow rate (engines with a reducing gas generator), the precombustion-chamber turbine can be partial ($n_{s\ т} < 50$-70); then it was made inpulse. As precombustion-chamber turbines radial-axial inward-flow turbines are also used.

4.8.2. SELECTION OF PARAMETERS AND THE ORDER OF CALCULATION OF AUTONOMOUS TURBINES

4.8.2.1. Autonomous Single-Stage Turbine

In Section 4.8.1.1 it was indicated that the autonomous turbine is made an impulse single-stage turbine when $u/c_{ад} > 0.2$-0.25. With smaller $u/c_{ад}$ the double-stage turbine with velocity stages has a larger operating factor and efficiency. However, from considerations of simplicity and a decrease in the mass of the construction and at smaller values of $u/c_{ад}$, the autonomous turbine can be made single-stage impulse.

A. INITIAL DATA AND THEIR SELECTION

The initial data for the calculating are:

1) N_T - the power of the turbine which is determined by the power required for the pump drive;

2) ω - frequency of rotation;

3) physical constants and temperature of the working medium of the turbine;

4) pressure ratio δ;

5) material of blades of the turbine and its strength data.

Frequency of Rotation and Peripheral Velocity

The frequency of rotation is determined by the value permissible for pumps at which the noncavitation work of the pump is ensured.

An increase in the frequency of rotation promotes an increase in the efficiency of the turbine because of an increase in the power-speed coefficient (see Fig. 4.58). Furthermore, with an increase in the frequency of rotation the dimensions of the turbine with the selected peripheral velocity are decreased. Therefore, an increase in acticavitation qualities of the pumps, which enables an increase in ω, favorably affects the autonomous turbine.

The independent selection of the frequency of rotation of the turbine, which provides for the pump drive through the reducers which reduce the frequency of rotation, did not justify itself. Such a design of the turbopump unit greatly loses with respect to the simplicity and mass of the construction.

It is advantageous to select peripheral velocity as maximum as possible. On the basis of considerations of strength u_{max} = = 350-400 m/s; let us note that the value u_{max}, as a rule, is

always less than the optimum value determined according to $c_{ад}$ and the optimum ratio $(u/c_{ад})_{opt}$ (see Fig. 4.58) at which $\eta_т$ and, therefore, $L_т = L^*_{ад}\eta_т$ reach a maximum.

In selecting $u = u_{max}$, it is possible to obtain at the assigned frequency of rotation the large mean diameter at which the diametrical dimensions of the turbopump unit will be inadmissibly great. Therefore, from considerations of permissible dimensions of the turbopump unit the mean diameter $D_{ср}$ should not exceed $(1.5\text{-}2)D_2$, where D_2 is the outside diameter of the wheel of the fuel pump. From the selected mean diameter and the frequency of rotation the peripheral velocity is determined.

Physical Constants and Temperature of the Working Medium of the Turbine

As a rule, the working medium of the turbine consists of combustion products of basic components (either with a fuel surplus or oxidizer surplus). Usually used as the working medium is gas with a fuel surplus - reducing gas (see Section 1.4.1).

Sometimes the working medium of the turbine can be the decomposition products of single-component, unitary fuels - hydrogen peroxide, hydrazine, etc.

Physical constants of working mediums of the turbine of the LPRE greatly depend on the relationship of components in the gas generator. The coefficient of the adiabatic curve is found within limits of $k = 1.2\text{-}1.4$. For fuels in which the combustible is a hydrocarbon compound and the oxidizer - on a nitric acid base, for the reducing gas RT^*_0 is approximately $(30\text{-}50)\cdot10^4$ J/kg. It is desirable to have the value of RT^*_0 high. The higher RT^*_0, the more the operating factor, and the less the flow rate of working medium.

In practice the value of the temperature in front of the turbine is limited by values of 1000-1200°K on the basis of the efficiency of the design. With a further increase in temperature an increase in specific work occurs. This circumstance and the possibility in the prospect for gas bleed from the combustion chamber for feeding the turbine make the problem of an increase in temperature in front of the turbine an actual one.

Pressure Ratio

The value δ - the pressure ratio - for the turbine is determined by the selection of the initial pressure p_0^* and pressure after the turbine p_2. The pressure ratio δ for autonomous turbines is usually 15-40.

An increase in the pressure ratio leads to an increase in the adiabatic work, but because of the drop in efficiency with an increase in the pressure ratio (decrease) in $u/c_{ад}$) the specific work $L_т$ with an increase in δ increases slowly (see Fig. 4.96).

The correlations established by the graphs given in Fig. 4.96 should be considered when selecting p_0^* and p_2, if there is the possibility of varying them.

The material of blades of the turbine and its strength data at temperature $T_{w_1}^*$ should be assigned for further calculation of the designed turbine for strength.

B. ORDER OF CALCULATION AND AN EXAMPLE OF THE CALCULATION

As a result of the calculation of the autonomous turbine of the LPRE such dimensions of elements of the turbine which are used when developing the design are determined. Apart from this, the flow parameters (temperature, pressure, velocity, normalized

speed, etc.) in the characteristic sections of the turbine are determined. Furthermore, the gas flow rate through the turbine necessary for providing the assigned power of the turbine should be determined.

Determination of the Required Gas Flow Rate Through the Turbine

In the first approximation, the gas flow rate is determined by means of the graphic dependences given in Fig. 4.58. For this according to the initial data one should determine the mean diameter of the wheel and the ratio of the velocities $u/c_{a\text{д}}$, knowing the peripheral velocity and adiabatic work (δ, T_0^*, k and R).

Then the value of the clearance between the wheel and the housing Δ = 1-3 mm is assigned. In the case of a wheel without a shroud - this is a radial clearance; for shrouded wheels Δ is understood as the minimum (axial or radial) clearance (see Section 4.5.1). According to the value of the clearance the relative value $\bar{\Delta} = \Delta/D_{\text{ср}}$.

Several values of the gas flow rate G are assigned in order to determine by equation (2.185) the values of $n_{s\ T}$, which should lie within limits of 10-40; the adiabatic volumetric flow rate of the gas at the inlet into the wheel $Q_{1a\text{д}}$, which enters into equation (2.185), is determined in the following manner:

$$Q_{1a1} = \frac{G}{\rho_{1a1}} = \frac{GRT_{1a1}}{p_1},$$

where

$$p_1 = p_0^*\left(1 - \frac{k-1}{k+1}\lambda^2_{c_{1a1}}\right)^{\frac{k}{k-1}}; \qquad (4.194)$$

$$T_{1a1} = T_0^*\left(1 - \frac{k-1}{k+1}\lambda^2_{c_{1a1}}\right). \qquad (4.194')$$

since

$$\rho_{1a1} = \frac{p_1}{RT_{1a1}}. \qquad (4.195)$$

Used as an autonomous turbine are impulse turbines ($\rho_т = 0$) (for the impulse turbine $c_{1ад} = c_{ад}$; $p_1 = p_2$). According to values $u/c_{ад}$, $\bar{\Delta}$ and $n_{s\ т}$, with the aid of Fig. 4.58 for each of the selected values of G, the efficiency of the turbine $\eta_т$ is determined. The flow rate G, at which the power of the turbine $N_т = GL^*_{ад}\eta_т$ will coincide with the assigned, is the required gas flow rate through the turbine. This value is used in further calculations. At the end of the calculation it can appear that the obtained power value is distinguished from the assigned by more than 5%. In this case one should repeat the calculation, having changed the initial value of the flow rate.

Calculation of Flow Parameters in the Axial Clearance Between the Nozzle Cascade and Cascade of the Wheel

The calculation of parameters in the axial clearance (outlet from nozzle cascade - inlet into the wheel) is necessary for determining dimensions of the nozzle cascade and cascade of the wheel.

The flow angle in the axial clearance is selected within limits of $\alpha_1 = 15°$-$20°$. The velocity factor of the nozzle cascade can be taken at $\phi = 0.92$-0.96.

The basic equation for calculating the flow parameters were given in Section 4.2.1.

Let us recall that the M number can be expressed by the normalized velocity λ:

$$M = \frac{c}{a}, \tag{4.196}$$

where a is the speed of sound,

$$a = \sqrt{kRT}; \tag{4.197}$$

$$M = \sqrt{\frac{\frac{2}{k+1}\lambda^2}{1-\frac{k-1}{k+1}\lambda^2}}. \tag{4.198}$$

The normalized flow rate $q(\lambda)$ can be determined with the aid of gas-dynamic tables or by equation

$$q(\lambda)=\lambda\left[\frac{k+1}{2}\left(1-\frac{k-1}{k+1}\lambda^2\right)\right]^{\frac{1}{k-1}}. \qquad (4.199)$$

Determination of Dimensions of the Nozzle Cascade

In the case of the turbine with the full gas feed ($\varepsilon = 1$), the span of nozzle cascade is determined according to equation (4.63).

It is advantageous to begin the determination of dimensions of the nozzle cascade of partial-admissions turbines with the presence of the span of the blade of the wheel according to equation (4.132). For this it follows to assign the width of the cascade of the wheel b and relative pitch $\bar{t}$ (in the first approximation). Subsequently, it is necessary to be convinced of the fact that ratio h_n/b was more than unity.

From the found span of the impeller vanes, taking into account the overlap, the span of the nozzle cascade h_c is determined from equation (4.71). A further course of the computation is clear from Section 4.3.3.2. Let us note that in the case of conical nozzles the width of the nozzle cascade is determined by the construction of the conical nozzle.

Determination of Dimensions of the Wheel Cascade

The airfoil cascade of the wheel is selected from the atlas of profiles (see source [4]). For the selection of the profile it is necessary to know the flow angles at the inlet into the cascade and at the outlet from it (β_1 and β_2), and the number $M_{w_{2д}} = M_{w_1}$. Profiles of cascades of the wheel of impulse

turbines are designated in the atlas by the letter P. The flow angle at the inlet β_1 is determined from the velocity triangle (see Section 4.2.1.1).

The flow angle at the oulet β_2 can be determined from equation (4.72), having selected the span of the blade at the outlet

$$h_{2a} = h_{1a} + (0 \div 5)\ \text{мм}. \qquad (4.200)$$

or, being assigned the angle β_2, it is possible to determine h_{2a} by equation (4.72).

For determining β_2 from equation (4.72), one should assign the velocity factor ψ, which makes it possible to find the value $q(\lambda_{w_2})$ [see equation (4.73)]; subsequently, value ψ is refined. The selected profile is changed geometrically in a similar way in connection with the calculated turbine. If the radii of the rounding of edges of the blades are too small (technologically unfavorable), then it follows to increase the radius by means of increasing the profile on the side of the face.

Having selected the cascade profile according to its characteristic curves (see the atlas of profiles [4]), we find the geometric parameters of the cascade. Having selected the value of the relative pitch $\bar{t}$ in the range of optimum values, we determine, according to the dependences given in the atlas, the angle of setting of the profile χ at which the necessary angle of departure β_2 is ensured. It is possible in this case to assume that

$$\beta_2 = \beta_{2\text{л}} - \arcsin\frac{o_2}{t}.$$

The value found of the setting angle makes it possible to determine the airfoil chord

$$b_1 = \frac{h}{\sin\chi}. \qquad (4.201)$$

the cascade pitch

$$t = \bar{t} b_2 \tag{4.202}$$

and the number of blades

$$z = \frac{\pi D_{cp}}{t}. \tag{4.203}$$

After this it is possible to determine the loss factor in the cascade ζ, using the characteristic curves of the selected profile. In this case one should consider the difference in the selected geometric parameters of the cascades from those with which the indicated characteristics are obtained. For this we utilize the generalized dependences given in atlas [4].

Flow Conditions from the Wheel

The absolute outlet velocity and flow angle α_2 are determined from the velocity triangle (Fig. 4.97d):

$$c_2 = \sqrt{(w_2 \sin\beta_2)^2 + (w_2 \cos\beta_2 - u)^2}; \tag{4.204}$$

$$\alpha_2 = \operatorname{arctg} \frac{w_2 \sin\beta_2}{w_2 \cos\beta_2 - u}. \tag{4.205}$$

The stagnation temperature is found from the equation

$$T_2^* = T_2 + \frac{k-1}{2kR} c_2^2 \tag{4.206}$$

The total pressure at the outlet can be found from the general expression

$$\frac{p}{p^*} = \left(1 - \frac{k-1}{k+1} \lambda^2\right)^{\frac{k}{k-1}}, \tag{4.207}$$

where

$$\lambda = \frac{c}{a_{kp}}; \quad a_{kp} = \sqrt{\frac{2k}{k+1} RT^*}; \tag{4.207a}$$

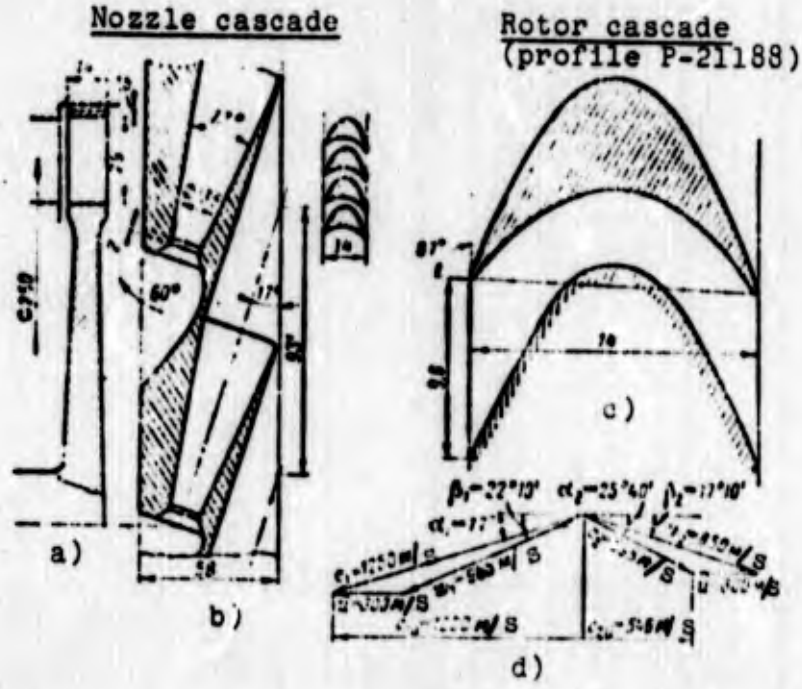

Fig. 4.97. Diagram of blading and velocity triangles for the calculated autonomous turbine of the LPRE: a - meridian section; b - developemnt of the nozzle cascade and cascade of the rotor wheel on the mean diameter; c - shape and vane channel of the rotor cascade; d - velocity triangles.

Determination of Work, Power and Efficiency

The power, work and efficiency of the turbine is calculated with the aid of the dependences given in Sections 4.4.2 and 4.5.

If the power value obtained as a result of the calculation will differ from that assigned by more than 5%, the calculation should be repeated, having changed the rate of discharge of gas through the turbine.

In more detail the order of the calculation can be observed according to the example of the calculation given in Table 4.3. The blading and velocity triangles for the calculated turbine are given in Fig. 4.97.

Table 4.2. Example of the calculation of an autonomous single-stage turbine of the LPRE.

No.	Name of value	Designation	Number of equation	Dimensionality	Value	Remark
1	2	3	4	5	6	7
	A. Initial data					
1	Power of the turbine	$N_т$	-	kW	1200	Assigned from calculations of pumps
2	Frequency of rotation	ω	-	s^{-1}	2410	The same
3	Total pressure at inlet	p_0^*	-	N/m^2	$60 \cdot 10^5$	Assigned from calculation of TU (see Chapter 5)
4	Outlet pressure	p_2	-	N/m^2	$2.5 \cdot 10^5$	Assigned
5	Stagnation temperature of gas at inlet	T_0^*	-	°K	1000	The same
6	Gas constant	R	-	J/(kg·°K)	400	" "
7	Adiabatic index	k	-	-	1.33	" "
	B. Calculated and selective values					
	a) Determination of required gas flow rate					
8	Circular velocity on mean diamter	u	-	m/s	300	Assigned
9	Mean diameter	$D_{ср}$	-	m	0.25	-
10	Pressure ratio	$\delta = p_0^*/p_2$	-	-	24	-
11	Adiabatic work	$L_{ад}^*$	(4.3)	J/kg	$89 \cdot 10^4$	-
12	Adiabatic velocity	$c_{ад}$	(4.102a)	m/s	1330	See Section 4.4.2
13	Ratio of velocity	$u/c_{ад}$	-	-	0.225	-

Table 4.3 (continued).

14	Minimum (axial or radial) clearance between the wheel and housing (turbine with shroud)	Δ	-	m	$1.5 \cdot 10^{-3}$	Assigned
15	Relative minimum clearance	Δ/D_{cp}	-	-	0.006	-
16	Required gas flow rate	G	-	kg/s	2.67	Determined by means of graphs given in Fig. 4.58
17	Power-speed coefficient of turbine	$n_{s\ T}$	(2.185)	-	22.4	-
18	Specific work of turbine	L_T	(4.1)	J/kg	$45 \cdot 10^4$	See also Section 4.8.1.1
19	Operating factor	$\bar{L}_T$	(4.2a)	-	4.97	See also Section 4.8.1.1

b) *Flow parameters in the axial clearance from the nozzle cascade and the wheel (outlet from the nozzle cascade to the inlet into the wheel).*

20	Flow angle	α_1	-	angular degrees	17	Assigned
21	Velocity factor	ϕ	-	-	0.94	The same
22	Outlet velocity from nozzle cascade	c_1	(4.33)	m/s	1250	-
23	Critical speed of sound for flow in nozzle cascade	$a_{1кр}$	(4.207a)	m/s	676	-
24	Normalized velocity	λ_{c_1}	(4.17)	-	1.84	-

Table 4.3 (continued).

25	Coefficient of total pressure	σ_1	(2.192)	-	0.584	-
26	Total pressure in axial clearance	p^*_{1c}	-	N/m^2	$35.7 \cdot 10^5$	See Section 4.3.1.1
27	Static temperature in clearance	T_1	(4.194)	°K	515	-
28	Gas density in clearance	ρ_1	(4.195)	kg/m^3	1.21	-
29	Speed of sound in clearance	a_1	(4.197)	m/s	520	-
30	M number	M_1	(4.196)	-	2.4	-
31	Relative velocity at inlet into wheel	w_1	-	m/s	965	See Section 4.2.1.1
32	Stagnation temperature in relative motion	$T^*_{w_1}$	(4.7)	°K	805	-
33	Critical velocity	$a_{кр\ w}$	(4.21)	m/s	605	-
34	Normalized velocity	λ_{w_1}	-	-	1.6	-
35	M number in relative motion	M_{w_1}	(4.198)	-	1.83	-
36	Total pressure in relative motion	$p^*_{w_1}$	(4.8)	N/m^2	$17.6 \cdot 10^5$	-

c) *Determination of optimum span of impeller vanes*

37	Width of cascade	b	-	m	0.014	Assigned
38	Relative width	b/D_{cp}	-	-	0.056	-
39	Relative cascade pitch (in the first approximation)	$\bar{t}$	-	-	0.6	Assigned

Table 4.3 (continued).

40	Reynolds number of wheel disk	$Re_д$	-	-	$5 \cdot 10^5$	Assigned
41	Reynolds number of shroud	$Re_б$	-	-	$5 \cdot 10^3$	The same
42	Relative span of blade	$\bar{h}_{1л}$	(4.132)	-	0.115	-
43	Span of blade	$h_{1л}$	-	m	0.0295	-
	d) *Determination of dimensions of the nozzle cascade which consists of conical nozzles*					
44	Overlap on periphery	$\Delta h_п$	-	m	0.001	Assigned
45	Overlap in hub	$\Delta h_{вт}$	-	m	0.0005	The same
46	Span of nozzle cascade	h_c	(4.71)	m	0.028	-
47	Total minimum cross section of nozzles	F_{min}	(4.40)	m^2	$4.24 \cdot 10^4$	We assume $\sigma_{кр} = 1$
48	Velocity factor of conical part of nozzle	ϕ'	-	-	0.98	Assigned
49	Nozzle expansion ratio	$\bar{f}_1'$	(4.53)	-	4	-
50	Area of nozzles at end of conical part	F_1'	(4.67)	m^2	$17 \cdot 10^{-4}$	-
51	Area of nozzle exit	F_c	-	m^2	$88.1 \cdot 10^{-4}$	See Section 4.3.3.2
52	Degree of admission	ϵ	(4.70)	-	0.264	-
53	Quantity of nozzles	z_c	(4.69)	-	3	-
54	Major axis of ellipse of cross section of nozzles at outlet	a_c	-	m	0.095	See Section 4.3.3.2

Table 4.3 (continued).

55	Pitch of nozzles	t_c	-	m	0.093	We assume $\frac{a_c - t_c}{t_c} = 0.02$
56	Minimum diameter of nozzle	d_{min}	-	m	0.0136	See Section 4.3.3.2

e) *Determination of parameters of wheel cascade*

57	Flow angle at inlet into wheel	β_1	-	Angular degrees	22°10'	See Section 4.3.2.1
58	Speed factor (in the first approximation)	ψ	-	-	0.88	Assigned
59	Flow velocity at outlet in relative motion	w_2	(4.27)	m/s	850	-
60	Normalized velocity	λ_{w_2}	-	-	1.41	-
61	Coefficient of total pressure	σ_2	(2.193)	-	0.635	-
62	Normalized flow rate	$q(\lambda_{w_2})$	(4.199)	-	0.83	-
63	Span of blade at outlet	h_{2n}	(4.200)	m	0.0295	Assigned $h_{2n} = h_{1n}$
64	Flow angle at outlet in relative motion	β_2	(4.72)	Angular degrees	17°10'	-
65	Cascade of profile P-2118B	-	-	-	-	Selected from atlas [4]
66	Relative cascade pitch	$\bar{t}$	-	-	0.684	Selected from the range of optimum values

Table 4.3 (continued).

67	Setting angle	χ	-	Angular degrees	87	Determined according to airfoil characteristics
68	Blade chord	$b_л$	(4.201)	m	0.014	-
69	Cascade pitch	t	(4.202)	m	0.0096	-
70	Quantity of blades	z	(4.203)	-	82	-
71	Relative length of blade	$h_л/b_л$	-	-	2.07	-
72	Loss factor in cascade	$\zeta_к$	-	-	0.22	Determined from profile characteristics
73	Velocity factor	ψ	(2.195)	-	0.88	-

f) *Flow parameters at outlet from wheel*

74	Static temperature	T_2	(4.194)'	°K	580	-
75	Absolute velocity	c_2	(4.204)	m/s	598	-
76	Flow angle at outlet in absolute motion	α_2	(4.205)	Angular degrees	25°40'	-
77	Stagnation temperature	T_2^*	(4.206)	°K	680	-
78	Critical speed of sound	$a_{2кр}$	(4.207a)	m/s	555	-
79	Normalized speed	λ_{c_2}	(4.207a)	-	1.07	-
80	Stagnation pressure	p_2^*	(4.207)	N/m^2	$5 \cdot 10^5$	-

Table 4.3 (continued).

g) *Determination of work, power and efficiency of the turbine*

81	Ratio of velocities	u/c_1	-	-	0.24	-
82	Circular efficiency	η_u	(4.97)	-	0.579	-
83	Circular work	L_u	(4.84)	J/kg	$51.5 \cdot 10^4$	-
84	Flow rate of leakages	G_y	(4.111)	kg/s	0.07	-
85	Gas flow rate through cascade of wheel	G'	(2.249)	kg/s	2.6	-
86	Flow efficiency	η_p	(2.255)'	-	0.975	-
87	Circular power	N_u	(2.234)	kW	1340	-
88	Power of disk friction	$N_{тр.д}$	(2.202)	kW	1.5	See Section 4.5.2.1 Assigned $Re_д = 5 \cdot 10^5$; $Re_б = 5 \cdot 10^3$
89	Friction power of shroud	$N_{тр.б}$	(4.116)	kW	0.13	
90	Power of losses connected with partial admission	N_ε	(4.118)	kW	71	-
91	Effective power of turbine	$N_т$	(4.120)	kW	1259.4	-
92	Effective work	$L_т$	(4.1)	J/kg	$47.1 \cdot 10^4$	-
93	Operating factor	$\bar{L}_т$	(4.2a)	-	5.22	-
94	Effective efficiency of turbine	$\eta_т$	(2.259)	-	0.53	-

Let us note that the order of calculation of the energy characteristics of the turbine is presented in sufficient detail in Section 4.7.2.3.

4.8.2.2. Features of the Calculation of a Two-Stage Autonomous Turbine with Velocity Stages

With small ratios $u/c_{ад}$ ($u/c_{ад} < 0.2$-0.25), for increasing the efficiency, it is advantageous to use a two-stage impulse turbine with velocity stages. These turbines, just as the single-stage turbines, are high-pressure and supersonic.

The required gas flow rate through the turbine is determined similar to the way in which the flow rate for a single-stage impulse turbine is determined (see Section 4.8.2.1) with the use of the dependences given in Fig. 4.75.

The profiles of the blades of the rotor cascades and the guide vane is selected from the atlas of profiles [4]. In the calculation it is possible to assume the spans of rotor blades of the first and second stages and stator blades to be identical or smoothly increasing.

Losses of power and efficiency of the double-stage turbine is calculated in accordance with the data given in Section 4.6.2.2. Let us note that rotor blades of the first and second stages can be located on one disk (see Fig. 4.67). In this case entering into disk losses of the turbine will be friction of the disk and cylindrical surface on the periphery of the disk. It is possible approximately to take the sum of these losses equal to double the friction losses of the disk.

In connection with the spreading of the gas on the arc, the degree of admission ε of the guide vane should be selected higher than that for the nozzle cascade of the first stage. Therefore,

the arc occupied by the guide vane should be more than the arc occupied by the nozzles. It is possible to assume that

$$t_{н.а} z_{н.а} \approx t_c z_c + (0{,}05 : 0{,}1)\pi D_{ср}$$

Let us note that at subsonic speeds and with a full gas feed, for a decrease in the losses (by means of a decrease in the flow velocity, the small degree of reaction for the first and second stages ($\rho_т$ = 0.02-0.08) is introduced. Such turbines are conditionally called active turbines with velocity stages, although according to the operating principle they are reaction multistage turbines with a low degree of reaction. Such turbines are used mainly in industrial power engineering. The introduction of reaction in partial-admission turbines of LPRE is inexpedient, since this leads to an increase in gas overflow along the inactive circular arc.

4.8.3. SELECTION OF PARAMETERS AND ORDER OF CALCULATION OF PRECOMBUSTION-CHAMBER TURBINES

4.8.3.1. Precombustion-Chamber Axial-Flow Turbine

In Section 4.8.1.2 it was indicated that the precombustion-chamber turbines correspond to small values of $L^*_{ад}$, and therefore the precombustion-chamber turbines, as a rule, can be made single-stage. For precombustion-chamber turbines $u/c_{ад} > 0.5$-0.6; in connection with this (see Fig. 4.48) for the obtaining of the maximum efficiency precombustion-chamber turbines can be made reaction. However, reaction turbines correspond to considerable axial forces, which impede the design of the turbopump unit. Therefore, during the calculation one should assume that $\rho_т = 0$ or introduce the low reaction ($\rho_т \leq 0.3$).

A. INITIAL DATA AND THEIR SELECTION

Such initial data as the power of the turbine, the frequency of rotation and the physical constants of the working medium are assigned and selected just as for the autonomous turbine (see Section 4.8.2.1).

For the precombustion-chamber turbine the gas flow rate is also assigned. The flow rate is determined by the design of the feed system (see Section 1.4.2) and the assigned temperature of the gas in front of the turbine. In feed system with the oxidizing gas generator, through the turbine passes the entire oxidizer flow and low fuel flow necessary for providing the assigned temperature of the gas. For the oxidizing gas R = 200-300 J/kg. The temperature of the oxidizing gas is selected within limits of $T_0^* = 600\text{-}800°K$.

With the reducing gas generator, passing through the turbine is the entire fuel flow and a small part of the oxidizer flow (in greater detail see further Section 5.1.2).

The outlet pressure of the turbine is determined by the combustion-chamber pressure of the LPRE. The inlet pressure is determined from the condition of the provision of the balance of powers of the pumps and turbine (see Section 5.1.2). The pressures at the inlet and at outlet determine the pressure ratio δ and adiabatic work of the turbine.

B. ORDER OF CALCULATION AND AN EXAMPLE OF THE CALCULATION

As a result of the calculation of the precombustion-chamber turbine there should be determined the geometric dimensions of elements of the turbines in which the assigned power with the assigned flow rate will be provided. These dimensions are

necessary for the design development of the turbine. Besides the dimensions, the flow parameters in the characteristic cross sections of the turbine are determined.

Determination of the Circular Velocity and Mean Diameter

It is advantageous to begin the calculation of turbine with the determination of the value of the circular velocity and mean diameter. For this it is necessary to assign the degree of the reaction of the turbine. If $n_{s\ т} > 50\text{-}60$, then the precombustion-chamber turbine can be made with a full gas feed ($\varepsilon = 1$) (see Section 4.5.4.2), and then the degree of reaction $\rho_т > 0$ can be assigned.

If it was found that $n_{s\ т} < 50\text{-}60$ (small-flow precombustion-chamber turbines; turbines on reducing gas), then for an increase in efficiency it is expedient to introduce partial admission ($\varepsilon < 1$). Then the calculation of the precombustion-chamber turbine is conducted similar to the calculation of the autonomous turbine (see Section 4.8.2.1).

For precombustion-chamber turbines with full feed ($\varepsilon = 1$) the circular efficiency is sufficiently similar in value to the effective efficiency. Therefore, the optimum ratio $u/c_{ад}$ at the selected value $\rho_т$ can be determined with the aid of Fig. 4.48. From the value $u/c_{ад}$ and $c_{ад}$ let us find the circular velocity u, and then $D_{ср}$, since the frequency of rotation is assigned.

Determining Dimensions of the Nozzle Cascade

It is advantageous to begin the calculation of dimensions of the nozzle cascade from the determination of height h_c. For this one should assign the angle of flow at the outlet $\alpha_1 = 20\text{-}25°$ and select in the first approximation the value of the velocity factor

ϕ. For the precombustion-chamber turbines ϕ = 0.96-0.98. The height of the nozzle cascade is determined from equation (4.65).

The width of the cascade is selected from design considerations. It is possible to assume that b_c = 10-30 mm.

The profile of the nozzle blades is selected from the atlas of profiles [4] according to values α_0, α_1 and $M_{c_{1ад}}$. (The flow angle at the inlet α_0 can be taken equal to 90°.) The profiles of the nozzle cascades are designated in the atlas [4] by the letter C. According to characteristics of the selected profile the relative pitch $\bar{t}$ is determined; it should be found in the range of the optimum values. According to the value of the relative pitch $\bar{t}$, we find the setting angle of the profile χ at which the necessary effective angle of the cascade $\alpha_{1эф}$ is provided. The effective angle $\alpha_{1эф}$ = arc sin (a/t) is connected with the angle of flow α_1 by the following relation, which results from equation (4.38):

$$\sin\alpha_{1\phi} = \frac{\sin\alpha_1}{\bar{t}}. \qquad (4.208)$$

The number of blades and loss factor in the cascade are determined just as in Section 4.8.2.1.

After this it is possible to approach the calculation of the flow parameters in the axial clearance between the nozzle cascade and the wheel.

Determining the Dimensions of the Cascade of Rotor Wheel

The span of the blade at the inlet is determined by taking into account the overlap (see Section 4.3.3.3).

The flow angles at the inlet and outlet are determined just as they are in the calculation of the autonomous turbine (see Section 4.8.2.1).

According to the values β_1, β_2 and $M_{w_{2ад}}$, in the atlas of profiles [4] working profile is selected.

According to characteristics of the selected profile, the parameters of the rotor cascade and loss are determined. For determining the effective angle of the rotor cascade the equation similar to equation (4.208) is used:

$$\sin\beta_{2эф} = \frac{\sin\beta_2}{m}. \qquad (4.208а)$$

The width of the rotor cascade can be selected in the range $b_н$ = 15-40 mm.

After this it is possible to calculate the parameters of flow at the outlet from the wheel, losses, power and efficiency of the turbine.

$$\text{When } i = 1 \quad N_1 = N_0 - N_{тр.1} \ldots N_{тр.ф} \qquad (4.209)$$

If the power obtained as a result of the calculations will differ from assigned by more than 5%, then one should repeat the calculation, having changed the pressure at the inlet into the turbine or gas temperature (with a change in temperature the gas flow rate will be changed). In the case of a considerable change in temperature and pressure, the balance of powers of the turbopump unit should be refined.

The order of the calculation can be observed in more detail according to the example of the calculation given in Table 4.4.

Table 4.4. Example of the calculation of an axial precombustion-chamber turbine of the LPRE.

No.	Name of value	Designation	Number of equation	Dimensionality	Value	Remarks
1	2	3	4	5	6	7
	A. Initial data					
1	Power of turbine	$N_т$	-	kW	4150	Assigned from calculations of pumps
2	Frequency of rotation	ω	-	s^{-1}	2410	The same
3	Gas flow rate	G	-	kg/s	85	Assigned from calculation of turbopump unit (See Chap. 5)
4	Total pressure at inlet	p_0^*	-	N/m^2	$140 \cdot 10^5$	The same
5	Outlet pressure	p_2	-	N/m^2	$100 \cdot 10^5$	" "
6	Stagnation temperature of gas at inlet	T_0^*	-	°K	700	Assigned
7	Gas constant	R	-	J/(kg·°K)	280	The same
8	Adiabatic index	k	-	-	1.33	" "
	B. Calculated and selective values					
	a) Determination of circular velocity and mean diameter of the turbine					
9	Pressure ratio	δ	-	-	1.4	-
10	Adiabatic work of turbine	$L_{ад}^*$	(4.3)	J/kg	$6.5 \cdot 10^4$	-

Table 4.4 (continued).

11	Power-speed coefficient	$n_{s\ т}$	(2.185)	-	137	-
12	Degree of admission	ε	-	-	1	We assume that $\varepsilon = 1$, since $n_{s\ т} >$ > 50-70 (see Section 4.5.4.2)
13	Degree of reaction	ρ_1	-	-	0.2	Assigned
14	Ratio of velocities	$u/c_{ад}$	-	-	0.52	Assigned with the aid of Fig. 4.48 (see Section 4.4.2)
15	Adiabatic velocity	$c_{ад}$	(1.102a)	m/s	360	
16	Circular velocity	u	-	m/s	188	See items 14 and 15
17	Mean diameter	$D_{ср}$	-	m	0.156	-

b) *Determination of height of nozzle cascade*

18	Adiabatic work of nozzle cascade	$L^*_{ад_1}$	(4.88)	J/kg	$5.2 \cdot 10^4$	-
19	Adiabatic discharge velocity from nozzle cascade	$c_{1ад}$	(4.103)	m/s	322.5	-
20	Velocity factor (in the first approximation)	ϕ	-	-	0.975	Assigned
21	Outlet velocity from nozzle cascade	c_1	(4.33)	m/s	314	In first approximation

Table 4.4 (continued).

22	Critical speed of sound	$a_{1кр}$	(4.207a)	m/s	472	The same
23	Normalized speed	λ_{c_1}	-	-	0.665	" "
24	Normalized flow rate	$q(\lambda_{c_1})$	-	-	0.865	" "
25	Coefficient of total pressure	σ_1	(2.192)	-	0.98	" "
26	Flow angle	α_1	-	angular degrees	24	Assigned
27	Height of nozzle cascade	h_c	(4.63)	m	0.024	In the first approximation
	c) *Determination of parameters of nozzle cascade*					
28	Flow angle at the inlet	α_0	-	angular degrees	90	Assigned
29	M number, calculated from the adiabatic velocity	$M_{c_{1ад}}$	(4.198)	-	0.652	-
30	Effective angle of the cascade	$\alpha_{1эф}$	(4.208)	angular degrees	22°10'	-
31	Name of profile C-9022A	-	-	-	-	Selected from atlas [4]
32	Relative pitch	$\bar{t}_c$	-	-	0.79	Assigned in the range of optimum values
33	Angle setting of the profile	χ	-	angular degrees	40°20'	Determined according to characteristics of the cascade

Table 4.4 (continued).

34	Width of the cascade	t_c	-	m	0.013	Assigned
35	Airfoil chord	$b_{л.c}$	(4.201)	m	0.0183	-
36	Cascade pitch	t_c	(4.202	m	0.0145	See items 32 and 35 of the table
37	Quantity of nozzle blades	z_c	(4.203)	-	34	-
38	Relative span of the blade	$h_c/b_{л.c}$	-	-	1.31	See items 27 and 34 of the table
39	Loss factor in the cascade	ζ_c	-	-	0.05	Determined from cascade characteristics
40	Velocity factor of the cascade	ϕ	(2.194)	-	0.975	-

d) *Flow parameters in the axial clearance*

41	Total pressure	$p^*_{1_c}$	-	N/m^2	$137 \cdot 10^5$	See Section 4.3.1.1
42	Static pressure	p_1	(4.194)	N/m^2	$108 \cdot 10^5$	-
43	Static temperature	T_1	(4.194)'	°K	657	-
44	Gas density	ρ_1	(4.195)	kg/m^3	58.7	-
45	Speed of sound	a_1	(4.197)	m/s	498	-
46	M number	M_1	(4.196)	-	0.63	-
47	Relative velocity at the inlet into the rotor cascade	w_1	-	m/s	158	See Section 4.2.1.1

Table 4.4 (continued).

48	Stagnation temperature in relative motion	$T^*_{w_1}$	(4.7)	°K	668	-
49	Critical speed of sound in relative motion	$a_{кр\ w}$	(4.21)	m/s	461	-
50	Normalized speed	λ_{w_1}	-	-	0.343	-
51	Normalized flow rate	$q(\lambda_{w_1})$	(4.199)	-	0.512	-
52	M number in relative motion	M_{w_1}	(4.198)	-	0.32	-
53	Total pressure in relative motion	$P^*_{w_1}$	(4.8)	N/m^2	$114 \cdot 10^5$	-

e) *Determination of parameters of the rotor cascade*

54	Span of blade at the inlet	$h_{1л}$	(4.71)	m	0.027	Assinged $\Delta h_п = 2 \cdot 10^{-3}$ m; $\Delta h_{вт} = 1 \times 10^{-3}$ m
55	Flow angle at inlet	β_1	-	angular degrees	52	See Section 4.3.2.1
56	Adiabatic outlet velocity from the wheel	$w_{2ад}$	(4.19)	m/s	226	-
57	Normalized adiabatic velocity	$\lambda_{w_{2ад}}$	(4.21)	-	0.493	-
58	M number calculated from adiabatic velocity	$M_{w_{2ад}}$	(4.198)	-	0.465	-
59	Velocity factor (in the first approximation)	ψ	-	-	0.95	Assigned

Table 4.4 (continued).

60	Relative outlet velocity from the wheel	w_2	(4.20)	m/s	215	-
61	Normalized velocity	λ_{w_2}	-	-	0.469	-
62	Normalized flow rate	$q(\lambda_{w_2})$	(4.199)	-	0.70	-
63	Coefficient of the total pressure	σ_2	(2.193)	-	0.99	-
64	Flow angle at outlet in relative motion	β_2	(4.72)	angular degrees	29	Assigned is $h_{2л} = h_{1л}$ and G_y is estimated according to equation (4.111)
65	Effective angle of the cascade	$\beta_{2эф}$	(4.208a)	angular degrees	24°30'	Assigned m = 1.08
66	Name of profile C-6030A	-	-	-	-	-
67	Relative pitch	$\bar{t}_k$	-	-	0.657	Assigned in the range of optimum values
68	Setting angle of profile	χ	-	angular degrees	66°40'	Determined from characteristics of the cascade
69	Width of the cascade	$b_к$	-	m	0.015	-
70	Blade chord	$b_{л.к}$	(4.201)	m	0.0165	-
71	Cascade pitch	$t_к$	(4.202)	m	0.0107	See items 67 and 70 of table
72	Quantity of impeller vanes	$z_к$	(4.203)	-	46	-

Table 4.4 (continued).

73	Relative span of blade	$h_л/b_{л.к}$	-	-	1.62	See items 54 and 70 of the table
74	Loss factor in the cascade	$\zeta_к$	-	-	0.095	Determined according to characteristics of the cascade
75	Velocity factor	ψ	(2.195)	-	0.95	-

f) *Parameters of flow at the outlet from the wheel*

76	Total pressure in relative motion	$p^*_{w_2}$	(4.207)	n/m^2	$113 \cdot 10^5$	-
77	Absolute outlet velocity from the wheel	c_2	(4.204)	m/s	106	-
78	Flow angle at outlet in absolute motion	α_2	(4.205)	angular degrees	86°50'	-
79	Static temperature	T_2	(4.194)'	°K	647	-
80	Stagnation temperature	T^*_2	(4.206)	°K	652	-
81	Critical speed of sound	$a_{кр_2}$	(4.207a)	m/s	455	-
82	Normalized velocity	λ_{c_2}	(4.207a)	-	0.233	-
83	Stagnation pressure	p^*_2	(4.207)	n/m^2	$102 \cdot 10^5$	-
84	Gas density	ρ_2	(4.195)	kg/m^3	55.2	-

Table 4.4 (continued).

g) *Determination of work, power and efficiency of the turbine*

85	Ratio of velocities	u/c_1	-	-	0.6	See items 16 and 21 of table
86	Circular efficiency	η_u	(4.95)	-	0.838	-
87	Circular work	L_u	(2.232)	J/kg	$5.44 \cdot 10^4$	-
88	Flow rate of leakages	G_y	(4.111)	kg/s	3.15	-
89	Flow rate through the cascade of the wheel	G'	(2.249)	kg/s	81.85	-
90	Flow efficiency	η_p	(2.255)'	-	0.963	-
91	Circular power	N_u	(2.234)	kW	4450	-
92	Friction power of disk	$N_{тр.д}$	(2.202)	kW	5.40	See Section 4.5.2.1. Assigned $Re_д = 5 \cdot 10^5$; $Re_б = 5 \cdot 10^3$
93	Friction power of shroud	$N_{тр.б}$	(4.116)	kW	1.3	
94	Effective power of turbine	$N_т$	(4.209)	kW	4443	-
95	Effective work of turbine	$L_т$	(4.1)	J/kg	$5.22 \cdot 10^4$	-
96	Operating factor	$\overline{L}_т$	(4.2a)	-	1.48	-
97	Overall efficiency of the turbine	$\eta_т$	(2.259)	-	0.802	-

The blading and velocity triangles for the calculated turbine are given in Fig. 4.98.

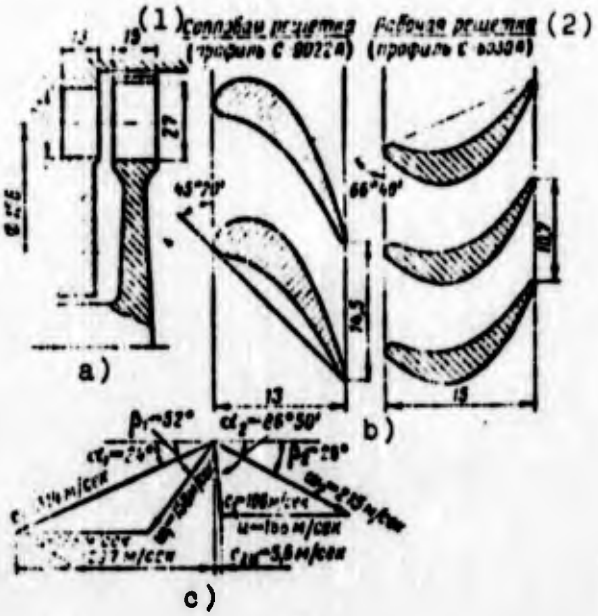

Fig. 4.98. Diagram of the blading and velocity triangles for the calculated precombustion-chamber axial-flow turbine of the liquid-propellant rocket engine: a) meridian section; b) development of nozzle and rotor cascades on the mean diameter; c) velocity triangles.
KEY: (1) Nozzle cascade (profile C-9022A); (2) Rotor cascade (profile C-6030A).
Designations: м/сек = m/s.

4.8.3.2. Features of the Calculation of Radial-Axial Turbines of LPRE. An Example of the Calculation

According to economy the radial-axial and axial-flow turbines are approximately equivalent. The diametric dimensions of the radial[1] turbine, due to the considerable dimensions of the feeding device, can exceed the dimensions of the axial-flow turbine. Used as the feeding devices of radial-flow turbines are spiral feeds (see Fig. 4.11). It is possible to decrease the dimensions of the turbine by the use of a toroidal feed (Fig. 4.99) with a radial connecting piece. Dimensions of toroidal feed are selected from design considerations. The cross section of the feed should be sufficient in order to obtain low velocities and a uniform velocity field at the inlet into the nozzle cascade.

---

[1]As earlier, by the radial-flow turbine we will understand as the radial-axial inward-flow turbine.

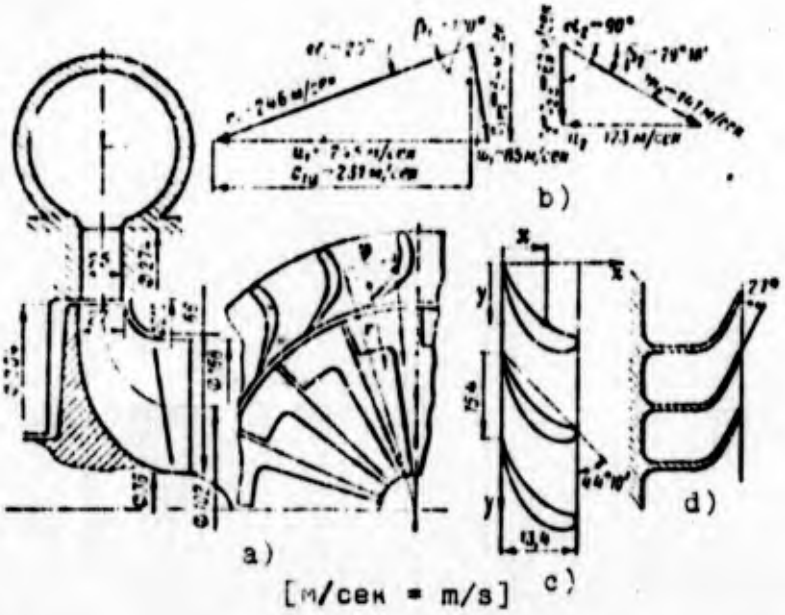

Fig. 4.99. An example of calculation of the inward-flow precombustion-chamber turbine: a) diagram of blading; b) velocity triangles; c) initial airfoil cascade; d) development of the cascade of the trailing edges of impeller vanes.

A shortcoming in the radial-flow turbines is the considerable temperature and power (from rotating blades) loading of the rear disk, which complicates the design of the turbine.

The use of a radial-flow turbine in LPRE can be dictated by design and technological considerations, for example, by the convenience of the layout of the turbine with the combustion chamber, the ease of manufacture, and so on.

Determination of the Ratio u_1/c_1

It is advantageous to begin the calculation of the radial-flow turbine with the determination of the ratio u_1/c_1. From considerations of strength, the impeller vanes at the outlet should be made radial ($\beta_{1л} = 90°$). In this case the defined ratio of velocities u_1/c_1 should be the provided [see equation (4.76a)]. Angle α_1 is selected within limits of 15°-22°.

By knowing u_1/c_1, it is possible to determine the value of the circular velocity u_1 if the discharge velocity from the nozzle cascade c_1 is known. To determine c_1, it is necessary to find the degree of the reaction of the turbine ρ_T.

Determination of the Degree of Reaction

The value of the degree of reaction should be such that at the selected value of u_1/c_1 the maximum of the overall efficiency would be reached. Taking into account the small distinction in the optimum conditions for the overall and circular efficiency, we will determine the value of the degree of reaction on the basis of the maximum of circular efficiency at the selected value of u_1/c_1.

Under conditions of the maximum of circular efficiency, the flow at outlet has an axial direction (minimum losses with the outlet velocity). Let us note that the axial flow is favorable for the operation of the combustion chamber arranged after the turbine.

For the axial outlet from the wheel it is possible to write:

$$w_2^2 = c_{2a}^2 + u_2^2 \tag{4.210}$$

Having substituted the expression (4.210) for w_2 into equation (4.9) and having used the relations

$$l_{adiab} = \frac{\psi_T}{2\varphi^2(1-\psi_T)} c_1^2 \tag{4.211}$$

and

$$w_1^2 = c_1^2 + u_1^2 - 2c_1u_1\cos\alpha_1, \tag{4.212}$$

after the conversions we will obtain the following expression:

$$\frac{\psi_T}{1-\psi_T} = 2\varphi\left(\frac{u_1}{c_1}\right)\cos\alpha_1 + \left(\frac{u_1}{c_1}\right)^2\left(\frac{u_2}{u_1}\right)^2\left(\frac{\varphi}{\varphi}\right)^2(1-\rho_T) + \\ + \left(\frac{\varphi}{\varphi}\right)^2\left(\frac{c_{2a}}{c_{1a}}\right)^2\sin^2\alpha_1 - \varphi^2. \tag{4.213}$$

Expression (4.213) makes it possible to determine the degree of the reaction of the turbine with the selected ratio u_1/c_1. For this one should assign the values ϕ, ψ, c_{2z}/c_{1m} and D_{2cp}/D_1 (see Section 4.3.4). Let us recall that ratio D_{2cp}/D_1 is selected within limits of $D_{2cp}/D_1 = 0.3\text{-}0.6$. Subsequently, the selected value, if necessary, is more precisely defined.

Having determined ρ_T, according to equation (4.33) we find the velocity c_1 and determine the circular velocity on the outside diameter of the wheel u_1. The speed should not exceed (from considerations of strength) 250-300 m/s. According to the known values of u_1 and the frequency of rotation, let us find the outside diameter of the wheel D_1.

Calculation of the Nozzle Cascade

The diameter of the oulet from the nozzle cascade d_1 is determined by the diameter of the wheel D_1. The radius of the inlet r_0 (see Fig. 4.41) is selected within limits of $\bar{r}_0 = r_0/r_1 = 1.2\text{-}1.4$ (where $r_1 = d_1/2$). We calculate the height of the nozzle cascade h_c from equation (4.74).

To obtain the nozzle cascade of a radial-flow turbine, one should use conformal mapping of the cascade (see Section 4.3.4). Therefore, in the calculation of the nozzle cascade, it is preliminarily necessary to calculate the airfoil cascade. Calculation of the cascade is made in a way similar to the calculation of the cascade for the axial-flow turbine (see Section 4.3.1.5). The profile of the airfoil cascade is selected from the atlas of profiles [4] from the number of profiles of group A (subsonic profiles). Nozzle profiles are designated by the letter C.

The selection of the profile is produced according to the M number, calculated according to the adiabatic velocity at the outlet from the nozzle cascade and according to values of angles α_1 and α_0. Angle α_0 should be selected equal to 90°. At the

angle α_0 different from 90°, to provide for a shock-free inlet of flow the nozzle cascade should be made from two sectors with different blades: the blades of one sector should be the mirror image of blades of the other sector.

Having assigned the cascade pitch within the optimum limits for the selected profile, according to the effective angle of the cascade $\alpha_{1э\Phi}$ [see equation (4.208)] we determine the incidence of the profile. For determining the pitch of the cascade t from the relative pitch, it is necessary to assign the airfoil chord $b_п$. The value of the chord is selected in such a way that the ratio of $h_c/b_п$ exceeds unity, i.e., in order that the losses caused by the vortex pair would be small. Along the chord of the profile we determine the width of the cascade $b_{пр}$ [see equation (4.201)].

The loss factor in the airfoil cascade is determined from the characteristics given in atlas [4]. Losses in the airfoil cascade and in the nozzle radial cascade, obtained by conformal mapping of the straight cascade, can be taken as identical. The number of blades of the nozzle cascade is found from the relation resulting from the conformal mappings (see source [7]):

$$z_c = \frac{2\pi}{\ln(r_0/r_1)} \frac{b_{пр}}{t}. \qquad (4.214)$$

The profile of radial nozzle cascade is plotted by the method of conformal mappings (see Section 4.3.4). The further order of the calculation is clear from the example given in Table 4.5. Figure 4.99 gives the blading and the velocity triangles of the calculated inward-flow radial-axial turbine.

Table 4.5. Example of the calculation of the precombustion-chamber radial-axial inward-flow turbine.

No.	Name of value	Designation	Number of equation	Dimensionality	Value	Remarks
1	2	3	4	5	6	7
	A. **Initial data**					
1	Gas flow rate	G	-	kg/s	85	
2	Power of turbine	$N_т$	-	kW	4200	Determined in the calculation of the balance of powers of the TU (see Chapter 5).
3	Stagnation temperature at inlet into turbine	T_0^*	-	°K	700	
4	Gas constant	R	-	J/(kg·°K)	280	
5	Adiabatic index	k	-	-	1.33	
6	Inlet pressure of turbine	p_0^*	-	N/m^2	$140 \cdot 10^5$	
7	Outlet pressure	p_2	-	N/m^2	$100 \cdot 10^5$	
8	Frequency of rotation	ω	-	s^{-1}	2410	Known from calculation of pumps
	B. **Calculated and selective values**					
9	Pressure ratio	δ	-	-	1.4	-
10	Adiabatic work of turbine	L_{ad}^*	(4.3)	J/kg	$6.5 \cdot 10^4$	-
11	Power-speed coefficient	$n_{s\,т}$	(2.185)	-	137	-
	a) *Determination of ratio* u_1/c_1					
12	Flow angle at outlet of nozzle cascade	α_1	-	angular degrees	20	Assigned

Table 4.5 (continued).

13	Angle of the impeller vanes at inlet	$\beta_{1л}$	-	angular degrees	90	The same
14	Flow angle at inlet into wheel	β_1	(4.76)	angular degrees	100°	Assigned is the angle of attack i = -10°
15	Ratio of velocities	u_1/c_1	(4.76a)	-	1	-

b) *Determination of the degree of reaction and outside diameter of the wheel*

16	Ratio of diameters	$D_{2ср}/D_1$	-	-	0.5	Assigned
17	Velocity factor of nozzle cascade	ϕ	-	-	0.975	The same
18	Velocity factor of wheel	ψ	-	-	0.9	" "
19	Ratio of velocities	c_{2z}/c_{1m}	-	-	0.82	" "
20	Degree of reaction	$\rho_т$	(4.213)	-	0.52	-
21	Adiabatic work of nozzle cascade	$b^*_{ад_1}$	(4.88)	J/kg	$3.19 \cdot 10^4$	-
22	Adiabatic discharge velocity from nozzle cascade	$c_{1ад}$	(4.103)	m/s	252	-
23	Outlet velocity from nozzle cascade	c_1	(4.33)	m/s	246	-
24	Circular velocity	u_1	-	m/s	246	See items 15 and 23 of the table
25	External diameter of wheel	D_1	-	m	0.204	-

Table 4.5 (continued).

c) *Calculation of nozzle cascade*

26	Diameter of oulet from nozzle cascade	d_1	-	m	0.21	Assigned is the radial clearance 0.003 m
27	Radius of inlet into nozzle cascade	r_0	-	m	0.137	Assigned is $\bar{r}_0 = 1.3$ (see Section 4.8.3.2)
28	Critical velocity of sound	$a_{1кр}$	(4.207a)	m/s	460	-
29	Normalized velocity	λ_{c_1}	(4.17)	-	0.535	-
30	M number	M_{c_1}	(4.198)	-	0.508	-
31	M number calculated from the adiabatic velocity	$M_{c_{1ад}}$	(4.33)	-	0.520	-
32	Normalized flow rate	$q(\lambda_{c_1})$	(4.199)	-	0.75	-
33	Coefficient of total pressure	σ_1	(2.192)	-	0.99	-
34	Height of nozzle cascade	h_c	(4.74)	m	0.025	-
35	Flow angle at inlet into the cascade	α_0	-	angular degrees	90	Assigned
36	Profile of cascade used for the radial nozzle cascade C-9022A.	-	-	-	-	Selected from atlas [4] with respect to α_0, α_1 and $M_{c_{1ад}}$
37	Effective angle of cascade	$\alpha_{1эф}$	(4.208)	angular degrees	18°30'	-

Table 4.5 (continued).

38	Relative pitch of cascade	$t/b_л$	-	-	0.8	Selected from optimum values (see Section 4.3.1.5)
39	Setting angle	χ	-	-	44°10'	Determined according to profile characteristics
40	Relative height of cascade	$h_c/b_л$	-	-	1.3	Assigned
41	The airfoil chord of cascade	$b_л$	-	m	0.0193	See items 34 and 40 of table
42	Pitch of airfoil cascade	t	-	m	0.0154	See items 38 and 41 of table
43	Width of the cascade	$b_{пр}$	(4.201)	m	0.0134	-
44	Loss factor of cascade	ζ_1	-	-	0.04	Determined according to profile characteristics
45	Speed factor of nozzle cascade	ϕ	(2.194)	-	0.975	-
46	Quantity of nozzle turbine blades	z_c	(4.214)	-	21	-

d) Parameters of flow in the radial clearance between the nozzle cascade and wheel

Table 4.5 (continued).

47	Stagnation pressure	$p^*_{c_1}$	(4.36a)	N/m^2	$139 \cdot 10^5$	-
48	Static pressure	p_1	(4.207)	N/m^2	$118 \cdot 10^5$	-
49	Static temperature	T_1	(4.194)'	°K	672	-
50	Density of gas	ρ_1	(4.195)	kg/m^3	62.8	-
51	Relative velocity	w_1	-	m/s	85	With respect to velocity triangle
52	Stagnation temperature in relative motion	$T^*_{w_1}$	(4.7)	°K	673	-
53	Critical speed of sound in relative motion	$a_{кр\ w_1}$	(4.21)	m/s	452	-
54	Normalized velocity	λ_{w_1}	-	-	0.188	-
55	Total pressure in relative motion	$p^*_{w_1}$	(4.8)	N/m^2	$119 \cdot 10^5$	-

e) *Parameters of flow at outlet from wheel*

56	Circular velocity on mean diameter	u_2	-	m/s	123	-
57	Adiabatic work of wheel	$L_{ад2}$	(4.79)	J/kg	$3.31 \cdot 10^4$	-
58	Relative outlet velocity from wheel	w_2	(4.80)	m/s	141	-
59	Axial velocity at outlet	c_{2z}	-	m/s	69	See item 19 of table
60	Flow angle at the outlet in absolute motion	β_2	(4.766)	angular degrees	29°18'	-

Table 4.5 (continued).

61	Absolute outlet velocity from wheel	c_2	(4.204)	m/s	69	-
62	Flow angle at outlet in absolute motion	α_2	(4.205)	angular degrees	90	-
63	Stagnation temperature in relative motion	$T^*_{w_2}$	(4.82)	°K	653	-
64	Critical speed of sound in relative motion	$a_{кр\ w_2}$	(4.207a)	m/s	445	-
65	Normalized speed	λ_{w_2}	-	-	0.317	-
66	Normalized flow rate	$q(\lambda_{w_2})$	(4.199)	-	0.48	-
67	Total pressure in relative motion	$p^*_{w_2}$	(4.207)	N/m^2	$105 \cdot 10^5$	-
68	Static temperature	T_2	(4.194)'	°K	642	-
69	Stagnation temperature	T^*_2	(4.206)	°K	645	-
70	Critical speed of sound	$a_{кр2}$	(4.207a)	m/s	442	-
71	Normalized velocity	λ_{c_2}	(4.207a)	-	0.156	-
72	Stagnation pressure	p^*_2	(4.207)	N/m^2	$102 \cdot 10^5$	-
73	Density of gas	ρ_2	(4.195)	kg/m^3	55.7	-

f) *Calculation of wheel*

74	Type of wheel - single shrouded	-	-	-	-	Assigned
75	Height of wheel at inlet	$h_{1л}$	(4.74a)	m	0.027	Assigned is the overlap of 0.002 m

Table 4.5 (continued).

76	Mean diameter at outlet	D_{2cp}	-	m	0.102	See items 16 and 25 of table
77	Height of blades at outlet	$h_{2л}$	(4.75)	m	0.066	-
78	Blade chord of wheel on diameter D_{2cp}	$b_{2л}$	-	m	0.041	Assigned is $0.2D_1$
79	Relative cascade spacing of wheel at outlet	$t_2/b_{2л}$	-	-	0.487	Assigned
80	Cascade pitch	t_2	-	m	0.02	See items 78 and 79 of table
81	Quantity of blades	$z_л$	(4.203)	-	16	-
82	Angle of blades	$\beta_{2л.cp}$	-	angular degrees	27	See item 60, assigned is the lag angle of 2°18'
83	Law of change in radius of the blade angle	$r\ tg\ \beta_{2л}$	-	m	0.026	
84	Mean value of front axial clearance	Δz_{cp}	-	m	0.0035	Assigned
85	Mean height of the impeller vane	h_{cp}	-	m	0.046	See Section 4.3.4.2
	g) *Determination of work, power and efficiency of the turbine*					
86	Circular efficiency	η_u	(4.94)	-	0.874	-
87	Circular work	L_u	(2.232)	J/kg	$5.69 \cdot 10^4$	-
88	Friction power of disk	$N_{тр.д}$	(2.202)	kW	27	Assigned is $Re_д = 5 \cdot 10^5$

Table 4.5 (continued).

89	Power of turbine with zero clearance ($\Delta z_{cp} = 0$)	$N_T(\Delta z_{cp}=0)$	(4.209)	kW	4813	-
90	Efficiency of turbine with zero clearance ($\Delta z_{cp} = 0$)	$\eta_T(\Delta z_{cp}=0)$	(2.259)	-	0.87	-
91	Relative drop in efficiency caused by axial clearance	$\frac{\Delta\eta_T}{\eta_T(\Delta z_{cp}=0)}$	(4.114)	-	0.1	-
92	Overall efficiency of turbine	η_T	-	-	0.784	See items 90 and 91 of table
93	Effective work of turbine	L_T	(4.1)	J/kg	$5.1 \cdot 10^4$	-
94	Work factor	$\bar{L}_T$	(4.2a)	-	0.84	-
95	Effective power of turbine	N_T	(2.259)	kW	4340	-

CHAPTER 5

OPERATION OF PUMPS AND TURBINE IN THE FEED SYSTEM OF LIQUID-PROPELLANT ROCKET ENGINES

5.1 SELECTION OF BASIC PARAMETERS OF THE TURBOPUMP UNIT FEED SYSTEMS OF LIQUID-PROPELLANT ROCKET ENGINES

The turbopump feed system of the liquid-propellant rocket engines [LPRE] (ЖРД) (see Section 1.4) can have an autonomous or precombustion-chamber turbine. The selection of one design or another is determined by the purpose of the LPRE. As a rule, in LPRE of average and high thrusts, the design with the precombustion-chamber turbine is used, which makes it possible to obtain a high specific thrust, since in the LPRE with the precombustion-chamber turbine it is possible to have high combustion-chamber pressures.

The feed system with the precombustion-chamber turbine can be carried out by different designs (see Section 1.4.2). Parameters of the feed system - the gas flow rate through the turbine, the outlet pressure of the pumps, the temperature and pressure in front of the turbine (in the gas generator), the frequency of rotation of the turbopump unit [TU] (ТНА) and so on - are determined by the design of the feed system. The design of the feed system also determines the design features of the pumps

and turbine of the turbopump unit. In this section let us examine the questions of the selection of the design of the feed system and the determination of the basic parameters of the feed system with the assigned thrust, specific thrust and relationship of the fuel components in the engine. The selection of the design of the feed system and the determination of its basic parameters always precedes the detailed calculation of the turbopump unit, since these factors determine those parameters for which the pumps and the turbine of the TU should be designed.

5.1.1. SELECTION OF PARAMETERS OF THE FEED SYSTEM WITH THE AUTONOMOUS TURBINE

In the feed system with the autonomous turbine, for driving the turbine a reducing gas produced in the gas generator is used. The use of the reducing gas is not connected with the danger of inflammation of the metal at high gas temperatures, which exists with the use of an oxidizing gas. Therefore, it is possible to allow a higher temperature of the reducing gas (1000°-1200°K) than that of the oxidizing gas (600°-800°K). Furthermore, the gas constant is more in the reducing gas. All this facilitates a decrease in the necessary gas flow rate through the turbine $G_т$.

The magnitude of the discharge $G_т$ is one of the basic parameters of the supply system with an autonomous turbine. The less $G_т$ is, the higher the specific thrust of the engine will be. The provision for the smallest value $G_т$ governs the selection of the type and parameters of pumps and turbine of the turbopump unit. The flow rate $G_т$ is found from the condition of the equality (balance) of powers of the pumps and turbine of the TU:

$$N_{ок} + N_{гор} = N_т \qquad (5.1)$$

where subscripts "ок," "гор," and "т" refer, respectively, to the oxidizer and fuel pumps and to the turbine.

Expression (5.1) can be rewritten in the form

$$\frac{i_{ок}H_{ок}}{\eta_{ок}} + \frac{i_{гор}H_{гор}}{\eta_{гор}} = i_1 l^*_{ад}\eta_т. \qquad (5.2)$$

The fuel component flow rates $G_{ок}$ and $G_{гор}$ are determined by the thrust, specific thrust and the relationship of the fuel components in the engine, taking into account the flow rate of components for driving the turbine (see Section 1.1). The pump pressures $H_{ок}$ and $H_{гор}$ can be found from the combustion chamber pressure $p_к$ and from the value of the resistance of the main pressure lines of the oxidizer and fuel (see Section 1.1).

The efficiency of the pumps $\eta_{ок}$ and $\eta_{гор}$ can be estimated with the aid of the dependences given on Figs. 3.38-3.40 according to the value of the power-speed coefficient [see equation (3.235)].

Let us express ω in terms of the cavitation parameters of the oxidizer pump with the aid of equation (3.163); then expression (3.235) will be rewritten in the form

$$n^*_s = 0{,}365\,\frac{(C_{спа})_{ок}\sqrt{i_{ок}}\left(\frac{\Delta h^*_{спа}}{\psi}\right)^{3/4}_{ок}}{\sqrt{Q_{ок}}}\,\frac{\sqrt{Q}}{(H/z)^{3/4}}, \qquad (5.3)$$

where $i_{ок}$ is the quantity of inlets into the first stage of the oxidizer pump and z is the number of stages of the pump.

Having substituted into relation (5.3) the appropriate values of Q, H and z for the oxidizer pump and fuel pump, we will obtain for them values of the power-speed coefficients $n^*_{s\ ок}$ and $n^*_{s\ гор}$ which usually do not exceed 40-60.

From Figs. 3.38-3.40 it follows that the larger values of n^*_s correspond to the large values of efficiency of the pumps,

and, therefore, less power inputs. A decrease in the pump power [see equation (5.2)] favorably affects the rate of discharge of gas through the turbine $G_т$, decreasing it, and therefore it is necessary to strive for an increase in efficiency of the pumps.

Let us recall how it is possible to raise the efficiency of the pumps by means of an increase in n_s^*. From expression (5.3) it follows that an increase in n_s^* is reached by an increase in the cavitation power-speed coefficient of the oxidizer pump $(C_{срв})_{ок}$. For this the oxidizer pump should be made with the overexpanded inlet into the screw conveyor (large values of K_{D_0}). Sometimes it is advantageous to make the oxidizer pump with a two-way inlet ($i_{ок} = 2$).

It is possible to increase n_s^*, and, therefore, to raise the efficiency by means of making the pumps not single-stage but multistage (for example, with two stages: $z = 2$). The greatest effect can be expected in relation to the fuel pump, which due to the low volume flow rate Q and high pressure H has in the single-stage version a small value of the power-speed coefficient $n^*_{s\ гор} = 25\text{-}35$.

Finally, having selected the design of the pumps and having determined [assuming $(C_{срв})_{ок} = 3500\text{-}4000$ and $K_{D_0} = 6.5\text{-}8$] their efficiency ($\eta_{ок}$; $\eta_{гор}$), it is possible from the equation of the balance of powers (5.2) to find the necessary gas flow rate through the turbine $G_т$. The determination of $G_т$ with the known pump power is examined in Section 4.8.2.1. Let us recall only that the inlet pressure from the oxidizer pump, which creates less pressure than does the fuel pump (with cooling of the combustion chamber by fuel).

The outlet pressure of the turbine depends on whether or not gas is ejected directly into the atmosphere or through additional

nozzles (see Section 1.4.1). To decrease the flow rate $G_т$, sometimes (see Section 4.8.2.2) it follows to use a two-stage impulse turbine with velocity stages, if this leads to an increase in efficiency of the turbine.

Usually in the determination of parameters of the feed system of LPRE with an autonomous turbine, one proceeds from the need to obtain the least gas flow rate through the turbine $G_т$. However, sometimes the gas flow rate through the turbine $G_т$ proves to be assigned. This takes place when the gas after the turbine is fed into the special control nozzles, which create thrust for the flight control of the rocket. In this case the gas flow rate through the turbine will be determined by the relationship

$$G_т = R_с / R_{уд.с},$$

where $R_с$, $R_{уд.с}$ - the thrust and specific thrust of the control nozzles respectively.

The outlet pressure of the turbine will also be assigned and it will be determined by the pressure at the inlet into the control nozzles. Under these conditions the power of the turbine necessary for the pump drive will be provided by the appropriate value of the adiabatic work of the turbine [see equation (5.2)], i.e., by the selection of the temperature and gas pressure at the inlet into the turbine. Since the gas flow rate through the turbine is considerable, the temperature and the pressure will be less than when it is attempted to obtain the least flow rate $G_т$. Sometimes with high thrusts of the control nozzles (high flow rate through the turbine $G_т$), for obtaining the necessary power of the turbine there is a bypass of part of the gas into the nozzles, by passing the turbine, since a further decrease in the temperature and pressure at the inlet into the turbine (in the gas generator) can lead to an unstable process of burning in the gas generator.

5.1.2. SELECTION OF PARAMETERS OF THE FEED SYSTEM WITH PRE-COMBUSTION-CHAMBER TURBINE

The feature of the feed system with the precombustion-chamber turbine consists in the fact that the gas flow rate through the turbine G_T is assigned. It is determined by the flow rate of that component of fuel, on the excess of which the gas generator operates. In the case of a design with an oxidizing gas generator - this is the oxidizer flow rate. For such a design (see Fig 1.19) the equation of the balance of powers will be written in the form

$$N_{ок} + N_{гор} = N_т \qquad (5.4)$$

or

$$\frac{G_{ок} H_{ок}}{\eta_{ок}} + \frac{G_{гор} H_{гор}}{\eta_{гор}} = G_{ок} \frac{1 + \varkappa_{тг}}{\varkappa_{тг}} L_{ад}^{*} \eta_т \qquad (5.5)$$

since

$$G_т = G_{ок} + G'_{гор} = G_{ок} + \frac{G_{ок}}{\varkappa_{тг}} = G_{ок} \frac{1 + \varkappa_{тг}}{\varkappa_{тг}};$$

here $G'_{гор}$ is the fuel flow rate into the gas generator; $\varkappa_{тг}$ is the relationship of the fuel components in the gas generator.

The flow rates of components $G_{ок}$ and $G_{гор}$ are determined by thrust, specific thrust and the relationship of fuel components in the engine (see Section 1.1).

The pump pressures depend on the pressure in the gas generator:

$$H_{ок} = \frac{(p_{ок.к} - p_{ок})_{ок}}{\rho_{ок}} = \frac{p_{тг} + \Delta p_{маг.ок} - p_{к.ок}}{\rho_{ок}}; \qquad (5.6)$$

$$H_{гор} = \frac{(p_{ок.к} - p_{ок})_{гор}}{\rho_{гор}} = \frac{p_{тг} + \Delta p_{маг.гор} - p_{ок.гор}}{\rho_{гор}}, \qquad (5.7)$$

where $\Delta p'_{маг.т}$ - losses of pressure in the main line, which discharges gas from the turbine to the combustion chamber [$\Delta p'_{маг.т} = (10\text{-}15)\cdot 10^5$ N/m^2]. Therefore, the adiabatic work $L^*_{ад}$ will depend on the temperature T^*_0 and pressure at the inlet into the turbine p^*_0, which is connected with the pressure in the gas generator: $p^*_0 = p_{гг} - \Delta p_{маг.т}$ [$\Delta p_{маг.т}$ - losses of pressure in the gas conductor, which discharges gas from the gas generator into the turbine; usually $\Delta p_{маг.т} = (10\text{-}5)\cdot 10^5$ N/m^2]. Let us note that by temperature T^*_0 the value $\kappa_{гг}$ is determined.

Thus, during the calculation of the feed system with precombustion-chamber turbine from parameters which determine the powers of the pump and turbine, the pressure in the gas generator $p_{гг}$ and the temperature of the gas in front of the turbine (in the gas generator) T^*_0 are unknown. Their values are determined from the condition of the balance of powers of the pumps and turbine (5.5).

Usually from considerations of strength the turbines are assigned by the gas temperature T^*_0 (for the oxidizing gas $T^*_0 \leq 600\text{-}800$°K), and the necessary value of pressure in the gas generator $p_{гг}$ is found from the balance of the powers. Sometimes $p_{гг}$ can be assigned; then the necessary temperature T^*_0 is determined.

At the assigned temperature T^*_0 it is difficult to find from equation (5.5) the analytical expression for the necessary pressure $p_{гг}$. Therefore value $p_{гг}$ is determined by graphic means. For a number of values $p_{гг}$ we determine the sum of the pump powers $N_{он} + N_{гор}$ and the power of the turbine $N_т$ (curve 1 on Fig. 5.1). The value of the pressure $p_{гг}$ at which the balance of the power will be observed [see equation (5.4) and (5.5)] is the true value of the pressure in the gas generator. If obtained are two values of $p_{гг}$ at which equality (5.4) is satisfied, then naturally the smaller value is accepted.

where $\Delta p_{маг.ок}$, $\Delta p_{маг.гор}$ are the main lines of the oxidizer and fuel, respectively, from the outlet of the pump to the inlet into gas generator (taking into account the resistance of the injectors). Usually $\Delta p_{маг.ок} = (10\text{-}20)\cdot 10^5$; $\Delta p_{маг.гор} = (30\text{-}40) \times \times 10^5$ N/m^2.

The pressure at outlet of the fuel pump $p_{вых.гор} = p_{гг} + \Delta p_{маг.гор}$ should not be less than the pressure necessary for the fuel feed in the combustion chamber $p'_{вых.гор} = p_к + \Delta p'_{маг.гор}$, where $\Delta p'_{маг.гор}$ is the resistance of main line from the outlet from the pump to the inlet of the combustion chamber, including the resistance of the coolant duct of the combustion chamber [$\Delta p'_{маг.гор} = (70\text{-}90)\cdot 10^5$ N/m^2]. If it appears that $p'_{вых.гор} > p_{вых.гор}$, then the pump pressure $H_{гор}$ should be determined from pressure $p'_{вых.гор}$.

The efficiency of the pumps can be estimated just as in the case of the feed system with an autonomous turbine (see Section 5.1.1), according to the power-speed coefficient n_s^* calculated according to equation (5.3). Let us note that since n_s^* depends on H, and H depends on $p_{гг}$ [see equations (5.6) and (5.7)], the efficiency of the pumps will depend on the pressure in the gas generator $p_{гг}$.

Since the flow rate $G_{ок}$ is known, and the efficiency of the precombustion-chamber turbines with full feed ($\varepsilon = 1$) is equal to 0.7-0.75, the power of the turbine will be determined by the adiabatic work $L^*_{ад}$.

The outlet pressure of the turbine p_2 is determined by the combustion-chamber pressure, into which the gas enters after the turbine:

$$p_2 = p_к + \Delta p'_{маг.г}$$

With an increase in the combustion-chamber pressure $p_к$ and at a constant value of $p_{гг}$, the pump power will not be changed [see equations (5.5) - (5.7)], but the power of the turbine will decrease, since with the same $p_{гг}$ with an increase in $p_к$ the degree of the pressure drop in the turbine

$\delta = \frac{p_0^*}{p_2} = \frac{p_{гг} - \Delta p_{маг.т}}{p_к + \Delta p_{маг.т}}$ will be decreased (curve 2 on Fig. 5.1). The pressure $p_{гг}$ at which there will be observed the balance of the powers will increase (see Fig. 5.1).

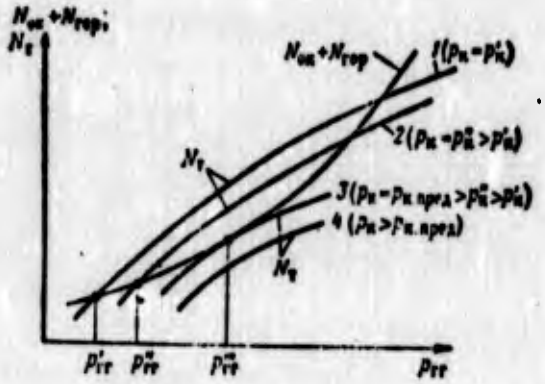

Fig. 5.1. Determination of pressure in the gas generator of the feed system with the pre-combustion-chamber turbine.

With a definite combustion-chamber pressure the curve of the dependence of the power of the turbine on $p_{гг}$ (curve 3 on Fig. 5.1) will touch at one point of the curve of the sum of the pump powers. This value of pressure will be maximum ($p_{к.пред}$, see source [150]), since at higher pressures the condition of the balance of powers will not be fulfilled (curve 4 on Fig. 5.1).

For an increase in the maximum pressure $p_{к.пред}$, it is necessary to increase the power created by the turbine (for example, an increase in the gas temperature T_0^* or by the transition to a design with two turbines - oxidizing and

reducing) or decrease the power consumed by the pumps (for example, by an increase in the efficiency of the pumps).

With the assigned $p_к$ with a decrease in the power consumed by the pumps, the pressure in the gas generator $p_{гг}$ decreases, since for the creation by the turbine of less power a smaller degree of a decrease in pressure in the turbine δ is necessary.

It is possible to decrease the pump power by an increase in its efficiency. Hence it follows that an increase in the efficiency of the pumps promotes a decrease in the pressure in the gas generator $p_{гг}$. The same effect on the pressure $p_{гг}$ is rendered by an increase in the efficiency of the turbine. Consequently in the feed system with the precombustion-chamber turbine, an increase in the economy of the pumps and turbine leads to a decrease in the pressure in gas generator (or to a decrease in the temperature in the gas generator if the pressure $p_{гг}$ is assigned).

In the feed system with the autonomous turbine, as was shown in Section 1.4.1, an increase in the efficiency of the pumps and turbine by means of a decrease in the flow rate through the turbine increases a specific thrust of the LPRE.

A decrease in pressure in the gas generator of the LPRE with the precombustion-chamber turbine promotes a decrease in the mass of the gas generator and turbopump unit, i.e., it allows making the engine lighter. It is possible to increase efficiency of the pumps by an increase in their power-speed coefficients n_s^* [see equation (5.3)]. This can be achieved by an increase in the number of stages of pump z, as can be seen from equation (5.3).

At high combustion-chamber pressures [$p_к > (250\text{-}300)\cdot 10^5$ N/m^2] the use of multistage pumps can prove to be advisable.

For the LPRE, which operate on liquid hydrogen, the use of a multistage fuel pump proves to be advisable already when $p_н = (45\text{-}50)\cdot 10^5$ N/m^2 (see source [31]), since due to the low density of hydrogen the fuel pump pressure will be considerable, and with one stage of the pump value n_s^* and, therefore, the value of the efficiency are low. Furthermore, the making of hydrogen pumps into multistage pumps makes it possible to decrease the circular velocity on the outside diameter of the wheel down to a value permissible from considerations of strength (u_2 < 400--450 m/s).

In LPRE with a precombustion-chamber turbine the anti-cavitation qualities of the feed system are increased by the use of booster jet and vane pumps. Their use increases the values of n_s^* [in equation (5.3) instead of $(C_{срв})_{он}$ one should substitute $(C_{с.п})_{он}$] and the efficiency of the pumps and in this way facilitates a decrease in pressure in the gas generator. However, the expenditure of the power for driving the booster pumps requires a certain increase in pressure $p_{гг}$. If the vane booster pump is driven by the gas turbine, then the gas after the turbine is ejected into the atmosphere, which lowers the specific thrust of the engine. However, since the gas flow rate for driving the booster pump is low, then this reduction is insignificant. Moreover, a definite gas flow rate can be required for tank pressurization of the rocket or for the control nozzles.

If in the feed system booster pumps are provided, then pumps of TU should be made with a one-way inlet, since although the use of a two-way inlet decreases the required pressure of the booster pumps (see Section 3.3.8), the complexity and mass of construction of TU will increase. For this reason there is no need to re-expand considerably the inlets into the pumps of the TU - it is possible to be limited to the value $K_{D_0} = 6.5\text{-}5.5$.

The pressure in the gas generator $p_{гг}$ and temperature T_0^* in other designs of the feed with the precombustion-chamber turbine (designs with a reducing gas generator, with two gas generators etc.) are determined in a way similar to that in which they are determined in the design with the oxidizing gas generator - on the basis of equation of the balance of powers for each of the designs.

For the design with the reducing gas generator (see Fig. 1.18), it is possible to write

$$N_{ок} + N_{гор} = N_т;$$

hence
$$\frac{G_{ок}H_{ок}}{\eta_{ок}} + \frac{G_{гор}H_{гор}}{\eta_{гор}} = G_{гор}(1-K)(1+\alpha_{1г})L_0^*\eta_т. \qquad (5.8)$$

where K is the coefficient which considers the fuel consumption for the internal cooling of the combustion chamber; usually K = 0.02-0.06.

Pump pressures $H_{ок}$ and $H_{гор}$ are determined from expressions (5.6) and (5.7), and the efficiency is determined by n_s^* [see equation (5.3)].

In connection with the fact that the gas flow rate through the turbine in the design with a reducing gas generator is less than that in the design with an oxidizing gas generator, the reducing turbine can prove to be partial ($\varepsilon < 1$). This will be observed (see Section 4.5.2.2) with the power-speed coefficient of the turbine $n_{s\,г} \leq 50\text{-}60$. Then $\eta_т$ will be able to be evaluated with the aid of the dependences given on Fig. 4.58.

Partial-admission precombustion-chamber reducing turbines are obtained at high pressures in the gas generator [high densities of gas, low volumetric flow rates, see equation (2.185)

for $n_{s\ T}$], which corresponds to high combustion-chamber pressures [$p_{к}^{*} > (200\text{-}250)\cdot 10^{5}$ N/m^{2}], and when using liquid hydrogen as a fuel. In the latter case the exhaust gas velocity from the nozzle cascade increases, which leads to a reduction in length of the turbine blade.

The balance of powers for the design with a low-flow pump of the gas generator, for example, for a design with an oxidizing gas generator (see Fig. 1.20) is written in the form

$$N_{ок} + N_{гор} + N'_{гор} = N_{т}, \qquad (5.9)$$

where $N'_{гор}$ is the power of the gas-producing fuel pump.

In expanded form expression (5.9) is written in the following form:

$$\frac{G_{ок}H_{ок}}{\eta_{ок}} + \frac{G_{гор}H_{гор}}{\eta_{гор}} + \frac{\frac{G_{ок}}{\nu_{гг}}H'_{гор}}{\eta_{гор}} = G_{ок}\frac{1+\nu_{гг}}{\nu_{гг}}L^{*}_{т}\eta_{т}, \qquad (5.10)$$

where

$$H_{ок} = \frac{p_{г} + \Delta p_{маг.ок} - p_{ок.вх}}{\rho_{ок}};$$

$$H_{гор} = \frac{p_{к} + \Delta p'_{маг.гор} - p_{гор.вх}}{\rho_{гор}};$$

$$H'_{гор} = \frac{(p_{гг} + \Delta p''_{маг.гор}) - (p_{к} + \Delta p'_{маг.гор})}{\rho_{гор}}$$

(here $\Delta p''_{маг.гор}$ is the resistance of the main line from the outlet of the gas-producing pump to the inlet into the gas generator).

The efficiency of the pumps is determined, as in other design, according to the power-speed coefficient n_{s}^{*}. Similarly

it is possible to write the balance equations also for other designs of the feed system with the precombustion-chamber turbine.

When selecting designs of the feed system, it is necessary to compare them with respect to the required value of pressure in the gas generator at the selected temperatures in front of the turbine (or the required magnitude of temperature at the selected pressure $p_{гг}$). The design which provides less pressure $p_{гг}$ should be given preference, since such a design will make it possible to obtain a lighter construction of the engine.

The answer to which of the designs - with the oxidizing or reducing gas generator - corresponds to less pressure $p_{гг}$ is immediately difficult. The flow rate through the oxidizing turbine is more than that through the reducing turbine, since $G_{ок} > G_{гор}$. But the working capacity of the reducing gas $\frac{k}{k-1} RT_0^*$, which determines the adiabatic work of the turbine $L_{ад}^*$, is higher than that of the oxidizing gas; as a rule, the product $G_г \frac{k}{k-1} RT_0^*$ is also more than that of the reducing gas. But, at the same time, the smaller value of the adiabatic index k, inherent usually to the reducing gas, decreases the adiabatic work of the turbine as a result of a decrease in the complex $[1-(1/\pi^{\frac{k-1}{k}})]$ [see equation (4.3)]. Furthermore, the reducing turbine can prove to be partial-admission, which will lower its efficiency.

Usually up to the pressure in the combustion chamber, which does not exceed $p_к = (140\text{-}180)\cdot 10^5$ N/m^2, lower pressures in the gas generator are obtained in the design with the oxidizing

gas generator, and at higher combustion-chamber pressures the advantages on the side of the design with a reducing gas generator. In hydrogen LPRE, in connection with the great work capacity of the reducing gas $\frac{k}{k-1}RT_0^*$, it is advantageous to use the design of the feed with a reducing gas generator (see source [31]).

When using a design with two gas generators and two turbines, reducing and oxidizing (see Fig. 1.21), because of the greater power created, it is possible to operate at lower pressures in the gas generators than when using a design with one gas generator. But the design with two gas generators is constructively more complex, and it corresponds to a large total mass of the gas generators and TU. Therefore, it is advantageous to use the design with the two gas generators for engines with high combustion-chamber pressures, when the assigned magnitude $p_к$ cannot be provided in the design with one gas generator, or when in the design with one gas generator pressures $p_{гг}$ unacceptable according to considerations of strength are obtained.

The design of the feed with a low-flow gas-generator pump (see Fig. 1.20) will correspond to less pressure $p_{гг}$ than in the design without such a pump. This is obtained because the pump power in the case of the use of a gas-generator pump decreases, since with the oxidizing gas generator, for example, the pressure of not the entire fuel flow is increased to a pressure of the gas generator but only a small part of it which enters into the gas generator.

The use of a low-flow gas-producing pump lowers the pressure in the gas generator by $(10\text{-}15)\cdot10^5$ N/m^2 when $p_к = (100\text{-}150)\cdot10^5$ N/m^2. At high pressures $p_к$ [$p_к > (250\text{-}300)\cdot10^5$ M/m^2] this reduction can consist of $(40\text{-}60)\cdot10^5$ N/m^2 and more. In the latter

case it is advantageous to proceed to a certain complication of the design of the TU, attaining a decrease in the pressure in the gas generator.

The question of the selection of one design or another of the feed system with the precombustion-chamber turbine is solved when designing specific LPRE by means of comparative calculations of different design, taking into account the complexity of the construction and its mass. In the comparison of designs throughout the mass of the construction, it is possible to use the relations given in Section 5.4.

5.2. OPERATION OF THE PUMPS AND TURBINE IN THE CONTROL OF LPRE

5.2.1. GENERAL INFORMATION

The purpose of the control system of the liquid-propellant rocket engine is to change the thrust with a specific relationship of the fuel components. Usually a change in the thrust is reached by a reduction in the flow of the fuel components fed by the pumps into the combustion chamber. A change in the quantity of components fed into the chamber can be realized by means of changing the operating mode of the pump. The method of a change in the frequency of rotation of the pump spindle by means of an effect on the turbine is most favorable.

Thus, the problem of control of the engine with respect to thrust is reduced to a change in the operating mode of the turbine. In this case the engine regulator changes the flow rate of the components entering into the gas generator of the turbine. The theory of the control process of the LPRE is not examined in the present course, and therefore in this section

only the general questions concerning the use of characteristics of pumps and turbines for the examination of the operation of the feed system and requirements for the characteristics of pumps and turbines on the basis of the control problems will be examined.

5.2.2. REQUIRED PRESSURE OF THE FEED SYSTEM

Figure 1.2 shows a diagram of the pump feed system of the LPRE. The pumps should provide the feed of the assigned quantity of fuel and oxidizer into the combustion chamber. The necessary pump pressure H, for providing the assigned flow rate Q through the system, is determined by the required increase in specific mechanical energy H_c. For brevity, subsequently this value will be called the required pressure of the system.

For the steady-state conditions

$$H = H_c; \tag{5.11}$$

$$Q_н = Q_c, \tag{5.12}$$

where the subscript "н" refers to parameters of the pump and subscript "с" to parameters of the system (we will write the pump pressure without a subscript).

The required pressure of the system H_c is determined by the resistance of the system, i.e., by the pressure in chamber $p_к$, by pressure drop on the injectors $\Delta p_ф$, by the flow friction of the system from the pump to the injectors $L_{\text{conp.вых}}$, by required high-speed energy $c^2_{\text{вых}}/2$, and by the available total pressures at the inlet $p^*_{\text{вх}}$:

$$H_c = \left(\frac{p_к}{\rho} + \frac{\Delta p_ф}{\rho} + L_{\text{conp.вых}} + \frac{c^2_{\text{вых}}}{2}\right) - \left(\frac{p^*_{\text{вх}}}{\rho} + \frac{c^2_{\text{вх}}}{2}\right). \tag{5.13}$$

The pressure at the inlet into the pump $p_{вх}$ is determined by the tank pressure $p_б$, an excess in the gravitational level of the tank above the level of the pump (energy of position), inertial pressure, and flow friction of the main line from the tank to the inlet into the pump $L_{конр.вх}$ [see equation (1.12)].

By comparing equations (5.13) and (1.12), let us find (disregarding by the difference in the values of $c_{вх}$ and $c_{вых}$):

$$H_{н} = \frac{p_к}{\varphi} - \frac{\Delta p_ф}{\varphi} - L_{\text{конр.вх}} - \frac{p_к}{\varphi} - l(\varphi\cos\varphi - f). \qquad (5.14)$$

With a change in the flow rate through the system the required pressure of system will be changed. Let us examine how the individual terms of equation (5.14) making up the required head of the system depend on the flow rate. The pressure $p_к$ in the combustion chamber is changed directly proportional to the rate of flow of the component (Fig. 5.2). It is thought that the relationship of the components is maintained constant. The drop on the injectors $\Delta p_ф$ determines with this flow cross-sectional area of the injectors $f_ф$ the rate of flow through them:

$$Q = n\mu f_ф \sqrt{2\frac{\Delta p_ф}{\varphi}},$$

where n is the number of injectors; μ is the coefficient of flow rate of the injectors.

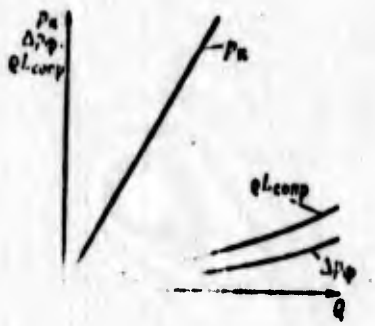

Fig. 5.2. Dependences of the combustion-chamber pressure, injector pressure drop and hydraulic losses in the feed system on the volumetric flow rate.

Graphically the quadratic dependence of Δp_{ϕ} on Q is shown on Fig. 5.2 (coefficient of the flow rate μ is taken in all conditions as being constant).

The hydraulic friction of the pipelines L_{conp} is proportional to the square of the speed of motion of the fluid:

$$L_{conp} = \xi \frac{c^2}{2}.$$

The speed of motion in the pipeline of this cross section is proportional to the fluid flow rate; consequently, by taking ξ = const, we will obtain

$L_{conp} = \text{const} \cdot Q^2$ (see Fig. 5.2).

The tank pressure, the energy of the position determined by the difference in the gravitational levels, and the value of the inertial pressure are not directly determined by the flow rate in these conditions.

The total dependence of the required increase in energy of the system (pressure of the system) on the value of volumetric flow rate for the feed system given on Fig. 1.3 is shown on Fig. 5.3. We will call this dependence the characteristic of the system. For the system of the LPRE the excess pressure in the tanks and the positive value of the gravitational and inertial pressures are characteristic; consequently, the curve of the required increases in energy of the system intersect the axis of the ordinates below zero. This means that the flow rate from zero to Q_1 (see Fig. 5.3) is provided only because of the input energy, without the participation of the pump. The flow rate which exceed Q_1 can be obtained in this system only with the installation of the pump.

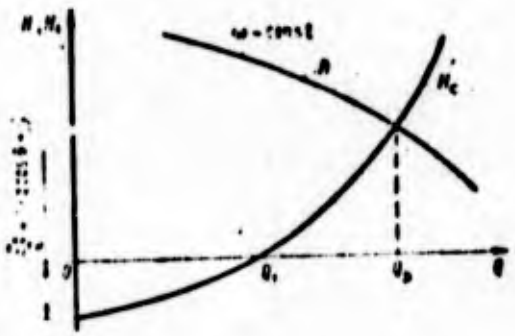

Fig. 5.3. Dependence of the required increase in energy of the system on the volumetric flow rate and the pump pressure characteristic.

For the stationary exhaust pump installations, the curve of the required energies will intersect the axis of the ordinates above zero. This means that in similar installations no flow can be obtained without the pump.

The pressure characteristic of the pump $H = f(Q)$, also given on Fig. 5.3, shows the dependence of the pump pressure on the flow rate at the constant frequency of rotation of the pump spindle. The point of intersection of the curves $H_c = f(Q)$ and $H = f(Q)$ when $\omega = \text{const}$ determines the flow rate Q_p which will be established in the system at this frequency of rotation of the pump spindle. At the assigned flow rate Q_p, according to the value of the required pump pressure, it is possible to find the necessary rotating frequency for providing the assigned mode.

For a thrust change of the engine, it is necessary to change the flow rate through the system. A change in the fuel consumption is one of the primary tasks of the control of the feed system of the LPRE. It can be achieved by different methods. By control of the feed system of the LPRE with the turbopump unit according to the flow rate we will understand as a change

in the system characteristic or the pump characteristic which provides transition to a new flow rate through the system.

5.2.3. METHODS OF CONTROL OF TURBOPUMP FEED SYSTEMS ACCORDING TO FLOW RATE

5.2.3.1. Control of the Pump

A change in the system characteristic is most simply achieved by the throttling of the main pressure line.

Let us assume that the flow rate in the new conditions will be equal to Q_2 (Fig. 5.4). The required pressure H_{c2} which the pump should insure in this case will be determined by the required pressure of the system with the flow rate Q_2 and the additional resistance of the throttle $L_{др}$:

$$H_{c2} = H'_{c2} - L_{др}.$$

The new characteristic of the system $H''_c = f(Q)$, taking into account the resistance of the throttle, passes more steeply, and the new steady-state mode (point 2) will take place at a smaller value of the flow rate (see Fig. 5.4).

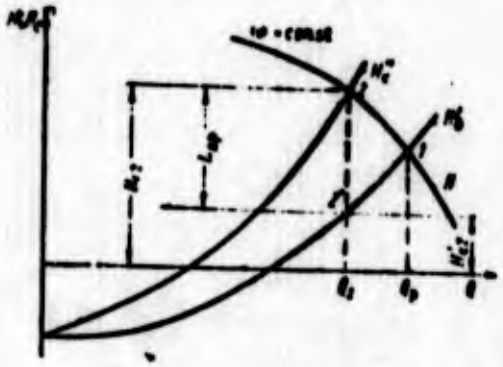

Fig. 5.4. Examination of the control of the system by throttling.

The introduction of the resistance of the throttle will require greater pump pressure for the assigned less flow rate and, thereby, greater power (in comparison with the power in the system without a throttle with the same flow rate). An additional expenditure of power can be caused not only by the fact that the pump pressure in new conditions is more than that required for a system without a throttle, but also by the fact that in new (off-design) conditions the pump usually operates with the less efficiency. The unproductive expenditure of the pump power while maintaining the previous frequency of rotation is accompanied by the unproductive gas flow rate through the turbine. The most considerable shortcoming of this method of control consists in the unproductive expenditure of power.

A change in the system characteristic by means of the introduction of an additional resistance is widely used in the adjustment of the engine. By means of installing washers on the main pressure line of the pipelines, we attain such a change in the flow rate in order that the assigned relationship of components would be maintained.

The throttle valve (adjustable resistor) is also widely used in the control systems for maintaining the assigned magnitudes of pressure and the relationship of components in the combustion chamber.

For a change in the conditions with respect to thrust, the method of throttling is used in conjunction with other methods of control - most frequently in the control of feed systems of LPRE the method of throttling is combined with the control by means of changing the frequency of rotation of the TU.

Another method of the conversion of the system into a new flow is possible, and this consists in the fact that part of

the fluid which passed through the pump will pass back into the pump and does not enter into the system (Fig. 5.5). In this case the excess energy will be spent, since the flow through the pump increases, and the operating point is displaced into the region of less efficiency.

In the feed system of the LPRE a bypass is frequently used not only for the control but also with the purpose of the avoidance of hydraulic shock in the system with the connection of the pump.

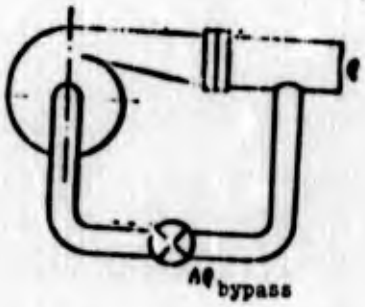

Fig. 5.5. Diagram of a pump with a bypass main line.

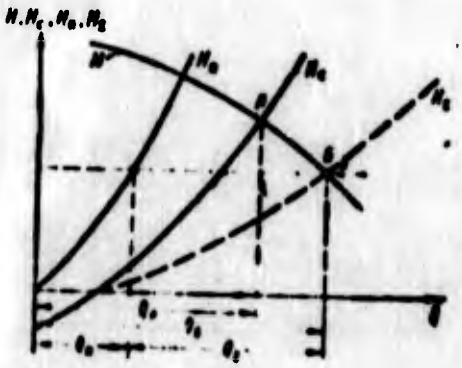

Fig. 5.6. Examination of control of the system with a bypass.

Figure 5.6 gives characteristics of the pump (H), the main system (H_c) and main bypass line ($H_п$). For the given required energy, the flows through the system and the main bypass line are totaled. The total characteristic is designated H_Σ. If the operational mode without a bypass is depicted by point A, then with the use of a bypass the operational mode is moved to point Б. The flow rate through the system is decreased ($Q_2 < Q_A$), while the flow rate through the pump increases ($Q_Б > Q_A$). The flow rate through the main bypass line will be equal to $Q_п$. By changing the resistance of the main bypass line by the throttle installed on it, it is possible to expand the range of the control.

The third method of the conversion of the system into a new flow rate consists in a change in the pump characteristic. In this case the minimum expenditure of power is provided.

A change in the pump characteristic can be achieved most simply by a change in the frequency of rotation (Fig. 5.7). The design conditions (ω': Q_p) are characterized by point 1: the frequency of rotation ω'' is found from value of the required pressure of the system at the new flow rate Q_2.

If for the pump there is a field of characteristics, then the new frequency of rotation will be found easily graphically according to the assigned flow rate with the known pressure of the system.

If there is only one experimental pump characteristic, then the frequency of rotation upon transition to new conditions can be found analytically. Let us draw a parabola of similar conditions through the point on the characteristic of the system which corresponds to the new flow rate Q_2 (dashed line on Fig. 5.7). It will cross the normal characteristic for the calculated frequency of rotation at point A. The new value of the frequency of rotation will be found from the relation (see Section 3.1.4.3)

$$\frac{\omega'}{\omega''} = \frac{Q_1}{Q_2}, \text{ or } \frac{\omega'}{\omega''} = \sqrt{\frac{H_1}{H_2}}.$$

The method of feed control of the pump by a change in the frequency of rotation in conjunction with the bypass or throttling is the most common in the feed system of the LPRE. A change in the frequency of the rotations of the pump is reached by the control of the turbine.

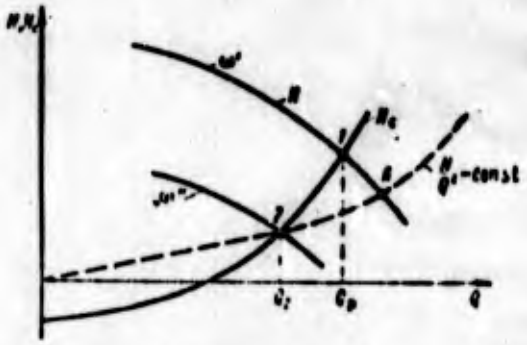

Fig. 5.7. Examination of control of the system by a change in the frequency of rotation.

In principle, the change in the slope angle of the blades and width of the wheel at the outlet can also be the method of control of the pump characteristic. In practice this can be used only when designing pumps. For the pump made it is complicated to carry out this method of the effect on the pump characteristic in a design respect. In industrial pump construction rotary rotor blades for the control of axial propeller pumps are used.

It is simpler to carry out control by the use of rotary guide blades at the inlet into the pump. In this case it is easy to change the circular velocity component at the inlet into the wheel c_{1u} and, as follows from the Euler equation (2.31), change the pump pressure. But in practice this method is not applicable for pumps of LPRE, since the rotary device at the inlet into the pump, by virtue of the additional flow friction, will make the anticavitation properties of pump worse. The method of controlling the characteristics of turbomachines by the use of deflectors at the inlet is easily used for compressor machines and hydraulic turbines.

5.2.3.2. Control of the Turbine

We will understand by control of the turbine the effect on its characteristic for the purpose of a change in the power and frequency of rotation. In principle, several methods of the control of the turbine are possible. The basic methods are: nozzle control, bypass control, a change in the pressure and temperature of the working medium at the inlet into the turbine or pressure at the outlet from it.

Nozzle control provides for a change in the quantity of the working medium passing through the turbine by means of changing the degree of admission, i.e., by means of the disconnection or connection of the individual groups of nozzles. Constructively this method of control is quite complex - it requires an independent feed of the working medium to the individual groups of nozzles. In the TU such a method of control can be achieved by the use of several gas generators operating on individual groups of nozzles. A change in the power, and with the assigned load and the frequency of the rotation of the turbine, is reached by the disconnection of the individual gas generators (Fig. 5.8). The advantage of this method of control consists in the fact that parameters of the working medium (pressure, temperature) in this case can remain calculated. In steam turbines and in turbojet engines such a variety of nozzle control as the rotation of the nozzle blades is used.

Another method of control with which basically changed is the quantity of working medium is the bypass of part of the gas past the turbine (Fig. 5.9, see source [158]). For autonomous turbines of LPRE this method is clearly disadvantageous, since it leads to a reduction in the specific thrust of the engine plant. In precombustion-chamber turbines this method of control, in principle, can be used. For any design of engine installa-

tions it is possible also to use the bypass of the liquid component into the inlet into the pump (see Fig. 5.5).

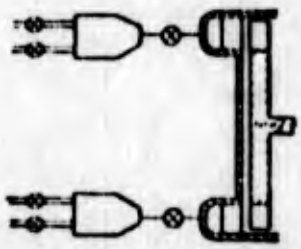

Fig. 5.8. Design of a turbine with feed from several gas generators (examination of the nozzle control of the turbine).

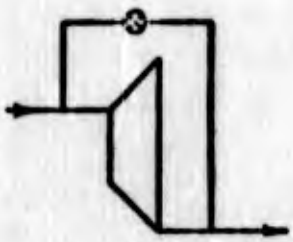

Fig. 5.9. Examination of the control of the turbine by a bypass.

With the control of the turbine by a change in parameters of the gas at the inlet there can be two cases: control by a change in the gas flow rate through the turbine at a constant temperature and control by a change in the temperature by means of a change in the relationship of the components.

In the first case of the control the flow rate of the components through the gas generator (turbine) is changed by a change, with the aid of throttles, in the resistance of the main lines feeding the components of fuel to the gas generator. In this case the relationship of the fuel components is maintained constant (constant temperature in the gas generator). With a change in the resistance of the main lines the pressure in the gas generator (in front of the turbine) is changed. Therefore, the power of the turbine will be changed both as a result of a change in the flow rate and also due to a change in the adiabatic work. This method of control is used for autonomous turbines.

Figure 5.10 shows a change in the initial parameters of the gas and available adiabatic works with the control of the turbine

by throttling at an inlet. The line $i_0^* = \text{const}$ corresponds to the process of throttling.

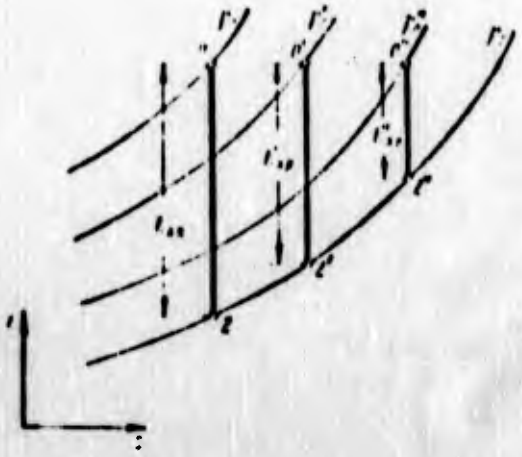

Fig. 5.10. Representation of the available adiabatic curves of works in the i - s diagram with control of the turbine by throttling at the inlet.

With the control by a change in the turbine inlet gas temperature, the temperature is changed by means of a change in the flow rate of the fuel component with a deficiency of which the gas generator operates. The flow rate is changed with the throttle valve (variable resistance). A change in the temperature leads to a change in the adiabatic work. With a change in the adiabatic work $L^*_{ад}$ the frequency of rotation of the turbine is changed. With an increase in $L^*_{ад}$ (increase in temperature), for example, the frequency of rotation will increase; the pump pressure and pressure in the gas generator are increased. This leads to a further increase in $L^*_{ад}$ and flow rate through the turbine (at constant pressure at the outlet), but since with an increase in the frequency of rotation the pump power also increases, then the TU emerges into a new steady-state mode with increased frequency of rotation. At the increased frequency

of rotation the fuel component flow increases, and the engine emerges into conditions of greater thrust. The examined method is used for the control of precombustion-chamber turbines.

Control by a change in conditions of the gas generator is most economical, since the operating mode of the turbine with respect to $u/c_{ад}$ with control can be changed insignificantly, and then efficiency of the turbine remains virtually constant.

5.2.3.3. Selection of Conditions with Control of the TU

With the known characteristics of the pump and turbine, the selection of their conditions with the control of the LPRE with respect to thrust can be produced graphically.

The assignment of the flow rate of one of the components in the other conditions makes it possible to select the new frequency of rotation of the TU. For the other component the required frequency of rotation is thus determined. However, it can be obtained so that the frequencies of rotation of pumps of the oxidizer and fuel necessary for providing for the assigned flow rate will be different in connection with the fact that the relationship of the components is maintained constant.

Let us assume that Fig. 5.7 shows the characteristics which refer to the control of the system of one of the components. The graphic representation of control for the other component is presented on Fig. 5.11. The characteristic of the system of the second component is designated H_{cII}; the pump performance is H_{II}. With the assigned characteristic of the system H_{cII} the new flow rate Q_{2II} is provided at the frequency of rotation of the pump ω''' less than ω''. The frequency of the rotation of the TU should be selected with respect to the higher frequency of

rotation (ω"), and it follows to transfer the system of the second component to the less flow rate by throttling. Figure 5.11 shows the required resistances of the throttle $L_{дрII}$. This throttle will be the control of the relationship of the components.

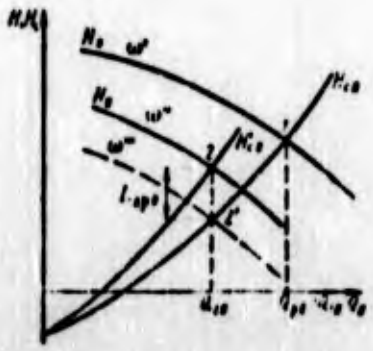

Fig. 5.11. Examination of the control of the feed system of the second component.

Fig. 5.12. Examination of the control of the TU by a change in the pressure at the inlet into the turbine.

The required change in the gas flow rate through the turbine for the case of the control by a change in the pressure at the inlet into the turbine can be found from an examination of the combined turbine and pump characteristics (Fig. 5.12), where plotted along the axis of the ordinates are the power of the turbine at different flow rates of the working medium and the total required pump power, but plotted along the axis of the abscissae is the frequency of rotation. The dependence of the pump power on the frequency of rotation in the assigned hydraulic circuit, which determines the change in the flow rate, can be obtained when using a field of the pump characteristic. From an examination of the joint operation of the pump and the system, Q and H for each of the pumps are known. By these parameters the required power of each pump is found:

$$N_{\text{н}} \frac{QH}{\eta_{\text{н}}};$$

$\eta_н$ - determined according to the assigned field of efficiency on the pump characteristic (see Fig. 3.61).

The mode of the joint operation of the pumps and turbine is determined by the equality of the powers. Having selected in accordance with the graph given on Fig. 5.12 the frequency of rotation of the second mode of the TU, we find the required flow through the turbine (point 2 on Fig. 5.12). The initial turbine characteristics, obtained as a result of the processing of experimental data, were given earlier (see Fig. 4.91). Let us note that these characteristics can be obtained by calculation (see Section 4.7.2.3).

Similar plottings can also be used in the adjustment of the engine to the assigned conditions.

A distinction in the course of characteristics of the fuel and oxidizer pumps requires the introduction of an additional control with respect to the relationship of the components during a change in the operating mode of the engine, as follows from Fig. 5.11 ($L_{дрII}$).

The characteristics of the oxidizer and fuel pumps with respect to flow rate and the frequency of rotation can be selected so that the relationship of the components upon the transition to other conditions will always be maintained without special control. In this case the pumps will be the regulators of the ratio of components. It is the simplest of all to achieve the maintaining of the assigned relationship of components without a special regulator with sloping characteristics $H = f(Q)$. The sloping characteristics $H = f(Q)$ correspond to larger angles at the outlet from the wheel $\beta_{2л}$ and larger width b_2 (less than q_p) (see Fig. 3.54).

5.2.4. STABILITY OF OPERATION OF THE PUMP IN THE FEED SYSTEM OF LPRE

Operation of the pump in the feed system of LPRE should be stable in all the operating modes of the engine. This means that parameters of the pump should be maintained constant for the assigned conditions, in spite of small deviations in their values caused by random effects.

If the centrifugal pump has the characteristic $H = f(Q)$ with an explicit maximum or bend (Fig. 5.13), then the emergence of the unstable operation of the pump is fundamentally possible (see source [151]). The unstable operation of the pump is characterized by the nonstationary displacements of the fluid in the system, which leads to a periodic change in the productivity and pressure, which is accompanied by hydraulic shocks.

Fig. 5.13. Question of the stability of the pump system.

Let us analyze the conditions which determine the static stability of the operation of the pump in general. The stability of the conditions depends on the characteristics of the pump and the system. Figure 5.13 gives the characteristics of the pump and system (network). Let us assume in general that the characteristics of the system intersect the characteristics of the pump at two points - A and Б.

Let us examine the effect of small deviations in parameters of the system on the stability of conditions of the pump in the region of points A and Б.

In the region of point A any small random decrease in the flow rate for value ΔQ (for example, as a result of the temporary clogging of an opening of one of the injectors) leads to the fact that the pump pressure will exceed the required pressure of the system; because of this the fluid flow in the system will be accelerated, and the flow rate will increase up to the previous value.

In the region of point Б a short-term decrease in the flow rate by value ΔQ, which arose for different reasons, will cause an excess in the required pressure of the system above the pump pressure, and, as a consequence of this, the stagnation of the flow and further reduction in the flow rate will arise. Similar considerations can be conducted also for the case of a short-term increase in the flow rate by value ΔQ.

Thus, in the region of point Б an unstable equilibrium takes place - a slight disturbance causes a sharp deviation from the conditions, and in the region of point A the conditions are stable (they possess the property of self-regulation), since a small deviation does not bring the system out of equilibrium.

Mathematically the condition of the stable static equilibrium of the operation of the pump in the system can be written by the following inequality:

$$\frac{\partial H_c}{\partial Q} > \frac{\partial H}{\partial Q}. \qquad (5.15)$$

Graphically this means that at the point of intersection of the characteristics of the pump and the system, the tangent to

the characteristic of the system should pass at a larger angle to the horizontal axis than does the tangent to the characteristic of the pump. A smaller angle of inclination of the tangent to the characteristic of the system at the point of intersection of it with the characteristic of the pump can take place only when the left increasing branch of the pump characteristic is present, (from point Д to point Б on Fig. 5.13).

In spite of the presence of the left increasing branch of the pump characteristic, the statically unstable conditions

$$\frac{\partial H_c}{\partial Q} < \frac{\partial H}{\partial Q}$$

will take place only with such an intersection with the system characteristic H_c of the left branch of the pump characteristic H, as is shown on Fig. 5.13. The steeper the characteristic of the network, the less the probability of an unstable operation, and therefore the throttling, which leads to a steeper increase in the system characteristic, can serve as a means of the elimination of the surge phenomena.

Systems of the LPRE have steep characteristics of the required pressures of the system which intersect the axis of the abscissae (dot-dash curves H_c' and H_c'' on Fig. 5.13), and therefore the feed systems of LPRE with turbopump feed, as a rule, are stable, since condition (5.15) is observed.

Questions of the stability of the joint operation with a change in the frequency of the rotation of the TU are analogously examined (see source [12]). The curve of the change in the required pump power in the frequency of rotation usually proceeds more steeply than the curve of the change in the power of the turbine (see Fig. 5.12), and therefore the stability condition (self-regulation) in the joint operation of the turbine and pumps in the TU

$$\frac{\partial N_1}{\partial Q} \cdot \frac{\partial N_2}{\partial Q}.$$

as a rule, is maintained.

In the operation of the LPRE examples of the unstable operation of the pump systems can be encountered. The feed system of the LPRE is a complex hydraulic network consisting of several pumps, a turbine, a gas generator and pipelines. Despite the fact that the condition of the static stability of the pump with the pipelines connected to it is usually maintained, a change in conditions of the TU can lead to a loss in stability of the system as a whole.

Thus, for instance, in the diagram of the feed system given on Fig. 1.17, if the pump of the gas generator has a characteristic of the form given on Fig. 5.13, then in the work on the increasing branch of the pressure characteristic of this pump, i.e., in the section where $\partial H/\partial Q > 0$, the increase in the flow rate Q, which is accompanied by an increase in pressure H, leads to an increase in the gas flow rate through the turbine. This leads to an increase in the frequency of rotation of the TU. An increase in the frequency of rotation leads to a further increase in the flow rate Q and pressure H of the pump of the monopropellant and, consequently, leads to a further increase in the gas flow rate through the turbine, which, in turn, again leads to an increase in the frequency of rotation and to the loss in stability of the feed system.

A similar pattern can also take place in the operation of the gas generator of the turbine on basic components. In the work of the pump on the increasing branch of the pressure characteristic, the deviation with respect to the flow rate, which leads to a deviation with respect to the pressure of the

same sign, will involve a change in the gas flow rate through the turbine, in consequence of which an increase or decrease in the frequency of rotation of the turbopump unit and the loss in stability of the engine can occur.

The presence of the volume being changed in value of cavitation cavities, the presence of reverse currents at the inlet into the pump, and the compliance of pipelines increase the possibility for low-frequency auto-oscillations (see source [153]).

The concurrence of frequencies of oscillations of a rocket body and the feed system can lead to the longitudinal instability of the rocket (see sources [159, 161]).

5.2.5. JOINT OPERATION OF PUMPS IN THE FEED SYSTEM

In feed systems of the LPRE the series connection of pumps can be encountered. The booster pump installed directly at the tanks (see the diagram given on Fig. 3.97), and the basic pump are two series-connected installed pumps. The series connection of pumps can be used in engines with high combustion-chamber pressures.

In the cooling of the chamber by the fuel component it can prove to be unsuitable (from considerations of strength) to feed the component to the cooling jacket under a pressure equal to the pressure in the chamber. Having used the two series-connected pumps, it is possible to avoid the high pressures in the cooling jacket.

In a number of cases it is advisable to feed the gas generator of the turbine, which operates on the basic components, from

the individual pumps, into which part of the components from the basic pumps will consecutively enter (see Fig. 1.20). Finally, the series and parallel connections of the pumps can be encountered on test stands when using finished pump units for operation in the general network.

For the full representation of possible conditions in the system, which has a series or parallel connection of the pumps, it is necessary to examine the course of their characteristics in a joint operation. With substantially different pump characteristics it can be found that the connection of the pumps will not give increases in pressure or flow rate.

Let us examine the joint characteristic of two series-connected pumps I and II having different initial characteristics (Fig. 5.14). Adding the values of pressures with the same flow rate, we obtain the characteristic $H = f(Q)$ of the unit (hatched curve on Fig. 5.14).

With the flow rates $Q < Q_B$ the total pressure is greater than the pressure of any of the pumps. In order to plot the characteristic on section Q_B-a, it is necessary to know the pump characteristic II when $Q > Q_B$ (see Fig. 5.14) With flow rates which exceed Q_B (and such flow rates will be driven through pump II by pump I), in pump II the pressure is negative, i.e., the energy of the fluid is decreased; the pump will operate in braking conditions and absorb the energy, i.e., the energy will be selected from the fluid. A reduction in pressure in pump II will cause drop in the total pressure. Beginning from the flow rate equal to Q_B and at greater flow rates, the total pressure of the two pumps will be less than the pressure of one pump I. Consequently, for the system with characteristic H''_c the use of two series installed pumps is advantageous ($H_A > H_Д$),

and for the system with the characteristic H_c' such a connection is inexpedient ($H_Б < H_Е$). Before applying the series connection of two different pumps, one should always explain what their joint characteristic will be.

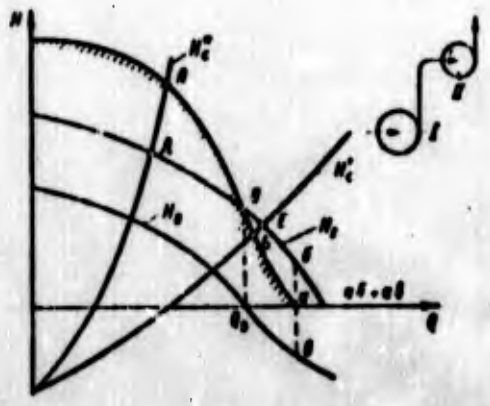

Fig. 5.14. Joint characteristic of two series-connected pumps.

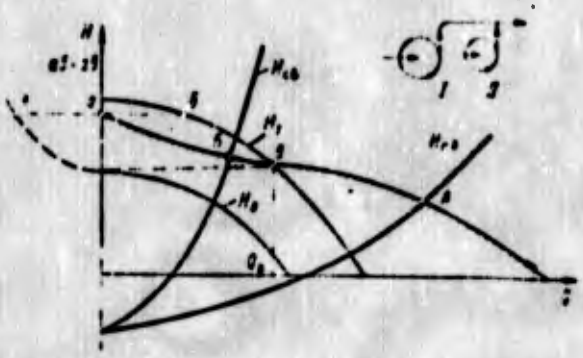

Fig. 5.15. Joint characteristic of two pumps operating in parallel.

Let us examine the joint characteristic of two different pumps with their connection in parallel (Fig. 5.15). In this case the flow rates are totaled, and the region of operational conditions is expanded to the side of the higher flow rates. Such a connection of the pumps is completely justified for the

required pressures of the system less than the pump pressure II with zero flow rate (on Fig. 5.15 the system characteristic H_{cA}). Beginning from the flow rate Q_B, which corresponds to the pressure for the pump when $Q = 0$, the fluid from the system being fed by the pump I with higher pressure will flow through pump II from the outlet to the inlet.

In order to plot a joint characteristic in the region of low flow rates, it is necessary to know the pump characteristic II with negative flow rates (see the dashed part of the pump characteristic H_{II} on Fig. 5.15). By comparing the rates of flow through both pumps at the same pressures, we will obtain the characteristic of their joint operation (see the hatched line 5A on Fig. 5.15). With the system characteristic H_{cB} the parallel connection of the two pumps which have different characteristics is inexpedient.

From the aforesaid it follows that for the solution of the question of the joint operation of two or more pumps having different ranges of pressures and flow rates, it is necessary to examine attentively the joint characteristic and determine the optimum operating modes of the system.

5.3. AXIAL AND RADIAL FORCES IN THE TU

The axial and radial forces which act on the rotor wheels of the pumps and turbine and impeller seals (see Section 2.7.4) are transmitted through the shaft to the bearings of the TU and load them. The selection of the bearings is produced by taking into account the acting forces, and therefore when designing the TU the values of the axial and radial forces should be known. For a decrease in the forces which act on the bearings, different design measures are used. We will examine some of them in this section.

5.3.1. AXIAL FORCES IN THE TU

5.3.1.1. Axial Force in the Pump

For determining the axial force from equation (2.72), it is necessary to know the pressure distribution p over the control surface (see Fig. 2.38). Let us examine the single-stage screw-centrifugal pump (see Fig. 2.38, I). Acting on the surface a-a is the pressure at the inlet into the screw conveyor p_1, while acting on surface б-б is the outlet pressure of the screw conveyor equal to $p_1 + \rho H_{ст.ш}$. Surfaces б-в and г-г are found in the cavity of high pressure, and high pressures affect them.

The cavity A (discharging cavity) detached by the seal (see Fig. 2.38, I) is connected by several openings B with the inlet into the centrifugal wheel. The pressure in the discharging cavity $p_{разгр}$ exceeds the pressure after the screw conveyor by the value of the pressure differential at the openings $\Delta p_{отв}$:

$$p_{разгр} = p_1 - \rho H_{ст.ш} + \Delta p_{отв}. \qquad (5.16)$$

Then the axial forces which act on the wheel will be virtually balanced.

I we displace the rear seal to a less radius, as is shown in 2.38, I, then the projection of the surface г-г on the p... perpendicular to the axis of rotation will become more than the projection of the surface б-в, and on the wheel there will emerge an axial force acting to the side of the inlet. The displacement of the seal to a larger radius gives a force acting to the side of the inlet. In this way it is possible to obtain axial force necessary in value and direction on the wheel. By this force it is possible to counterbalance, for example, the axial force acting on the turbine, and it is possible to unload the bearings of the TU from the axial force.

Let us note that for the elimination of the adverse effect on the flow in the centrifugal wheel of leakages fed through the openings B (see source [102]), the discharging cavity A is sometimes connected by the pipeline with the inlet into the pump. In this case the pressure $p_{разгр}$ will be equal to the sum of pressure at the inlet into the pump and the losses of pressure in coupling pipeline $\Delta p_{труб}$:

$$p_{разгр} = p_{вх} + \Delta p_{труб}. \tag{5.17}$$

In the single-stage pump the overflowings in the axial clearance between the wheel and the housing are directed from the periphery to the center. Therefore, the pressure p, which acts on the surface б-в and г-г (see Fig. 2.38, I), will be determined by expressions (3.40) and (3.41).

By knowing the pressure distribution with respect to elements of the control surface, it is possible to pass to the determination of the axial force in a single-stage pump. On the basis of that given above, the integral in equation (2.72) can be presented in terms of components of the axial force in the form

$$\int_{F_в} p\,dF_z = \frac{\pi d_{вт}^2}{4} p_1 + \pi\left(R_{з1}^2 - \frac{d_{вт}^2}{4}\right)(p_1 + \psi\rho_{ст.т}) - \\ -(R_{з1}^2 - R_{т1}^2)\,p_{разгр} + J_1 - J_2, \tag{5.18}$$

where

$$J_1 = \int_{F_z(б-в)} p\,dF_z; \qquad J_2 = \int_{F_z(г-г)} p\,dF_z.$$

With the aid of expressions (3.40) and (3.41) we will obtain the general equation for integrals J_1 and J_2 (making up the axial forces acting on the surface б-в and г-г, see Fig. 2.38, I):

$$J = \pi\rho\Pi_{ст}(r_2^2 - R_{з1}^2) - A, \tag{5.19}$$

where $H_{ст}$ is the static head of the wheel [see equation (3.39)]:

$$J = 2\pi r_2^2 \left\{ \frac{b_2}{r_2} \left[\left(1{,}96 \frac{R_y}{r_2} - 1\right)(p_2 - p_{r=0{,}85r_2}) - \right.\right.$$

$$\left.\left. - \left(2{,}3 \frac{R_y}{r_2} - 1\right)(p_2 - p_y) \right] + 0{,}85 (p_2 - p_{r=0{,}85r_2}) \right\}$$

- when $R_y < 0{,}85r_2$:

$$J = 4\pi r_2^2 \left[p_2 - p_{r=0{,}85r_2} \left(\frac{1 - (0{,}85)^2}{2} - \frac{1 - (0{,}85)^3}{3} \right) \right]$$

- when $R_y > 0{,}85r_2$.

The pressure differences $(p_2 - p_y)$ and $(p_2 - p_{r=0.85r_2})$ are determined respectively from equations (3.40) and (3.41). In the calculation of forces J_1 and J_2 we substitute the corresponding values of the radius of the seal R_y and coefficients α and β, depending on the flow rate per second of overflowings through the axial clearance (see Fig. 3.31). With an increase in the overflowings the pressure in the axial clearance falls, and the axial force acting on the surface б-в (or г-г, see Fig. 2.38, I) is decreased. Therefore with an equal radial extent of the surfaces б-в and г-г and different overflowings, the axial forces which act on these surfaces will be different.

Experience shows that with the aid of relations (2.72), (5.18) and (5.19), it is possible to calculate the axial force acting on the wheel of the pump under conditions which are found in the region of the flow rate $Q > (0.7\text{-}0.8)Q_p$. With low flow rates [$Q < (0.7\text{-}0.8)Q_p$] at the outlet from the wheel, the parameters are substantially nonuniform over the circumference. The wheel begins to operate partially: the flow from the inlet to the outlet occurs not in all the channels of the wheel, and in a number of channels the fluid flows from the outlet from the wheel to the inlet into it. With a decrease in the flow rate the quantity of such channels increases.

Under these conditions the flow in the axial clearances is shaped basically by the effect of the wheel disks and not by the overflowings and conditions on the outside diameter of the wheel. Then in the axial clearance the fluid will be rotated with an angular velocity equal to half of the angular velocity of the wheel, and the pressure distribution on the radius will be determined by equation (3.35). Bearing this in mind, for conditions $Q < (0.7\text{-}0.8)Q_p$ we will obtain the following expression for forces J_1 and J_2 acting on the surfaces б-в and г-г (see Fig. 2.38, I):

$$J = \pi\rho\left(r_2^2 - R_{c1}^2\right)\left[H_{c.c} - \frac{\omega^2}{16}\left(r_2^2 - R_{c1}^2\right)\right]. \qquad (5.20)$$

Having the relations (5.16) and (5.17) in mind, it is possible to convert expression (5.18) respectively for cases of the connection of the discharging cavity of the pump A (see Fig. 2.38, I) with the inlet into the wheel and the inlet into the pump:

$$\int_{F_a} p\,dF_a = \pi\left(R_{y1}^2 - R_{c1}^2\right)p_1 + \pi\rho\left(R_{c1}^2 + R_{y1}^2 - R_{c2}^2 - \frac{D_{вт}^2}{4}\right)H_{c.вт} - \pi\left(R_{c2}^2 - R_{c1}^2\right)\Delta p_{вт} - J_1 - J_2; \qquad (5.21)$$

$$\int_{F_a} p\,dF_a = \pi R_{c1}^2 p_1 + \pi\left(R_{c2}^2 - R_{c1}^2\right)p_{вх} + \pi\rho\left(R_{c1}^2 - \frac{D_{вт}^2}{4}\right)H_{c.вт} - \pi\left(R_{c1}^2 - R_{y1}^2\right)p_{вх.вт} - J_1 - J_2. \qquad (5.22)$$

In expressions (2.27), (5.21) and (5.22) all the components except the terms which contain pressures p_1 and $p_{вх}$, in kinematically similar conditions are changed similarly. Therefore, for the pump in kinematically similar conditions of its operation (Q/ω = const), values of the criterial complex (see sources [154]) will be identical:

$$\frac{R_e \quad \pi\left(R_{y1}^2 - R_{c1}^2 - R_{c2}^2\right)p_1}{\rho\omega^2}$$

- in the connection of the discharging cavity with the inlet into the centrifugal wheel or

$$R_z \; [illegible]$$

- in the connection of the discharging cavity with the inlet into the pump.

5.3.1.2. Axial Force in the Turbine

Let us discuss the determination of the axial force in the turbine (see Fig. 2.38, II). For calculation of the axial force according to equation (2.72), it is necessary to know the pressure distribution over surfaces a-a and б-б. Acting on the surface a-a is the outlet pressure from nozzle cascade p_1, and acting on surface б-б is the outlet pressure from the turbine p_2. Then on the surface a-a the axial force equal to $F_{z(a-a)}p_1$ will arise, and on the surface б-б - the axial force $F_{z(б-б)}p_2$. The equation (2.72) for the axial force on the turbine wheel takes the form

$$R_z = G(c_{1z} - c_{2z}) + \frac{\pi}{4}[D \; [illegible] \; d^2]p_1 - \frac{\pi}{4} \; [illegible] \; p_2 \qquad (5.23)$$

In the reaction turbine $p_1 > p_2$, and therefore on the wheel a considerable axial force appears, acting in the direction of the gas flow. In the impulse turbine pressures p_1 and p_2 are almost identical and the axial force is virtually close to zero. The latter fact is frequently the decisive one for the selection of the impulse turbine as a precombustion-chamber turbine of the LPRE, since in the reaction precombustion-chamber turbines these forces can be great. Let us note that in the partial impulse turbine $p_1 < p_2$ (see Section 4.5.2.2) the axial force will appear on the side of the outlet.

For a decrease in the axial force in the reaction axial-flow turbine, it is possible to provide in the disk several discharge openings depicted on Fig. 2.38, I by a dashed line. In the presence of the openings the pressures on both sides of the disk are equalized, and the axial force on the wheel is decreased. For a decrease in the gas leakages on the side of the inlet into the wheel through the openings, the axial clearance between the front surface of the disk and the housing should be packed. The use of discharging openings is undesirable, since the openings, in concentrating the stresses, reduce the strength of the turbine disk.

5.3.1.3. Axial Force in the Impeller Seal

In the design of the TU impeller seals of the shaft are frequently used (see Fig. 3.33). In connection with the fact that the wheel of the impeller seal (impeller) maintains a definite pressure differential, an axial force appears on it. Let us determine this force. Since through the impeller seal there is no discharge flow of fluid the expression for the axial force (2.72) will be rewritten in the form

$$R_z = \int_{F_z} p\,dF_z = \int_{F_{c-c}} p\,dF_z - \int_{F_{a-a}} p\,dF_z. \qquad (5.24)$$

The direction of the axial force on the side of the smooth disk of the impeller is taken as being positive.

In the axial clearance on the side of the finned disk (see Fig. 3.33, A) the fluid moves with an angular velocity $\omega_ж = \alpha^{1/2}\omega$, where ω is the angular velocity of the impeller (see Section 3.1.2.1). Then the pressure distribution in the space occupied by the fluid will be found by the integration of expression (3.34):

$$p = p_{1имп} + \rho \frac{\omega^2}{2}(r^2 - r_м^2). \qquad (5.25)$$

With the aid of expression (5.25) let us find the axial force acting on the finned disk. Bearing in mind that acting on the surface limited by radii $r_в$ and $r_м$ (see Fig. 3.33, A) is the pressure $p_{1имп}$, we obtain

$$P_{1осев} = \pi(r_{2имп}^2 - r_в^2)\, p_{1имп} + \pi\rho \frac{\omega^2}{4}(r_{2имп}^2 - r_м^2)^2. \qquad (5.26)$$

With great clearance on the side of the smooth disk pressure $p_{2имп}$ will act. With small clearance the fluid on the side of the smooth disk (in connection with the absence of the discharge flow) moves with an angular velocity equal to half of the angular velocity of the impeller ω. Therefore a change in the pressure along the radius will be found with the aid of the integration of relation (3.34):

$$p = p_{2имп} - \rho \frac{\omega^2}{8}(r^2 - r_в^2). \qquad (5.27)$$

With the aid of expression (5.27) it is possible to determine the force which acts on the surface 6-6 (see Fig. 3.33, A) (with a small clearance on the side of the smooth disk):

$$P_{2осев} = \int_{r_в}^{r_{2имп}} p 2\pi r\, dr = \pi(r_{2имп}^2 - r_в^2)\, p_{2имп} - \pi\rho \frac{\omega^2}{16}(r_{2имп}^2 - r_в^2)^2. \qquad (5.28)$$

Substituting equations (5.26) and (5.28) into (5.21), we will obtain the expression for the axial force acting on the impeller:

$$R_z = \pi(r_{2имп}^2 - r_в^2)(p_{2имп} - p_{1имп}) + \pi\rho \frac{\omega^2}{16}(r_{2имп}^2 - r_в^2)^2 - \pi\rho \frac{\omega^2}{8}(r_{2имп}^2 - r_м^2)^2. \qquad (5.29)$$

The radius of the fluid $r_ж$ is determined by a pressure differential on the impeller seal ($p_{2имп} - p_{1имп}$) with the aid of equation (3.45). With the maximum pressure differential $(p_{2имп} - p_{1имп})_{max}$ the axial clearance on the side of the finned disk will be completely filled with fluid ($r_ж = r_{1имп}$). By disregarding the distinction between the radii $r_{1имп}$ and $r_в$, let us find the equation for the axial force with an impeller completely filled with fluid. Having substituted relation (3.46) into expression (5.29), we obtain

$$R_z = \pi \frac{4m+1}{16} \rho \omega^2 (r_{2имп}^2 - r_в^2)^2. \qquad (5.30)$$

The axial thrust on the impeller can reach a significant magnitude.

Sometimes the impeller is made as one whole with the rear wheel disk (see source [18] and Fig. 3.91). Then the force on the wheel will be directed toward the inlet. Let us note that at small values of n_s^* such a design can raise the efficiency because of the prevention of leakages on the rear disk.

5.3.1.4. Unloading of the Rotor of the TU from Axial Force

In the TU the axial force which acts on the thrust bearing will be found with the vectorial addition of axial forces from the pumps, turbine and impellers of the impeller seals. For the unloading of the bearing from the axial force or for its decrease, selected in a definite manner is the position on the radius of rear seals of the centrifugal wheels of the pumps. Thus, it is possible to completely unload the bearing from the axial force only in one operating mode of the turbopump unit - as a rule, in design conditions. In order to carry out the unloading in other conditions close to design in the design of

the TU it is possible to provide an automatic flowing hydraulic unloading mechanism (see, for example, source [158]).

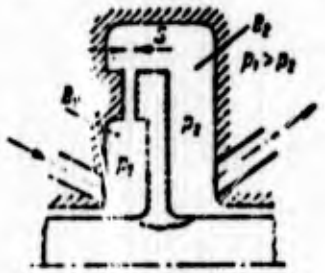

Fig. 5.16. Diagram of an automatic hydraulic unloading mechanism.

The operating principle of such a device can be explained in the following way. The element connected with the shaft, in the particular case, the disk (Fig. 5.16), divides by a small clearance S cavities B_1 and B_2. Cavity B_1 is connected with the high-pressure cavity of the pump; cavity B_2 has a sufficiently large volume and is connected with the low-pressure cavity. Let us assume that on the shaft there arose an axial thrust directed from right to left. The shaft will move under the action of this force, and the clearance S is decreased. Losses with the overflowing of the fluid through the clearance will increase (the process of throttling), and pressure p_2 will decrease. This decreases the force directed from right to left. The shaft is turned to the initial position. If there appears an axial force acting from left to right, the clearance S is increased, pressure p_2 increases, and the axial force decreases.

A shortcoming of the use of an unloading mechanism is in the decrease in the discharging efficiency of the pump connected with the additional hydraulic leakages of high pressure in the low-pressure cavity.

5.3.2. RADIAL FORCES IN THE TU

5.3.2.1. Radial Force in the Pump

In the centrifugal pump with a spiral branch the pressure and the velocity over the circumference of the outlet from the

wheel are uniform only near the design conditions. For flow rate less than the design, the cross sections of the spiral branch prove to be overexpanded. Therefore, the flow in the branch is braked, and the pressure along the length of the spiral collector increases. In this case the axial symmetry of the flow is disturbed - on the side of the outlet part of the collector increased pressure will act on the wheel. This leads to an emergence on the wheel of a radial force directed on the side of the exit sections of the collector.

For the flow rates which exceed the calculated flow rate, the cross sections of the branch become narrowed. The pressure along the length of the collector falls, and there appears a radial force directed on the side of the initial part of the collector. It is possible to determine the value and direction of the radial force on the basis of the theorem about a change in the momentum in a radial direction, if the pressure distribution and velocity over the circumference of the outlet from the wheel are known (see source [155]). Since in the designing of a pump the distribution of these parameters is not known, then for calculating the radial force R_r it is possible to use the empirical relation:

$$R_r = K_{R_r} \rho g H D_2 b_д, \qquad (5.31)$$

where K_{R_r} is the coefficient of radial force; H is the pump pressure in the conditions in question; $b_д$ is the width of the wheel taking into account the width of the disk (see Fig. 3.24).

The value K_{R_r} is determined from the power-speed coefficient n_s with the aid of the generalized experimental dependences (Fig. 5.17). The dependence of K_{R_r} on n_s for $Q = (0\text{-}1)Q_p$ is given in work [156], and for $Q = (1.3\text{-}1.5)Q_p$ it is obtained by means of the processing by the authors of experimental data of the source [156].

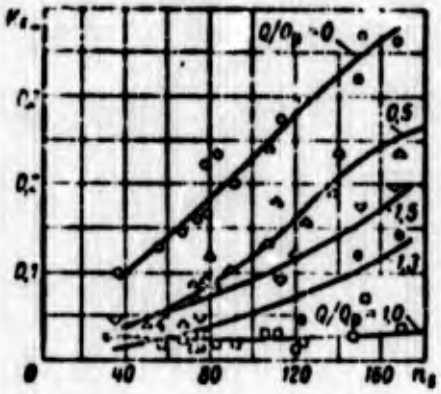

Fig. 5.17. Dependence of the coefficient of radial force on the power-speed coefficient and flow rate.

In design conditions the radial force R_r is not equal to zero ($K_{R_r} > 0$, see Fig. 5.17), since in design conditions there is a certain nonuniformity of pressures and velocities along the circumference of the wheel caused basically by the streamline flow of the "tongue." The minimum value of R_r is found in the region of the design conditions. The experimental data given in work [156] make it possible to evaluate the flow rate at which the radial force is minimum:

$$Q_{(R_r)_{min}} = (0{,}7 + 0{,}0025 n_s) Q_p. \qquad (5.32)$$

From equation (5.32) it follows that when $n_s < 110$-130 the flow rate at which the radial force is minimum will be less than the calculated and when $n_s > 110$-130 more than the calculated. Experimental data show that the less the value of n_s, the more the range of flow rates in which the radial force is close to the minimum value. The greatest nonuniformity of flow in the branch will be with low flow rates, when the wheel of the pump begins to operate partially. Therefore, the radial force R_r reaches a maximum value at zero flow rate ($Q = 0$). Having divided the expression (5.31) by $\rho\omega^2$, we obtain

$$\frac{R_r}{\rho\omega^2} = K_{R_r} D b_2 \frac{H}{\omega^2}. \qquad (5.33)$$

In kinematically similar conditions (Q/ω = idem) values of H/ω^2 are identical (see Section 3.1.4.3), and values of the coefficient K_{R_r} will be identical, since when Q/ω = idem and Q/Q_p = idem.

From expression (5.33) it follows that in kinematically similar conditions of the pump (Q/ω = idem) values of criterial complex $R_r/\rho\omega^2$ will be equal.

Let us examine the possibilities for a decrease in the radial force. From equation (5.31) it follows that the radial force is decreased with a decrease in the area of the outlet from the wheel $\pi D_2 b_д$. It is possible to decrease the radial force by a change in the design of the outlet branch device of the pump.

Fig. 5.18. Diagram of a spiral branch with an additional blade: 1-additional blade.

Figure 5.18 depicts a spiral branch with an additional wall (blade) 1. The setting of such a blade provides the axial symmetry of the flow areas of the branch along the circumference of the wheel. This facilitates the setting of the axial symmetry of the flow parameters along the circumference of the wheel. However, as an experiment shows (see source [155]), the full symmetry is not provided in this case. But the value of the radial force at such a branch is decreased in comparison with the branch without an additional blade.

Leading to a reduction in the radial force are also the setting into the branch of a vaned diffuser (see Fig. 3.19) and the use in the spiral branch of a vaneless diffuser of considerable

radial extent (D_2/D_2^1 = 1.3-1.4) - in both cases the axial symmetry of the initial section of the branch will take place.

5.3.2.2. Radial Force in the Turbine

In turbines the radial force will appear with the partial gas feed. Let us examine the axial-flow turbine, assuming that the pressure along the outside diameter of the wheel is uniform. With the partial gas feed, emerging from the nozzle cascade, there is flow around only those impeller vanes which are found on the arc of the feed. Therefore, the circular forces on the blades will give the moment with respect to the axis of rotation and radial force. Thus, the force dR_u (Fig. 5.19) will give the moment

$$dM = r_{cp} dR_u \qquad (5.34)$$

and the radial force $$dR_r = dR_u. \qquad (5.35)$$

Let us assume that each element of the arc of the feed creates the same value of the moment. Then

$$dM = \frac{M}{\varphi_1} d\varphi = \frac{M}{2\pi} d\varphi. \qquad (5.36)$$

The moment M is equal to the moment on the circumference of the wheel with the subtraction of the moment of resistance caused by losses to "ejection." The moment M differs from the moment on the shaft of the turbine M_T by the value of the moment caused by the friction of the disk against the gas and ventilation losses. By disregarding these losses, let us write approximately:

$$M \approx M_1 = \frac{N_T}{\omega}, \qquad (5.37)$$

where N_T is the power of the turbine.

Fig. 5.19. Calculation of the radial force in an axial-flow partial-admission turbine.

In using expressions (5.34), (5.35), (5.36) and (5.37), we find

$$dR_r = \frac{N_1}{2\pi u} d\varphi. \qquad (5.38)$$

The projections of the force dR_r on the x and y axis:

$$dR_{rx} = dR_r \cos\varphi = \frac{N_1}{2\pi u} \cos\varphi d\varphi; \qquad (5.39)$$

$$dR_{ry} = -dR_r \sin\varphi = -\frac{N_1}{2\pi u} \sin\varphi d\varphi. \qquad (5.40)$$

Projections of the resulting radial force R_r will be found by integration over the arc of the feed of dR_{rx} and dR_{ry} respectively:

$$R_{rx} = \frac{N_1}{2\pi u} \int_0^{\varphi_0} \cos\varphi d\varphi = \frac{N_1}{2\pi u} \sin\varphi_0 = \frac{N_1}{2\pi u} \sin 2\pi i; \qquad (5.41)$$

$$R_{ry} = -\frac{N_1}{2\pi u} \int_0^{\varphi_0} \sin\varphi d\varphi = -\frac{N_1}{2\pi u} (1 - \cos\varphi_0) = -\frac{N_1}{2\pi u} (1 - \cos 2\pi i). \qquad (5.42)$$

The radial force R_r, which acts on the wheel of the partial axial-flow turbine, will be equal to:

$$R_r = \sqrt{R_{rx}^2 + R_{ry}^2},$$

or, after the substitution of expressions (5.41) and (5.42),

$$R_r = \frac{N_1}{\pi} \sqrt{\frac{1}{2i} - \cos 2\pi i}. \qquad (5.43)$$

With a decrease in the degree of the admission ε the radial force R_r increases. The direction of the radial force R_r will be determined graphically according to its projections of R_{rx} and R_{ry}.

It is possible to decrease the radial force R_r down to zero by means of the dividing of one arc of the gas feed into two symmetrically located arcs of the feed. However, with this the efficiency of the turbine will decrease (see Section 4.5.2.2). In a radial-flow turbine with partial admission the radial force can be determined if the pressure distribution along the circumference of the inlet into the wheel is known. Reliable data on the pressure distribution can be obtained by experimental means.

Having determined the values of the radial forces which act on wheels of the pumps and turbine, it is possible to find radial stresses on the bearings. For this one should examine the shaft as a beam located on supports (bearings).

5.4. RELATIONSHIP OF THE MASS OF THE TU WITH HYDRODYNAMIC PARAMETERS OF THE FEED SYSTEM

The mass of the turbopump unit is largely determined by hydrodynamic parameters of the unit.

Elements of the feed, branches, wheels, etc., of the pumps and the turbine of the TU can be conditionally divided into complete cylinders and disks. The mass of the hollow cylinder is defined as

$$m_{цил} = \rho_м \pi D_{цил} \delta_{цил} l_{цил} \text{ [кг]}. \qquad (5.44)$$

where $\rho_м$ is the density of the material; $D_{цил}$, $\delta_{цил}$, $l_{цил}$ - characteristic diameter, thickness and length of the cylinder, respectively.

The mass of the disk $m_д$ can be expressed in the following way:

$$m_д = \rho_м \frac{\pi D_д^2}{4} \delta_д, \qquad (5.45)$$

where $D_д$ and $\delta_д$ are the characteristic diameter and thickness of the disk, respectively.

If we refer, for example, for the pump of thickness $\delta_{цил}$ and $\delta_д$ to its characteristic thickness $\delta_н$, and the remaining linear dimensions - to the characteristic diameter of the pump $D_н$, then expressions (5.44) and (5.45) are converted into the following form:

$$m_{цил} = \rho_м \pi \bar{D}_{цил} \bar{l}_{цил} \bar{\delta}_{цил} l D_н^2 \delta_н = \rho_м K_{цил} l D_н^2 \delta_н;$$
$$m_д = \rho_м \frac{\pi}{4} \bar{D}_д^2 \bar{\delta}_д l D_н^2 \delta_н = \rho_м K_д l D_н^2 \delta_н.$$

The mass of the pump is expressed in the form of the sum of masses of cylindrical and disk elements:

$$m_н = \sum m_{цил} + \sum m_д = l D_н^2 \delta_н (\sum \rho_м K_{цил} + \sum \rho_м K_д), \qquad (5.46)$$

or, having designated the parenthesis in expression (5.46) by coefficient $K'_н$ we will obtain

$$m_н = K'_н l D_н^2 \delta_н. \qquad (5.47)$$

In the mass of the pump a considerable portion is occupied by casings of the feed and branch. Therefore, the characteristic dimensions of the pump $D_н$ and $\delta_н$, which enter into expression

(5.47), will be determined according to the feed and the branch of the pump.

It is natural that at the high pressures developed by pumps of the LPRE, the mass of the discharge devices will always comprise a large portion of the mass of the pump. The effect of feed on the mass of the pump will be considerable with great flow rates of the component, when the feed has large geometric dimensions, and less considerable at low flow rates.

Let us determine the characteristic diameter $D_н$ with respect to the feed and the thickness $\delta_н$ with respect to the branch. The dimensions of the feed depend on the volumetric flow rate, and therefore it is possible to write:

$$\frac{\pi D_н^2}{4} = K_{подв} \frac{Q}{c_{подв}}, \qquad (5.48)$$

where $c_{подв}$ is the characteristic velocity of the fluid in the feed.

The characteristic thickness of the branch which is loaded by considerable forces from internal pressure $p_{отв}$ will be determined according to the equation known from a course on the strength of materials for a short cylinder loaded by internal pressure:

$$\delta_н = \frac{p_{отв} D_{отв}}{R_z}, \qquad (5.49)$$

where R_z is the tensile strength of the material.

The diameter of the branch $D_{отв}$ in the relation (5.49) is determined by the diameter of the wheel of the pump D_2, and the pressure $p_{отв}$ can be taken as proportional to ρH; then expression (5.49) will take the following form:

$$\delta_н = \frac{K'_{отн}(HD_2)^3}{R_t}, \qquad (5.50)$$

or, having substituted for D_2 expression (3.223), after the conversions we obtain

$$\delta_н = \frac{K_{отн}QH^2}{\omega}. \qquad (5.51)$$

Having substituted expressions (5.48) and (5.51) into the relation (5.47), after uniting the constants of the pump into the coefficient of the pump, we obtain

$$\eta_н = K_н \frac{QH^{3/2}}{\omega}. \qquad (5.52)$$

From equation (5.52) the effect of the hydrodynamic parameters of the pump on its mass is clearly evident. With an increase in the pump pressure H and flow rate Q and with a decrease in the frequency of the rotation ω the mass of the pump increases.

Such an effect of the hydrodynamic parameters is explained in the following manner. With an increase in pressure the pressure in the pump increases which requires a thickening of the housing of the branch. Besides this, for the creation of high pressure a large diameter of the centrifugal wheel is necessary, and therefore, in this case dimensions of the branch increase. A decrease in the frequency of rotation ω also leads to an increase in the dimensions of the wheel and branch. The effect of the flow rate Q on the mass of the pump is developed basically in terms of dimensions of the feed connecting piece. With an increase in Q the dimensions of the connecting piece increase.

Assuming that the oxidizer and fuel pumps have close values of $K_н$, it is possible with the aid of equation (5.52) to write the expression for the total mass of the pumps:

$$m_{ок} + m_{гор} = \frac{K_н}{\omega}(\varrho_{ок} Q_{ок} H_{ок}^{1/2} + \varrho_{гор} Q_{гор} H_{гор}^{1/2}). \qquad (5.53)$$

where subscripts "ок" and "гор" refer to the oxidizer and fuel pumps, respectively.

Having expressed the mass of the turbine of the TU in the form of a fraction of the total mass of the pumps, it is possible to obtain the following equation for the mass of the TU:

$$m_{ТНА} = \frac{K_{ТНА}}{\omega}(\varrho_{ок} Q_{ок} H_{ок}^{1/2} + \varrho_{гор} Q_{гор} H_{гор}^{1/2}). \qquad (5.54)$$

In equation (5.54) it is possible to assume that $K_{ТНА} = (0.3\text{-}0.35) \times 10^{-3}$ s^3/m^3 for single-shaft TU with one turbine and single-stage pumps with a one-way inlet, which have a total volumetric flow rate of $(Q_{ок} + Q_{гор}) > 0.06\text{-}0.07$ m^3/s.

With the less flow rates of the components the effect of the flow rate on the mass of the TU proves to be insignificant. For such a TU equation (5.54) takes the following form:

$$m_{ТНА} = \frac{K_{ТНА}}{\omega}(\varrho_{ок} H_{ок}^{1/2} + \varrho_{гор} H_{гор}^{1/2}). \qquad (5.55)$$

where $K_{ТНА} = (0.12\text{-}0.18) \cdot 10^{-4}$ $[s^2]$.

For pumps with a two-way inlet values of $K_{ТНА}$ should be accepted at 10-15% more.

Equations (5.54) and (5.55) make it possible, in the first approximation, to estimate the mass of the turbopump unit according to hydrodynamic parameters of the feed system, without resorting to a designer's study of the TU. With the aid of these

parameters it is possible in the calculation of different variants of the TU to estimate the effectiveness of each of the variants according to the mass of the design.

5.5. EFFICIENCY OF THE TURBOPUMP UNIT

We will understand by efficiency of the turbopump unit the ratio of the sum of the net power of the pump to the available adiabatic power of the turbine:

$$\eta_{\text{ТНА}} = \frac{\sum G_i H_i}{G_т L^*_{ад}}.$$

For the simplest TU, which consists of a turbine and two pumps - oxidizer and fuel pumps, we will obtain

$$\eta_{\text{ТНА}} = \frac{G_{ок} H_{ок} + G_{гор} H_{гор}}{G_т L^*_{ад}}.$$

Having expressed, respectively, the products of GH in terms of $N_н \eta_н$ and $G_т L^*_{ад}$ in terms of $N_т/\eta_т$, we will obtain

$$\eta_{\text{ТНА}} = \left(\frac{N_{ок}}{N_т} \eta_{ок} + \frac{N_{гор}}{N_т} \eta_{гор} \right) \eta_т.$$

If we assume that the efficiency of the pumps is equal to $\eta_{ок} = \eta_{гор} = \eta_н$, then the efficiency of the TU will be the product of the efficiency of the turbine by the efficiency of the pump, since $N_т = N_{ок} + N_{гор}$,

$$\eta_{\text{ТНА}} = \eta_н \eta_т.$$

Depending on the values of the efficiency of the pumps and turbine, the value of the efficiency of the TU can lie within limits of 0.25-0.45.

BIBLIOGRAPHY

A. Recommended bibliography

1. Абианц В. Х. Теория газовых турбин реактивных двигателей. Изд. 2-е. М., «Машиностроение», 1965.

2. Дейч М. Е. и Самойлович Г. С. Основы аэродинамики осевых турбомашин. М., Энергоиздат, 1959.

3. Дейч М. Е. и Трояновский Б. М. Исследование и расчет ступеней осевых турбин. М., «Машиностроение», 1964.

4. Дейч М. Е., Филиппов Г. А. и Лазарев Л. Я. Атлас профилей решеток осевых турбин. М., «Машиностроение», 1965.

5. Емин О. Н. Выбор параметров и расчет осевых активных турбин для привода агрегатов. М., Оборонгиз, 1962.

6. Жирицкий Г. С. и др. Газовые турбины двигателей летательных аппаратов. М., «Машиностроение», 1971.

7. Зарянкин А. Е. и Шерстюк А. Н. Радиально-осевые турбины малой мощности. М., Машгиз, 1963.

8. Кириллов И. И. Теория турбомашин. Л., «Машиностроение», 1964.

9. Ломакин А. А. Центробежные и осевые насосы. Л., «Машиностроение», 1966.

10. Матвеев Г. А. и др. Аэродинамика проточной части судовых турбин. М., Судпромгиз, 1961.

11. Митрохин В. Т. Выбор параметров и расчет центростремительных турбин. М., «Машиностроение», 1966.

12. Мошкин Е. К. Нестационарные режимы работы ЖРД. М., «Машиностроение», 1970.

13. Овсянников Б. В. Теория и расчет насосов жидкостных ракетных двигателей. М., Оборонгиз, 1960.

14. Певзнер Б. М. Судовые центробежные и осевые насосы. М., Судпромгиз, 1958.

15. Пфлейдерер К. Лопаточные машины для жидкостей и газов. (Пер. с нем.). М., Машгиз, 1960.

16. Самойлович Г. С. и Трояновский Б. М. Переменный режим паровых турбин. М., Госэнергоиздат, 1955.

17. Самойлович Г. С. и Трояновский Б. М. Паровые турбины. Сборник задач. М., Госэнергоиздат, 1957.

18. Степанов А. Центробежные и осевые насосы. (Пер. с англ.). М., Машгиз, 1960.

19. Степанов Г. Ю. Основы теории лопаточных машин комбинированных и газотурбинных двигателей. М., Машгиз, 1958.

20. Степанов Г. Ю. Гидродинамика решеток турбомашин. М., Физматгиз, 1962.

21. Стечкин Б. С. и др. Теория реактивных двигателей. Лопаточные машины. М., Оборонгиз, 1956.

22. Траупель В. Тепловые турбомашины. (Пер. с нем.). М., Госэнергоиздат, 1961.

23. Холщевников К. В. Теория и расчет авиационных лопаточных машин. М., «Машиностроение», 1970.

24. Шерстюк А. Н. Паровые турбины. М., «Энергия», 1967.

Б. Used bibliography

Chapter 1

25. Байбаков О. В. К вопросу о разработке теоретических методов расчета шнековых насосов. Труды ВНИИНЕФТЕМАШ. Вып. 35. М., «Машиностроение», 1967.

26. Васильцов Э. А. и Шевелев В. В. Герметические электронасосы. Л., «Машиностроение», 1968.

27. Добровольский М. В. Жидкостные ракетные двигатели. М., «Машиностроение», 1968.

28. Перельман Р. Г. и Поликовский В. Н. Основы теории насосов дискового типа. Известия АН СССР. Серия «Энергетика и транспорт», 1963, № 1.

29. Раздолин М. В. Агрегаты воздушно-реактивных двигателей, жидкостные объемные насосы. М., Оборонгиз, 1959.

30. «Aeronautique et astronautique», 1968, n°. 3.

31. «Aviation Week», 1962, vol. 76, No. 14.

32. «Aviation Week», 1964, vol. 79, No. 11.
34. «Interavia Air Letter», 1958, No. 6558.
34. «Journal of Spacecraft and Rockets», 1965, No. 1.
35. «Journal of the Royal Aeronautical Society», 1961, No. 605
36. «Weltraumfahrt», 1956, Nr. 2.

Chapter 2

37. Абрамович Г. Н. Прикладная газовая динамика. М., «Наука», 1969.

38. Борисенко А. И. Газовая динамика двигателя. М., Оборонгиз, 1962.

39. Боровский Б. И. О свойствах коэффициента быстроходности центробежных насосов. — «Энергомашиностроение», 1958, № 11.

40. Боровский Б. И. и Овсянников Б. В. Параметры обращения напора и к. п. д. центробежных насосов. — «Вестник машиностроения», 1957, № 4.

41. Быков Н. Н. Исследование турбин с различными законами профилирования. Известия ВУЗов. Серия «Авиационная техника», 1961, № 1.

42. Лорфман Л. А. Гидродинамическое сопротивление и теплоотдача вращающихся тел. М., Физматгиз, 1960.

43. Караваев А. Е. Очерки по истории развития лопастных насосов. М., Машгиз, 1958.

44. Кромов А. Г. Влияние периодической нестационарности потока в турбинной ступени на потери активных лопаток. «Известия Всесоюзного теплотехнического института», № 1. М., Госэнергоиздат, 1950.

45. Марков Н. М. Теория и расчет турбинных ступеней. М., Машгиз, 1963.

46. Мидзумати Н. Исследование радиальных газовых турбин. (Пер. с япон.). М., Машгиз, 1961.

47. Миролюбов Н. В. Расчет характеристик осевых предвключенных насосов. Известия ВУЗов Серия «Авиационная техника», 1959, № 1.

48. Никитин А. А. и Зыков В. Н. К исследованию аэродинамики проточной части центробежных компрессоров методом электромоделирования. Ученые записки аспирантов и соискателей ЛПИ. Серия «Энергомашиностроение». Л., «Машиностроение», 1964.

49. Овсянников Б. В. Сила напора колеса радиальной машины с моментом кориолисовых сил инерции. Известия ВУЗов, Серия «Авиационная техника», 1961, № 2.

50. Овсянников Б. В. и Боровский Б. И. К вопросу о передаче энергии в центробежных и осе-центробежных насосах циркуляционными и кориолисовыми силами. Известия ВУЗов. Серия «Авиационная техника», 1960, № 4.

51. Покровский Б. В. и Жемчугов В. Н. О влиянии шероховатости на энергетические и виброакустические характеристики центробежных насосов. Труды ВНИИГидромаш. Вып. 36. М., «Машиностроение», 1967.

52. Рис В. Ф. Центробежные компрессорные машины. М., «Машиностроение», 1964.

53. Седов Л. И. Методы подобия и размерности в механике. М., «Наука», 1965.

54. Селезнёв К. П., Подобуев Ю. С. и Анисимов С. А. Теория и расчет турбокомпрессоров. М., «Машиностроение», 1968.

55. Суханов Л. Я. Работа лопастных насосов на вязких жидкостях. М., Машгиз, 1952.

56. Тарышкин В. Г. Исследование законов закрутки турбинного облопачивания. М., Машгиз, 1953.

57. Уваров В. В. Профилирование длинных лопаток газовых и паровых турбин. М., Оборонгиз, 1945.

58. Целиков В. А. Моделирование турбин тяжелым газом. Известия АН СССР, ОТН, 1957, № 10.

59. Чебаевский В. Ф. и др. Отклонение потока на выходе из колеса центробежного насоса. — «Энергомашиностроение», 1969, № 2.

60. Черняк А. П. Зависимость коэффициента р реактивного колеса центробежного насоса от его геометрических параметров и режима работы. Сб. «Лопаточные машины и струйные аппараты». Вып. 1. М., «Машиностроение», 1965.

61. Шерстюк А. Н. Расчет течения в элементах турбомашин. М., «Машиностроение», 1967.

62. Шлихтинг Г. Теория пограничного слоя. (Пер. с нем.). М., Изд-во иностр. лит., 1956.

63. SAE Nat. Aeronaut. Reprints, 1959, No. 545.

64. Байбаков О. В. Кавитация в отводе центробежного насоса. Сб. МВТУ «Гидромашиностроение», М., Машгиз, 1960.

65. Белоусов [illegible] Определение осевого расхода жидкости при работе [illegible]. Известия [illegible]. Серия «Авиационная техника», 1961, № 3.

66. Васильев А. П. и др. Основы теории и расчета жидкостных ракетных двигателей. М., «Высшая школа», 1967.

67. Вероцкая О. А. Распределение давлений в боковых полухах центробежных насосов с учетом утечек. Переговой научно-технический и производственный опыт. Изд. ВНИИГПН МН СССР, 1957.

68. Вуд Дж. и др. Влияние зазора по свободным кромкам лопаток у открытых колес центробежных насосов. Trans. ASME. Серия D (Русский перевод), 1965, № 4.

69. Голубев А. П. Современные уплотнения вращающихся валов, М., Машгиз, 1963.

70. Горгидзиани С. А. и Зимницкий В. А. О расчете осевых предвключенных колес для питательных насосов. — «Энергомашиностроение», 1967, № 4.

71. Дворниченко В. В. К вопросу о скорости звука в двухфазной [illegible]. — «Теплоэнергетика», 1966, № 10.

72. Джекобсон Дж. О механизме срыва напора на входном участке [illegible] насосов. Trans. ASME. Серия D (Русский перевод), 1964, № 2.

73. Лиманг П. М. Расчет спрямляющего аппарата центробежных [illegible] и насосов. Научные доклады высшей школы. Серия «Энергетика», № 2, Минск, 1960.

74. Лумон В. И. Повышение антикавитационных свойств центробежных ступеней насосов при помощи осевых предвключенных ступеней. — «Теплоэнергетика», 1957, № 4.

75. Лумон В. И. Расчет центробежных ступеней насосов с предвключенными осевыми колесами, обладающими высокими антикавитационными свойствами. — «Теплоэнергетика», 1959, № 6.

76. Лумон В. И. и Пешкин М. А. Некоторые результаты исследования работы осевых винтовых колес. — «Энергомашиностроение», 1962, № 2.

77. Ефимакова В. Ф. Спиральный отвод центробежной компрессорной ступени. Труды ВНИИКИМАШ, Вып. 1. М., Машгиз, 1959.

78. Ершов Н. С. О возможности моделирования кавитационных явлений при испытаниях центробежных насосов на газах. Известия ВУЗов. Серия «Авиационная техника», 1967, № 4.

79. Ершов Н. С. О механизме кавитации в центробежных насосах. Известия ВУЗов Серия «Авиационная техника», 1959, № 3.

80. Кинг Дж. Испытания насосов на воздухе. Trans. ASME. Серия А (Русский перевод), 1958, № 2.

81. Королев П. П. Исследование работы жидкостного эжектора. Труды ЦИАМ. М., Оборонгиз, 1948.

82. Локшин Н. Л. Применение результатов исследования вращающихся круговых решеток к аэродинамическому расчету колес центробежных вентиляторов. «Промышленная аэродинамика». Вып. 25. М., Оборонгиз, 1963.

83. Махин В. А., Присняков В. Ф., Белик И. П. Динамика жидкостных ракетных двигателей. М., «Машиностроение», 1969.

84. Михеев Н. П. Моделирование работы центробежного насоса на воздухе. Труды МАИ № 95, М., Оборонгиз, 1958.

85. Никитин А. А., Селезнев К. П. и Шкарбуль С. П. Исследование входных патрубков центробежных компрессоров. — «Энергомашиностроение», 1966, № 9.

86. Numachi F. Влияние шероховатости поверхности на кавитационные характеристики гидропрофиля. Trans. ASME. Серия D (Русский перевод), 1965, № 2; 1967, № 1.

87. Овсянников Б. В. и Чебаевский В. Ф. Некоторые результаты испытаний высокооборотных центробежных насосов. Известия ВУЗов. Серия «Авиационная техника», 1958, № 2.

88. Перник А. Д. Проблемы кавитации. М., Судпромгиз, 1963.

89. Потиковский В. Н., Перельман Р. Г., Иванов Ю. А. Об одной возможности уменьшения длины эжектора. — «Теплоэнергетика», 1957, № 9.

90. Полоцкий Н. Д. О коэффициенте сопротивления кольцевых цилиндрических щелей. Сб. научно-технической информации по гидромашиностроению. Труды ВНИИГИДРОМАШ Вып. 5 (11). М., Машгиз, 1959.

91. Полоцкий Н. Д., Богницкая Ф. А., Агульник Р. М. Расчет отводящих устройств центробежных насосов. М., «Машиностроение», 1967.

92. Райт М. Расчет и результаты экспериментальных исследований [illegible] с высокими кавитационными коэффициентами быстроходности. Trans ASME. Серия А (Русский перевод), 1964, № 2.

91. Руднев С. С. и Матвеев Н. В. Некоторые соображения по проблеме увеличения оборотности лопастных насосов. Труды ВНИИГИДРОМАШ. Вып. 32. М., Машгиз, 1963.

94. Семенов Н. И. и Костерин С. И. Результаты исследования скорости звука в движущихся газожидкостных смесях. — «Теплоэнергетика», 1964, № 6.

95. Столярский М. Т. Обобщенная зависимость для определения потерь в спиральной камере центробежного нагнетателя. — «Теплоэнергетика», 1965, № 8.

96. Стриплинг Л. и Акоста А. Кавитация в лопаточных насосах. Trans. ASME. Серия А (Русский перевод), 1962, № 3.

97. Уилд Р. и Акоста А. Исследование кавитирующих решеток профилей. Trans. ASME. Серия D (Русский перевод), 1967, № 4.

98. Фаррел Е. и Кинг Дж. Переходные характеристики предвключенного насоса с приводом от гидротурбины. — «Вопросы ракетной техники», 1970, № 5.

99. Чебаевский В. Ф. К вопросу о механизме кавитации в центробежных насосах. — «Теплоэнергетика», 1957, № 9.

100. Черных А. П. Влияние геометрических параметров и режима работы на величину коэффициента μ рабочего колеса центробежного насоса. Сб. «Лопаточные машины и струйные аппараты». Вып. 3. М., «Машиностроение», 1968.

101. Шапиро А. С. и Некл[illegible] гидравлического торможения при входе в колесо центробежного насоса. — «Вестник машиностроения», 1968, № 5.

102. Шемель В. Б. Оптимальные параметры, определяющие кавитационные качества центробежных насосов. Труды ВНИИГИДРОМАШ. Вып. 22. М., Машгиз, 1968.

103. Шатс Г. и Брапкар Ч. Многоступенчатый аксиальный жидкостный насос с разрезными лопатками. Trans. ASME. Серия А (Русский перевод), 1966, № 2.

104. Шкловер Г. Г. и Росинский А. З. Экспериментальное исследование водоструйных эжекторов, работающих на кипящей воде. — «Энергомашиностроение», 1966, № 4.

105. Шнидман В. Н. О работе центробежных насосов с отводами различной пропускной способности. — «Энергомашиностроение», 1966, № 3.

106. Яловой Н. С. К вопросу об исследовании всасывающих патрубков центробежных насосов. Труды ЛКИ. Вып. 47. Л., «Машиностроение», 1965.

107. AIAA Reprint, 1966, No. 66-621.

108. Aeronaut. Research Council Papers, 1961, No. 527.

109. «Advances in Cryogenic Eng». 1960, No. 12.

110. «Missiles and Rockets», 1963, vol. 12, No. 2.

111. Roder H. Weber L., Goodwin R. Thermodynamic and Related Properties of Parahydrogen from the Triple Point to 100° K at Pressures to 340 Atmospheres. National Bureau of Standarts, Washington, 1965.

112. «Technology Week», 1967, vol. 30, No. 11.

113. «The Journal of the Royal Aeronautical Soc., 1961, vol. 65, No. 612.

114. Trans. Japan Soc. Mech. Engrs., 1964, No. 210.

Chapter 4

115. Гольцев В. В. Потери в сверхзвуковых сопловых решетках на нерасчетных режимах. — «Инженерный журнал», 1963, № 3.

116. Губарев А. В. Исследование рабочих решеток турбин при сверхзвуковых скоростях. Известия ВУЗов. Серия «Авиационная техника», 1963, № 2.

117. Давыдов А. Б. и Епифанова В. И. Экспериментальное исследование решетки профилей-тандем с парциальным подводом газа. Труды ВНИИГИДРОМАШ. Вып. [illegible]. «Машиностроение», 1965.

118. Дейч М. Е. Техническая газодинамика. М.-Л., Госэнергоиздат, 1961.

119. Дейч М. Е. и Губарев А. В. Исследование рабочих решеток турбин при сверхзвуковых [illegible]. — «Теплоэнергетика», 1958, № 12.

120. Дейч М. [illegible] Шейнкман А. Г. К определению оптимальной величины первой ступени обводненной турбинной ступени. — «Теплоэнергетика», 1962, № 1.

121. Деннис Г. Коттас Г. и Моди А. Влияние числа Re на эффективность лопаточных машин. — «Вопросы ракетной техники», 1952, № 4(10).

122. Емин О. Н. и Моравский М. В. Исследование кольцевых активных решеток при частичном подводе газа. — «Теплоэнергетика», 1967, № 8.

121. Зайдель Р. Э. Турбомашины [illegible] установок. М., Машгиз, 1940.
124. Залу Г. А. и Замгинадзе В. В. Тепловой расчет паровых турбин. М., Машгиз, 1961.
125. Зарянкин А. Е. и Зарянкин О. Е. К расчету потерь в осевых турбинах, вызванных радиальным зазором. Известия ВУЗов. Серия «Энергетика», 1965, № 1.
126. Заикворонов В. Н. и Подгорнов В. А. Исследование парциальных турбин. Известия ВУЗов. Серия «Авиационная техника», 1964, № 2.
127. Зарянкин А. Е. и Зарянкин М. Ф. О влиянии зазора между корпусом и рабочим колесом на к. п. д. ступени радиально-осевой турбины. — «Энергомашиностроение», 1964, № 3.
128. Зарянкин А. Е., Шерстюк А. Н. и Зарянкин М. Ф. Некоторые пути повышения экономичности радиально-осевых турбин. — «Теплоэнергетика», 1962, № 5.
129. Кириллов И. И. и Клячкин А. Л. Потери энергии в турбинных ступенях с бандажом и без бандажа. — «Теплоэнергетика», 1961, № 2.
130. Ключников Г. М. и Струнки В. А. О влиянии радиального зазора на эффективность турбинной ступени. Известия ВУЗов. Серия «Авиационная техника», 1966, № 4.
131. Ковалевская А. Е. Влияние степени парциальности на работу центростремительной турбины. Известия ВУЗов. Серия «Авиационная техника». 1966, № 3.
132. Крылов Е. П. и Сирицкий Я. Л. О влиянии зазора между рабочими лопатками и корпусом радиальной турбины на ее показатели. Известия ВУЗов. Серия «Энергетика», 1965, № 7.
133. Курзон А. Г. и Левенберг В. Д. О выборе параметров парциальной ступени малой мощности. Известия ВУЗов. Серия «Авиационная техника», 1967, № 3.
134. Курзон А. Г. и др. Исследование парциальных сверхзвуковых турбинных ступеней. — «Энергомашиностроение», 1964, № 10.
135. Линхардт Г. и Стельцери Д. Расчет активных осевых турбин с парциальным впуском. — Русский перевод журнала ARS Journ. «Ракетная техника», 1961, № 3.
136. Локай В. И. Зависимость профильных потерь в решетке от угла атаки. Известия АН СССР. ОТН, 1954, № 6.
137. Наталевич А. С. Течение газа в косом срезе единичных сопел и сопловых аппаратах турбин. Труды МАИ. Вып. 95, М., Оборонгиз, 1958.
138. Павлов А. П. Влияние высоты лопаток и формы каналов на концевые потери в сверхзвуковых рабочих решетках турбин. Труды ЛПИ № 297. Л., «Машиностроение», 1968.
139. Поликовский М. В. и Шеколдин А. В. О выборе конструкции соплового аппарата для сверхзвуковой регулирующей ступени. — «Теплоэнергетика», 1958, № 11.
140. Пшеничный В. Д. Исследование двухвенечных ступеней скорости с различными формами сопловых аппаратов. — «Теплоэнергетика», 1963, № 10.
141. Пшеничный В. Д. Оптимальный выходной угол сопел одновенечной активной ступени небольшой пропускной способности. — «Энергомашиностроение», 1964, № 2.
142. Розенберг Г. Ш., Костыркин В. Ф., Кастальский С. А. Результаты исследования радиальных турбин с лопаточными и безлопаточными направляющими аппаратами. Сб. «Судовые газовые турбины». М., «Морской транспорт», 1961.
143. Синярев Г. Б. и Добровольский М. В. Жидкостные ракетные двигатели. М., Оборонгиз, 1957.
144. Шерстянников В. А. Исследование активных парциальных турбин. — «Теплоэнергетика», 1963, № 10.
145. Юсупов Э. Н. и Соколов Б. Г. Об оптимальном расположении сопел в сегменте сверхзвуковой турбинной ступени. — «Энергомашиностроение», 1969, № 4.

146. Horlock J. H. Axial Flow Turbines. London, Butterworths, 1966.
147. Lancaster O., Bates C. Trans. ASME. Ser. A, 1959, vol. 81, No. 3.
148. Trutowsky K. «Konstruction», 1956, Nr. 10.
149. Winkler K. «Energietechnik», 1958, Nr. 9—12.

150. Добровольский М. В. и Крылов Ю. В. Определение наибольшего возможного давления в камере ЖРД, работающего по замкнутой схеме газ+жидкость. Известия ВУЗов. Серия «Машиностроение», 1967, № 4.
151. Поляковский М. В. [illegible] критерии устойчивости характеристик лопаточных машин. Известия АН СССР. ОТН. Серия «Энергетика», 1960, № 1.
152. Поляковский М. В. Переменные режимы и динамика запуска турбонасосов. — «Теплоэнергетика», 1962, № 11.
153. Сак Л. и Потсейдж Г. Колебания в системе, вызванные кавитацией на шнековом насосе. Trans. ASME. Серия D (Русский перевод), 1965, № 4.
154. Шемель В. Б. Экспериментальное определение осевых сил в центробежных насосах. — «Вестник машиностроения», 1958, № 6.
155. Шемель В. Б. и Агульник Ф. М. Исследование радиальных сил в центробежных насосах. Труды ВНИИГИДРОМАШ. Вып. 24. М., Машгиз, 1959.
156. Agostinelli A., Nobles D., Mockridge C. An Experimental Investigation of Radial Thrust in Centrifugal Pumps, Items ASME. Ser A., 1960, vol. 82.
157. «Aviation Week», 1963, vol. 78, No. 15—16.
158. «Mech. Design Eng.», 1964, No. 2.
159. «Missiles and Rockets», 1966, vol 18, No. 14.
160. Strub R. A. Trans. ASME. Ser. A, 1964, No. 2.
161. Wick S. The Effect of Vehicle Structure on Propulsion System Dynamics and Stability. «Jet Propulsion», October, 1956.